ICSS12

12th INTERNATIONAL CONFERENCE on SANDWICH STRUCTURES ICSS-12

Proceedings

19-22 August 2018 — EPFL Lausanne, Switzerland

Editors: Thomas Keller, Sonia Yanes-Armas, Leif A. Carlsson and Yeoshua Frostig

ÉCOLE POLYTECHNIQUE FÉDÉRALE DE LAUSANNE
CCLAB
AIREX BALTEK BANOVA
Office of Naval Research GLOBAL Science & Technology

12th INTERNATIONAL CONFERENCE on SANDWICH STRUCTURES ICSS-12

Proceedings

19-22 August 2018 — EPFL Lausanne, Switzerland

Edited by:

Thomas Keller	EPFL, Switzerland
Sonia Yanes-Armas	EPFL, Switzerland
Leif A. Carlsson	Florida Atlantic University (FAU), USA
Yeoshua Frostig	Technion - Israel Institute of Technology, Israel

Organized by:

Composite Construction Laboratory (CCLab)

École Polytechnique Fédérale de Lausanne (EPFL)

ISBN: 978-2-8399-2435-1 (PDF)
DOI: 10.5075/epfl-ICSS12-2018-1-275

Published by
Composite Construction Laboratory (CCLab)
École Polytechnique Fédérale de Lausanne (EPFL)
BP 2225 (Bâtiment BP), Station 16
1015 Lausanne
Switzerland
https://cclab.epfl.ch/

Cover
Rolex Learning Center
© Alain Herzog, EPFL

Cover Design
Composite Construction Laboratory (CCLab)
École Polytechnique Fédérale de Lausanne (EPFL)
Lausanne, Switzerland

PREFACE

This publication comprises the printed versions of the scientific articles presented at the 12th International Conference on Sandwich Structures, ICSS-12, and is compiled according to the Technical Program. The conference was organized by the Composite Construction Laboratory (CCLab) of the École Polytechnique Fédérale de Lausanne (EPFL) and took place at EPFL in Lausanne on August 19-22, 2018.

Following the previous conference in Fort Lauderdale (USA) in 2016, ICSS-12 was the 12th in this series, which started in Stockholm (Sweden) in 1989. It was the second to be held in Switzerland, the first being ICSS-5 in Zurich in 2001. The ICSS conferences represent one of the largest and most prestigious events covering the general topic of sandwich structures in the naval, aerospace, automotive, mechanical and civil engineering and architecture fields.

ICSS-12 aimed to provide a state-of-the-art overview, identify knowledge gaps and develop a vision for the future directions of research and development in sandwich structures. It was intended to provide a forum for world leaders in sandwich structures for the exchange and discussion of their latest research results and developments in such different sectors as aircraft, spacecraft, train and automotive applications, wind turbine blades, boat/ship hulls and superstructure, bridge and building construction.

The Technical Program comprised 84 presentations given in two parallel sessions during the three days. The total of 22 sessions covered a wide range of topics related to sandwich construction, including delamination/disbond, impact, fatigue, thermal effects, design, modeling, core materials, manufacturing and applications, and three special sessions organized by the U.S. Navy Office of Naval Research (ONR). Furthermore, four keynotes were presented by Prof. Amir Fam (Queen's University, Canada), Prof. João R. Correia (Technical University of Lisbon, Portugal), Dr. Ronald Krueger (National Institute of Aerospace, USA), and Prof. Christian Berggreen (Technical University of Denmark). The authors and participants represented 25 countries from four continents - America, Asia, Europe and Oceania.

We would like to thank i) all the authors and participants, for their valuable contributions to a successful conference, ii) the International Scientific Committee for their support in the review process, thus ensuring the high scientific standard of the conference, iii) the sponsors for their generous financial support, enabling the conference registration fee to be maintained at a reasonable level, and iv) the Local Organizing Committee for its strong commitment to the conference organization.

Thomas Keller, Leif A. Carlsson and Yeoshua Frostig
Conference chairs

Hosting Organization

Composite Construction Laboratory (CCLab), École Polytechnique Fédérale de Lausanne (EPFL)
https://cclab.epfl.ch

Conference Chairs

Chair:
Prof. Thomas Keller, EPFL, Switzerland
Co-Chairs:
Prof. Leif A. Carlsson, Florida Atlantic University (FAU), USA
Prof. Yeoshua Frostig, Technion - Israel Institute of Technology, Israel

International Scientific Committee

Dr. Mark Battley, University of Auckland, New Zealand
Prof. Christian Berggreen, Technical University of Denmark (DTU), Denmark
Dr. Magnus Burman, Royal Institute of Technology (KTH), Sweden
Prof. Leif A. Carlsson, Florida Atlantic University (FAU), USA
Prof. Pascal Casari, University of Nantes, France
Dr. Zhi-Ming Chen, FAA Tech Center, USA
Dr. Peter Davies, IFREMER, France
Mr. Russell Elkin 3A Composites, USA
Prof. Yeoshua Frostig, Technion - Israel Institute of Technology, Israel
Dr. Jörg Hohe, Fraunhofer IWM, Germany
Mr. James Jones, Diab International, USA
Prof. George A. Kardomateas, Georgia Institute of Technology, USA
Prof. Thomas Keller, EPFL, Switzerland
Dr. Ramesh Kolar, Office of Naval Research Global, USA
Dr. Ronald Krueger, National Institute of Aerospace (NIA), USA
Prof. Dayakar Penumadu, University of Tennessee, USA
Prof. Oded Rabinovitch, Technion - Israel Institute of Technology, Israel
Dr. Yapa D.S. Rajapakse, Office of Naval Research, USA
Dr. Ralf Schäuble, Fraunhofer IMWS, Germany
Prof. Arun Shukla, University of Rhode Island, USA
Prof. Jack R. Vinson, University of Delaware, USA

Local Organizing Committee

Prof. Thomas Keller, CCLab, EPFL, Switzerland
Dr. Julia de Castro, CCLab, EPFL, Switzerland
Dr. Sonia Yanes-Armas, CCLab, EPFL, Switzerland
Saira Mohamed, CCLab, EPFL, Switzerland

Sponsors

Major Sponsors:
3A Composites Core Materials, https://www.airexbaltekbanova.com
Office of Naval Research Global (ONRG), https://www.onr.navy.mil/

Sponsors:
ThermHex Waben GmbH, http://www.thermhex.com
Diab International AB, https://www.diabgroup.com

Institutional Partners

International Institute for FRP in Construction (IIFC), https://www.iifc.org
Society for the Advancement of Material and Process Engineering (SAMPE) Switzerland, http://www.sampe.ch
Carbon Composites Schweiz (CC Schweiz), https://www.carbon-composites.eu

CONTENTS

PLENARY LECTURES

DOI: 10.5075/epfl-ICSS12-2018-2

SANDWICH STRUCTURES WITH SYNTHETIC AND NATURAL FIBER COMPOSITE SKINS UNDER FLEXURAL AND AXIAL LOADING

Dr. Amir Fam, FASCE, CSCE, FIIFC, FACI, FCAE, FEIC, PEng[1]
[1]Donald and Sarah Munro Chair Professor, Civil Engineering, and Associate Dean (Research),
Faculty of Engineering and Applied Science, Queen's University, Canada, Email: amir.fam@queensu.ca

This paper is an overview of research activities at Queen's University, Canada, over the past ten years, pertaining to sandwich panels with both glass fiber reinforced polymer (GFRP) and flax-FRP (FFRP) skins. The research addressed flexural performance and behavior under axial compression loading, including slenderness effect. Both short and long term behaviors, including fatigue performance [1,2] and durability under thermal cycles and in salt solution [3], have been studied. The effects of core density [4-6], skin-to-core thickness ratio, particularly with FFRP skins [7,8], and internal rib configuration [9,10] were explored, followed by a full scale test on cladding wall panel under air pressure [11]. The effect of reversed bending fatigue representing wind pressure and suction was studied [12]. The experimental work was complemented by analytical and numerical investigations accounting for both material and geometric non-linearity arising from the soft core [13-16]. The research showed that sandwich panels with FFRP skins can indeed provide equivalent flexural and axial strength to panels with GFRP skins; however, thicker skins by about 20% are necessary. Tensile strength and modulus of FFRP are sensitive to number of layers. As the layers increased from one to five, the properties also increased but plateaued at three layers. Vacuum bag (VB) molding resulted in an apparent increase in tensile strength of FFRP coupons; however, when applied to sandwich panels there is a decrease in ultimate load of the panel of up to 27%, compare to wet layup (WL) because the VB thinner skins are more susceptible to skin wrinkling. VB specimens also demonstrated a higher susceptibility to environmental degradation than WL specimens. Tensile strength retentions of FFRP are better than GFRP at elevated temperatures. The 300 days retentions of FFRP at 23°C, 40°C, and 55°C were 81, 76 and 72%, while for GFRP were 86, 72 and 61%, respectively. Fatigue threshold of panels without ribs was 37% of the ultimate static capacity. In order for panels to sustain at least two million cycles, load should be limited to about 45% of the static capacity (and 30% for fully reversed bending). The benefit of ribs was more significant in low cycle fatigue (from zero to approximately 1,000 cycles). From 1,000 cycles to infinite fatigue life (high cycle fatigue), the contribution of ribs to strength reduced gradually to zero. Increasing core density from 32 to 96 kg/m^3, increased axial strength of panels by 116-176% at various slenderness ratios.

REFERENCES

[1] Mathieson, H. and Fam, A. (2014) "Static and Fatigue Behavior of Sandwich Panels with GFRP Skins and Governed by Soft Core Shear Failure", ASCE Journal of Composites for Construction, 18(2):04013046.
[2] Mathieson, H. and Fam, A. (2015) "Effect of Internal Ribs on Fatigue Performance of Sandwich Panels with GFRP Skins and Polyurethane Foam Core", ASCE Journal of Materials in Civil Engineering, 27(2):A4014005 (Invited paper).
[3] Mak, K., Fam, A., and MacDougall, C. (2016) "The Effects of Long Term Exposure of Flax Fiber Reinforced Polymer to Salt Solution at High Temperature on Tensile Properties", Polymer Composites, 37(11):3234–3244.
[4] Sharaf, T., Shawkat, W., and Fam, A. (2010) "Structural Performance of Sandwich Wall Panels with Different Foam Core Densities in One-Way Bending", Journal of Composite Materials, 44(19):2249-2263.
[5] CoDyre, L., and Fam, A. (2017) "Axial Strength of Sandwich Panels of Different Lengths with Natural Flax Fiber Composite Skins and Different Foam Core Densities", ASCE Journal of Composites for Construction, 21(5):04017042.
[6] CoDyre, L., and Fam, A. (2016) "The Effect of Foam Core Density at Various Slenderness Ratios on Axial Strength of Sandwich Panels with Glass-FRP Skins", Composites Part B: Engineering, 106:129-138.
[7] Mak, K., Fam, A., and MacDougall, C. (2015) "Flexural Behavior of Sandwich Panels with Bio-FRP Skins Made of Flax Fibers and Epoxidized Pine Oil Resin", ASCE Journal of Composites for Construction, 19(6):04015005.
[8] CoDyre, L., Mak, K. and Fam, A. (2016) "Flexural and Axial Behaviour of Sandwich Panels with Bio-Based Flax-FRP Skins and Various Foam Core Densities", Journal of Sandwich Structures and Materials, DOI:10.1177/1099636216667658.
[9] Fam, A. and Sharaf, T. (2010) "Flexural Performance of Sandwich Panels Comprising Polyurethane Core and GFRP Skins and Ribs of various Configurations" Composite Structures, 92(12):2927-2935.
[10] Mathieson, H. and Fam, A. (2016) "Analytical Modeling and Experimental Validation of Axially Loaded Slender Sandwich Panels with Soft Core and Various Rib Configurations", Engineering Structures, 118:195-209.
[11] Sharaf, T. and Fam, A. (2011) "Experimental Investigation of Large Scale Cladding Sandwich Panels under Out-of-Plane Transverse Loading for Building Applications", ASCE Journal of Composites for Construction, 15(3):422-430.
[12] Mathieson, H. and Fam, A. (2014) "High Cycle Fatigue under Reversed Bending of Sandwich Panels with GFRP Skins and Polyurethane Foam Core", Composite Structures, 113:31-39.
[13] Sharaf, T. and Fam, A. (2012) "Numerical Modelling of Sandwich Panels with Soft Core and Different Rib Configurations", Journal of Reinforced Plastics and Composites, 31(11):771–784.
[14] Sharaf, T. and Fam, A. (2013) "Analysis of Large Scale Cladding Sandwich Panels Composed of GFRP Skins and Ribs and Polyurethane Foam Core", Thin-Walled Structures, 71:91-101.
[15] Mathieson, H. and Fam, A. (2015) "Axial Loading Tests and Simplified Modeling of Sandwich Panels with GFRP Skins and Soft Core at Various Slenderness Ratios", ASCE Journal of Composites for Construction, 19(2):04014040.

DOI: 10.5075/epfl-ICSS12-2018-3-5

COMPOSITE SANDWICH PANELS FOR BUILDING FLOORS: RECENT DEVELOPMENTS AND MAIN CHALLENGES

João R. Correia[1] and Mário Garrido[2]
[1]CERIS, Instituto Superior Técnico, University of Lisbon, Portugal. joao.ramoa.correia@tecnico.ulisboa.pt
[2]CERIS, Instituto Superior Técnico, University of Lisbon, Portugal. mario.garrido@tecnico.ulisboa.pt

1. INTRODUCTION

Sandwich structures have a long history of successful use in various applications, namely in automotive, aerospace and naval industries [1]. For civil engineering applications, sandwich structures also present very high potential, due to their high strength- and stiffness-to-weight ratios, lightness and potential multi-functionality, *i.e.* their ability to fulfil multiple functions in a single element [2]. In addition, when made of fibre reinforced polymer (FRP) skins, this type of construction also offers durability and low maintenance requirements.

The above-mentioned features are particularly useful for the rehabilitation of existing buildings, namely those made of masonry walls with degraded timber floors. In these cases, replacing timber floors with FRP sandwich panels does not represent significant weight increase, which can be a very important advantage, especially in seismic regions [3]. However, for building applications, composite sandwich panels need to meet specific requirements, namely (i) those concerned with the connection technology; (ii) the ability to present limited deformations during service life, (iii) the acoustic comfort afforded by partition elements; and (iv) the behaviour when exposed to elevated temperatures or fire. These different requirements constitute a main challenge towards the use of FRP sandwich panels in buildings. This presentation summarizes some of the research made in recent years at Instituto Superior Técnico - University of Lisbon (IST-UTL) regarding the prospects of composite sandwich floors in addressing such challenges.

2. CONNECTION TECHNOLOGY

Recent investigations at IST focused on the connection technology for sandwich panel floors at two levels: (i) panel-to-supports; and (ii) panel-to-panel.

At the panel-to-supports level, connection systems were designed, tested and simulated, aiming at joining sandwich floor panels to masonry walls of old buildings in the scope of rehabilitation projects [4]. These systems involve bolting and/or bolding the panels to the load-bearing walls through metallic angle section members along the contour of the walls (Fig. 1). This follows the same intervention principle used when replacing timber floors, where angle profiles are also used to brace the walls, thus improving their resistance to out-of-plane loads.

At the panel-to-panel level, connection systems have been developed and investigated with the following main requirements: (i) easy and fast panel installation in confined spaces, by means of vertical movements (instead of horizontal/sliding movements); (ii) adequate structural performance; and (iii) possibility of integration in the production process. Two main types of connection systems were designed, tested and simulated: adhesively bonded (Fig. 2) [5] and snap-fit or interlock. While the former system provides higher stiffness, the latter offers quicker installation times and the possibility of disassembly.

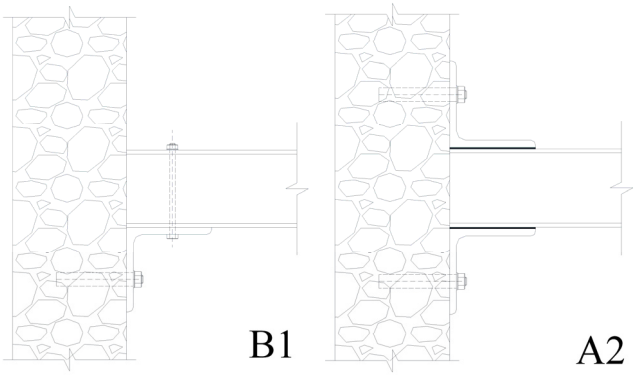

Fig. 1: Detail of two of the panel-to-wall connection systems tested (B1 – bolted, single profile; A2 – adhesive, two profiles) [4].

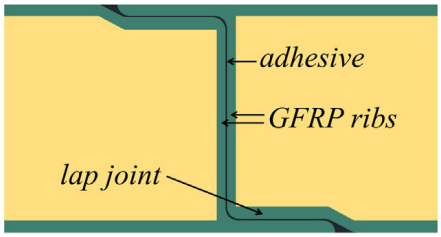

Fig. 2: Detail of a Z-shaped adhesively bonded panel-to-panel connection [5].

3. LONG-TERM STRUCTURAL BEHAVIOUR

Sandwich panels used in building floors need to be designed to fulfil service limit states requirements during service life, which is generally set as 50 years. This period is much longer than that considered in other more typical

applications of sandwich panels. This explains the very limited information available in the literature and in existing design guidance about the creep behaviour of sandwich panels and their constituent materials.

Previous research at IST in this domain focused on the characterization of the creep response of (i) different core materials – polyurethane (PUR) and polyethylene terephthalate (PET) foams and balsa wood – in shear [6]; (ii) GFRP skins in bending [7]; and (iii) full-scale sandwich panels in bending [8,9]. In each case, the influence of the load level and of the service temperature on the creep behaviour were investigated. Results of experiments were used to derive design-oriented creep coefficients and simple analytical models to predict the long-term structural response of sandwich panels [6-9].

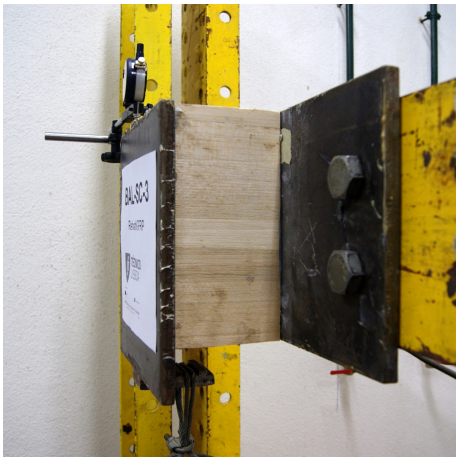

Fig. 3: Shear creep test in balsa wood.

Fig. 4: Flexural creep tests of web-core FRP sandwich panel.

4. ACOUSTIC BEHAVIOUR

For building applications, a very relevant requirement for user's comfort is the acoustic performance of partition members, such as walls and floors. In this respect, due to their inherent lightness, there are concerns about the acoustic insulation provided by FRP sandwich panels.

In this domain, recent and on-going research at IST has two main goals: (i) to understand and characterize the acoustic performance of FRP sandwich panels and, whenever needed, (ii) to define and assess constructive strategies towards the fulfilment of acoustic-related building regulation requirements, either adjusting the characteristics of the panels or adopting complementary constructive measures. To that end, full-scale experimental tests were recently conducted to assess the acoustic insulation of FRP sandwich panels for both airborne and impact sounds (Fig. 5). These experiments were complemented with finite element (FE) models that were used to simulate the response measured in those tests (Fig. 6) and to assess the effectiveness of different improvement measures.

Fig. 5: Full-scale acoustic tests in FRP sandwich panels.

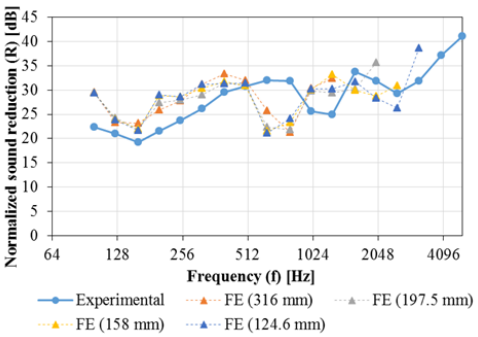

Fig. 6: Numerical FE simulation of airborne sound insulation of FRP sandwich panel for different mesh sizes.

5. BEHAVIOUR AT ELEVATED TEMPERATURE AND UNDER FIRE EXPOSURE

The behaviour of FRP sandwich panels at elevated temperature and under fire exposure is one of the most serious challenges regarding their use in buildings, where elements must fulfil relatively strict requirements in terms of both fire resistance and fire reaction. Indeed, when exposed to moderately elevated temperature, the mechanical properties of both FRP skins and most core materials are significantly decreased. Accordingly, under fire exposure, the integrity of

structural members can be compromised in relatively short periods. Moreover, most materials ignite under such temperatures, releasing heat, smoke and potentially toxic gases.

In this domain, research at IST has focused on three main issues: (i) the mechanical behaviour at elevated temperature of the constituent materials of sandwich panels - FRP skins, and polymeric foam and balsa wood cores [10,11]; (ii) the fire resistance behaviour of tubular and multicellular structural elements in bending [12,13]; and (iii) the fire reaction behaviour of FRP panels. For the last two issues, the influence of different passive fire protection systems was experimentally and numerically assessed, indicating the conditions under which fire-related building regulation requirements may be met.

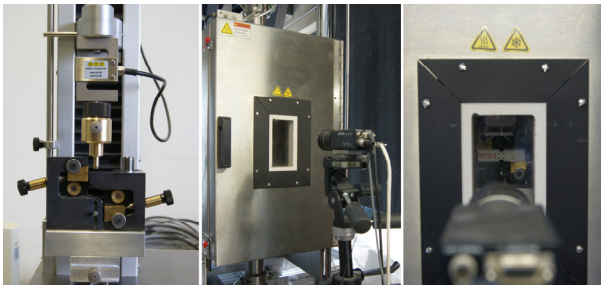

Fig. 7: Shear (Iosipescu) test in PUR foam at elevated temperature [10].

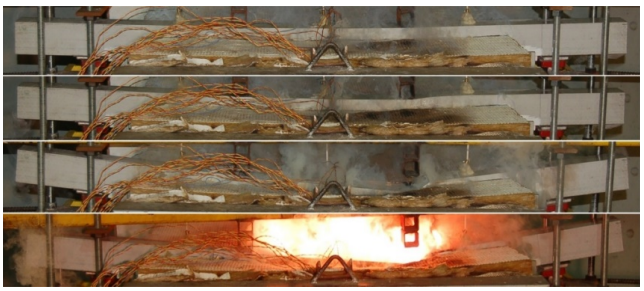

Fig. 8: Fire resistance test in tubular FRP profile [13].

6. CONCLUDING REMARKS

Sandwich construction is a very interesting solution for civil engineering structural applications, for both new constructions and the rehabilitation of existing ones. Composite sandwich panels in particular offer many advantages for this specific application, namely for the replacement of degraded timber floors of old buildings. This presentation describes the results of recent research activities conducted at Instituto Superior Técnico in order to address a number of challenges towards the use of composite sandwich panels in building floors: the connection technology, the creep behaviour, the acoustic performance and the fire behaviour. The results obtained confirm the potential of composite sandwich panels for this application, but also point out the need to take those aspects into account in their design.

ACKNOWLEDGEMENTS

The authors would like to acknowledge the financial support of the Portuguese National Innovation Agency (ANI) – project 2015/03480 (EasyFloor).

REFERENCES

[1] D. Zenkert, *The Handbook of Sandwich Construction*. Engineering Materials Advisory Services (EMAS), Worcestershire, UK: 1997, 442p.

[2] S. Yanes-Armas *et al.*, “Long-term design of FRP-PUR web-core sandwich structures in building construction”, *Compos. Struct.*, 2017; 181: 214-228.

[3] M. Garrido, *Composite Sandwich Panel Floors for Building Rehabilitation*, PhD Thesis in Civil Engineering, Instituto Superior Técnico, 2016.

[4] M. Garrido *et al.*, “Connection systems between composite sandwich floor panels and load-bearing walls for building rehabilitation”, *Eng. Struct.*, 2016; 106: 209-221.

[5] M. Garrido *et al.*, “Adhesively bonded connections between composite sandwich floor panels for building rehabilitation”, *Compos. Struct.*, 2015; 134: 255-268.

[6] M. Garrido *et al.*, “Effect of service temperature on the shear creep response of rigid polyurethane foam used in composite sandwich floor panels”, *Constr. Build. Mater.*, 2016; 118: 235-244.

[7] M. Garrido *et al.*, “Effect of service temperature on the flexural creep of vacuum infused GFRP laminates used in sandwich floor panels”, *Compos. Part B Eng.*, 2016; 90: 160-171.

[8] M. Garrido *et al.*, “Elastic and viscoelastic behaviour of sandwich panels with GFRP faces and PET foam core”, *J. Sandw. Struct. Mater.*, DOI: 10.1177/1099636216657388.

[9] M. Garrido *et al.*, “Creep of sandwich panels with longitudinal reinforcement ribs for civil engineering applications: experiments and composed creep modelling”, *J. Compos. Constr.*, 2017; 21: 04016074.

[10] M. Garrido *et al.*, “Effects of elevated temperature on the shear response of PET and PUR foams used in composite sandwich panels”, *Constr. Build. Mater.*, 2015; 76: 150-157.

[11] J.R. Correia *et al.*, “Mechanical behaviour of pultruded glass fibre reinforced polymer composites at elevated temperature: experiments and model assessment”, *Compos. Struct.*, 2013; 98: 303-313.

[12] T. Morgado *et al.*, “Numerical modelling of the thermal response of pultruded GFRP tubular profiles subjected to fire”, *Compos. Part B Eng.*, 2018; 137: 202-216.

[13] T. Morgado *et al.*, “Experimental study on the fire resistance of GFRP pultruded tubular beams”, *Compos. Part B Eng.*, 2018; 139: 106-116.

DOI: 10.5075/epfl-ICSS12-2018-6-7

FACE SHEET TO CORE SEPARATION CAUSED BY INTERNAL CORE PRESSURE: AN IMPORTANT FAILURE MODE FOR AEROSPACE STRUCTURES MADE OF HONEYCOMB SANDWICH

Ronald Krueger
National Institute of Aerospace, Hampton, Virginia, USA. rkrueger@nianet.org

Sandwich structures exhibit high stiffness and strength-to-weight ratios and therefore are widely used as structural components, especially within the aerospace industry [1, 2]. Sandwich structures become most effective with thick, low density cores. The volume of light-weight honeycomb core materials typically consist of up to 95% enclosed air. If this honeycomb sandwich structure is subjected to varying ambient pressure, temperature and/or humidity, and if airflow into and out of the honeycomb core is prohibited, the resulting pressure difference causes mechanical stress. During the ascent of an aircraft to cruise altitude and the launch of space systems, their honeycomb sandwich structures are subjected to tensile stress in the core, as well as in the bondline between face sheet and core, caused by the decreasing ambient pressure. Although a major concern for aircraft honeycomb structures today, the first problems related to internal pressurization arose in space systems. Since their use in the early 1960's, several honeycomb sandwich structures of space systems have failed during launch due to face sheet/core disbonding [3, 4]. A major recommendation that arose from the subsequent accident investigations was the use of fully vented sandwich constructions for space systems. This means that the sandwich should not only be vented between each core cell but also through the face sheets. If the use of a vented design is not possible, the structural integrity should be verified via in-flight condition testing and non-destructive testing of the face sheet/core bond [4]. However, large-scale face sheet/core disbonding in unvented sandwich construction occurred again in the liquid hydrogen tank of the X-33 technology flight demonstration vehicle during the protoflight test in 1999 [5, 6]. The internal pressurization of the core in this case was caused by gases which had entered the honeycomb core due to an external leak path and then condensed to the cold surfaces, reducing the internal pressure. This phenomenon called *cryopumping* allowed more gas to enter the honeycomb core. During the warm-up phase of the tank after the test, the gases expanded and created much higher loads than the atmospheric pressure. This structural failure was cited as one of the reasons to stop the *VentureStar* suborbital spaceplane program.

Due to their lower operating altitude, aircraft honeycomb sandwich structures experience lower loads during flight compared to space systems. However, the use of fully vented sandwich constructions often is not possible or practical. Although intact honeycomb sandwich structures have been widely used in aircrafts for many years, face sheet/core disbonding can be critical when the bondline between face sheet and core is weak or damaged due to impacts or inadequate repairs. In the last decades, face sheet/core disbonding in honeycomb sandwich structures have occurred in large passenger aircrafts [7-11]. Among initial disbonds, or weak face sheet/core interfaces, internal pressurization was another major cause of the disbond propagation. In another example, the loss of a rudder on a commercial airliner (as shown in Fig. 1) was found to be caused by disbonding within the sandwich structure of the rudder, growth of which was driven by internal pressurization at flight altitude [10, 11]. A key conclusion of these incidents is that critical face sheet disbond size and the parameters affecting disbond growth become very important for the damage tolerance evaluation of an aircraft sandwich component during its design phase and in service.

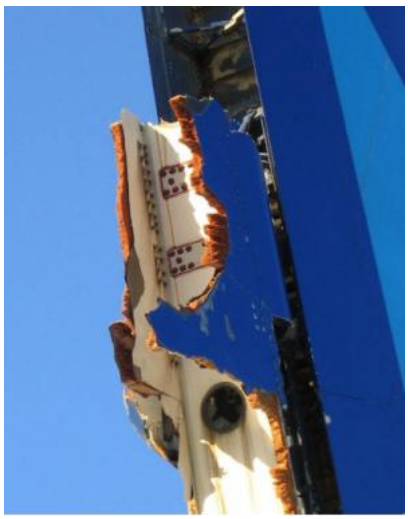

Fig. 1: Loss of rudder in a commercial airliner [10].

In this presentation, a historical background is provided. In addition, an overall methodology to address face sheet to core separation in sandwich structures is presented. Steps taken by an international group of experts include the development of test methods that yield a critical strain energy release rate associated with disbonding, with a current focus on mode-I dominated loading conditions. Further steps include the development of analysis methods to compute energy release rates along an arbitrarily shaped disbond front. Finally, an outlook is provided.

REFERENCES

[1] Vinson JR. Sandwich Structures: "Past, Present, and Future. In: Sandwich Structures 7: Advancing with Sandwich Structures and Materials," *Proceedings of the 7th International Conference on Sandwich Structures*, Aalborg, Denmark, 29-31 August 2005, pp. 3-12.

[2] Herrmann AS, Zahlen PC and Zuardy I: "Sandwich Structures Technology in Commercial Aviation. In: Sandwich Structures 7: Advancing with Sandwich Structures and Materials," *Proceedings of the 7th International Conference on Sandwich Structures*, Aalborg, Denmark, 29-31 August 2005, pp. 13-26.

[3] Low GM. Apollo 6 Anomaly Report No. 6: "Abnormal Structural Performance During Launch Phase," *NASA-TM-X-70374,* National Aeronautics and Space Administration, Houston, TX, USA, April 1969.

[4] Epstein G and Ruth S. "Honeycomb Sandwich Structures: Vented Versus Unvented Designs for Space Systems," *Aerospace Report No. TR-93(3904)-1*, The Aerospace Corporation, El Segundo, CA, USA, October 1993.

[5] Goetz et al. "Final Report of the X-33 Liquid Hydrogen Tank Test Investigation Team," National Aeronautics and Space Administration, Huntsville, AL, USA, May 2000.

[6] Glaessgen EH, Reeder JR, Sleight DW, Wang JT, Raju IS and Harris CE: "Debonding. Failure of Sandwich-Composite Cryogenic Fuel Tank with Internal Core Pressure," *Journal of Spacecraft and Rockets* 2005, vol. 42, no. 4, pp. 613-627.

[7] Air Accident Investigation Branch. *AAIB Bulletin 8/92 Ref: EW/A92/5/1*, Air Accident Investigation, UK, 1992.

[8] Air Accident Investigation Branch. *AAIB Bulletin 2/95 Ref: EW/C94/8/3*, Air Accident Investigation, UK, 1995.

[9] Air Accident Investigation Branch. *AAIB Bulletin 10/96 Ref: EW/C96/6/6*, Air Accident Investigation, UK, 1996.

[10] Transportation Safety Board of Canada. *Aviation Investigation Report A05F0047*, Minister of Public Works and Government Services Canada, 2007.

[11] Hilgers R: "Substantiation of Damage Growth within Sandwich Structures," *FAA Workshop for Composite Damage Tolerance & Maintenance*, Tokyo, Japan, 1-5 June 2009.

10.5075/epfl-ICSS12-2018-8-10

FRACTURE MECHANICS METHODS FOR ASSESSMENT OF DAMAGE TOLERANCE OF DEBONDED/DISBONDED SANDWICH STRUCTURES

Christian Berggreen[1]
[1]Department of Mechanical Engineering, Technical University of Denmark, Denmark. cbe@mek.dtu.dk

In the last 40 years sandwich composites have seen a growing popularity in a wide spectrum of different industries. Areas of application have first of all been aircraft and spacecraft, but with a decreasing fiber material price of the most commonly used fiber types, composite materials have eventually been applied on a larger scale in ships, cars, trains, wind turbine blades, off-shore installations, etc. Common to most of these weight critical applications is the need for reducing the weight of the structure to increase the strength-to-weight and stiffness-to-weight ratios and thus obtain better performance and/or an increased loading capacity. With regard to these strength- and stiffness-to-weight ratios, composites and especially sandwich composites possess a superior performance. Other advantageous properties are thermal and acoustic insulation, fatigue, corrosion and easy manufacturing of aero- and hydro-dynamically superior shapes.

One of the key aspects in a design, which does not only apply to composite weight-critical structures but in general, is to be able to take advantage of the construction materials and utilize them to their limits. This, in turn, leads to requirements for theoretical tools for accurate prediction of the loads, the structural response as well consequences of damages in the structure. However, with the increasing ability to optimize the structures to the performance limit of the construction materials and with the willingness to do so in practice, the reserve margin for structural degradation and damage tolerance becomes significantly smaller. In Fig. 1 the reliability index, Y, versus the ageing of the structure is shown for a typical structural lifetime of a structure optimized to the material performance limit. For this particular example it may be observed that the reliability index is reduced as the ageing of the structure increases. However, the structural integrity is regained because of repair every time the reliability index reaches the accepted minimum value.

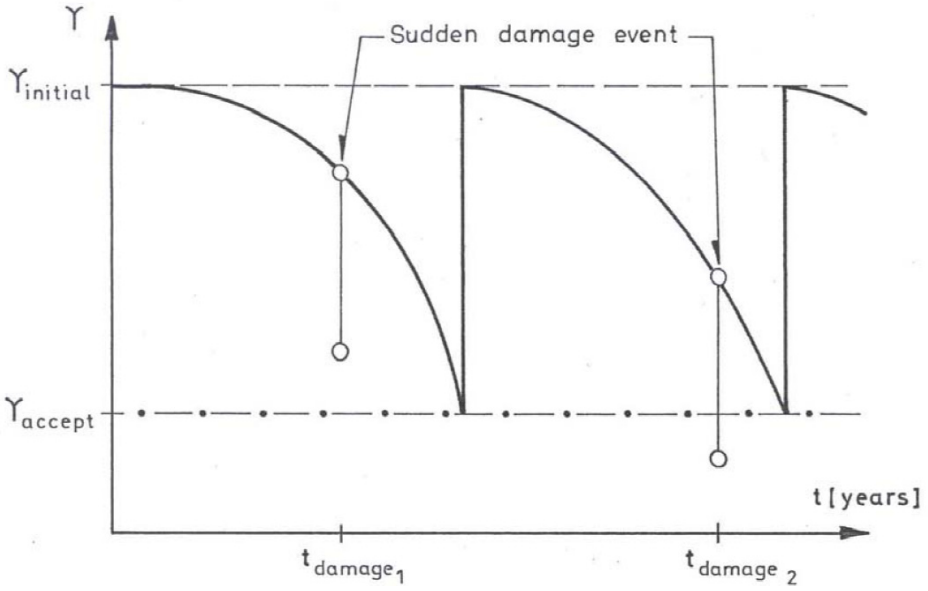

Fig. 1: The structural reliability index versus the ageing of the structure. Additionally, the effect of a sudden damage event is indicated.

In Fig. 1 the effect of the same sudden damage to the structure is indicated for two different times during the structural lifetime. The damage to the structure means that the structural integrity is suddenly reduced and the reliability index is therefore dropping. As indicated in Fig. 1, the damage is seen to be non-critical to the first damage case but critical to the second damage case, as the reliability instantly drops below the accepted value. The example emphasizes the importance of being able to evaluate the criticality of a given damage in connection with the redundancy of the structure. Furthermore, it is evident that in order to achieve highly optimized structures, which are able to operate in a stochastic loading environment, damage tolerance evaluation is needed. Furthermore, the damage tolerance approach does not only apply to the design and optimization of composite structures, but is also highly relevant to composite

structures already in service and exposed to minor or major damages. Is a given damage critical for the structural integrity, or is the damage negligible? These questions are especially relevant for sandwich structures, which by nature are highly optimized structures with a high number of possible damage scenarios and consequent failure mechanisms.

Among the most critical damages to sandwich structures is debonding or disbonding (the choice of term depends on the industry segment) of the face and core layer (loss of connection between them), see Fig. 2. This kind of damage can be highly critical for the sandwich structure as the basic sandwich principle is compromised when the connection between the face and the core layer is lost. Over the last 30 years, investigations of this damage type have been carried out within a range of industry segments, beginning with Zenkert (1990) [1], who investigated the strength of foam core sandwich beams with various debonds and interface propagated shear cracks using the finite element method and experimental testing. A wide range of other investigations have over the years been presented in the literature aiming at different sandwich material systems within marine, wind energy, aeronautical and space applications, using both experimental and numerical tools to model debond propagation using experimental fracture mechanical characterization data from a range of different fracture characterization specimens.

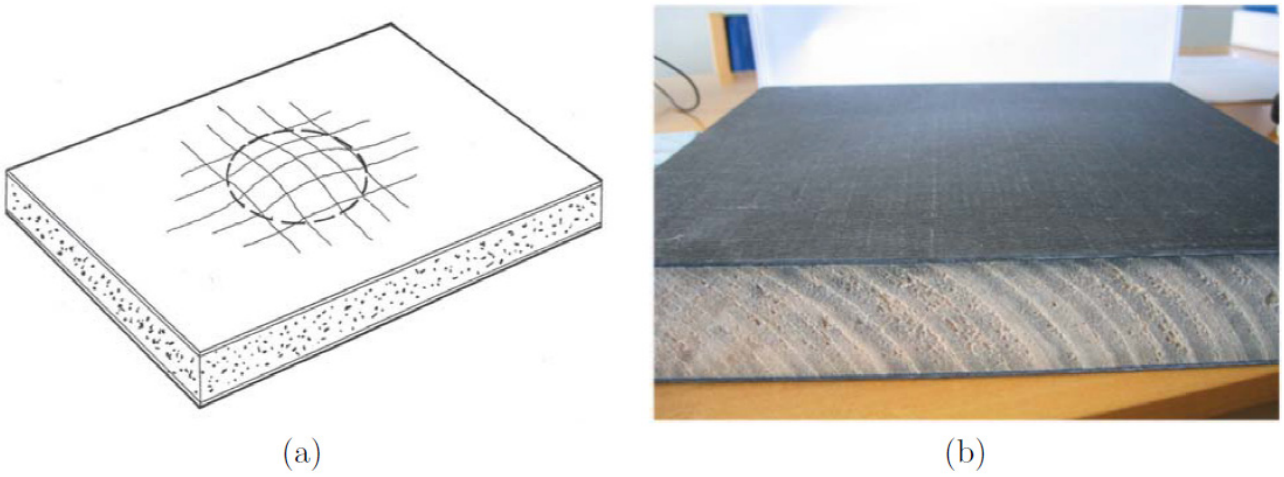

Fig. 2: Example of a debond in a CFRP/PVC foam core panel. (a) Schematic representation, (b) photo courtesy of Royal Institute of Technology, Sweden.

In addition, the underpinning generic fracture mechanics for an interface crack between two dissimilar materials has over the same time span developed from the fundamental work by Professor J. W. Hutchinson and Professor Z. Suo, who were the first to establish a firm foundation for the analytical description of the bi-material interface fracture mechanics, Hutchinson and Suo (1992) [2], Suo (1990) [3] and Suo and Hutchinson (1990) [4]. Their work have the recent years been expanded by a number of authors to address sandwich specimens with a full set of external loading configurations, opening the door for possible standardization of fracture characterization specimens and methods for sandwich composites.

The current plenary talk will include a review and overview of the work performed in the field of damage tolerance of debonded sandwich structures focusing on the development of fracture mechanics based analysis and test methods for the assessment of residual strength and life-time of typical sandwich structures. Analysis and test methods both on the coupon, component and structural length-scale will be presented and recommendations will be given for safe engineering analysis and assessment of debond damages in a range of typical debond damage cases from the marine, wind energy and aeronautical industries, see Figs. 3-5.

Fig. 3: Debond damages as a result of slamming on the wet-deck bottom structure in a catamaran ship.

Fig. 4: Disbond damage in a wind turbine blade as a result of torsional induced panel breathing in the max-cord section.

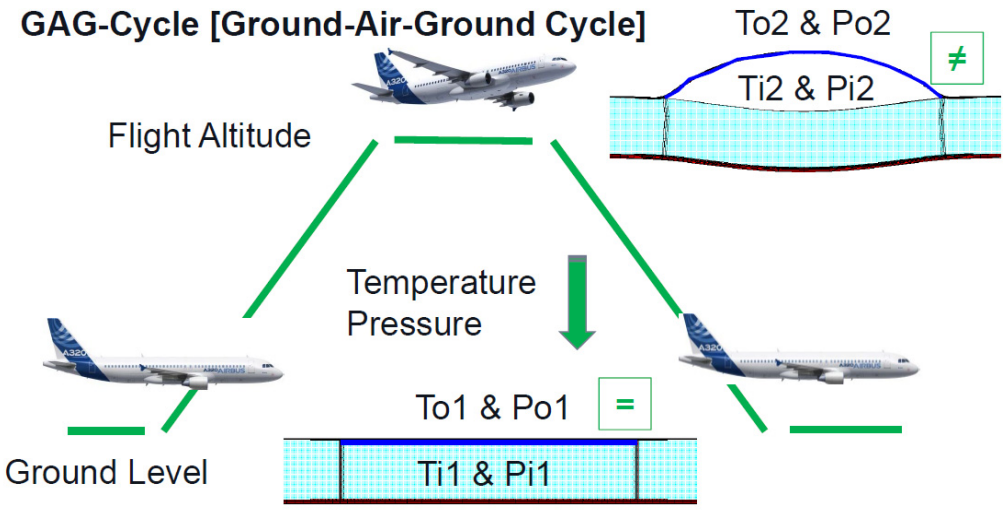

Fig. 5: Disbond damages in an aircraft honeycomb sandwich panel as a result of Ground-Air-Ground flight operational induced pressure differences. Photo courtesy of Airbus.

REFERENCES

[1] Zenkert, D. (1990), Damage Tolerance of Foam Core Sandwich Constructions, PhD thesis, Department of Aeronautics, Royal Institute of Technology, Sweden.

[2] Hutchinson, J.W. and Suo, Z. (1992), Mixed Mode Cracking in Layered Materials, Advances in Applied Mechanics, J.W.Hutchinson and T.Y.Wu (eds.), 29:63–191.

[3] Suo, Z. (1990), Singularities, Interfaces and Cracks in Dissimilar Anisotropic Media, Proc. Royal Society of London, A(427):331–358.

[4] Suo, Z. and Hutchinson, J. W. (1990), Interface Crack Between Two Elastic Layers, Int. Journal of Fracture, 43:1–18.

SESSION 1A: ONR SPECIAL SESSION – MECHANICS

DOI: 10.5075/epfl-ICSS12-2018-12-14

NONLINEAR BUCKLING AND POST-BUCKLING BEHAVIOR OF SANDWICH BEAMS/WIDE PANELS

Zhangxian Yuan[1] and George A. Kardomateas[2]
[1] Georgia Institute of Technology, USA. yuanzx@gatech.edu
[2] Georgia Institute of Technology, USA. george.kardomateas@aerospace.gatech.edu

1. INTRODUCTION

The advantages in strength, stiffness and overall response of the sandwich structure can be realized only if it is stabilized against buckling. The compressibility of the core significantly affects the stability response and contributes to the local instability phenomenon. Therefore, despite the global buckling (Euler buckling), very common in ordinary beams and plates, wrinkling, also known as local buckling, may occur in sandwich structures. Wrinkling manifests itself as short-wave buckling of the face sheets.

In the literature, the sandwich theories, especially high order theories, have been applied to investigate the stability behavior of sandwich structures, e.g., High-order Sandwich Panel Theory (HSAPT) [1-3], Extended High-order Sandwich Panel Theory (EHSAPT) [4, 5]. Perhaps due to the complexity of the stability of sandwich structures, assumptions are usually adopted to simplify modelling and solving efforts, i.e., the anti-plane assumption [1-3] in the core, and membrane pre-buckling state [4, 5]. The anti-plane assumption assumes the axial rigidity of the core is negligible since its magnitude is usually about two to three orders of magnitude smaller than that of the faces. Although the validation of anti-plane assumption is approved for the static and dynamic behavior, there is no clear evidence that the effect caused by the axial rigidity of the core is negligible to the stability response. As a compound structure containing layers made of different materials, the sandwich structure may also have a non-membrane pre-buckling state even when subjected to axial compressive loading. Therefore, it is of crucial importance to investigate the stability property of sandwich panels comprehensively without applying these simplifications.

The Extended High-order Sandwich Panel Theory (EHSAPT) accounts for the axial, transverse, and shear rigidity of the core. It shows high accuracy and yields identical displacement and stress to the elasticity for both static behavior and dynamic response. Therefore, a general and comprehensive investigation about the stability of sandwich panels is carried out based on the EHSAPT. The weak form governing equations are formulated based on EHSAPT-based finite element [6]. Both faces and core undergo large displacements with moderate rotations.

2. MATHEMATICAL FORMULATION

The stability analysis is based on the equilibrium equations of sandwich panels, which are derived from the nonlinear EHSAPT. The high stiffness thin faces follow the Euler-Bernoulli assumptions and the thick core has a high order displacement pattern. In the core, the axial displacement and transverse displacement are assumed to be a third order polynomial and a second order polynomial in terms of the transverse coordinate, z, respectively. The geometric nonlinearity is considered in both faces and core, and the Lagrange strain is used as the kinematic relation. In faces, only the axial normal strain is considered as the result of the Euler-Bernoulli assumption,

$$\varepsilon_{xx}^{t,b} = u_{,x}^{t,b} + \frac{1}{2}\left(u_{,x}^{t,b}\right)^2 + \frac{1}{2}\left(w_{,x}^{t,b}\right)^2 \tag{1}$$

and in the core, the nonlinear axial normal strain, transverse normal strain, and shear strain are,

$$\varepsilon_{xx}^{c} = u_{,x}^{c} + \frac{1}{2}\left(u_{,x}^{c}\right)^2 + \frac{1}{2}\left(w_{,x}^{c}\right)^2 \tag{2a}$$

$$\varepsilon_{zz}^{c} = w_{,z}^{c} + \frac{1}{2}\left(u_{,z}^{c}\right)^2 + \frac{1}{2}\left(w_{,z}^{c}\right)^2 \tag{2b}$$

$$\gamma_{xz}^{c} = u_{,z}^{c} + w_{,x}^{c} + u_{,x}^{c}u_{,z}^{c} + w_{,x}^{c}w_{,z}^{c} \tag{2c}$$

Together with the EHSAPT-based element, which has 10 DOFs at each node, the weak form nonlinear governing equations are obtained from the variational principle of total potential energy. It is given as,

$$\left\{\mathbf{G}\left(\{\mathbf{U}\},\lambda\right)\right\} = \left[\mathbf{K}\left(\{\mathbf{U}\}\right)\right]\{\mathbf{U}\} - \lambda\{\mathbf{R}\} = \{\mathbf{0}\} \tag{3}$$

where $[\mathbf{K}(\{\mathbf{U}\})]$ is the stiffness matrix, $\{\mathbf{U}\}$ is the displacement vector, $\{\mathbf{R}\}$ is the unit load vector and λ is a load scalar. Since the geometric nonlinearity is considered, the stiffness matrix $[\mathbf{K}(\{\mathbf{U}\})]$ depends on the deformation, $\{\mathbf{U}\}$. Eq. 3 gives the governing equations of sandwich panels in arbitrary equilibrium state, including the pre-buckling state, buckling state, and post-buckling state. Therefore, it is used to determine the critical load and buckling mode, and will also be used to obtain the post-buckling response.

In the buckling analysis, the pre-buckling state is determined via a nonlinear static analysis. Thus, the pre-buckling state is not necessary to be a membrane state. The global buckling and wrinkling are not treated separated, and thus, the interaction between the global buckling and wrinkling can be captured. The critical load is calculated by solving an eigen-value problem and the corresponding eigen-vector gives the buckling mode.

The post-buckling response of sandwich structures can be regarded as an extension of the geometric nonlinear static behavior. Therefore, it is obtained from the weak form nonlinear governing equations. The path following procedure together with branch switching technique or imperfections is considered to capture the bifurcation phenomenon.

3. NUMERICAL EXAMPLES

Several sandwich panels with different lengths subjected to axial compressive loads are considered to study the stability properties. To investigate the effect of the axial rigidity of the core, additional numerical examples are considered by setting the core axial rigidity to be a very small amount. It shows that the core axial rigidity, although its magnitude is about two to three orders smaller than that of the faces, has a significant effect upon the stability response of sandwich panels. Although the core axial rigidity is usually negligible in the static analysis, it does affect the critical load, buckling mode, and the corresponding post-buckling response.

Fig. 1 plots the first buckling mode shape of a sandwich panel of 300 mm length. Fig. 1(a) is the mode shape given by the commercial FEA software ADINA, which is the same as the result given by the present approach, shown in Fig. 1(b). Fig. 1(c) is the mode shape when neglecting the core axial rigidity (by setting $E_1^c=52.0\times10^{-5}$ MPa instead of $E_1^c=52.0$ MPa). It is seen that the wrinkling appears as the first buckling mode when the core axial rigidity is neglected. This wrinkling mode shape agrees with the results given in the literature [3], in which the core axial rigidity was neglected.

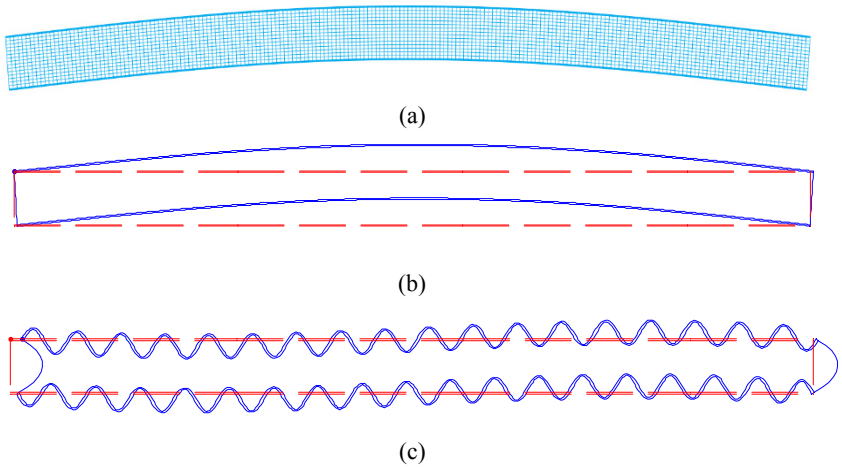

Fig. 1: First buckling mode of a=300 mm sandwich panel: (a) ADINA; (b) EHSAPT, $E_1^c=52.0$ MPa; (c) EHSAPT, $E_1^c=52.0\times10^{-5}$ MPa.

Both global buckling and local wrinkling are observed in the numerical examples. The examples also show that the sandwich panels have non-membrane pre-buckling state, and the buckling mode may have a non-uniform sine wave pattern.

The post-buckling analysis reveals that the sandwich panels have different nonlinear post-buckling response when it shows global buckling or local wrinkling. Although sandwich panels may have similar global buckling shapes as ordinary beams, as shown in Fig. 1(b), they cannot retain the stable post-buckling response for a long duration as ordinary beams do. When global buckling occurs, the post-buckling response is stable at the beginning. However, with the growing of the deformation, sandwich panels may be destabilized due to the imperfections and localized effects. When wrinkling occurs, sandwich panels lose their load carrying capability immediately, and the required axial compressive load level for further deformation is lower than that needed to maintain current deformation.

The present study gives a comprehensive investigation on the nonlinear buckling and post-buckling response of sandwich panels. With several numerical examples, some conclusions and new finds are given.

ACKNOWLEDGEMENT

The financial support of the Office of Naval Research, Grant N00014-16-1-2831, and the interest and encouragement of the Grant Monitor, Dr. Y.D.S. Rajapakse, are both gratefully acknowledged. The authors would also like to acknowledge very useful discussions with Prof. Yeoshua Frostig of Technion-Israel as well as the valuable input of Prof. Izhak Sheinman of Technion-Israel regarding ADINA.

REFERENCES

[1] Y. Frostig et al., "High-order buckling analysis of sandwich beams with transversely flexible core", *J. Eng. Mech.*, 1993; 119: 476-495.
[2] V. Sokolinsky et al., "Nonlinear behavior of sandwich panels with a transversely flexible core", *AIAA J.,* 1999; 37: 1474-1482.
[3] V. Sokolinsky et al., "Branching behavior in the nonlinear response of sandwich panels with a transversely flexible core", *Int. J. Solids Struct.*, 2000; 37: 5745-5772.
[4] C. N. Phan et al., "Global buckling of sandwich beams based on the extended high-order theory", *AIAA J.*, 2012; 50:1707-1716.
[5] C. N. Phan et al., "Wrinkling of sandwich wide panels/beams based on the extended high-order sandwich panel theory: formulation, comparison with elasticity and experiments", *Arch. Appl. Mech.*, 2012; 82: 1585-1599.
[6] Z. Yuan et al., "Geometric nonlinearity effects in the response of sandwich wide panels", *J. Appl. Mech.*, 2016; 83: 091008.

DOI: 10.5075/epfl-ICSS12-2018-15-17

NORMAL AND SHEAR ELASTIC FOUNDATION CONSTANTS FROM ELASTICITY AND THE EXTENDED HIGH-ORDER SANDWICH PANEL THEORY

George A. Kardomateas[1], Zhangxian Yuan[2] and Leif A. Carlsson[3]
[1]Georgia Institute of Technology, USA. george.kardomateas@aerospace.gatech.edu
[2] Georgia Institute of Technology, USA. yuanzx@gatech.edu
[3]Florida Atlantic University, USA. carlsson@fau.edu

1. INTRODUCTION

One of the approaches that could be used to analyze a face/core debond is the elastic foundation approach. In this approach, the top debonded face is considered to rest on an elastic foundation, which is provided by the rest of the structure, i.e., the core and the bottom face. Such elastic foundation models have been used from the 70s for the study of crack propagation. Kanninen [1,2] used such a model for the study of the double cantilever beam (DCB) test specimen in a homogeneous material with the crack at mid-thickness. A "crude" approximation of the elastic foundation modulus, based on the half-thickness of the beam, as outlined in the Results section, was used. Williams [3] extended Kanninen's model by using the Timoshenko beam theory in a homogeneous material and he used a formula for the elastic foundation constant similar to Kanninen's [3] based on the thickness of the debonded layer. In a more recent paper on the subject, Li and Carlsson [4] used the elastic foundation analysis on the tilted sandwich debond specimen. In a sandwich section, which is non-homogeneous, with varying properties and geometry of the two faces and the core, it is sensible to assume that the elastic foundation constant will depend on the mechanical properties and thicknesses, etc of all the constituent layers. Thus, the objective of this research is to provide a formula that answers this question.

2. FORMULATION

Extended High Order Sandwich Panel Theory (EHSAPT) Solution

The details of the EHSAPT theory are in [5]. We also use the same notation as in [5]. Let us consider the loading configuration that would be most appropriate for the normal elastic foundation constant. The one that would most first come to mind is a single face loading, in which case the normal spring constant would be defined by the transverse displacement of the top face/core interface and the transverse normal stress at the same place, after subtracting the transverse displacement at the bottom bounding surface, i.e. from a relationship of the form

$$k_n(x)\ \left[w(x,c)-w(x,-c-f_b)\right]=b\sigma_{zz}^{c}(x,c) \tag{1a}$$

This relationship would, however, include the bending deformation of the bottom face and thus would not represent the pure transverse compression of the structure below the top face. A symmetric loading configuration would, however, create a reference surface of uniform zero transverse displacement (i.e. the bending deformation would be eliminated and it would be like resting on a "rigid" surface. This reference surface would be at the middle of the core for a symmetric sandwich construction. Then, the normal spring constant would be defined from

$$k_n(x)\ w(x,c)=b\sigma_{zz}^{c}(x,c) \tag{1b}$$

Furthermore, if we consider a simply supported sandwich panel under transversely applied symmetric sinusoidal loading i.e. of the form:

$$q^t(x)=q_0\sin\frac{\pi x}{a};\qquad q^b(x)=-q_0\sin\frac{\pi x}{a}; \tag{2}$$

then the seven differential equations of the EHSAPT become seven algebraic equations for the seven constants: $U_0^{t,c,b}$, $W_0^{t,c,b}$ and Φ_0^c. Eliminating the $\sin(\pi x/a)$ from both sides of the resulting equation gives an expression of a constant k_n:

$$k_n=\frac{b}{W_0^t}\left[-c_{13}^{c}\left(\frac{\pi}{a}U_0^t+\frac{f_t\pi^2}{2a^2}W_0^t\right)+c_{33}^{c}\left(-\frac{2}{c}W_0^c+\frac{3}{2c}W_0^t+\frac{1}{2c}W_0^b\right)\right] \tag{3}$$

The shear constant of the elastic foundation (shear spring constant) expresses the relationship between the axial displacement, u, and the transverse shear stress, τ_{xz}, at the face/core interface. In the same spirit as for the normal spring constant, we need to refer to a zero axial displacement reference surface (i.e., again as resting on "rigid" surface). This can be achieved with an anti-symmetric loading. The reference surface is at the middle of the core for a symmetric sandwich construction. The shear spring stiffness can then be found from the relationship

$$k_s(x)\left[u(x,c)+\left(c-z_{ref}\right)w^c_{,x}(x,c)\right]=b\tau^c_{xz}(x,c) \tag{4}$$

Eliminating the $\cos(\pi x/a)$ from both sides of the resulting equation gives a constant value of the shear spring constant as

$$k_s=c^c_{55}\left|\frac{\left[-2\Phi^c_0-\frac{1}{2c}U^b_0-\frac{2}{c}U^c_0+\frac{5}{2c}U^t_0+\frac{\pi f_b}{4ca}W^b_0+\left(1+\frac{5f_t}{4c}\right)\frac{\pi}{a}W^t_0\right]}{U^t_0+\frac{\pi f_t}{2a}W^t_0}\right| \tag{5}$$

Since the shear stress can be negative, the absolute value is taken in Eq. 5.

Elasticity Solution

The elasticity solution is given in detail in [6,7]. The analysis is done in complex variables. In this solution, the displacements in each layer are as follows:

$$u=\sum_{j=1,2,3,4}e^{\lambda_j z}a_j\cos px \tag{6a}$$

and

$$w=\sum_{j=1,2,3,4}\frac{c_{11}p^2-c_{55}\lambda_j^2}{\left(c_{13}+c_{55}\right)p\lambda_j}e^{\lambda_j z}a_j\sin px \tag{6b}$$

where p = π/a and λ_j are the four roots of the characteristic equation of each layer:

$$c_{33}c_{55}\lambda^4+p^2\left[\left(c_{13}+c_{55}\right)^2-c_{11}c_{33}-c_{55}^2\right]\lambda^2+p^4c_{11}c_{55}=0 \tag{6c}$$

The roots of the characteristic equation (Eq. 6c) are either all real or complex conjugates. Regarding the a_j constants in the previous equations, within each layer i, where $i = t, c, b$, there are four constants: $a_{ij}, j = 1,2, 3, 4$. Therefore, for the three layers, this gives a total of 12 constants to be determined. These are found from the continuity conditions at the faces/core interfaces and the traction conditions at the bounding surfaces

Again, eliminating the $\sin(\pi x/a)$ from both sides of the resulting equation, gives an expression of a constant k_n:

$$k_n=b\frac{\sum_{j=1,2,3,4}\left[-c^c_{13}p+c^c_{33}\frac{c^c_{11}p^2-c^c_{55}\lambda^2_{cj}}{\left(c^c_{13}+c^c_{55}\right)p}\right]e^{\lambda_{cj}c}a_{cj}}{\sum_{j=1,2,3,4}\frac{c^t_{11}p^2-c^t_{55}\lambda^2_{tj}}{\left(c^t_{13}+c^t_{55}\right)p\lambda_{tj}}e^{\lambda_{tj}c}a_{tj}} \tag{7}$$

The shear spring constant is defined in Eq.4. Assuming symmetric construction, for which $z_{ref} = 0$, and subsequently eliminating the $\cos(\pi x/a)$ from both sides of the resulting equation, gives the following expression of a constant k_s:

$$k_s=b\frac{\sum_{j=1,2,3,4}c^c_{55}\left[\lambda_{cj}+\frac{c^c_{11}p^2-c^c_{55}\lambda^2_{cj}}{\left(c^c_{13}+c^c_{55}\right)\lambda_{cj}}\right]e^{\lambda_{cj}c}a_{cj}}{\sum_{j=1,2,3,4}\left[1+c\frac{c^c_{11}p^2-c^c_{55}\lambda^2_{cj}}{\left(c^c_{13}+c^c_{55}\right)\lambda_{cj}}\right]e^{\lambda_{tj}c}a_{tj}} \tag{8}$$

3. RESULTS

Table 1 shows the elastic foundation "normal spring" constant from Elasticity (benchmark), EHSAPT and the Kanninen-type simple formula based on the core. It can be seen that the agreement between Elasticity and EHSAPT is excellent. There is only a case of moderate discrepancy, namely a 10% discrepancy in the isotropic homogeneous case, which is to be expected, considering that the EHSAPT is a sandwich panel theory and makes assumptions regarding the faces and the core. The Kanninen-type simple formula has a varying accuracy, which depends on the core type, and in all cases predicts a less stiff foundation.

Table 1: Elastic Foundation Constant – "normal spring", k_n, MPa. Comparison of Elasticity, EHSAPT and Kanninen-type formula.

	Elasticity	EHSAPT	Kanninen [core] bE_3^c/c
Aluminum Faces H100 Core	692.0	698.1 +0.88%	520 -24.8%
Carbon Epoxy Faces H100 Core	692.6	698.5 +0.85%	520.0 -24.9%
Aluminum Faces Balsa Wood Core	31,248.1	31,308.4 +0.19%	30,880.0 -1.18%
Aluminum Faces Honeycomb Core	1,220.8	1,221.5 +0.06%	1,200.0 -1.70%
Aluminun Faces Aluminum Core (homogeneous isotropic)	313,936.2	346,387.4 +10.3%	276,000.0 -12.1%

ACKNOWLEDGEMENTS

The financial support of the Federal Aviation Administration though the National Aerospace Institute Cooperative Agreement 16-P-0012, and the interest and encouragement of the Grant Monitors Drs. Zhi-Ming Chen, Ronald Krueger, Larry Ilcewicz, Peter McHugh and Curtis Davies, and that of the Office of Naval Research, Grants N00014-16-1-2831 and N00014-16-1-2448, and the interest and encouragement of the Grant Monitor, Dr. Y.D.S. Rajapakse, are both gratefully acknowledged.

REFERENCES

[1] M.F. Kanninen, M.F. "An augmented double cantilever beam model for studying crack propagation and arrest", *International Journal of Fracture*, 1973, vol. 9, no. 1, pp. 83-92.

[2] M.F. Kanninen, M. F. "A dynamic analysis of unstable crack propagation and arrest in the DCB test specimen", *International Journal of Fracture*, 1974, vol. 10, no. 3, pp. 415-430.

[3] J.G. Williams, J.G. "End corrections for orthotropic DCB specimens", *Composites Science and Technology*, 1989, vol. 35, pp. 367-376.

[4] X. Li X. and L.A. Carlsson L.A. "Elastic Foundation Analysis of Tilted Sandwich Debond (TSD) Specimen", *Journal of Sandwich Structures and Materials*, 2000, vol. 2, pp. 3-32.

[5] C.N. Phan, C.N., Y. Frostig, Y. and G.A. Kardomateas "Analysis of Sandwich Panels with a Compliant Core and with In-Plane Rigidity-Extended High-Order Sandwich Panel Theory versus Elasticity", *Journal of Applied Mechanics* (ASME), 2012, vol. 79, no 041001 (11 pages).

[6] N.J. Pagano N.J. "Exact Solutions for Composite Laminates in Cylindrical Bending", *J. Composite Materials*, 1969, Vol. 3, pp. 398-411.

[7] G.A. Kardomateas and C.N. Phan "Three Dimensional Elasticity Solution for Sandwich Beams/Wide Plates with Orthotropic Phases: the Negative Discriminant Case", *Journal of Sandwich Structures and Materials*, 2011, vol.13, no.6, pp. 641-661.

DOI: 10.5075/epfl-ICSS12-2018-18-20

FULL-FIELD SURFACE AND INTERIOR DEFORMATION MEASUREMENT OF SANDWICH CORE MATERIAL USING DIGITAL SPECKLE PHOTOGRAPHY

Lingtao Mao[1], Rui Guo[1] , Yanqi Song[1] and Fu-pen Chiang[2]
[1] State Key Laboratory of Coal Resources and Safe Mining, Beijing, 100083, China; mlt@cumtb.edu.cn
[2] Dept. of Mechanical Engineering, Stony Brook University, Stony Brook, NY 11794-2300, USA; fu-pen.chiang@stonybrook.edu

1. INTRODUCTION

Composite materials are becoming more ubiquitous as engineering materials in aircraft, ships, bridges, and motor vehicles, because of their superior strength to weight ratio. Composite sandwich plates comprising of two face sheets and a polymer foam core are particularly advantageous as a ship building and wind turbine blade material because of its high bending rigidity. Knowing sandwich material's failure mechanism is, of course, of paramount importance in a safety design. Several experimental studies have been carried out to investigate the mechanical properties and failure mechanisms of composite sandwich plates and beams [1-3]. As a full-field measurement technique, DSP (Digital Speckle Photography) and DIC (Digital Image Correlation) have been used to analyze local core deformations and damage mechanisms [4,5]. However, these two techniques only provide the surface deformation. In order to fully appreciate the deformation mechanism of sandwich structures, it is paramount that the interior deformation be mapped and quantified. Recently the X-ray Computed Tomography (CT) technique has been used for in-situ testing of composite structures and in detecting interior damages [6,7]. However most of these studies are qualitative in nature. By taking advantage of the 3D volumetric imaging capability of X-ray CT, we recently developed an effective experimental strain analysis technique called DVSP (Digital Volumetric Speckle Photography) [8], whereby we can probe quantitatively and in detail the interior deformation of most opaque materials. DVSP is an extension of DSP technique in interior 3D displacement assessment. While DVSP was first developed to probe the interior deformation of geomaterials, we have also successfully applied it to probing the interior deformation of a woven composite beam and a composite sandwich plate [9, 10].

In this paper, we apply DSP and DVSP to mapping the deformation of a short and thick sandwich beam under three-point bending, respectively, and evaluate the results from those two methods and provide a comparison of the pros and cons of these techniques

2. MATERIALS AND METHODS

A Sandwich Beam under Three-Point Bending

Fig.1 shows the sandwich beam specimens under three-point bending. The specimen is made of E-glass Vinyl Ester composite face sheet with a polymer foam core [1]. The size is 50.0×20.0×32.0 mm^3. There are two specimens, one for DSP measurement, and the other for DVSP measurement combined with CT scanning. Fig.1(b) and (c) show the image with a digital camera and the X-ray reconstructed 3D image, respectively. Dark spots are the speckles sprayed on the surface of the specimen for the DSP method.

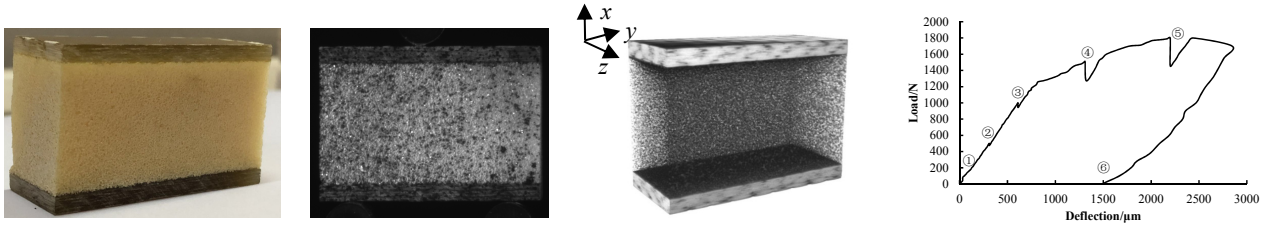

(a) specimen (b) the specimen in DIC experiment (c) X-ray reconstructed 3D image (d) loading history

Fig.1 : Images of the specimen.

In the experiment for DSP measurement, a sequence of images were captured by using a digital camera during the loading. The physical size of a pixel is 25×25 μm^2. In the experiment with CT scanning, the whole loading process was divided into 6 steps shown in Fig.1(d). In each step, the load is kept constant during the x-ray scanning. The reconstructed volumetric images have 890×360×530 voxels with the physical size of a voxel being 55×55×55 μm^3.

Theory of Digital Volumetric Speckle Photography(DVSP)

After a 3D volumetric image of an opaque specimen is recorded digitally via an X-ray CT before and after the application of load, the images are divided into sub-images with an arbitrarily selected unit volume of 32×32×32

voxels, for example. A 3D FFT (Fast Fourier Transform) is applied to a selected (one before and one after loading) sub-image pairs to reveal their spatial frequency spectrum. An numerical "filtering" process is performed on them. And then a further application of 3D FFT on the spectrum gives rise to a delta function G(ξ, η, ζ) whose coordinates (*u*, *v*, *w*) of the crest are nothing but 3D components of the displacement vector of all the volumetric speckles within the selected voxel array. The procedure is repeated over the entire volume of voxel array pairs. The result is a set of displacement vectors within the entire calculated volume. A schematic of the algorithm is illustrated in Fig.2.

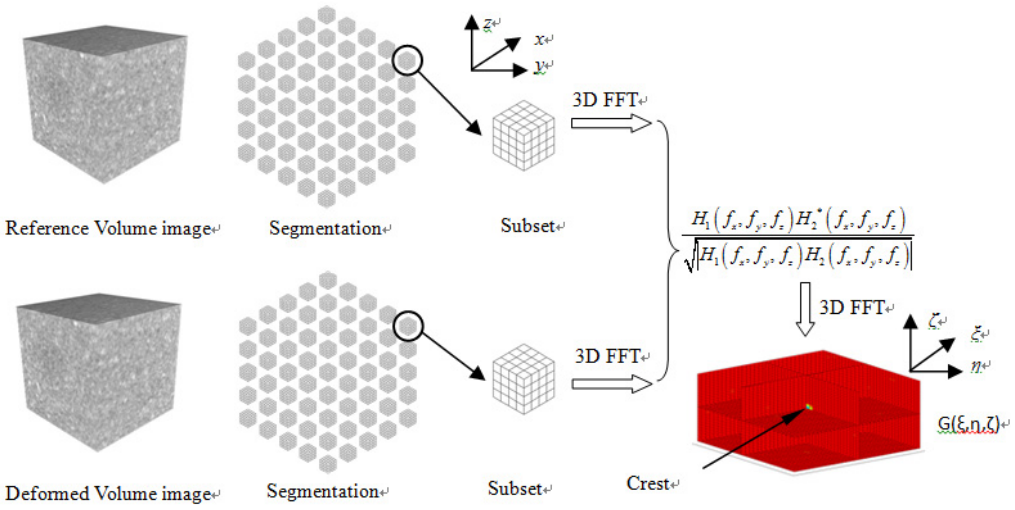

Fig.2: Schematics demonstrating the processing algorithm of DVSP.

3. RESULTS AND DISCUSSIONS

Based on the images from the two experiments, the displacement fields were calculated by using DIC and DVSP methods, respectively. In DSP method [11], the size of a subset is 128×128 pixels whereas in the DVSP method, the micro-structure of the core was treated as volumetric speckles and the size of a volume subset is 32×32×32 voxels. The deformation of the core region was calculated. Fig.3 shows the displacement fields of *u* and *v* corresponding to *x* and *y* axis based on the DSP results, and Fig.4 shows the displacement fields *u*, *v* and *w* of 3 sections along *z*=1.8mm, 9.7mm and 17.6mm of the beam as calculated by DVSP. The loading in both cases was 500N.

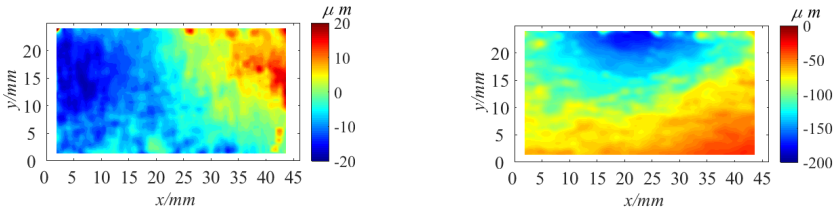

(a) *u* field (b) *v* field

Fig.3 : Displacement fields of the surface with DSP.

Compared Fig.3 with Fig.4, *u* and *v* field contours from DVSP are much smoother than these from DSP. The reason is that the volumetric subset in DVSP has much more information than the subset in DSP, which improves the robust of correlation searching. In Fig.4(c), (f) and (i), it is noted that the specimen has the deformation along *z* axis. In 2D DSP method, it is assumed that only the in-plane deformation occurs in the surface, and the out-plane deformation will be neglected. The actual deformation along z axis would result in measurement errors of DSP.

Due to the transverse shear stress effects, warping phenomenon will occur on the transverse section of a composite beam. DVSP is a good choice to validate those phenomenon. In Fig.5, *u* fields of the section at the middle length between the upper and the left supports are shown. With the loading increment, the warping section is clearly visible.

Using the surface measurement technique such as DIC or DSP the size of the speckles can be varied because they are spread onto the specimen surface artificially. For a volumetric technique such as DVSP or DVC (Digital Volume Correlation) [12] the speckles are part of the material's interior structure. Thus, it cannot be modified. If the interior texture of a material does not lend itself to be treated as volumetric speckles these techniques are not applicable at all. When the material's internal texture can be treated as volumetric speckles and the internal deformation of the specimen is needed DVSP or DVC technique is obviously a superior choice. But if only the surface deformation is the only needed information, DIC or DSP is a better one in that one can optimize the size and contrast of the speckles to yield better results.

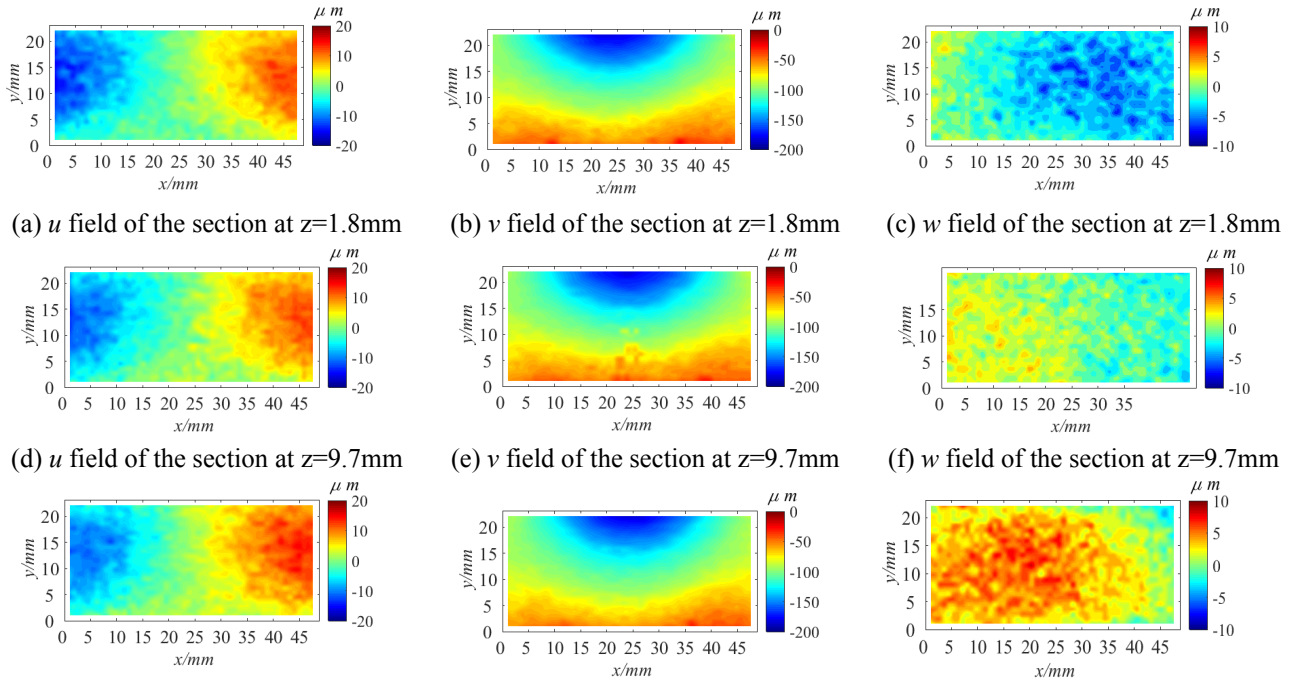

(a) *u* field of the section at z=1.8mm (b) *v* field of the section at z=1.8mm (c) *w* field of the section at z=1.8mm

(d) *u* field of the section at z=9.7mm (e) *v* field of the section at z=9.7mm (f) *w* field of the section at z=9.7mm

(g) *u* field of the section at z=17.6mm (h) *v* field of the section at z=17.6mm (i) *w* field of the section at z=17.6mm

Fig.4: Displacement fields of three different sections with DVSP.

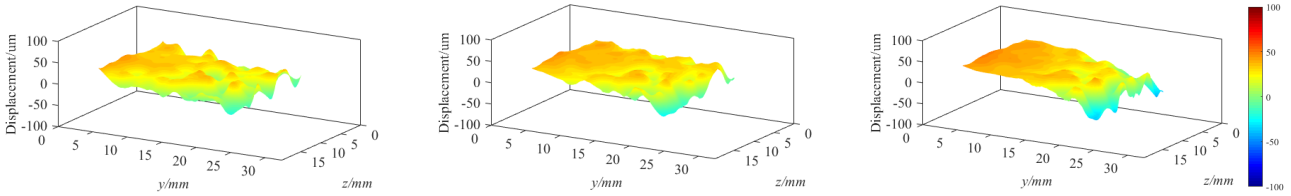

(a) Loading 1000N (b)Loading 1500N (c) Loading 1800N

Fig.5: u fields of the middle section between the upper and left support of the sandwich specimen.

ACKNOWLEDGEMENT

This project was supported by the National Natural Science Foundation of China (51374211), and ONR Solid Mechanics Program grant N0014-17-1-2873 directed by Dr.Yapa Rajapakse,

REFERENCES

[1] E. Wang, et al. “Blast performance of sandwich composites with in-plane compressive loading”. *Experimental Mechanics,* 2012; 52: 49–58.

[2] S. Gupta, et al. “Blast Performance of Marine Foam Core Sandwich Composites at Extreme Temperatures”. *Experimental Mechanics,* 2012; 52:1521-1534

[3] Z.B. Li, et al. Deformation and failure mechanisms of sandwich beams under three-point bending at elevated temperatures. *Composite Structures,* 2014; 111: 285–290.

[4] Chang S., et al. “Macro and micro deformations in a sandwich foam core”. *Composites: Part B*, 2004;35: 503–509

[5] Fathi A., et al. “Full-field shear analyses of sandwich core materials using Digital Image Correlation (DIC)”. *Composites: Part B* , 2015; 70:156–166.

[6] Dietrich S., et al. “Measurement of sub-surface core damage in sandwich structures using in-situ hertzian indentation during x-ray computed tomography”. *Experimental Mechanics,* 2014; 54:1385–1393

[7] Dietrich S., et al. “3D tomographic characterization of sandwich structures”. *NDT&E International* , 2014; 62:77–84

[8] Chiang F.P., et al. “Development of interior strain measurement techniques using random speckle patterns”. *Meccanica,* 2015; 50(2) :401–410.

[9] Mao L.T., et al. “Interior strain analysis of a woven composite beam using x-ray computed tomography and digital volumetric speckle photography”. *Composite Structures,* 2015;134: 782-788.

[10] Mao L.T., et al. “Mapping interior deformation of a composite sandwich beam using digital volumetric speckle photography with x-ray computed tomography”. *Composite Structures*, 2017; 179:172-180

[11] Chen D.J., et al. “Digital speckle-displacement measurement using a complex spectrum method”, *App. Opt.*, 1993;32:1839-1849

[12] Pan B., et al, “Research progress in digital volume correlation method”. *Chinese Science Bulletin*, 2017; 62: 1671-1681

SESSION 1B: MODELING

DOI: 10.5075/epfl-ICSS12-2018-22-24

MECHANICAL AND ACOUSTIC RESEARCH OF SOUND-ABSORBING COMPOSITE SANDWICH STRUCTURES FOR AIRCRAFT ENGINES

Aleksandr N. Anoshkin, Valery Yu. Zuiko, Pavel V. Pisarev, Mikhail A. Alikin and Evgenia N. Shustova
Perm National Research Polytechnic University, Russian Federation,
aan-02@yandex.ru; zuyko81@mail.ru; pisarev85@live.ru; alik87miha@gmail.com; evgenianicolaevna@gmail.com

1. INTRODUCTION

Nowadays sandwich structures are widely used for the casing parts of aircraft engines. The initial primary function of such parts was the mechanical fastening of engine assemblies. Accordingly, they were required to ensure high mechanical properties - strength and rigidity. Then the International Civil Aviation Organization developed standards for noise emission of civil aircraft and now the second no less important function of these parts is to reduce the noise of the aircraft engines. It was found that the cells of the sandwich structure, when perforated by one of its shells, can interact with acoustic wave like a Helmholtz resonator. By varying the dimensions of the cells, the thickness of the shells and the diameter of the perforation holes, one can select the resonant frequency of the sandwich structure cells so that it corresponds to one of the main frequencies of the aircraft engine. Thus sandwich structures for casing parts of aircraft engines require effective sound absorption in a given frequency range and mechanical strength. The requirements of weight reduction for all aircraft structures lead to the use of composite materials for the manufacture of the sound-absorbing sandwich structures. The present work is devoted to solving of the actual problem of the modeling and development of effective aviation sound-absorbing sandwich structures, made of composite materials.

2. ACOUSTIC RESEARCH

The modern aviation sound-absorbing composite sandwich structures consist of glass-fiber or carbon-fiber laminate skins and a core sandwiched between, which can have a tubular, cellular, honeycomb structure etc. (Fig.1).

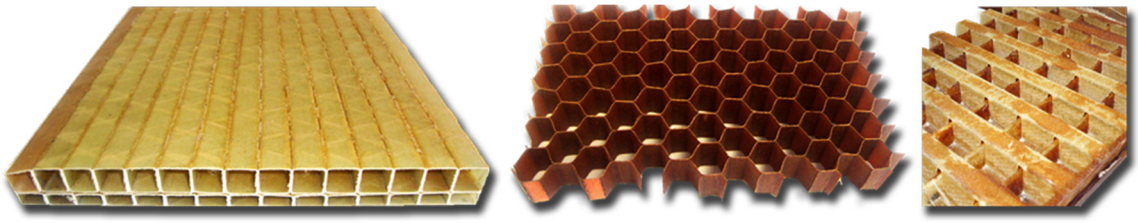

(a) *(b)* *(c)*

Fig. 1: Types of core: tubular (a), honeycomb (b) and cellular (c).

The core cells interact with acoustic wave like a Helmholtz resonator and absorbing acoustic energy. For a given resonant frequency, the cell parameters are preliminarily calculated by the Helmholtz formula. After that the samples of the cells for testing on an interferometer are made. As a result of the tests, the sound absorption coefficient of the cells at different frequencies is determined. Then the numerical simulation of mono- and polychromatic acoustic wave interaction with one and group of the cells in the model channel was performed. As a result of numerical simulation, the effect of the shape of the cells on the coefficient of sound absorption was established. Distribution of the acoustic pressure inside the channel and on sidewall cell was found, loss factor of output acoustic pressure wave was calculated for variety of geometric forms of cell's chamber and neck (Fig. 2). Analysis of the acoustic pressure fields revealed that cell neck geometry strongly influences on cell resonant frequency and on outlet acoustic pressure loss factor. It was concluded that for effective sound absorption of sandwich structures, it is necessary to select not only the geometric parameters but also the shape of the core cells.

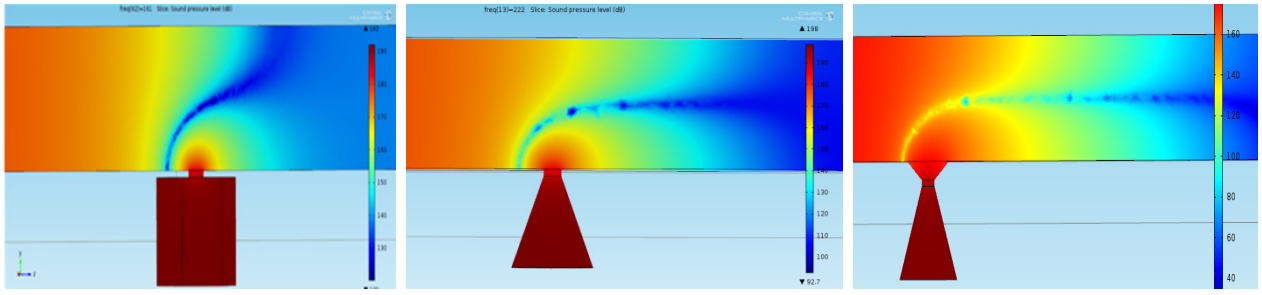

(a) *(b)* *(c)*

Fig. 2: Acoustic pressure fields inside the channel for various cell shapes: honeycomb (a), conical (b) and bi-conical (c).

3. MECHANICAL RESEARCH

The sound-absorbing composite sandwich structures serve also as load-bearing casing parts of aircraft engine. Therefore, ensuring their performance and structural integrity under various loading conditions is an important task which needs the solution of composite material mechanics problems. Depending on the purpose of the part and the nature of the loads, the solution of this task can be carried out in two directions.

The first way – the effective mechanical properties can be found for various types of core, which will simplify the further numerical modeling of complex structures. In present work, using analytical methods for isotropic materials, the verification of the developed algorithms for numerical analysis of the effective properties of honeycomb core made of both isotropic and orthotropic material, was performed (Fig.3).

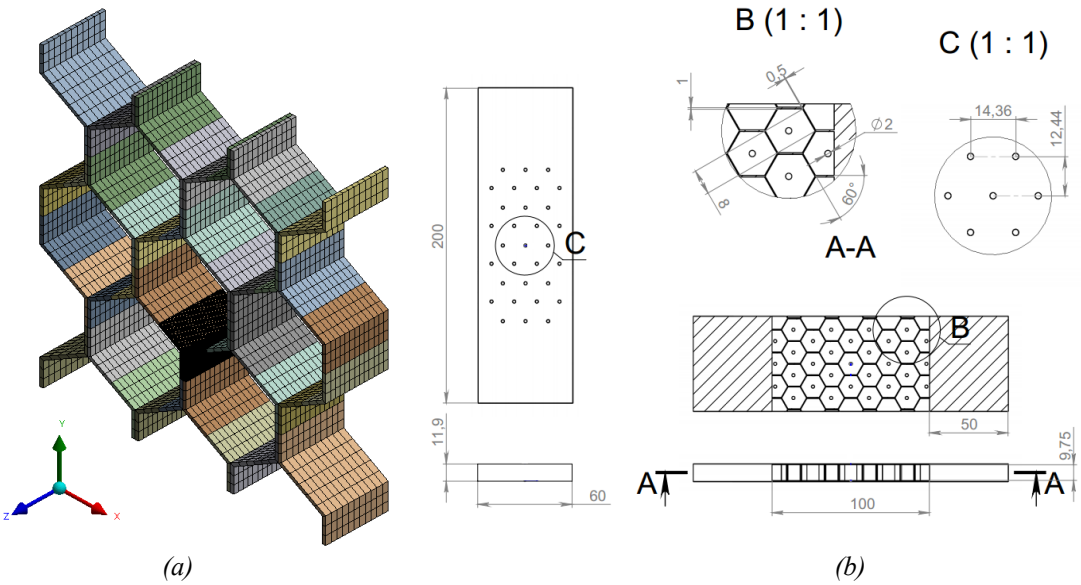

Fig. 3: Finite element model of honeycomb core (a) and scheme of sandwich panel (b).

The second way - the whole model, including the structure of core and laminated composite face sheets, can be used for simulation. Thus, the multilevel 3D models (Fig. 4) of panels with various types of core corresponding to full-scale samples used for mechanical tests were created for numerical prediction of their effective mechanical properties and analysis of non-uniform stress-strain fields distribution [1-2]. The numerical stress-strain analysis of panels under various loading condition was obtained with ANSYS Workbench software using the ACP module. Initial mechanical properties and strength characteristics of the materials used in numerical studies were obtained in in-house tests.

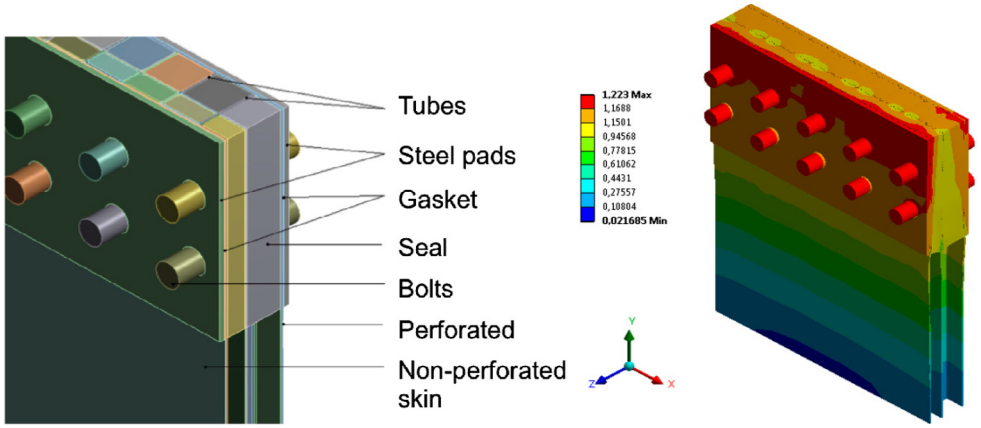

Fig. 4: 3D model of sandwich panel for FEM analysis.

The experimental verification of the developed numerical models was carried out with the help of specimens of panels made of ABS plastic and produced by 3D printing (Fig. 5). Static tensile tests were conducted on Zwick / Roell ProLine Z100 testing machine. The results of numerical simulation were compared to results of samples tension tests – good correlation was found.

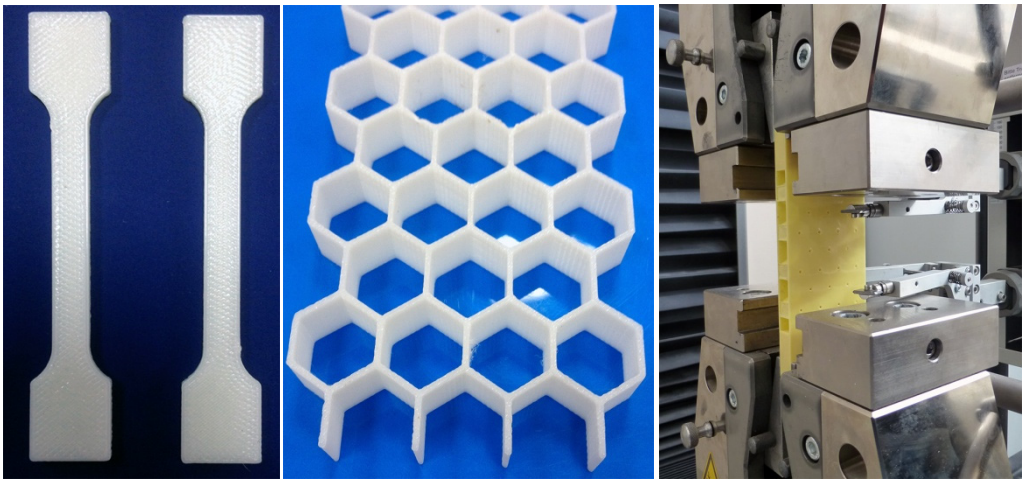

Fig. 5: Testing specimens made of ABS plastic.

4. CONCLUSIONS

Numerical models of sandwich structures from composite materials have been developed. The models allow solving problems of propagation of acoustic waves in sandwich structures and problems of mechanical deformation of sandwich structures. As a result of solving these problems, it is possible to predict absorption coefficients of acoustic waves and mechanical properties for different sandwich structures. It is supposed to use the developed models for the design of sound-absorbing composite casing parts of aircraft engines.

ACKNOWLEDGMENTS

The results were obtained within the framework of the state task of Russian Ministry of Education and Science (project no. 11.2391.2017/4.6)

REFERENCES

[1] A.N. Anoshkin et al., "Repair of damage in aircraft composite sound-absorbing panels", *Compos. Struct.*, 2015, 120: 153–166

[2] A.N. Anoshkin et al.,"Experimental-theoretical research of mechanical properties of perforated composite sandwich panels", *Solid State Phenom.*, 2016, 243: 1–10.

DOI: 10.5075/epfl-ICSS12-2018-25-27

ON REMARKABLE LOSS AMPLIFICATION MECHANISM IN SANDWICH PANELS WITH COMPOSITE FACE SHEETS REINFORCED WITH COATED FIBERS

Yury O. Solyaev[1], Sergey A. Lurie[2] and Anastasia D. Ustenko[3]
[1]Institute of Applied Mechanics of Russian Academy of Science, Moscow Aviation Institute, Russia. yos@iam.ras.ru
[2]Institute of Applied Mechanics of Russian Academy of Science, Moscow Aviation Institute, Russia. salure@mail.ru
[3]Institute of Applied Mechanics of Russian Academy of Science, Moscow Aviation Institute, Russia. audlord@yandex.ru

1. INTRODUCTION

Effective vibrational and noise control structures are important in aerospace and automotive industry. Less vibrational energy leads to longer life of components and structures while less noise means comfort to passengers as well as to surrounding environments. In aerospace industry, the requirement for high vibrational damping and high strength/stiffness composites now seems to be mandatory especially when more aircraft structural components are designed with reinforced polymer-matrix composite materials. As a result, various design optimizations to improve both damping and stiffness properties of composite structure have been proposed in the frame of micromechanics and structural mechanics [1, 2]. In the present work, we concern ourselves with traditional way of optimizing dynamic properties of sandwich panels but solution is addressed from the nanotechnology perspective where an ultra-thin coating layer of viscoelastic material on the reinforced fibers in the composite face sheets is considered. With this optimization, a remarkable high loss amplification effect can be observed on the levels of lamina, laminate and sandwich panel structure with such composite face sheets.

Reinforced polymer composite material, apart from its high strength and stiffness to weight ratio characteristic, is naturally a good damping material. In such composite, polymer-matrix is the source of damping mechanism [2]. The contribution of inclusions to damping can be very significant when high volume fraction of inclusions is present. In general, a comparably higher or the same level of damping as the matrix can be obtained for composite structure that has inclusions, about hundred times stiffer than the matrix [3]. To further increase damping capacity of composite, a hybrid concept of combining composite and viscoelastic material is examined. With viscoelastic composite material, good combination of high damping and high stiffness properties might be achievable [4]. In the last decade, various authors have investigated this hybrid concept analytically and numerically [3-10]. At micromechanical level, their basic strategy is to have viscoelastic lossy layer coated between stiffer phases [6, 7], while at macromechanical level, viscoelastic layer is selectively placed between sheets or laminates [8]. Nevertheless, the results showed that although higher damping capacity of composite is obtainable, retaining sufficiently high stiffness is proved difficult [1, 5].

Searching for optimum balance between loss and stiffness, Gusev and Lurie [7] examined the effect of thickness of viscoelastic coating layer surrounding spherical inclusions that are embedded in epoxy matrix system. It is found that at extremely thin coating layer, the effective shear loss modulus of composite increases substantially. At the same time, the decrease in its effective storage modulus is minimal. This high loss amplification effect is so extreme that its effective loss modulus value significantly exceeds the loss moduli of constituents in the composite. Later the similar effects was found in fiber reinforced composites [8] and in wavy layered composites [9] containing ultra-thin viscoelastic layers. Clearly, this approach of optimization shows that high loss and high stiffness composite structure might be attainable, and this is due to the presence of high shearing damping mechanism in viscoelastic layer [4, 7, 9].

In the present work, we provide a further development of the proposed strategy for the increase of damping and stiffness properties for the sandwich panels which composite face sheets reinforced with coated fibers. Overall stiffness and damping properties of the foam filled panels are examined by the analytic and numerical means. Rational design method is proposed. Optimal values of microscopic and macroscopic parameters of considered composite structures are found. It is shown the significant influence of the ultra-thin viscoelastic coatings on the overall properties of the panels.

2. MODELLING METHODOLOGY AND RESULTS

We consider a flat sandwich panel with polyurethane foam core and with face sheet that consists of epoxy matrix reinforced with coated glass fibers. Coating is made of rubber-toughened epoxy with improved damping behavior. All materials except the fibers are assumed to be viscoelastic, and their behavior is described by frequency-dependent complex moduli. To analyze micromechanical behavior of lamina, we use a micromechanical model of coated cylindrical inclusion. Generalized self-consistent method with elastic-viscoelastic correspondence principle are involved in the analytical estimations (Fig. 1(c)). Classical theory of laminates is involved to study the mechanical performance of face sheets with symmetric angle-ply lay-up (Fig. 1(b)). First-order shear deformation analysis of simply-supported sandwich plates is performed to investigate the overall properties of sandwich structures under consideration (Fig. 1(a)). Using proposed multiscale analytical model an optimal set of the model parameters (coating thickness, fiber volume fraction,

lamination angle of face sheets, core thickness) are found for the best damping behavior of sandwich plate. Fundamental modal loss factor of the panel is considered as the target function in maximization problem.

Numerical verification for the obtained optimal sandwich structure is given. We consider a sandwich panel model with solid second order hexahedral elements for the core layer and with Mindlin-Reissner plate elements for the faces. In the finite-element modeling we use the frequency dependent storage modules and loss factors of the face plates material found from preliminary micromechanical analysis. Viscoelastic properties of the core are taken from known experimental data. Vibrational behavior of the panel is simulated in frequency domain using frequency/harmonic response analysis in the Femap/Nastran system. We consider a lateral vibrations of simply-supported panel with prescribed harmonically varying displacements of supported ends. Based on numerical solution we found a frequency response function for the panel vibrations amplitude and estimate the modal loss factor of the panel based on "half-power" method. Comparison between obtain finite element and analytical predictions allows us to check the accuracy of the last one as well as to check the significance of longitudinal and rotatory inertia effects, high order shear effects in the core etc. that are neglected in the analytical model.

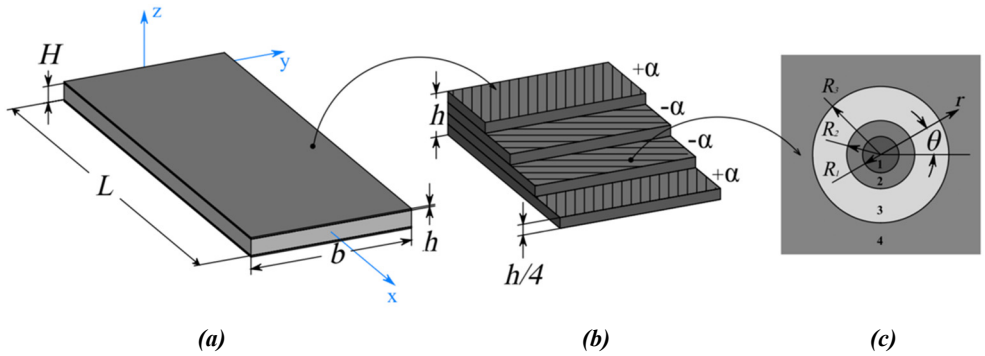

Fig. 1: Modeling scheme. (a) Three-layer sandwich panel, (b) four-layer laminated face plates with a symmetric angle-ply lay-up, (c) model of a coated cylindrical inclusion in the framework of the generalized self-consistent method (1 - fiber, 2 - coating, 3 - matrix, 4 - equivalent homogeneous medium)

Analytical and numerical study reveals that at ultra-thin coating layer, the laminas exhibits very high loss characteristics where its effective loss moduli significantly exceed the loss moduli of both coating and matrix materials (Fig. 2). High shearing dissipation mechanism in ultra-thin layer of viscoelastic coating material is found to be responsible for this peculiar behavior. This remarkable loss amplification effect is technologically appealing as such composites with high damping and high stiffness properties might be attainable. From Fig. 2, it is clear that both effective transverse Young's and shear loss moduli (E_T, G_T) have two distinct peaks. One of the peaks, as before occurs at extremely thin coating layer. Here, the possibilities of obtaining enhanced composite's damping capacity while maintaining sufficiently high stiffness characteristic can be observed. In this case, the loss moduli increase more than 10 times, and the decrease in stiffness is between 15 and 20 % only. These effects are studied then at the laminate and sandwich structure levels. It is found a strong relation between overall damping properties of the sandwich panel and parameters of the microscopic viscoelastic coatings.

Analytical design methodology is proposed to find optimal values of micromechanical and structural parameters of the model to provide a highest stiffness and damping behavior of the panels. Example of the panel fundamental modal loss factor estimation for different coating thicknesses (micro parameter) and lamination angles (macro parameter) are given in Fig. 3. It is found that a balance between the damping improvement and the stiffness decrease can be achieved by using thin viscoelastic coatings, a lamination angle close to $\alpha = 20^\circ$–30° and a sufficiently thick core. The panel with the maximum loss factor is realized with a [±45] lay-up. For the considered panels with glass-fiber-reinforced epoxy face plates and polyurethane cores, it is shown that the application of thin rubber-toughened epoxy coatings to the fibers should allow one to increase the fundamental modal loss factor of a panel by a factor of greater than ten. The optimal relative coating thickness for the fibers is approximately 0.1 times the fiber radius. For a typical glass fiber radius (5-10 μm), this means that the coating thickness should be approximately 0.5-1 μm.

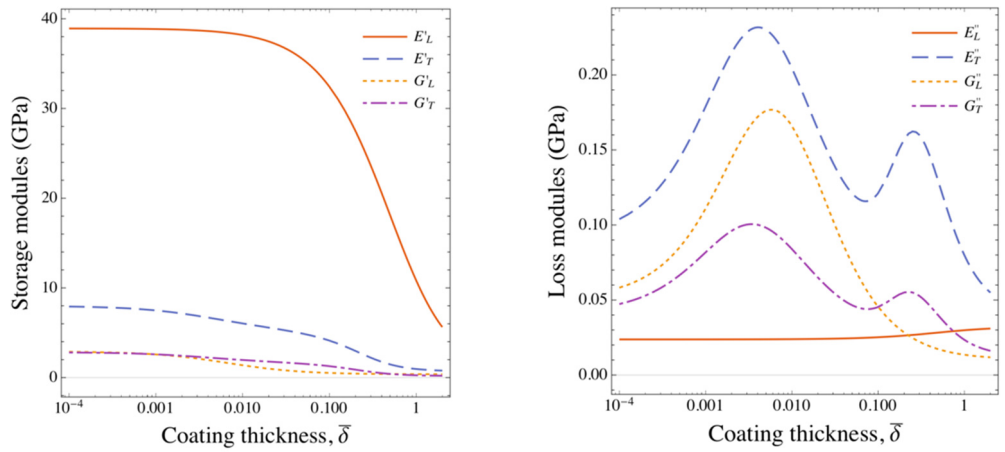

Fig. 2: Effective storage and loss moduli of the lamina vs. relative coating thickness (divided on the fibers radius).

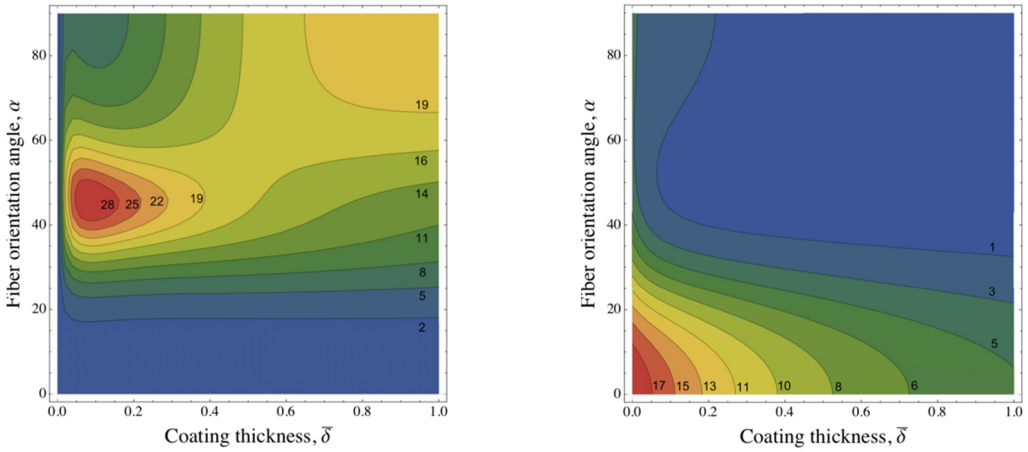

(a) ***(b)***

Fig. 3: Sandwich panel properties vs. coating thickness and lamination angle. (a) Fundamental modal loss factor, (%); (b) bending stiffness per unit width, (10^3 Nm); property values are shown by colors and labels on the contours.

REFERENCES

[1] I.C. Finegan et al., "Recent research on enhancement of damping in polymer composites", *Compos. Struct.,* 1999; 44; 89–98.
[2] R. Chandra et al., "Damping studies in fiber-reinforced composites – a review", *Compos. Struct*., 1999; 46; 41–51.
[3] C. Remillit, "Damping mechanism of polymers filled with elastic particles", *J. Mech. Mater.*, 2007; 39; 525–537.
[4] J. Meaud et al., "Analysis and optimal design of layered composites with high stiffness and high damping" *Int. J. Solids Struct.*, 2013; 50; 1342–1353.
[5] R.S. Lakes, "High damping composite materials: Effect of structural hierarchy", *J. Compos. Mater*., 2003; 36; 287–297.
[6] F.T. Fisher et al., "Viscoelastic interphases in polymer-matrix composites: theoretical model and finite element analysis", *Compos. Sci. Technol.*, 2001; 61; 731–748.
[7] A. Gusev et al., "Loss amplification effect in multiphase materials with viscoelastic interfaces", *Macromolecules*, 2009; 42; 5372–5377.
[8] S. Lurie et al., "On remarkable loss amplification mechanism in fiber reinforced laminated composite materials", *Appl. Compos. Mat.*, 2014; 21; 179-196.
[9] J. Yang et al., "Vibration and damping characteristics of hybrid carbon fiber composite pyramidal truss sandwich panels with viscoelastic layers", *Compos. Struct.*, 2013; 106; 570-580.
[10] A.A. Gusev, "Optimum microstructural design of coated sphere filled viscoelastic composites for structural noise and vibration damping applications", *Int. J. Sol. Struct.*, 2017; 128; 1-10.

DOI: 10.5075/epfl-ICSS12-2018-28-30

PREDICTING THE DAMAGE TOLERANCE OF NOMEX® HONEYCOMB SANDWICH STRUCTURES BASED ON DETAILED FINITE ELEMENT MODELS

Chris Fischer[1], Falk Hähnel[2] and Klaus Wolf[3]
Institute of Aerospace Engineering, Technische Universität Dresden, 01062 Dresden, Germany.
[1]Email: chris.fischer@tu-dresden.de, [2]Email: falk.haehnel@tu-dresden.de, [3]Email: klaus.wolf@tu-dresden.de

1. INTRODUCTION

The application of structural sandwich is an important design solution for load-carrying lightweight components. In aircraft structures sandwich made of graphite/epoxy face-sheets and aramid honeycomb cores is often used [1] due to features such as high strength- and stiffness-to-weight ratios as well as a good fatigue behaviour. Owing to the rather weak core material, this kind of sandwich is prone to a range of defects and damages as a result of impact loading which may accidentally occur during assembly or operation of aircraft. These damages and their effect on the load carrying capability of structures have to be considered in the damage tolerant design of airplanes and helicopters.

For the analysis of the impact damage process and the damage tolerance behaviour, numerical simulations are increasingly used and have been the focus of previous studies [2-6]. As long as only the global behaviour of sandwich components is investigated by finite element methods, it is sufficient to model the structure by using shell elements for the skins and solid elements for the core [2, 7]. Nevertheless, local failure phenomena especially of the honeycomb core structure have to be considered in the damage tolerance behaviour of the structure. Such a detailed finite element model requires not only a thorough knowledge about the basic material properties of the sandwich constituents [8, 9] but also information about the honeycomb geometry [10]. Therefore, the cell walls have to be idealised with shell elements and the resin corners with solids. Such a finite element (FE) model has to be validated following a step-by-step approach as shown in Fig. 1. Once validated, the simulation model can be applied for further investigations regarding the impact behaviour and the residual strength of honeycomb sandwich structures (Fig. 1).

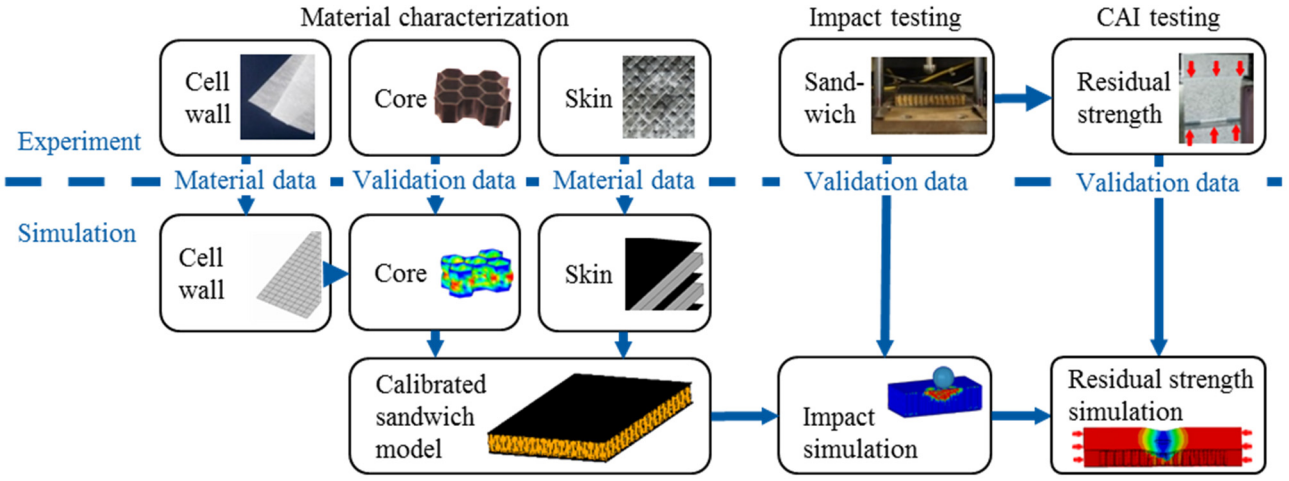

Fig. 1: Calibration process for sandwich FE models used to simulate the impact and residual strength behaviour.

In this paper a step-by-step approach is proposed to validate detailed finite element (FE) models of honeycomb sandwich structures for impact and residual strength simulations using the commercial simulation software LS-Dyna.

2. MATERIAL CHARACTERIZATION

Cell Wall

Honeycomb cores used in aerospace structures usually have cell walls consisting of three layers (resin-paper-resin) resulting from the impregnation process. In the applied simulation model this wall structure has been modelled using shell elements with 3 layers, where each layer has the material properties of the relevant constituent. Hence, the specific material properties of the pure as well as the impregnated aramid paper had to be determined by compressive, tension and shear tests (Fig. 2). Based on these experimental data the properties of the Nomex® paper as well as the phenolic resin were identified. These data are required as input parameters of the orthotropic elastic-plastic user-defined material law for paper-like materials, which has been developed at the Institute of Aerospace Engineering. Using this material model, simulations of the tests have been performed showing a very good agreement with the experimental data.

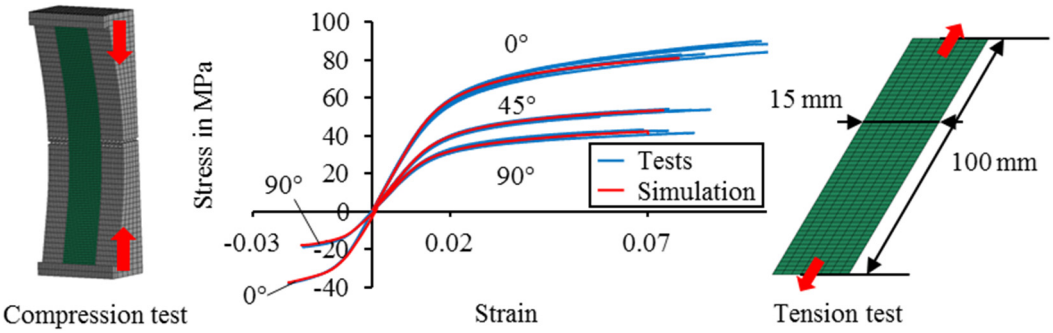

Fig. 2: Material test of Aramid paper: examples of simulation results under compression and tension.

CFRP Skin Material

The face sheets investigated were made of both unidirectional and woven CFRP fabric plies (Hexcel M18/1-G939 and M18/1-G947). Already known intra-laminar data have been complemented through additional experiments: impact tests for the failure analysis as well as mode I, mode II and mixed mode delamination tests in relevant ply and angle configurations. Finally, the properties required for the material models were determined for all relevant skin lay-ups.

The fabric composite material has been modelled using the LS-Dyna orthotropic material formulation for layered composite materials. Delamination interfaces have been considered between the fibre shell layers using solid elements in combination with the LS-Dyna cohesive mixed-mode material. Both impact behaviour and delamination propagation obtained by simulation agree very well with the experiments (Fig. 3).

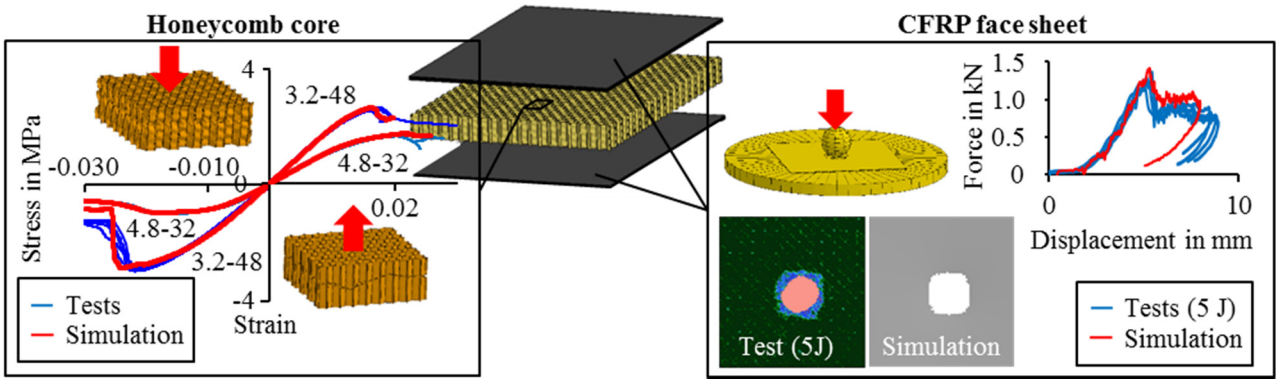

Fig. 3: Coupon test of honeycomb core and CFRP face sheet: examples of test and simulation.

Honeycomb Core Structure

These test specimens consisted of Nomex® honeycombs with cell widths of 3.2 mm and 4.8 mm and densities of 48 kg/m³ and 32 kg/m³, respectively. Both core types were tested under compression, tension and shear loading using 40 by 40 mm test specimens. Imperfections were analysed from the procedure described in [10] on different honeycomb configurations and were considered in the simulation models. The numerical results show a very good agreement with the nonlinear behaviour of honeycomb cores obtained from the experiments (Fig. 3).

3. IMPACT TEST ON SANDWICH SPECIMENS

Extensive low velocity impact tests were conducted at different energy levels from 2 J to 15 J in order to determine the impact behaviour of honeycomb sandwich structures. These experiments were performed according to standard CAI test procedures. A rectangular window frame support of 75 mm in width and 125 mm in length and an impactor with a semi-spherical head of 1-inch diameter has been used. A force transducer recorded the force-displacement-histories.

The models of the sandwich structure were build up using the validated models for the honeycomb core and the CFRP skins in combination with a tied bonding interface of skin and core (Fig. 4). Investigations showed that it is important to model the meniscus resulting from the sandwich manufacturing process in order to get reliable simulation results of the core damage depth. Both impact testing and impact simulations were performed on different sandwich configurations. A good correlation has been obtained as shown in Fig. 4 using the example impacted at 5 J.

4. COMPRESSION AFTER IMPACT

After being impacted the damaged samples were prepared for residual strength testing (Fig. 4). During these experiments the compressive strain was measured on the skin surface using a three-dimensional digitisation system. As a result, the stress-strain-curves as well as the failure loads were obtained. During the compression tests, stability failure modes such as shear crimping and wrinkling have been observed. Typical test results for samples with a 0.9 mm CFRP skin are given in Fig. 4 where the compression after impact force is shown as a function of the displacement.

Residual strength simulations were conducted using LS-Dyna applying a multi-step simulation approach. Following the impact simulation, the simulation model is modified: specimen supports were added on the edges of both face sheets to prevent premature buckling. Additionally, solid elements were placed at both ends to model the load introduction. The compressive load was simulated by prescribed displacements of the load introduction surfaces longitudinal to the sandwich sample. As shown in Fig. 4 the analysis results agree very well with the experimental data achieved by the residual strength tests using the 5 J impact example.

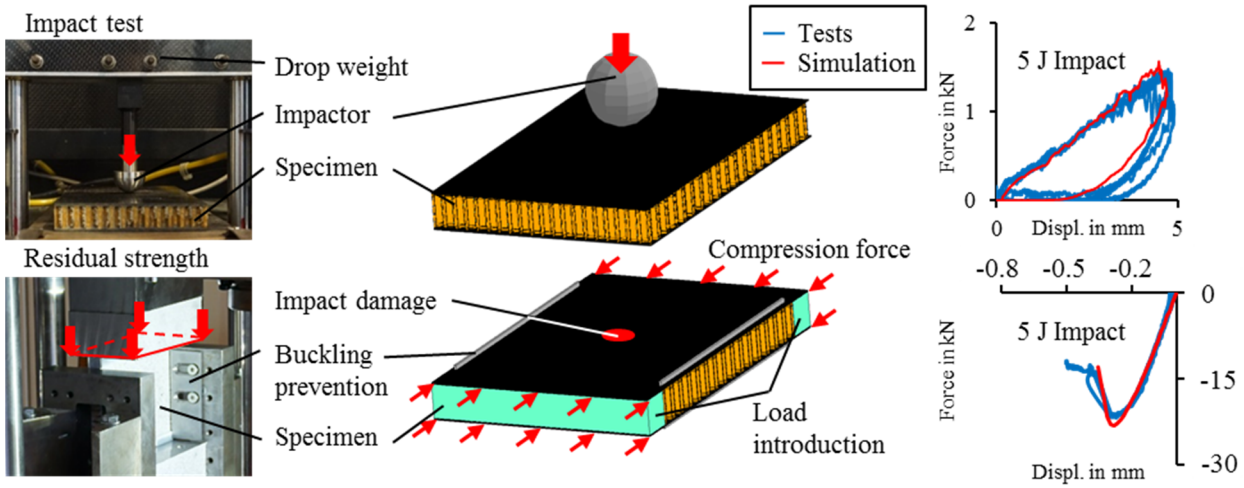

Fig. 4: Comparison of test and simulation: effect of a 5 J impact on the response and residual strength of a sandwich sample.

5. CONCLUSIONS

The experimental study performed in the presented research project provided a comprehensive database on impact-force time relations for a range of impact energies. The data were obtained for sandwich configurations typical for aircraft applications. Particularly, the knowledge gained on the quantitative magnitude is useful for the evaluation of residual strength simulations as a function of the structural damage severity.

Based on these experimental data a step-by-step simulation approach has been developed which is applicable to predict the impact behaviour as well as the residual strength of damaged sandwich structures. As numerical method, explicit finite shell elements have been used. The comparison with experimental results revealed a very good agreement.

The developed simulation approach was applied particularly to examine systematically the failure processes in honeycomb sandwich structures. The obtained knowledge on the effective mechanisms are very useful for the development of better macro-mechanical simulation methods.

ACKNOWLEDGEMENTS

This research was performed within the LuFo V-1 project SCHACH funded by the German Federal Ministry for Economic Affairs and Energy. The simulations were performed on the Bull HPC-Cluster of the Center for Information Services and High Performance Computing (ZIH) of TU Dresden. Both the financial support as well as the computing capacity provided is gratefully acknowledged.

REFERENCES

[1] R. Boyer et al., *Aircraft Materials*, Reference Module in Material Science and Material Engineering, Elsevier: 2016.
[2] C. Menna et al., "Numerical assessment of the impact behaviour of honeycomb sandwich structures", *Composite Structures*, 2013; 106: 326-339.
[3] A. Akatay et al., "The influence of low velocity repeated impacts on residual compressive properties of honeycomb sandwich structures", *Composite Structures*, 2015; 125: 425-433.
[4] D. Zhang et al., "Experimental and numerical investigation on indentation and energy absorption of a honeycomb sandwich panel under low-velocity impact", *Finite Elements in Analysis and Design*, 2016; 117-118: 21-30.
[5] D. Zhang et al., "Drop-weight impact behaviour of honeycomb sandwich panels under spherical impactor", *Composite Structures*, 2017; 168: 633-645.
[6] M. Meo et al., "The response of honeycomb sandwich panels under low-velocity impact loading", *Int. Journal of Mechanical Sciences*, 2005; 47: 1301-1325.
[7] S. Heimbs et al., "Towards the Accurate Numerical Prediction of Impact Damage and Residual Strength of Helicopter Sandwich Structures", *ICSS-11*: 2016.
[8] F. Hähnel, *Ein Beitrag zur Simulation des Versagens von Honigwaben aus Meta-Aramid-Papier in schlagbelasteten Sandwichstrukturen*, Shaker Verlag: 2016.
[9] R. Seemann et al., "Numerical modelling of Nomex honeycomb sandwich cores at meso-scale level", *Composite Structures*, 2017; 159: 702-718.
[10] C. Fischer et al., "Influence of imperfections on the structural behaviour of honeycomb cores", *ECCM-17*: 2016.

SESSION 2A: ONR SPECIAL SESSION – DELAMINATION / DISBOND

DOI: 10.5075/epfl-ICSS12-2018-32-34

DAMAGE ASSESSMENT SCHEMES FOR NAVAL SANDWICH STRUCTURES WITH FACE-CORE DEBONDS CONSIDERING RESIDUAL STRENGTH AND FATIGUE LIFE

Brian Hayman[1] and Christian Berggreen[2]
[1]Technical University of Denmark, Denmark. bhayman@mek.dtu.dk
[2]Technical University of Denmark, Denmark. cbe@mek.dtu.dk

1. INTRODUCTION

Face-core debonds in sandwich structures of naval vessels may occur in production or result from unfavourable events or environmental conditions during service. A debond may be large enough to cause failure of a loaded sandwich component, while an initially harmless debond may grow under fatigue loading until it becomes critical. Thus, for cyclic loading, it is important to understand the way that debonds grow, the extent to which the component strength is reduced, and the remaining fatigue life at any given stage. It is also important to be able to include these in a damage assessment scheme for practical application when decisions have to be made, sometimes urgently, on corrective measures. Extensive studies have been performed at the Technical University of Denmark (DTU) into the behaviour of sandwich structures with face-core debonds. Fracture properties of the interface have been determined for several material combinations relevant to wind turbine blades and ship and aircraft structures. For hull and deck panels of naval vessels the dependence of residual strength on the debond size has been determined, and subsequently used in a damage assessment scheme [1-3]. DTU's research is now focusing especially on fracture and crack growth under cyclic loading.

Material and interface fracture properties are generally obtained from tests on small-scale specimens, often simple sandwich beams. Real sandwich ship structures consist of assemblies of panels. While extensive physical testing and numerical modelling have been performed on sandwich panels and joints with debonds for static loadings, much fewer studies have been performed for cyclic loading. In principle, once the interface fracture properties have been obtained, a structure can be modelled and its fatigue life estimated. However, in practice this can be demanding and time-consuming, so that ways of reducing the computational effort are needed [4-6]. The work reported here considers practical ways of assessing the consequences of defects and damage, as a basis for determining appropriate corrective measures. Procedures developed earlier for static or quasi-static loading [1] have been refined, and ways of adapting and extending them to damage growth and residual life under cyclic loading are explored.

2. THE "SANDI" APPROACH TO DAMAGE ASSESSMENT BASED ON RESIDUAL STRENGTH

The SaNDI Project, *Inspection and Repair of Sandwich Structures in Naval Ships*, was performed in 2001-4 with participants in Norway, Sweden, Denmark, Finland and the United Kingdom. Methodologies for production control and in-service damage inspection were developed, and acceptance criteria established for defects and damage [4,5]. Several types of defects and damage were considered, including face-core debonds as well as various types of impact damage and production defects such as face sheet wrinkles. Damage assessment procedures developed for residual strength in the SaNDI Project use almost exclusively pre-calculated information that can be made readily available in decision support tools and/or manuals on board a ship and at its onshore support facilities.

In the SaNDI damage assessment procedure [1,2], four levels of damage severity are defined: level 1 (small local damage, covering a small part of a panel so that its influence on the panel stiffness and the stresses at remote points on the panel can be neglected); level 2 (as level 1 but involving a larger part of a panel); level 3 (confined to one panel but affecting its stiffness); level 4 (affecting two or more panels and/or supporting structure). The procedure involves consideration of strength reduction factors at up to three scales as illustrated in Table 1. Figure 1 shows local strength reduction factors for debond damage on some sandwich layups with GFRP faces and three types of foam core, from a later study [3]. Debonds may be of level 1, level 2, or level 3 damage. When they are within level 1, the local factor R_l can be combined with a local location and load type sensitivity factor S_p to give the panel strength reduction factor R_p:

$$R_p = R_l S_p \text{ with a maximum value of 1.0} \quad (1)$$

Table 1: Three scales to be considered when assessing damage in a naval sandwich structure

Schematic	Scale	Strength reduction factor
	Local (for level 1 only)	$R_l = \dfrac{\text{Nominal (far field) stress or strain to cause failure with damage}}{\text{Nominal (far field) stress or strain to cause failure without damage}}$
	Panel	$R_p = \dfrac{\text{Maximum allowable load on damaged panel}}{\text{Maximum allowable load on intact panel}}$
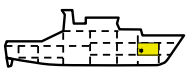	Ship	$R_s = \dfrac{\text{Maximum allowable load on damaged ship}}{\text{Maximum allowable load on intact ship}}$

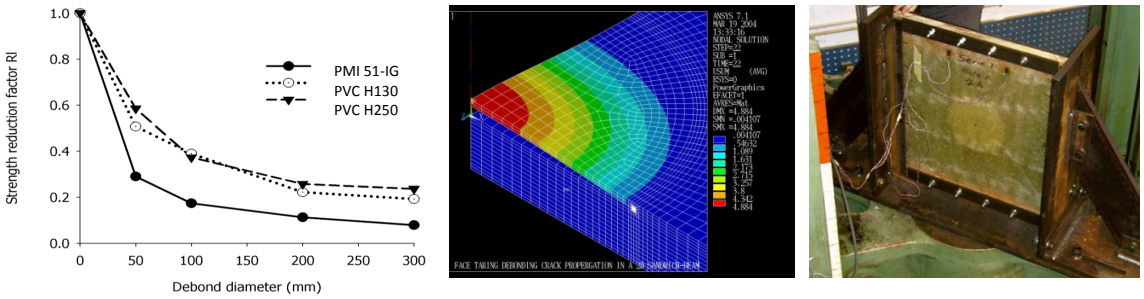

Fig. 1: Local strength reduction factors for face-core debond damage on sandwich layups with GFRP face sheets and three different foam core materials, with in-plane compressive loading [3]. FE analysis and physical testing.

The factor S_p is defined as the ratio of the value of the load on the panel that would cause the critical stress or strain component *at the damage location* to reach its maximum allowable value, *ignoring the damage*, to the maximum allowable value of load on the intact panel (i.e. the load that causes the critical stress or strain component to reach its maximum allowable value at the most highly stressed location). Even if parts of the panel are at their design strength limit under the maximum design loading, other, less severely stressed parts may be able to sustain damage without consequences for the panel as a whole. The variation of S_p over the panel depends on its boundary conditions and type of loading. It will always be on the conservative side to assume $S_p = 1.0$ since, by definition,

$$S_p \geq 1 \tag{2}$$

Any panel that experiences damage should be checked by comparing R_p with a minimum allowable value R_{pa}:

$$R_p \geq R_{pa} \text{ where } R_p = \min\left(R_l S_p, 1\right) \tag{3}$$

R_{pa} represents the minimum residual load-carrying capacity that can be allowed for the panel concerned in order to maintain its functionality. Such a limit can be defined for either local or global loading cases, or both.

If the damaged panel contributes to the global strength of the ship, the overall consequences for the ship must also be assessed. Then the ship strength reduction factor R_s is estimated for one or more global loading cases. For level 1 and 2 damage types, this can be done using a panel location and load type factor S_s that is analogous to the factor S_p so that

$$R_s = R_p S_s \text{ with a maximum value of 1.0.} \tag{4}$$

S_s represents the reserve of strength at the panel in which the damage occurs, calculated for the intact condition. Analysis of the intact ship can provide a map showing the reserve of strength and the S_s value for each panel. For level 3 damage, an approximate method has been proposed [1] for estimating R_s. For level 4 damage, a direct assessment of the damaged ship must be performed. Finally the ship strength reduction R_s has to be compared with an allowable value R_{sa} based on evaluation of the required margin of safety for the design of the ship as a whole:

$$R_s \geq R_{sa} \text{ where } R_s = \min\left(R_p S_s, 1\right) \tag{5}$$

Apart from establishment of the strength reduction at the lowest level, all the factors required can be obtained from prior analysis of the intact ship and its components, considering the relevant loading conditions on the ship in service, as part of the design calculations. Once the above checks have been performed, a decision can be made on further actions.

Subsequent studies have shown that it may be preferable to transform the global strength criterion to either the panel or the local level, so that R_{sa} is used to establish an allowable panel strength reduction factor R_{paG} and, where appropriate, an allowable local strength reduction factor R_{laG}, for global loads. From Eqs. 1-5 it can be shown that

$$R_{paG} = \max\left(\frac{R_{sa}}{S_s}, \frac{1}{S_s}\right) \quad \text{and} \quad R_{laG} = \max\left(\frac{R_{sa}}{S_p S_s}, \frac{1}{S_p}\right) \tag{6}$$

Then the condition $R_s \geq R_{sa}$ can be applied at either the panel or the local level:

$$R_p \geq R_{paG} = \max\left(\frac{R_{sa}}{S_s}, \frac{1}{S_s}\right) \quad \text{or} \quad R_l \geq R_{laG} = \max\left(\frac{R_{sa}}{S_p S_s}, \frac{1}{S_p S_s}\right) \tag{7}$$

Since normally $R_{sa} \leq 1$ these criteria normally reduce to

$$R_p \geq R_{paG} = \frac{1}{S_s} \quad \text{or} \quad R_l \geq R_{laG} = \frac{1}{S_p S_s} \tag{8}$$

Application at the panel level is often most convenient. However, the formulation at the local level is relevant for the extension to damage growth under cyclic loading (see Section 3). The allowable strength reduction factors for local load cases are designated R_{paL} and R_{laL}, and those for global load cases R_{paG} and R_{laG}. By similar arguments to the above,

$$R_{laL} = \max\left(\frac{R_{paL}}{S_p}, \frac{1}{S_p}\right) \tag{9}$$

3. APPLICATION TO CYCLIC LOADING

With cyclic loading on level 1 damage, the local strength reduction curve should in principle be replaced by a *residual life reduction curve*. This would have to be drawn for a given load level (as amplitude of load or stress cycles) and a given minimum/maximum load or stress ratio, most appropriately that for the far-field stress. Figure 2(a) shows schematically a set of such curves. These intersect with the horizontal axis at the points where the applied maximum load is equal to the residual strength of the component in its *initial damaged* state. For a given observed damage size and load amplitude, this shows the expected residual life. This can be compared with the minimum acceptable residual life considering the situation in which the vessel is operating. If the relevant load level is not known, it is still possible to use R_{laG} given by Eq.6, or the value of R_{laL} given by Eq. 9, to give a maximum allowable load value. This is given by multiplying the intact static strength by R_{laG} or R_{laL}. As load values above this would violate the static strength acceptance criterion, this must give a conservative estimate for the residual fatigue life.

Although the initial damage may be level 1, growth under cyclic loading might possibly increase the size beyond this level. However, if the same type of damage has been considered under static loading and found to give failure while the size is within level 1, this is unlikely to be a problem, though change of shape of the damage during growth might invalidate this assumption. Such situations will, however, become clear during the analysis or testing at the local scale.

Another approach is to use the same data as presented in Fig. 2(a) but plot the load level (amplitude) against the initial size of damage, for a series of values of residual life. The load level can be made dimensionless by dividing it by the intact strength, as shown schematically in Fig. 2(b). This is the inverse of what is normally calculated, because the residual life would be calculated based on a given load amplitude. The inversion process would require interpolation between actual calculated cases. This approach allows the SaNDI damage assessment procedure to be applied directly, with use of the load type and location factors as for static loading. We now have a series of local strength reduction curves for given desired values of residual life. For level 2 damage types, similar curves can be drawn at the panel level.

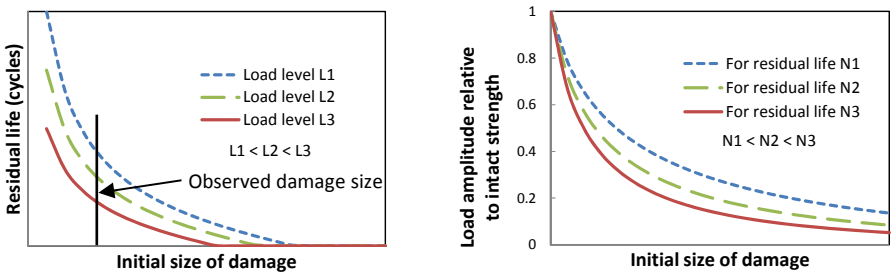

Fig. 2: (a) Residual life reduction curves; (b) Strength reduction curves for different values of residual life.

4. CONCLUSION

Previously developed schemes for assessing damage experienced by sandwich structures in naval ships and their influence on residual structural strength have been described and discussed. Possibilities for devising similar procedures for assessing residual fatigue life following a damage event have been explored. It is important to bear these schemes in mind when performing research into the effects of damage (under both static and cyclic loading) on structural performance, in order to ensure that the results can be used by navies in the operation of their ships. In particular there is a need for research into the way that damage grows in realistic, three-dimensional sandwich structures; knowledge and experience of such processes is essential if approaches to damage assessment are to be tried and tested.

ACKNOWLEDGEMENTS

The support of the Office of Naval Research Solid Mechanics Research Program (Program Manager Dr. Y.D.S. Rajapakse, grants N00014-14-10253 and N00014-16-1-2977) is gratefully acknowledged.

The SaNDI Project (JP 3.23 Inspection and Repair of Sandwich Structures in Naval Ships) was led by Det Norske Veritas AS and supported by the Ministries of Defence of Norway, Sweden, Denmark, Finland and the United Kingdom.

REFERENCES

[1] B. Hayman, "Approaches to Damage Assessment and Damage Tolerance for FRP Sandwich Structures", *J. Sandw. Struct. Mater.*, 2007; 9: 571-596.

[2] D. Zenkert et al., "Damage Tolerance Assessment of Composite Sandwich Panels with Localised Damage", *Compos. Sci. Technol.*, 2005; 65: 2597-2611.

[3] R. Moslemian et al., "Failure of Uniformly Compression Loaded Debond Damaged Sandwich Panels - an Experimental and Numerical Study", *J. Sandw. Struct. Mater.*, 2012; 14: 297-324.

[4] R. Moslemian et al., "Accelerated Fatigue Crack Growth Simulation in a Bimaterial Interface", *Int. J. Fatigue*, 2011; 33: 1526-32.

[5] R. Moslemian et al., "Face/Core Debond Propagation in Sandwich Panels Under Cyclic Loading - Part I: Numerical Modeling and Part II: Experimental Validation", *10th Int. Conf. Sandwich Structures*: 2012, 41-44.

[6] R. Moslemian et al., "Interface Fatigue Crack Propagation in Sandwich X-joints – Part I: Experiments and Part II: Finite Element Modeling", *J. Sandw. Struct. Mater.*, 2013; 15: 1-36.

10.5075/epfl-ICSS12-2018-35-37

DEVELOPMENT OF A MODE I/II/III TEST FIXTURE FOR COMPOSITE LAMINATES AND SANDWICH FACE/CORE FRACTURE CHARACTERIZATION

Pietro Sabbadin[1], Christian Berggreen[2] and Brian Nyvang Legarth[3]
[1]Department of Mechanical Engineering, Technical University of Denmark, Denmark. pisabb@mek.dtu.dk
[2]Department of Mechanical Engineering, Technical University of Denmark, Denmark. cbe@mek.dtu.dk
[3]Department of Mechanical Engineering, Technical University of Denmark, Denmark. bnle@mek.dtu.dk

1. INTRODUCTION

Sandwich structures are considered as key enablers for future and present lightweight structural applications in naval ships because of their superior stiffness/weight and strength/weight ratios compared with traditional metallic concepts as well as monolithic composite materials. Naval vessels are expected to encounter a large variety of load scenarios, which can cause different types of damages within the sandwich structure.

The most common and severe type of damage that a composite sandwich structure can experience is the lack of adhesion (a crack develops) between the face sheets and core known as a "debond". Therefore, the fracture characterization of the face/core surface is fundamental to predict the remaining life of a debond damaged sandwich structure.

The aim of this work consists in developing a test rig and a test procedure which is able to carry out the fracture characterization on a delaminated or debonded specimen (monolithic or sandwich composite specimen) in the most general loading scenario where all three types of loadings at the crack tip are present (Mode I-II-II).

2. THE TEST RIG

The test rig geometry (Fig. 1) is inspired from the STB test rig presented in [1] since in that work experimental results agreed well with the FEM analyses regarding pure Mode III and multiaxial (Mode I+III, II and II+III) fracture characterization of delaminated composite laminates.

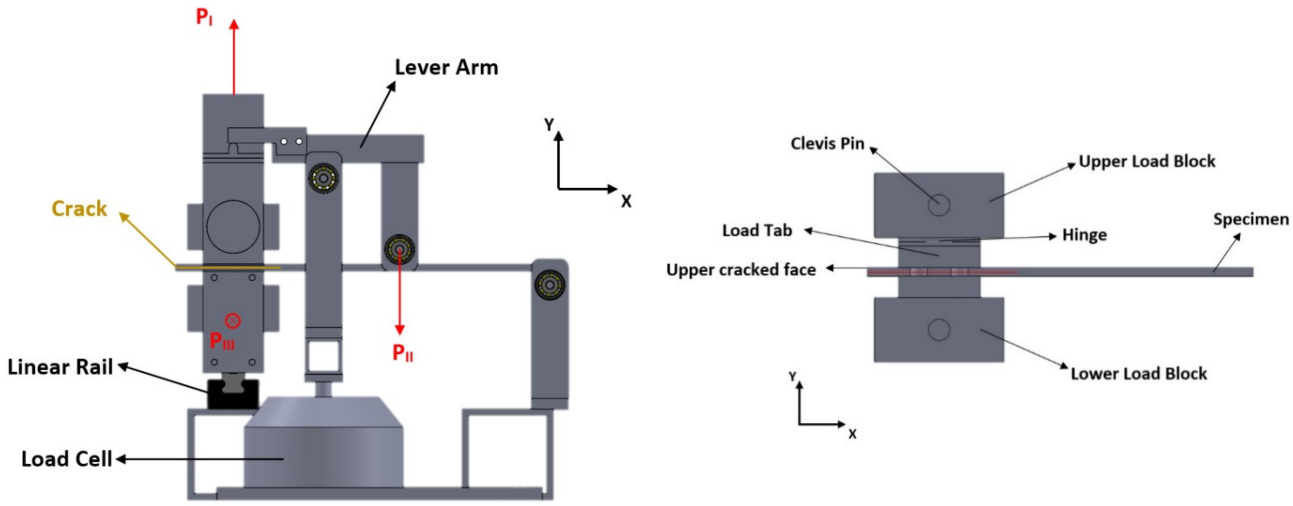

Fig. 1: Mode I-II-III test rig on the left and a detailed view of the cracked specimen with load tabs on the right.

The STB geometry was analyzed by building a 3D FEM model in order both to benchmark the strain energy release rate (SERR) distributions against those in the literature [1] and to understand how geometric parameters of the specimen influence SERR distributions along the debonded front.

The extraction of SERR values from the debond front in the FE model has been carried out by applying the CSDE method [2]. Experimental tests jointly with results from the FE model will be capable of gaining new and important insight regarding pure Mode III as well as multi-mode fracture characterization of face/core interfaces in composite sandwich structures.

3. NUMERICAL MODEL AND PRELIMINARY NUMERICAL RESULTS

This work will initially focus on the analytical/numerical analysis and experimental measurement of the Mode III fracture toughness regarding composite laminates (CFRP and GFRP, see table 1 for the material properties). Secondly, Mode III fracture toughness analysis will be extended also to foam cored composite sandwich specimens. Finally, the complete analysis will be addressed (analytical, numerical and experimental) regarding mixed-mode I/II/III fracture characterization utilizing the new test rig.

A 3D FE model (Fig. 2) of a CFRP and GFRP laminate specimen was built in order to extract the SERR trend along the crack front under pure mode III load conditions, using the CSDE method [2]. This procedure was adopted in order to check if a pure mode III state was present along the crack front with the external load imposed by the test rig. Material properties used in the FE model are reported in Table 1.

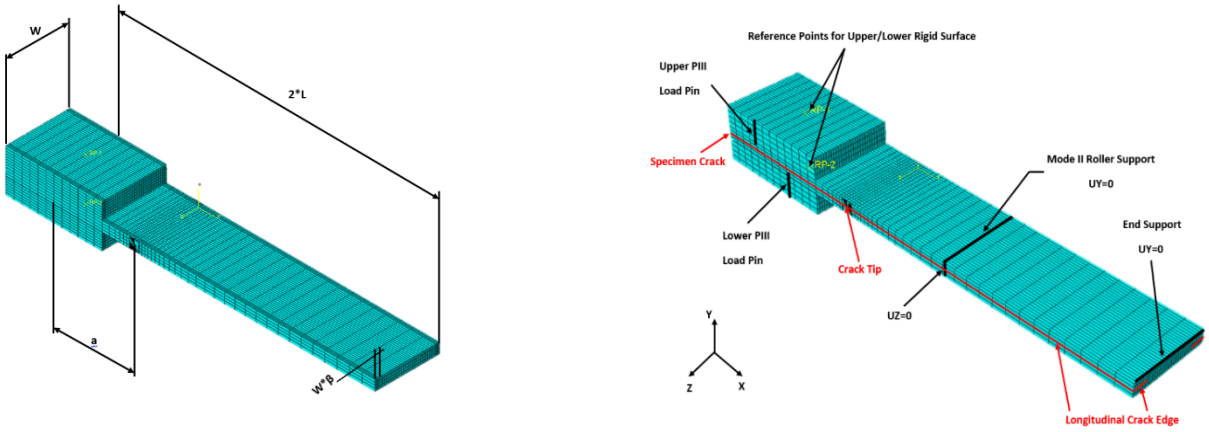

Fig. 2: 3D FEM model showing the principle geometrical parameters of the model and the boundary conditions applied.

The SERR values extracted along the crack front with the CSDE method [2] for CFRP and GFRP laminates are reported in Fig. 3. The ratio G_{III}/G_{TOT} (where G_{TOT} accounts for all three modes contributions, i.e. mode I-II and III) along the crack front is approximately equal to unity, thus indicating a pure mode III state is achievable with this preliminary design. Further numerical investigations will be carried out regarding the introduction of mode I and II.

Table 1: Material properties of the two laminates.

Laminate	Elastic Moduli [GPa]						Poisson´s ratios		
	E_{11}	E_{22}	E_{33}	G_{12}	G_{13}	G_{23}	ν_{12}	ν_{13}	ν_{23}
Unidirectional GFRP	48.00	8.00	8.00	4.00	4.00	3.00	0.285	0.285	0.333
Unidirectional CFRP	150.00	10.00	10.00	5.36	5.36	3.75	0.330	0.330	0.333

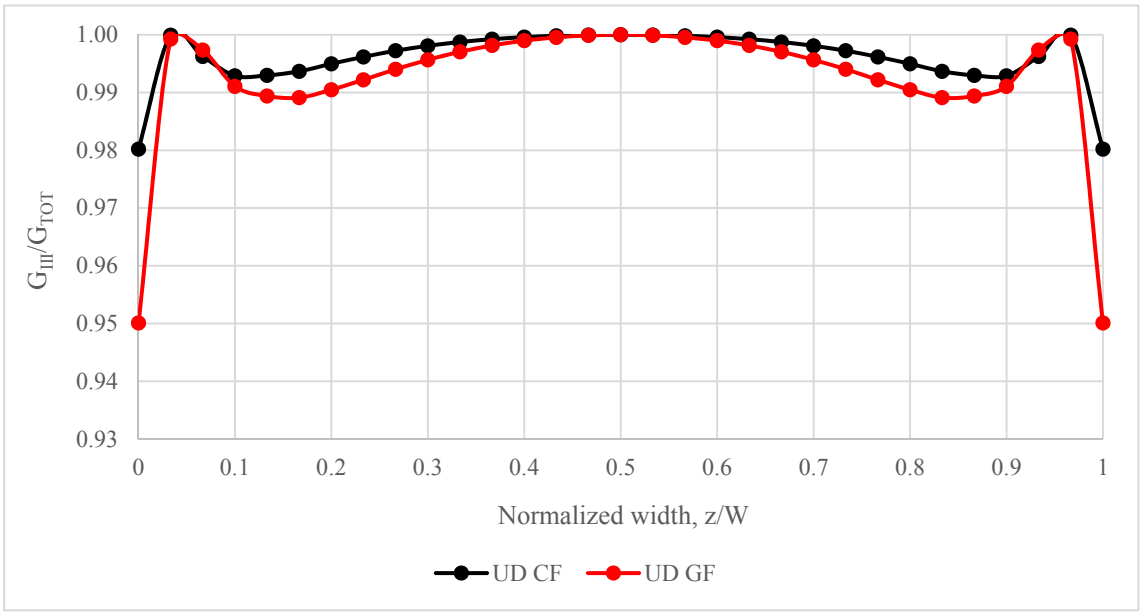

Fig. 3: G_{III}/G_{tot} trend along the crack front under pure mode III external load for two different composite laminates.

ACKNOWLEDGEMENTS

Financial support from the US Navy Office of Naval Research, Grant N00014-16-1-2977, and the interest of the Grant Monitor, Dr. Y.D.S. Rajapakse, are gratefully acknowledged.

REFERENCES

[1] Barry D. Davidson, Felipe O. Sediles, Mixed mode I-II-III delamination toughness determination via shear-torsion-bending test, Composites Part A-applied Science and Manufacturing — 2011, Volume 42(6), pp. 589-603.

[2] C. Berggreen, B. C. Simonsen, K. K. Borum, Experimental and Numerical Study of Interface Crack Propagation in Foam-cored Sandwich Beams, Journal of Composite Material, Vol. 41, No. 4/2007.

DOI: 10.5075/epfl-ICSS12-2018-38-40

INVESTIGATION OF THE INFLUENCE OF FACE THICKNESS ON FACE/CORE FRACTURE TOUGHNESS OF FOAM AND HONEYCOMB CORE SANDWICH

Mohammad Tauhiduzzaman[1], Laura J. Duarte Mendoza[2] and Leif A. Carlsson[3]
[1]Florida Atlantic University, FL, USA. mtauhiduzzam2016@fau.edu
[2]Florida Atlantic University, FL, USA. lduartemendo2018@fau.edu
[3]Florida Atlantic University, FL, USA. carlsson@fau.edu

1. INTRODUCTION

A critical failure mode of sandwich structures is crack propagation at the interface between face and core. Fracture toughness, G_C, i.e. the critical value of the energy release rate, is used to characterize the resistance to such crack propagation. Several tests method are available to study the interfacial fracture of sandwich. The Single Cantilever Beam (SCB) test, Fig. 1, has emerged during recent years as a potential ASTM test standard [1].

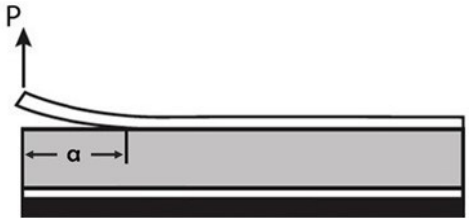

Fig. 1: Schematic of SCB test.

The loading and support conditions lead to mode I dominated crack propagation at or near the face/core interface. When a crack advances between two dissimilar materials, it will experience mixed mode conditions i.e. both tension and shear. Under such loading, unless the crack is trapped at a certain plane, the crack will try to find a new plane where mode I exists [2]. The possibility of oblique crack propagation is known as kinking behavior for sandwich structures, see Fig. 2. Interfacial crack growth occurs when crack propagates under mode I dominance and when the face/core bonding is weak. As discussed by He and Hutchinson [2] a tough core material will also prevent kinking. Crack propagation inside the core may occur when the bonding of face and core is strong enough. Kinking into core may occur due mode II loading if the core material is brittle.

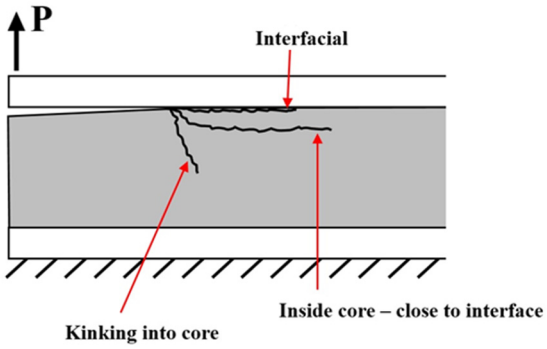

Fig. 2: Different crack propagation scenarios.

In this study, SCB tests will be conducted on PVC H100 foam and honeycomb core SCB specimens with aluminum face sheets with a range of thicknesses. As discussed by e.g. Li et al. [3], increased face thickness will promote shear loading (mode II) which would lead to crack kinking into the core. Furthermore, thicker face sheets are expected to promote linear load-displacement response allowing use of the MBT method with more confidence. These issues are fundamental for the design of the SCB test and wider acceptance of the test method as an ASTM standard.

2. EXPERIMENTAL

PVC H100 foam core panels of 25.4 *mm* thickness were provided by DIAB. HC core panels of the type ECA- HC $3/16^{"}$ with 12.7 *mm* thickness were obtained from Eurocomposites. The thickness of top face sheets was varied from 3 to 6.35 *mm*. The thickness of bottom face was same for all specimens, 3.20 *mm*. An artificial precrack was defined by placing a 250 μm thick Teflon film of 3.18 *cm* length between top face and core. The bottom face sheet was bonded to

the core with Araldite 2015, while the top face sheet was bonded with Hysol EA 9309.3NA adhesive. To accommodate load application, a hinge was mounted to the top face sheet above the precrack. The test program is presented in Table 1.

Table 1: Material properties of sandwich elements.

Materials	Mechanical Properties	Thickness *(mm)*	Density (kg/m^3)
Top Facesheets (6061-T6 Aluminum)	$E = 68.9GPa$ $\sigma_y = 240MPa$	3, 4.76, 6	2700
PVC-H100 Core	$E_c = 130MPa$	25.4	100
ECA- HC $3/16^{"}$ Core	$E_c = 140MPa$ (Out of plane)	12.7	48

The SCB specimens were $5.1\ cm$ wide, and $30.5\ cm$ long. All HC specimens were tested with the L direction along the specimen. A SCB test fixture was mounted to the base of a Tinis-Olsen test frame of $133\ kN$ load capacity. Sharp edge clamps of the fixture hold the lower face sheet during loading. A $30\ cm$ long loading rod attached to the moving crosshead of the test machine was attached to the edge of the face using a pinned connection. Displacement was measured by a linear voltage differential transducer (LVDT). Load was recorded by a $13.3\ kN$ load cell mounted on the moving crosshead.

During the experiments, the crosshead was moved at a constant speed of $2.5\ mm$/min. Load-displacement data was recorded throughout the test using a LabVIEW data acquisition system. Crack growth was monitored by visual observation of the crack tip region on both sides of the specimen. The location of the crack front was marked by pencil after each cycle allowing for subsequent evaluation of crack length. The testing was conducted by loading-unloading cycles with propagation of the crack in increments of about $1-2\ cm$.

3. FRACTURE TOUGHNESS DETERMINATION

Fracture toughness G_C is estimated for each loading cycle by using the modified beam theory (MBT) [1, 4] and area methods [1, 5]. MBT is based on multiple compliance measurements. Therefore, several crack growth cycles are considered to generate a plot of cube root compliance, $C^{1/3}$, vs. disbond length, a which allows determination of the offset crack length Δ. The fracture toughness from MBT method is determined for each crack increment by

$$G_C = \frac{3P_C\delta_C}{2b(a+\Delta)} \tag{1}$$

where P_C is the load at the onset of debond growth, δ_C is corresponding displacement, b is the width of the specimen and a is the crack length. It is straight-forward to evaluate the critical load P_C for an ideal linear load-displacement curve, where the crack propagates at a well defined point. However, the actual $P-\delta$ curve display nonlinear response prior to the crack growth. The nonlinear response could be attributed to several reasons such as slow stable crack growth etc. When the nonlinear response is softening, P_C is considered as the load at the onset of a distinct nonlinearity in the curve. The toughness value , G_C , is referred to as initiation toughness. Thin face sheets, however, promote a stiffening nonlinearity which obscures determination of P_C and δ_C.

The area method provides a direct measure of G_C from the energy dissipation ΔU required to achieve a disbonded area increment ΔA.

$$G_C = \frac{\Delta U}{b\Delta a} \tag{2}$$

where ΔU is the area enclosed within a loading-unloading cycle and Δa is the increment in crack length. The fracture toughness value G_C represents an average value including both initiation and propagation of the crack.

At the time of writing this abstract, we have tested only a few specimens, and more specimen will be tested before we can assess the importance of face thickness in the SCB test.

ACKNOWLEDGEMENT

Support from NIA/FAA and ONR is gratefully appreciated. The NIA program manager, Dr. Ronald Krueger, and FAA program manager Dr. Zhi-Ming Chen provided also useful technical support. This research is partly managed by Dr. Yapa Rajapakse from ONR. We also wish to thank DIAB (James Jones) and Euro-Composites (Barry Millward) for donation of core materials.

REFERENCES

[1] ASTM Standard XXXXX-XX, Draft Standard "Interfacial Fracture Toughness of Peel Loaded Sandwich Constructions," American Society for Testing and Materials, March 9, 2017.

[2] M.Y. He et al., "Kinking of a crack out of an interface", *Journal of Applied Mechanics*, 1989, 56(2): 270-278.

[3] S. Li et al., "The effects of shear on delamination in layered materials", Journal of the Mechanics of Physics and Solids, 2004, 52, 193-214.

[4] ASTM Standard D5528- 01, "Mode I Interlaminar Fracture Toughness of Unidirectional Fiber-Reinforced Polymer Matrix Composites," *American Society for Testing and Materials*, 2007; ASTM Annual Book of Standards, Vol. 15.03.

[5] K. Shivakumar et al., "In situ fracture toughness testing of core materials in sandwich panels", *Journal of Composite Materials*, 2004; 38(8):655-668.

DOI: 10.5075/epfl-ICSS12-2018-41-42

SHEAR AND FOUNDATION EFFECTS IN SCB SANDWICH SPECIMEN

Leif A. Carlsson[1], Vishnu Saseendran[2], Christian Berggreen[3] and Laura J. Duarte Mendoza[4].
[1]Department of Ocean and Mechanical Engineering, Florida Atlantic University, USA. carlsson@fau.edu,
[2]Department of Mechanical Engineering, Technical University of Denmark, Denmark vsas@mek.dtu.dk,
[3]Department of Mechanical Engineering, Technical University of Denmark, Denmark. cbe@mek.dtu.dk.
[4]Department of Ocean and Mechanical Engineering, Florida Atlantic University, USA. lduartemendo2018@fau.edu

1. INTRODUCTION

Failure of the face/core interface in a sandwich structure needs consideration in design of damage-tolerant sandwich structures. The large elastic stiffness mismatch between the face sheets and core leads to mixed mode (combined opening and shear) loading. Experimental studies have shown that the face/core fracture resistance and the tendency of the crack to kink into the core depend on the mode mixity. Li et al. [1] and Andrews and Massabo [2] conducted finite element analysis of a beam-like element under axial a transverse forces and pure bending moments Li et al. [1] found that shear may greatly influence energy release rate and mode mixity and that these quantities depend on localized deformation in the crack tip region termed “root rotation”, see Fig. 1.

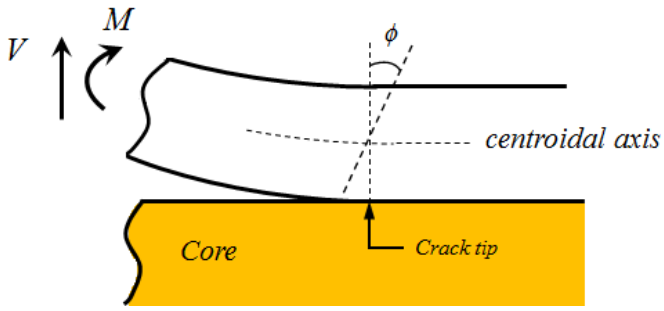

Fig. 1: Illustration of crack root rotation.

Analysis of crack root rotation in the SCB test specimen, Fig.2, has recently been conducted by Saseendran et al. [3].

Fig. 2: Schematic representation of SCB test for face/core disbanding characterization.

Notice that for this test, the crack tip shear force and moment (both per unit width) are defined in Eqs.1a and 1b:

$$V = P / b \tag{1a}$$

$$M = Pa / b \tag{1b}$$

where P is the load applied, b is the specimen width and a is the crack length (Fig. 2). Hence, for short crack lengths, shear will dominate the loading, while at long crack lengths, we can neglect the influence of shear, and consider only the applied moment.

In this presentation, we will extend the results by Saseendran et al.[3] to show how they apply to SCB specimens with a range of foam and honeycomb cores. The conditions when shear becomes a significant factor influencing energy release rate and mode mixity will be discussed.

2. RESULTS

A symmetrical SCB sandwich specimen with aluminum face sheets $(E_f = 68.9\ GPa, h_f = 6.35mm)$ and a PVC H100 foam core $(E_c = 130\ MPa, h_c = 25.4\ mm)$ was initially considered. Total length of specimen was L = 305mm, and the crack length was varied in the range: a = 1-50 mm. The foundation model was used to analyze crack root rotation. In addition, a 2D plane stress finite element model of the SCB specimen was constructed. The model utilized 4-node parabolic elements in the crack tip region.

Results for the crack root rotation for this specific SCB specimen are presented in Fig. 3. The FEA results agree very well with analytical results from the foundation model. Notice that the pure shear effect can be determined by extrapolation of the results to a = 0. It is noted that shear dominates the rotation for crack lengths less than about 15 mm $(\frac{a}{h_f} \leq 2.4)$.

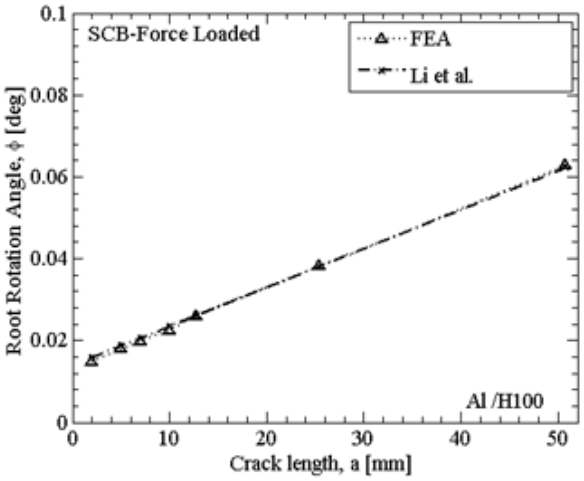

Fig. 3: Crack root rotation angle (ϕ) for SCB sandwich specimen (P = 1N/mm) calculated from FEA and Li et al. [1] approach.

Results for a wide range of face, core materials, and thickness will be presented.

ACKNOWLEDGEMENTS

Support from ONR and NIA/FAA is gratefully appreciated. This research is managed by the ONR program officer, Dr. Yapa Rajapakse, who has provided much encouragement and support. Grant and technical support from NIA/FAA is also appreciated. Thanks go to Drs. Krueger and Chen from NIA/FAA.

REFERENCES

[1] Li, S.et al., "The effects of shear on delamination in layered materials." Journal of the Mechanics and Physics of Solids, 2004, vol. 52, no. 1, pp. 193-214.

[2] Andrews, M.G. and Massabo, R., 2007, The Effects of Shear and Near–Tip Deformations on Energy Release Rule and Mode Mixity of Edge–Cracked Orthotropic Layers, Eng. Fract. Mech., 74, 2700–2720.

[3] Saseendran, V.et al., "Shear and foundation effects on crack root rotation and mode-mixity in moment- and force-loaded single cantilever beam sandwich specimen", Journal of Composite Materials, DOI: 10.1177/0021998317749714.

SESSION 2B: MECHANICS / MODELING

DOI: 10.5075/epfl-ICSS12-2018-44-46

1D COUPLING ELEMENT FOR EFFECTIVE MODELLING OF SANDWICH PANELS

Alexander N. Nordas[1], Luis Santos[2], Bassam A. Izzuddin[3] and Lorenzo Macorini[4]
Department of Civil and Environmental Engineering, Imperial College, London SW7 2AZ, UK
[1]alexandros.nordas13@imperial.ac.uk, [2]ls3715@ic.ac.uk, [3]b.izzuddin@imperial.ac.uk, [4]l.macorini@imperial.ac.uk

1. INTRODUCTION

The considerably superior specific strength and stiffness of sandwich panels in relation to conventional structural components makes their employment for deck systems and two-way spanning structural applications a highly attractive alternative. An accurate description of the mechanical response and encountered failure modes in a sandwich panel deck system requires high-fidelity detailed finite element models, capable of capturing geometric and material nonlinearity both globally and locally. In this context, besides the detailed modelling of the panel geometric domain, the accurate representation of compatibility between deformable deck components, such as along weld lines, is essential for the local response evaluation. Considering all-steel sandwich decks, the welded connection between the panel core and faces, the edgewise connection of adjacent panels, as well as the connection of the panel deck with the underlying grillage of supporting beams and the load patches transferring the equipment loading to the panel top surface require a sophisticated modelling approach.

When modelling connected deformable components, the geometric complexity of the system often imposes severe constraints on the meshing of the respective interfaces to achieve coupling, such as the requirement for nodal alignment, compliance of element shapes and density, proportionality of element sizes and the implementation of geometrically complex transitional meshes. This paper presents an efficient and highly accurate computational strategy for coupling shell surfaces modelled with non-matched Finite Element (FE) meshes along a line interface of arbitrary spatial orientation. The developed formulation allows independent meshing of the coupled domains, enabling a more efficient discretisation procedure to be achieved and overcoming the previously noted modelling shortcomings. It is therefore particularly applicable in the modelling of deformable components which are independently meshed and coupled along a weld line, as well as in the case of partitioned models with a different level of discretisation detail in each child partition, dictated by the geometry, applied loading and the specific boundary conditions.

2. 1D LINE COUPLING ELEMENT FORMULATION

The coupling constraint is introduced along the line interface in the weak form of the global boundary value problem, by using a two-field Lagrangian functional which represents the contribution of the tied interface to the total potential energy of the system. An element-to-element coupling is introduced along the intersections of the tied interface with the faces of a different subset of active elements for each independently discretised domain. This mesh-tying formulation has been implemented in the form of a coupling element which consists of two arbitrary 2D solid FE faces, located at opposite sides of the 1D line interface. The constraint over the tied interface is enforced by employing the augmented Lagrangian multiplier formulation, where the total potential energy contribution of the element to the system includes a second-order penalty regularisation [1]:

$$\Pi_{\boldsymbol{ALM}} = \int_{\boldsymbol{\Gamma_c}} \left[\boldsymbol{\lambda} \cdot \mathbf{g}(\mathbf{u}) + \frac{1}{2} \cdot \varepsilon \cdot \mathbf{g}(\mathbf{u}) \cdot \mathbf{g}(\mathbf{u}) \right] \mathrm{d}\boldsymbol{\Gamma_c} \tag{1}$$

In the above expression, $\boldsymbol{\lambda}$ is an independent variable field of Lagrangian multipliers introduced along the coupled interface $\{\Gamma_c\}$, $\mathbf{u} = \{\mathbf{u}^1, \mathbf{u}^2\}$ is the domain displacement field, $g(\mathbf{u}) = \mathbf{u}^1 - \mathbf{u}^2$ is the gap vector field, and $\varepsilon \geq 0$ is a penalty parameter. The coupling interface contributions to the first order variations of the total potential energy in Eq. 1 with respect to $\mathbf{u}$ and $\boldsymbol{\lambda}$, which relate to resistance forces and constraint equations respectively, are obtained as**:**

$$\delta\Pi^{\boldsymbol{u}}_{\boldsymbol{ALM}} = \int_{\boldsymbol{\Gamma_c}} [\boldsymbol{\lambda} + \varepsilon \cdot \mathbf{g}(\mathbf{u})] \cdot \frac{\partial \mathbf{g}(\mathbf{u})}{\partial \mathbf{u}} \cdot \delta\mathbf{u} \ \mathrm{d}\boldsymbol{\Gamma_c} \tag{2}$$

$$\delta\Pi^{\boldsymbol{\lambda}}_{\boldsymbol{ALM}} = \int_{\boldsymbol{\Gamma_c}} \delta\boldsymbol{\lambda} \cdot \mathbf{g}(\mathbf{u}) \ \mathrm{d}\boldsymbol{\Gamma_c} = \mathbf{0} \tag{3}$$

The expressions of the element stiffness matrix and resistance force vector are obtained by expressing the Lagrangian multiplier and displacement fields in a discrete form. This is achieved by means of interpolating the values obtained at *a priori* defined collocation points and nodal locations, using Lagrangian polynomial shape functions. The concept is illustrated in Fig. 1(a), where two independently discretised regions $\{\Gamma_h^{(i)}\}$, i=1,2, are coupled along the 1D interface $\{\Gamma_c\}$. The active subset of elements in each mesh are denoted as $\{\Gamma_{c,h}^{(i)}\}$.

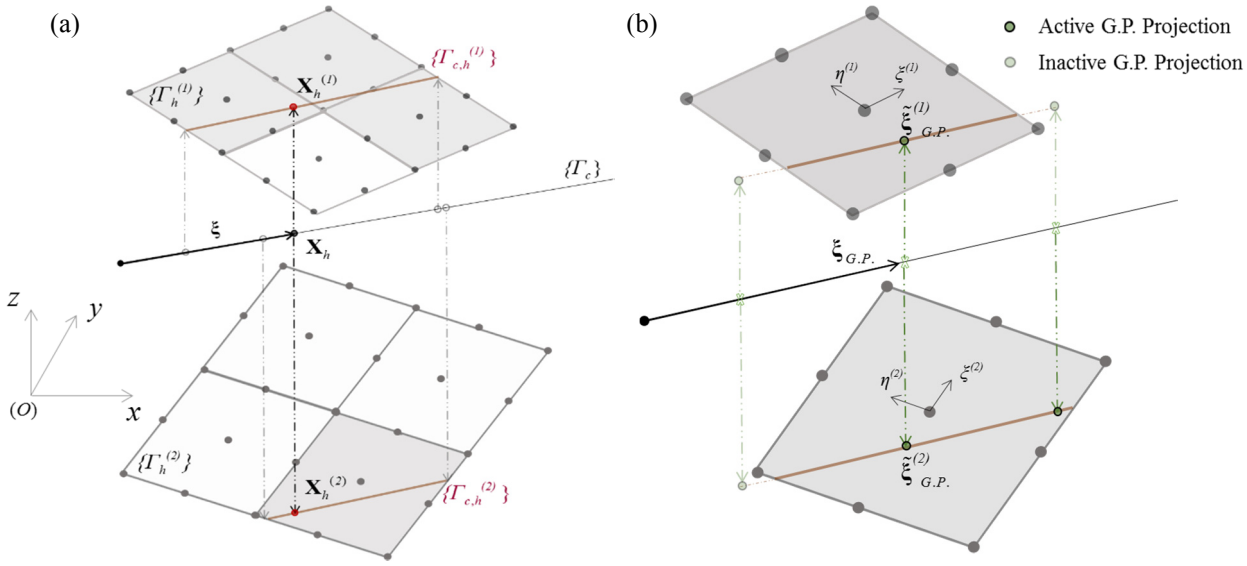

Fig. 1: (a) 1-D coupling element consisting of two 9-noded shell finite elements faces, (b) Gauss Point projection procedure for numerical integration of the stiffness matrix.

For the numerical integration of the stiffness matrix along the interface Gaussian quadrature is employed. The interface is sub-divided into a finite number of regions where Gauss points are defined and are subsequently projected on the element faces. The component matrices are evaluated at the Gauss point projections, $\xi^{(i)}_{\mathrm{G.P.}}$, expressed in the respective natural coordinate system of the two elements on the coupled surfaces, as illustrated in Fig. 1(b).

3. NUMERICAL EXAMPLES

The effectiveness and accuracy of the proposed coupling element formulation are illustrated using detailed models at critical regions of an all-steel sandwich panel deck system, where a thorough investigation of the connection between discrete plated components is required, as illustrated in Fig. 2. The sandwich panels comprise a rectangular honeycomb core configuration, consisting of a grid of 3 mm thick rectangular steel strips, laser-welded to the top plates, also of 3 mm thickness. The panel compartments, underlying beams and loading patch plates used as equipment supports have been discretised using 9-noded co-rotational curved shell nonlinear elements [2] in accordance with a high-fidelity modelling strategy for metal sandwich panels [3]. The deformed shapes, contour plots and graphs have been obtained using ADAPTIC [4], in which the coupling element has been implemented.

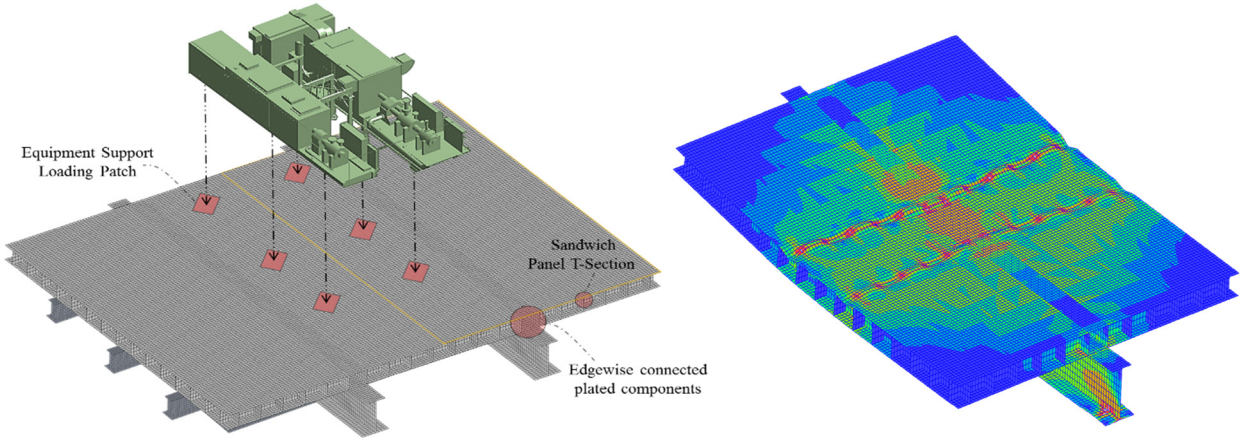

Fig.2: High-fidelity modelling of all-steel sandwich panel deck system and identification of critical contact regions.

Fig. 3(a) illustrates the element application in modelling the coupling of non-matching meshes in locations of different plated component edgewise contact. The contour plot highlights the ability of the element to effectively transfer a planar stress field between the two non-matched meshes in contact. An independent meshing of adjacent sandwich panel domains is thereby allowed without necessitating the implementation of complex transitional mesh regions. Fig. 3(b) illustrates the element application in modelling the coupling of sandwich panel plates and core strips for an arbitrary orientation of the weld line, where clearly the intersection of the line interface with the element edges of the top plate are non-coincident with nodal locations over the core strip. This enables the independent meshing of the various panel compartments, with a

higher level of discretisation detail being employed in regions characterised by high stress variation and potential instability. Lastly, Fig.3(c) illustrates the element application in coupling independently meshed shell surfaces along a line interface. A load patch skewed by 45° in the x-y plane underneath an equipment support is coupled to the top panel plate along four weld lines on the patch perimeter. The use of the coupling element allows a significantly reduced mesh density (left), as compared to the case where a fine compliant mesh is required for the application of conventional node-to-node coupling or continuous meshing at coincident nodal locations. Evidently, the response obtained at the patch centre with the use of the proposed coupling element is comparable to that obtained using conventional translational joint elements for nodal coupling. The presented examples clearly illustrate the numerous modelling benefits associated with the employment of the proposed formulation, in addition to its accuracy and effectiveness. Beyond leading to a simple and effective discretisation procedure, the proposed approach leads to a more efficient use of computing time and resources.

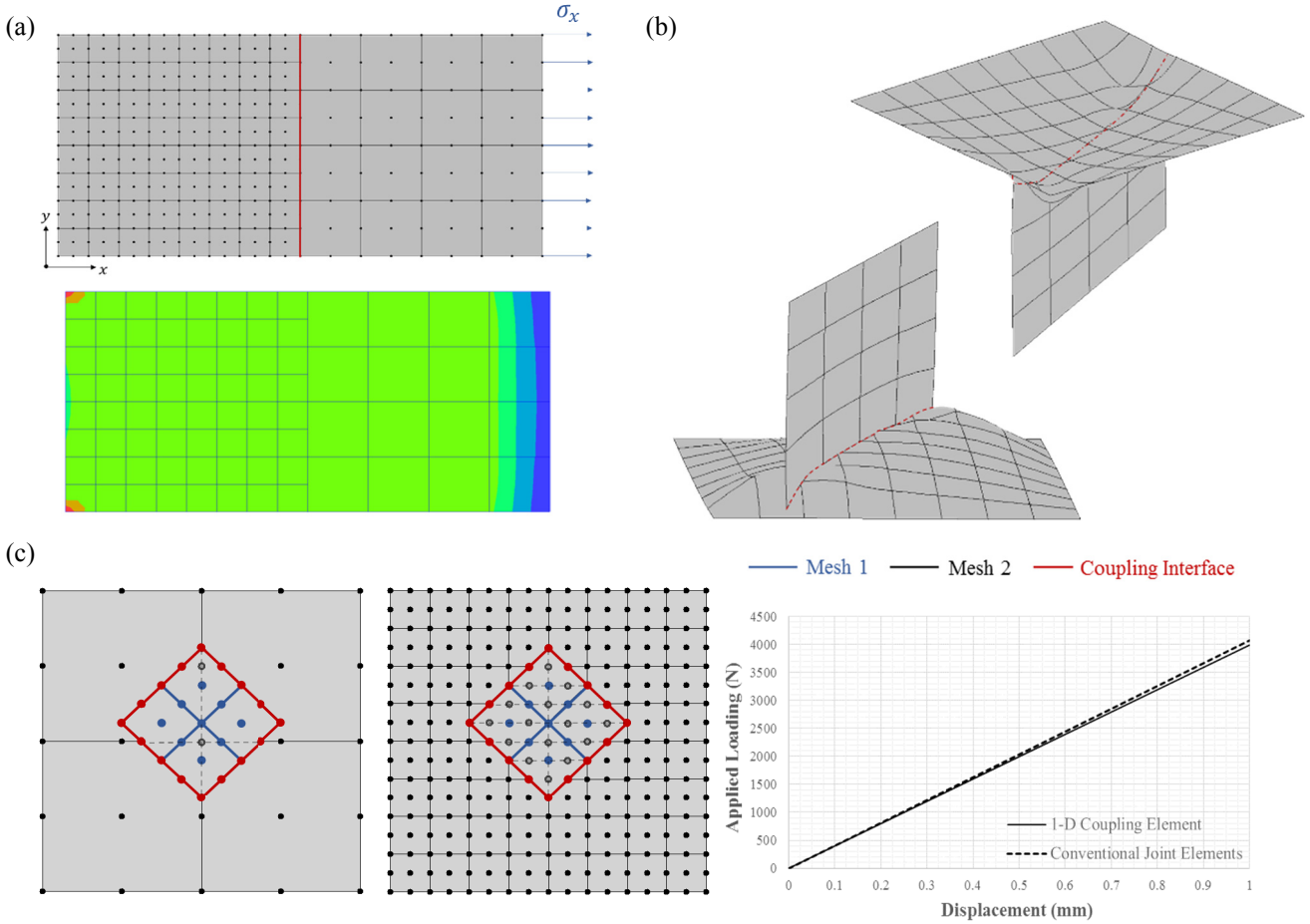

Fig.3: Applications of the 1D coupling element in modelling of contact problems with non-matching meshes: (a) Edgewise plate contact, (b) weld line modelling in rectangular honeycomb sandwich panel plate and core strip T-sections, (c)weld line modelling in load patch – sandwich panel plate contact regions.

4. CONCLUSIONS

This paper presents a novel formulation for translational coupling of two surfaces discretised with non-matching shell element meshes along a line interface with any spatial orientation, which has particular applications in the modelling of sandwich systems. The formulation is developed as a coupling element consisting of two arbitrary 2D element faces on either side of the interface, where the overall interface is discretised into several coupling elements. It is therefore particularly applicable in the modelling of independently discretised components that are welded and to partitioned models with different levels of discretisation detail in each child partition. The presented approach addresses major shortcomings in conventional coupling of surfaces along a line, thus achieving significant modelling benefits.

REFERENCES

[1] P. Wriggers, Computational Contact Mechanics. Springer Science & Business Media, 2006.

[2] B. A. Izzuddin and Y. Liang, "A hierarchic optimisation approach towards locking-free shell finite elements," Computers & Structures, 2017. . DOI: https://doi.org/10.1016/j.compstruc.2017.08.010.

[3] A. N. Nordas et al, "Effective high-fidelity nonlinear analysis of metal sandwich panels using partitioned modelling," Ukacm 2017, 2017, pp. 284-287.

[4] B. A. Izzuddin, "Nonlinear Dynamic Analysis of Framed Structures." , Imperial College, University of London, 1991.

DOI: 10.5075/epfl-ICSS12-2018-47-49

AN ALTERNATE STATE VECTOR FORMULATION FOR THERMO-ELASTIC DEFORMATION ANALYSIS OF SANDWICH PANELS

Balavishnu Udayakumar[1] and K.V. Nagendra Gopal [2]
[1]Aerospace Engineering, Indian Institute of Technology Madras, India. balavishnu.iitm@gmail.com
[2]Aerospace Engineering, Indian Institute of Technology Madras, India. gopal@iitm.ac.in

1. INTRODUCTION

Mathematical models based on exact thermo-elasticity equations and their solutions act as benchmark for analytical, semi-analytical and numerical solutions based on approximate models. Analytical methods used for solving the exact thermo-elastic models for advanced layered, multi-functional panels, including sandwich construction, should have the capability to incorporate any number of layers with arbitrary material properties (structural, functional, and/or multiple fields like elastic, thermal, electro-magnetic, etc.) and thickness. Compared to other analytical methods [1], the state space method [2, 3], based on the idea of converting boundary value problems to equivalent initial value problems, has been shown to be very efficient for the analysis of layered panels, including multi-field problems [4, 5].

In linear un-coupled thermo-elasticity, the conventional procedure followed by most analytical methods is to solve the elastic and thermal and fields separately [6, 7]. The same procedure has also been implemented in the state space formulation for obtaining analytical solutions to single layer [5] and sandwich panels [8].

In this paper, an alternate state vector formulation is presented in which an augmented state vector is defined including the displacements, transverse stresses, temperature and transverse heat flux. The present formulation is a more general method with advantages like provision for fully coupled response, ability to incorporate multiple edge boundary conditions and loading simultaneously. Thus, all the state variables can be obtained simultaneously by solving a single set of vector differential equation. The method is validated using the thermo-elasticity solutions for simply-supported panels obtained using Eshelby-Stroh formalism [7]. The alternate state vector formulation is found to provide accurate numerical results. After validation, the procedure is applied for the thermo-mechanical analysis of a sandwich panel with thin aluminum face-sheets and a soft-core of divinycell H35 foam.

2. AN ALTERNATE STATE VECTOR FORMULATION FOR THERMO-ELASTICITY

The governing state vector equation and associated derived variables within the framework of the three-dimensional, linear un-coupled thermo-elasticity in the absence of body forces and internal heat sources can be obtained by combining and re-arranging the following equilibrium equations, constitutive laws and strain-displacement relations.

$$\left(\sigma_{jm,m}=0\right),\left(q_{m,m}=0\right),\left(\sigma_{jm}=C_{jmqr}\varepsilon_{qr}-\beta_{jm}T\right),\left(q_m=-\kappa_{mr}T_{,r}\right),\left(\varepsilon_{qr}=\frac{1}{2}\left(u_{q,r}+u_{r,q}\right)\right),\left(j,m=1-3\right)$$

The variables in the above equations have their usual meaning (refer [7] for further details).

The present study is however limited to two-dimensional plane strain thermo-elastic deformation analysis. The non-dimensionalized state vector and derived equations, for any layer of a multi-layered panel consisting of specially orthotropic materials, are given in Eqs. 1 - 3.

$$\xi=\frac{x}{L},\eta=\frac{z}{H},\lambda=\frac{H}{L},\ \left(u,w\right)=\left(\bar{u},\bar{w}\right)\left(T_0\alpha_0H\right),\ \left(\sigma_z,\tau_{xz}\right)=\left(\bar{\sigma}_\eta,\bar{\tau}_{\xi\eta}\right)\left(E_0\alpha_0T_0\right),\ \left(q\right)=\left(\bar{q}\right)\left(\frac{\alpha_0\kappa_0}{H}\right) \tag{1}$$

$$\bar{u}_{,\eta}=-\lambda\bar{w}_{,\xi}+\frac{E_0}{C_{55}}\bar{\tau}_{\xi\eta};\quad \bar{\sigma}_{\eta,\eta}=-\lambda\bar{\tau}_{\xi\eta,\xi};\quad \bar{T}_{,\eta}=\frac{-\alpha_0\kappa_0}{T_0\kappa_\eta}\bar{q}_\eta;\ \bar{q}_{\eta,\eta}=\frac{\kappa_\xi T_0\lambda^2}{\kappa_0\alpha_0}\bar{T}_{,\xi\xi};$$

$$\bar{w}_{,\eta}=-\frac{C_{13}\lambda}{C_{33}}\bar{u}_{,\xi}+\frac{E_0}{C_{33}}\bar{\sigma}_\eta+\frac{\beta_\eta}{C_{33}\alpha_0}\bar{T};\ \bar{\tau}_{\xi\eta,\eta}=\left(\frac{C_{13}^2}{C_{33}}-C_{11}\right)\frac{\lambda^2}{E_0}\bar{u}_{,\xi\xi}-\frac{C_{13}\lambda}{C_{33}}\bar{q}_{\eta,\xi}+\left(\beta_\xi-\frac{C_{13}}{C_{33}}\beta_\eta\right)\frac{\lambda}{E_0\alpha_0}\bar{T}_{,\xi} \tag{2}$$

$$\bar{\sigma}_\xi=\left(C_{11}-\frac{C_{13}^2}{C_{33}}\right)\frac{\lambda}{E_0}\bar{u}_{,\xi}+\frac{C_{13}}{C_{33}}\bar{q}_\eta-\left(\beta_\xi-\frac{C_{13}}{C_{33}}\beta_\eta\right)\frac{1}{E_0\alpha_0}\bar{T} \tag{3}$$

The in-plane and transverse coordinates in physical and normalized coordinate systems are denoted, respectively, by the variables (x, z) and (ξ,η). The displacements and stress variables with and without over-line, respectively, denote those in the normalized and physical coordinate systems. The variables E_0, T_0, α_0, κ_0 denote, respectively, the reference stiffness constant, temperature, coefficient of thermal expansion and thermal conductivity; whereas H, L are the total thickness and length of the panel.

Exact solutions are obtained for a panel with simply-supported edge boundary conditions ($SS: \bar{w}=0, \bar{\sigma}_{\xi}=0$) by expanding the state variables into a trigonometric series (Eq. 4), where '*c*' and '*s*' denote $\cos(m\pi\xi)$ and $\sin(m\pi\xi)$ respectively and satisfying both the governing state vector equations (Eq. 2) and SS edge boundary conditions and loads on lateral faces. On substituting the expanded state variables into the governing equation, a first order ordinary vector differential equation with constant coefficients is obtained for each layer of the panel (Eq. 5).

$$\left[\bar{u} \quad \bar{\sigma}_{\eta} \quad \bar{T} \quad \bar{q}_{\eta} \quad \bar{w} \quad \bar{\tau}_{\xi\eta}\right]^{T} = \sum_{m=1}^{\infty}\left[U_m c \quad Z_m s \quad T_m s \quad Q_m s \quad W_m s \quad R_m c\right] \tag{4}$$

$$\delta_{m,\eta} = [K]\delta_m, \quad \delta_m(\eta) = \left[U_m \quad Z_m \quad T_m \quad Q_m \quad W_m \quad R_m\right]^{T}, \quad [K] = \begin{bmatrix} [0] & [A] \\ [B] & [0] \end{bmatrix} \tag{5}$$

$$[A] = \begin{bmatrix} 0 & -\lambda m\pi & \dfrac{E_0}{C_{55}} \\ 0 & 0 & \lambda m\pi \\ -\dfrac{\alpha_0\kappa_0}{T_0\kappa_{\eta}} & 0 & 0 \end{bmatrix} \quad [B] = \begin{bmatrix} 0 & 0 & -\dfrac{\kappa_{\xi}T_0(\lambda m\pi)^2}{\kappa_0\alpha_0} \\ \dfrac{C_{13}}{C_{33}}(\lambda m\pi) & \dfrac{E_0}{C_{33}} & \dfrac{\beta_{\eta}}{C_{33}\alpha_0} \\ \left(C_{11}-\dfrac{C_{13}^2}{C_{33}}\right)\dfrac{(\lambda m\pi)^2}{E_0} & -\dfrac{C_{13}}{C_{33}}(\lambda m\pi) & \left(\beta_{\xi}-\dfrac{C_{13}}{C_{33}}\beta_{\eta}\right)\dfrac{\lambda m\pi}{E_0\alpha_0} \end{bmatrix}$$

The solution to Eq. 5 for any layer '*i*' of an '*n*' layered panel is given by Eq. 6; called the local transfer matrix relation for the i^{th} layer. Using these local transfer matrix relations and the interface continuity conditions between any two adjacent layers '*i*' and '*i*+1' (Eq. 7), the global transfer matrix for the entire panel (Eq. 8) can be obtained. Further, on relating the state vectors and load vectors at the top and bottom surface of the panel, the final set of algebraic equations to be solved can be obtained.

$$\delta_m^{(i)}(\eta) = \left[TM(\eta)\right]^{(i)}\delta_m^{(i)}(0), \left[TM(\eta)\right] = \exp\left([K]\eta\right), 0 \le \eta \le h^{(i)}; \delta_m^{(i)}\left(h^{(i)}\right) = \left[TM\left(h^{(i)}\right)\right]^{(i)}\delta_m^{(i)}(0) \tag{6}$$

$$\delta_m^{(i)}\left(h^{(i)}\right) = \delta_m^{(i+1)}(0) \tag{7}$$

$$\delta_m^{(n)}\left(h^{(n)}\right) = [TM]_G\,\delta_m^{(1)}(0), \quad [TM]_G = [TM]_n[TM]_{n-1}\ldots[TM]_1, \quad [TM]_i = \left[TM\left(h^{(i)}\right)\right]^{(i)} \tag{8}$$

3. RESULTS AND DISCUSSIONS

The alternate state vector formulation for two dimensional plane strain thermo-elastic deformation analysis of simply-supported panels is implemented in MATLAB®. Validation studies (Table 1) are conducted using analytical solutions obtained using Eshelby-Stroh formalism [7]. A very good match between the results is observed. The material and geometric parameters of the composite laminate, subjected only to a sinusoidal temperature increase of the form $T(x,H) = T_0\sin(\pi x/L)$ on the top surface, are as follows [7]:

$$\frac{L}{H}=5, \quad \frac{(C_{11})_0}{E_0}=1.0169, \quad \frac{(C_{13})_0}{E_0}=0.0339, \quad \frac{(C_{55})_0}{E_0}=0.05, \quad \frac{(C_{33})_0}{E_0}=\frac{(C_{11})_{90}}{E_0}=\frac{(C_{33})_{90}}{E_0}=0.1078$$

$$\frac{(C_{13})_{90}}{E_0}=0.0278, \quad \frac{(C_{55})_{90}}{E_0}=0.02, \quad \frac{(\beta_{\xi})_0}{\alpha_0E_0}=1.5051, \quad \frac{(\beta_{\eta})_0}{\alpha_0E_0}=\frac{(\beta_{\xi})_{90}}{\alpha_0E_0}=\frac{(\beta_{\eta})_{90}}{\alpha_0E_0}=1.0102, \quad \frac{(\kappa_{\xi})_0}{\alpha_0E_0}=100$$

$$\frac{(\kappa_{\eta})_0}{\alpha_0E_0}=\frac{(\kappa_{\xi})_{90}}{\alpha_0E_0}=\frac{(\kappa_{\eta})_{90}}{\alpha_0E_0}=1$$

After validation, the method is used for thermo-elastic analysis of a simply supported symmetric sandwich panel (L/H =5) made of aluminium face sheets (E = 70GPa, υ = 0.3 , α = 23x10^{-6}K^{-1}, κ =180 W/(mK), h_f/H =1/20) and a Divinycell H35 core (E=0.04GPa, υ = 0.3 , α =40x10^{-6}K^{-1}, κ =0.028W/(mK), h_c/H =18/20) under a sinusoidal temperature increase $T=T_0\sin(\pi x/L)$ on the top surface. The numerical results are given in Table 2, where the non-dimensionalized field variables at different locations are displayed. In Table 2, the variable 'x^*' denotes location in the x-coordinate at which the field variables are maximum (that is, x^*=0 for $\tilde{u}$, $\tilde{\tau}_{xz}$ and x^*=$L/2$ for others) and '$(.)^{(f)}$', '$(.)^{(c)}$'

denote the numerical values of in-plane normal stress, respectively, in the face sheet and the core at the top face sheet-core interface.

Table 1: Comparison of displacements and stresses (non-dimensionalized as in [7]) obtained using alternate state vector formulation (Present) and Eshelby-Stroh formalism (ESF [7]) at specific locations for a simply-supported 3-ply laminate.

Variables	Present	ESF [7]
$10\tilde{u}\left(L/4,H\right)$	-1.7428	-1.743
$\tilde{w}\left(L/2,H/2\right)$	0.4049	0.405
$10\tilde{\sigma}_{xx}\left(L/2,0\right)$	-4.0829	-4.083
$10\tilde{\sigma}_{xx}\left(L/2,0\right)$	-0.7945	-0.795
$100\tilde{\tau}_{xz}\left(L/4,H/2\right)$	0.1336	0.134
$1000\tilde{\sigma}_{zz}\left(L/2,H/2\right)$	0.2795	0.279

Table 2: Displacements and stresses at specific locations (non-dimensionalized as in [7]) of a simply-supported, symmetric sandwich panel with isotropic layers under a sinusoidal temperature increase at the top surface using present formulation.

Locations \ Variables	(10x) $\tilde{u}$	$\tilde{w}$	(10^2x) $\tilde{\sigma}_{xx}$	(10^4x) $\tilde{\tau}_{xz}$	(10^5x) $\tilde{\sigma}_{zz}$
$\left(x^*,\frac{19H}{20}\right)$	-1.854	0.376	-1.909[f] -0.029[c]	0.414	-0.401
$\left(x^*,\frac{H}{2}\right)$	-0.951	0.296	-0.013	-0.173	-0.633

4. CONCLUSIONS

An alternate state vector formulation was introduced for thermo-elastic analysis of multi-layered panels. The proposed procedure successfully predicted the two-dimensional thermo-elastic deformation response of simply-supported sandwich panels.

REFERENCES

[1] C. P. Wu et al., "A review on the three-dimensional analytical approaches of multilayered and functionally graded piezoelectric plates and shells", *Comput. Mater.Continua.*, 2008; 8: 93-132.

[2] L. Y. Bahar, "A state space approach to elasticity", *J. of Franklin Inst.*, 1975; 299(1): 33-41.

[3] F. Jiarang et al., "An exact solution for the statics and dynamics of laminated thick plates with orthotropic layers", *Int. J. of Solids and Struct.,* 1990; 26(5): 655-662.

[4] Z. Zhong et al., "Three-dimensional exact analysis of a simply supported functionally gradient piezoelectric plate", *Int. J. of Solids and Struct.,* 2003; 40(20): 5335-5352.

[5] A. Alibeigloo, "Exact solution for thermo-elastic response of functionally graded rectangular plates", *Comp. Struct.*, 2010; 92: 113-121.

[6] J. N. Reddy et al., "Three-dimensional thermomechanical deformations of functionally graded rectangular plates", *Eur. J. Mech. A – Solids*, 2001; 20: 841-855.

[7] S. S. Vel et al., "Generalized plane strain thermo-elastic deformation of laminated anisotropic thick plates", *Int. J. of Solids and Struct.*, 2001; 38(8): 1395-1441.

[8] A. Alibeigloo, "Three-dimensional thermo-elasticity solution of sandwich cylindrical panel with functionally graded core", *Comp. Struct*, 2014; 107: 458-468.

DOI: 10.5075/epfl-ICSS12-2018-50-51

A NOVEL SANDWICH COMPOSITE WITH GRADED LAYERED CORE PREDICTED BY EXTENDED COHESIVE DAMAGE MODEL

Surya Ghimire and Jiye Chen*
School of Civil Engineering and Surveying, University of Portsmouth
Portland Street, Portsmouth PO1 3AH, UK
*Corresponding author: Jiye.chen@port.ac.uk

1. INTRODUCTION

Graded sandwich composites have drawn extensive attention from academics and engineers in the composite society in the last twenty years. The graded sandwich composite consists of two fibre laminates on top and bottom respectively and the foam core between two laminates. In traditional sandwich structures, the core is single foam material with homogeneous property. This sandwich construction has two interfaces between core and the top and the bottom laminates respectively, in which there is a big gap between two different materials. This miss matched materials at interfaces may bring interfacial fractures e.g. delamination which leads sandwich structures losing loading capacity. In this investigation, the foam core is proposed to be graded material mimicked from bio-tube composites to have good behavior in failure mechanism. To achieve the best mechanical behaviour, understanding its detailed failure mechanism is essential. It is challenging to predict the multiple crack in the foam core because the core is multilayer graded and weak material comparing to top and bottom laminates. This paper presents a highly efficient approach in predicting multiple crack mechanism in graded sandwich composites using an extended cohesive damage model (ECDM). Examples given in this investigation show that the detailed failure mechanism of graded sandwich composites was studied well by the ECDM, and an excellent outcome was achieved through the modelling prediction, which shows the loading capacity of the proposed sandwich composite with graded multiplayer foam core is increased by 45% compared to traditional sandwich composites with single or normal foam core. This investigation also shows that the extended cohesive damage model is a highly efficient approach in predicting fracture behavior of sandwich composites.

2. THE FORMULATIONS OF THE ECDM

A brief description of the ECDM formulations is given in this section. Its detailed theory can be referred to the [1, 2]. The displacement approximation within a specified cracked element can be expressed by Eq. (1):

$$\begin{Bmatrix} u \\ v \end{Bmatrix} = \sum_{i=1}^{4} N_i(\xi,\eta) \begin{Bmatrix} u_i \\ v_i \end{Bmatrix} + \sum_{i=1}^{4} step_i(\xi,\eta) N_i(\xi,\eta) \begin{Bmatrix} u_i' \\ v_i' \end{Bmatrix} \tag{1}$$

In which u and v are the displacement along x axis and y axis in 2D domain, respectively. In Eq. 1 the **H** is standard Heaviside step function. Using the weak form of equilibrium equation from Bubnov-Galerkin method, the discrete form of equilibrium equation for static analysis can be written as shown in Eq. (2).

$$\begin{bmatrix} \mathbf{K}^{uu} & \mathbf{K}^{ua} \\ \mathbf{K}^{au} & \mathbf{K}^{aa} \end{bmatrix} \begin{bmatrix} \mathbf{u} \\ \mathbf{a} \end{bmatrix} = \begin{bmatrix} \mathbf{f}_{ext}^{u} \\ \mathbf{f}_{ext}^{a} \end{bmatrix} \tag{2}$$

Where, $\mathbf{K}^{uu}$ and $\mathbf{K}^{aa}$ are the stiffness matrices associated with the standard FE approximation and the enriched approximation, respectively; $\mathbf{K}^{ua}$ and $\mathbf{K}^{au}$ account for the coupling between the standard FE approximation and the enriched approximation; $\mathbf{f}_{ext}^{u}$ and $\mathbf{f}_{ext}^{a}$ are the equivalent nodal force vectors for standard FEM DoFs and enriched DoFs, respectively; **u** denotes the standard DoFs while **a** denotes the enriched DoFs. In a fully condensed equilibrium system, the additional enrichment term **a** is eliminated, thus the equilibrium equation with the standard FEM unknown quantities can be consequently obtained as shown in Eq. 3:

$$\left(\mathbf{K}^{uu} - \mathbf{K}^{ua}\left(\mathbf{K}^{aa}\right)^{-1}\mathbf{K}^{au}\right)\mathbf{u} = \mathbf{f}_{ext}^{u} - \mathbf{K}^{ua}\left(\mathbf{K}^{aa}\right)^{-1}\mathbf{f}_{coh} \tag{3}$$

Where, the internal nodal force vector $\mathbf{f}_{coh}$ due to cohesive traction on the crack surface $\mathbf{\Gamma}_{element}^{crack}$ can be expressed as:

$$\mathbf{f}_{coh} = \int_{\Gamma_{element}^{crack}} \mathbf{N}_{\mathrm{STD}}^{T}\mathbf{t}\,d\Gamma \tag{4}$$

in which **t** is the traction between the two crack surfaces within the specified failure element.

3. GRADED LAYERED SANDWICH COMPOSITES

Fig. 1(a) shows a cross section view of proposed novel sandwich panel. Its core is a graded layered foam material. The top and the bottom laminates are normal glass fibre laminates with $0^0/90^0$ lay-up. The basic foam material has Young's modulus 89MPs. The core was designed as a multilayered in terms of bio-mimicked construction [3]. Multilayered cases with 6, 12, 16, 18, 24, 48 layers in the core were investigated. The Yang's modulus at each layer is varied by either increased or decreased grade. At the two interfaces, the material gap was much reduced thus materials miss matched problem was mitigated.

The ECDM technique was used to investigate the fracture behavior of the graded layered sandwich panel. Fig. 1(b) shows a half model with shearing failure mode in the core predicted by the ECMD. The shearing failure started from the interface between the core and the bottom laminates then propagated toward the middle of the core. The shearing fracture initiated at the edge and moved to the centre of the panel. The failure responses can be seen from Fig. 1(c) in which 5 layered core cases are presented and compared to the case of normal core case. It can be seen from Fig. 1(c) that all graded layered core cases have higher loading capacity compared to the normal core case. It should be noted that the core with 6, 12 and 16 graded layers have a macro crack at the displacement of 0.5mm, while, the core with 24 and 48 layers have a micro crack at the same displacement, their corresponding macro crack occurs at the displacement of 0.7mm. Compared the loads at the macro crack state, the case with 48 graded layers increases loading capacity by 45% from the one of normal core case presented by dash line with label of "average" in Fig. 1(c).

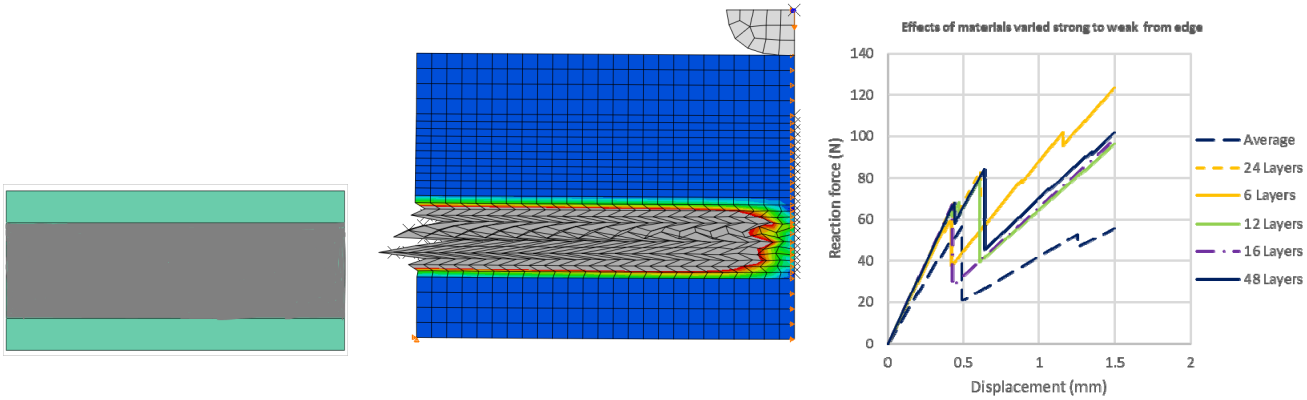

Fig. 1: (a) A cross section of the proposed sandwich panel with layered core from 6 to 48 layers; (b) shearing failure mode in core, grey color area is shear delamination; (c). failure responses.

4. CONCLUSIONS

The proposed sandwich composites with graded layered core was successfully investigated using the ECDM model. The investigation shows a very promising outcome in increasing loading capacity. In the future, this proposed sandwich panel can be manufactured using additive manufacture technology to conduct proposed graded layered core. This would be a cost-effective approach for the next generation of sandwich composites.

REFERENCES

[1] X Li and J Chen, "An extended cohesive damage model for simulating multicrack propagation in fibre composites", *Composite Structures*, 2016, 143, 1–8.

[2] J. Chen, "Predicting progressive delamination of stiffened fibre-composite panel and repaired sandwich panel by decohesion model", *Thermoplastic Composite Materials*, 2002, 15, 429 - 442.

[3] J Chen, "Improvement of damage resilience of composites", *Bio-Based Composites for High-Performance Materials: From Strategy to Industrial Application*, CRC press, Taylor and Francis Group, 2013, Chapter 11.

DOI: 10.5075/epfl-ICSS12-2018-52-54

THE INFLUENCE OF INHOMOGENEITY OF THE CORE MATERIAL ON THE BEHAVIOR OF THE SANDWICH PANEL

Monika Chuda-Kowalska[1] and Michal Malendowski[2]
[1]Institute of Structural Engineering, Poznan University of Technology, Poland. monika.chuda-kowalska@put.poznan.pl
[2]Institute of Structural Engineering, Poznan University of Technology, Poland. michal.malendowski@put.poznan.pl

1. INTRODUCTION

Polymer foams are widely used in various areas of engineering. In this paper sandwich panels, composed of thin metal sheets and a thick foam core, are considered. In the literature, it is possible to find many papers focused on sandwich structures, their applications, experimental tests or different approaches for modelling. The vast majority of them assume that the core consist of an isotropic, linear-elastic and homogenous foam [1-3]. Then, only two independent material parameters are needed to describe the material. Usually, they are the Young's modulus E and the shear modulus G. These parameters play significant role in a structural response. In fact, when the material has porous structure, like a polyurethane foam, the identification of mechanical properties is an intricate task [4]. The main problem is in their intrinsic anisotropy and non-homogeneity. Previous works concern the anisotropy of the core in sandwich panels [5-6]. Therefore, the aim of the present work is to extend this knowledge by studying the changeability of Young's modulus on the thickness of the sample and their influence on the wrinkling stress of sandwich panels. The impact of the size of geometric imperfections is discussed.

2. PROBLEM FORMULATION

Observing the sample during the tensile (or compression) test, changes in distribution of deformation on the thickness of the sample can be observed (Fig. 1). Intrinsically, it reflects the inhomogeneity of the material properties.

The aim of this work is to experimentally determine the variability of the Young's modulus on the thickness of the sample. Next, the impact of their variability on the load-bearing capacity of the sandwich panel will be studied. The analysis will be carried out for plates with various thicknesses and two different spans: L = 3.0 m and L = 5.0 m.

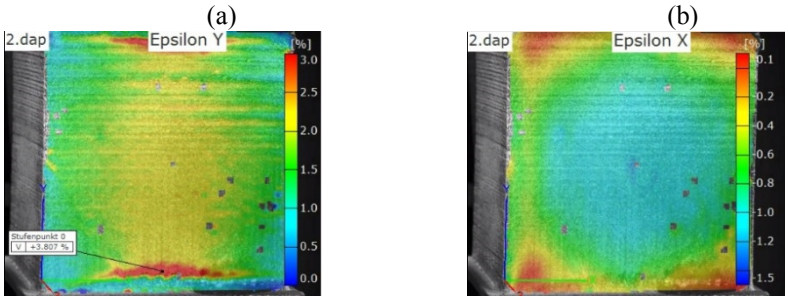

Fig. 1: Tension test (a) longitudinal strains, (b) transverse strains.

3. NUMERICAL MODEL

Finite element method models are created in Abaqus simulation software package [7]. The geometrically nonlinear static analysis is used. The problem is solved using Newton-Raphson procedures. Numerical instability is used as a failure criterion. Geometric imperfections are introduced as a combination of five buckling modes with the multiplier equal to 1 mm, 0.5 mm and 0.1 mm.

In this paper, steel faces are modelled using four node thin shell nonlinear finite elements, referred as S4, with the size of 2 x 2 cm. The core is modelled using eight node linear brick elements C3D8 (3D element) with the size of 2 x 2 x 2 cm. S4 and C3D8 elements with full integration in stiffness computation are used in order to avoid non-physical phenomenon like hourglassing. Additionally, these elements give more accurate results in stress field for deformed elements, especially, when wrinkling phenomenon occurs. The "tie" interaction has been used between the layers facing-core-facing, what correspond to constrained degrees of freedom of corresponding sheet and core nodes. The core is divided into the parallel regions to enable the possibility of assigning various materials to core's layers. Each region corresponds to the particular layer of finite elements on the core's thickness.

The panel is supported by two basing plates (b = 100 mm) modelled as rigid bodies. The right supporting basing plate is free to rotate with respect to Y axis, whereas the left basing plate differs only in that, it has the possibility to move in the X direction (Fig. 2). The contact interaction between supports and sandwich panel (lower sheet) is used, with the friction coefficient equal to 0.3 and no penetration allowed. The panel is loaded by uniform pressure q.

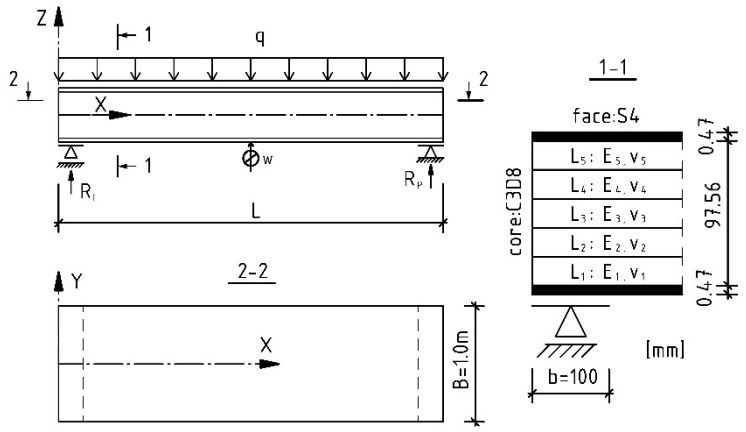

Fig. 2: Geometry and the scheme of simply-supported panel with layered core.

4. NUMERICAL SIMULATIONS

In numerical analyses, the steel facings are assumed flat and covered by zinc, what results in Young's modulus $E_F = 195$ GPa and Poisson's ratio $\nu_F = 0.3$. Moreover, the actual stress-strain relationship is introduced based on the laboratory test. In the tensile test, the obtained yield strength is equal to 360 MPa and the ultimate strength reached 436 MPa. These relationships are used for modelling of the elastic and plastic behavior of sheets. Foam material is assumed to be isotropic. The basic parameters are obtained from test performed in thickness direction of a sandwich panel. Young's modulus E_C and shear modulus G_C play crucial role if an isotropic material model is used for core modelling. These parameters are taken as: $E_C = 5.26$ MPa and $G_C = 3.0$ MPa [6].

The first example corresponds to the panel, which has non-layered core. So, the material parameters do not changes on the thickness. Panels with two different spans are analyzed: $L_1 = 3.0$ m and $L_2 = 5.0$ m. In the first step the influence of the size of imperfection is analyzed. Obtained results are shown in Fig. 3 and summarized in Table 1.

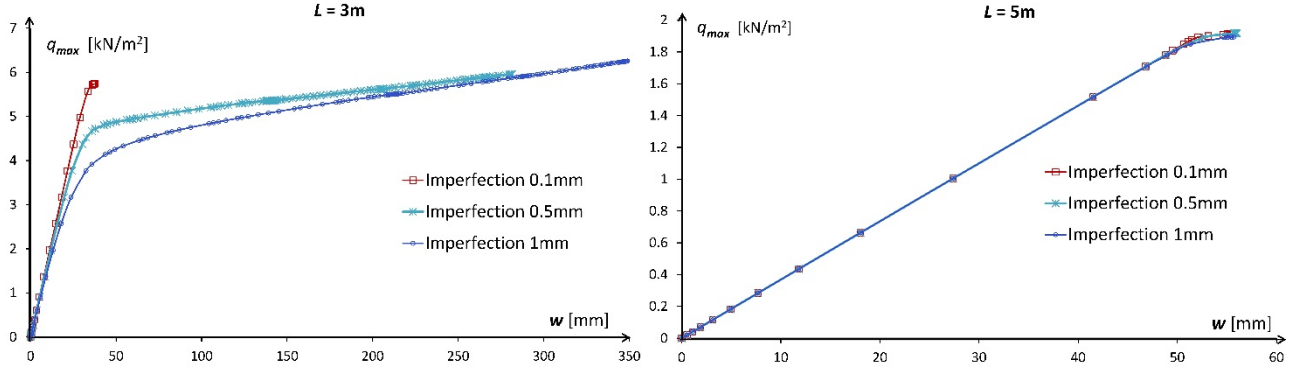

Fig. 3: The influence of the size of imperfections multiplier.

Table 1: Results.

Span	Imperfection [mm]	q_{max} [kN/m^2]	w [mm]	σ_x [MPa]
$L_1 = 3$m	0.1	5.74	37.58 / 35.40*	141.0 / 138.71*
	0.5	5.96	281.44 / 36.77*	199.2 / 143.92*
	1.0	6.25	348.93 / 38.55*	212.6 / 151.09*
$L_2 = 5$m	0.1	1.91	55.71 / 54.78*	126.5 / 128.48*
	0.5	1.92	56.07 / 54.86*	128.5 / 128.68*
	1.0	1.89	55.81 / 54.18*	127.5 / 127.07*

* Value obtained from analytical equation [3]

It is observed, the long panel, where the bending deflection dominated, is less affected by the size of imperfections multiplier. However, for shorter panels the size of imperfection has to be chosen very carefully. Further analyzes are carried out for panels with the span of 3 and 5 m and for imperfection 0.1 mm.

In the next step, the influence of Young's modulus variability on the load-bearing capacity of the sandwich panel is studied. Value of Young's modulus in each layer is changed in accordance with the rule given in the Table 2. For isotropic material model only two out of three parameters are independent. Hence, operating on the Young's modulus and shear

modulus changes the value of Poisson's ratio. So, the Poisson's ratios in individual layers are selected to remain G_C constant and equal 3.0 MPa.

Table 2: Adopted material parameters of the foam core.

Layer	Example 1	Example 2	Example 3	Example 4
	E_C [MPa]			
L_5	5.26	6.31	6.31	6.31
L_4	5.26	5.26	4.56	5.00
L_3	5.26	5.26	4.56	5.00
L_2	5.26	5.26	4.56	5.00
L_1	5.26	6.31	6.31	5.00
Average value	5.26	5.68	5.26	5.26

Obtained results are summarized in Table 3 and Fig. 4.

Table 3: Results.

	Example 1		Example 2		Example 3		Example 4	
	σ_x [MPa]	w [mm]	σ_x [MPa]	w [mm]	σ_x [MPa]	w [mm]	σ_x [MPa]	w [mm]
L = 3m	141.0	37.58	146.9	38.71	141.8	40.04	146.9	38.67
L = 5m	126.5	55.71	131.5	57.41	131.5	57.36	131.5	57.36

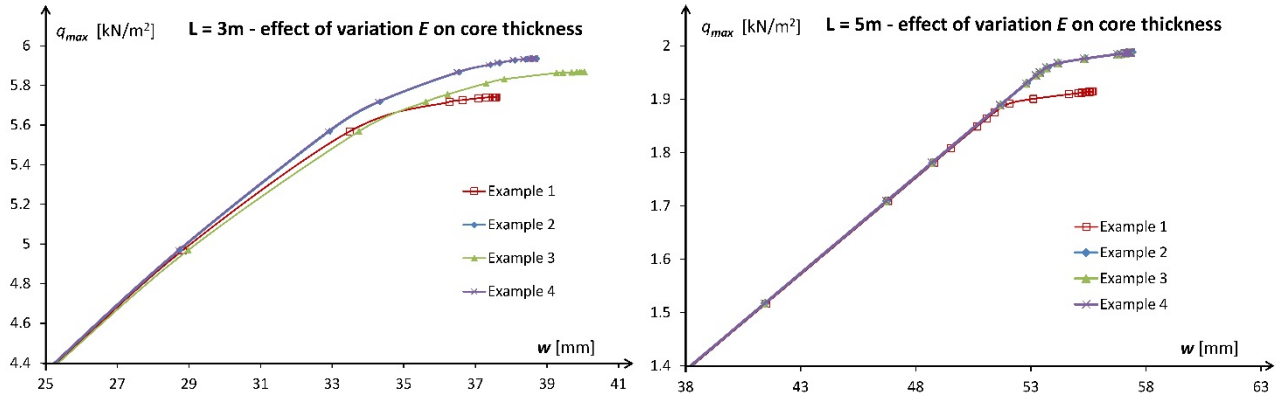

Fig. 4. The effect of E_C variation.

The load-displacement curves presented in Fig. 4 indicate that the Young's modulus of the layer situated directly under the compressed face is crucial for the structural behavior of the panel. It is observed, for longer panel the modification of E parameter in other layers are less influential.

5. FINAL REMARKS

Initial analyzes show that the change of the Young's modulus on the core thickness affects the behavior of the loaded sandwich panel. Considering this variability in the FE model contributes to a more accurate analysis of the sandwich panels. However, using nowadays methods, material parameters on the core's thickness can be experimentally determined. Hence, the next our step is to experimentally validate the model and use it to more comprehensive analyses. Obtained results will be presented during the conference.

REFERENCES

[1] R.F. Gibson, "A simplified analysis of deflections in shear deformable composite sandwich beams", *Journal of Sandwich structures & Materials,* 13(5), 2011, 579-588.
[2] R. Juntikka and S. Hallström, "Shear Characterization of Sandwich Core Materials Using Four-point Bending" *Journal of Sandwich structures & Materials,* Vol.9, 2007, 67-94.
[3] EN 14509 Self-supporting double skin metal faced insulating panels – Factory made products – Specifications.
[4] L. Gibson, and M. Ashby, *Cellular Solids. Structure and Properties*. Cambridge University Press, 1997, pp.510.
[5] M. Chuda-Kowalska and M. Urbaniak, "Orthotropic Parameters of PU Foam Used in Sandwich Panels", *Chapter IV in Continuous Media with Microstructure 2*, edited by B. Albers and M. Kuczma, Springer International Publishing, 2016, pp. 343-353.
[6] M. Chuda-Kowalska and M. Malendowski, "The influence of rectangular openings on the structural behaviour of sandwich panels with anisotropic core" *Journal of Applied Mathematics and Computational Mechanics*, Vol.15(3), 2016, 15-25.
[7] Dassault Systemes, Abaqus Documentation, 2014.

DOI: 10.5075/epfl-ICSS12-2018-55-58

ANALYSIS OF SANDWICH BEAMS WITH HOMOGENEOUS OR GRADED CORES UNDER FLEXURAL LOADING

Efstathios E. Theotokoglou[1] and Vasilios K. Mantzaroudis[2]
[1,2]Department of Mechanics – Laboratory of Testing and Materials, School of Applied Mathematical and Physical Science, National Technical University of Athens, Zografou Campus 15773, Athens, Greece
E-mail: stathis@central.ntua.gr, v.mantzaroudis@gmail.com

1. INTRODUCTION

Sandwich structures have been in the center of interest for several industries, such as the automotive, aerospace or marine ones during the last decades. Characteristics like their increased stiffness to weight ratio have made them eligible for a number of applications as substitutes of traditional structures, like metallic ones. Different kinds of sandwich structures exist, depending on the materials used to construct their skin panels and cores, the two components that they consist of. Common materials for the skin panels are metal alloys, carbon fiber reinforced polymers (CFRPs) or glass fiber reinforced polymers (GFRPs). On the other hand, a variety of materials is also used for the core construction, such as honeycombs, woods (e.g. Balsa core), polymers or foams [1-4]. An aspect of sandwich structures that has been attending interest is the effect that the technique of "gradation" has in their mechanical behavior under a variety of loads they are subjected to. This concept of gradation appeared in the work presented by Kaboglu et. al. [5] in the 20th International Conference on Composite Materials in Copenhagen. Their primary aim was to study the effect of changing the skin-core configuration on the mechanical response of the sandwich structures tested, which consisted of GFRP skin panels and PVC foam cores. More specifically, their interest focused on the sandwich structure behavior when different core configurations were used in three and four-point bending experiments. In the study of Kaboglu et al. [5] four core configurations were used : a) Core with a single layer of uniform density b) Core with three uniform density layers c) Graded core with three distinct layers in a high-low-high configuration d) Graded core with three distinct layers in a low-high-low configuration. For reasons of comparison, the mean densities of all the configurations were kept approximately the same. Using the technique of Digital Image Correlation (DIC), critical regions were identified and the effect of the core configuration was highlighted. Their results showed that the uniformity of core leads to higher load-bearing capabilities, but the graded core configurations provides a smoother failure process in regard with the uniform case. The importance of this result lays in the usefulness of the concept of gradation to ensure the achievement of a failure mode that is preferable according to the application where the sandwich structure is used.

2. PRESENT STUDY

Intention of this study is to perform a thorough investigation of the capabilities of the commercial Finite Element explicit code LS-DYNA [6], in the prediction of the mechanical response of the sandwich structures [7]. The challenging part of this investigation is the effort to combine the highly nonlinear behavior of the PVC foam cores in fundamental experiments such as uniaxial tension, uniaxial compression or shear, with the solution capabilities provided by LS-DYNA©. The lack of direct experimental results on the materials comprising the sandwich structures leads to another challenge. As the material models provided by the software need a non-negligible amount of experimental data, our effort is also focused on predicting experimental results based on engineering assumptions, analytical calculations, research conducted by others or data provided by the manufacturers in the literature. Furthermore, due to the fact that the experimental configuration is reproduced in the LS-DYNA© interface in a 3D manner, numerical aspects of the problem, such as the correct definition of the contacts between the different materials, add more interest to the whole project. In this study the behavior of the sandwich structures is being investigated under three-point bending loading.

3. GEOMETRIC FEATURES AND MATERIALS

Skin Panels

The GFRP skin panels of the sandwich structures comprise of Gurit XE603 +/-45 biaxial E-glass fiber reinforcement fabrics and a mixture of Prime 20 LV epoxy resin and slow hardener. They are stacked in a [0/90]/[-45/45]/[90/0] lay-up [5].

Foam Core

The PVC foam core used is AIREX C.70, a closed cell, cross-linked PVC foam. The specific products that are used are the C70.55, C70.75 and C70.90, which are designated as "low density" (60 kg/m^3), "middle density" (80 kg/m^3) and "high density" (100 kg/m^3) foam core for the present study. Properties for these cores were directly obtained from the manufacturer Airex Baltek Banova [5].

Core Configurations

The core configurations under consideration are presented in Table. 1.

Table 1: The core configurations examined in the study.

Configuration	[80]	[80/80/80]	[60/100/60]	[100/60/100]
Layup	6 layers of glass fiber ([0/90/-45/45/90/0] layup with epoxy matrix			
	80 kg/m^3 foam (15 mm thick)	80 kg/m^3 foam (5 mm thick)	60 kg/m^3 foam (5 mm thick)	100 kg/m^3 foam (5 mm thick)
		80 kg/m^3 foam (5 mm thick)	100 kg/m^3 foam (5 mm thick)	60 kg/m^3 foam (5 mm thick)
		80 kg/m^3 foam (5 mm thick)	60 kg/m^3 foam (5 mm thick)	100 kg/m^3 foam (5 mm thick)
	6 layers of glass fiber ([0/90/-45/45/90/0] layup with epoxy matrix			
Average core density (kg/m^3)	80	80	73	87

Three-point Bending Configuration

The geometric features of the specimens used for three-point bending experiments are presented in Table 2.

Table 2: Geometric features of the three-point bending experiments.

Specimen dimensions (L x W x T) (mm x mm x mm)	300 x 75 x 18
Span of cylindrical supports (mm)	200
Diameter of cylindrical supports and indentor (mm)	12
Velocity of the indentor (mm/min)	6

4. FINITE ELEMENT MODELING

Material Models

The material models examined in the LS-DYNA code [6] for their applicability are the following ones:

- MAT_COMPOSITE_DAMAGE (MAT 22) for the GFRP skin panels, which is a relatively simply defined material model for composite materials. Properties such as elastic moduli and fracture stresses in tension, compression and shear are required for its definition.
- MAT_HONEYCOMB (MAT 26) for the PVC foam core, which is a material model applying to honeycombs or anisotropic foams, like the C.70 ones. Its consideration of a zero Poisson ratio for the material is under investigation, as experiments show an elastic Poisson ratio >0.3 for the foams under investigation. Values of the elastic moduli are required for its definition, as well as stress-strain curves of uniaxial compression and shear experiments.
- MAT_TRANSVERSELY_ISOTROPIC_CRUSHABLE_FOAM (MAT 142) for the PVC foam core, which is a material model applying to anisotropic foams as an alternative to the honeycomb model mentioned above. The same input are required for its definition, and their only difference lies in the way the foam yield criterion is applied.
- MAT_RIGID (MAT 20) for the indentor and supports, which is the standard choice for parts that are practically non-deformable in the simulation.

It is noted that a third material model for the PVC foam core was examined, the MAT_CRUSHABLE_FOAM, which is an isotropic foam model, defined by elastic moduli and a single uniaxial compression stress-strain curve. This material model failed to sufficiently simulate the sandwich structures bending response, probably due to the fact of the important role that the shear stresses which play in these cases.

Element Type

The elements used are 3D hexahedral solids with reduced integration for computational efficiency for both the skin panels and the core. In the LS-DYNA environment [6], this option is characterized as “constant stress solid element”.

Three-point Bending Model

A graphic representation of the geometry of a typical Finite Element model for the problem (high-low-high foam configuration) is presented in Fig. 1. In this case, the total number of elements for the 3D model is 56700 (16200 for each skin panel and 24300 for the core). Other mesh densities were examined as well, in order to show the effect they have on the results, especially on the post-yielding region.

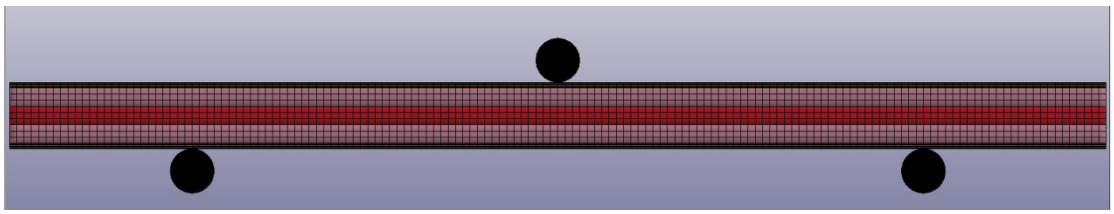

Fig. 1: Side view of the 3D model used for the three-point bending simulation of the high-low-high core configuration.

5. RESULTS

From our analysis the load-displacement curves extracted by the simulation are compared to the experimental ones. It is noted that in the work of Kaboglu et. al. [5] shear stress-displacement curves are given, which are transformed to load-displacement curves for direct comparison with the LS-DYNA results. For example, Fig. 2 shows the currently achieved correlation between the experimental and simulation results for the high-low-high core configuration, using the MAT_HONEYCOMB material. Linear results from another solver, the static of ANSYS© have been added for validity. The simulations have been performed for the first 20 mm of vertical displacement of the indentor, where no failure has appeared yet.

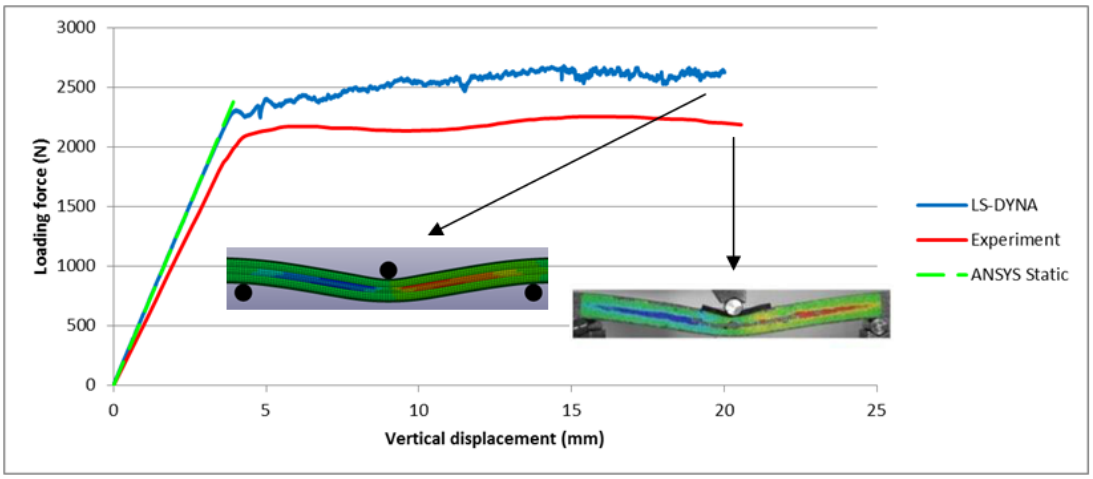

Fig. 2: Comparison of the load-displacement curves of the experiments and the simulations for the high-low-high core configuration. A linear curve from the static solver of ANSYS is included for comparison as well. The shapes of the beam at the 20 mm displacement are also added.

6. INVESTIGATIONS IN PROGRESS

As it was earlier stated, not all the desired results have been obtained yet. The two main directions in which our efforts are currently focused are the following ones:

- Modeling the catastrophic failure in the specimens under consideration. In the experimental procedure, catastrophic phenomena in either the skin (skin rupture) or the core (core shear cracking) were observed, based on the core configuration used. This process is simulated in LS-DYNA by using the MAT_ADD_EROSION option provided, which practically is a virtual tool to remove elements that fulfill a certain criterion. Such criteria are the maximum principal strain criterion, the maximum shear strain criterion, the maximum principal stress criterion etc. However, there is practically no straightforward way to determine which criterion is more preferable than others, as well as which value should be used as the critical one. Besides, and depending on the constitutive material model selected, the removal of elements may be highly dependent on the level of meshing used. Common practice in the literature is the calibration of the MAT_ADD_EROSION option according to the experimental results available [8, 9]. The failure criterion is selected by the catastrophic failure mode it produces, and the critical value is iteratively calibrated in order to "fit" the experimental results. This method is followed in the present work as well.
- After examining the level of applicability of the LS-DYNA material models under consideration, effort will be given in the extension of the simulations in a variety of specimens, by examining the effect that the core gradation combined with the specimen overall dimensions has in the bending response. However, the applicability of the MAT_ADD_EROSION option in this case is questionable. As it was stated above, it is a tool that is commonly calibrated according to experimental results available, and is difficult to be used "a priori" to accurately predict the catastrophic failure behavior. As a result, it is probable that the analysis will be limited to the prediction of the initial yield/failure phenomena and not the catastrophic ones.

REFERENCES

[1] H.G. Allen, *Analysis and Design of sandwich Panel,* Oxford: Pergamon Press, 1969.

[2] I. M. Daniel et. al. **"**Deformation and failure of composite sandwich structures", Journal *of Thermoplastic Composite Materials*, 2003,16, 345-364.

[3] A. Quispitura, et. al. "A debonded sandwich specimen under mixed mode bending", In Proceedings of the 8th International Conference of Sandwich Structures (ICSS8), A. J. M. Ferreira (Editor), Porto, Portugal, 2008, 186-198 .

[4] E.E. Theotokoglou et. al. "Crack kinking in sandwich structures under three point bending", *Theoretical and Applied Fracture Mechanics*, 2010*,* 53, 158-164.

[5] C. Kaboglu et. al., "Strain visualization of composite sandwich structures with core materials for wind turbine blades", *20th International Conference on Composite Materials:* Copenhagen, 19-24th July 2015, 225-236.

[6] Ansys/LS-Dyna, *Reference Manual*, Ansys, Inc. 2017.

[7] V. K. Mantzaroudis, "Analysis of sandwich beams under flexural loading" Master Thesis under preparation, Interdisciplinary Postgraduate Course of the National Technical University of Athens "Computational Mechanics – Solids Division", 2018, 1-100.

[8] A.G. Mamalis, "Finite element investigation of the influence of material properties on the crushing characteristics of in-plane loaded composite sandwich panels", *Thin-Walled Structures*, 2013, 63, 163-174

[9] R. Brooks et. al., "Predictive Modeling of the Impact Response of Thermoplastic Composite Sandwich Structures", *Journal of Sandwich Structures and Materials*, 2010, 12, 449-476

SESSION 3A: MODELING

DOI: 10.5075/epfl-ICSS12-2018-60-63

ELASTO-PLASTIC BENDING ANALYSIS OF SANDWICH TIMOSHENKO BEAM USING GENERALIZED DIFFERENTIAL QUADRATURE METHOD

Sattar Jedari Salami[1], Mahmoud Shakeri[2] and Mehrdad Movahedi[3]
[1] Department of Mechanical Engineering, Damavand Branch, Islamic Azad University, Damavand, Iran. sattar.salami@aut.ac.ir
[2] Department of Mechanical Engineering, Amirkabir University of Technology, Iran. shakeri@aut.ac.ir
[3]Department of Mechanical Engineering, Amirkabir University of Technology, Iran. Eng.movahedi@aut.ac.ir

1. INTRODUCTION

Sandwich construction has been a strong option whenever specific stiffness and/or strength has been an important design consideration. In 2003 an elastic–plastic stress analysis and the expansion of plastic zone in layers of stainless steel woven fiber- reinforced thermoplastic matrix composite laminated plates with square hole are carried out by using finite element method (FEM)[1]. Also, Nonlinear material response of a sandwich beam with bilinear elasto- plastic constitutive relations for the transverse normal and shear stresses of the core is studied in 2015 [2]. In the present project, flexural analysis of sandwich beam by considering the bilinear elasto-plastic behavior for axial normal stress of the sandwich beam in different boundary condition is studied. The governing equations according to first shear deformation theory (FSDT) for both face sheets and the core are obtained and generalized differential quadrature method (GDQ) has been used to solve them. Two types of boundary conditions are considered, simply supported and immovable clamped edges. In each type of boundary conditions, based on plastic modulus of bilinear material, expansion of plastic regions and axial normal stress have been investigated.

2. GOVERNING EQUATIONS

A sandwich beam of length (L) with a core of thickness (h_c), width of (b) and top and bottom face sheet thicknesses (h_l)is considered. Based on FSDT, the displacement components of face sheets and the core are described as follows:

$$u(bottom) = u_0 - \frac{h_c + h_L}{2}\psi_x \tag{1}$$

$$u(top) = u_0 + \frac{h_c + h_L}{2}\psi_x \tag{2}$$

$$w = w_0 \tag{3}$$

The stress–strain relations for the top and bottom face sheets based on linear elastic behavior can be defined as:

$$\sigma_x = Q_{11}\varepsilon_x \tag{4}$$

$$\tau_{xz} = Q_{55}\gamma_{xz} \tag{5}$$

$$Q_{11}^{(k)} = E_x^{(k)} \tag{6}$$

$$Q_{55}^{(k)} = G_{xz}^{(k)} \tag{7}$$

According to the displacement fields, the strains are derived [3]. The Ritz method is adopted to derive governing equations from total potential energy function of the sandwich beam. The total potential energy (Π) includes the strain energy (U) and the potential of external works (W) [4].

$$\Pi = U - W \tag{8}$$

$$U = \frac{1}{2}\int \left(\sigma_x\varepsilon_x + \tau_{xz}\gamma_{xz}\right)dv \tag{9}$$

$$W = \int_0^l q(x)w\,dx \tag{10}$$

Finally, by substituting Eqs. 4 -7 into Eqs. 9 and 10 and finally inserting into generalized Lagrange equations the governing equations of elastic analysis can be derived as follows [5]:

$$A_{11}\frac{\partial^2 u_0}{\partial x^2} = 0 \tag{11}$$

$$\frac{\partial}{\partial x}\left[D_{11}\frac{\partial \psi}{\partial x}\right] = KA_{55}\left(\psi + \frac{\partial w}{\partial x}\right) \tag{12}$$

$$\frac{\partial}{\partial x}\left[KA_{55}\left(\psi + \frac{\partial w}{\partial x}\right)\right] + q(x) = 0 \tag{13}$$

In elastic-plastic analysis by considering the bilinear material behaviour for the axial normal stress for the both face sheets and the core is:

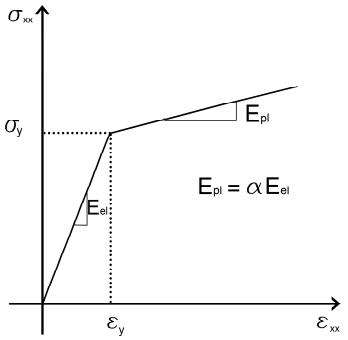

Fig. 1: A bilinear normal stress strain diagram.

$$\sigma_{xx}^{pl} = (signum(\sigma_{xx})\sigma_{xx}^{y} + E_{pl}(\varepsilon_{xx} - signum(\sigma_{xx})\frac{\sigma_{xx}^{y}}{E_{el}}) \tag{14}$$

Finally, the GDQ method is applied for solving Eqs. 7-9.

For normalization of boundary condition two type of boundary condition are considered herein.

a) simply support edge

$$w(x=0)=0, w(x=l)=0, u_0(x=0)=0, u_0(x=l)=0, M_x(x=0)=0, M_x(x=l)=0 \tag{15}$$

b) clamped edge

$$w(x=0)=0, w(x=l)=0, u_0(x=0)=0, u_0(x=l)=0, \psi(x=0)=0, \psi(x=l)=0 \tag{16}$$

3. RESULTS AND DISCUSSION

The geometrical characteristics of the studied beam are: length L =1000 mm, width b =20 mm and material properties of face sheet and core is according to Table 1.

Table 1: Material properties of face sheets and core.

part	MATERIAL	MECHANICAL PROPERTY	THICKNESS
core	foam	$E = 217Mpa, G = 76Mpa$ $\upsilon = 0.43, \sigma_{xx}^{y} = 3.9Mpa$	10 mm
face sheets	aluminum	$E = 70.15Gpa, G = 26.37Gpa$ $\upsilon = 0.33, \sigma_{xx}^{y} = 324Mpa$	2.5 mm

In order to validate the theoretical model comparison between elastic analysis, elasto-plastic theoretical analysis and elasto-plastic analysis using ABAQUS finite element software as shown in Fig.2. The sandwich beam is modelled as a 3D elasticity with the same loading and boundary conditions with present elasto- plastic modelling. At first, the three dimensional beam was modelled and then the face sheets and the core were separated with PARTITION comment in ABAQUS. As seen, the results are in good agreement for elastic and, elaso-plastic regions based on present analysis and ABAQUS one.

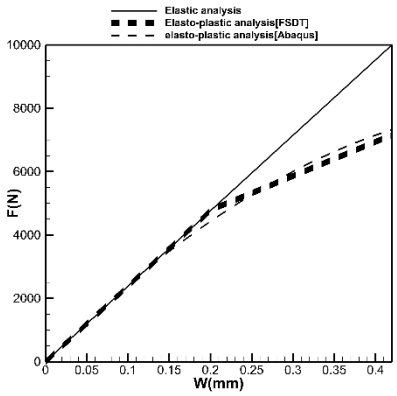

Fig. 2: A comparison of load–displacement response for simply supported sandwich beam.

For a case study, the distributed load q=100 N/m has been applied upper surface of the top face sheet.

Figs 3 -6 show the plastic regions and axial normal stress diagrams in the x- and y-plane for bilinear normal stress-strain behaviour in simply supported and clamped sandwich beams. At first, Eqs. 11- 13 are solved simultaneously and the plastic regions based on elastic solution, in which the axial normal stresses are beyond yielding stress, are obtained. According to iteration procedure, as the Eq. 14 is adopted for plastic regions, the resulted plastic regions from elastic analysis follow Eq. 14 and by inserting Eq. 14 into Eqs. 9 and 10 the solution procedure is modified. Thus, the resulted equations corresponding to elastic and plastic zones are solved simultaneously. Finally, after some iterations, the boundaries of exact elastic and plastic regions are obtained. Results show that, in clamped one, the plastic region initiate from edge of faces and expand in each iterate till convergence .On the other hand, for simply supported case, plastic region appear from center of faces and grows in all directions and after five iterations the size of plastic region is converged. Besides, as may be concluded, maximum elastic, plastic, and normal stress components belongs to the top and bottom surfaces for both boundary cases.

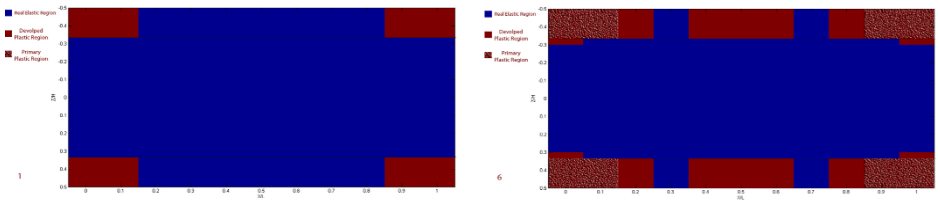

Fig. 3: Initiation and expansion of Plastic regions for clamped sandwich beam ($\alpha = \frac{E_{pl}}{E_{el}} = 0.1$).

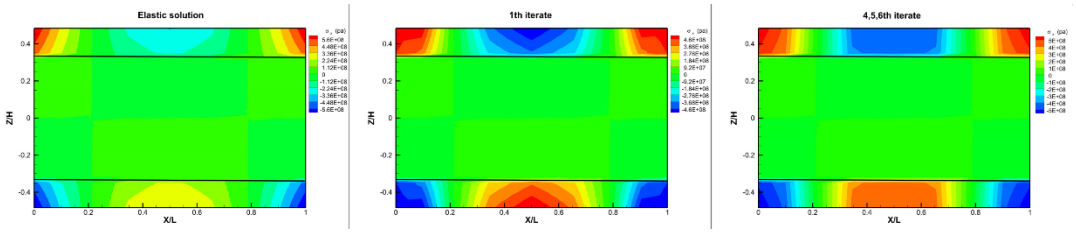

Fig. 4: Distribution of axial normal stress in elastic and plastic analyses for clamped sandwich beam ($\alpha = \frac{E_{pl}}{E_{el}} = 0.1$).

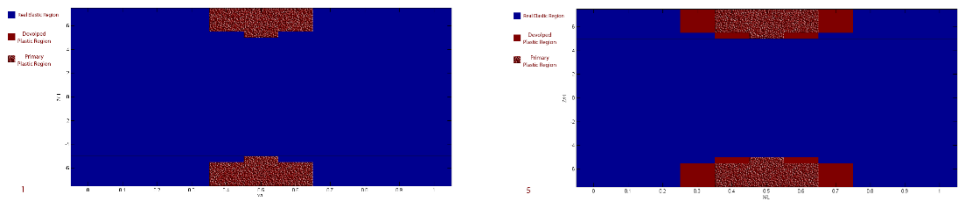

Fig. 5: Initiation and expansion of Plastic region for simply supported sandwich beam ($\alpha = \frac{E_{pl}}{E_{el}} = 0.1$).

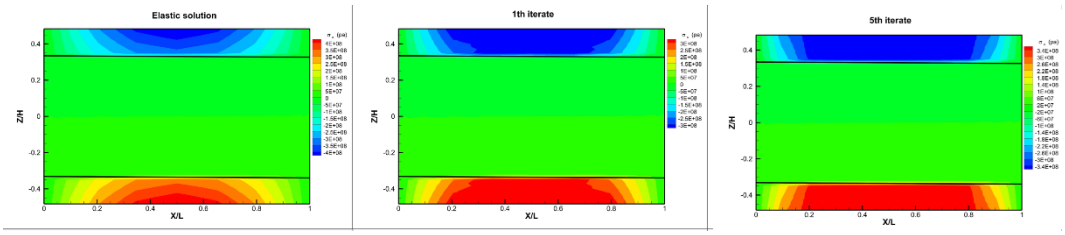

Fig. 6: Distribution of axial normal stress in elastic and plastic analyses for simply supported sandwich beam ($\alpha = \frac{E_{pl}}{E_{el}} = 0.1$).

4. CONCLUSION

The results show that with respect to plastic region and iterative process, the amounts of total deformation has absolutely increased and maximum amount of normal stress is reduced. Also plastic region is exceeding in comparison with elastic solution. Effect of boundary conditions indicate that by increasing the boundary constraint, global deformation are decreased while normal stresses are increased. The results can be concluded as below:

1. Based on bilinear normal stress- strain behavior for sandwich beam, after some iteration of analysis, plastic region expand in all directions.
2. The plastic regions initiate from the upper and lower surfaces of the face sheets. In other words, in the same level of axial strain for both face sheets and the core, axial normal stresses of the face sheets are so much larger than that created in the core due to the stiffness of the face sheets are several times of the stiffness of the core.
3. The highest plastic normal stress are obtained at the top and bottom surfaces for both boundary conditions.
4. The plastic regions expand away from the mid plane and the largest regions belong to the top and bottom surfaces.

REFERENCES

[1] N. Arslan et al., Elastic-plastic stress analysis and expansion of plastic zone in clamped and simply supported thermoplastic-matrix laminated plates with square hole, *Compos. Sci. Tech*., 2004; 64:1147-1166,.
[2] S. J. Salami et al., Improved high order analysis of sandwich beams by considering a bilinear elasto-plastic behavior of core: an analytical and experimental investigation, *Int. J. Mech. Sci*., 2015; 93, 270-289,.
[3] H.-T. Thai et al., A simple first-order shear deformation theory for laminated composite plates, *Compos. Struct.*, 2013; 106, 754-763.
[4] M. R. Eslami, Finite elements methods in mechanics: Springer, 2014.
[5] H. Altenbach et al., *Mechanics of composite structural elements*: Springer Science & Business Media, 2013.

DOI: 10.5075/epfl-ICSS12-2018-64-66

HOMOGENIZATION OF ISOLATED HONEYCOMB CORE AND SANDWICH BY FINITE ELEMENT ANALYSIS AND CLASSICAL LAMINATION THEORY

Mohammad Tauhiduzzaman[1] and Leif A. Carlsson[2]
[1]Florida Atlantic University, FL, USA. mtauhiduzzam2016@fau.edu
[2]Florida Atlantic University, FL, USA. carlsson@fau.edu

1. INTRODUCTION

Nomex honeycomb (HC) core is composed of Kevlar fiber paper impregnated by a phenolic resin organized in a periodic hexagonal cell structure. The macroscopic mechanical response of the HC core may be considered orthotropic or transversely isotropic with the principal directions, L, W and T. To simplify analysis of HC core sandwich, it is common practice to consider the honeycomb layer as an effective homogeneous solid that behaves as the actual HC core. This approach will by-pass the need for detailed structural analysis of the cell structure. Our main purpose of homogenization is to determine the effective in-plane extensional properties of the HC core. Such properties are essential for analysis of debonding failure. In homogenization analysis, the smallest representative part of the periodic honeycomb structure known as a unit cell is modeled. The main assumptions of homogenization are that the unit cell must be repetitive and small compared to the whole structure. A large number of studies have been performed to predict the effective mechanical properties of HC core. Gibson and Ashby [1] used beam analysis of HC core unit cells to determine equivalent in-plane and out-of-plane elastic properties. Malek et al. [2], and Masters and Evans [3] employed both analytical and numerical approaches to investigate the elastic behavior of periodic hexagonal honeycomb cores. Such studies have shown that isolated HC core has very large in-plane Poisson ratios. For a HC core bonded to two face sheets, it has been recognized that the in-plane deformation of the core is significantly constrained by face sheets [4-6]. This constraint causes an increase of the effective core stiffness compared to the unconstrained isolated core.

In this paper, homogenization analysis of isolated HC core and HC core bonded to face sheets is conducted using FEA. FE modeling of a representative volume element (RVE) is established. Extension of the analysis to HC core sandwich determines the interaction of core and face sheets.

2. GEOMETRY AND HOMOGENIZATION ANALYSIS

For a periodic structure like HC core, the smallest representative element is considered as the unit cell. In order to compare our results with previous analytical estimates [1], a single wall HC core is considered, see Fig. 1. The rectangular domain marked by dashed lines refers to the unit cell geometry. All cell walls have same wall thickness (h). Unit cell selection from the HC cores assembly results in eight wall blocks with two horizontal walls having half of the thickness (h/2).

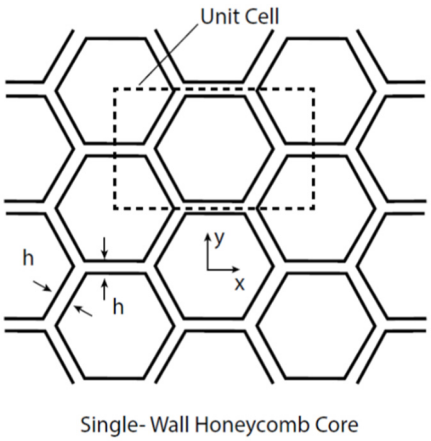

Fig. 1: HC core unit cell with single cell wall thickness.

Geometric models of isolated HC core and constrained HC core elements were created in FE program ANSYS v17.2 [7]. The HC core unit cell was modeled in both 2D and 3D, as shown in Fig. 2. All the corner angles are 120° and cell size is 4.80 mm. The height of the unit cell is 8.413 mm and the width is 4.852 mm (W- direction). The cell wall material is assumed to be isotropic with a Young's modulus (E) of 3.15 GPa and Poisson's ratio (v) 0.4. Projection of the 2D unit cell along the thickness (T) direction creates the 3D unit cell Fig. 2(b). The 3D unit cell is 12.7 mm in the thickness (T)

direction, see Fig. 2(b). The HC core sandwich elements consists of two $0.052\ mm$ thick aluminum face sheets attached the 3D unit cell of HC core (Fig. 3(a)). The face material has $E = 70\ GPa$ and $v = 0.3$.

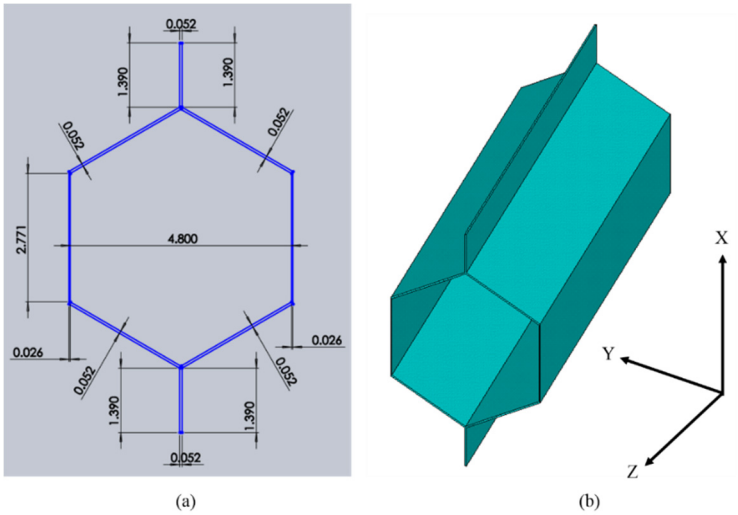

Fig. 2: HC unit cell representations (a) two-dimensional (2D) (b) three dimensional (3D).

The 2D unit cell, Fig. 2(a), was meshed with 8 node Plane 183 elements configured in plane stress. The 2D model was discretized into a total of 2615 elements and 9809 nodes. For the 3D unit cell model, Fig. 2b, 20-node Solid 186 elements with reduced integration were used. The 3D unit cell was discretized into 51054 solid elements and 282022 nodes. To determine the effective in-plane modulus and Poisson ratio (E and v) in the x and y directions, displacement and constraints were imposed on the unit cells to represent uniaxial extension in the x and y directions, while fulfilling compatibility requirements.

Homogenization concept was also applied to the sandwich elements, Fig. 3. The effective in-plane properties (E_x and v_{xy}) of the structural core element, Fig. 3(a), were determined by imposing a x- axis displacement of the nodes on top edges while the corresponding nodes on the bottom edge were constrained in the x direction. Coupling degrees of freedom of nodes located on the unloaded surfaces, consistent with uniaxial loading in the x-direction and compatibility with neighboring cells were defined. Finite element analysis of a sandwich element with homogenized core was also conducted.

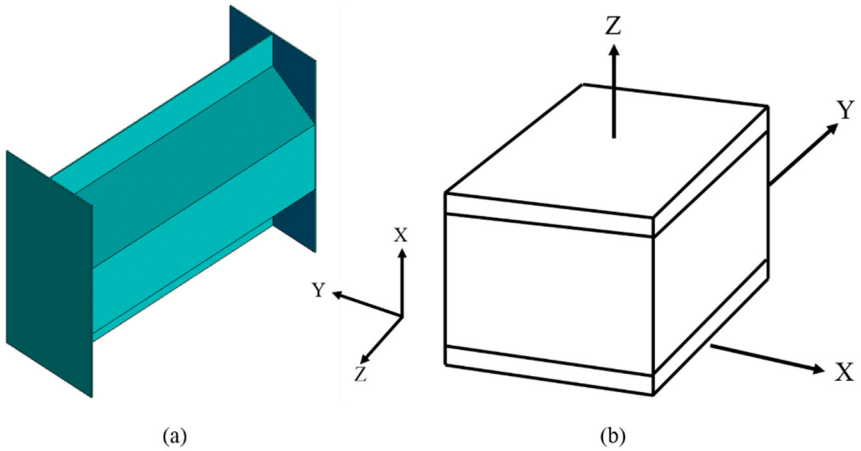

Fig. 3: HC core sandwich elements a) FE model, b) laminate model.

The sandwich element consisting of two face sheets and homogenized core was also modeled by classical laminated plate theory (CLPT) as a three layer symmetric laminate. Fig. 3(b) shows the sandwich element considered. Assumption of plane stress in each layer ($\sigma_z = 0$) and analysis of a load case representative for extensional loading along the x-axis enables derivations of closed-form expressions for the effective in-plane properties of the sandwich [8].

3. RESULTS

The isolated HC core and the sandwich element were analyzed using the material properties and geometry of the constituents defined above. The effective elastic constants determined for the 2D and 3D unit cells of the isolated core element are listed in Table 1 along with predictions from Gibson and Ashby [1].

Table 1: Homogenized elastic properties (E and ν) for HC core.

Type	2D Unit Cell		3D Unit Cell	
	Young's modulus (MPa)	Poisson's ratio	Young's modulus (MPa)	Poisson's ratio
FEA	$E_x = 0.048$	$\nu_{xy} = 1.0$	$E_x = 0.048$	$\nu_{xy} = 1.0$
	$E_y = 0.048$	$\nu_{yx} = 1.0$	$E_y = 0.056$	$\nu_{yx} = 1.0$
Gibson-Ashby [1]	$E_x = E_y = 0.048$	$\nu_{xy} = 1.0$		

It is observed that the results predicted by Gibson and Ashby [1] are in very good agreement with our 2D FEA results. The results from the 3D analysis of the HC core similarly show good agreement with Gibson and Ashby predictions and the 2D FEA results. The 3D analysis provides similar results as the 2D analysis. Based on the results, it is concluded that the homogenization analysis based on 2D finite element approach provides a reasonable prediction of homogenized in-plane extensional stiffness properties of HC core.

The HC core sandwich was first analyzed by FEA with the actual HC core structure and a solid core with the homogenized properties obtained from 3D analysis (Table 2). E_x and v_{xy} of the sandwich with orthotropic homogenized core was also determined by CLPT. Table 2 presents model results for the HC core sandwich. The results from all models are consistent.

Table 2: Effective properties of HC core sandwich.

Type	Young's modulus (MPa)	Poisson's ratio
HC Core Sandwich (FEA)	$E_x = 576$	$\nu_{xy} = 0.34$
	$E_y = 565$	($\nu_{yx} = 0.44$)
Homogenized Core Sandwich (FEA)	$E_x = 576$	$\nu_{xy} = 0.30$
CLPT	$E_x = 568$	$\nu_{xy} = 0.30$

Notice also the constraint imposed by the face sheets on the deformation of the core. The isolated core has Poisson ratio of 1.0, while the sandwich has Poisson ratio of about 0.3, similar to that of the face sheets.

ACKNOWLEDGEMENT

Support from NIA/FAA is gratefully appreciated. The NIA program manager, Dr. Ronald Krueger, and FAA program manager Dr. Zhi-Ming Chen provided also useful technical support. We also wish to thank Euro-Composites (Barry Millward) for donation of core materials.

REFERENCES

[1] L.J. Gibson et al., "The Mechanics of Honeycombs-Chapter 4", In *Cellular Solids Structure and Properties*, Pergamon Press: 1988.
[2] S. Malek et al., "Effective elastic properties of periodic hexagonal honeycombs", *Mechanics of Materials*, 2015; 91(226-240).
[3] I.G. Masters et al., "Models for the elastic deformation of honeycombs", *Composite structures*, 1996; 35(4): 403-422.
[4] W. Becker, "The in-plane stiffnesses of a honeycomb core including the thickness effect", *Archive of Applied Mechanics*, 1998; 68.5: 334-341.
[5] J. Hohe et al., "Effective stress-strain relations for two-dimensional cellular sandwich cores: Homogenization, material models, and properties", *Applied Mechanics Reviews*, 2002; 55(1):61-87.
[6] J. W. Sue et al., "Effect of sandwich configuration on behavior of honeycomb core. Journal of Sandwich Structures & Materials", 2008; 10(4): 311-329.
[7] ANSYS Mechanical user's guide, ANSYS, Inc., Southpointe, PA, 2015.
[8] L.A. Carlsson et al., "Experimental *characterization of advanced composite materials*", CRC Press, Boca Raton, FL, 2014.

DOI: 10.5075/epfl-ICSS12-2018-67-69

MODELING AND ASSESSMENT OF FOLDED THERMOPLASTIC HONEYCOMB CORE SANDWICH STRUCTURES USING A REPRESENTATIVE VOLUME ELEMENT

Marianne John[1], Matthias Petersilge[2], Anne Geyer[3], Ralf Schlimper[4] and Jochen Pflug[5]
[1]Fraunhofer Institute for Microstructure of Materials and Systems IMWS, Germany. marianne.john@imws.fraunhofer.de
[2]Fraunhofer Institute for Microstructure of Materials and Systems IMWS, Halle, Germany. matthias.petersilge@imws.fraunhofer.de
[3]Fraunhofer Institute for Microstructure of Materials and Systems IMWS, Halle, Germany. anne.geyer@imws.fraunhofer.de
[4]Fraunhofer Institute for Microstructure of Materials and Systems IMWS, Halle, Germany. ralf.schlimper@imws.fraunhofer.de
[5] ThermHex Waben GmbH, Halle, Germany. jochen.pflug@econcore.com

1. INTRODUCTION

To achieve the climate targets in transport industry a consistent implementation of lightweight construction is necessary. That's why the use of composites sandwich structures in automotive applications is increasing constantly due to their excellent specific mechanical properties and the resulting weight saving potential. Beside the ecological awareness, the economic effectiveness plays an important role for the choice of the most appropriate material. Sandwich structures with folded thermoplastic honeycomb cores and fiber-reinforced face sheets can be produced in an automated process with short cycle times [1, 2]. Furthermore the meltability of thermoplastics leads to further process relevant advantages like thermoformability and a high recyclability [3]. They are therefore of great interest to the automotive industry. EconCore (Leuven, Belgium) developed a novel and innovative semi-finished material combination which combines the advantages of a sandwich structure with the high specific mechanical properties of a thermoplastic FRP composite which enhances light weight potential and production effectiveness significantly [4].

These novel sandwich materials consisting of a folded Polypropylene (PP) honeycomb core and glass fiber reinforced PP face sheets were investigated in this study. A finite element model was built to simulate the mechanical performance and to validate correlation between mesoscopic honeycomb core structure and overall sandwich behavior. A Representative Volume Element (RVE) of the folded honeycomb core structure was defined in a Finite Element Model. The main objective was the determination of effective material properties for folded honeycomb core sandwich panels.

2. HONEYCOMB GEOMETRY AND PROPERTIES

The regular hexagons resulting in an optimal geometric arrangement of the honeycomb structure are inherently suited for saving material. In Fig. 1 is shown the geometry in principle on the left, the blue marked lines are the double walled surfaces, that are connected in the top and bottom region to the face sheets. On the right side in Fig. 1 is shown the cross section of the honeycomb structure, the L-direction is the stiffer and stronger direction along the double walls, across to them is defined the weaker W-direction. The red marked frame illustrates the selected region of the Representative Volume Element (RVE) for the Finite Element Model.

The folded PP- honeycomb core >THPP< is available form the company ThermHex Waben GmbH with different nominal densities, cell sizes and heights. In this work the densities of 60 kg/m^3 and 80 kg/m^3 THPP60 and THPP80 were investigated. They have nominal cell sizes of 8.0 mm or 9.6 mm and core heights of 10.0 mm and 20.0 mm. Some of these selected honeycomb cores and its mechanical properties are shown in Table 1. The material properties were determined by semi-analytical assumptions for honeycomb cores by Gibson and Ashby [5]. For the RVE model were assumed linear isotropic PP properties with an E-Modulus of 1800 MPa. The face sheets of two unidirectional sheets in 0° and 90° are made of glass fiber reinforced Polypropylene. The properties of the face sheet layers were measured by tensile testing, see Table 1.

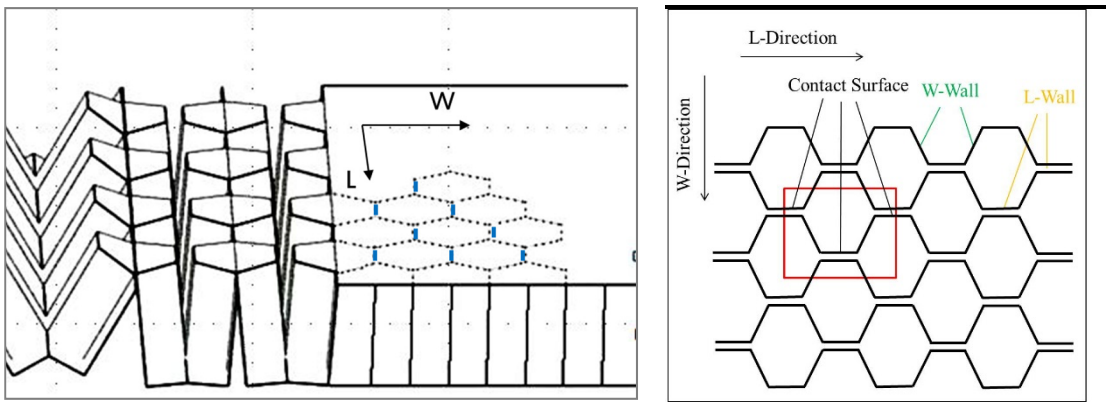

Fig. 1: Geometry of the honeycomb structure with double walls (blue lines left) and cross section of the honeycomb structure with region of RVE (red frame right).

Table 1: Properties of the sandwich components.

Sandwich Elements	E-Modulus [MPa]			Poisson ratio [-]			Shear Modulus [MPa]		
	E_1	E_2	E_3	ν_{12}	ν_{13}	ν_{23}	G_{12}	G_{13}	G_{23}
GFRP-PP face sheet	29˙233	3514	3514	0.33	0.005	0.005	3798	2000	2000
THPP60-10-8 –L	0.247	0.247	98.0	0.99	0.001	0.001	0.137	20.0	12.0
THPP60-10-8 –W								12.0	20.0
THPP80-20-9.6-L	0.583	0.583	130.4	0.99	0.002	0.002	0.320	26.1	16.9
THPP80-20-9.6-W								16.9	26.1

It has been found that the homogenized honeycomb properties are not suitable to estimate the global sandwich behavior in a FE model. That's why a simulation of the mesoscopic structure of the honeycomb core was made.

3. FINITE ELEMENTE MODEL

The overall objective was the determination of the effective material properties for honeycomb core sandwich panels as well as the components of the orthotropic stiffness matrix from 6 experiments (compression, shear, tension, bending) on the RVE model in comparison with experiment and global sandwich simulation.

The complexity of the geometry results from the continuous production process of the folded structure, see Fig. 2 on the left. This creates double walls at certain places as well as top-side caps one the honeycomb structure. The RVE can be arbitrarily laterally put together to expand larger models or provided laterally with periodic boundary conditions, see Fig. 2 on the right. The honeycomb walls as well as the top caps were modeled as shell elements. Between the double walled surfaces, there are defined contact elements in that region they are not glued together. At the face sheets they were assumed to be glued by hot press process during the face sheet application. The face sheets were assumed with linear elastic material properties and modeled as layered shell elements, too.

For the first steps the following load cases were regarded:

(1) Compression in the thickness direction

(2) Shear in W-direction.

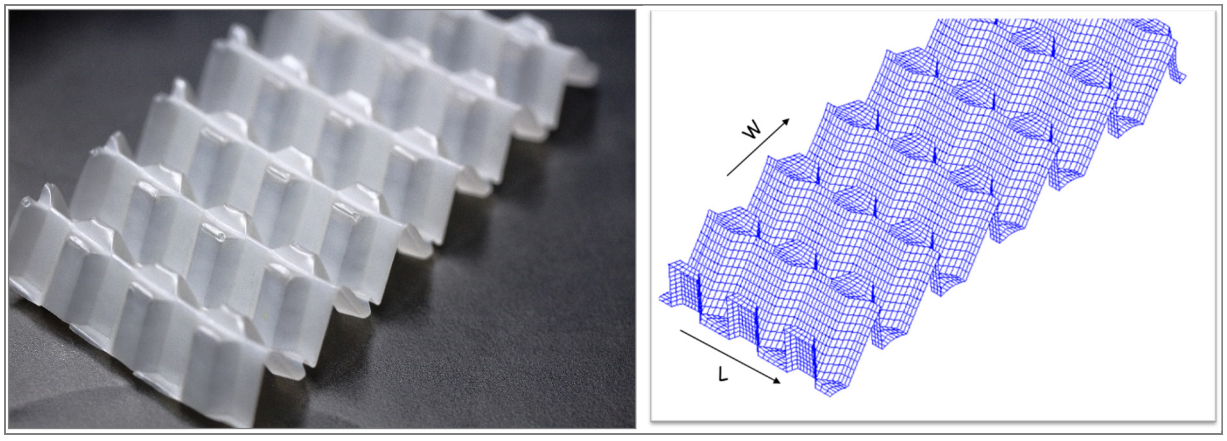

Fig. 2: Folded PP-Honeycomb core (left) and model mesh of 3x6 honeycomb elements without face sheets (right).

4. RESULTS

At first the general deformation behavior of the honeycomb structure was observed qualitatively. In Fig. 3 is shown the displacement of the honeycomb core in lateral direction at compression load of the whole sandwich structure in thickness direction, the core is plotted without top caps and face sheets. It is visible that the double walls of the honeycomb core buckles in s-shape formation.

In Fig. 4 is shown the deformation behavior in case of shear load of the sandwich structure in w-direction. The deformation behavior as well as the force-deflection performance from the simulation has to be compared to experimental results of compression and shear load tests. Depending on these results it has to be decided if a nonlinear material behavior of the PP material has to be implemented. Due to the fact that the folded honeycomb is produced by deep drawing of the PP material, it may happen that in certain areas deviating material properties occur within the PP honeycomb or varying

thicknesses could result in varying stiffness's. This has to be proofed for example by computer-tomographic analysis of the honeycomb structure. In addition, it will be investigated which influence the double walls have on the bonding behavior to the face sheet layers.

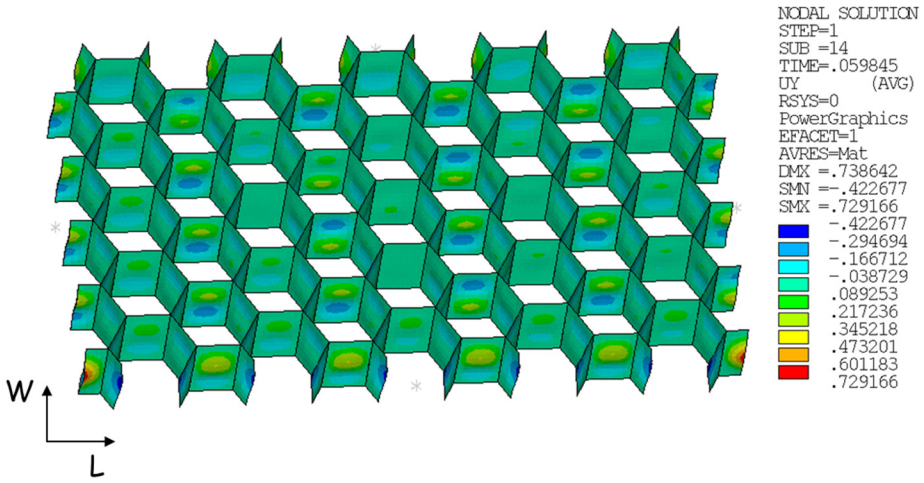

Fig. 3: Nodal Displacement of honeycomb core in lateral direction at out of plane compression load of the sandwich element.

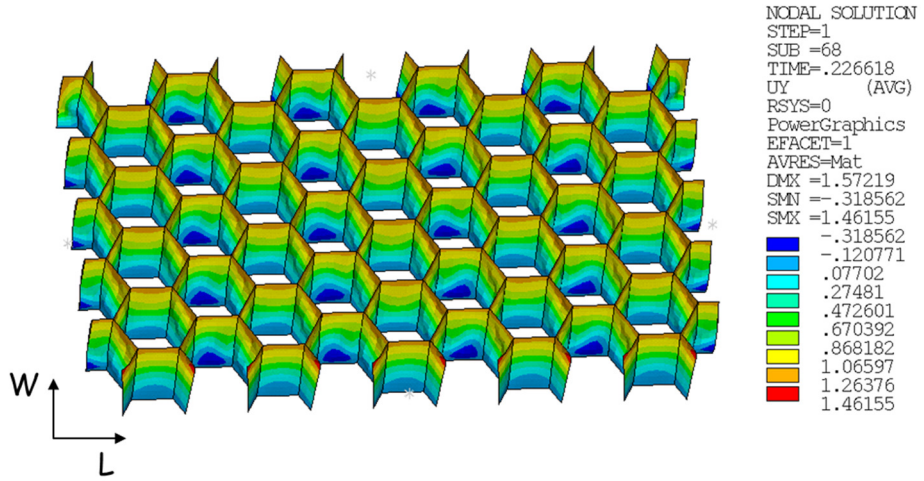

Fig. 4: Nodal displacement of honeycomb core in lateral direction at shear load in w-direction of the sandwich element.

ACKNOWLEDGEMENT

The authors wish to thank for the financial support for this research project which was funded by the EU in terms EFRE program via the "Investionsbank Sachsen-Anhalt" under grant no. 1604/00019.

REFERENCES

[1] M. Schuck, Kombination von Materialleichtbau mit konstruktivem Leichtbau, In: Lightweight Design 5, 2012, 2, 54–59
[2] J. Pflug, I. Verpoest, Sandwich Materials Selection Charts, Journal of Sandwich Structures and Materials 8, 2006, 5
[3] A. Geyer, Th. Gläßer, J. Pflug, R. Schlimper, M. Zscheyge, Mechanical Behavior of novel Organo-Sandwich Components for Lightweight Structures in automotive Applications, *ITHEC*, 2016
[4] G. Kopp, J. Kuppinger, H. E. Friedrich, Sandwich-Strukturen für den funktionsintegrierten Leichtbau. In: Lightweight Design 2, 2009, 3, 38-43
[5] L. Gibson, M. Ashby, Cellular Solids. *Cambridge University Press*, 1997

SESSION 3B: APPLICATIONS

DOI: 10.5075/epfl-ICSS12-2018-71-73

RESULTS OF THE PRELIMINARY TESTS CARRIED OUT ON THE PROTOTYPE OF A FRP COMPOSITE SHIPPING CONTAINER

Flavio Bono[1], Eugenio Gutiérrez[2], Pablo Sánchez Sierra[3] and Carlo Paulotto[4]
[1]European Commission - JRC, Italy. flavio.bono@ec.europa.eu
[2]European Commission - JRC, Belgium. eugenio.gutierrez@jrc.ec.europa.eu
[3]Acciona Costrucción S.A., Spain. pablo.sanchez.sierra@acciona.com
[4]Acciona Costrucción S.A., Spain. carlo.paulotto@acciona.com

1. INTRODUCTION

The use of shipping containers over the last five decades has radically changed world shipping. The latest figures from the World Shipping council report that in 2010 container traffic stood at approximately 110 million shipments, which would correspond to a throughput of the order of 380-400 million individual container movements: hundreds of millions of opportunities to either defraud customs, introduce illicit cargo, smuggle people, or breach security protocols.

Containers are now considered as a weak link in the supply chain with the potential to be exploited as a major security threat. Within this context, a number of national and international programmes and agreements have been drafted to limit the potential of intermodal containers for the transport of weapons ─or illegal substances─ that can be used to attack populations or public assets [1].

The ideal scenario for container shipping is one that continues to provide a fast, smooth-running, world supply chain whilst maximizing security. The combination of the structural manufacturing and design flexibility of advanced composites, allied to the wide variety of miniaturized sensor technologies opens up the possibility of developing structural components capable of providing more than one functionality in a manner that had, hitherto, not been possible. For example, it is possible of including antitamper diagnostics into the structure of the container by exploiting nonstructural physical properties of materials; for example, carbon fibre is an excellent conductor and therefore an ideal material for an antenna, which, if broken or damaged by malicious intrusion, will change its transmitting reception properties. In contrast, glass fibre is transparent to radar so that a panel made from hybrid (glass/carbon fibres) could provide a triple function both as a radar-transparent structural component fitted with an antenna [1].

2. DESCRIPTION OF THE PROTOTYPE OF THE FRP COMPOSITE SHIPPING CONTAINER

Shipping containers are required to carry noticeable load and are subject to severe forces during their lifetime. When containers are stacked in port terminals or on ships, they have to carry the load of several full containers, each capable of carrying up to 235 kN. Dynamical forces also occur during transportation due to the sea-faring conditions so that ensuring the structural stability of the containers is mandatory in order to avoid collapse and to ensure safety. Standard dry shipping containers are manufactured to comply with rigorous design codes such as [2] [3], but if we consider that containers are usually made from steel, the adoption of new materials leads to new challenges. The Joint Research Centre designed a nearly 100% FRP composite 1CC shipping container, with standard ISO corner blocks [4], glass fibre sandwich panels and carbon fibre tubes.

The container is assembled by bonding preformed sandwich panels onto a frame as seen in Fig. 1(a). The frame is made from pultruded carbon fibre tubes which are slotted and bonded onto steel tubes which, in turn are welded to the ISO corner blocks. The sandwich panels are made from medium density polyurethane (PUR) core with fibre reinforced composite skins. Panels have a wide top-hat cross-section and are dimensioned to fit and slot into the perimeter of the carbon fibre tubes. The panel dimensions differ because (a) the container has a non-square width-to-height ratio and (b) the fibre type, lay-up and orientation are selected to suit the type of service load specific to each panel (top, floor sides and back).

The frame, shown in Fig. 1(b), consists of twelve tubular-section pultrusions, comprised of eight short bars of approximately 2.5 m length and four bars of approximately 6 m. The container frame consists of 100x100x8 mm pultruded carbon fibre tubes. The tube lay–up is given as 0°, ±45° in proportions of 70 and 30 percent respectively, i.e. a predominantly 0° unidirectional lay-up for axial stresses and the ±45° fibres for radial confinement. The tubes have been cut to length in accordance with the ISO-specified container dimensions so that they press against the inner-facing surfaces of the connector blocks. The carbon fibre is a low modulus, high strength stitched mat. The resin system is an epoxy system specially formulated for pulling the carbon fibre tubes. The inner tolerances of the tubes are within 1 mm to accommodate the steel connectors, but leaving a small gap for the thixotropic adhesive interface. The data from tests on the pultruded material can be found in [5]. On the basis of the current lay-up, the axial modulus of the tubes is of the order of 110 GPa. The twelve pultruded sections are assembled by inserting a specially adapted standard container end-block fitted by a three-pronged tubular connection made in steel. Each block is fitted with an 80x80x8 mm tubular steel section of 120 mm length. The three end fitting are arranged orthogonally to fit into the hollow pultrusions in the vertical, longitudinal and cross-frame directions (Fig. 1(b)).

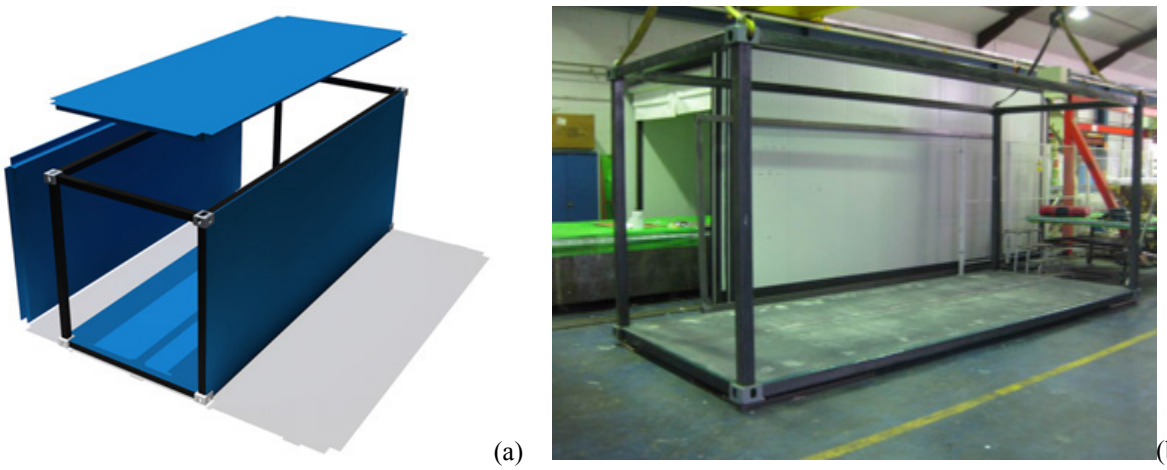

(a) (b)

Fig. 1: The modular design of the container panels (a); container frame (b).

Although the pultruded frame is expected to carry the main compressive loads, the container walls and, especially the floor are also subjected to considerable forces; for example, we can briefly point out that the floor will be subjected to loads of the order of 19 kN/m^2. The container walls are made up of modular sandwich panels. The philosophy is the same for all, with minor changes for skin and core dimensions and properties. The geometry consists of a flat panel with wing extensions adhesively bonded to the frame. The corner formed by the wing extension and the side of the panel is meant to fit onto the contiguous corner sides of the corresponding pultrusion beams and columns. The panel will therefore slot into place within the perimeter of each panel's corresponding frame. All but the floor sandwich panels are made with a nominal thickness of the glass-fibre skins of 5 mm. For all the panels the core consists of 80 kg/m^3 PUR. The fibre lay-up of each panel is based on preferential directions based on the certification's load requirements. In all cases the lay-up is balanced symmetric.

The panels are manufactured using vacuum-assisted resin infusion with the container frames used as a pattern, to try to achieve rectified angles and compatible tolerances required to fit each panel within its own frame. For the sides a fibre layout of ±45° is the preferred orientation in order to support the shear forces along with a minor amount of fibres in 0°/90° to provide some quasi-isotropic balancing. The front panel takes the same fibre lay-out. For the floor panel, the main fibre strength is required across the container in the 0° direction to support the major component of the plate stresses; to provide some quasi-isotropic properties. Additional transversal stiffeners composed of laminates of 2 layers of +/-45º glass fibre were added to the sides of each core.

3. TEST DESCRIPTION AND RESULTS

The scope of the test campaign was to verify the suitability of the container to undergo the type of tests required to obtain the Convention for Safe Container (CSC) certification. In the first instance it was decided to devise a test campaign with a view for a certification process consistent with a standard 8-high stacking and racking loads as well as a 117.7 kN payload.(for floor and side panels)

During the payload tests the container was positioned onto four load cells to acquire the variation of the total vertical force during the loading and unloading operations. Four 98.1 kN GS504 load cells were positioned in correspondence of the container's corner blocks. To measure the axial and bending strains on the door-front frame, strain gauges were mounted on the pultrusion columns and beams both at mid-span and at the corner sections. In addition to these, it was also decided to check the participation of the panel edges closest to the putrusion columns, where strain gauges were mounted on the panel at mid-point along the edge between the floor and side panels. To monitor the deflection of the panels during loading, the floor or the side panels, potentiometric displacement transducers (Gefran model PZ12-A-025) were placed between the floor and the composite sandwich panel. More details about the test instrumentation can be found in [5].

Floor Payload Test

A convenient way that simulates the type of load commonly carried by containers is to introduce the payload in the form of pallets. For this purpose it was decided to use standard 1m^3 tanks mounted on pallets (Fig. 2 right frame). Each tank, when fully loaded with water, weighs just over 9.81 kN and the dimensions are such that, given the internal dimensions of the container, a total of sixteen containers can be fitted on a grid of four-by-two and stacked two high; the total load is therefore just under 166.7 kN. This value although smaller than the 212 kN required by CSC for the 12 ton certification (i.e. 117.7 kN times 1.8 overload factor) was considered sufficiently high to obtain a good estimate of the serviceability performance and the overall strength of the container floor and load transfer to the corner blocks and side panels. The manner of loading was such that the water pallets were loaded progressively from the back first and from the lowest container first the set-up is that shown in Fig. 2 (left frame) .Whereas the rate of loading is limited by

the available water pressure and hoses (about 245 N /min), the discharge is somewhat faster as is flushed directly to the drainage system of the laboratory. In addition to the loading and unloading phases, the container was also monitored, fully loaded, over a 60-hour period during which it was possible to check for signs of creep and other phenomena. The container floor mid-point displacement was 2.5 mm for a total load 166.7 kN (Fig. 2 right). It is expected that the displacement for 117.7 x 1.8 kN rating load should not exceed 3mm and will therefore fall well within the limit established by CSC certification. Upon unloading the container returned to its original deformation status and had not suffered any damage either visually or from the recorded instrumentation signals. More details about the test can be found in [5].

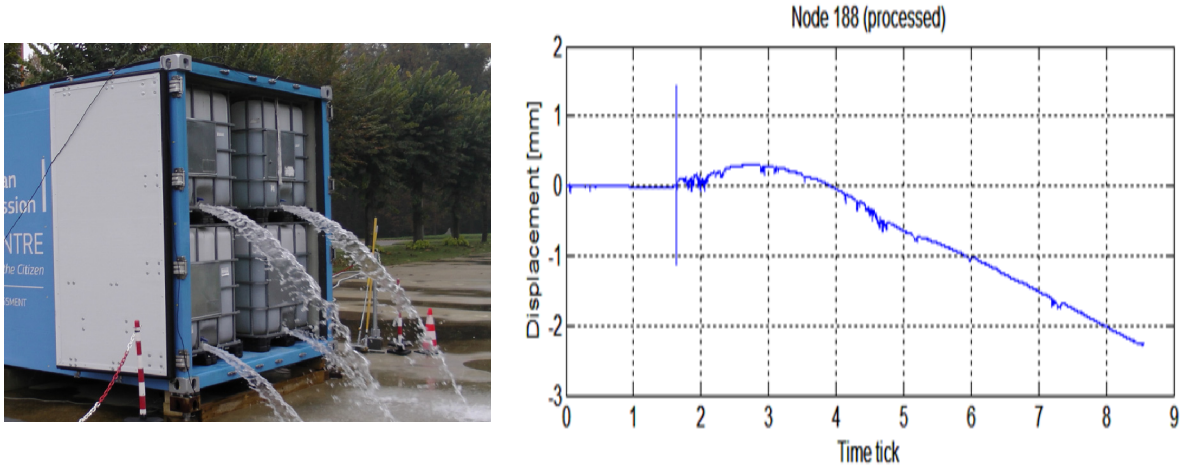

Fig. 2: Container floor loaded by water tanks (left); results of the floor payload test (right).

Vertical and Diagonal Load Tests

The verticals load bearing capacity is crucial whenever the container is positioned at the bottom of the stacking. Vertical loads can be as high as 848 kN per each corner post for nine high stacking of 24 t rated container. The prototype container was provided with a vertical tensioning system that connects the two opposite corner blocks, top and bottom, at the doors side. Tensioning loads are applied to the prototype container by means of hydraulic cylinders controlled with an oil pump. A vertical load of 250 kN per column was applied and the maximum measured strains were less than 600 με in correspondence of the base column. More details about the test can be found in [5].

Similarly to the previous test, a diagonal test was performed in order to verify the prototype's response to shear forces. The tensioning setup was places at the doors side (Fig. 3(a)) to induce a horizontal force component to the structure. Results are shown in Fig. 3(b). Only the first linear part can be considered valid, since the remaining part is affected by the uplifting of the bottom corner block opposite to the one which the hydraulic jack is connected to.

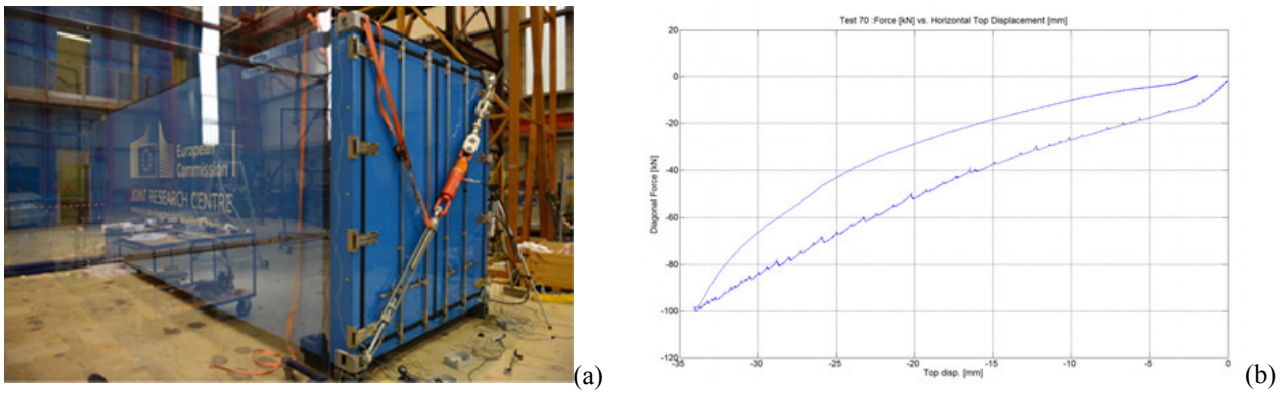

Fig. 3: Position of the hydraulic cylinder for the diagonal (racking) test (a); a typical result from a test up to 9.81kN (b).

REFERENCES

[1] E.Gutiérrez, W. van Heeswijk and D. Arrowsmith., *An overview of research programmes and prospective technology in the development of more secure supply chains: The Case of Shipping Containers*, European Commission: 2012, 32 pp.
[2] ISO, *International Standard ISO 1496 3, Series 1 freight containers. Specification and testing*, 1995.
[3] ISO, *International Standard ISO 668, Series 1 freight containers. Classification, dimensions and ratings*, 2013.
[4] ISO, *International Standard ISO 1161, Series 1 freight container. Corner fittings Specification*, 1984.
[5] F.Bono and E.Gutiérrez, *JRC Composite Container, Technical Documentation*, European Commission: 2017, 142 pp.

DOI: 10.5075/epfl-ICSS12-2018-74-76

APPLICATION OF CARBON FIBER REINFORCED POLYMER SANDWICH STRUCTURES IN MULTIAXIAL TESTING MACHINES

Eduard Relea[1,*], Ralph Kussmaul[2,*], Lukas Weiss[1], Markus Zogg[1], Paolo Ermanni[2]and Konrad Wegener[1,3]
[1]inspire AG, Switzerland. relea@inspire.ethz.ch
[2]ETH Zurich, CMASLab, Switzerland. kralph@ethz.ch
[3]ETH Zurich, Institute of Machine Tools and Manufacturing (IWF), Switzerland.

1. INTRODUCTION

Hardware-in-the-loop (HWIL) simulations of inertial navigation systems, gyroscopes and accelerometers commonly employ highly-dynamic multiaxial testing machines (MATMs). The development progress of the systems to be tested is driving the demand for better performing testing machines, achieving higher angular accelerations and velocities without precision and stability losses. Strict requirements for the eigenfrequencies have to be fulfilled, as the tests must not be influenced by the natural vibrations of the testing machine. So far, the moving machine axes are mostly shaped as aluminum or magnesium classic box beam designs. This article investigates the potential and challenges of the application of carbon fiber reinforced polymer (CFRP) sandwich structures for the moving structural parts of MATMs.

2. REFERENCE SYSTEM

The testing machine under study consisted of a steel base structure on which three aluminum cardanic axes were mounted as can be seen in Fig. 1(a). The outer and middle axes are hydraulically-driven, whereas the small inner axis is driven by an electric motor. In order to analyze the dynamics of the machine, a parameterized rigid body model was created and calibrated by experimental modal analysis data. A subsequent sensitivity analysis revealed the outer cardanic axis (OCA) to be the most influencing substructure for the lowest eigenfrequencies of the machine. As a consequence, the OCA was primarily targeted for the machine optimization that is presented in the following.

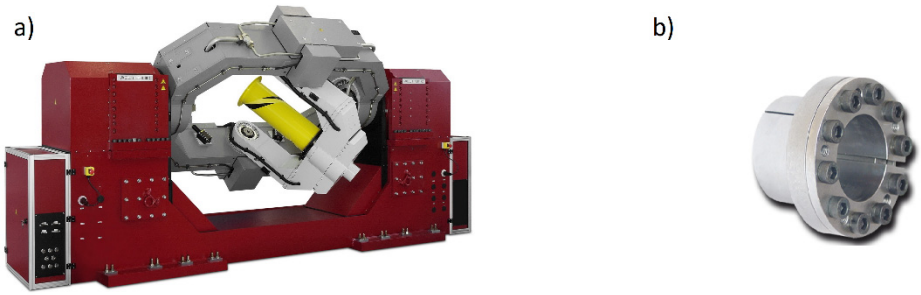

Fig. 1: (a) Reference aluminum testing machine, (b) Cone clamping element (Ringspann GmbH).

3. STRUCTURAL CONCEPT

The existing aluminum OCA design was not a convincing structural concept for a CFRP component. FRPs are typically processed in a mold-based manufacturing process. This allows for much higher freedom of design regarding geometrical complexity. According to [1], the introduction of curvatures into a structure leads to a significant increase of stiffness and buckling strength. The same was found for the reinforcement of free edges or the stiffening of large-area shells by ribs and stringers, as stated by [2]. Thus, by carrying out a systematic concept study, a structural model is presented, which exploits the geometrical potential of the FRP approach better than the reference design.

The first step included the development, analysis and assessment of design concepts of lightweight beams, shells and framework structures. After assessing these designs in terms of mechanical performance and expected manufacturing effort, curved sandwich shell concepts were identified as the most promising.

The second step aimed at investigating the effect of design parameters such as shell curvature and thickness, position and configuration of stiffeners, and material distribution. Thereafter, weaknesses in the design were systematically eliminated. As a final design, visible in Fig. 2(a), a double-curved sandwich shell was obtained, which offered a promising combination of high performance and reasonable manufacturing effort. The sandwich shell shape was based on an ellipsoid and flat surfaces were introduced at the flange areas to allow for the mounting of the motors. The shell structure was carried out as a sandwich with a foam core of 50 mm thickness. The stiffness was enhanced by introducing edge stiffeners. The foam runs out at the shell edge, as can be seen in the section view in Fig. 2(a). The face sheets followed a 90° bend to the inside of the shell and were joined to form a thick edge reinforcement of the shell.

[*] Both authors contributed equally to the work.

In a third step, laminate optimization of the CFRP sandwich shell structure was carried out. Optimization target was a maximum lowest eigenfrequency, while constraints on laminate thickness and the inertia of the structure were applied. After the optimization run, the element-wise optimal results were transferred to a producible layup solution. Local layups acting as reinforcements of critical areas of the sandwich were created, mainly the flanges and the edge stiffeners. The total thickness distribution after post-processing the optimization result is shown in Fig. 2(b).

As a result of the redesign of the outer cardanic axis of the MATM, a fundamental frequency of 139.1 Hz was measured for the optimized CFRP sandwich shell structure, whereas the aluminum reference structure showed a lowest eigenfrequency of 78.6 Hz. The frequency-to-inertia ratio of the system could be increased from 1.52 to 3.93 Hz/kg m^2 (+160%). A significant improvement of stiffness and margin of safety against structural failure of the structure could be guaranteed as well.

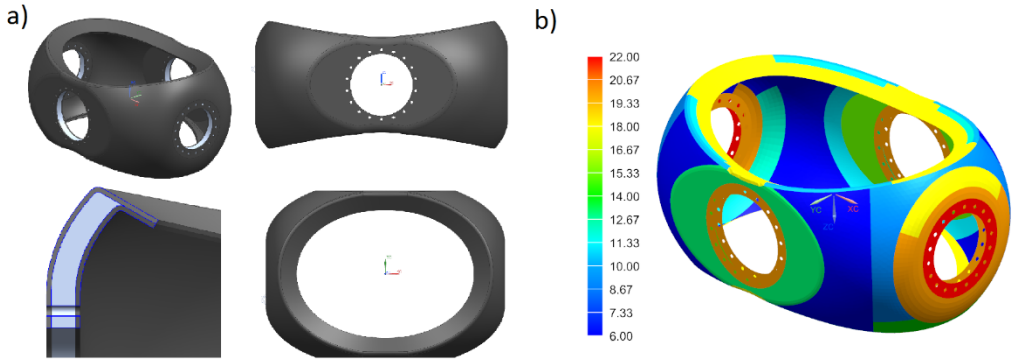

Fig. 2: (a) Double-curved CFRP sandwich structure for the outer cardanic axis, (b) laminate thickness of optimized sandwich shell structure [mm].

4. LOAD INTRODUCTION AND INSERTS DEVELOPMENT

The sandwich structure lacks inherently of precision in thickness, and its core is unable to bear large local pressures. Therefore, the load introduction in the CFRP tub lead to considerable difficulties. Flanges and cone clamping elements (Fig.1(b)) are the most common way of load introduction and transfer between elements. However, they are disadvantaged when a lower weight, adjustability and scalability are required, caused by their massive and specific design for each application. Hence, inserts have been developed to satisfy the need of more compact dimensions, lower mass and higher freedom of design [3]. Stiffness and strength can be easily adjusted by varying the type and number of the inserts. As the inserts were originally developed in the aerospace and automotive industry [4], the precision of the parts was an order of magnitude lower than required for precision machines, typically in the 10 µm range. Besides, as safety has priority in aerospace and automotive applications, the design of the original inserts followed a design for strength rather than for stiffness. These two main differences induced the development of a new insert type for precision machines, object of this chapter.

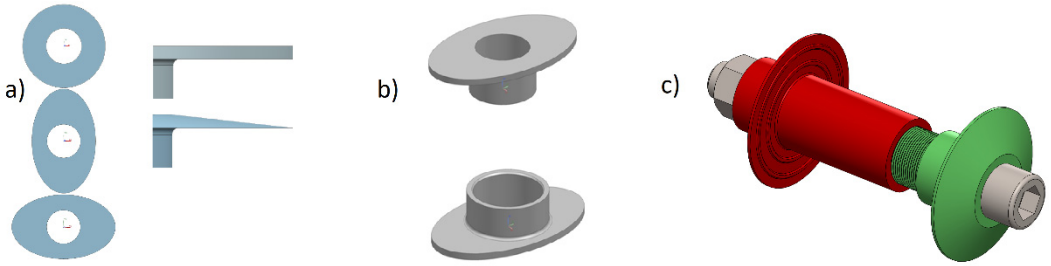

Fig. 3: (a) Design variation of the inserts, (b) Prototype inserts, (c) Prestressed stiffness optimized inserts.

The development of these new inserts was stiffness-driven with minimum strength requirements in the case of a 4 kN in-plane shear load case. The inserts are made of steel (42CrMo4) due to its high strength and stiffness, can be manufactured through an economic, automated turning process, and are of the through-the-thickness type. They consist of two pieces with concentric tubes and external flanges at both ends. The flanges distribute the load more evenly on the sandwich structure, thus preventing premature failure according to [5]. An increase of the loads with reduced stress concentrations is possible by implementing the geometry optimization of the inserts carried out by Shipsha et al [6].

Analytic considerations and FEM software allow for accurate and reliable stiffness calculations, whereas strength simulation is more complex and requires failure criteria and validation. Consequently, right from the beginning, it was fundamental to first of all guarantee the minimum strength requirement and understand how the different geometry variations influence the strength of the whole element. If the bonding fails, the whole solution would fail, causing the

optimization regarding stiffness to be useless. In this first phase, preliminary sandwich samples and prototype inserts were manufactured, and the most influential geometric parameters for strength were experimentally determined through pull-out testing. As depicted in Fig. 3(a), circular, oval parallel and oval perpendicular to the load case direction flanges were employed. Two thickness variations of the flanges were also tested: constant flange thickness and linear thickness variation. The pull-out results indicated that the flange thickness variation leads to a considerably better load (+25%) introduction in the structure. Oval shaped flanges showed just a minor advantage (7%). Thus, a circular shape was favored, due to advantages in manufacturing and assembly.

Following the minimum strength requirements, a stiffness optimization was carried out. In this second phase, the results from the previous study were applied to a parametrically designed insert, employing the Design Step SolidWorks algorithm. The inserts were developed with respect to high stiffness, low mass, scalability, adjustability, ease of manufacture, and cost effectiveness. A first addition to the prototype design includes a fine thread connecting the bolt prestressed tubes, as visible in Fig. 3(c). This ensures a precise axial compensation for the CFRP sandwich thickness variation, and predominantly protects the sandwich core from damaging. Other additions include millable overhangs for further axial compensation and improved mating with other components, as well as back spacers on flanges to guarantee an optimal bonding layer thickness with the CFRP sandwich.

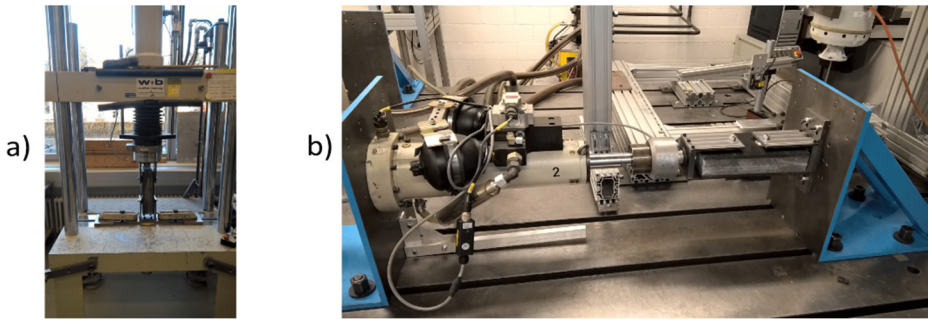

Fig. 4: (a) Static and (b) Fatigue testing in the hydropulser machine.

In the last development phase, static and dynamic characteristics of the stiffness-optimized through-the-thickness stainless steel inserts for CFRP sandwich structures with a foam core were investigated. A conclusive pull-out test with a load of 45 kN was passed in order to ensure the essential strength requirement (Fig. 4(a)). As shown in Fig. 4(b), fatigue tests at room temperature with a 2 Hz sinusoidal load were also successfully conducted in a hydropulser machine: the first round comprised of one million cycles with a +/-2.5 kN load, followed by another half a million cycles at +/-5 kN load.

ACKNOWLEDGEMENT

This work was supported by Acutronic Switzerland Ltd and the Swiss Commission for Technology and Innovation (CTI Project 15096.1 PFIW-IW).

Fig. 5: (a) CFRP MATM, (b) Newly developed inserts.

REFERENCES

[1] T. v. Karman, “The influence of curvature on the buckling characteristics of structures”. *J. Aer. Sci.*, 1940; 7(7):276–289.
[2] B. Klein, *Konstruktive Versteifungen: Leichtbau-Konstruktion*. Springer; 2011, p. 259–274.
[3] D. Zenkert, *The handbook of sandwich construction*, EMAS Publishing: 1997.
[4] ECSS – European Cooperation for Space Standardization, *Space Engineering Insert Design Handbook,* 2011.
[5] J.K. Byoung et al., “Characteristics of joining inserts for composite sandwich panels”, *Composite Structures*, 2008, 86:55–60.
[6] A. Shipsha et al., “Shape Optimisation of an Internal Metal Doubler for Load Introduction in Sandwich Structures”, *Sand. Const. 4: Fourth Int. Conf. on Sand. Constr.*: 1998, 839–51.

DOI: 10.5075/epfl-ICSS12-2018-77-79

CHARACTERISATION OF THERMOPLASTIC FOAM CORE MATERIALS FOR SANDWICH APPLICATIONS UNDER CRASH LOAD

Michael Schaeffer[1], Gerhard Kopp[2], Ralf Sturm[3] and Horst E. Friedrich[4]
[1]German Aerospace Center (DLR), Institute of Vehicle Concepts, Germany, michael.schaeffer@dlr.de
[2]German Aerospace Center (DLR), Institute of Vehicle Concepts, Germany, gerhard.kopp@dlr.de
[3]German Aerospace Center (DLR), Institute of Vehicle Concepts, Germany, ralf.sturm@dlr.de
[3]German Aerospace Center (DLR), Institute of Vehicle Concepts, Germany, horst.friedrich@dlr.de

1. ABSTRACT

Based on the requirements on the overall vehicle like driving dynamics, comfort, safety, ergonomics, costs, environmental safety and image the specific requirements on body-in-white components can be derivate. An important task of the material pre-selection is the mechanical properties and the structural requirements for each specific component. In the presented talk the developed method for material pre-selection is described for a firewall, which functions as a shear field. A firewall influences significantly the torsional stiffness of the body-in-white and as secondly protects the occupants during for all front crash load cases. Due to the main advantages of fiber reinforced thermoplastics, which have improved impact resistance compared to thermoset composites, a thermoplastic composite, consisting out of a PA6 skins and a homogeneous PA6 core is chosen as material.

In the presentation the characterization of the foam material and the subsequent development of the numerical description of PA6 sandwich core for dynamic loading conditions are shown.

2. INTRODUCTION

In the research project Next Generation Car (NGC) at the German Aerospace Center (DLR), three different novel vehicle concepts are being developed: Urban Modular Vehicle (UMV), Safe Light Regional Vehicle (SLRV) and Inter Urban Vehicle (IUV). The objective of this project is the cross-linking of different technologies, methods and tools for the holistic development of vehicles of the future in terms of vehicle design, vehicle structure, power and thermal management, vehicle intelligence and power train. The concept considered in this work is the Urban Modular Vehicle (Fig. 1) with a modular and multimaterial body-in-white.

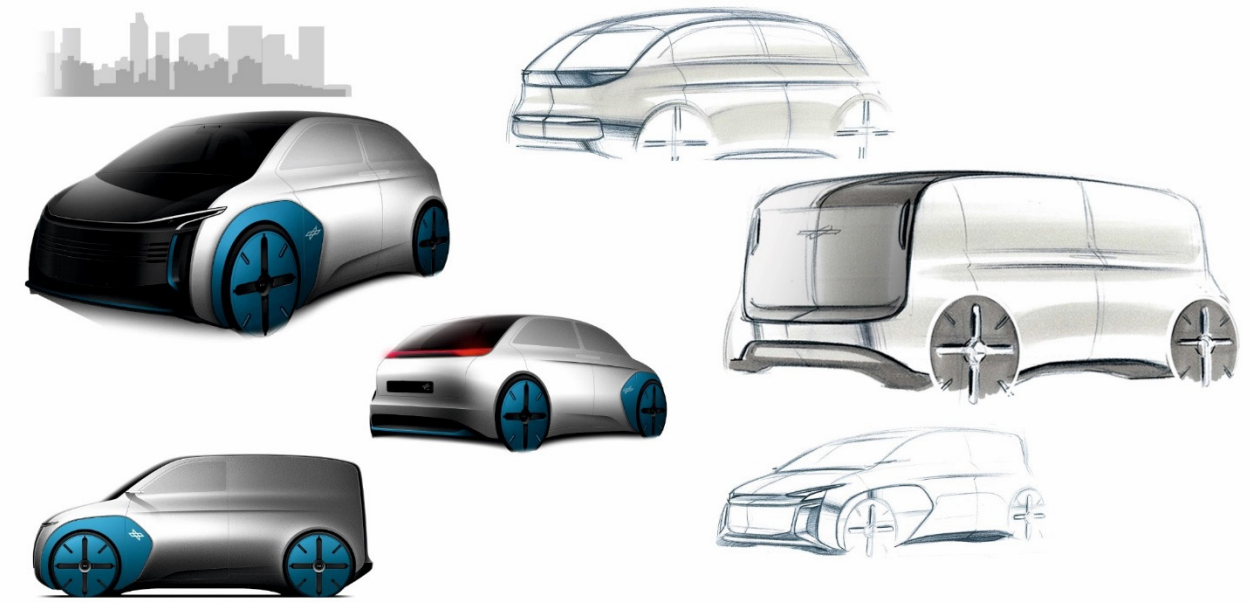

Fig. 1: Concept design of the Urban Modular Vehicle [1].

One starting point to reduce CO2 emissions is to reduce vehicle mass and related driving resistances by using lightweight construction methods and new material combinations and manufacturing technologies [2].

3. REQUIREMENTS FOR BODY-IN-WHITE PARTS UNDER CRASHLOAD

Based on the requirements on the overall vehicle like driving dynamics, comfort, safety, ergonomics, costs, environmental safety and image the specific requirements on body-in-white components can be derivate. An important issue of the pre-selection is the mechanical property objective (Fig. 2) of the specific component which will be investigated. The different body-in-white components can be divided into several groups. For example, a firewall is

especially a shear field. It influences the torsional stiffness of the body-in-white and as a second objective it has to have low intrusions to protect the occupants during a front crash load case.

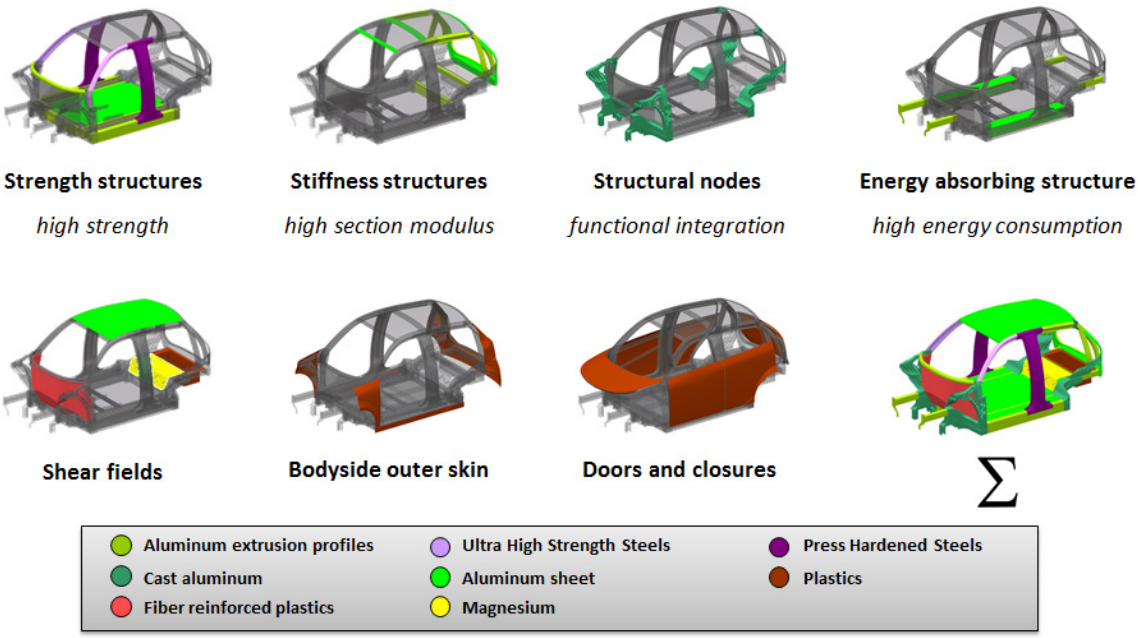

Fig. 2: Specific requirements of body-in-white components [3].

Taking into account the further requirements of the firewall (separation of front end and passenger compartment, low noise emissions, integration of attachment parts and etc.) the sandwich construction is preferred due to the offer of major potential for weight reduction, the possibility of the integration of different functions, high energy absorption capacity as well as the high thermal and acoustic isolation [4].

Due to the variety of core geometries and the materials available, there is a wide range of cores that can be used for sandwich structures.

In terms of geometric design, sandwich can be distinguished at the macroscopic level between homogeneous and structured cores. If they are further classified according to the degree of support / stabilization to the face sheets, they can be derived into five core geometries [2, 5-7]:

1. Cores with a homogeneous structure and therefore providing homogeneous support (e.g. balsa wood and various polymer foams)
2. Cores providing local support for the face sheets (e.g. textile and wire cores)
3. Cores providing partly local support (e.g. 'drilled out' foam and balsa cores, hump plates and hollow cone structures)
4. Cores providing unidirectional support (e.g. corrugated sheet, longitudinal bars or tubular structures)
5. Cores providing multidirectional support for the face sheets (e.g. core materials with a honeycombed structure)

Due to the major advantages of thermoplastics a thermoplastic PA6 composite with a homogeneous PA6 core and PA6 composite skin was selected for this application. The main advantages of thermoplastic resins are its less brittle which results in a higher toughness than thermosets and are improved impact resistance compared to thermoset composites [8].

Another advantage is that thermoplastic composites can be shaped easily after heating up. Using this technique complex three-dimensional shaped sandwich parts can be created [8].

4. CHARACTERISATION OF THE THERMOPLASTIC CORE MATERIAL

For the evaluation of the potential of possible sandwich structure three different PA6 core densities (35 kg/m³, 50 kg/m³ and 70 kg/m³) were characterized. The closed cell and cross-linked polyamide-6 foams were tested under the following test conditions:

- Compression test perpendicular to DIN EN ISO 604 [9]
- Dynamic compression test according to [10]
- Tensile test perpendicular to DIN EN ISO 1798 [11]

Some results of the tensile tests are shown in Fig. 3. The results indicate a significant influence of the specimen preparation procedure on the material behavior under tension loading. A further strain-rate dependent material behavior was identified under tensile loads.

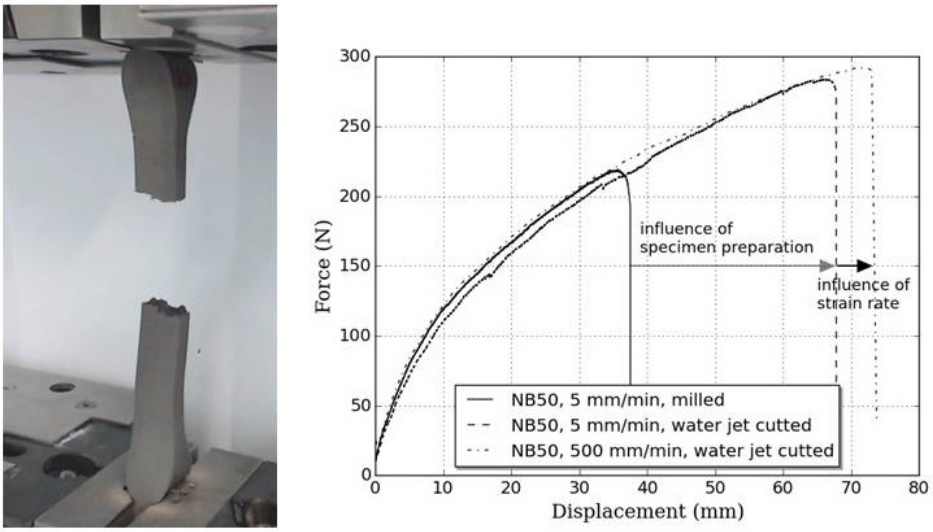

Fig. 3: Results of the tensile tests with influences of specimen preparation and strain rate.

5. SIMULATION OF THE MATERIAL BEHAVIOUR

For the simulation of the sandwich structure three virtual material descriptions have to be developed. Firstly, the facesheets made of fiber reinforced thermoplastics, secondly the thermoplastic foam core, which has a recoverable material behavior. And finally the interface between these two partners. The scope of this presentation is on the dynamic material behavior of the thermoplastic foam.

For the generation of the strain rate dependent foam material card the 4a impetus was used. This system enables the automatic mechanical characterization of dynamically loaded test specimens [10].

For the simulation a strain rate dependent hyperelastic material description was selected which is implemented in the nonlinear FEM Solver LS-DYNA from LSTC.

6. APPLICATION IN CRASH

For the evaluation of the potential of the thermoplastic sandwich structure under crash load a thermoplastic sandwich firewall will be virtually tested in a full vehicle crash simulation and finally compared with a currently build version made out of steel.

For the comparison the mass and the intrusions into the passenger compartment are considered. It is expected that the sandwich solution has less weight by similar mechanical performance. Due to the use of thermoplastics this solution is also suitable for a high-volume production.

ACKNOWLEDGEMENTS

The research leading to these results received funding from the Helmholtz Association of German Research Centres within the research topic Next Generation Car. The responsibility for the content of this publication lies with the authors.

REFERENCES

[1] Münster, et al: „Modulare Karosseriebauweise für ein Stadt-Elektrofahrzeug“, ATZ – Automobiltechnische Zeitschrift, Ausgabe 5/2017, Springer Fachmedien Wiesbaden.
[2] Ge. Kopp: „Auslegung und Dimensionierung von großflächigen polyurethanbasierten Sandwichbauteilen unter Berücksichtigung von konzeptionellen und fertigungstechnischen Einflüssen“, Universität Stuttgart (Germany), PhD-Thesis, 2015, DLR-Forschungsbericht. ISRN DLR-FB--2015-27.
[3] Schäffer, M., et al: „Projekt Next Generation Car“, Lightweight Design, Ausgabe 1/2017, Springer Fachmedien Wiesbaden.
[4] Knöchel, J.: MAI-Sandwich, MAI Carbon, Augsburg, Germany, 2017.
[5] Lutz, D.: „Anwendungen und Innovationen bei Kernwerkstoffen für den Leicht- und Sandwichbau“, Internationale AVK-Tagung, Stuttgart (Germany), 26. - 27. September 2011.
[6] Roth, M.: „Strukturelles Nähen: Ein Verfahren zur Armierung von Krafteinleitungen für Sandwich-Strukturen aus Faser-Kunststoff-Verbund“, TU Kaiserslautern (Germany), Dissertation, 2005.
[7] Friedrich, H. E., (Hrsg.), et al: „Leichtbau in der Fahrzeugtechnik“, Springer Vieweg und Salzgitter AG. 2013, ISBN 978-3-8348-1467-8, Kap. 7.3 Verbund und Sandwichlösungen, 519 – 538.
[8] Vogler, M.: “Anisotropic Material Models for Fiber Reinforced Polymers”, Leibniz Universität Hannover, Germany, PhD Thesis, 2015, ISSN 1862-4650.
[9] N., N.: DIN EN ISO 604,”Plastics - Determination of compressive properties”, 2003.
[10] Fertschej, A., et al: „Versagen von Thermoplasten Teil 1 – Charakterisierung, Versuche“, DYNAFORUM 2014, Bamberg, Germany, 2014.
[11] N., N: DIN EN ISO 1798, “Flexible cellular polymeric materials – Determination of tensile strength and elongation at break”, 2008.

SESSION 4A: ONR SPECIAL SESSION – DYNAMIC BEHAVIOR

DOI: 10.5075/epfl-ICSS12-2018-81-83

HYDROSTATIC IMPLOSION PHENOMENA IN SANDWICH COMPOSITE STRUCTURES

Shyamal Kishore[1] and Arun Shukla[2]
[1]Dynamic Photomechanics Laboratory, Department of Mechanical, Industrial and Systems Engineering, University of Rhode Island, USA, shyamal_kishore@uri.edu
[2]Dynamic Photomechanics Laboratory, Department of Mechanical, Industrial and Systems Engineering, University of Rhode Island, USA, shuklaa@uri.edu

1. INTRODUCTION

Composite sandwich structures have been of considerable interest for underwater applications. In general composite materials have high specific strength and stiffness, as well as very good corrosion resistance. Sandwich structures comprise of relatively low density material bonded between two face-sheets of higher strength or density. They offer several benefits in cases where buckling is the critical mode of failure. Underwater implosion phenomenon has been gaining recent attention especially for structures made of composite materials. Studies show that implosion of structures can release potentially dangerous high pressure pulse waves and can damage nearby structures [1]. Due to the improved buckling strength and low stiffness to weight ratio of composite structures they are ideal for underwater hydrostatic applications. It is hence imperative that the implosion behavior of these structures be well understood for such applications.

Some studies addressing this need have been performed, however they all have dwelled on the problem either analytically or numerically [2]–[5]. Additionally, though there has been some work on the shock initiated implosion of underwater cylinders, there is still no experimental work that investigates implosion of composite sandwich structures [6]–[9]. Recently, DeNardo et al. [10], carried out hydrostatic and shock initiated implosion experimental studies on double-hull composite structures. However, the authors considered only the case where the composite facesheets were not bonded to the foam core. The strength of the structure and the mechanics of its collapse can be altered by the inclusion of adhesive bonding between the layers of the sandwich. This study aims to address this knowledge gap experimentally by carrying out hydrostatic implosion experiments of sandwich structures made out of concentric carbon-epoxy cylinders with adhesively bonded light-weight closed cell PVC foam cores of different densities.

2. EXPERIMENTAL DETAILS

All the specimens in this study use filament-wound carbon-fiber/epoxy cylinders for their inner and outer facesheets, and are manufactured by Rock West Composites (West Jordan, UT). Both the inner and outer cylinders have a general purpose [±15/0/±45/±15] layup, with a 1.7 mm wall thickness. The outer cylinder has a 60.4 mm ID and the inner cylinder a 38.6 mm ID. In hydrostatically-initiated implosion experiments, the specimens have a 279-mm unsupported length, which encourages a mode 3 collapse and gives more foam core crushing. The outer cylinder has a random, black-and-white speckle pattern for DIC. The PVC foam cores used in the specimens are from the closed-cell Divinycell H series of foams, as produced and provided by DIAB, Inc. (DeSoto, TX). Foam cores are bonded to composite cylinders using a two part epoxy supplied by Loctite, and achieve 24.13 MPa strength after 24 hours of curing time. The adhesive is applied between the inner surface of the outer tube and the outer surface of the foam core and between the outer surface of the inner cylinder and inner surface of the foam core (see Fig. 1). The weight changes due to the application of epoxy in the assembly were recorded.

All implosion experiments are conducted in a 2.13m diameter spherical pressure vessel with a maximum pressure rating of 6.89MPa designed to provide constant hydrostatic pressure throughout the collapse event (see Fig. 2). Several Plexiglass windows mounted about the midspan of the pressure vessel allow the specimens to be viewed by cameras and adequately lit by two high-powered lights. The specimens are sealed using two aluminum end caps and suspended horizontally in the center of the pressure vessel. To measure the changes in local pressure during the collapse event, several high-pressure blast transducers (PCB 138A05, PCB Piezotronics, Inc., Depew, NY) are mounted at different locations about the specimen both axially and circumferentially (see Fig. 1). The vessel is then flooded with filtered water, leaving a small air pocket at the top. Once the vessel is filled, nitrogen gas is introduced into the air pocket to pressurize the enclosed water. The pressure inside the vessel is increased at a gradual rate until the specimen collapses.

Two digital high-speed cameras (Photron SA1, Photron USA, Inc.) are mounted normal to the viewports outside the tank and at an angle of 17° from one another. These are used to record stereoscopic images of the collapse event at frequencies on the order of 40,000 frames per second, and the images are later analyzed using 3-D DIC software (VIC 3D 2012, Correlated Solutions Inc.) to determine full field displacements across the outer surface of the specimen.

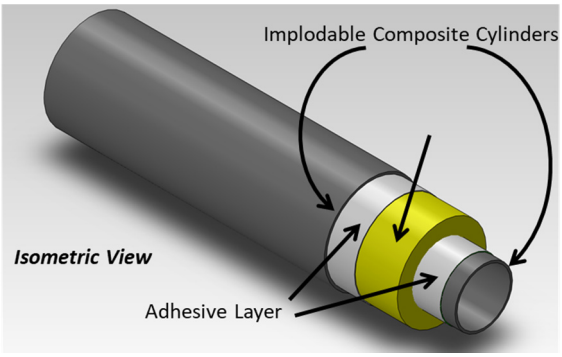

Fig. 1: Schematic of the Sandwich Composite Structure geometry.

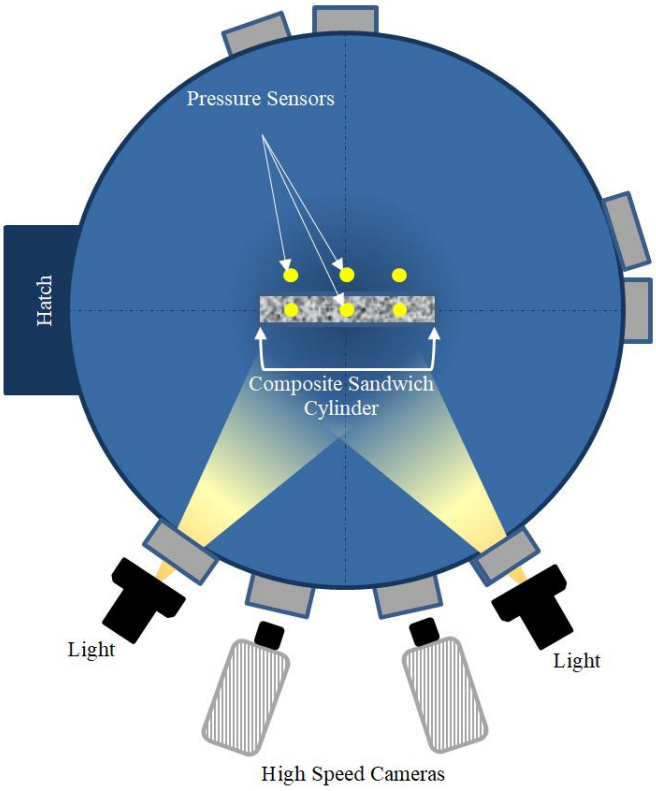

Fig. 2: Experimental facility.

3. RESULTS AND CONCLUSIONS

Experiments have been performed with increasing core foam densities. The outer and the inner tubes collapsed in all cases of the experiments performed. A typical experiment is shown in Fig. 3, showing the progressive stages of collapse of a sandwich structure with H35 foam filled core. Adding the adhesive bonding significantly increased the collapse pressures of the sandwich structures, as in the case of H35 foam filled core, where the collapse pressure was increased by 22% when compared with the case of H35 foam filled double hull structure reported by DeNardo et al [10]. Similarly, in the case of H60 foam filled core, the same comparison showed a 48% increase. As the foam density was increased the collapse pressures increased non-linearly and the improvement to the buckling strength performance was greater for the cases of higher foam densities.

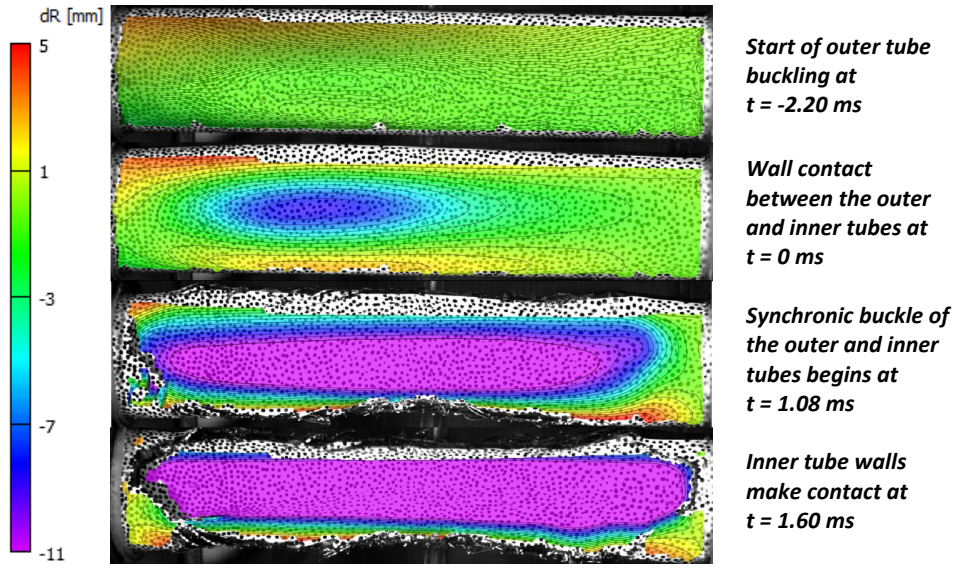

Fig. 3: dR contours (showing change in radial location of a point) of collapse of H35 foam filled Sandwich Composite Structure.

In all of cases, the outer tube as well as the inner tube collapsed in mode 3. DeNardo et al [10], reported that in cases where the inner tube imploded, they always did in mode 2. Due to the significant increase in the buckling strength there was also much greater energy in the primary collapse, i.e., collapse of the outer tube, which affected the stability of the inner tube. This indicates that the inclusion of bonding between different constituents not only increased the stiffness but also drove the collapse mode of the second tube.

4. ACKNOWLEDGEMENTS

The authors would like to acknowledge the Office of Naval Research and Dr. Yapa D.S. Rajapakse for providing financial support to conduct this research under the Grant No # N00014-17-1-2080.

REFERENCES

[1] S. E. Turner and J. M. Ambrico, "Underwater Implosion of Cylindrical Metal Tubes," *J. Appl. Mech.*, vol. 80, p. 11013, 2012.
[2] J.-H. Han, G. a. Kardomateas, and G. J. Simitses, "Elasticity, shell theory and finite element results for the buckling of long sandwich cylindrical shells under external pressure," *Compos. Part B Eng.*, vol. 35, pp. 591–598, 2004.
[3] G. A. Kardomateas and G. J. Simitses, "Buckling of Long Sandwich Cylindrical Shells Under External Pressure," *Jam*, vol. 72, no. 4, pp. 493–499, 2005.
[4] M. Ohga, A. Sanjeewa Wijenayaka, and J. G. A. Croll, "Reduced stiffness buckling of sandwich cylindrical shells under uniform external pressure," *Thin-Walled Struct.*, vol. 43, no. 8, pp. 1188–1201, 2005.
[5] K. Arjomandi and F. Taheri, "Stability and post-buckling response of sandwich pipes under hydrostatic external pressure," *Int. J. Press. Vessel. Pip.*, vol. 88, no. 4, pp. 138–148, 2011.
[6] N. G. Pegg, "Effects of impulse duration and combined impulse-hydrostatic pressure on buckling stability of cylindrical structures," *Sh. Res.*, vol. 38, no. 2, pp. 164–171, 1994.
[7] J. M. Brett and G. Yiannakopolous, "A study of explosive effects in close proximity to a submerged cylinder," *Int. J. Impact Eng.*, vol. 35, pp. 206–225, 2008.
[8] C. F. Hung, B. J. Lin, J. J. Hwang-Fuu, and P. Y. Hsu, "Dynamic response of cylindrical shell structures subjected to underwater explosion," *Ocean Eng.*, vol. 36, no. 8, pp. 564–577, 2009.
[9] M. Pinto, S. Gupta, and A. Shukla, "Study of implosion of carbon/epoxy composite hollow cylinders using 3-D Digital Image Correlation," *Compos. Struct.*, vol. 119, pp. 272–286, 2015.
[10] N. DeNardo, M. Pinto & A. Shukla, "Hydrostatic and shock-initiated instabilities in double-hull composite cylinders", *Journal of the Mechanics and Physics of Solids,* https://doi.org/10.1016/j.jmps.2017.10.020

DOI: 10.5075/epfl-ICSS12-2018-84-86

A TRANSVERSELY ISOTROPIC MATERIAL MODEL FOR FOAM CORES IN MARINE COMPOSITE SANDWICH PANELS UNDER BLASTS

Michelle S. Hoo Fatt[1], Chong Zhong[2], Xiaolong Tong[3] and Prasanna C. Gadepalli[4]
[1]University of Akron, USA. hoofatt@uakron.edu
[2]University of Akron, USA. cz29@zips.uakron.edu
[3]University of Akron, USA. xt7@zips.uakron.edu
[4]University of Akron, USA. pg62@zips.uakron.edu

1. INTRODUCTION

Structural polymeric foams are used as the core material in lightweight composite sandwich ship structures. Traditional sandwich theory suggests that the primary function of the foam core is to transmit shear to the fachesheets, thereby rendering high bending stiffness and strength from a panel with minimum weight penalty. Recent analysis on the underwater blast response of PVC foam-core composite sandwich panel, however, shows that in addition to the above, PVC foams have blast mitigation effects via energy absorption during plastic core crushing [1]. Sandwich panels with softer more ductile foam cores can offer better blast resistance than panels with stiffer and stronger foams because of the associated energy dissipation due to core crushing. This is especially true in water blast cases where yielding of the foam is under transverse shear and compression and in all three principal directions. Furthermore, a foam-core sandwich panel is able to resist blast loading even after the foam has plastically deformed, as long as fracture has not ensued. Plastic deformation of the foam parent material, which is semi-rigid PVC for Divinycell PVC H100 foam, leads to permanent changes in the geometry of the foam cells and hence, a corresponding change in the overall material behavior of the foam. Such behavior after permanent, plastic deformation has not been addressed until very recently [2-5].

Chen and Hoo Fatt [2] characterized the out-of-plane (transverse) and in-plane, elastic-plastic hysteresis behavior of PVC H100 foam under cyclic, uniaxial compression and simple shear. This foam exhibited transversely isotropic properties, with a ratio of out-of-plane to in-plane stiffness and yield strength for the PVC H100 foam to be approximately 3/2 in both the compression and shear modes. Once yielding occurred, the foam underwent permanent damage and exhibited hysteresis, mainly in the form of viscoelasticity. Similar behavior was reported for the form under combined transverse compression and shear in Refs. [4-5]. The objectives of this research are (1) to design pressure vessel experiments for obtaining multi-axial, elastic-plastic and hysteresis properties of PVC foams, and (2) to use the experimental results to develop 3D crushable foam core constitutive models that account for transverse isotropy, plasticity, damage and hysteresis.

2. PRESSURE VESSEL EXPERIMENTS

In order to obtain tri-axial material properties of PVC H100 foam, a pressure vessel apparatus shown in Figs. 1(a) and (b), was built to encase specimens in a servo-hydraulic MTS machine. The air pressure in the vessel was controlled through a micro-controller circuit board and two solenoid valves. Output signals from the MTS controller were fed into the micro-controller circuit board and used to synchronize the pressure with the MTS actuator motion. The pressure inside the cylinder was measured by a pressure transducer. Signals from the pressure transducer were directly fed into the data acquisition of the MTS machine controller itself. As shown in Fig. 1(a), sight-windows in the end-caps of the pressure vessel were used to enable Digital Image Correlation (DIC) measurements of strains in a wide assortment of specimens, which are shown in Fig. 2. Figure 1(b) shows an Arcan specimen inside the cylinder. Nozzle-guided pistons pass straight through the body pressure chamber in order to achieve good alignment of these specimens. The pistons were sealed with a specially-designed, low friction lip seals.

Extensive testing of the PVC foam was done under uni-, bi- and tri-axial loading in both out-of-plane and in-plane material directions. As described in Fig. 2, Arcan butterfly specimens were used for shear loading (0 deg), as well as combined shear and compression (15-75 degs) and compression (90 deg). A dogbone specimen was used for tension. Pressurizing the air in the chamber allowed for tri-axial loading, and DIC allowed for strains to be measured in the neck regions of the Arcan and dogbone specimens.

3. CYCLIC STRESS-STRAIN CURVES

Tri-axial compression and shear stress-strain were obtained by enclosing the 0 deg Arcan specimen in the pressure chamber and pressurizing it. The strain distributions in the specimen are shown in Figs. 3(a)-(c), and the resulting stress-strain behaviors are given in Figs. 4(a)-(c). These strains were obtained using 2D DIC measurements. It was assumed that in-plane behavior of the foam would be similar, although 3D DIC will be used later to confirm this. Elastic-plastic response followed by viscoelastic hysteresis can be seen in Figs. 4(a)-(c).

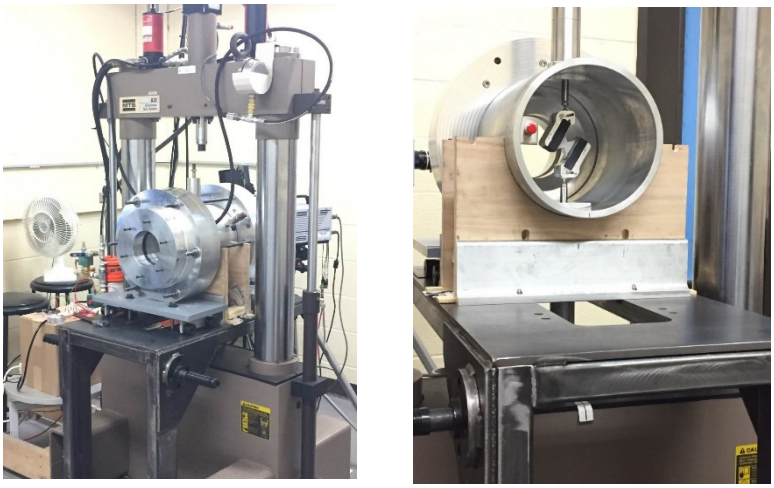

(a) (b)

Fig. 1: Pressure vessel experiments to obtain multi-axial hysteresis of PVC foam: (a) pressure chamber and (b) Arcan specimen inside chamber.

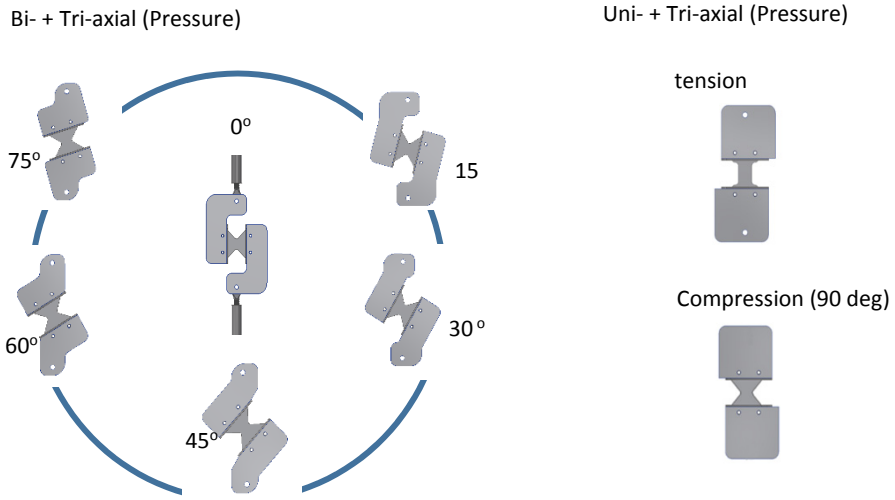

Fig. 2 Specimens used to determine uniaxial, biaxial and tri-axial material properties of PVC H100 foam.

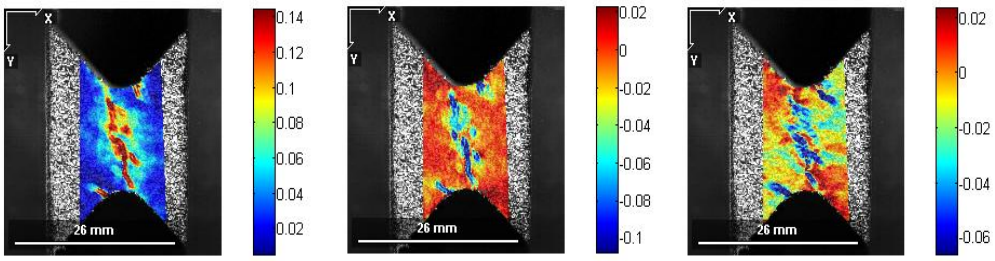

(a) (b) (c)

Fig. 3: Strain distributions in pressurized Arcan specimen: (a) transverse shear, (b) transverse compression and (c) in-plane compression.

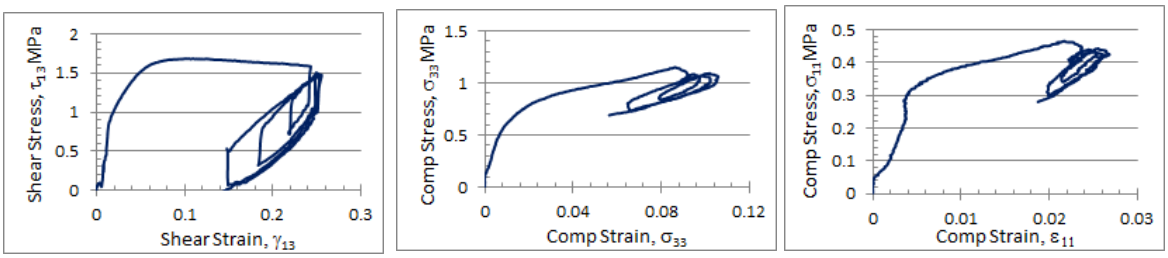

(a) (b) (c)

Fig. 4: Cyclic stress-strain curves: (a) transverse shear, (b) transverse compression and (c) in-plane compression (1- and 2-directions assumed same because of foam transverse isotropy).

4. CONSTITUTIVE MATERIAL MODEL

The foam exhibited elastic-plastic with viscoelastic hysteresis and damage after initial yielding. The onset of plasticity and damage occurred simultaneously, and before these occurred, the foam experienced linear elastic behavior. A material model based on coupled Tsai-Wu plasticity, with mixed kinematic and isotropic hardening, and linear viscoelasticity after yielding/damage was developed for the PVC H100 foam. Good agreement can be seen between the predicted response based on the above constitutive model and the combined shear-compression test data of the 45 deg Arcan specimen in Figs. 5(a) and (b). Similar good agreement was also found for other angles, and the model is currently being applied to the tri-axial test data.

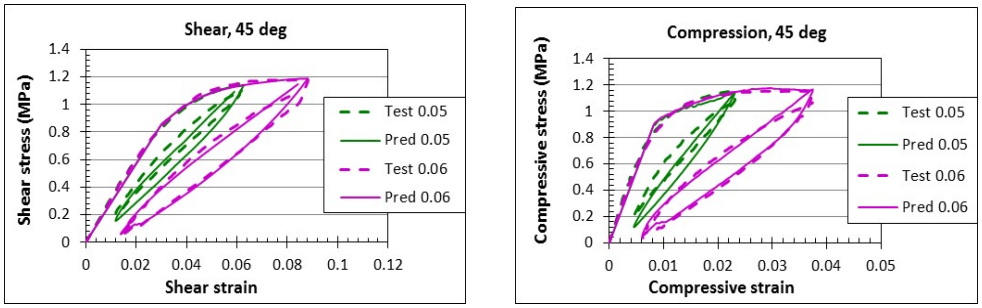

(a) (b)

Fig. 5: Comparison between predicted and experimental results for 45 deg Arcan specimens: (a) transverse shear and (b) transverse compression.

5. CONCLUDING REMARKS

Experiments were done to determine the multi-axial, elastic-plastic and hysteresis behavior of Divinycell PVC H100 foam. The foam, which was transversely isotropic, exhibited elastic-plastic response followed by damage and viscoelastic hysteresis. A Tsai-Wu plasticity model, including combined kinematic and isotropic hardening, was coupled with viscoelasticity and damage to describe the foam behavior. This constitutive model will be used to simulate the response of composite sandwich panels subjected to underwater blasts.

REFERENCES

[1] M.S. Hoo Fatt et al., "Marine composite sandwich plates under air and water blasts," *Mar Struct, 2017* 56: 63-185.
[2] L. Chen et al., "Transversely isotropic mechanical properties of PVC foam under cyclic loading," *J Mat Sci, 2013,* 48: 6786-6796.
[3] M.S. Hoo Fatt et al., "A viscoelastic damage model for hysteresis in PVC H100 foam under cyclic loading," *J Cell Plast*, 2015, 51: 269–287.
[4] M.S. Hoo Fatt et al., "Underwater blast resistance and energy absorption of PVC foams in sandwich panel constructions," ICSS-11, *2016.*
[5] M.S. Hoo Fatt et al.. "Blast mitigation effects of foam-core, composite sandwich structures," in S. Gopalakrishnan and Y.D.S. Rajapakse (Ed.), *Blast Mitigation Strategies for Marine Composite and Sandwich Structures*, Springer Science & Business Media Singapore Pte Ltd, Singapore, 2017, 265-280

DOI: 10.5075/epfl-ICSS12-2018-87-88

COMPARING THE BLAST TOLERANCE OF HYBRID COMPOSITE SANDWICH PANELS

Emily Rolfe[1], Hari Arora[2], Paul A. Hooper[1] and John P. Dear[1]
[1]Department of Mechanical Engineering, Imperial College London, London, United Kingdom. emily.rolfe11@imperial.ac.uk
[2]Zienkiewicz Centre for Computational Engineering, College of Engineering, Swansea University, United Kingdom

1. INTRODUCTION

Due to the advantageous properties of composite sandwich panels, including high strength-to-weight ratio and low radar signature, these materials are of increasing interest in the naval sector along with many other industries. Naval vessels, however, must be able to withstand a variety of loads including very destructive loads, such as explosive blast loading. Representative materials must be tested under real blast conditions to ascertain whether the proposed composite sandwich materials are suitable for such applications. Arora et al [1] have performed full-scale blast experiments on composite sandwich panels with glass-fiber reinforced polymer (GFRP) face-sheets and on GFRP tubular laminates. The results demonstrated that sandwich structures are able to effectively resist blast loading and strain gauges are able to record the dynamic response of such structures. The same authors investigated the effect of different parameters, for example core thickness, on composite sandwich panels under air blast loading [1]. The research presented here focusses on full scale air blast testing on two types of composite sandwich panel with different combinations of glass- and carbon-fiber reinforced composite face-sheets.

2. EXPERIMENTAL METHOD

Two types of composite sandwich panel were subjected to air blast loading. The skin layups of these two panels are shown in Fig. 1. All panels had a total of 8 fiber plies in each skin, 4 glass-fiber and 4 carbon-fiber arranged quadriaxially. Both panels had a 30 mm polyvinyl chloride (PVC) foam core and the panels were 1.75 m × 1.55 m. During blast testing the panels were bolted side-by-side into a steel cubicle at a 15 m stand-off distance away from a 100 kg nitromethane charge. 5 mm thick steel frames were adhered to the front and back of the panels and the panels were bolted to the front of the steel cubicle. A pair of high speed cameras was placed behind each panel to record the full field out-of-plane displacement of the panels. To enable processing of the high speed images as 3D DIC data, the panels were speckled. Additionally, the edges of the steel cubicle were speckled to track movement of the boundaries. A pressure gauge block was placed at the same stand-off distance as the charge to record the blast wave pressure profiles. In addition, 14 foil strain gauges were adhered to the front skin of each panel. This would enable a comparison between the front and rear skin strain at certain locations.

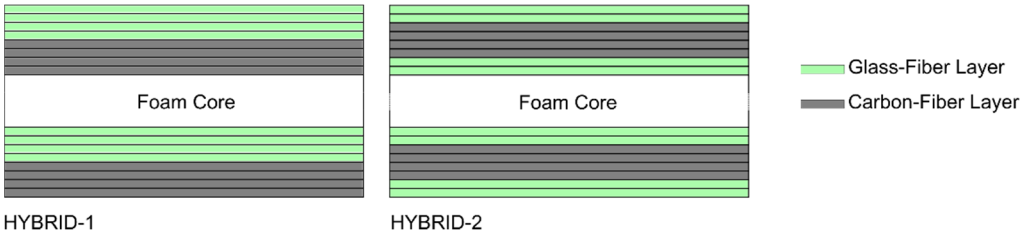

Fig. 1: Schematic of the two types of hybrid skin adopted in the full scale air blast panels.

3. RESULTS

The DIC contour plots for Hybrid-1 are shown in Fig. 2. Fig. 3 shows the displacement of the central horizontal cross-section of the panel, both the initial deflection and first rebound. Each displacement curve is 0.25 ms apart, the arrow on the right hand side of each diagram show the direction of movement of the panel. During the initial deflection, the panel deforms in the expected bath-tub shape before adopting a parabolic shape. The center point reaches a maximum displacement of 75 mm. Sharp changes in gradient observed during the rebound stroke indicate damage within the panel. The movement of the steel cubicle has been removed from the displacement of the panel. The performance of Hybrid-2 is very similar with a maximum out-of-plane deflection of 73 mm and comparable values of major strain. The out-of-plane displacement of the central point of the two panels is shown in Fig. 4. The panels both reach a maximum velocity of approximately 37 ms^{-1} during deflection.

The strain gauge data revealed that overall, the front skins undergo greater strain compared to the rear skin. As expected, the front skins experience compression and the rear skins tension during blast loading. The support offered by the steel cubicle is not equally stiff around the perimeter of the panel due to its design. This is highlighted by the strain gauge data where the edge bolted to the central support of the cubicle experience less strain.

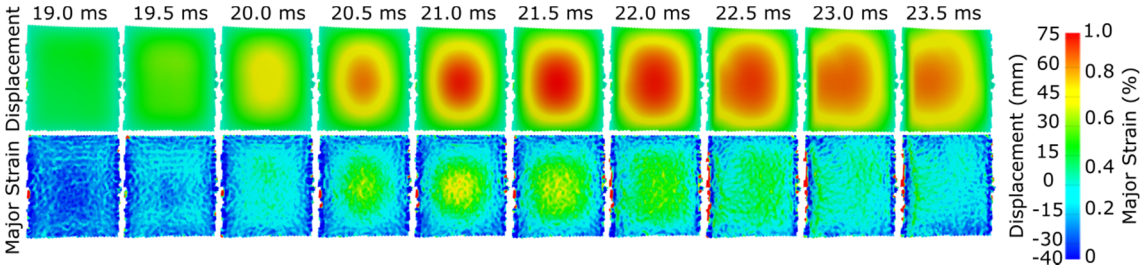

Fig. 2: DIC contour plots for out-of-plane displacement and major strain for Hybrid-1.

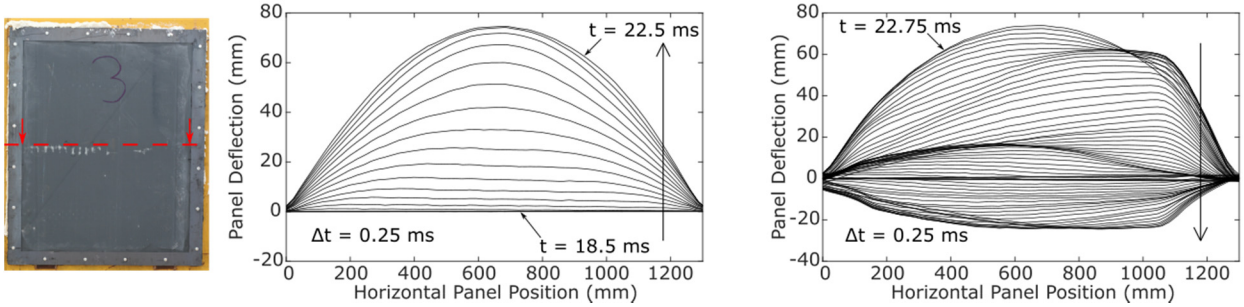

Fig. 3: Displacement of the central horizontal cross-section at 0.25 ms time intervals for Hybrid-1.

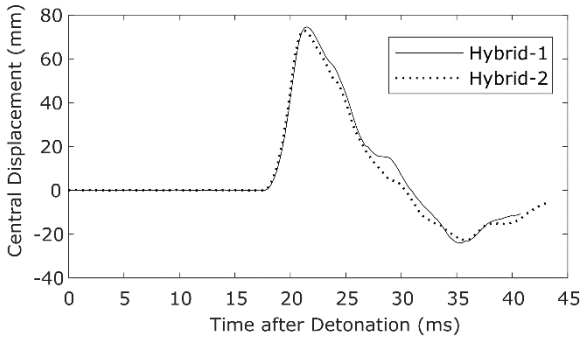

Fig. 4: Central out-of-plane displacement of Hybrid-1 versus Hybrid-2 panels.

4. DISCUSSION

The behavior of the two composite sandwich panels with different hybrid skins was very similar overall. The panels demonstrated comparable deflection, pull-out, velocity and discontinuous deflection gradients at the quarter points across the panel width. These panels can be compared to previous blast testing on sandwich panels with purely glass- and carbon-fiber reinforced polymer skins. The hybrid demonstrated a significantly lower deflection, even when variations in blast pressure are taken into account, and significantly less skin damage. The results suggest that on such a large scale, the incorporation of the two fiber types is the key factor in improving blast resilience rather than the layup order.

5. CONCLUSION

In conclusion, the use of hybrid glass-/carbon-fiber skins acted to attenuate blast energy and reduce the central deflection of the panel. The use of foil strain gauges on the sandwich panel front skins reveals the difference in strain experienced by the front and rear skins and across the front of the panel due to non-rigid boundary conditions. By speckling the steel cubicle and recording the blast event with high speed cameras, it is possible to accurately measure the displacement of the panel and subsequently remove the rigid body motion of the cubicle structure.

ACKNOWLEDGEMENTS

The authors would like to thank Dr Yapa Rajapakse of the Office of Naval Research for supporting Emily Rolfe, Dr Mark Kelly and Dr Hari Arora during their PhDs; EPSRC for supporting Emily Rolfe during her PhD. Additionally, much appreciated is the assistance from DNV GL during blast testing, GOM UK for their support with DIC and Slowmo Ltd for high speed camera hire and expertise.

REFERENCES

[1] H. Arora et al., “The effects of air and underwater blast on composite sandwich panels and tubular laminate structures”, *Exp. Mech.*, 2012;52:59-81.

DOI: 10.5075/epfl-ICSS12-2018-89-91

IMPACT AND POST-IMPACT FLEXURAL BEHAVIOR OF COMPOSITE SANDWICH STRUCTURES IN EXTREME LOW TEMPERATURE ARCTIC CONDITIONS

Kwek-Tze Tan[1] and Md. Mahfujul Khan[2]
[1]Department of Mechanical Engineering, The University of Akron, USA, ktan@uakron.edu
[2]Department of Mechanical Engineering, The University of Akron, USA, mhk11@zips.uakron.edu

1. INTRODUCTION

The reduction in arctic sea ice region over the last three decades has opened new sailing routes which are more efficient and economical. This has resulted in the increased use of marine and naval vessels in extreme low temperature arctic conditions. The fundamental challenge of operating in such cold and harsh environment lies in the understanding of how materials and structures behave and perform in extreme low temperature. In recent years, structural sandwich composites have been widely used in many applications such as aircraft structures, ship hulls, wind turbine blades and bridge decks. This is due to their superior bending stiffness, low weight, excellent thermal insulation and acoustic damping properties. They are commonly used in many engineering fields because they are more superior over the conventional structural construction materials such as having high bending stiffness and good weight saving. The behavior of sandwich beams depends on the properties of the core material, especially under impact loading. They typically consist of two thin, stiff, and strong faces which are separated by a thick, light, and shear-resistant core. However, one of the major concerns in the use of sandwich composites such as in the conventional polymer matrix composites is the impact-induced damages which may occur during normal maintenance operations or during service conditions. Even a relatively minor impact could drastically reduce the residual-strength of the material. In this study, we experimentally investigate the impact response and post-impact flexural behaviour of Divinycell H-100 foam core sandwich panel with woven carbon fiber reinforced polymer (CFRP) facesheets in low temperature arctic conditions.

2. EXPERIMENTAL METHODOLOGY

Materials

The composite sandwich structure specimens have face sheets made of 0°/90° woven carbon fiber epoxy matrix composite. The sandwich core is PVC Divinycell H-100 foam core. The facesheets are either 0.01 inch or 0.03 inch thick, while the foam core is 0.25 inch thick. Individual composite panels were cut into 6 inch x 4 inch specimen size for impact test. The impacted specimens were further cut into 6 inch x 1 inch bending specimen for three point bending test.

Impact Tests

Impact tests were conducted using Instron CEAST 9350 drop tower with an environmental chamber. The samples were impacted across three different temperatures: 23°C (baseline room temperature); -30°C (arctic average temperature); -70°C (arctic coldest temperature). Drop height of the striker was adjusted to control the impact energy level. Each sample type was impacted at two different energy levels at 4 J and 8 J. Impact response data was collected using DAS64K system, in terms of force, time, deflection, velocity and energy.

Bending Tests

Three point bending tests were conducted to evaluate the residual strength and stiffness of the samples. Test procedure was in accordance to ASTM C 393 with a crosshead speed of 0.5 mm/min and a span of 100mm. Samples were flexural tested at room temperature, -30°C and -70°C, at the same respective temperatures as they were impacted.

3. RESULTS AND DISCUSSION

Results show that exposure to low temperature generally causes more severe damage in the specimens. Post-mortem inspection using x-ray micro-computed tomography revealed complex failure mechanisms in the composite facesheets (such as matrix crack, delamination and fiber breakage) and foam core (core crushing, core shearing and interfacial debonding).

Impacted specimens were then subjected to three point bending test to examine their residual flexural properties. Bending characteristics were analysed on both sides of the specimens (front impact face and back distal face), as depicted in Fig. 1. Bending test data suggests that residual flexural properties after impact are more sensitive to the in-plane compressive property of the CFRP facesheet than the in-plane tensile property, as shown in Fig. 2. Results also indicate that degradation of flexural rigidity of the sandwich composite panel strong depends on existing damage state of prior impact test. Analogous to impact behavior, specimens have much reduced flexural properties when exposed to extreme low temperature conditions (-70°C).

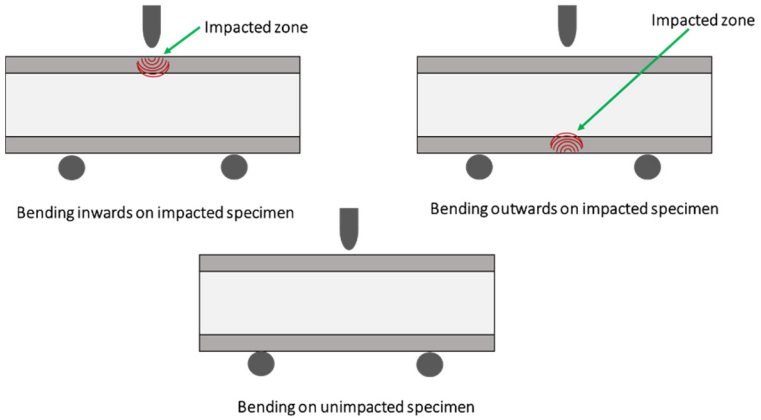

Fig. 1: Schematic view of three point bending test configuration.

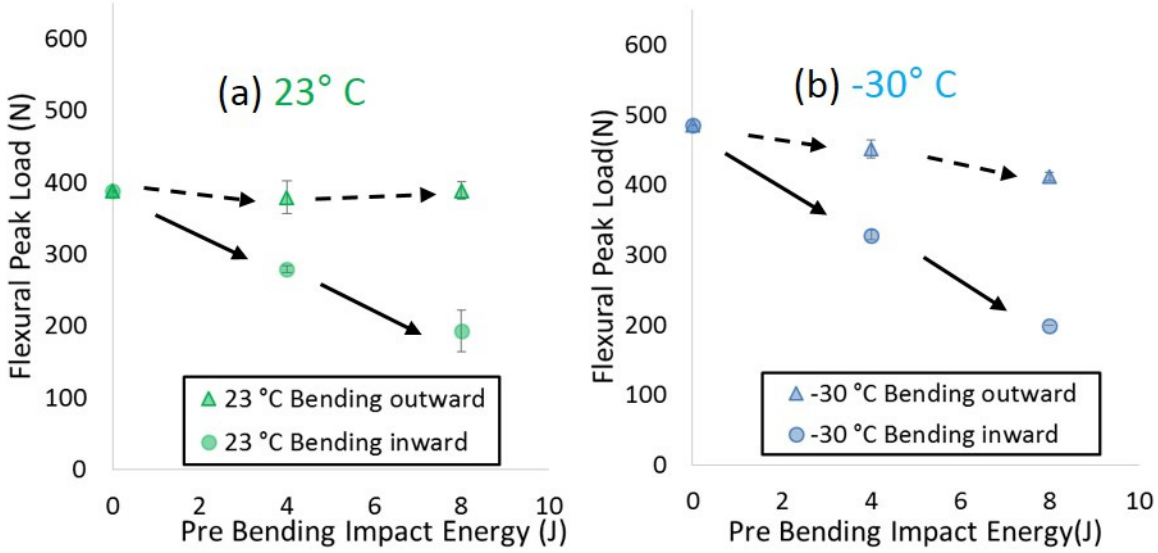

Fig. 2: Flexural load against impact energy plots (a) 23°C; (b) 30°C.

Experimental results obtained in this work are further compared and validated with analytical models that can predict the competing collapse mechanisms for simply support sandwich beams with composite faces and PVC foam core subjected to three point bending [1-2]. Figure 3 shows the peak load prediction based on different failure mechanisms. For the specimens tested in this study, they failed by indentation. Experimental data (shown in markers) are plotted to compare with analytical prediction (linear lines). It is clear that there is good agreement with both experimental and analytical results. The predicted collapse loads for face yielding or microbuckling; core shear failure; face wrinkling and indentation are examined with the physical-based mechanisms obtained in experiments. The analytical models aim to reveal knowledge on the coupling effect of low temperature with damage mechanisms.

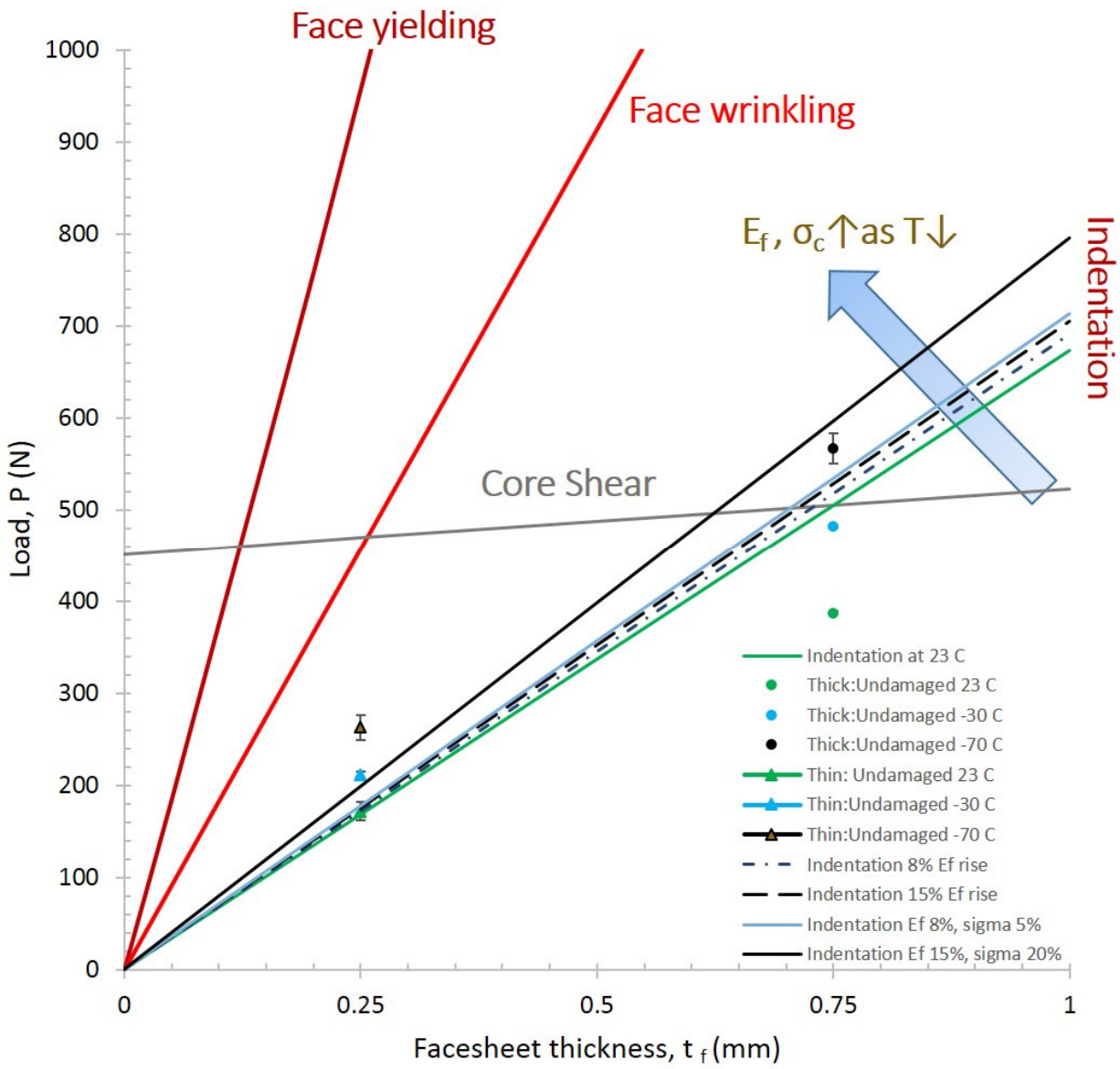

Fig. 3: Flexural load prediction based on analytical models and validation with experimental results.

4. CONCLUSIONS

The findings from this work will lead to better understanding of the dynamic response and failure of composite sandwich structures at extreme low temperature conditions, which will subsequently lead to improved design for naval structures and materials that can operate safely and effectively in arctic environment.

ACKNOWLEDGEMENTS

The authors acknowledge the research grant N00014-16-1-3202 provided by the U.S. Office of Naval Research (ONR Program Manager: Dr. Yapa Rajapakse).

REFERENCES

[1] C.A. Steeves et al., "Collapse mechanisms of sandwich beams with composite faces and a foam core, loading in three-point bending. Part I: analytical models and minimum weight design", *Int. J. Mech. Sci.*, 2004; 46: 561-583.

[2] C.A. Steeves et al., "Collapse mechanisms of sandwich beams with composite faces and a foam core, loading in three-point bending. Part II: experimental investigation and numerical modelling", *Int. J. Mech. Sci.*, 2004; 46: 585-608.

SESSION 4B: APPLICATIONS – CIVIL ENGINEERING

DOI: 10.5075/epfl-ICSS12-2018-93-95

MODULAR FRP SANDWICH ASSEMBLIES FOR ONE-WAY AND TWO-WAY SLAB AND COMPOSITE BEAM APPLICATIONS

Yu Bai[1] and Sindu Satasivam[2]
[1]Professor, Department of Civil Engineering, Monash University, Clayton, Melbourne, Australia. Tel: ++61 3 9905 4987; Fax: +61 3 9905 4944; Email: yu.bai@monash.edu
[2]Former research fellow in the Department of Civil Engineering, Monash University; currently Structural Engineer at Lendlease Australia; Email: s.satasivam@gmail.com

1. INTRODUCTION

Fibre reinforced polymer (FRP) composite materials have become as primary load-carrying structural members in civil construction [1]. They provide high strength, come in a variety of colours and transparencies and are lightweight, chemically unreactive and resistant to corrosion [2]. FRP composites, particularly if glass fibres are used (i.e. glass fibre reinforced polymers, or GFRP), also exhibit low thermal conductivity and embodied energy. However, in comparison to steel, GFRP materials are associated with a low material stiffness resulting from a low elastic modulus (10-20% that of steel). This makes the deflection criteria in serviceability limit state (SLS) design of GFRP structures even more critical than strength design. GFRP is a linear-elastic material, resulting in sudden and brittle failures. The fibre architecture of GFRP materials also bring stiffness of the longitudinal direction (also known as the pultrusion direction, in which the majority of the fibres run) much larger than that in the transverse direction.

A modular sandwich design concept is developed to consider such specific material features for building construction, where built-up beam or slab sections consisting of pultruded GFRP box or I-profiles are sandwiched between GFRP flat panels to form a web-flange structure. This section has an improved second moment of area, thereby improving the stiffness of GFRP at the structural level. The use of pre-fabricated built-up profiles provides greater flexibility in designing floor systems, which may be advantageous than pultruded FRP decks with constant sections for varying load conditions. This design flexibility can also allow for the incorporation of two different pultrusion orientations into the one structure, which may improve strength in transverse direction and avoid premature cracking in this direction. In addition, by using built-up GFRP members, pre-fabricated foam blocks can be easily incorporated during fabrication of the modular assembly to further enhance structural performance. Finally, the inclusion of steel as a supporting girder to form composite beams may provide ductile responses if properly designed.

The paper summarizes the investigations on the mechanical performance under static loading for such modular GFRP sandwich structures in applications of one-way spanning slabs (or beams), two-way spanning slabs and GFRP-steel composite beams [3-6]. The bending stiffness, load-carrying capacity, failure mechanism and composite action were evaluated and analyzed. In addition, two different pultrusion configurations were achieved and examined in the two-way slabs and GFRP-steel composite beams: flat panels with pultrusion directions either parallel or perpendicular to the web-core profiles. The latter can effectively avoid premature cracking along the pultrusion direction of the face flat panels. Furthermore, the GFRP-steel composite beams were appropriately designed since they showed ductile load-deflection responses that resulted from yielding of the steel girder, which commenced prior to failure of the GFRP slabs.

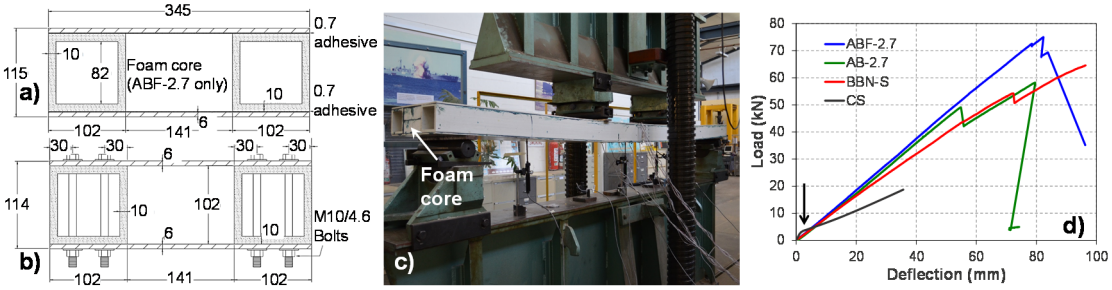

Fig. 1: Modular FRP sandwich beams (a) sections for AB-2.7 and ABF-2.7; (b) section for BBN-2.7; (c) specimen ABF-2.7 under bending and (d) load displacement curves for all specimens compared with a designed reinforced concrete one way slab.

2. ONE-WAY BENDING APPLICATIONS

Three modular sandwich beams (AB-2.7, ABF-2.7 and BBN-2.7) were fabricated from pultruded GFRP materials (box sections and flat panels as shown in Fig. 1(a) and (b)), consisted of E-glass fibres and polyester resin with volume fraction of 42-48% and 53-58% respectively. The material properties of the GFRP materials were determined as 306 MPa for tensile strength, 30 GPa for Tensile modulus, and 27 MPa for the interlaminar shear strength. Araldite 420 epoxy adhesive with a 25 MPa shear strength was utilized for the bonding. Divinycell P150 Foam, supplied by DIAB Australia, was utilized as a core material (only for ABF-2.7 see Fig. 1(c)). Zinc-plated M8 and M10 steel bolts were used for

preparation of specimen BBN-2.7 (Fig. 1(b)). The bolts were class 4.6 with a bolt diameter of 8mm (M8) or 10 mm (M10), a nominal tensile strength of 400 MPa and a proof load stress of 225 MPa.

All specimens (both adhesively bonded and bolted) had lengths of 2.7m (therefore with span-to-depth ratios about 25) and widths of 345mm. For specimens AB-2.7 and ABF2.7 with adhesive bonding, a layer of Araldite epoxy adhesive with a thickness of 0.7mm was used to adhesively bond the GFRP components and foam components. M10 bolts were used in a staggered configuration to connect the flat panels to the box profiles at a spacing of 150mm for specimen BBN-2.7. All specimens were simply supported and loaded in four-point bending, with the distance of 900mm between the point loads and the supports. Loading was applied as a displacement control mode of 3.5mm/min.

The load P_1, in which material failure of the upper panel (rather than structural ultimate failure) arose due to local buckling, occurred in specimen ABF-2.7 at 73kN (see Fig. 1(d)). A smaller P1 load seen in AB-2.7 is because the upper panel of AB-2.7 was bonded only to the box profiles; whereas the whole upper panel of ABF-2.7 was restrained as it was bonded to both the box-profiles and the foam core. Furthermore the presence of foam in this study represents an increase in weight of only 15%, the addition of such lightweight materials can improve the load-carrying capacity of GFRP sandwich structures. Both adhesively bonded specimens AB-2.7 and ABF2.7 demonstrated a higher bending stiffness than that of the bolted specimen BBN-2.7 especially at later loading stages as shown in Fig. 1(d), due to a partial composite action. All specimens finally failed at the web flange junction followed by the web buckling.

A RC member, designated CS, was designed according to AS3600 with the same cross-section dimensions (345 × 115mm reinforced by six N10 tensile bars and four N10 compressive bars) and same span length (2.7m) as those of the GFRP sandwich specimens. Under four-point bending, the failure load of CS was calculated to be 20kN per point load, which is equivalent to an ultimate moment capacity of 18kNm. The cracking moment of the concrete slab was calculated as 2.8kNm, corresponding to a load of 3kN under four-point bending. After the cracking moment, deflections were calculated based on the effective second moment of area of the cracked section. The load-deflection curve of CS is provided in Fig. 1(d) for comparison.

It can be seen that GFRP sandwich specimens showed favourable properties compared to the one-way spanning RC slab of the same sectional size. The sandwich specimens AB-2.7 and ABF-2.7 were about 80% lighter than CS (which weighed 100 kg/m), but their ultimate loads were about 2 to 2.5 times greater than that of CS. Prior to cracking, the bending stiffness of CS was 13.9×10^{11} Nmm^2, larger than that of sandwich specimens AB-2.7 and ABF-2.7 (at 6.2×10^{11} Nmm^2 and 6.9×10^{11} Nmm^2 respectively). However, once cracking occurred for CS, its effective section and therefore stiffness was greatly reduced as shown in Fig. 1(d). The SLS is reached in this post-cracking stage, where the effective bending stiffness of the cross-section is 5.2×10^{11} Nmm^2, up to 25% less than the stiffness of the GFRP specimens.

3. TWO-WAY BENDING APPLICATIONS

Four modular GFRP sandwich two-way spanning slabs were fabricated and tested. Each specimen was made from seven 50×50×6 mm GFRP box profiles sandwiched between 6 mm-thick flat GFRP panels. Each sandwich slab had a total depth of 62 mm, an overall length and width of 1.5×1.5 m, a span of 1.45×1.45 m, and was supported on all four sides by steel rollers. Three sandwich slabs (UA, BA and BAF) had an adhesively bonded connection. Sandwich slab UA had a unidirectional pultrusion orientation where the pultrusion direction of the upper and lower flat panels lay parallel to the pultrusion direction of the box profiles (Fig. 2(a)). Sandwich slabs BA, BAF and BB all had bidirectional pultrusion orientations, where the pultrusion direction of the upper and lower flat panels lay in the transverse slab direction, perpendicular to that of the box profiles (Fig. 2(b)). In addition, BAF also had six prefabricated foam blocks as the core of the structure between each box profile (see Fig. 2(b)). These foam blocks were adhesively bonded to the inner surfaces of the specimen. Finally, sandwich slab BB was fabricated by connecting the GFRP components with blind bolts at a practical spacing of 150 mm along the longitudinal slab direction to achieve partial shear interaction.

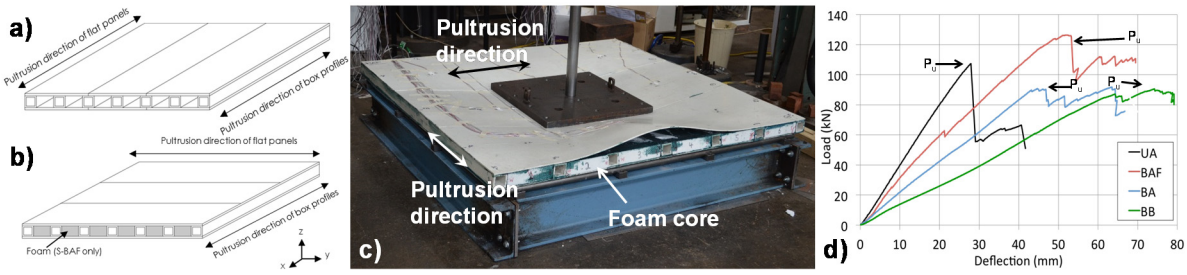

Fig. 2: Modular GFRP sandwich slabs (a) and (b) specimen configurations; (c) specimen BAF at failure and (d) load displacement curves for all specimens.

Load was applied at the central region of the slabs through a steel plate. The resulting bending caused cracking along the pultrusion direction between the fibres within the flat panel for the unidirectional sandwich slab UA at 65 kN. This longitudinal crack continued to elongate as loading increased. Slab UA failed at the ultimate load P_u of 107 kN, with the final failure occurred via in-plane shearing of box profiles. No premature local cracking was observed in the bidirectional

slabs BA, BAF and BB. Instead, local out-of-plane buckling arose at the edges of those slabs as shown in Fig. 2(c). This local buckling continued to increase, causing the failure of the connection between the upper panel and the central box profile. Such progressive failures developed in the connection region until in-plane shear failure of box profiles occurred at the ultimate loads of 90 kN for specimen BA, of 126 kN for BAF, of 88 kN for BB.

As shown in Fig. 2(d), the sandwich slab with the greatest stiffness was UA (unidirectional pultrusion orientation and adhesive bonding). When the pultrusion direction of the flat panel was placed perpendicular to that of the box profiles, the bending stiffness was reduced obviously as in BA. The stiffness of the slab BAF, with the foam core and adhesive bonding, was 45% greater than that of BA and 20% less than that of UA. The addition of foam provided a significant increase in stiffness, even though the foam core was associated with a low elastic modulus of 115 MPa (corresponding to only 0.4% of that of the GFRP box profiles). The slab with the lowest stiffness was BB, in which the stiffness was 40% less than that of BA, because of bolted connections provided partial composite action in comparison to the full composite action offered by the adhesive bonding.

4. COMPOSITE BEAM APPLICATIONS

Four GFRP-steel composite beams (UA, BA, UB and BB) were fabricated, with the first letter refers to the pultrusion configuration of the sandwich slab (U=unidirectional, B=bidirectional) and the second letter refers to the connection type between the slab and the steel beam (A=adhesive, B=bolted). A reference steel beam was also tested.

The overall length of each specimen was 3 m, and the span length was 2730 mm. The depth of each sandwich slab was 62 mm, and they were connected to steel beams with a depth of 155 mm, giving an overall composite beam depth of 217 mm. The width of each FRP slab was 500 mm. Fig. 1(a) shows the side view for the bidirectional beams BA and BB (bolts between the slab and steel beam used only for BB and UB); and Fig. 1(b) shows that for UA and UB.

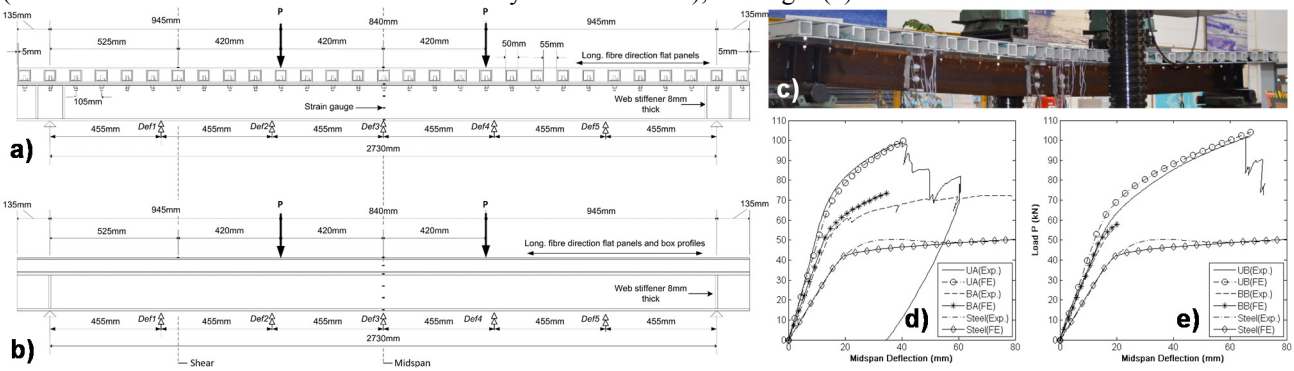

Fig. 3: Modular GFRP-steel composite beams (a) specimen BB and (b) UA in side view; (c) deformed shape of specimen BB with yielding of steel girder; (d) and (e) load displacement curves for all specimens.

Composite beam BA experienced local crushing of a box profile situated directly beneath a loading point at a load of 53 kN. Further increase in load until 72 kN was associated with a large increase in deformation due to the yielding of steel girder (Fig. 3(d)). This load (72kN) was recorded as its maximum load (Pmax), and was 40% higher than the maximum load of the reference steel beam (52 kN). Composite beam BB presented a maximum load of 79 kN (not recorded in Fig. 3(e)) and failed via in-plane shearing of the GFRP slab and then the experiment was manually stopped because of excessive large bending deformation (Fig. 3(c)). The local crushing of box profiles beneath the point load that was observed in BA was avoided in BB by the use of a greater steel plate width of 200 mm. The maximum failure load of unidirectional composite beam UA and UB was reached at 99 kN and 102 kN respectively, when the beams failed via longitudinal shear of the upper and lower panels. Again such failures of FRP sandwich slabs occurred after the excessive yielding of the supporting steel girders.

ACKNOWLEDGEMENTS

The authors thank the supports from the Australian Research Council through DE120101913 and DP180102208.

REFERENCES

[1] L.C. Bank, *Composites for construction: structural design with FRP materials*. John Wiley & Sons, Inc., 2007.
[2] T. Keller, C. Haas and T. Vallée. “Structural concept, design and experimental verification of a GFRP sandwich roof structure”, *Journal of Composites for Construction*, 2008; 12/4: 454-468.
[3] S. Satasivam, Y. Bai, X.L. Zhao. Adhesively bonded modular GFRP web–flange sandwich for building floor construction. *Composite Structures*, 2014; 111: 381-392.
[4] S. Satasivam, Y. Bai. Mechanical performance of bolted modular GFRP composite sandwich structures using standard and blind bolts. *Composite Structures*, 2014; 117: 59-70.
[5] S. Satasivam, Y. Bai, Y. Yang, L. Zhu, X.L. Zhao. Mechanical performance of two-way modular FRP sandwich slabs. *Composite Structures*, 2018; 184: 904-916.
[6] S. Satasivam, Y. Bai. Mechanical performance of modular FRP-steel composite beams for building construction. Materials and Structures, 2016; 49(10): 4113-4129.

DOI: 10.5075/epfl-ICSS12-2018-96-98

REFURBISHMENT OF THE VORDERRHEIN-ROADBRIDGE NEAR VALENDAS IMPLEMENTING A GFRP-WOOD HYBRID SLAB

Thomas J. E. Ekwall[1] and Gernot Weis[2]
[1]«thomas ekwall tragwerksplaner eth», office for structural engineering, Switzerland. info@tekwall.ch
[2]«Leichtbauweis», manufacturing company, Switzerland. gernot.weis@leichtbauweis.ch

1. INTRODUCTION

The road bridge crossing the Vorderrhein close to the railway station Valendas-Sagogn (CH) is a steel truss from 1903, which was refurbished in 2017 for an expected design working life of 70 years. A GFRP-wood hybrid slab replaced the existing bridge deck, increasing the allowed service loads from 9 t to 18 t. The refurbishment was planned by the engineering consortium thomas ekwall tragwerksplaner eth and Flückiger + Bosshard AG. The sandwich slab was produced and assembled on site by the company LeichtbauWeis AG. The project was supervised by the infrastructure department of the Raetian Railway RhB, which transferred the ownership of the bridge to the contiguous municipalities Safiental and Sagogn after completion.

This is just the second road bridge in Switzerland after the Avançon-bridge [1] which has been built using this manufacturing process. Besides dealing with horizontal loads such as stalling and impacts in statical verifications, the consequences of high temperatures caused by asphalting on the GFRP was evaluated in preliminary tests.

Fig. 1: Asphalted GFRP-Wood slab with steel guard rails.

2. PLANNING

Construction

The bridge slab is 62.07 m long with 3.30 m effective width. Considering weight and transportation boundaries, the slab was subdivided in ten elements with maximal length of 6.81 m (The expansion joints are independent from the slab). Each element has a 170 to 210 mm thick glulam spruce core GL 24h spanning transversally, enwrapped in a 6 mm thin matrix of vinyl ester synthetic resin. Glass fiber mats Saertex U-E-1751g/m^2 are integrated to the matrix (with a 55% ratio) using the vacuum infusion technique. Guard rails in steel are structurally glued to the GFRP on the lateral sides. The elements are separated to each other by 6 mm transversal joints and fixed to the steel substructure underneath using wood screws. The drainage occurs by longitudinal and transversal slopes, without perforating the slab elements.

Statics

The GFRP-Layer was not considered in the slab dimensioning. The wooden core was dimensioned for self-weight (slab 1.0 kN/m^2 + asphalt 1.6 kN/m^2) and trafic loads (surface loads 2.7 kN/m^2 + Axle 2x126 kN). Transverse compression at the supports as well as fatigue due to bending were determining for the ultimate limit state (ULS). The deformations in middle span satisfied the comfort criteria L/500 of the serviceability limit state (SLS).

The M16 wood screws (36 Pcs. in each element) transmit stalling loads up to 222 kN in the substructure by shear resistance. The guard rail transmit up to 100 kN impact loads in the slab elements, activating the shear and tensile resistance of the Sikadur 30 LP structural glue. [2]

Pavement

The sandwich elements have a surface coating Sikadur-188 Resin broadcasted with Quarz sand 0.7-1.2mm, so-called Hessensiegel. The slab joints are sealed with Dilatec stripes and Sikaflex PRO-3 mastic. Warm rolled asphalt AC TD 16 N

(combined asphalt base and surface layer) of 60 mm at 160°C was applied on the slab, which was recovered preliminarily with glass fleece.

3. PRELIMINARY TESTS

Three preliminary tests were implemented to measure the temperature and estimate the behavior of the GFRP-Layer during asphalt works, thus defining the maximal allowed paving temperature and various constructive details. [3]

Test with Rolled Asphalt on a Big Sample

The purpose of the first test was to estimate the temperature in the GFRP-Layer during asphalting on a sample with the measurements L=1.40 m, B=0.80 m, H=0.14 m and 12% moisture content. Wooden core, GFRP-Layer, Guard rails and transition joints and surface coating (Hessensiegel) were constructed according to the bridge slab. Six temperature sensors NiCrNi Type K with glass silk wire were applied on the lower surface of the GFRP, next to the core. The rolled asphalt was poured on the sample and compacted manually (the weight of the combination roller wasn't simulated).

Fig. 2: Sample of the first preliminary test before asphalting.

The installation temperature of +157°C sank immediately to +141.8°C before compacting. The maximal measured Temperature in the GFRP-layer (measuring device DTH-TYPK-2K) was +112.6°C and in the structural glue +54.0°C, barely satisfying the accepted upper limits of +120°C for the GFRP (noticeable stiffening losses) and +54°C for the glue (thermolability). On site, it was therefore decided to add a layer of glass fleece to increase temperature losses.

The guard rail didn't move and the structural glue remained hard, although the glass transition temperature (+45°C) was exceeded for approximately 90 min. Although these effects are reversible, the ten slab elements were placed in an isolated containment during seven days at +35°C to increase the glass transition limit to +55°C.

The influence of high temperatures in the wooden core was not specifically analyzed, since estimated as uncritical: The massive spruce core quickly spreads the heat and the vapor pressure. Since the GFRP-layer is completely sealed and bonded to the wooden core and air pockets are chased during the vacuum infusion process, the risk of damages due to blistering and delamination can be avoided.

Table 1: Results of the preliminary tests with rolled asphalt on a big sample.

t [min]	0	10	20	30	40	90	max
Asphalt [C°]	141.8	116.0	104.4	98.8	91.1	75.2	141.8
at GFRP/wood [C°]	27.5	95.5	109.6	112.6	108.6	85.5	112.6
in structural glue [C°]	26.0	49.5	53.6	54.0	51.1	42.5	54.0

Test with Hot Grout on the Big Sample

The purpose of the second test was to measure the temperature of the GFRP-Layer due to pouring of hot grout in the transition joints located next to the slabs front face. This was effectuated on the sample of the first test, whereas one half of the front face was covered with 2 mm thick tar paper. The 80 mm thick joint was progressively filled with Risoplast 164 at +174°C. The temperature of the GFRP-Layer only increased to +90.0°C under the Hessensiegel and +80.3°C where the tar paper was added. This area is therefore uncritical.

Table 2: Results of the preliminary tests with hot grout on the big sample.

t [min]	0	10	40	75	105	max
Under seal [C°]	27.3	81.2	89.1	90.0	89.2	90.0
Under tar+seal [C°]	26.5	51.1	79.0	80.3	79.8	80.3

Test with Hot Grout on Small Samples

The purpose of the third and final test was to measure the temperature and evaluate the behavior of the GFRP-layer alone due to the heat. Two samples of 4.8 mm thick GFRP-plates were supported on two sides each, whereas the second sample also received a Hessensiegel. The +174°C hot grout was poured into a 60 mm high square frame, whereas the temperature of the upper surface (grout) and lower surface (GFRP) were measured with a laser device Bosch PTD-1.

Thanks to the Hessensiegel, the lower surface of the second sample got -13°C colder than the first sample. The GFRP-plates had a plastic deformation of approximately 5 mm, without indication of fire or liquefaction and remained waterproof. Since the GFRP-Layer will be supported by the wooden core, a temporarily low stiffness shouldn't be problematic.

Table 3: Results of the preliminary tests with hot grout on small samples.

Measurement	0	45	55	75	105	max
Grout 1st Plate [C°]	30	177	157	–	–	–
Under 1st Plate [C°]	30	103	106	–	–	106.0
Grout 2nd Plate [C°]	30	190	111	–	–	–
On 2nd Plate [C°]	30	–	115	116.0	112.1	116.0
Under 2nd Plate [C°]	30	83	93	–	–	93.0

4. ASSEMBLY

The slab elements including the guard rails were transported from Arbon to Valendas using motor truck and train carriage. Placement, calibration and assembly were effectuated with truck crane in 10 hours. The next day, the elements were fixated from underneath and sealed according to following steps: Predrilling of the GFRP with diamond bits, wood drilling, sealing of the bored hole with epoxy resin, screwing of the wood screws and sealing of the slab joints.

Fig. 3: Assembly of a sandwich slab element.

The pavement company completed the structure with draining rails, drain troughs, grouting of the expansion joints and placing the glass fleece. The rolled asphalt was placed in one stage with one small paver and one combination roller. The installation temperature of the asphalt didn't exceed 160°C, as assumed in the preliminary tests.

5. CONCLUSION

This project demonstrates that a hybrid GFRP-wood bridge slab can be realized with the conventional methods of rolled asphalting. In contrast to the Avançon-bridge, where the asphalt was tempered with adjuvants to preserve the statically activated, 22 mm thick GFRP-chords, the GFRP-envelope in Valendas was chosen only for its sealing qualities, thus reducing the layer thickness to 6 mm. Static calculations were limited to the wooden core and therefore based on established norms. These advantageous boundaries, including the short spans of 57 cm between the beams of the substructure, made the hybrid slab economically attractive compared to a steel orthotropic plate and more durable compared to a conventional wood plate. The bridge in Valendas is a reference object to observe the behavior of such a bridge slab and asphalt layer under high humidity and temperature changes.

REFERENCES

[1] S. Nendaz et al., “Tablier composite du pont sur l'avançon”, *Revue Tracés*, 2012; Vol. 138: 6 Pages.
[2] J. Stelcl, “Vorderrheinbrücke Valendas Ausführungsstatik”, *sjb kempter fitze*, 2017; 31 Pages.
[3] G. Weis, “Temperatureinfluss auf die GFK-Schutzschicht”, *Leichtbauweis AG*, 2017; 12 pages.

DOI: 10.5075/epfl-ICSS12-2018-99-101

EVALUATION OF STRENGTH AND STIFFNESS OF A FRP SANDWICH BRIDGE DECK

Tomasz W. Siwowski[1], Maciej Kulpa[2] and Lech Wlasak[3]
[1]Rzeszow University of Technology, Poland. siwowski@prz.edu.pl
[2] Rzeszow University of Technology, Poland. kulpa@prz.edu.pl
[3]Mostostal Warszawa S.A., Poland. l.wlasak@mostostal.waw.pl

1. INTRODUCTION

Bridge decks are one of the most promising fields of fibre reinforced polymers (FRP) structural application in construction nowadays [1]. Some of the favourable characteristics of these decks involve high strength-to-weight ratio, high durability (particularly large tolerance for de-icing salt), short installation time as well as possible increase of the carrying capacity of existing bridges due to replacement of the heavy concrete decks into the lightweight FRP decks. Many different FRP deck systems have been already developed, but these two main structural forms can be identified: decks made of pultruded structural shapes glued together and sandwich slabs with different face/core structures [1].

Only the latter type could be considered in the R&D project presented herein, due to current possibilities of the Polish composite manufacturers. The sandwich deck was proposed and implemented in the construction of the first Polish road bridge fully made of FRP composites [2]. The all-composite bridge superstructure is formed by four FRP composite girders with an overlying 130 mm thick FRP sandwich deck slab. The FRP deck slab is bonded to the top flanges of the girders with epoxy adhesive.

The stiffness of the proposed sandwich deck system and its resistance to wheel loads were investigated within a research project presented in this paper. Further aims were to structurally optimize the deck system according to Eurocode loads and to assess the global safety coefficients for future applications.

2. SANDWICH DECK CONFIGURATION

According to previous authors' experience [3], the best structural solution that takes both structural as well as manufacturing aspects into account, seemed to be the sandwich plate made of GFRP faces and foam core stiffened with the internal vertical GFRP ribs. The total thickness of the deck panel (130 mm) and the division between faces and core were determined by the initial composite plate analysis. As a result, the sandwich bridge deck panel consists of two 12 mm thick GFRP faces and 105 mm thick PUR foam core. To obtain the high bearing resistance to patch loading, the core is stiffened with the 2-3 mm thick vertical GFRP ribs spaced at 25 mm (Fig.1). In order to find the most economical solution of the deck, two structural parameters have been changed during this research: foam density and thickness of vertical ribs, i.e. architecture of fabrics used to fabricate the deck.

The reinforcement of panels' composites consists of two types of glass fabrics:

- bi-directional braided fabric B-E 0/90 with the grammage g=800 g/m^2;
- bi-directional knitted fabric X-E ±45 with the grammage g=600 g/m^2.

The fabric architecture in the faces and ribs are as follows:

- faces: total of 15 fabrics, [0/90$_3$, ±45, 0/90$_3$, ±45, 0/90$_3$, ±45, 0/90$_3$];
- internal vertical ribs: panel A and C – 2 fabrics, [0/90, ±45], panel B - 1 fabric, [0/90].

The core is made of PUR foam and usability of two foam's densities have been checked in this research: ρ=30 kg/m^3 and ρ=105 kg/m^3. Considering the manufacturer's experience, the VARTM technology that uses the epoxy resin as a matrix, has been chosen to fabricate the FRP sandwich deck (Fig.1).

Fig. 1: Sandwich panel configuration (left) and panel prepared for VARTM.

The different structural parameters of tested panels are shown in Table 1. Three deck panel specimens (A-C) with the overall dimensions of 130 x 1200 x 2750 mm were manufactured to find the best structural solution in terms of stiffness

and strength of the FRP sandwich deck. Bending, shear and bearing tests were performed for each panel type. The plate behavior of the specimens was ensured by applying the span length of 2.4 m during bending tests.

Table 1: Structural parameters of the tested panels.

Panel	Foam density (kg/m^3)	Ribs reinforcement
A	105	2 fabrics [0/90; ±45]
B	105	1 fabric [0/90]
C	30	2 fabrics [0/90; ±45]

3. DECK PANELS TESTING

Loading Schemes

Four loading schemes were applied for each panel type to evaluate panel behavior under bending, shear and bearing, namely (Fig.2):

- scheme 1 – four point bending according to LM-1 Eurocode model;
- scheme 2 – three point bending according to LM-2 Eurocode model;
- scheme 3 – shear loading (short beam);
- scheme 4 – bearing on the load path 0.4 x 0.4 m according to Eurocode models.

Panels' displacements and strains in several points of the top and bottom faces were measured during static tests.

Fig. 2: Loading schemes of panel specimens: scheme 1 to scheme 4 from left to right.

Panel Behavior

The behavior of all specimens under loading was very similar, regardless the panel structure (A, B, C). Both "load-displacement" and "load-strain" plots were almost linear until failure (Fig.3). The initial plot curvature is due to support adjustment in the first loading phase. However, in some cases a small "knee" effect was also observed.

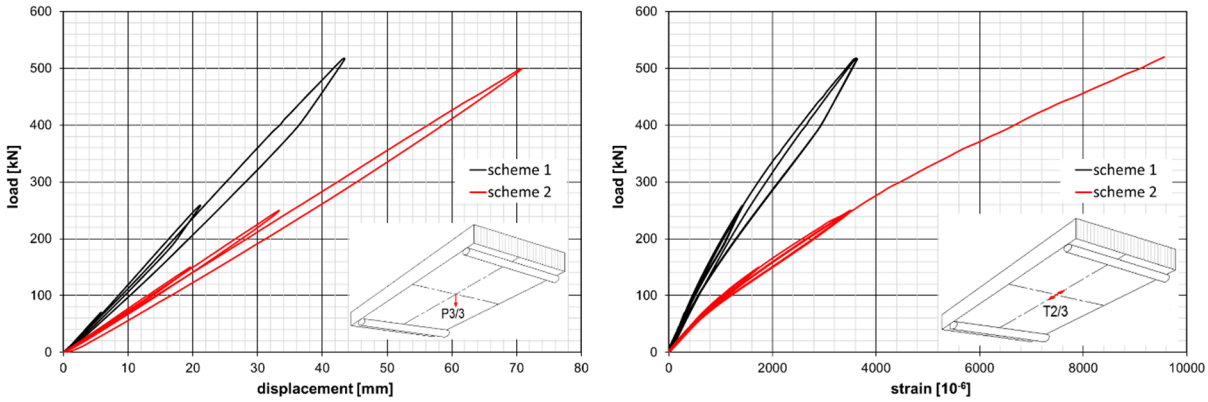

Fig. 3: Exemplary "load- displacement" (left) and "load- strain" (right) plots for scheme 1 and 2.

Failure Modes

Failure mode for each panel depended strongly on the loading scheme, i.e. the decisive inner force. For bending schemes (1 and 2), the failure in the middle of the panel was observed in the form of top face delamination along with crushing of the core foam beneath (Fig.4(a-b)). The delamination between top face and foam core at the support was observed as a shear failure mode in the scheme 3 (Fig.4(c)). Total crushing of the core, both foam and ribs, was the obvious failure mode in the scheme 4 under bearing path load (Fig.4(d)). The failures of all panels (except in scheme 4) occurred suddenly, without any warning, with loud sound of delamination. No earlier damages, neither in faces nor in core, were observed before final failure took place. In the scheme 4, slow but incremental damage of the core proceeded, until the loading was stopped. For all loading schemes, the failure mode was independent on the panel structure, i.e. foam density and rib thickness in the core. However, the panel structure has considerable influence on the total carrying capacity as well as global safety coefficient of various panel types, which is discussed below.

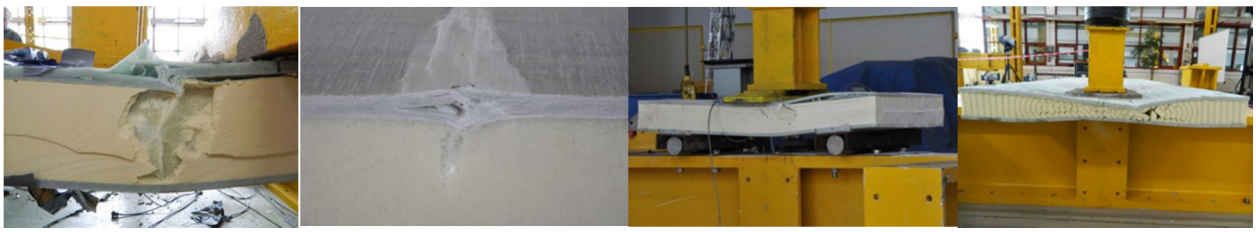

Fig. 4: Failure modes in particular loading schemes: scheme 1 to scheme 4 from left to right.

4. DISCUSSION OF RESULTS

Strength & Global Safety Coefficients

Experimentally determined strength of each panel was assumed as equal to the relevant inner force (bending moment, shear force, bearing load), calculated for the failure load of each panel under particular loading scheme. This experimental strength was divided by the characteristic inner force, calculated in the panel design under the LM-1 load model (as applied in the bridge design). The result represents the global safety coefficient of the panel in each type/loading scheme. The results for all cases under consideration are summarized in Table 3.

Table 2: Global safety coefficients of the tested panels for relevant strength cases.

Strength	Panel A	Panel B	Panel C
Bending	22.86	10.07*)	17.75
Shear	10.33	3.32	3.82*)
Bearing	5.18	3.97	2.74

*) minimum value, panel was not damaged

Taking the partial safety factors and conversion factors applied in FRP bridge design according to new European rules [4] into account, the minimum value of global safety coefficient should be greater than 3.375. Thus, only the A panel may be considered in this particular design circumstances and no material savings are allowed in the sandwich deck for the all-FRP composite bridge.

Stiffness

To compare the resultant A deck panel to another FRP sandwich decks, the approximate stiffness of the deck was assessed, basing on mid-span displacements measured in the tests of scheme I and II. No shear deformation was taken into account in this initial assessment. The plate stiffness was calculated for the panel width of 1.2 m. The stiffness calculation for the panel A is shown in Table 3.

Table 3: FRP sandwich deck stiffness calculation according to measurements (panel A).

Scheme	Max. load	Max. displacement	Stiffness	Average stiffness
	[kN]	[mm]	$[Nm^2/m]x10^6$	$[Nm^2/m]x10^6$
I	517	43,52	7,105	4,406
II	500	70,26	1,708	

The obtained plate stiffness of the tested panel is similar to another FRP sandwich decks [5]. However, the tested sandwich deck is only 130 mm deep, what means its stiffness is relatively higher than the others, considerably deeper (180 – 250 mm). Moreover, its mid-span deflection under service design load is only L/633, which is more than two times less than the allowable value assumed in design (L/300).

5. CONCLUSIONS

The tests carried out on the novel FRP sandwich deck panel confirmed its satisfying strength, stiffness and global safety coefficient to be implemented on site in the first Polish all-composite bridge. However, to obtain this good structural performance, no material savings in core may be allowed, comparing to the originally designed structure (panel A). The novel sandwich deck is also relatively stiffer than the others, implemented on various bridges worldwide.

REFERENCES

[1] M. Zoghi (Ed.), *The International Handbook of FRP Composites in Civil Engineering*, CRC Press: 2014.
[2] T.W. Siwowski et al., "The all-composite road bridge – a proposal for rapid urbanisation", *IABSE Conf. – Engineering the Developing World, Kuala Lumpur:* 2018, 8 p.
[3] M. Kulpa et al., "Structural shaping of FRP bridge decks", J. C.Eng., Env. Arch., 2015; volume: XXXII, 21 p. (in Polish).
[4] L. Ascione et al., *Prospect for new guidance in the design of FRP*, JRC Sci & Tech. Rep. No. 27666: 2016, 176 p.
[5] P. Alagusundaramoorthy et al., "Structural behavior of FRP composite bridge deck panels", *J. Bridge Eng.*, 2006; 11: 384–393.

DOI: 10.5075/epfl-ICSS12-2018-102-104

TESTING AND FEM ANALYSIS OF A NOVEL FRP SANDWICH BRIDGE DECK

Maciej Kulpa[1] and Tomasz W. Siwowski[2]
[1]Rzeszow University of Technology, Poland. kulpa@prz.edu.pl
[2] Rzeszow University of Technology, Poland. siwowski@prz.edu.pl

1. INTRODUCTION

The feasibility and potential of FRP sandwich systems in civil engineering and construction have been successfully demonstrated by various applications including bridge decks and girders [1]. The growing need of durability enhancement of the Polish road bridges has recently caused the big impulse for research on new, durable, lightweight and easy to handle bridge decks, made of FRPs (fibre reinforced polymers). Therefore, within the framework of UE 7FP PANTURA project, three structural solutions of FRP sandwich deck fabricated by VARTM technique were elaborated, fabricated and tested under static load (Fig.1). On the basis of initial test results, the stiffness, load carrying capacity and dynamic behaviour of panels were estimated and the best solution for further research was chosen [2].

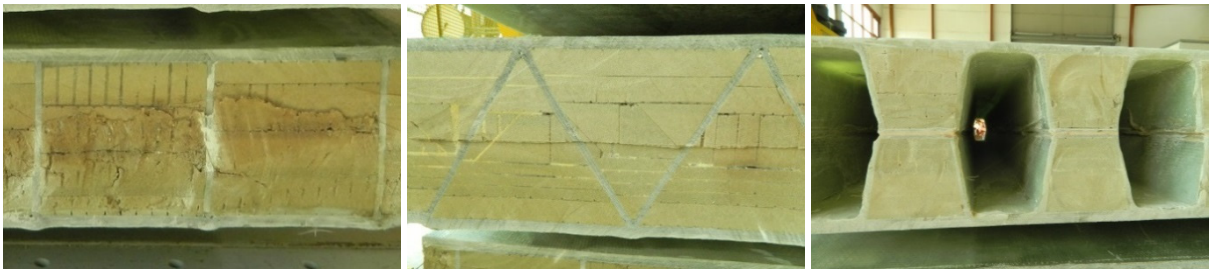

Fig. 1: Three structural solutions of sandwich FRP bridge deck elaborated within the framework of PANTURA project.

The best solution was tested on full-scale specimens to evaluate its behaviour under service, ultimate as well as dynamic load. The panel fulfilled the required criteria for ultimate capacity, serviceability and safety, therefore its application in prototype bridge construction is planned. The detailed FEM model of the panel was also elaborated and after validation against the test results, it is planned to be used in designing of the actual FRP bridge. The deck structure, some test results of the full-scale panel as well as FEM model validation procedure is presented in the paper.

2. SANDWICH DECK CONFIGURATION

According to comprehensive research works [3] and taking manufacturing aspects into account, the deck with trapezoidal ribs and internal openings turned out to be the best solution (Fig.1, right). Except for the best structural behavior, considering strength and stiffness, the following manufacturing aspects also heavily contributed to choosing this solution: simplifying the VARTM fabrication process and its control, improving panel faces quality and savings of core material. The panel is made of two symmetrical parts which are bonded together in the panel's mid-plane. Thus, the resultant sandwich deck is made of GFRP faces and foam core stiffened with the internal GFRP ribs.

The structural form and material selection for faces and core were determined by the initial plate analysis [3]. As a result, the sandwich bridge deck consists of two 17 mm thick GFRP faces and 222 mm thick PVC foam core, having the total thickness of 256 mm. The deck laminates are made of two types of glass fabrics: bi-directional braided fabric B-E 0/90 with the grammage g=800 g/m^2 and bi-directional knitted fabric X-E ±45 with the grammage g=800 g/m^2, and epoxy resin as the matrix. The fabric architecture as well as the overall dimensions of faces and ribs are shown in Fig.2. The 3 mm thick layer of standard epoxy adhesive was used to bond two parts of the deck.

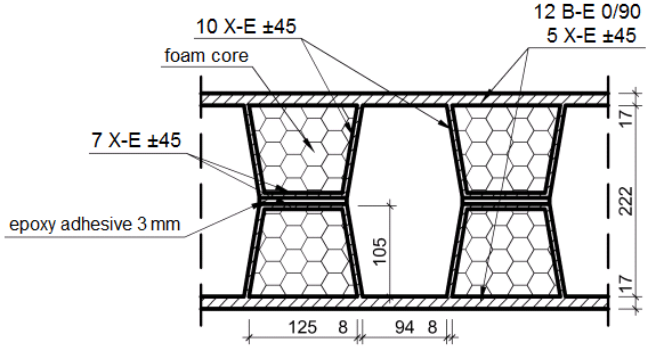

Fig. 2: FRP sandwich deck configuration.

3. FULL-SCALE DECK PANEL TESTING

Test Scheme

The static tests were carried out on the full-scale deck panel with the dimensions of 5.3 × 1.9 m. To simulate the actual bridge deck behavior, the two-span scheme of the panel 2 x 2.4 m was applied in the test. The LM-1 loading scheme according to Eurocode [4] was chosen to evaluate panel static behavior under bending and shear (Fig.3). Panel displacements and composite strains of the top and bottom faces were measured in several dozen points of the panel.

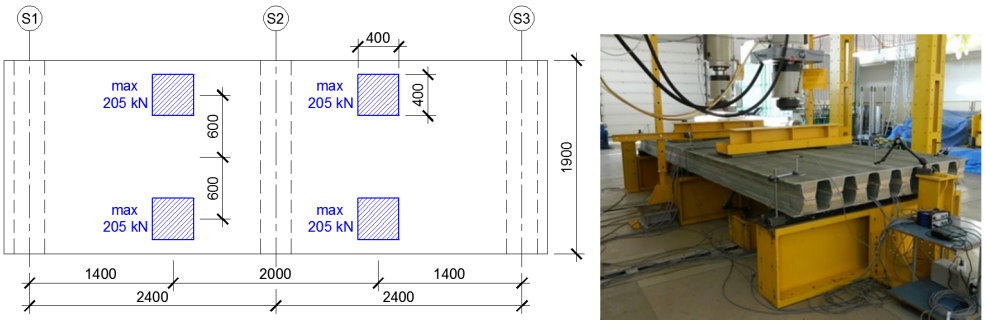

Fig. 3: LM-1 loading scheme and the full-scale panel on the test stand.

Panel Behavior

The behavior of the panel under static load was linear until failure. The exemplary "load-displacement" and "load-strain" plots in full range of static loading are shown in Fig.4. The initial plot curvature is due to support adjustment in the first loading phase. The mid-span deflection under service design load was only L/627, which is more than two times less than the allowable value assumed in design (L/300). Maximum mid-span strain in composite of the bottom face was about 1.25 ‰, which constitutes only 7% of the GFRP failure strain. No failure of the panel was observed under the full-range loading, i.e. the total load of 820 kN, which corresponds to the design load of LM-1 model according to Eurocode [4].

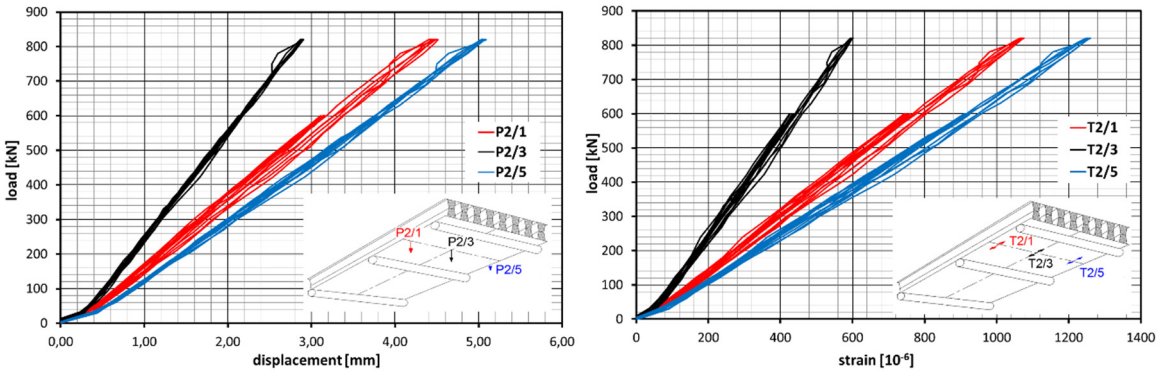

Fig. 4: Exemplary "load- displacement" (left) and "load- strain" (right) plots.

4. FEM ANALYSIS

ABAQUS code was used for FEM analysis of the panel. All panel laminates were modelled with 4-node shell elements based on Mindlin's plate theory. The 25 × 25 mm shell elements had the assumed thickness taking the actual number of laminas into consideration. Additionally, the 8-node solid elements were used to model the bondline as well as supporting steel plates and contact elements. To simplify the FEM calculations, foam core was not modelled but this is a safe side design assumption. The numerical model of the FRP sandwich panel consisted of total of 75 072 shell elements and 13 008 solid elements (Fig.5).

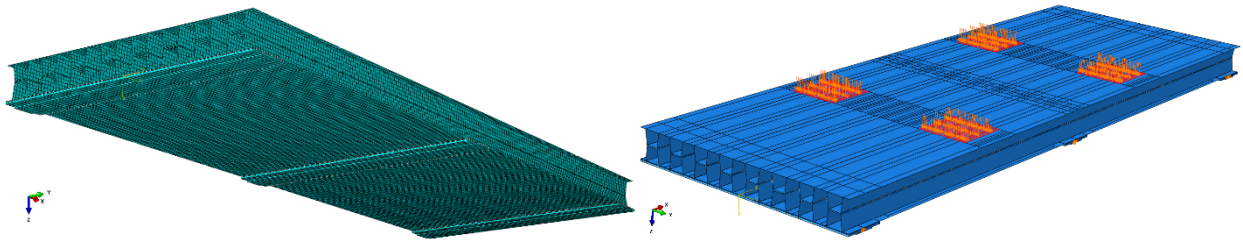

Fig. 5: FEM model of the panel and the loading.

The characteristic parameters for the both bi-directional glass-fiber laminas were determined by material testing and used to define the orthotropic layers in shell elements. The testing load was modelled by means of uniform pressure applied on four squares with the dimensions of 0.4 x 0.4 m according to Eurocode [4].

The FEM analysis results were obtained in the form of displacement or strain maps in each particular laminas of all panel composites (faces and core ribs). The exemplary displacement and strain maps are shown in Fig.6.

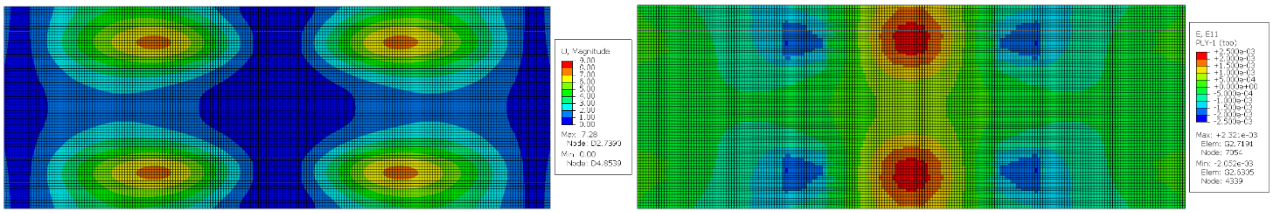

Fig. 6: Displacement map of the bottom face laminate (left) and longitudinal strain map of the top face laminate under the LM-1 characteristic loading.

5. FEM MODEL VALIDATION

The FEM model validation was performed by comparing the experimental and numerical results obtained in each discrete displacement and strain measurement point. Two plots of arbitrary displacements and strains in the mid-section of panel span under the characteristic LM-1 loading are shown in Fig.7, to compare experimental and numerical values.

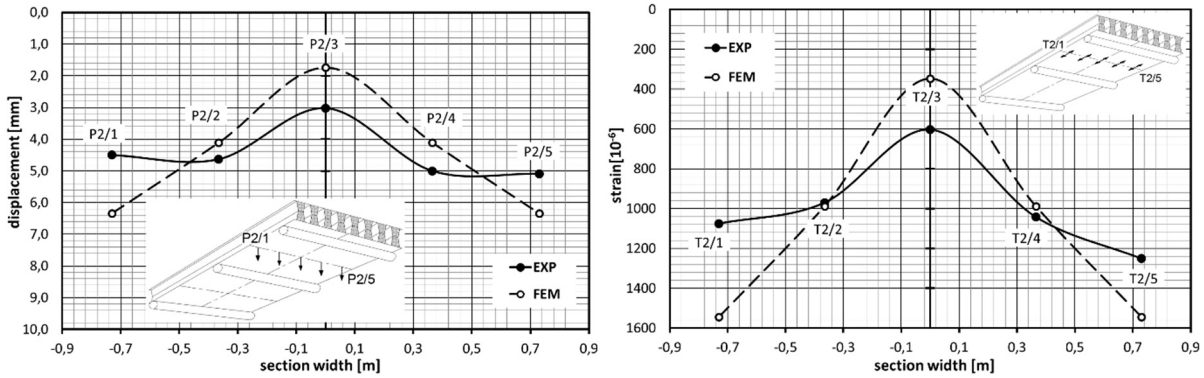

Fig. 7: Experimental versus numerical displacements (left) and strains (right) comparison.

The comparison shows that experimental displacements and strains close to panel edges are 25% lower than the numerical ones but the latter are as high as in the panel's longitudinal axis. The transverse stiffness of the actual panel was higher than the relevant stiffness obtained numerically. The basic reasons of the difference between experimental and numerical behavior of the FRP sandwich panel are: foam core was not modelled and the "pressure" patch load did not exactly simulated the actual bearing. Moreover, the material parameters applied in FEM analysis were determined for laminas not laminates. Finally, some internal flaws and geometrical nonconformities decreasing the overall quality of the actual panel also influenced these differences. Because the average differences for particular load cases were too big, it was decided to modify the numerical model. However, having in mind the application of the FEM model in practical design, the numerical model that does not increase the computation time has been created.

As the transverse stiffness of panel was the main reason of FEM/experiment discrepancy, the material parameter adjustment seemed to be the most efficient way to modify numerical model. Using *lamina* material model implemented in ABAQUS code, trial and error procedure was applied to find equivalent material properties in particular laminas and to obtain the displacement and strain compatibility in most load cases and points of the panel. The procedure was stopped if the average discrepancy between experimental and numerical values was below 15 %. In this way, the final design model was created without increasing the number of finite elements and computation time [5]. Moreover, the further research carried out on the novel FRP deck panel confirmed its satisfactory strength and stiffness to be implemented on site in bridge redecking.

REFERENCES

[1] A.Manalo et al., "State-of-the-art review on FRP sandwich systems for lightweight civil infrastructure", *J. Comp. Constr.*, 2017; 21: 16 p.
[2] M.Kulpa et al., "Structural shaping of FRP bridge decks", *J. Civ. Eng., Env. Arch.*, 2015; XXXII: 21 p. (in Polish).
[3] M.Kulpa et al., "Modelling and numerical analysis of GFRP composite panels of bridge deck", *3rd Polish Congress of Mechanics & 21st Computer Methods in Mechanics*: 2015, 2p.
[4] PN-EN 1991-2: *Eurocode 1: Actions on structures. Part 2: Traffic loads on bridges*, PKN, Warsaw: 2011.
[5] M.Kulpa, Strength and stiffness of FRP bridge decks, Dissertation, Faculty of Civil and Environmental Engineering and Architecture, Rzeszow University of Technology, Poland, 2017 (in Polish).

SESSION 5A: DELAMINATION / DISBOND

DOI: 10.5075/epfl-ICSS12-2018-106-108

FROM DYNAMIC DEBONDING FAILURE TO INTERFACE CHARACTERIZATION IN SANDWICH SYSTEMS

Gilad Mulian[1] and Oded Rabinovitch[2]
[1] PhD student, Faculty of Civil and Environmental Engineering, Technion Israel Institute of Technology, Technion City, Haifa, 32000, Israel. giladmu@technion.ac.il
[2]Professor, Abel Wolman Chair in Civil Engineering, Faculty of Civil and Environmental Engineering, Technion Israel Institute of Technology, Technion City, Haifa, 32000, Israel. cvoded@technion.ac.il

1. INTRODUCTION

Sandwich structures are layered structural systems that are composed of distinct material layers that considerably differ in thickness, stiffness, strength, thermomechanical properties, density, and role in the structural assembly. Due to their layered nature, such sandwich systems include interfaces that combine the physical layers together. Examples of such interfaces are found al the link between the core and the face sheets in classical sandwich applications but also between the adhesive layers and the adherents in adhesively bonded structural forms.

The functioning of all such forms critically depends on the ability to transfer tractions across the interfaces and on their ability to maintain compatibility of deformations and the composite action of all components. Failure of those interfaces and the evolution of a debonding mechanisms has fatal implications on the performance of the sandwich structure and, even more important, on its safety. The criticality of the debonding mechanism becomes particularly prominent when the failure of the interfaces diminishes the sandwich action and yields a sudden release of elastic energy. This effect is directly converted into a rapid growth of the debonding crack with crack front velocities that may reach the order of 10^3 m/s [1-3], abrupt evolution of a new structural state with time scales in the sub-ms range, and a significant dynamic response.

The aforementioned characteristics clearly define the debonding failure as dynamic by nature. The analysis and design of sandwich structures therefore has to take into account the presence and the behavior of interfaces as well as their dynamic failure mechanism and its impact on the layered structure. Specifically, the analysis has to span between service state performance where the interfaces maintain the integrative nature of the sandwich structure and the ultimate state behavior where they govern the dynamic debonding mechanism.

An attractive concept that introduces interfaces into the analysis while reflecting the physics of their behavior and the potential debonding mechanism is the cohesive interface approach. The cohesive interface defines the tractions that evolve across the interface between two adjacent components as nonlinear functions of the interfacial displacement jumps across that interface (tangential slip and normal separation). The nature of the nonlinear traction-displacement jump relations is such that under relatively small levels of slip and separation, the system reacts in a quasi-linear form with a rather stiff interfacial behavior. This phase minimizes the displacement jumps in the sense of a penalty method aiming to maintain compatibility of deformations across the interface. Under increasing levels of slip and/or separation, the tractions grow up to a maximum and then decay up to total fading. This phase simulates debonding.

While the cohesive interface is a powerful analytical and computational tool, it is a phenomenological one that necessitates calibration and assessment of the governing parameters. The smallest set of such interfacial properties includes the characteristic length parameter that defines the point of peak traction, the specific work of separation (fracture energy), and the functional form of the nonlinear cohesive laws. Additional features are the tangential-normal coupling, different shear and normal fracture energies, different shear and normal critical displacements and strengths, damage accumulation, rate dependent effects, etc.

The concept of the cohesive interface can be directly implemented the structural model, but the determination of the interfacial parameters is a challenge that necessitates the combination of two critical components. The first one is a sound set of experimental observations, measurements, and data that quantifies the debonding failure mechanism. Due to the dynamic nature of that mechanism, the experimental basis has to reside in the dynamic region providing observations on the kinematics of the debonding process. The second component is an analytical model and its numerical counterparts. The model should reflect the physical features of the debonding phenomenon, host the cohesive interfaces, and quantify the response of the test specimens and the target application. Also here, the dynamic nature of the problem necessitates its handling using dynamic analytical and numerical methodologies. The combination of experiment and modeling aims at throwing light on the nature of the failure mechanism, provide a framework for its quantification, and set the rules for the assessment of the latent parameters of the structure.

The aim of this paper is twofold. First, it aims to explore, quantify, describe, and characterize the dynamic debonding phenomenon in layered and sandwiched structures. Second, it aims to set forth an approach for using the direct experimental observations and the analytical/numerical data regarding the dynamic nature of the debonding process for the characterization the latent properties of the cohesive interfaces implemented in the framework. The specific sandwich

application that is investigated in this paper focuses on beams strengthened with externally bonded layers of FRP. The bonded FRP layer serves here as supplemental tensile resisting reinforcement while the layered layout that includes the original substrate beam, the FRP layer, and the adhesive layer defines it as a sandwich beam. The role that is played by the interfaces in such configuration, and the fact that dynamic debonding failures are among its most common and yet critical modes of failure, draw the attention to that type of application.

2. METHODOLOGY

Following the dual objective of the paper, the methodology adopted for achieving its goals also combines two components. The first one integrates analytical modeling, numerical methodologies, and experimental methods that are all focused on the dynamic interfacial failure of the sandwich beam. The analytical model is based on the extended high-order sandwich theory that is extended to account for the dynamic effects and the interfacial nonlinearity associated with the debonding mechanism [4-5]. The numerical approach converts the analytical model and its physical modeling concepts into a specially tailored high-order finite element form [1]. The experimental method uses four point bending tests of sandwich beams specimens made of steel, epoxy, and FRP for the detection of the interfacial debonding kinematics. This is achieved using high-speed photography, digital image processing, and detection of the movement of the debonding front in time and in space [2-3].

The second objective of the paper is faced by the development of an algorithmic approach that uses the experimental observations and the analytical/numerical tools for the interfacial characterization. Specifically, it uses the experimentally detected critical load and critical displacement where the debonding mechanism initiates, the duration of the process up to its arrest, the crack length at arrest, the averaged crack front velocity, and the temporal crack front velocity as features incorporated into the objective function. The characterization approach uses those experimental observations as target parameters for the calibration of the interfacial properties implemented in the analytical/numerical model. On the one hand, for simplicity, the implemented cohesive laws are taken in a rather simple form where the functional basis and the coupling effects are pre-determined, the shear fracture energy and the work of separation are equal, and the only "free" variables are the characteristic length parameter and the specific work of separation. On the other hand, the calibration algorithm resides in a highly nonlinear and dynamic regime that necessitates adequate analytical and numerical tools. The effectiveness of the aforementioned procedure is examined through comparison of the behavior described by the calibrated model and the one observed in an independent experiment. This aims to look into the dynamic aspects of the response and to explore additional features that are beyond the scope of the experimental method.

3. RESULTS

To illustrate the above methodologies, and mainly the experimental approach to the detection of the debonding kinematics, the experimental setup developed and presented in Mulian and Rabinovitch [2,3] is revisited. The setup is schematically illustrated in Fig. 1. A sketch of the tested specimen and a photo of the specimen on the testing rig before loading are also depicted in Fig. 1. The test specimen is a three-layer structural system comprised of a steel base plate, a 3-4 mm thick epoxy adhesive layer, and a 1.2 mm thick CFRP layer. The mechanical monitoring of the test specimen is limited to measurement of the load, the displacement of the loading piston, and the midspan displacement of the specimen. The main crack monitoring methodology uses high-speed photography with a rate of about 88,000 frames per second. The resulting snapshots are then digitally processed in attempt to trace the debonding front and thus to capture the debonding failure in progress. Analysis of the specimen, which is intentionally designed with some level of a-symmetry, reveals that failure is expected to initiate near the left FRP edge, take the form of an interfacial debonding, and propagate at the adhesive-substrate interface [2]. This allows focusing the monitoring efforts on the left side of the specimen aiming to capture the process in a smaller photographed window, see Fig. 1. More details about the experimental methodology and the test setup are given [2].

An illustrative set of experimental results [3] is shown in Fig. 2 where a set of snapshots taken by the high-speed camera at intervals of $11.36 \cdot 10^{-6}$ s is depicted. The green cross-marks shown in the figure designate the location of the crack tip. The processing of such experimental results allows tracing the evolution of the crack length and mainly the velocity of the crack front and its variation in time. The relevance of the experimental results is therefore threefold. First, it allows to gain insight into the debonding failure and to assess its dynamic nature. Second, it inspires the development of analytical and numerical models that can further explore the dynamic features of the response. Third, it provides direct experimental data that can be used for the calibration and validation of the analytical and numerical models and particularly for the detection of the latent properties of the interfaces. The three aspects, and particularly those that are focused on the interfaces, are at the focus of the current investigation.

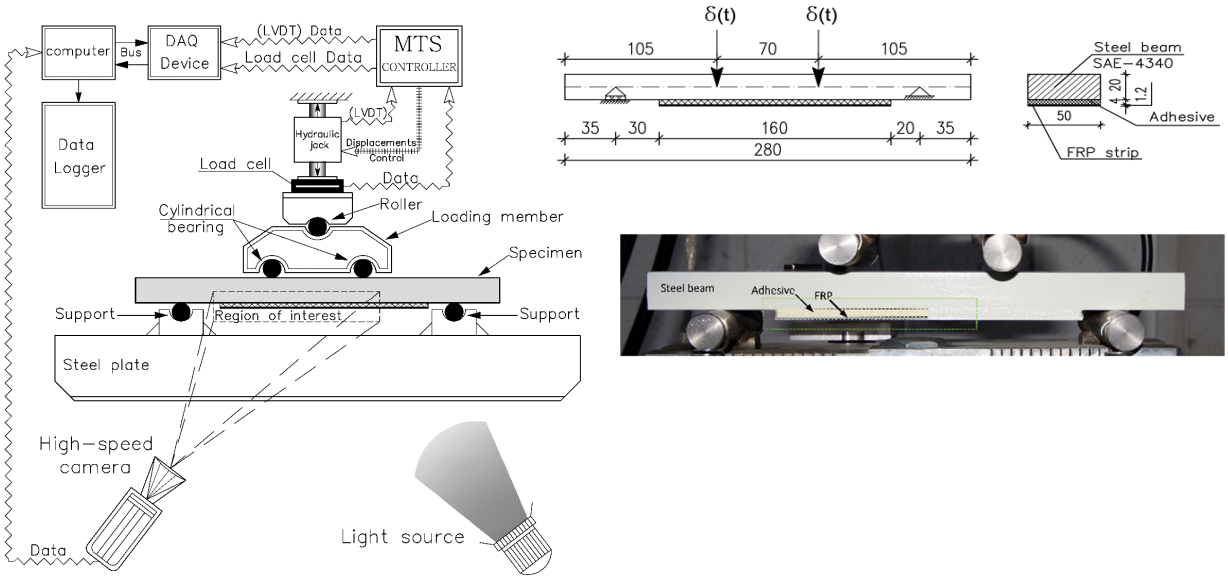

Fig. 1: Experimental setup and the test specimen (adapted from Mulian and Rabinovitch [2,3]).

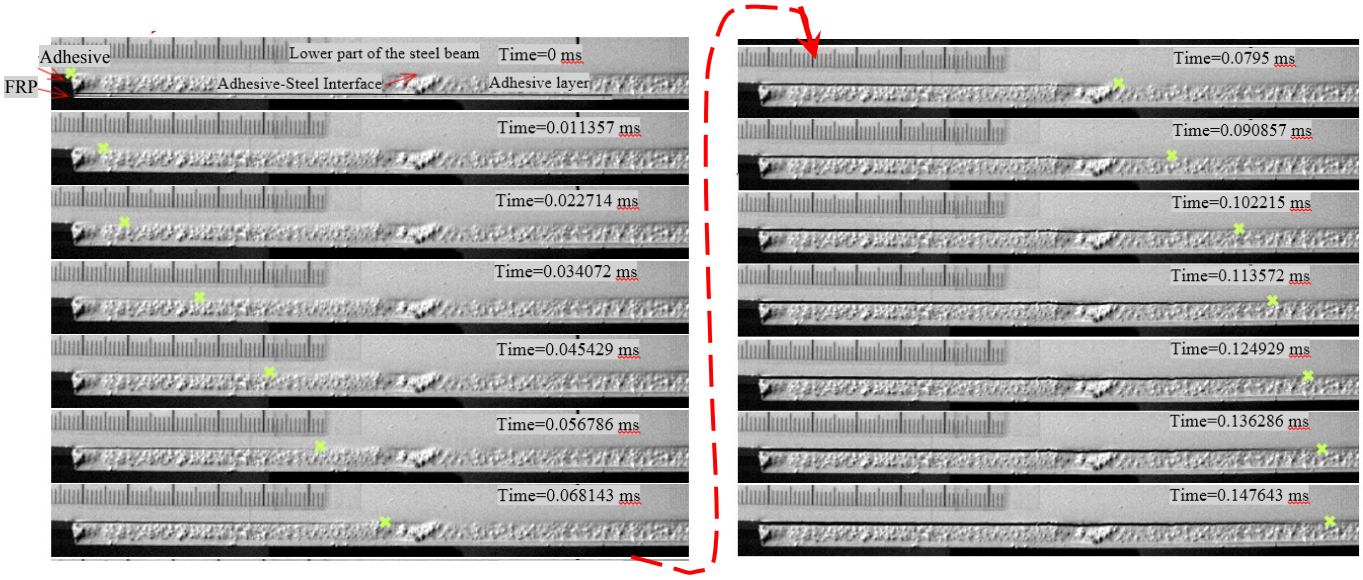

Fig. 2: Evolution of the interfacial debonding crack in time – experimental results (adapted from Mulian and Rabinovitch [3]).

REFERENCES

[1] Mulian, G. and Rabinovitch, O. (2015) "Debonding Dynamics in FRP Plated Beams: High Order Cohesive FE Formulation and Parametric Sensitivity", International Journal of Fracture, 195(1):53-78.

[2] Mulian, G. and Rabinovitch, O. (2016) "Experimental and Analytical Study of the Dynamic Debonding in FRP Plated Beams", International Journal of Solids and Structures, Volumes 92–93, 15 August 2016, Pages 121-134

[3] Mulian, G. and Rabinovitch, O. (2017) "Impact of Interfacial Non-Uniformity on the Dynamic Debonding in FRP Plated Beams", Journal of Engineering Mechanics, 143(9): 04017084-1:15

[4] Rabinovitch, O. (2014a) "Dynamic Edge Debonding In FRP Strengthened Beams", European Journal of Mechanics, 47: 309–326.

[5] Rabinovitch, O. (2014b) "An extended high order cohesive interface approach for the debonding analysis of FRP strengthened beams", International Journal of Mechanical Sciences, 81: 1-16.

DOI: 10.5075/epfl-ICSS12-2018-109-111

INTERFACIAL CRACK PROPAGATION IN AXIALLY COMPRESSED SANDWICH PANELS - EXTENDED HIGH-ORDER SANDWICH PANEL THEORY APPROACH

Itay Odessa[1], Yeoshua Frostig[2] and Oded Rabinovitch[3]
[1]Faculty of Civil and Environmental Engineering, Technion - Israel Institute of Technology, Haifa 32000, Israel. itay.od@campus.technion.ac.il
[2]Ashtrom Engineering Company Chair in Civil Engineering, Technion - Israel Institute of Technology, Faculty of Civil and Environmental Engineering, Haifa, 32000, Israel. cvrfros@technion.ac.il
[3]Abel Wolman Chair in Civil Engineering, Technion - Israel Institute of Technology, Faculty of Civil and Environmental Engineering, Haifa, 32000, Israel. cvoded@technion.ac.il

1. ABSTRACT

The investigation presents a nonlinear model for the analysis of the interfacial debonding propagation in sandwich panels. The model combines the Extended High-Order Sandwich Panel Theory with a cohesive interface modeling. The model derived using the first order shear deformation kinematic assumptions for the face-sheets and high order small deformations kinematic ones that include out-of-plane compressibility for the core. The cohesive interfaces join the three components of the sandwich panel and introduce the interfacial nonlinearity into the model. These interfaces are governed by nonlinear traction-displacement gap laws that allow capturing the failure mechanism of interfacial debonding propagation. This effect is combined with the geometrical nonlinearity and the instability associated with the buckling of the thin delaminated face-sheet. The cohesive interface parameters are calibrated to match to experimental results available in the literature. The results are compared with experiments of three specimens and loading configurations: Double Cantilever Beam (DCB), Cracked Sandwich Beam (CSB), and end-shortening (ES) test. In the DCB case, the crack tip is subjected to a global mode I and in the CSB case global mode II. This mode requires the consideration of interfacial contact conditions that prevent penetration of the delaminated face-sheet into the core. In the ES test case, the sandwich panel is subjected to an in-plane compression loading that introduces geometrical instabilities. This effect, along with the presence of pre-existing delaminated regions trigger buckling of the compressed face-sheet, evolution of a debonding mechanism, and a further growth of the delaminated region. The comparison of the analytical results with the experimental ones focuses on the linear response, the nucleation of the interfacial debonding crack, the phase of interfacial crack progression, and the local/global interfacial and geometrical instabilities. The analytical model, which is validated through the comparison with the experiments explores additional features of the debonding mechanism in sandwich panels that are beyond the capabilities of the experimental technique.

2. RESULTS

The experimental results of the DCB specimens in terms of load vs. displacement [1,2] and the numerical results of the extended high order model [3] appear in Fig. 1. The results are presented for two DCB specimens: one with a 15 mm thick core and other with a 20 mm core.

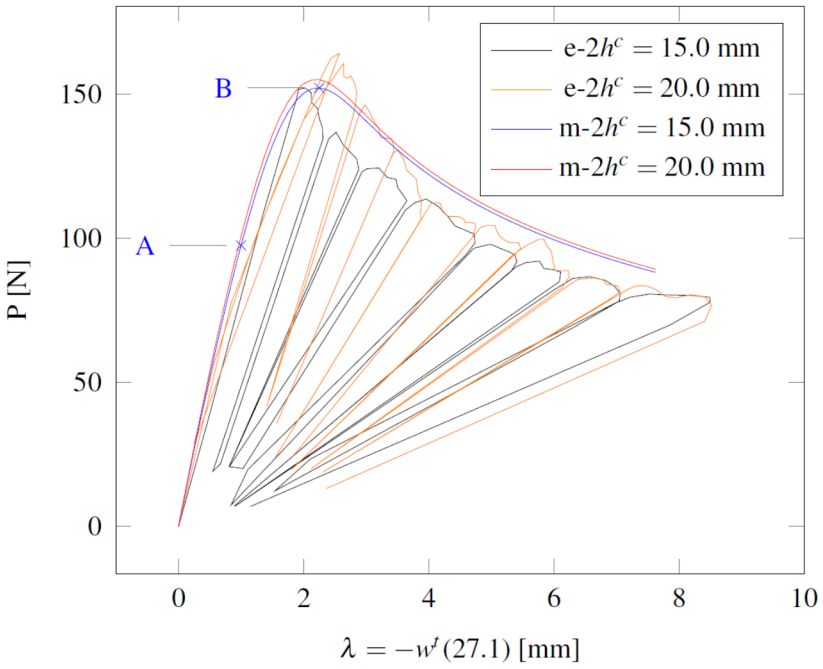

Fig. 1: Experimental [1-2] and model [3] load-displacement curves of two DCB sandwich specimens (e-experiment, m-model).

The load-displacement curves in Fig. 1 (black and blue curves) show that the numerical results are in good agreement with the global envelope of the experimental ones. The correlation includes the initial linear stage, the ultimate load, and the descending branch of the load. This branch, which reflects a decrease in load and is attributed to the interfacial crack propagation phase. In the experiment, this phase is associated with unloading and re-loading cycles which are not considered here. However, the theoretical results of the analysis match the envelope of those experimental cycles very well. The comparison with the experiments allow to calibrate the properties of the cohesive interface. In this case, the properties are calibrated using the experimental results of the thinner core. Using the same calibrated cohesive interface parameters for thicker core yields satisfactory results that well compare with the experimental measurements (orange and red curves in Fig. 1).

The analytical [3] and experimental [4] results of load vs. mid-span displacement for the CSB specimens appear in Fig. 2.

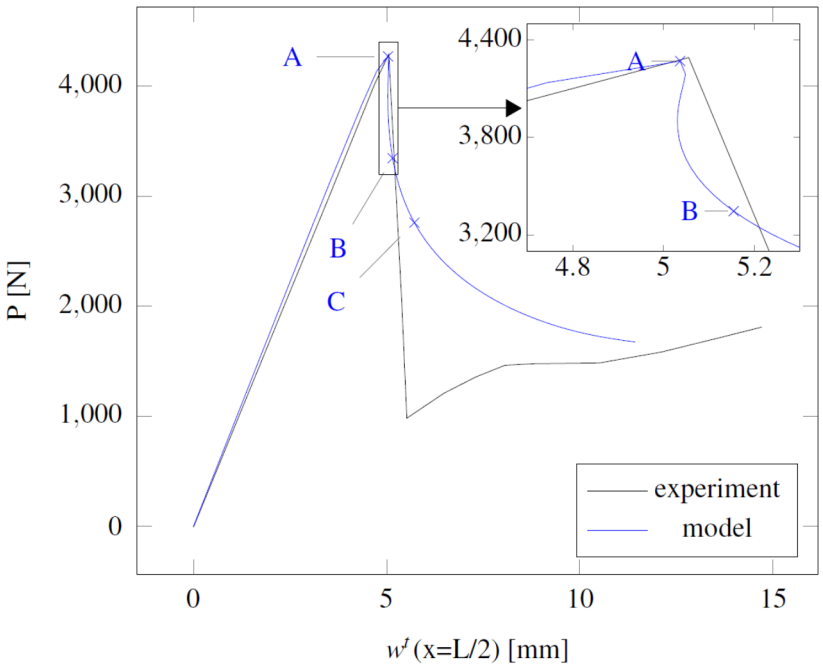

Fig. 2: Experimental [4] and model [3] load-displacement curves for CSB sandwich specimen.

The results of the model for the CSB case are in good agreement with the experimental ones, see Fig. 2. This correlation includes the linear phase, the ultimate load, and the initial phase of the debonding where the load drops. Notice that in the experiment, the load drop is sharper than in the model and it may be attributed to the dynamic effects of the response. Rinker et al. [4] noted that the crack propagation is not stable and it has occurred in one-step of expansion up to mid-span. This crack propagation drove the specimen into the dynamic regime, which is not discussed here. Yet, the model captures the instability reflected by the load drop and the snap-back of the response beyond the peak load.

The experimental setup of the ES specimen [5] appears in Fig. 3. In general, this setup reflects an axial compression test where a sandwich panel is axially loaded through stiffened clamps at its edges, denoted as edge-beam. Yet, the layout of the sandwich panel, the presence of pre-existing delaminated regions, the slenderness of the compressed face-sheet in the delaminated region, and the geometrical and interfacial nonlinearities yield a response of buckling instability, out-of-plane deformations, and evolution of a debonding process. The real boundary conditions (BCs) are modelled using the concept of an edge-beam with a rotation spring that enables a range of conditions from fixed edges to hinge ones.

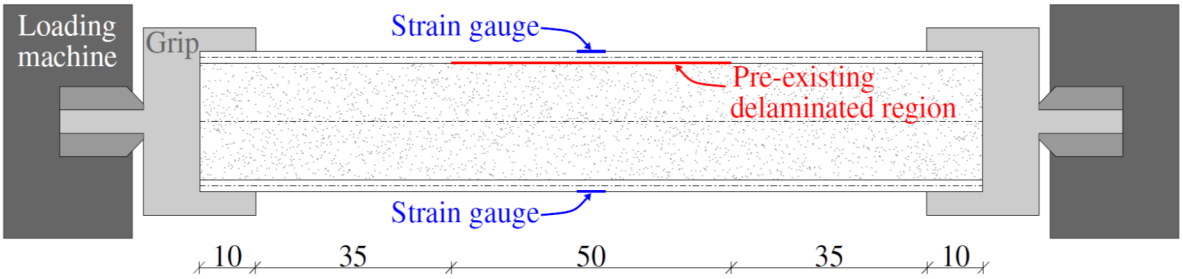

Fig. 3: ES specimen [5].

The numerical and experimental [5] results of the ES specimen in terms of load vs. strains of outer fibers of ES sandwich panel at mid-span appear in Fig. 4.

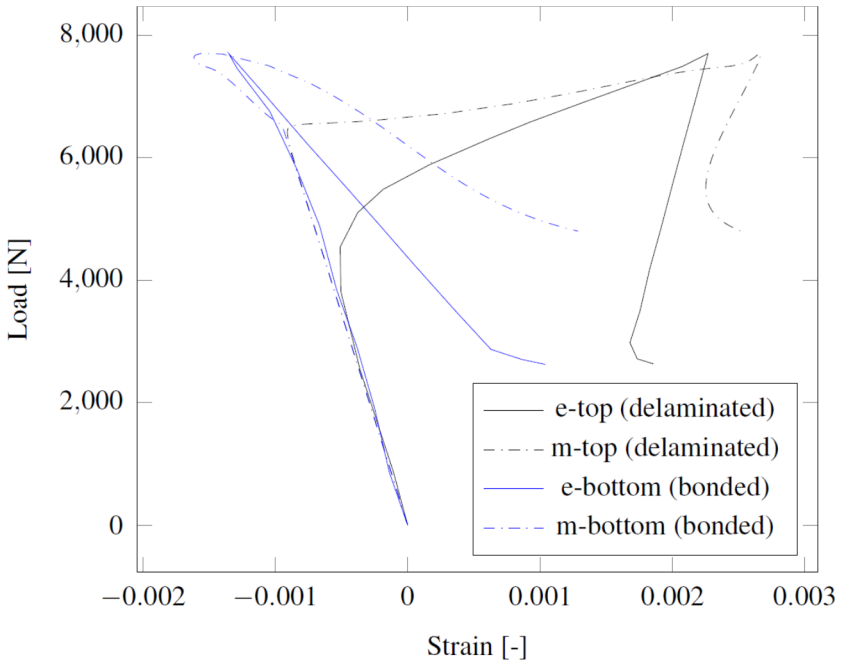

Fig. 4: Load vs. strains of outer fibers of an ES sandwich panel at mid-span, experimental [5] and model results (e-experiment, m-model).

The numerical results are in good agreement with the experimental ones, see Fig. 4. This comparison includes the linear phase and the ultimate load. In addition, the buckling and post-buckling behavior of the delaminated face-sheet that are observed in the experiment are reflected by the strains of the top face-sheet. The numerical results compare well with the experimental ones for the debonding phase where the load drops. The strains of the top face-sheet (delaminated) beyond the peak load alter their trend twice, similar to experiment's measurements. The strains of the bottom face-sheet (bonded) also follow the behavior of the experiment. Beyond the peak load, the strains are growing and even become positive. The deformed shape of the modelled sandwich panel consists of an "opening" mode, where the two face-sheets move in opposite directions similar to that of the experiment (see [5]). Please notice that the numerical results are highly sensitive to the exact definition of the BCs. Minor changes in the BCs may alter the response significantly. This sensitivity requires an enhanced investigation when modelling compressed delaminated sandwich panels of combined geometrical and interfacial instabilities.

REFERENCES

[1] Prasad S., “Investigation of Debonding and Crack Kinking in Foam Core Sandwich Beams”, *Florida Atlantic University Master’s Thesis*, 1993.

[2] Prasad S., Carlsson L.A, “Debonding and crack kinking in foam core sandwich beams-II. Experimental investigation”, *Eng. Fracture Mech.*, 1994, 47 (6), 825–841.

[3] Odessa I., Frostig Y., Rabinovitch O., “Modeling of interfacial debonding propagation in sandwich panels”, *International Journal of Solids and Structures*, 2017, *In Press*, https://doi.org/10.1016/j.ijsolstr.2017.10.014.

[4] Rinker M., John M., Zahlen P.C., Schäuble R., “Face sheet debonding in CFRP/PMI sandwich structures under quasi-static and fatigue loading considering residual thermal stress”, *Eng. Fracture Mech.*, 2011, 78 (17), 2835–2847.

[5] Nieh, Y.-H., Lai, Y.-K., Tsai, J.-L., “Characterizing failure behaviors of debonded composite sandwich structures under compressive loading”, *Journal of Sandwich Structures & Materials*, 2015, 17 (5), 578–594.

DOI: 10.5075/epfl-ICSS12-2018-112-113

KINEMATIC STUDY OF DCB-UBM SANDWICH FRACTURE SPECIMEN

Vishnu Saseendran[1], Christian Berggreen[2] and Leif A. Carlsson[3]
[1]Department of Mechanical Engineering, Technical University of Denmark, Denmark. vsas@mek.dtu.dk
[2] Department of Mechanical Engineering, Technical University of Denmark, Denmark. cbe@mek.dtu.dk
[3] Department of Ocean and Mechanical Engineering, Florida Atlantic University, USA. carlsson@fau.edu

1. INTRODUCTION

The face/core disbond or debond problem in sandwich composites has received wide attention in recent years as many in-service structural failures have been attributed to debonds [1, 2]. There is a need to address the disbond problem under generalized loading conditions for sandwich structural components employed across various sectors. In order to understand the phenomenon of face sheet/core debonding, reliable methodologies to characterize the interface debond must be developed. One such methodology, which have been proven to be robust for mixed-mode fracture characterization of sandwich debonding is the Double Cantilever Beam loaded with Uneven or unequal Bending Moments (DCB-UBM) specimen, which was first introduced by Sorensen et al. [3] for laminate composites and later extended to sandwich composites by Lundsgaard-Larsen et al. [4] (see Fig.1).

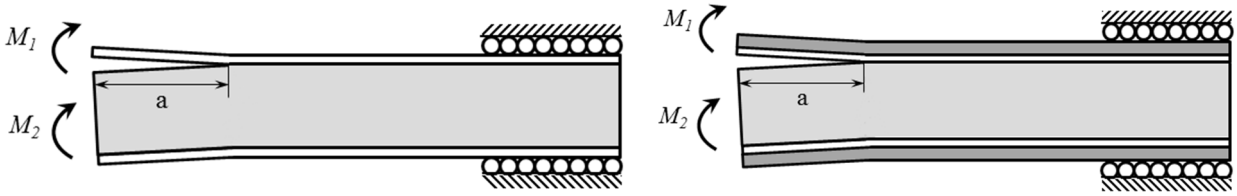

(a) (b)

Fig. 1: Schematic illustration of DCB-UBM sandwich specimen: (a) un-reinforced, (b) reinforced with doubler layers.

The DCB-UBM sandwich specimen has been proven to be robust for interface characterization of typical sandwich configurations [5, 6]. It should be noted that the energy-release rate of a moment loaded beam is independent of crack length [7]. There are many ways in which the DCB specimen can be subjected to uneven or unequal bending moments, such as through special jig and fixture design, long wires or through direct independent torsional actuators. A modified DCB-UBM test method in which the specimen is subjected to moments through independent actuators have been shown to achieve a wide range of mixed mode conditions. However, the kinematic solution of the DCB-UBM specimen has not been developed yet. Without any closed-form kinematic expressions, it has become a difficult task to characterize the kinematics of various test rigs. The aim of the current investigation is to derive the kinematic solution of a DCB-UBM sandwich specimen, using the beam on elastic foundation approach.

2. FOUNDATION MODEL APPROACH ON MOMENT-LOADED SCB SPECIMEN

A simplified analysis of DCB-UBM specimen was carried out by assuming the lower face sheet to be fixed. Such a simplification leads to a typical Single Cantilever Beam (SCB) sandwich specimen loaded with an edge couple, M_1. The Winkler mechanical model which was first utilized by Kanninen [8] for homogenous DCB specimens, was employed to obtain the deformation characteristic of a moment-loaded SCB sandwich specimen by Saseendran et al. [7]. A schematic illustration of the beam on elastic foundation approach is shown in Fig. 2. The compliance of a moment loaded SCB specimen can be expressed as the ratio of rotation to the applied moment as [7]:

$$C = \frac{|\theta(-a)|}{M_1} \tag{1}$$

The deflection of the moment loaded SCB specimen (see Fig. 2) is given by [7]:

$$w(x) = M_1 \begin{cases} \dfrac{x^2}{2EI} - \dfrac{4\lambda^3 x}{k} + \dfrac{2\lambda^2}{k}; (-a \le x \le 0) \\ \dfrac{2\lambda^2}{k}\left[f_1(\lambda x) - f_2(\lambda x)\right]; (0 \le x \le \infty) \end{cases} \tag{2}$$

where $f_1(\lambda \mathrm{x}) = e^{-\lambda x}\cos(\lambda \mathrm{x})$ and $f_2(\lambda \mathrm{x}) = e^{-\lambda x}\sin(\lambda \mathrm{x})$, and λ is defined by:

$$\lambda = \sqrt[4]{\frac{k}{4E_f I}} \tag{3}$$

where k is the elastic foundation modulus.

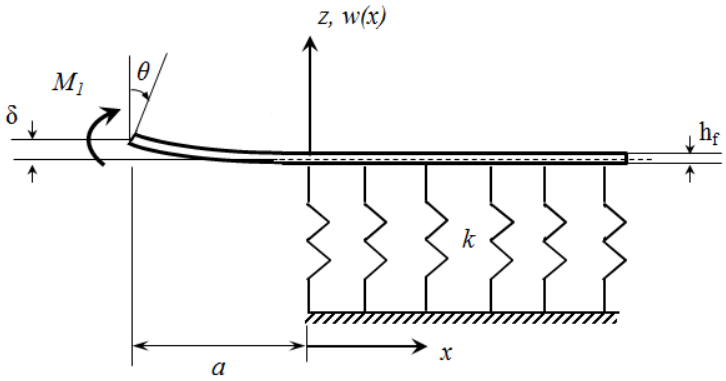

Fig. 2: Beam on elastic foundation approach of a moment-loaded SCB sandwich specimen.

Progressive derivative of Eq. 2 will yield rotation which make it possible to calculate the compliance, C, in Eq. 1. The analysis will be extended to a DCB specimen acted upon by unequal bending moments, representing the case for a DCB-UBM specimen. A full compliance solution of the DCB-UBM specimen will aid in understanding direct comparison of experimental results with the analytic solution. Such a direct comparison will enable in estimating the efficacy of DCB-UBM test rigs. To extend the kinematic analysis to a DCB-UBM specimen case, the crack root rotation should also be take into account. The crack root rotation have been shown to significantly affect the near tip deformation characteristics, especially for specimens with thin cores [9]. The crack tip root rotation angle (φ) can be expressed as [9]:

$$\phi_A = c_M \frac{M}{\bar{E}_f h_f^2} + c_N \frac{N}{\bar{E}_f h_f} + c_V \frac{V}{\bar{E}_f h_f} \tag{4}$$

where c_M, c_P and c_V depend on the face and core stiffnesses. M is the moment, N the axial load and V, the shear force in the upper face (all per unit width) at the crack tip. A comprehensive approach in which the full compliance solution based on the rotations and moments of a DCB-UBM sandwich specimen will be provided followed by a comparison with numerical results for typical sandwich configurations.

REFERENCES

[1] Transportation Safety Board of Canada, “Loss of Rudder in Flight,” Aviation Investigation Report A05F0047: Minister of Public Works and Government Services, Canada, 2007.
[2] E. H. Glaessgen et al., “Debonding Failure of Sandwich-Composite Cryogenic Fuel Tank with Internal Core Pressure,” J. Spacecraft and Rockets, 2005, vol. 42, no. 4, pp. 613-627.
[3] B. F. Sørensen et al., "DCB-specimen loaded with uneven bending moments." International Journal of Fracture, 2006, vol. 141, no .1, pp. 163-176.
[4] C. Lundsgaard-Larsen et al.,”A modified DCB sandwich specimen for measuring mixed-mode cohesive laws”. Engineering Fracture Mechanics, 2008, vol. 75, no. 8, pp. 2514-2530.
[5] V. Saseendran et al. "Fracture Characterization of PVC Foam Core Sandwich Specimen Using the DCB-UBM Test Method.", 21st International Conference on Composite Materials (ICCM-21). 2015.
[6] V. Saseendran et al. “Honeycomb Sandwich Face/Core Fracture Toughness Measurements using the DCB-UBM Test Method – DoSS Project”, 2017, Technical Report, Dept. of Mechanical Engineering, Technical University of Denmark.
[7] V. Saseendran et al., “Shear and foundation effects on crack root rotation and mode-mixity in moment- and force-loaded single cantilever beam sandwich specimen”, Journal of Composite Materials, DOI: 10.1177/0021998317749714.
[8] M. F. Kanninen, "An augmented double cantilever beam model for studying crack propagation and arrest." International Journal of fracture , 1973, vol. 9, no. 1, pp. 83-92.
[9] S. Li et al., "The effects of shear on delamination in layered materials." Journal of the Mechanics and Physics of Solids, 2004, vol. 52, no. 1, pp. 193-214.

SESSION 5B: APPLICATIONS

DOI: 10.5075/epfl-ICSS12-2018-115-117

MECHANICAL RESPONSE OF SANDWICH STRUCTURES BASED ON CORRUGATED COMPOSITE CORES FILLED WITH PVC FOAM

Jin Zhou[1], Lei Peng[1], Zhong Wei Guan[1] and Wesley James Cantwell[2]
[1] School of Engineering, University of Liverpool, Liverpool, L69 3GH. United Kingdom. Email: jinzhou@liv.ac.uk
[1] School of Engineering, University of Liverpool, Liverpool, L69 3GH. United Kingdom. Email: sglpeng2@liv.ac.uk
[1] School of Engineering, University of Liverpool, Liverpool, L69 3GH. United Kingdom. Email: guan@liv.ac.uk
[2]Aerospace Research and Innovation Center, Khalifa University of Science Technology and Research, 127788 Abu Dhabi, United Arab Emirates. Email: cantwell@liv.ac.uk

1. INTRODUCTION

Sandwich structures have been used in a number of light-weight aerospace structures. In recent years, there has been a drive to develop sandwich structures based on novel designs, for example truss, lattice and prismatic structures [1, 2]. For example, researchers have developed stretch-stretch hybrid hierarchical cores that include pyramidal lattice sandwich panels in macroscopic truss designs [4]. More recently, researchers have studied the possibility of employing corrugated composite panels in the design and manufacture of morphing structures and energy-absorbing components [3, 4]. Kazemahvazi and co-workers characterized the properties of hierarchical corrugations manufactured from a carbon fibre reinforced epoxy resin [3]. The sandwich structures exhibited different failure mechanisms as the geometry of these novel structures was changed. Rejab and Cantwell [4] used a steel mould with a triangular profile to manufacture a number of corrugated cores with differing wall thicknesses and compared the resulting properties to those associated with a comparable aluminium system. It was concluded that the carbon fiber-based core offer superior properties of that of the metallic system. Malcom et al [5] tested a number of foam-filled and plain corrugated core structures produced from 3D glass fiber fabrics where it was shown that slender struts failed in an elastic buckling mode and thicker struts in a plastic microbuckling mechanism. Finally, Zhou et al [6] a broad range of tests on integrated woven corrugated sandwich composites and showed that the compressive properties of these sandwich structures, offer stiffness and strength characteristics that vary with the relative density squared. The aim of the work presented in this paper is to investigate the mechanical properties of sandwich structures consisting of curvilinear composite cores filled with PVC foam. Here, the effect of density of filled PVC foam and geometrical parameters on the mechanical properties of the sandwich structures is investigated.

2. EXPERIMENTAL PROCEDURE

The corrugated core sandwich structure tested in this study were fabricated using a woven glass fibre reinforced plastic (GFRP), and a woven carbon fibre reinforced plastic (CFRP). The sinusoidal-shaped composite cores with varying diameter and thickness were manufactured by wrapping sheets of composite prepreg around an array of Teflon-coated steel tubes, as shown schematically in Fig. 1. The skins of the sandwich structures were introduced by laying composite plies on the top and bottom surfaces of the uncured tubular array.

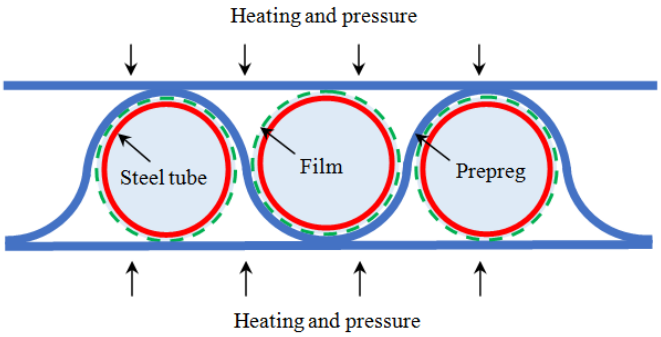

Fig. 1: Schematic of the corrugated core sandwich structure.

Subsequently, the entire structure was cured in a hot press. Here, the panels were heated to 125 ºC at a heating rate of 1.5 ºC/minute. This temperature was then maintained for 90 minutes, before allowing the samples to cool to room temperature. The sandwich panels were then moved to oven and post-cured for 90 minutes at 125 ºC. The PVC foam varying density from 40 to 130 kg/m^3 used in this investigation, were supplied by Airex AG. PVC foams were machined by CNC machine and filled in the curvilinear composite core structures. The specimen investigated in this study is shown in Table 1.

Table 1: Summary of the specimen investigated in this study.

Thickness of corrugation.	C40 PVC	C80 PVC	C130 PVC
CF1	C40CF1	C80CF1	C130CF1
CF2	C40CF2	C80CF2	C130CF2
CF3	C40CF3	C80CF3	C130CF3
CF4	C40CF4	C80CF4	C130CF4
CF5	C40CF5	C80CF5	C130CF5
GF1	C40GF1	C80GF1	C130GF1
GF2	C40GF2	C80GF2	C130GF2
GF3	C40GF3	C80GF3	C130GF3
GF4	C40GF4	C80GF4	C130GF4
GF5	C40GF5	C80GF5	C130GF5

Compression tests were undertaken at a crosshead displacement rate of 1 mm/min using a universal Instron 4045 test machine. A crosshead displacement rate of 1 mm/min was employed during testing. Potential changes in failure mode were photographed at regular intervals during testing in order to elucidate the modes of failure and fracture. The dynamic impact response of the sandwich structure was investigated through a series of drop-weight impact tests on foams had nominal densities of 40 and 130 kg/m^3. During impact loading, the displacement and force of the impact head were measured using a high speed video camera and a piezoelectric load cell respectively.

3. RESULTS AND DISCUSSION

The Influence of Corrugation Thickness

Typical stress-strain traces following compression tests on GFRP and CFRP samples with corrugation thicknesses ‘t’ between 0.25 and 1.25 mm. An examination of the response of those structures, indicates that increasing the value of ‘t’ serves to increase the compression strength of the core. Further increases in thickness precipitated a change in the shape of the stress-strain trace, with the curves exhibiting stable plateau before the onset of final densification.

The Influence of Foam Density

The comparison of the failure modes in GFRP samples with web thicknesses of 1.25 mm filled with 40 and 130 kg/m^3 PVC foams are shown in Fig. 2. Failure in the 40 kg/m^3 foams samples involved initial buckling and creasing close to the upper skin, followed by a buckling failure of the webs at their mid-points. Failure in the 130 kg/m^3 foams samples involved the formation of a hinge at the vertical alignment of the webs and the top surface. These re-aligned webs were capable of supporting significant load before failing, leading to distinct peak in the stress-strain trace. The filled PVC foam enhance the mechanical performance.

Fig. 2: Typical failure of GFRP samples for C40GF3 and C130GF5.

4. CONCLUSIONS

The mechanical response of sandwich structures base on corrugation core filling with PVC foam have been investigated experimentally and numerically. The mechanical response of the sandwich structures was modelled using finite element model. Sandwich structures based on varying thickness of corrugated core have been manufactured by compression molding an array of wrapped metallic cylinders. Tests on the resulting samples indicated that the compression strength increased with the thickness of the corrugation and density of filled PVC foam. The stress-strain traces for the PVC foam filled c samples exhibited less peak, failure mechanisms that were associated with buckling of the web. It indicates that the carbon fiber reinforced corrugated structures offered superior compressive properties to its glass-based counterpart. It also clears that compression strength increased rapidly with the thickness of the corrugation and foam density. The final part of this study focused on investigating the dynamic response of the glass and carbon/epoxy

structures. This study suggests that the mechanical response of the hybrid sandwich structures can be predicted by using FE modelling.

REFERENCES

[1]. J. Xiong, B. Wang, L. Ma, J. Papadopoulos, A. Vaziri and L. Wu, "Three-dimensional composite lattice structures fabricated by electrical discharge machining" Experimental mechanics, 2013;54:405–412.
[2]. S. Yin, L. Wu and S. R. Nutt, "Compressive efficiency of stretch-stretch-hybrid hierarchical composite lattice cores", Materials and Design 2014; 56:731–739.
[3]. S. Kazemahvazi, D. Tanner and D. Zenkert, "Corrugated all-composite sandwich structures. Part 2: Failure mechanisms and experimental programme", Composites Science and Technology 2009;69:920-925.
[4]. M. R. M. Rejab and W. J. Cantwell, "The mechanical behaviour of corrugated-core sandwich panels", Composites. Part B Engineering 2013;47:267–277.
[5]. A.J. Malcom, M.T. Aronson, V.S. Deshpande and N.H.G. Wadley, "Compressive response of glass fiber composite sandwich structures", Composites Part A – Applied Science and Manufacturing 2013;54:88-97.
[6]. F.N. Jin, H.L. Chen, L. Zhao, H.L. Fan, C.G. Cai and N. Kuang, "Failure mechanisms of sandwich composites with orthotropic integrated woven corrugated cores: Experiments", Composite Structures 2013;98: 53-58.
[7]. Z. Hashin, "Failure criteria for unidirectional fiber composites", Journal of Applied Mechanics 1980;47:329-334.
[8]. E. Sitnikova, Z.W. Guan, G.K. Schleyer, W.J.Cantwell, "Modelling of perforation failure in fibre metal laminates subjected to high impulsive blast loading", International Journal of Solids and Structures 2014; 51: 3135-3146.
[9]. T. P. Vo, Z. W. Guan, W. J. Cantwell, G. K. Schleyer. "Modelling of the low-impulse blast behaviour of fibre–metal laminates based on different aluminium alloys", Composites: Part B 2013;44: 141–151.
[10]. J. X. Zhang, Q. H. Qin and T. J. Wang, "Compressive strengths and dynamic response of corrugated metal sandwich plates with unfilled and foam-filled sinusoidal plate cores", Acta Mechanica 2013;224:759–775.

DOI: 10.5075/epfl-ICSS12-2018-118-120

LOCALISATION OF DAMAGE TO A ROTOMOULDED PE SANDWICH STRUCTURE BY ACOUSTIC EMISSION SUBJECTED TO INTERNAL PRESSURE

Eric Lainé[1], Anne-Laure Gorge[2], Maxime Cruz[3], Jean-Claude Grandidier[4], Eric Maziers[5], Geert Vaes[6] and Simon Karam[7]
[1]Institut Pprime, CNRS, ISAE-ENSMA, Université de Poitiers, F-86962 Futuroscope, France, eric.laine@ensma.fr
[2]Institut Pprime, CNRS, ISAE-ENSMA, Université de Poitiers, F-86962 Futuroscope, France, anne-laure.gorge@ensma.fr
[3]Institut Pprime, CNRS, ISAE-ENSMA, Université de Poitiers, F-86962 Futuroscope, France, maxime.cruz@ensma.fr
[4]Institut Pprime, CNRS, ISAE-ENSMA, Université de Poitiers, F-86962 Futuroscope, France, jean-claude.grandidier@ensma.fr
[5]Total Research & Technology Feluy, Zone Industrielle Feluy, B-7181 Seneffe, Belgique, eric.maziers@total.com
[6]Total Research & Technology Feluy, Zone Industrielle Feluy, B-7181 Seneffe, Belgique, geert.vaes@total.com
[7]Total Research & Technology Feluy, Zone Industrielle Feluy, B-7181 Seneffe, Belgique, simon.karam@total.com

1. INTRODUCTION

Sandwich materials are increasingly used in industrial applications. They generally consist of two thin skins of relatively high tenacity materials and a thicker lightweight core (low density). These sandwich materials can take many shapes by combining different skin types (aluminium, steel, wood, polymer, composites...) and core materials together with different geometries (honeycombs (aluminium, polymer, Nomex), cellular foams, balsa...). This makes it possible to produce optimal sandwich materials for specific applications. Generally, the mechanical behavior of these sandwich structures (skin-core-skin) is determined by bending tests (3 or 4 points) and impact tests (weight drop) in both static and dynamic modes. In literature, many works are devoted to the determination of the damage on these sandwich materials using the technique of acoustic emission (AE). For example, Burman et al. [1] studied the initiation and progression of damage in cellular foam sandwich composites. The acoustic characteristics of mode I and mode II on PVC foam fracture were determined by both single notch and end notch bending tests. Ben Ammar et al. [2] studied the mechanical behaviour under static (4-point bending) and dynamic loads and also evaluated the damage of two types of sandwich composite materials. However, there are very few articles in the literature on EA for sandwich polymers. One reason may be that polymers strongly attenuate ultrasonic waves and are less energetic. However, acoustic emission was used to analyze plastic deformation and damage in pure semi-crystalline polymers [3,4] above their glass transition temperature and vitreous polymers (PET) [5-6]. If a very low acoustic activity was observed [3,4], Ronkay et al. [6] attribute the signals to the formation of cavities, which appear with propagation through the neck during tensile tests. Recently, Casiez et al. [7] showed for two types of PE samples that AE can be sensitive enough to analyze the initiation of plastic deformation, including cavitation, on semi-crystalline polymers above their glass transition temperature. The challenge is to verify that this technique (AE) is able to apprehend damage in a polymer sandwich material. This is the purpose of this paper. Beforehand, tensile tests have been carried out on PE material at different constant strain rates and our results are consistent with those of Casiez et al. [7]. A static test on a rotomoulded PE sandwich structure (bottle) subjected to increasing internal water pressure is carried out up to an acoustic level sufficient to develop damage without failure of the structure (external skin). The acoustic activity of this instrumented test appears to agree with the observed structural damage.

2. SANDWICH MATERIAL (SKIN-FOAM-SKIN) AND SANDWICH OR MULTILAYER STRUCTURE (BOTTLE)

Researchers from one of the WW major Oil company 'Total' have developed a new sandwich material consisting of a foamed polyethylene (PE) layer between two PE skin layers. The PE skins and foam have a density of 0.935 g/cm^3 and 0.200 g/cm^3 respectively. The structure (bottle) is made by rotational moulding, a polymer conversion technology specifically designed to produce hollow plastics parts. This type of sandwich material (skin-foam-skin, Figs. 1(a) and 1(b)) dramatically increases the stiffness for the same weight.

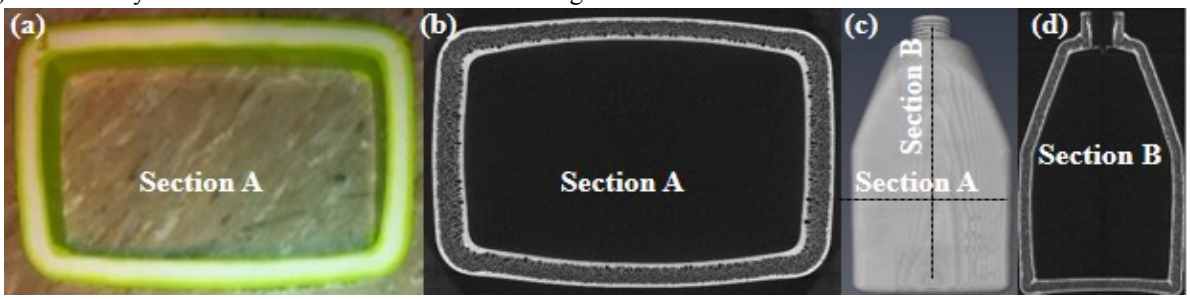

Fig. 1 : Sandwich material: (a) photo and (b) tomography of a bottle section - Sandwich structure: tomography of (c) the bottle and (d) a section.

This new technology offers the opportunity to use lightweight polyethylene in structural parts which is interest particularly for the automotive, aeronautical, storage and transport industries. The sandwich structure used in this study

is a multilayer bottle with dimensions: height 330 mm, width 200 mm and depth 140 mm (Figs. 1(c) and 1(d)). The PE skins and foam have a thickness of 2 and 10 mm respectively. This is a reference test structure for the company Total. It is used during the development of new materials to define and optimize the processing parameters, to extract specimens for a thermo-mechanical characterization and to perform tests under different loading conditions (creep ...).

3. EXPERIMENTAL PROCEDURE

The experimental test bench ENDOMAT (Fig. 2(a)) implements a mechanical testing machine including tensile-compressive (1200 kN) and internal pressure (1200 bars). The axes impose stress loads in static and dynamic possibly synchronized over a frequency range up to 10 Hz according to the amplitude of monitored efforts. The useful dimensions of the testing machine are (700x700x1800 mm) with a volume of 882 L allow fastening large-dimension structures on the bench test. As of the pressure axis, it has two devices in parallel, each transforming the hydraulic power into oil to the hydraulic power circuit and into water in contact with the structure to be tested. The first is a transfer accumulator (oil or water) that transfers the pressure supplied by the oil circuit with a storage tank (hydraulic operating pressure: 300 bars). The second device is a booster which multiplies the pressure by four thanks to the piston surfaces. The system can convert the oil operating pressure from 300 bars to 1200 bars in the water circuit, but at a lower rate. A specific assembly (Fig. 2(a)) has been developed to connect the bottle to the test bench, allowing positioning, maintenance and sealing during an internal pressure test. With this system, the bottle can be loaded with mechanical compression and internal pressure in different ways: monotonous, load-unload, creep, fatigue (cyclical). In addition, it is possible to couple mechanical compression and internal pressure simultaneously.

An 8-channel Express System Mistras is used to record AE signals during bottle testing (Figs 2(b)-2(e)). The test is carried out with eight "micro80" piezoelectric acoustic sensors with a PAC 1220A preamplifier with a gain of 40 dB. The peak sensitivity of the sensor is approximately 450 kHz for pressure waves and 250 kHz for Rayleigh (surface) waves. The signals are digitized with a sampling rate of 5 MHz. The sensors are fixed with silicone and attached to the bottle by tape strips. They are positioned in a "triangle" (Fig. 2(b)-2(e)) to locate the acoustic signals as well as possible because the localization system works by calculating the time difference of the acquisition of a wave for two different sensors. When recording AE signals, the user sets a detection threshold (32 dB) below which no signal is recorded. The acquisition system is calibrated before each test using the mine breakage procedure [8].

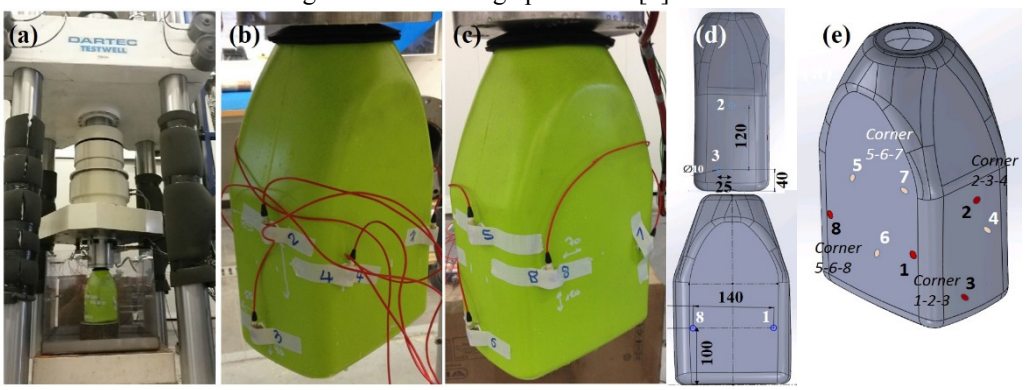

Fig. 2 : (a) Endomat and Specific assembly, (b) - (c) - (d) & (e) Bottle equipped with EA sensors and Position of EA sensors.

4. RESULTS AND DISCUSSIONS

A test with monotonous loading under internal pressure was carried out. The objective was to interrupt it when the acoustic activity would become high without the complete break on the bottle. Thus, from 6 bar pressure (Fig. 3(a)), the AE signals increase rapidly (Fig. 3(a)) mainly on sensors 1, 2 and 3 (Figs. 2(b)-2(e)), a very low activity on sensor 6 is observed and no activity is detected on sensors 4, 5, 7 and 8. When disassembling the structure, it can be observed that the inner skin of the bottle displayed several large cracks (Fig. 3(b)). The AE signals detected by sensors 1, 2 and 3 appear to correspond to damage in the inner skin at the vertical edge and the two horizontal edges (Fig. 4(a)) framed by these three sensors. On the other vertical edges, no damage is observed, which may explain why the other sensors (4, 5, 7, 8) did not detect any signal. It is not possible here to distribute the signals perceived by the sensors in relation to the damaged areas. However, it is certain that the signals are weak that sensor 6 (Fig. 3(b)) has detected damage to the horizontal edge of the bottle bottom (Fig. 4(a)). The crack is only 10mm long. Finally, it is likely that the signals perceived by sensor 1 correspond to the damage to the vertical edge (breaking length approximately 110 mm) but also to the two horizontal corners (1 and 2) of the bottom of the bottle which have a crack length of 80 and 70 mm respectively. Fig. 4(b) shows the AE signals count (N) and amplitude (V) obtained during the static internal pressure test. The data at $N \geq 5$ was plotted, since a few AE signals were generated due to the swelling process. The AE signals count (N) and amplitude (V) verify the following relationship where A and m are constants (Fig. 4(b)). This correlation corresponds to a crack growth during the test [9]. The value of the parameter m is equal to 1.88 (Fig. 4(b)). This one is close to that determined by Yamabe et

al. [10] for rubber material (m=1.8) under the static crack growth test on classical specimen (for metal material, m=2 [11]). Fracture behaviour is correlated with this slope; consequently the value obtained for this polymer material is representative of crack growth of an energy which is between steel and rubber [10].

The use of AEs for polymers such as PE allows tracking, damage and/or structural failure. These results are definitively complementary to the work of the literature [3-7]. The passage from a tensile specimen to an industrial sandwich structure is therefore validated. In a complex environment (pressurized water), using this PE sandwich structure, it is possible to detect the first stages of damage at 6 bar and the propagation of cracks up to the high breaking stage of the inner skin with acoustic emission. It seems that only one mechanism is captured by AE in the ruin process.

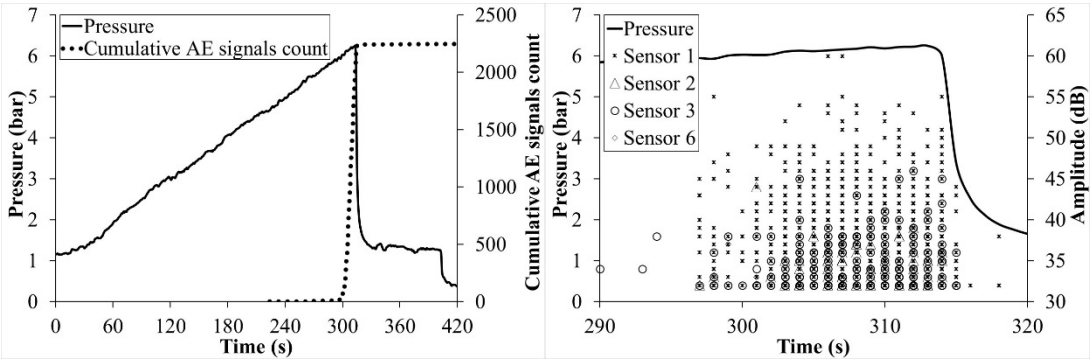

Fig. 3 : (a) Pressure vs. Time and Cumulative AE signals count vs. Time, (b) Zoom of Fig. 3(a) between 290 and 320s - Pressure vs. Time and AE amplitude vs. Time.

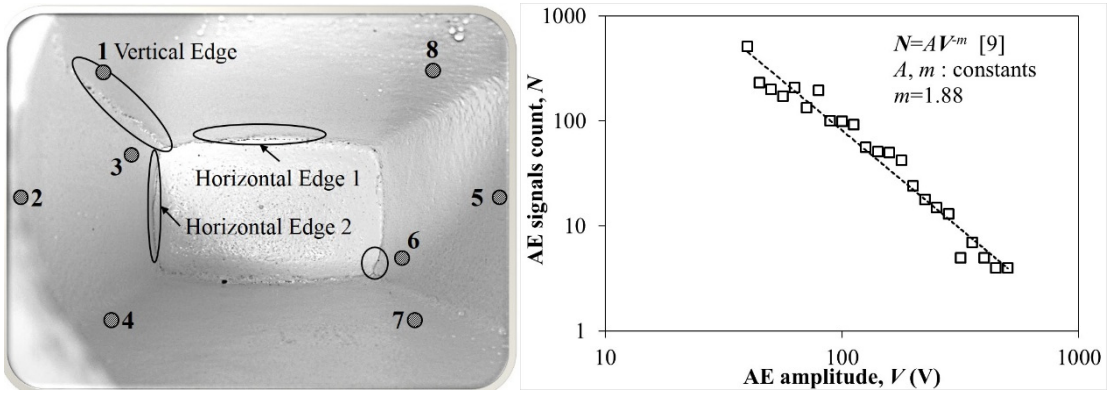

Fig. 4 : (a) Photo of the inside of the bottle after testing and disassembly – (b) Relationship between AE signals count and amplitude obtained from static pressure test.

ACKNOWLEDGMENTS

This work was funded by the French Government program “Investissements d’Avenir” (EQUIPEX GAP, reference ANR-11-EQPX-0018). The authors would like to thank Total Petrochemicals for their financial support for this research and for the provision of structures (bottles).

REFERENCES

[1] M. Burman et al., “Acoustic Emission Monitoring of Foam Core Sandwich Composites”, *J Sand. Struct. Mat*., 1999; 1:147-175.
[2] I. Ben Ammar et al., “Mechanical behavior and acoustic emission technique for detecting”, *App. Acoustics*, 2014; 86: 106-117.
[3] J. Bohse, “Acoustic emission characteristics of micro-failure processes in polymer blends and composites”, *Compos. Sci. Technol.*, 2000; 60:1213-1226.
[4] R. Qian et al., “Acoustic emission during stretching of polymers, *J Polym Sci* , 1983; 2:168-175.
[5] D. Betteridge et al., “Analysis of acoustic emissions from polymers”, *Polymer*, 1983; 24:1206-1212.
[6] F. Ronkay et al., “Cavity formation and stress-oscillation during the tensile test of injection molded specimens made of PET”, *Poly. Bull*, 2006; 57: 989-998.
[7] N. Casiez et al., “Acoustic emission from the initiation of plastic deformation of Polyethylenes during tensile tests”, *Polymer*, 2014; 55: 6561-6568.
[8] K. Jemielniak, “Some aspects of acoustic emission signal pre-processing”, *J. Mat. Proc. Tech.*, 2001; 109: 242-247.
[9] M. Ohtsu, “The history and development of acoustic emission in concrete engineering”, *Mag. Conc. Res*., 1996; 48: 321-330.
[10] J. Yamabe et al., “Application of acoustic emission method to detection of internal fracture of sealing rubber material by high-pressure hydrogen decompression”, *Poly. Testing*, 2011; 30: 76-85.
[11] S. Yuyama et al., “Effect of environmental, mechanical conditions, and materials characteristic on AE behavior during corrosion fatigue processes of an austenitic stainless steel”, *Nucl. Eng. Des*, 1984; 81: 345-355.

DOI: 10.5075/epfl-ICSS12-2018-121-123

MODELLING PERFORMANCE OF SANDWICH PIPE JOINTS UNDER INSTALLATION LOADINGS

Maria Kashtalyan[1], Ikechukwu Onyegiri[2] and Igor A. Guz[3]
[1] School of Engineering, University of Aberdeen, Scotland, UK, m.kashtalyan@abdn.ac.uk
[2] School of Engineering, University of Aberdeen, Scotland, UK, r01ico15@abdn.ac.uk
[3] School of Engineering, University of Aberdeen, Scotland, UK, i.guz@abdn.ac.uk

1. INTRODUCTION

As oil and gas production moves to deep- and ultra-deep waters, new pipeline configurations are required to meet simultaneous demands for thermal insulation and structural integrity to ensure safe and reliable transportation of hydrocarbons. Over the past two decades pipe-in-pipe systems have been developed for fields with flow assurance challenges [1, 2]. However, with increasing water depths and associated increasing demands on structural performance, the pipe wall thickness in pipe-in-pipe systems will have to increase, with pipe-in-pipe systems becoming exceedingly heavy and uneconomical [3], and lightweight alternatives will need to be sought.

The significant benefits of the sandwich pipe as an alternative to conventional pipe-in-pipe systems and single wall pipes has been researched and documented over the last decade. The bulk knowledge of this research has focused on the intended benefits of cost savings and increased capacity-to-weight ratio for deepwater pipeline installation and operation with respect to external pressure capacity, internal pressure capacity, pure bending capacity and reel-lay analysis. Developing a suitable method that permits the joining of sandwich pipes in an efficient manner, preserving the integrity of the insulation and the mechanical properties, is essential for successful application of sandwich pipes, however joining of sandwich pipes has received considerably less attention in the literature. The aim of this study is to analyse, by means of finite element method, performance of a swaged joint between sandwich pipes and establish the effect of both geometrical and mechanical properties of joint components on the strain concentration at the joint.

2. METHODOLOGY

Strain concentration at the field joint is a result of variation in bending stiffness along the pipe [4]. On the application of a bending moment, longitudinal strains in tension and compression are experienced and can be analysed starting from the girth weld connecting two adjacent inner pipe ends to some distance along the inner pipe where the swaged weld toe is encountered. The magnitude of strain especially in the girth weld is dependent on weld shape, wall thickness variation, pipe ovality and weld metal mismatch [5].

In order to gain a thorough understanding of the response of the joint components to installation based loadings, parametric studies are carried out to establish the effect of the inner pipe thickness, cutback length, and stiffness of the field joint filler on the strain concentration at the joint, with particular focus on the swaged weld region and the girth weld region. The base three-dimensional axisymmetric model used in this study can be seen in Fig 1. A uniform bending moment was applied at the pipe ends and the variation of the longitudinal strain in the inner pipe was studied; for this paper, we use the term strain concentration factor (SCF) to quantify this variation, defined as: $\varepsilon_{\max\_FJ}/\varepsilon_g$ where $\varepsilon_{\max\_FJ}$ is the maximum longitudinal strain at the field joint and ε_g is the global bending strain calculated by the Euler bending theory for a simple beam. The yield curvature for the inner pipe was defined by the expression: $k_y = \sigma_y/E.r_i$. The mechanical properties for the base model sandwich pipe are shown in Table 1.

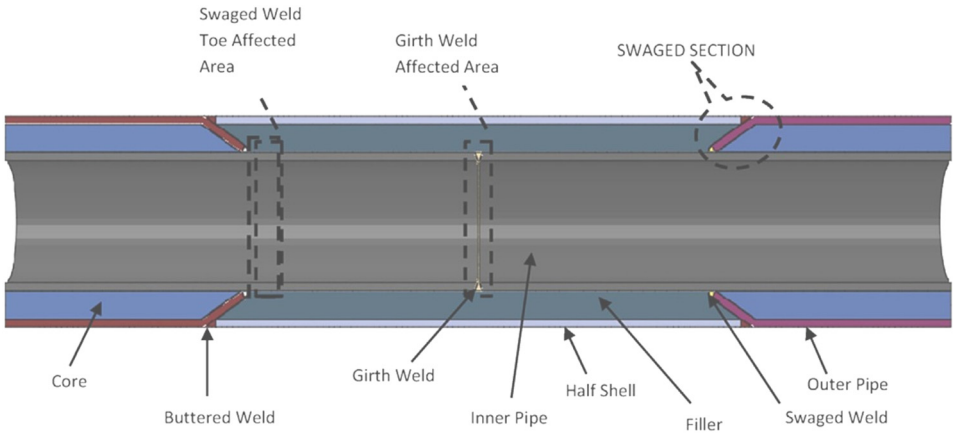

Fig. 1: Sandwich pipe swaged joint.

Table 1: Mechanical properties for the base model sandwich pipe.

Component	Material	Young's Modulus E (GPa)	Yield strength σ_y (MPa)	Ultimate tensile strength σ_{UTS} (MPa)	Poisson's ratio v
Inner Pipe, Outer Pipe, Half Shell	Steel	207	448	603	0.3
Core	Polymer	1.0	Perfectly elastic	Perfectly elastic	0.43
Filler	Polymer	0.9	Perfectly elastic	Perfectly elastic	0.43

The analysis was carried out using the commercial FE software Abaqus, with only a quarter of the field joint modelled due to geometric axial symmetry. The base model was developed as an 8" x 12" sandwich pipe. Mesh convergence studies and model de-featuring were carried out to produce a robust model that closely matched experimental results as carried out by [6]. 52 elements along the circumferential direction proved to be enough when predicting the system instability for convergence (Fig. 2). The mesh for the steel parts was generated using 3D solid elements C3D20R while that for the core polymeric layer was meshed with C3D20H elements. Post yield behaviour for the steel layers was modelled by J2 plasticity theory with isotropic hardening with true stress-strain data evaluated by an elastic response followed by a Ramberg-Osgood plasticity response with strain index fitted from experimental results for API X65 pipes.

3. RESULTS AND DISCUSSION

Longitudinal strain distribution along the length of the inner pipe is shown in Fig. 2 starting from the girth weld interface. As is expected, strain localisation at the girth weld interface due to weld-pipe metal mismatch and hi-lo is observed. Moving further away, the strain appears constant and then elevates signifying the beginning of the stiffening enhanced region due to the presence of the swaged weld. The swaged weld can be characterised as a stiffener ring acting on the surface of the inner pipe thus allowing for higher strain just adjacent to the weld toe as can be seen in Fig. 2.

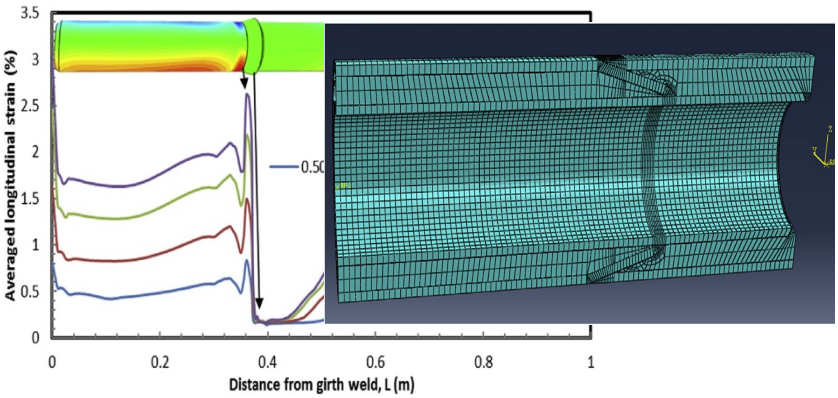

Fig. 2: Strain variation along the pipe for a range of global strain values (left), Finite element mesh of a sandwich pipe swaged joint (right).

The parametric studies [7] involved varying the studied parameter whilst keeping the other parameters as is in the base model. The influence of the inner pipe's diameter-to-thickness ratio on the SCF was studied and showed that reducing the ratio would lead to a decrease in the SCF as the bending stiffness of the pipe would increase. Also, increasing the filler-to-core stiffness ratio was seen to have a decreasing effect on the SCF at the swaged weld region of the inner pipe. This added structural advantage was more pronounced after the yielding of the inner pipe and thus supports the argument for a stiffer field joint region for sandwich pipes during installation by reel-lay or S-lay.

The effect of the cutback length on the strain concentration of a conventional swaged sandwich pipe joint is generally different from that expected for concrete coated pipe or wet insulation pipelines. This is due to the complex geometry and varying sectional profiles of the swaged weld field joint. The ratio of the inner pipe radius to the cutback length (r_i/L_f) was used as the defining parameter. Increasing the cut-back length would yield significant advantages by reducing the SCF but is not always favourable (a long cut-back length) as that leads to increased offshore time in making a tight connection. Utilising shorter cut-back lengths $r_i/L_f > 0.5$ avails lower SCF to the swaged weld region but greatly increase the SCF at the girth weld region for high reel curvatures. From the sensitivity studies, $r_i/L_f = 0.3 - 0.4$ would be suitable as they produce a good balance between the SCF at the swaged region and girth region. The effect of interlayer adhesion is shown in Fig. 3 where FB: fully bonded layers, FJ-NB: filler not bond, C-NB: core layer not bond and A-NB: no bond between the layers.

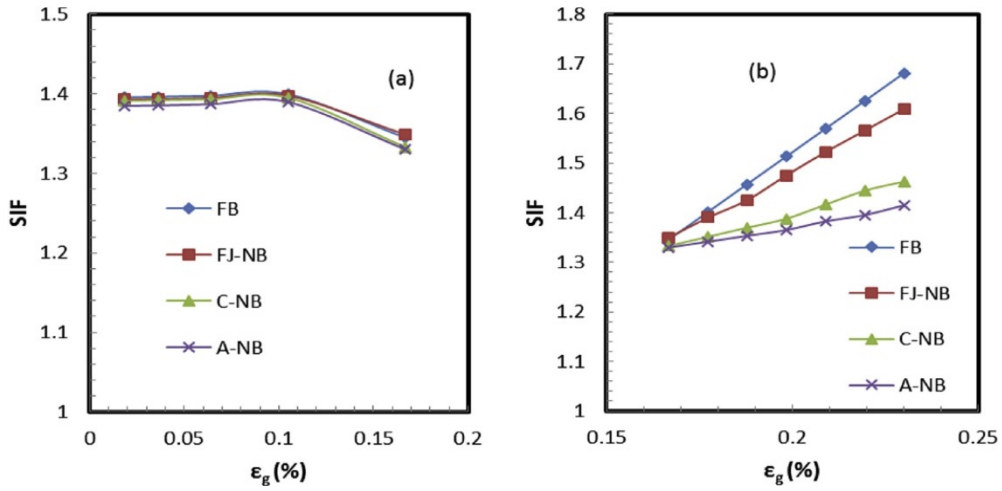

Fig. 3: Effect of interlayer adhesion on SCF at the swaged weld region: Elastic regime (left), Post-yield regime (right).

The choice of weld material and welding procedure will definitely have an impact on the SCF, and as such results showed that utilising a weld metal with a greater yield strength than that of the adjacent pipe would increase the SCF at the swaged weld region but this is only of significance for bending strains below the yield point of the swaged weld. Further research into the effect of the geometry of the swaged weld on the SCF is recommended, looking into dynamic loading (as with the reel installation procedure).

REFERENCES

[1] Bai, Q., Bai, Y., *Subsea Pipeline Design, Analysis, and Installation*. Elsevier, 2014

[2] Sriskandarajah, T., Ragupathy, P., Rao, V., "Design aspects of pipe-in-pipe systems for HP-HT applications". In: *Offshore Technology Conference*, 2–5 May 2016, Houston TX, USA. OTC 27046

[3] Bruschi, R., Vitali, L., Marchionni, L., Parrella, A., Mancini, A., 2015. "Pipe technology and installation equipment for frontier deep water projects", *Ocean Engineering* 2015; 108: 369–392.

[4] Roberts, C., Rathbone, A., Timmins, D., Cumming, G., Tørnes, K., "Strain intensification due to material discontinuity at field joints adjacent to thick wall insulation coating". In: *Proceedings of the ASME 28th International Conference on Ocean, Offshore and Arctic Engineering*, 31 May – 5 June 2009, Honolulu HI, USA. OMAE2009–79779.

[5] Dixon, M., Jackson, D., El Chayeb, A., "Deepwater installation techniques for pipe-in-pipe systems incorporating plastic strains". *Offshore Technology Conference*, 5–8 May 2003, Houston TX, USA. OTC 15373

[6] Jones, R.L., Geertsen, C., Booth, P., Mair, J.A., Sriskandarajah, T., Rao, V., Pipe-in-Pipe swaged field joint for reel lay. In: *Offshore Technology Conference*, 2013. OTC 24077.

[7] Onyegiri, I., Kashtalyan, M., "Finite element analysis of a sandwich pipe joint", *Ocean Engineering* 2017; 146: 363-374.

SESSION 6A: DELAMINATION / DISBOND

DOI: 10.5075/epfl-ICSS12-2018-125-127

DEVELOPMENT OF A METHODOLOGY TO ADDRESS FACE SHEET TO CORE SEPARATION IN SANDWICH STRUCTURES

Ronald Krueger[1] and Zhi-Ming Chen[2]
[1]National Institute of Aerospace, Hampton, Virginia, USA. rkrueger@nianet.org
[2]Federal Aviation Administration, Atlantic City, New Jersey, USA. Zhi-Ming.Chen@faa.gov

1. INTRODUCTION

Typical damage modes in honeycomb sandwich structures include face sheet wrinkling and dimpling, shear crimping, core crushing and core shear failure as well face sheet to core separation (also called disbonding) and core fracture [1]. Face sheet to core separation and core fracture are of particular interest to certification authorities since several in-service occurrences, such as rudder structural failure [2] and other control surface malfunctions [3] have been attributed to face sheet to core separation. Extensive studies have shown that face sheet to core separation can lead to damage propagation caused by internal pressure changes in the core. These internal pressure changes in the core may be due to ground-air-ground (GAG) cycles [4, 5] or may be caused by cryopumping [6, 7]. The increasing use of composite sandwich construction in aircraft applications for instance, composite sandwich construction of the fuselage of business jets that experience higher altitudes than transport aircraft, thus makes it vitally important to understand the phenomenon of disbond growth under generalized load conditions including maneuvers and gust conditions.

In this paper, a detailed problem description is provided first. Second, the overall methodology to address face sheet to core separation in sandwich structures is presented. Third, an overview is given on the development of test methods that yield a critical strain energy release rate associated with disbonding, with a focus on mode-I dominated loading conditions. Forth, an analysis approach is discussed to compute energy release rates along an arbitrarily shaped disbond front. Finally, an outlook is provided.

2. DETAILED PROBLEM DESCRIPTION

A sketch of flat sandwich panel, consisting of laminated composite face sheets and a honeycomb core with an initial disbond at the upper face sheet to core interface is shown in Fig. 1. The honeycomb core is assumed to be unvented. Air flow and rapid pressure equalization with the outside environment is prevented. For this reason, the pressure is initially assumed equal inside and outside the sandwich and thus the sandwich structure is not loaded (and is undeformed), as shown in Fig. 1(a).

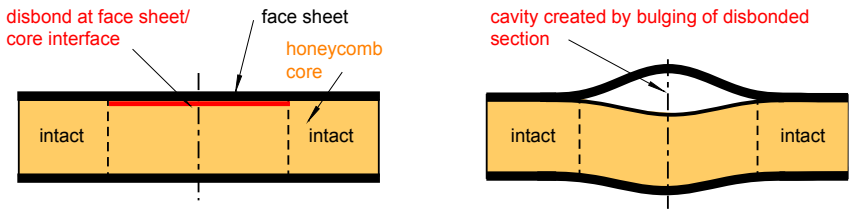

(a). Initial configuration at ground elevation *(b). Deformed configuration at cruising altitude*

Fig. 1: Deformation behavior of a sandwich panel with disbond.

When the ambient pressure decreases rapidly, for instance during the launch of a spacecraft or the ascent of an aircraft, the resulting pressure difference between the entrapped air and the ambient surrounding air causes the sandwich to expand. In the disbonded section, the thin face sheets with low bending stiffness can easily be deformed by the pressure load and bulge the sandwich as shown in Fig. 1(b). The out-of-plane deformation results in an increased volume, V, creating a cavity and a resulting decrease in internal pressure, p. At the same time, the decreasing ambient temperature cools the entrapped air, causing the honeycomb sandwich to shrink. This combined effect can be calculated using the ideal gas law

$$pV = nRT \tag{1}$$

where T is the temperature of the gas, R = 8.314 J/(mol K) is the universal gas constant and n is the amount of substance of gas (also known as number of moles) [8]. For the face sheet core separation case, the amount of gas is the entrapped air inside the honeycomb cells. Bulging is considered negligible in the intact section. Hence, volume increase is only possible due to out-of-plane deformation of the core. Thus, the pressure change in the intact section is dominated mainly by the temperature change and can easily be calculated using equation (1). For the disbonded section, however, a coupled pressure-deformation problem has to be solved. Therefore, a non-linear finite element analysis has to be performed which couples the ideal gas law for the air-filled cavity with the deformation analysis of the sandwich [9].

3. OVERALL METHODOLOGY

In order to identify, describe and address the phenomenon associated with face sheet to core separation, a reliable method of characterizing this damage mode must be developed. In monolithic laminates, delamination is typically characterized by measuring a critical strain energy release rate, G_c. A similar approach is proposed here, whereby G_c for face sheet to core fracture toughness is measured for a sandwich composite with thin face sheets typically applied in aircraft. However, unlike delamination in unidirectional monolithic laminates, face sheet core separation in a sandwich will not necessarily be confined to the bondline or a particular interface. Studies have shown that disbond growth location can be significantly affected by parameters such as core thickness, face sheet thickness, mode-mix and crack driving force [10, 11]. Characterization tests must therefore be developed that ensure that disbond growth occurs at the location observed in service. Further considerations include identification of a global loading scenario that would be most critical for potential face to core separation, the effect of environmental degradation and thermal residual stresses on disbonding, the potential reduction in disbond growth resistance of a repaired sandwich, and the characterization of disbond growth rates (*da/dN* vs. ΔG) under cyclic loading conditions. In addition to the characterization tests, analysis tools are required, to help assess the likelihood of a structure exhibiting critical disbonding. These analysis tools need to be verified and validated.

4. DEVELOPMENT OF STANDARD FRACTURE TEST METHODS

Face sheet to core separation generally takes place under mixed-mode loading conditions owing to effects from geometry and the typically disparate properties of the constituent materials of a sandwich structure. Test methods have therefore been developed for measuring fracture toughness associated with mixed-mode loading and also pure mode-II loading [12 ,13]. However, as is the case with delamination in monolithic laminates, the most critical disbonding process in sandwich structure is likely to be mode I dominated, corresponding to loading scenarios where the face sheet is peeled from the core. The literature contains many examples of test methods designed to measure the critical strain energy release rate associated with face sheet/core peel [13-15]. In a recent study, the suitability of five test methods for measuring disbond toughness associated with face sheet/core peel was evaluated [16]. A single cantilever beam (SCB) type configuration, as shown in Fig. 2 was identified as the most appropriate test. This determination was based on the following findings: (1) the test involves a simple loading fixture, (2) disbond front loading conditions were found to be independent of disbond length, (3) disbonding was found to take place along or near to the face sheet/core interface, rather than kinking into the core, (4) the data reduction for computing the fracture toughness can be accomplished using a compliance calibration procedure or the area method [17].

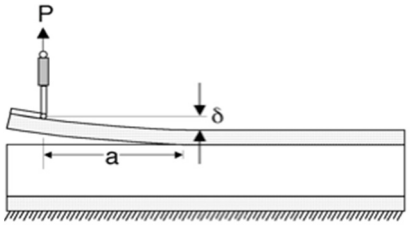

Fig. 2: Single Cantilever Beam Specimen (SCB).

Partly in response to these findings, a recent work item was created in ASTM to develop an ASTM standardized test method for a mode I dominated fracture toughness of sandwich constructions (ASTM WK 47682). As part of the standard development, an *ASTM Draft Standard* was developed, which was used in a round robin activity by seven research laboratories in the US and Europe [18].

5. ANALYSIS METHODOLOGY

Analysis methods are required to help assess the tendency of a structure to exhibit disbond growth. In monolithic laminates, the measured fracture toughness from simple tests is compared to computed values along the delamination front which were calculated from a finite element model (FE) of the real structure. Propagation of the front is predicted to occur when the computed value exceeds the measured fracture toughness of the material. A similar approach is proposed here, where G_c for face sheet to core separation from an existing disbond is measured using the SCB specimen geometry illustrated in Fig. 2. The Virtual Crack Closure Technique (VCCT) is used to calculate the total energy release rate along the disbond front based on the results obtained from a finite element analysis of the disbonded sandwich panel. A typical 3D model of a quarter of a flat panel containing a circular disbond is shown in Fig 3 [19]. Due to the symmetry of the problem, a simple model of a quarter of the panel was used for most analyses to reduce computational time as shown in Fig. 3a. The core was homogenized and 3D volume elements were used for the entire model.

This model was used for an initial study of Ground-Air-Ground-Cycle (GAG) effects in honeycomb sandwich structures. An approach that uses fluid-filled cavities was developed to include the effect of pressure-deformation coupling (recursive process in which deformation results in cavity volume change and thus affects cavity pressure) in the

disbonded area of the panel [9]. Therefore, the model was split into two cavities with one representing the intact and the other cavity representing the disbanded section of the panel as shown in Fig. 3b. The influence of the face sheet thickness and core thickness as well as the influence of several honeycomb core materials on the crack tip loading of the disbonded sandwich was investigated. Internal pressure due to GAG-cycle and in-plane loading due aircraft maneuver and gust loads were also applied to the panel [19].

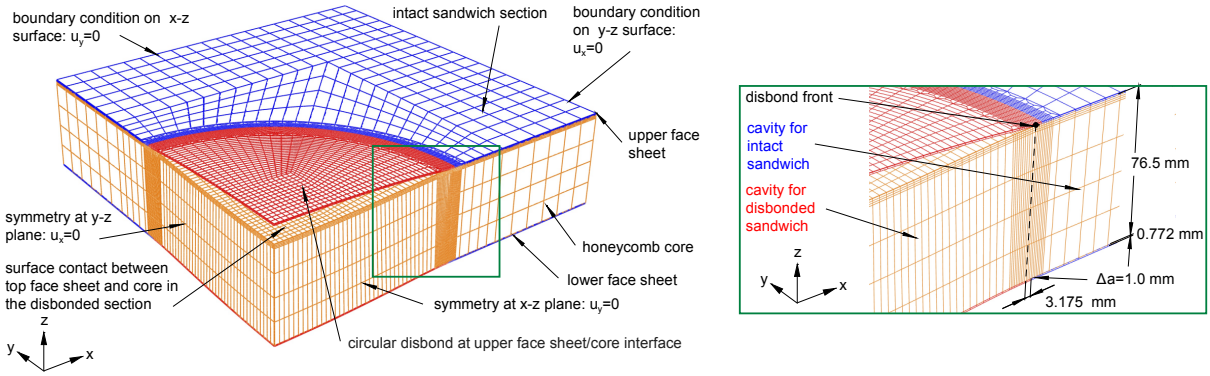

(a). Quarter of a sandwich panel with circular disbond *(b). Local mesh detail around disbond front*

Fig. 3: Finite element model of disbonded honeycomb sandwich panel.

6. OUTLOOK

Once developed, standardized test methods will be published as *ASTM Standards*. These *ASTM Standards* will be referenced, and methodology, analysis approach, case studies, and guidelines for best practice will be documented in new chapters of CMH-17 Vol. 6 [1].

ACKNOWLEDGEMENTS

This research has been supported by the Federal Aviation Administration (FAA). Funding through the Aviation Research Grants Program, Research Grant Number 16-G-006 is gratefully acknowledged.

REFERENCES

[1] *Composite Materials Handbook CMH-17, Volume 6. Structural Sandwich Composites*. SAE International: 2013.
[2] Transportation Safety Board of Canada, "Loss of Rudder in Flight," *Aviation Investigation Report A05F0047:* Minister of Public Works and Government Services, Canada, 2007.
[3] Air Accident Investigation Branch. AAIB Bulletin 8/92 Ref: EW/A92/5/1: Air Accident Investigation, UK, 1992.
[4] R. Hilgers, "Substantiation of Damage Growth within Sandwich Structures," *FAA Workshop for Composite Damage Tolerance & Maintenance,* Tokyo, Japan, 2009.
[5] V. Goyal et al., "Failure Analysis of Unvented Honeycomb Structures," *29th ASC Technical Conference*, 2014.
[6] E. H. Glaessgen et al., "Debonding Failure of Sandwich-Composite Cryogenic Fuel Tank with Internal Core Pressure," *J. Spacecraft and Rockets*, 2005, vol. 42, no. 4, pp. 613-627.
[7] Goetz et al., "Final Report of the X-33 Liquid Hydrogen Tank Test Investigation Team," NASA Marshall Space Flight Center, Huntsville, AL, USA, 2000
[8] J. M. Moran, *Fundamentals of Engineering Thermodynamics*: Wiley, 4th Edition, 2000.
[9] M. Rinker et al., "Analysis of an Aircraft Honeycomb Sandwich Panel with Circular Facesheet/Core Disbond Subjected to Ground-Air Pressurization," NASA/CR-2013-217974, 2013.
[10] S. Prasad et al., "Debonding and Crack Kinking in Foam Core Sandwich Beams-II. Experimental Investigation," *Engineering Fracture Mechanics*, 1994, Vol. *47*, no. 6, pp.825-841.
[11] M. Rinker et al., "Characterizing Facesheet/Core Disbonding in Honeycomb Core Sandwich Structure," NASA/CR-2013-217959, 2013.
[12] C. Lundsgaard-Larsen et al., "A Modified DCB Sandwich Specimen for Measuring Mixed-Mode Cohesive Laws," *Engineering Fracture Mechanics*, 2008, vol. 75 no. 8, pp. 2514-2530.
[13] W.J. Cantwell et al., "Interfacial Fracture in Sandwich Laminates," *Composites Science and Technology*, 1999, vol. 54, no. 14, pp. 2079-2085.
[14] X. Li et al., "The Tilted Sandwich Debond (TSD) Specimen for Face/Core Interface Fracture Characterization," *Journal of Sandwich Structures and Materials*, vol. 1, 1999, pp. 60-75.
[15] A.T. Nettles et al. "Using the Climbing Drum Peel (CDP) Test to Obtain a GIc Value for Core/Face Sheet Bonds," *Journal of Composite Materials*, vol. 41, no. 24, 2007, pp. 2863-2876.
[16] C. Weaver, "Evaluation of Mode I Fracture Mechanics Test Methods For Sandwich Composites," M.Sc Thesis, University of Utah, Salt Lake City, UT, 2009.
[17] J. G. Ratcliffe et al., "Sizing a Single Cantilever Beam Specimen for Characterizing Facesheet-Core Debonding in Sandwich Structure," *Journal of Composite Materials, 2011,* vol. 45, pp. 2669-2684.
[18] R. Krueger et al., "Characterizing Face Sheet/Core Disbonding Using the Single Cantilever Beam Test: Results from an International Round Robin," NASA/TM-2018-xxxxx, *NASA Langley Research Center, under review*, 2018.
[19] Z. M. Chen, R. Krueger, and M. Rinker, "Face Sheet/Core Disbond Growth in Honeycomb Sandwich Panels Subjected to Ground-Air-Ground Pressurization and In-Plane Loading," in *NAFEMS World Congress, paper #43*, San Diego, CA, 2015.

DOI: 10.5075/epfl-ICSS12-2018-128-129

GROUND-AIR-GROUND (GAG) MODELLING AND TESTING OF DISBONDED HONEYCOMB AIRCRAFT SANDWICH PANELS

Arash Farshidi[1], Christian Berggreen[1] and Ralf Hilgers[2]
[1]Department of Mechanical Engineering, Technical University of Denmark,
Nils Koppels Allé, Building 404, DK-2800 Kgs. Lyngby, Denmark.
Email: arfa@mek.dtu.dk & cbe@mek.dtu.dk
[2]Airbus GmbH, Hamburg, Germany. ralf.hilgers@airbus.com

1. ABSTRACT

On March 2005, an Airbus A310-300, experienced separation of its rudder in-flight (see Fig. 1). The investigation ruled out that the most probable root cause of the rudder loss was a sandwich disbond grown during the flight This incident together with a few other similar cases triggered extensive research into disbond fracture in honeycomb core sandwich composites [1, 2]. The presented experimental work here is part of an industrial partnership between AIRBUS and DTU in order to investigate disbond damages in aircraft honeycomb sandwich structures.

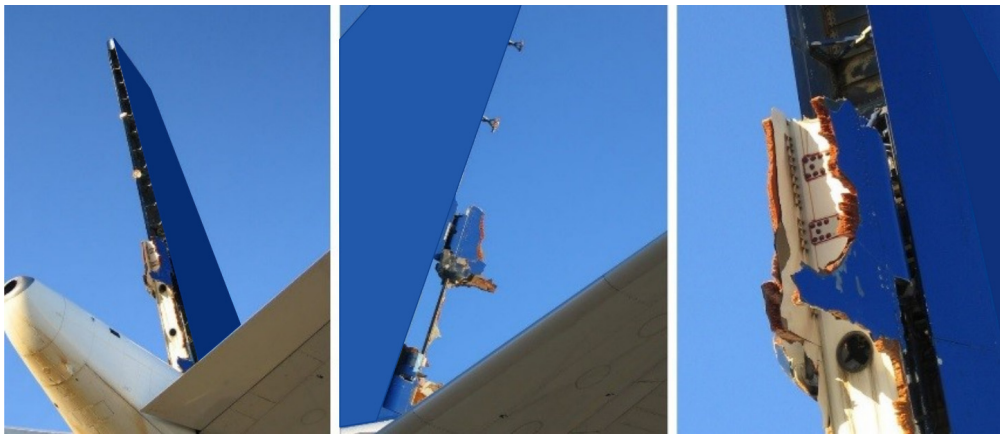

Fig. 1: Airbus A310-300 rudder failure.

Aircraft honeycomb sandwich structures are subjected to Ground-Air-Ground (GAG) loading cycles along their operation, as the relative pressure of the air inside their unvented honeycomb core varies due to different pressure at sea level and flight altitude. Cyclic change in relative internal pressure leads to fatigue loading and propagation of disbonds which may have been introduced during service or manufacturing process. This highlights the necessity of investigation of static and fatigue disbond propagation. To this end, CFRP/Nomex sandwich composite panels with circular disbond in centre were manufactured. A state of the art vacuum chamber was utilized to impose the cyclic pressure together with in-plane compression loading (see Fig. 2).

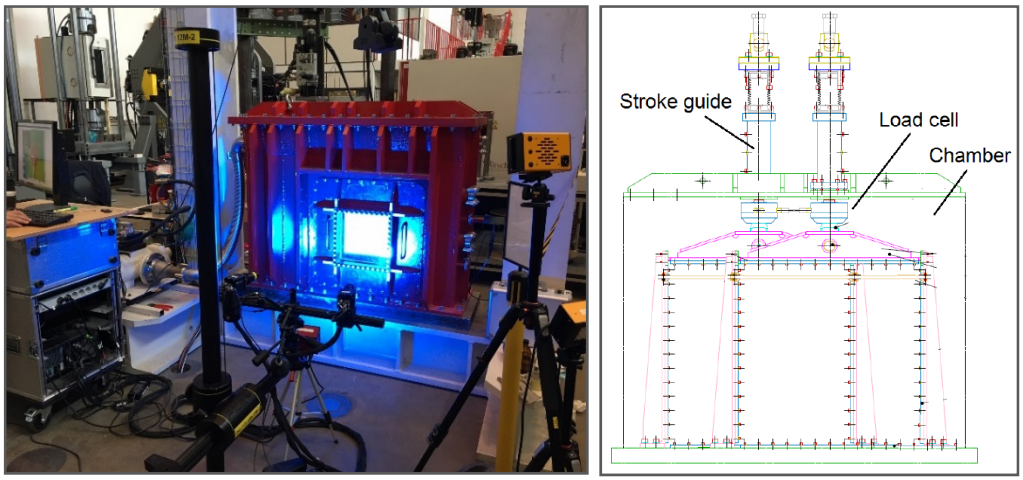

Fig. 2: Test setup using vacuum chamber and DIC.

The crack growth rate was measured for different load conditions. The sandwich panels were tested both in pure cyclic pressurization and also with cyclic in-plane compression. The disbond growth has been monitored using Digital Image Correlation (DIC) and the results have been compared with numerical analysis using Abaqus. Fig. 3 shows the out-of-

plane displacement measurement of a vacuum loaded sandwich panel with an artificial circular disbond. The DIC revealed the accurate position of the Teflon film. The FE model was constructed accordingly.

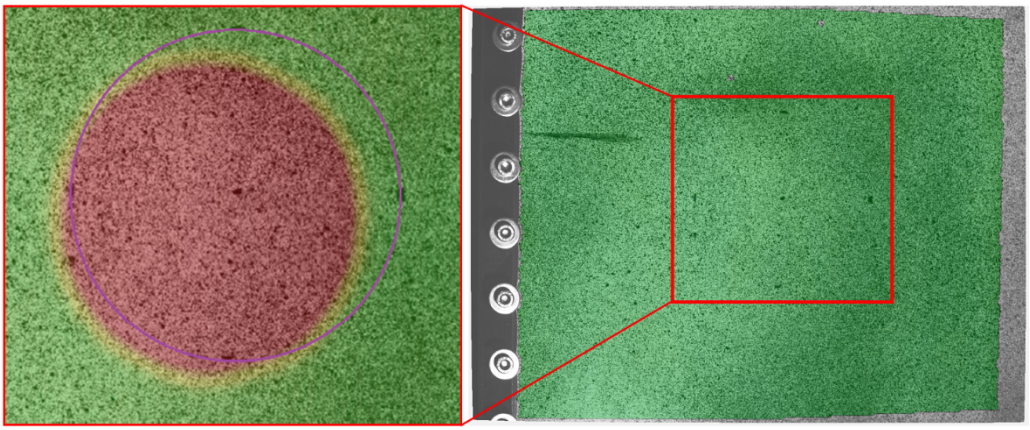

Fig. 3: Disbond front monitoring using DIC.

Pilot sandwich specimens were tested to validate the pressure control inside the vacuum chamber. Fig.4 shows the command and actual pressure versus time for a single cycle on left and for multiple cycles on right. The pressure was cycled between 1000 hPa corresponding to the see level air pressure and 150 hPa corresponding to the environment pressure at flying altitude.

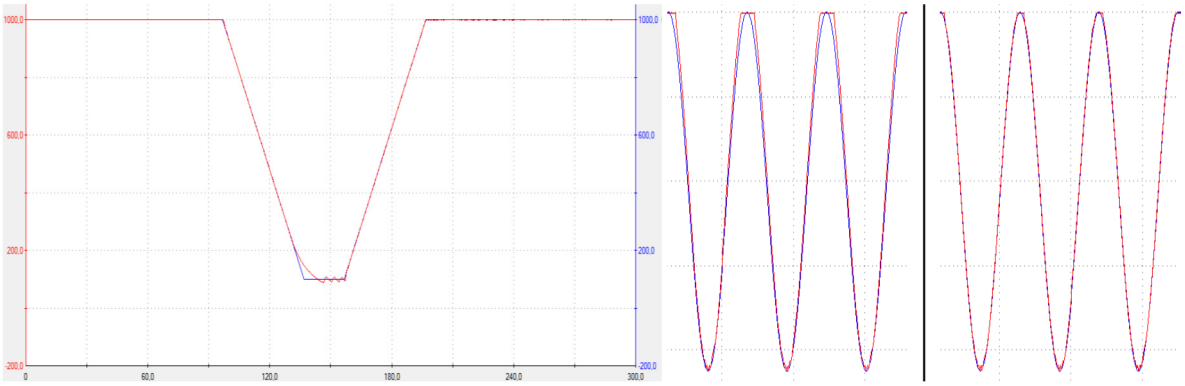

Fig. 4: Command pressure (blue) and actual pressure (red) for single (left) and multiple (right) cycles.

An advanced 3D model of disbonded panels subjected to Ground-Air-Ground (GAG) and in-plane loading was also constructed using the Abaqus software (see Fig. 5). The CSDE method and a sub-modeling technique as well as the cycle-jump method [3] were employed to handle arbitrary shape disbonds (i.e. not necessarily a circle or an ellipse) subjected to various fatigue loading scenarios (i.e. any combination of cyclic GAG, in-plane and out-of-plane loadings). Numerical results were validated against experiments carried out using the vacuum chamber facility.

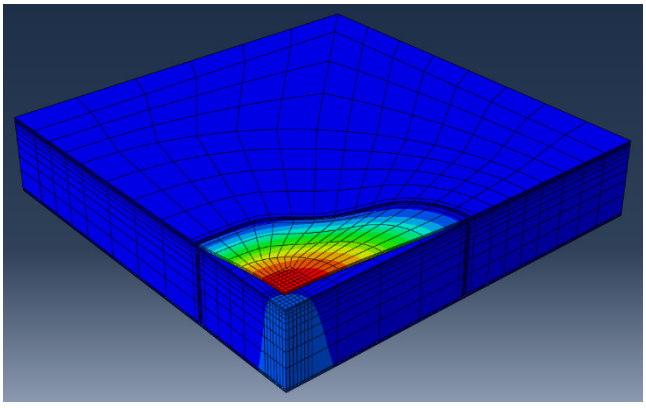

Fig. 5: Global model of the advanced 3D disbond model.

REFERENCES

[1] Transportation Safety Board Of Canada. Aviation Investigation Report A05F0047, Minister Of Public Works And Government Services Canada, 2007.

[2] R. Hilgers, "Substantiation Of Damage Growth Within Sandwich Structures," FAA Workshop For Composite Damage Tolerance & Maintenance, Tokyo, Japan, 1-5 June 2009.

[3] R. Moslemian et al., "Interface fatigue crack propagation in sandwich X-joints – Part II: Finite element modelling", *Journal of Sandwich Structures and Materials*, 2013, 15: 451-463

DOI: 10.5075/epfl-ICSS12-2018-130-132

2D QUASI-STATIC DELAMINATION IN GFRP LAMINATES: EXPERIMENTAL INVESTIGATION

Aida Cameselle-Molares[1], Anastasios P. Vassilopoulos[1] and Thomas Keller[1]
[1]Composite Construction Laboratory (CCLab), École Polytechnique Fédérale de Lausanne (EPFL), Switzerland.
aida.camesellemolares@epfl.ch, anastasios.vasilopoulos@epfl.ch, thomas.keller@epfl.ch

1. INTRODUCTION

Composite materials are commonly used for load-bearing structural elements because of their high stiffness- and strength-to-weight ratios. The successful use of fiber reinforced polymers (FRP) in primary structural parts depends on their integrity and reliability. Delamination in laminated composites is one of the most critical types of damage. Research efforts and standards [1-2] to investigate delamination fracture behavior have focused on beam-like specimens where the crack propagates with a constant width in only the longitudinal direction. Double cantilever beam specimens have been typically employed to study delamination under opening mode (Mode I) and the derived fracture values are used in structural design [3]. However, provided that delamination in real structures is not restricted to one direction but spans all around the contour of the defect, new fracture experimental designs capable of better approaching reality are needed. In this study, the main objective was the experimental investigation of the 2D delamination behavior in GFRP plates. A novel design and experimental set-up suitable for laminates with internal disbonds and subjected to opening loads was developed. Similar out-of-plane stresses are likely to appear in real applications such as local face sheet wrinkling in sandwich panels or curved face sheets (also in sandwich panels) with interlaminar defects.

2. EXPERIMENTAL INVESTIGATION

Material and Specimen Description

Three different types of glass fiber reinforcements were used to fabricate the laminates: two types of woven fabrics with different proportions of reinforcement in the warp/weft directions (50/50 (W50.50) and 60/40 (W60.40)); and a long continuous filament mat (CFM). The experimental program was conducted on six GFRP plates, two for each type of reinforcement. The layup and geometrical description of the plates are presented in Table 1.

Table 1: Description of GFRP plates.

Plate type	No. of layers	Dimensions (mm, width x height x avg. thickness)
W50.50.1/W50.50.2	8	460x460x3.33/480x480x3.53
W60.40.1/W60.40.2	6	410x410x3.33/410x410x3.06
CFM.1/CFM.2	6	420x420x7.50/420x420x6.99

All the GFRP laminates were symmetric with respect to both the midplane and each of the halves. The plate configuration is shown in Fig. 1(a). To introduce the load, two steel inserts were placed in the center and the midplane of the reinforcements. Between them, a Teflon film was placed to introduce the pre-crack of 55-mm radial length (see Fig. 1). The procedure developed for the introduction of the out-of-plane load into the plates is detailed in Figs. 1(b, c).

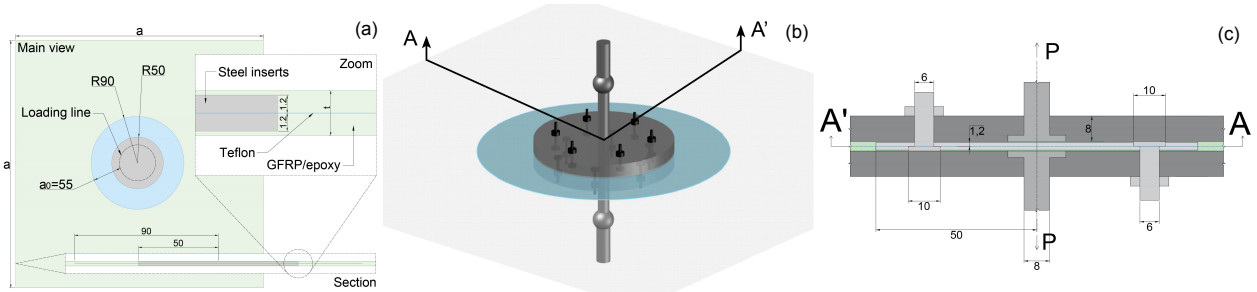

Fig. 1: (a) GFRP plate configuration; (b) general 3D view of the loading system; (c) A'A section view. Dimensions in mm.

Experimental Set-Up, Instrumentation and Measurements

The experimental set-up and instrumentation layout are shown in Fig. 2 (a, b). Once the load-introduction system was assembled, the plate was placed and fixed within the grips of the machine. Due to the difficulty of measuring the entire contour of the crack, three different measuring systems were employed: a 3D Digital Image Correlation System (DIC), a digital camera and visual measurements (see Fig. 2(c)).

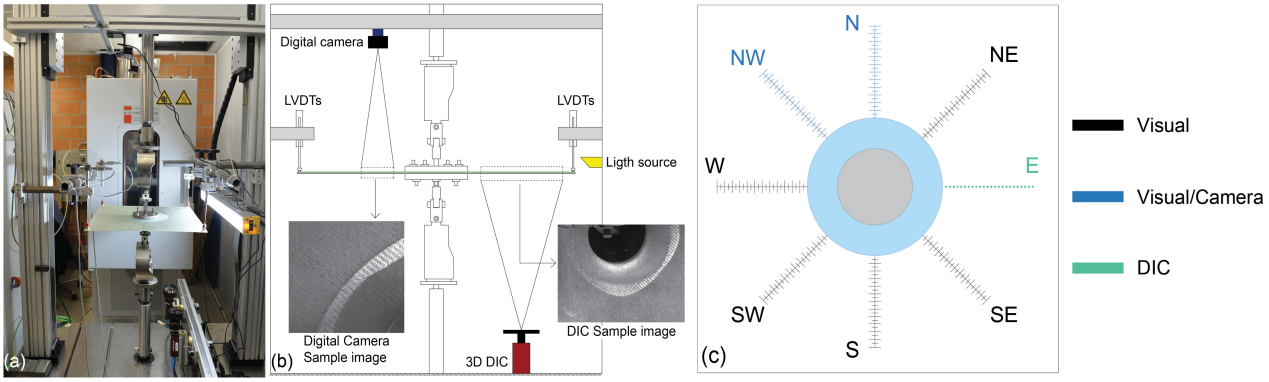

Fig. 2: (a) Experimental set-up; (b) instrumentation layout; (c) layout of crack measuring system.

EXPERIMENTAL RESULTS AND DISCUSSION

Load-Displacement Responses and Crack Propagation Measurements

Continuously increasing load-opening displacement curves were obtained for all the experiments (Fig. 3) as a result of the disproportionate growth of the crack area, whose increments were higher as the crack advanced, forcing the load to increase to continue the propagation of the crack. Only one specimen of each pair of plates is shown here. The other specimen of each pair of plates behaved similarly.

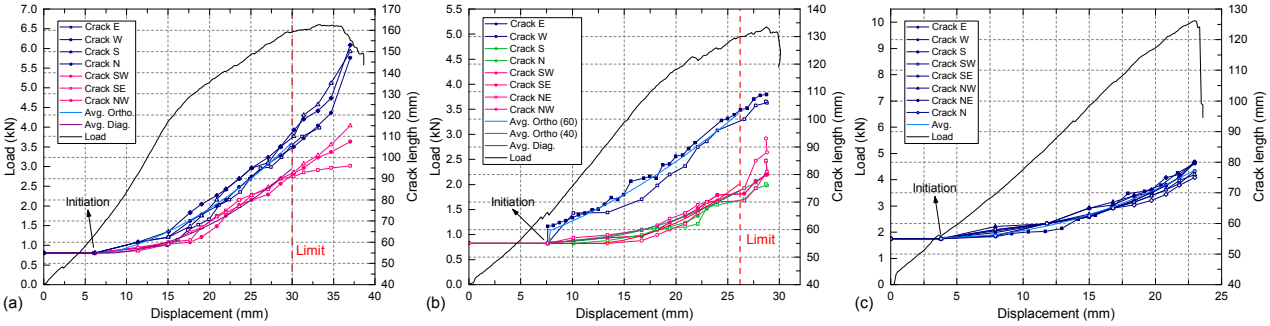

Fig. 3: Load and crack lengths vs opening displacement curves: (a) W50.50.1; (b) W60.40.1; and (c) CFM.1.

The crack lengths vs opening displacement response of the W50.50.1 plate is shown in Fig. 3(a). The blue lines represent the orthogonal directions and the magenta lines represent the diagonal directions. It can be observed that the measured lengths along the diagonal directions remained fairly consistent with each other as well as for the orthogonal directions, indicating a practically symmetric growth of the crack front. The limit of the symmetric behavior corresponded to a 30-mm opening displacement and is marked with a dashed vertical red line. The same representation is shown in Figs. 3(b, c) for the W60.40.1 and CFM.1 plates respectively. For the first, the blue lines represent the orthogonal directions with 60% reinforcement, the green lines the orthogonal directions with 40% of reinforcement and the magenta lines the diagonal directions. For the CFM.1, due to the concentric growth of the crack, the values of the crack lengths showed the same trend.

Crack Propagation Patterns

Crack propagation in the W50.50 and W60.40 plates advanced symmetrically to the orthogonal axes up to the symmetric limit (see Fig. 3). The shapes of the crack fronts for the last symmetric contours are drawn in blue in Figs. 4(a, b). For the CFM laminates, Fig. 4(c), a concentric circular crack front propagation was observed.

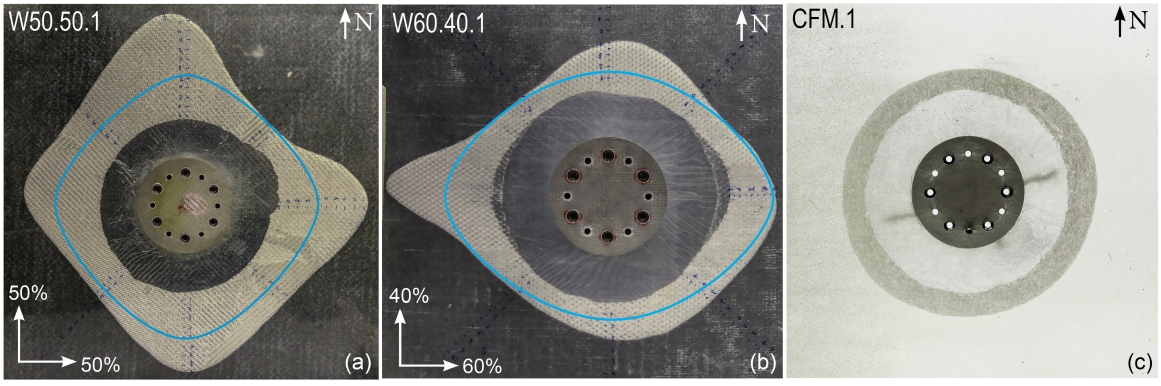

Fig. 4: Crack propagation pattern for (a) W50.50.1; (b) W.60.40.1; and (b) CFM.1.

Compliance Behavior and Stiffness-Related Mechanisms

The compliance plotted against the crack area is shown for W50.50, W60.40 and CFM plates in Figs. 5(a, b and c respectively). All laminates exhibited comparable behavior, i.e. first a descending branch down to a minimum and then an ascending branch corresponding respectively to a stiffening and subsequent softening of the system.

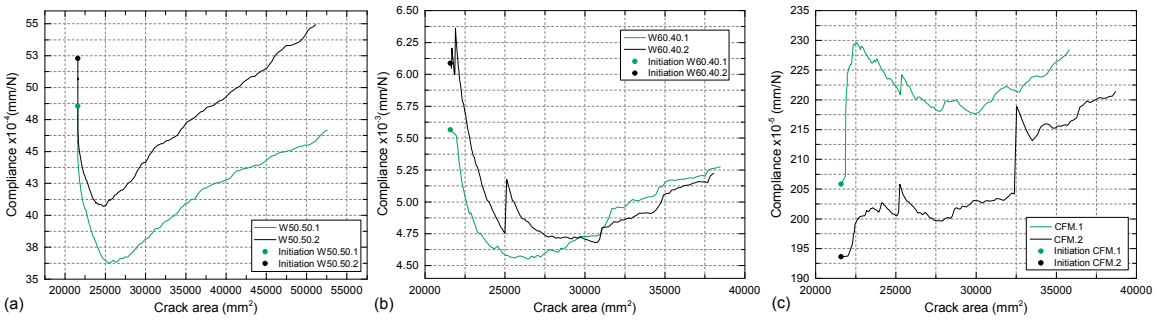

Fig. 4: Compliance vs crack area for (a) W50.50; (b) W60.40; and (c) CFM pairs

Based on the compliances, two main different regions could be differentiated, i.e. A and B in Fig. 6(a). In region A, a decreasing behavior of the compliance was observed (i.e. stiffening of the plate) down to a minimum value (transition point, TP). From the TP onwards (Region B), the compliance started to increase (i.e. softening of the plate). The changes in the stiffness were caused by three different mechanisms activated during the opening of the plates: stretching, fiber-bridging and crack propagation. The boundary conditions of the plates led to the radial and circumferential stretching of the out-of-plane deforming open part of the plates. Once the crack started propagating, the other two mechanisms were activated: the fiber-bridging, contributing to the stiffening of the plate, and the crack propagation itself, causing the softening of the system. The stiffening mechanisms prevailed over the softening up to the TP. Beyond the TP, the softening was the dominant mechanism. These two regions can be likewise identified in the load-displacement curves (see Fig. 6(b)). The same differentiation procedure in the compliance vs crack curve can be established for the W60.40 and CFM plates.

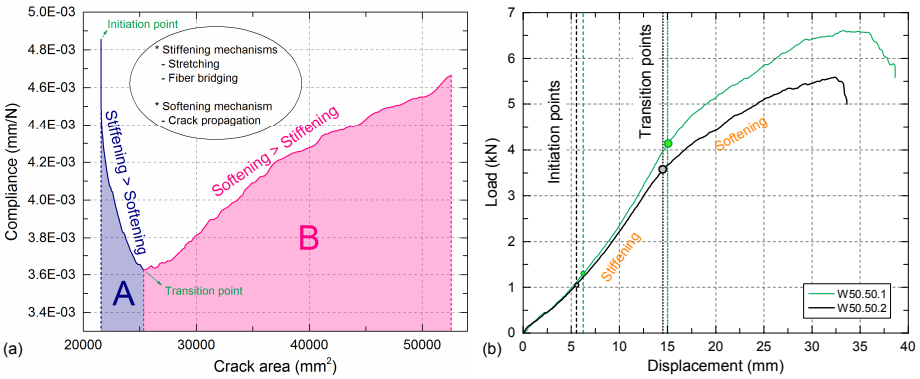

Fig. 6: Stiffening and softening regions on W50.50: (a) compliance vs crack area; (b) load vs displacement.

CONCLUSIONS

The 2D delamination behavior of composite laminates with a circular embedded pre-crack under quasi-static out-of-plane loading has been experimentally investigated. The following conclusions were drawn:

1. An experimental design suitable for investigating the 2D propagation of an embedded pre-crack under out-of-plane opening loading was successfully developed.
2. Increasing loads were obtained as a result of a continuously increasing crack front length and a consequently disproportionate increase in the propagation area.
3. As the plates started to deform, stretching stresses appeared in both the radial and circumferential directions as a result of the geometrical constraints. Consequently, the plates were subjected to a dual stiffening effect.
4. Stretching of the specimens and fiber bridging (both stiffening mechanisms) were capable of delaying the general softening of the system that typically occurs once the crack starts to propagate.

REFERENCES

[1] M.L. Benzeggagh et al., "Measurement of mixed-mode delamination fracture toughness of unidirectional glass/epoxy composites with mixed-mode bending apparatus", *Comp. Sci. and Tech.*, 1996; 56: 439-449.

[2] ASTM D5528-13: Standard test method for mode I interlaminar fracture toughness for unidirectional fiber-reinforced polymer matrix composites, in Annual book of ATM standards: adhesive section 15.03.

[3] K.F. Nilsson et al., "A theoretical and experimental investigation of buckling induced delamination growth", *J. Mechan. Phys. Solids,* 2017; 41: 749-782.

DOI: 10.5075/epfl-ICSS12-2018-133-135

2D QUASI-STATIC DELAMINATION IN GFRP LAMINATES: NUMERICAL INVESTIGATION

Aida Cameselle-Molares[1], Anastasios P. Vassilopoulos[1], Jordi Renart[2], Albert Turon[2] and Thomas Keller[1]
[1]Composite Construction Laboratory (CCLab), École Polytechnique Fédérale de Lausanne (EPFL), Switzerland.
aida.camesellemolares@epfl.ch, anastasios.vasilopoulos@epfl.ch, thomas.keller@epfl.ch
[2]AMADE, Mechanical Engineering and Industrial Construction Department, Universitat de Girona, Spain.
jordi.renart@udg.edu, albert.turon@udg.edu

1. INTRODUCTION

Delamination in laminated components is one of the most critical types of damage. Thus, significant efforts have been devoted to investigate delamination in laminated composites [1], mostly in beam-like specimens, which have been widely investigated and standardized [2]. However, some of the conditions required by these types of experiments (e.g. constant crack width or single direction of propagation) may not correspond to the actual damage growth in FRP structures where delamination may develop all around the contour of a defect.

The experimental fracture behavior of laminated FRP plates with an embedded circular pre-crack (i.e. 2D delamination) and subjected to quasi-static out-of-plane opening loads is presented in another abstract of this conference [3]. This abstract focuses on the numerical investigation of the 2D in-plane crack propagation in two of these laminated plates. To compare and to understand the transition from standard 1D fracture experiments to 2D crack propagation scenarios, DCB specimens were further experimentally and numerically investigated.

2. EXPERIMENTAL METHODS, RESULTS AND DISCUSSION

Experimental Investigation of Laminated Plates

The 2D delamination behavior of GFRP laminated plates under quasi-static out-of-plane opening loading was experimentally investigated and presented in [3]. The experimental results obtained for the two laminated plates studied here (with long continuous filament reinforcement, CFM) are summarized in Fig. 1, where the load vs displacement and average crack-length vs displacement curves are shown for both CFM plates (Fig. 1(a)). Likewise, the curves illustrating the crack area vs the compliance of the plates are shown in Fig. 1(b). The minimum value in these curves (changing from decreasing to increasing behavior) was named “transition point” (TP) (see [3]).

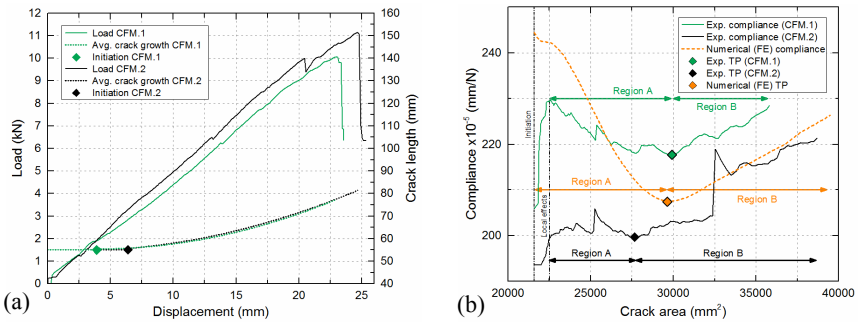

Fig. 1: (a) Experimental load and crack length vs displacement curves and (b) Comparison of experimental and numerical crack area vs compliance of CFM plates.

Experimental Investigation of Mode I DCB Specimens

Double cantilever beam specimens were used to determine the Mode I strain energy release rate (SERR). The same material system and lay-up (6 layers of CFM) as those of the plates were used. A Teflon film was placed at the midplane to introduce the pre-cracks. Specimens of 250-mm length and of different widths (25, 40, 60 and 100 mm) were investigated.

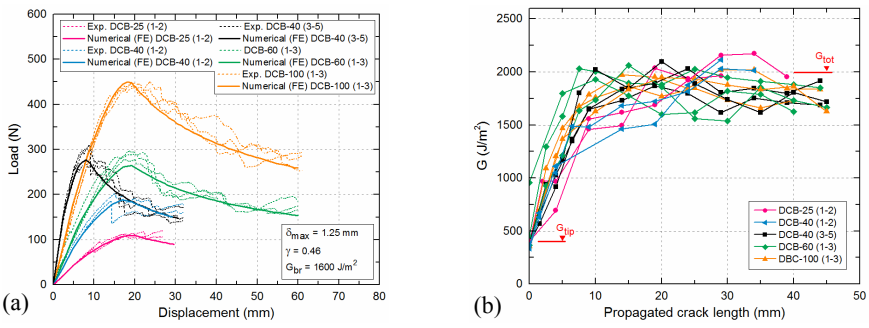

Fig. 2: (a) Comparison of experimental and numerical load-displacement curves; (b) experimental R-curves.

The experimental load-displacement responses of DCB specimens are shown in Fig. 2(a) and the experimental R-curves in Fig. 2(b). The total SERR, G_{tot}, derived from the experiments is the sum of the SERR at the crack tip, G_{tip}, and the SERR due to the fiber-bridging, G_{br}. According to these curves, values of 400 and 2000 J/m^2 respectively were assigned to G_{tip} and G_{tot}. A value of ~10 mm for the fiber-bridging length was obtained along with a maximum crack-opening displacement (COD), δ_f, of ~1.25 mm. Similar R-curves were obtained independently of the specimens' width.

NUMERICAL METHODS, RESULTS AND DISCUSSION

Cohesive Zone Modeling

The type of traction-separation law used to define the behavior of the cohesive elements is shown in Fig. 3(a). The first part of the law (orange) is attributed to the initial damage and the area equals SERR at the crack tip, G_{tip} (i.e. the energy required for crack initiation). The second part (blue) corresponds to the SERR due to the fiber-bridging, G_{br}. Details of the formulation can be found in [4].

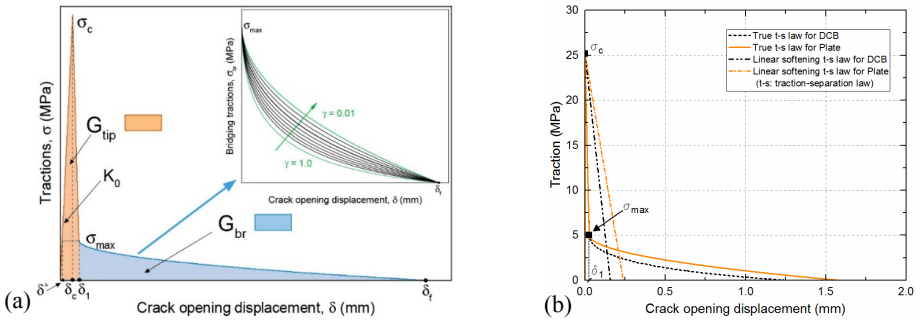

Fig. 3: Traction-separation curves; (a) general description and (b) used in numerical models.

Numerical Investigation of Mode I DCB Specimens

A finite element (FE) model was developed to simulate the delamination behavior of the DCB experiments using the commercial analysis software ABAQUS 6.14.1. The two GFRP beams were modeled with 3D built-in continuum shell elements and a single zero-thickness layer of three-dimensional cohesive elements was implemented at the midplane in the un-cracked region. Further details concerning this FE model can be found in [4]. The experimentally obtained SERR values of G_{tip}=400 J/m^2 and G_{tot}=2000 J/m^2 (i.e. G_{br}=1600 J/m^2) and the maximum COD (δ_f =1.25 mm) were assigned. The maximum traction for damage initiation was assumed to be equal to 30% of the tensile strength of the matrix, i.e. σ_c =25.2 MPa. The initial cohesive stiffness, K_0, was taken as being equal to 10^5 MPa/mm. The values of the maximum bridging traction, σ_{max}, and the bridging traction decay ratio, γ, were estimated iteratively. Corresponding values of 5 MPa and 0.46 were obtained. The resulting traction-separation law is presented in Fig. 3(b). The obtained numerical load-displacement curves (in good agreement with the experimental ones) are shown in Fig. 3(a).

Numerical Investigation of Laminated Plates

For the simulation of the CFM plates ABAQUS 6.14.1 was also employed. The FE model is described in Fig. 4.

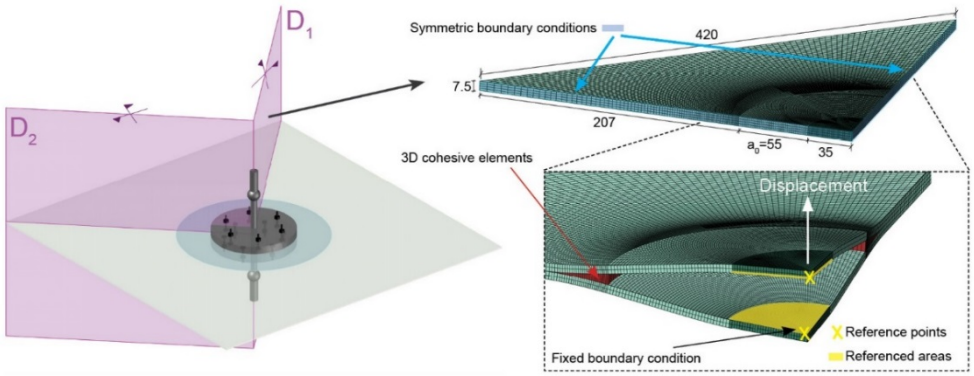

Fig. 4: Description of finite element model of laminated plate.

The built-in continuum shell element of eight nodes from Abaqus/Standard was used to mesh the bulk material. Two through-thickness elements were assigned to each of the halves of the plate. A single zero-thickness layer of 3D cohesive elements of eight nodes was implemented at the midplane of the un-cracked region. Further details of the model can be found in [4].

Initially, the same traction-separation law obtained for the DCB specimens was used (Fig. 3(b)), the total value of the SERR being therefore equal to G_{tot} =2000 J/m^2. However, the numerical load-displacement response obtained with these values did not correspond to the experimental curves, as shown in Fig. 5(a).

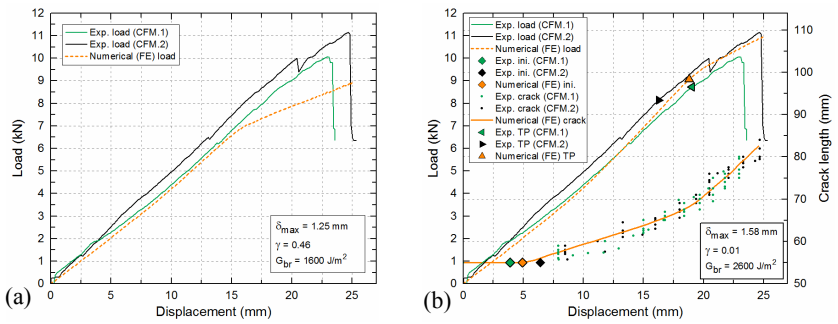

Fig. 5: Comparison of experimental and numerical results of CFM plates; (a) load-displacement curves using cohesive parameters and G_{tot} from DCBs and (b) load and crack length vs opening displacement curves with the adjusted parameters.

To better approach the experimental behavior, a fitting process was carried out. The values of K_0, G_{tip}, σ_c and σ_{max} (matrix-dominated values) were kept constant and the same as those obtained from the DCB specimens. The adjustment of the law was accomplished by fitting the value of G_{br} and therefore modifying the values of γ and δ_f. The values that allowed the FE model to approach the experimental behavior were γ = 0.01 and δ_f =1.58 mm, which lead to a G_{br} value of 2600 J/m^2 and therefore to a G_{tot} value of 3000 J/m^2 (see Fig. 3(b)). The revised numerical load-displacement and crack length-displacement curves are shown in Fig. 5(b). The numerical compliance vs crack area is shown in Fig. 1(b).

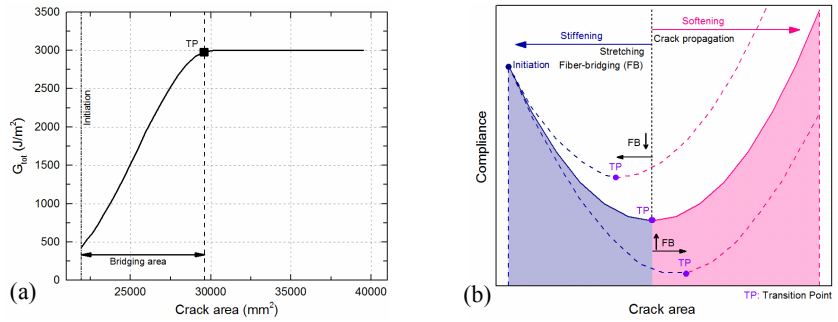

Fig. 6: (a) Numerical R-curve of laminated plate; (b) description of general behavior of crack area vs compliance curves.

The numerical value of the crack area at the TP in Fig. 1(b) coincides with the numerical value of the fully developed bridging area in the numerical R-curve (Fig. 6(a)). Consequently, with the value of the area at the TP obtained from the compliance vs crack area curve, the value of the bridging area can be directly obtained (here ~29600 mm^2 corresponding to a propagated radial length of ~13.2 mm). As a result, any decrease or increase in the bridging area would lead the compliance vs crack area curve moving to the left or right respectively (Fig. 6(b)).

The total value of the SERR obtained from the FEM of the plates was 50% higher than the total SERR derived from the DCB specimens (2000 vs 3000 J/m^2). This increase in the G_{tot} was directly related to the difference in stiffness between the DCB specimens and the plates. Furthermore, the stretching of the deformed part of the plate resulted in a "stress stiffening" effect. Consequently, more fiber-bridging than in the DCB specimens developed in the plates.

CONCLUSIONS

A numerical investigation of the 2D crack propagation in laminated plates was carried out to simulate the fracture behavior of the same plates that were previously experimentally investigated [3]. Additional DCB experiments were performed to study the transition from 1D to 2D crack propagation scenarios. The following conclusions can be drawn:

1. The selected shape of the traction-separation law was able to model the fracture behavior of the plates.
2. The stress stiffening of the plates and the increase in the flexural stiffness led to an increase of the fiber-bridging area, causing a 50% increase of the total SERR compared to the total SERR obtained from the DCB specimens.
3. The fully developed fiber-bridging area in the plates was correlated with the crack area at the transition point of the compliance vs crack area curves.

REFERENCES

[1] A.J. Brunner, "Experimental aspects of Mode I and Mode II fracture toughness testing of fiber-reinforced polymer-matrix composites", *Comput. Methods Appl. Mechs. Eng.*, 2000; 185: 161-172.

[2] ASTM D5528-13: Standard test method for mode I interlaminar fracture toughness for unidirectional fiber-reinforced polymer matrix composites, in Annual book of ATM standards: adhesive section 15.03.

[3] A. Cameselle-Molares et al., "2D quasi-static delamination in GFRP laminates: experimental investigation", *Extended abstract in the 12th International Conference in Sandwich Structures (ICSS12)*, 2018; 19-22 August, Lausanne, Switzerland.

[4] A. Cameselle-Molares et al., "Numerical simulation of two-dimensional in-plane crack propagation in FRP laminates", *Compos. Struct.*, 2018; 200:396-407

DOI: 10.5075/epfl-ICSS12-2018-136-138

UNSTABLE, 2D DEBONDING IN SANDWICH-LIKE TILING SYSTEMS

Shai Feldfogel[1] and Oded Rabinovitch[2]
[1] PhD student, Faculty of Civil and Environmental Engineering, Technion Israel Institute of Technology, Technion City, Haifa, 32000, Israel. shaifeldfogel@gmail.com
[2]Professor, Abel Wolman Chair in Civil Engineering, Faculty of Civil and Environmental Engineering, Technion Israel Institute of Technology, Technion City, Haifa, 32000, Israel. cvoded@tx.technion.ac.il

1. INTRODUCTION, MOTIVATION, AND OBJECTIVES

Tiling systems have been used by builders since ancient times, serving functional, structural, and aesthetic purposes as building cladding, floors, walls, and roofs coverings, artwork, mosaics, and more. In recent decades, along with their traditional uses, they have found growing application as thermal barriers systems in space-crafts and nuclear facilities [1, 2]. They have also been increasingly used for building facade cladding, due to the increase in high-rise building on the one hand, and their relatively low maintenance costs on the other.

As is typically the case in adhesively bonded sandwich plate structures, interfacial debonding is among the main failure mechanisms of tiling systems. In mild cases, interfacial damage may be limited and go unnoticed for quite some time. However, in more severe cases, interfacial debonding may propagate, leading to the detachment of the tile from its substrate and to its eventual falling. Falling of thermal barriers tiles from the space shuttle Columbia in the year 2003 led to its catastrophic disintegration and the death of all 13 astronauts upon reentry into the Earth's atmosphere [3]. Falling of tiles from building facedes on bystanders is another cause of injuries and death [4].

The main causes of interfacial debonding damage in tiling systems, which is *the* precondition for the eventual falling of tiles, are hygro-thermal effects. Exposure to large thermal differentials cycles, as well as to moisture and drying cycles, causes differential shrinkage of the constituent layers. This differential shrinkage results in interfacial traction concentrations, which, in turn, drive the interfacial debonding mechanisms.

Considering the extensive and increasing use of tiling systems on the one hand and the possible grave consequences of their failure on the other, understanding the evolution of interfacial debonding mechanisms is indispensable in the design of this ubiquitous layered structural form. Essential questions that arise in this regard are: What are the hygro-thermal loading levels under which interfacial damage begins to accumulate in a given tiling system? How does the two-dimensional (2D) debonding region change in size, location, and shape as the load levels increase? Is the growth of interfacial damage a stable process or an unstable one? How do the tile's geometry, the interfacial parameters, and the substrate's boundary conditions affect the debonding mechanism's evolution? The focus of the present paper is to help shed new light on and gain new insight into these pertinent questions.

The main challenges in addressing the raised questions regarding the evolution of interfacial debonding mechanisms in tiling systems are due to their salient physical features, the three most notable of them being:

1. A relatively soft adhesive mortar layer is sandwiched between two much more rigid substrate and tile layers;
2. The interfacial interactions that drive the debonding mechanism are governed by a small length scale while a much larger length scale defines the layered system's lineal dimensions; and
3. The interfacial tractions in this layered plate problem are 3D while the debonding region's evolution is 2D and geometrically irregular by nature.

2. METHODOLOGY

Specially tailored analytical and computational tools are developed in the present paper to address the salient physical features and to explore the nature of the problem at hand. Their totality comprises an analytical computational platform which includes a multilayered plate theory, and a corresponding triangular finite element (FE). To capture the high stress and deformation gradients in the soft adhesive mortar layer and the interfacial tractions at its interfaces, the formulation adopts the extended high-order plate theory for that layer [5,6,7]. Other specially tailored methodologies included in the formulation are plate-like cohesive interfaces to capture the 3D nature of the interfacial interactions, a pseudo arc-length procedure to explore the stability features of the debonding process, and a mode decomposition procedure to alleviate shear locking in the triangular FE [8,9,10].

3. NUMERICAL EXAMPLE

The numerical example focuses on the triggering and evolution of interfacial debonding in single tile configurations under uniform heating [9]. These simple conditions allow studying the problem in pure form and are therefore conducive to shedding light on the fundamental nature of the debonding mechanisms in this structural context. Emphasis is placed on the effects of different tile geometries, interfacial properties, and substrate boundary conditions on the geometrically irregular nature and the stability characteristics of the debonding mechanism. More details are given in [9].

Fig. 1 shows the configuration of Case A - a 200mm and 20mm thick square tile, connected by a 10mm thick adhesive mortar layer to a 200mm thick substrate layer. The three layers are subjected to a uniformly distributed heating differential $\Delta\theta$. Taking advantage of the double symmetry conditions, only the upper tight quadrant is analyzed, see Fig. 1(c).

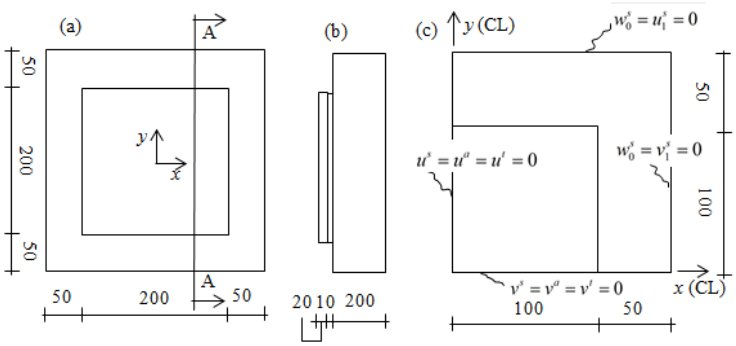

Fig. 1: Configuration of a square tile – Case A (a) plan; (b) cross-section AA; and (c) analyzed quadrant and the double symmetry boundary conditions (adapted from [9] with permission from Elsevier).

The evolution of the debonded area as a function of the temperature differential $\Delta\theta$ is depicted in Fig. 2. Fig. 2 can be thought of a type of "equilibrium" path, showing the normalized debonded area (debonded area divided by originally bonded area) A_d against $\Delta\theta$. Capturing the non-monotonous and highly irregular behavior in Fig. 2 is made possible through the use of the pseudo arc-length procedure. It can be seen that up to Point A1, at approximately 55°C, only negligible debonding occurs. From Point A1 to Point A2, the debonding process becomes much more "rapid", until a snap occur between Points A2 and A3. This zoom-in on the snap region, indicated by dashed lines, reveals an increase of debonded area without increase in thermal load. This type of behavior signifies an unstable nature of the debonding mechanism. The corresponding thermal load $\Delta\theta_{snap}$=75.53°C, well within service conditions in some cases, can therefore be considered as the debonding failure load of the layered system. The subsequent stabilization between Points A3 and A4 can be explained as an artificial product of the quasi-static analysis and is not very significant from a physical stand point.

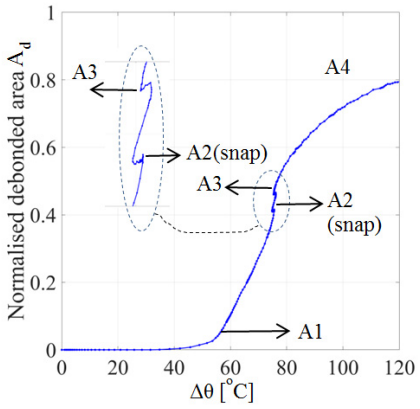

Fig. 2: Equilibrium path of case A: Normalized debonded area A_d Vs. the temperature differential $\Delta\theta$ (adapted from [9] with permission from Elsevier).

The geometrically irregular evolution of the debonding mechanism described in Fig. 2 is depicted in Fig. 3. Fig. 3 shows the progression of the debonding front, which is represented by the contour maps of the interfacial peeling traction at the substrate-adhesive interface. Figs. 3a-d show snap-shots of the debonding fronts that correspond to Points A1-A4, defined in Fig. 2 and referred to above. It can be seen that the debonding starts at the corner of the tile (Fig. 3(a)) and later propagates towards its center. The evolution in debonded area corresponding to the snap region between Points A2 and A3, is shown in Fig. 3(b) and 3(c). It seems that the snap is associated with a debonding front coalescence from the adjacent left and bottom quadrants (not shown in the figure). This suggests that the unstable nature of the mechanism is associated with the geometrical nature of the debonding area. At the end of the process, Fig. 3(d), the remaining bonded region becomes circular.

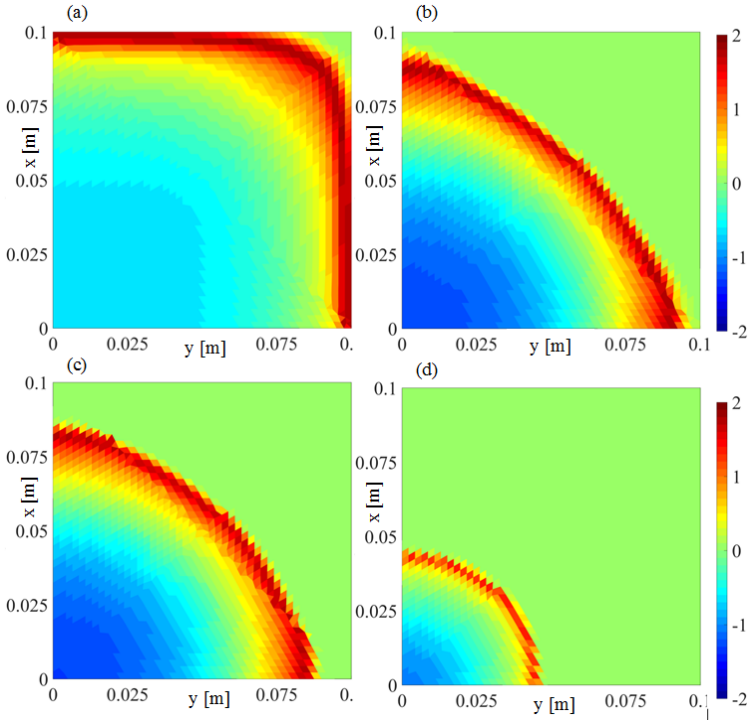

Fig. 3: debonding fronts: (a) Point A1; (b) Point A2; (c) Point A3; and (d) Point A4; (reprint from [9] with permission from Elsevier).

4. SUMMARY AND CONCLUSIONS

The numerical study reveals the unstable and the geometrically irregular nature of debonding mechanisms in tiling system. As is shown in the full paper, this observation is quite general as it applies to a wide range of tile geometries, boundary conditions, and interfacial properties. Understanding that instabilities are an inherent characteristic in the debonding mechanism is significant, especially because this aspect of the structural response is often overlooked in the design phase. Differently from other approaches, the present paper focuses directly on the 2D evolution of the debonding mechanism and on its relation to the observed instabilities.

REFERENCES

[1] E. Pate-Cornell et al., "Probabilistic risk analysis and risk-based priority scale for the tiles of the space shuttle", *Reliability Engineering and System Safety*, 1993; 40.3: 221-238.
[2] R. Mitteau et al., "Allowable heat load on the edge of ITER first wall panel beryllium flat tiles", *Nuclear Materials and Energy*, 2017
[3] A. M. Capece et al., "failure analysis of a thermal tile on the space shuttle Columbia", *Journal of Failure Analysis and Prevention*, 2006; 6.1: 55-60.
[4] D. C. Ho et al., "The causes of external wall tiling defects in Hong Kong", *Structural Survey*, 2005; 23.5: 386-402.
[5] C. Phan et al. "Blast response of a sandwich beam/wide plate based on the extended high-order sandwich panel theory and comparison with elasticity", *Journal of Applied Mechanics*, 2013; 80.6.
[6] O. Rabinovitch, "An extended high order cohesive interface approach to the debonding analysis of FRP strengthened beams", *International Journal of Mechanical Sciences*, 2014; 81: 1-16.
[7] S. Feldfogel et al. "Thermally induced wrinkling in orthotropic layered plates with irregular delaminations", *International Journal of Nonlinear Mechanics*, 2017; 92: 127-143.
[8] S. Feldfogel et al. "Full scale analysis of FRP strengthened plates with irregular layouts", *International Journal of Mechanical Sciences*, 2016; 113: 239-259.
[9] S. Feldfogel et al (2018) "Two Dimensional Debonding Failure in Adhesively Bonded Tiles" *International Journal of Solids and Structures*, In press.
[10] T. Belytschko et al., "A c0 triangular plate element with one quadrature point", *International Journal for Numerical Methods in Engineering*, 1984; 20.5: 787-802.

SESSION 6B: APPLICATIONS – CIVIL ENGINEERING

DOI: 10.5075/epfl-ICSS12-2018-140-142

POTENTIAL OF SHELL STRUCTURES MADE OF LINEAR MANUFACTURED UNIAXIALLY CURVED SANDWICH PANELS

Sören Grimm[1] and Jörg Lange[1]
[1]Technische Universität Darmstadt, Institute for Steel Structures and Materials Mechanics, Germany.
grimm@stahlbau.tu-darmstadt.de

1. INTRODUCTION

Today lightweight steel constructions made of sandwich panels are a common solution for roof and wall claddings. Due to the excellent weight to load ratio, their good heat insulation, their high load-bearing capacity as well as the economical manufacturing and erection process, sandwich constructions are build frequently. Besides the mentioned advantages the linear manufacturing process of sandwich panels, normally limits the possible building cubature to rectangular shapes.

Another construction form coming with an even lower ratio of weight to load are shell structures. In the 20th century, many of these structures were built, following the technical and scientific progress of that time. Disadvantages of most realized structures were that large and unique temporary constructions as well as large installation expense was necessary. In times of growing importance of construction time, the growing costs of construction site equipment and wage, building an economical efficient structure requires high levels of prefabrication and short assembly times.

In an interdisciplinary project, architectural, civil engineering and mechanical engineering institutes of Technische Universität Darmstadt are working on combining the advantages of these two forms of design. The research is aimed on the development of a concept to build shell structures out of linear manufactured uniaxially curved sandwich panels. This paper focuses on presenting the work status of the Institute for Steel Structures and Materials Mechanics, which consists of research on the load-bearing capacities of these structures.

2. STATE OF THE ART

In 1970, Otto Jungbluth presented a lightweight construction dome made of sandwich panels [2]. The shell structure has a span width of 45 m and was built of 120 panels. Each panels is uniaxially curved, has a variable width und was produced by Hoesch AG in single item fabrication.

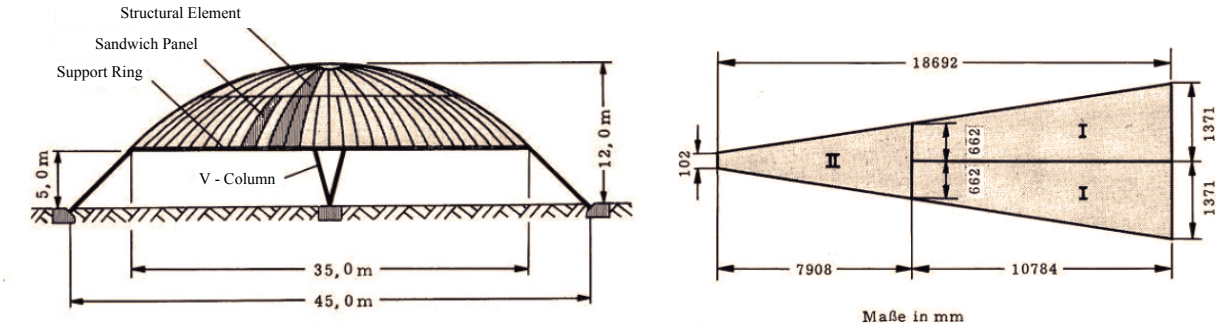

Fig. 1: Dome by O. Jungbluth and a Structural Sandwich Element. Figs. 1 and 2 in [2].

The panels with a length of approx. 8 m or 11 m are approx. 0.1 m to 1.4 m wide (see Fig. 1) and have metal faces with a thickness of 1 mm and polyurethane foam core in between the face sheet with a thickness of 150 mm. The structure is joined by pop rivets and bolted connections, which causes high local stresses in the face sheets.

On the site, 40 structural elements were merged to a shell structure (see Fig. 1), assembled by three sandwich panels, each. The connection of the panels to the structural elements as well as the connection of the elements had to be foamed after fixing them with the mentioned fasteners in situ.

After several reconstruction works, the dome is today the Information Center of Hannover Fairs. Taking into account that, according to German codes, facilities have to be designed to operate up to 50 years, it can it be concluded that the dome is a permanent light-weight shell structure with viable performance efficiency. However, despite its high performance a structure like the dome of Otto Jungbluth can hardly be built economically, considering todays boundary conditions.

Nevertheless, in 2010 Klaus Berner reported about established hall structures built with a roof structure made of linear manufactured uniaxially curved sandwich panels in Italy [1]. In this context, he also reminded of the structural potential of arched structures, which let expect a larger span of the panels.

3. ASPIRED DESIGN FORM

This research work is aiming on solutions realizing shell structures out of linearly manufactured uniaxially curved sandwich panels with plane face sheets and a polyurethane core taking advantage of their high load capacity and high level of prefabrication. This includes developing a design tool, a manufacturing process as well as the determination of the load bearing performance of these structures.

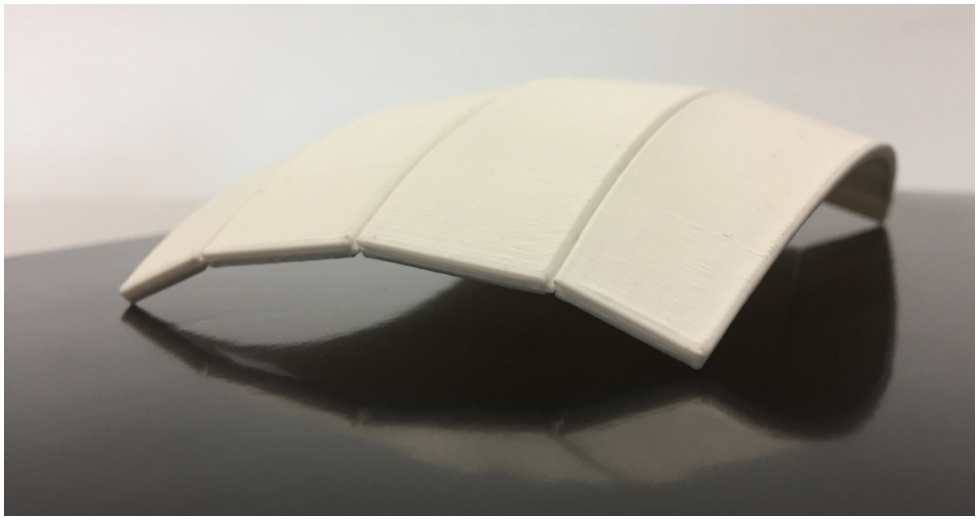

Fig. 2: Exemplary Design Model – Spherical Segment.

As an example, a roof structure could be designed as a spherical segment. Along the longitudinal direction, the panels are curved and in transverse direction, the curvature is approximated by a polygon. This design principle requires that the sandwich panels are produced with variable width as well as inclined joint planes. All features of the panels can be pre-engineered in computer models. The design tool will be targeted on holding the basic information for the manufacturing as well as the static model. Thus an integral design process is developed, which allows a close cooperation between architectural design, structural engineering and the manufacturer.

4. POTENTIAL OF LOAD-BEARING CAPACITIES

At this time, preliminary investigations on the load bearing capacity of arched sandwich beams indicate their high structural potential compared to single span sandwich beams. The load bearing capacity of these two kinds of structure was determined by loading them with the same unit dead load cases. Single span as well as arched sandwich beams, with different ratios of radius of curvature to span, have been loaded over their entire length respectively over half of their length. They were analysed in two-dimensional numerical models using the finite element method. Following up the model of the arched sandwich beam is described in detail.

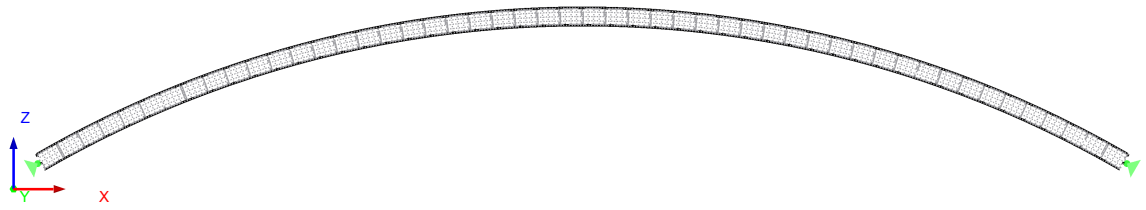

Fig. 3: 2D Finite Element Model.

The supports of the two-hinged arch where modeled by rigid beam elements connecting the two face sheets of the sandwich cross section similar to an end-plate connection (see Fig. 3). The end-plates them self were simply supported in the centroid of the sandwich cross section (see Fig. 4). The steel face sheets of the sandwich panels were modeled with curved beam elements using a common ideal-elastically isometric material with a Young's modulus of 210000 N/mm² and a Poisson's ratio of 0.3. The core of the sandwich panel was modeled using shell elements. Taking into account the simplified two-dimensional model, the core material was modeled ideal-elastically isometric as well. Deviating from the material of the deck layers the shear modulus of the core was defined as 2.5 N/mm² or 4.0 N/mm² and in consideration of a Poisson's ratio of 0.25, the belonging Young's modulus was calculated, isotropic material behavior presumed. The Poisson's ratio of the core material was set according to [3].

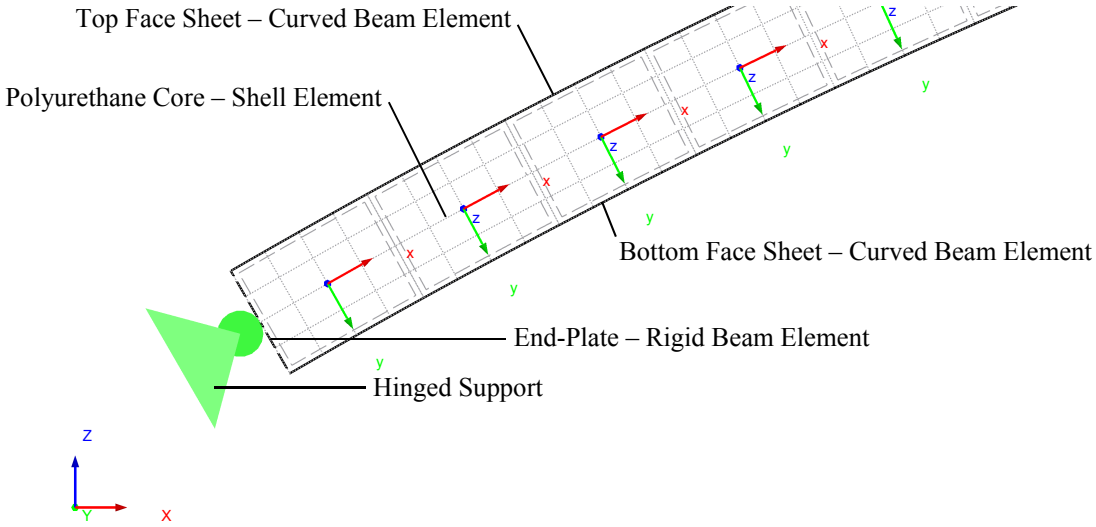

Fig. 4: 2D Finite Element Model – Detail at Support.

Since the material parameters of the core are defined vertically to the member axis, the plane of the core is modeled by trapezoidal shell elements which approximate the curved form like a polygon. According to [4] the limit values for the length of these elements are determined as the depth respectively twice the depth of the sandwich panel. The axis of each shell element is aligned with the longitudinal axis of the sandwich panel at the associated location. The axis and the mesh of the shell elements can be seen in Fig. 4.

To compare the load bearing capacity, the normal stresses in the face sheets of the two structures, resulting from the corresponding load cases, have been determined. They were compared to the yield stresses of usual face sheet material, as well as the wrinkling stress belonging to the modeled face sheets. Wrinkling stresses were calculated according to equation 8.50 in Stamm & Witte [5].

The comparison showed that the load bearing stresses of many two-hinged arch sandwich beams are significantly lower than in the single span beam. The actual amounts of stresses in the arched beam are essentially depending on the relation between the radius of curvature and the span of the sandwich panel. For example, sandwich beams were the radius of curvature and the span have approximately the same amount, are showing the highest potential of load bearing capacity.

5. CONCLUSIONS

Almost 50 years ago, Otto Jungbluth built a dome using lightweight sandwich panels, which have been produced in single item fabrication. Although his structure has a high potential of load bearing capacities, it seems not be possible to build a similar shell structure economically these days.

In a current project, three institutes of Technische Universität Darmstadt are working on a new design principle to build shell structures using economically manufactured sandwich panels with a high level of prefabrication.

A preliminary study showed that arched sandwich beams have a high potential regarding the load bearing capacity. The comparison between an arched and a single span sandwich beam showed that, even for asymmetric load, resulting bearing stresses in the arched beam are significantly lower than in the single span beam.

In the course of the project it is planned to produce uniaxially curved sandwich panels and verify the results of the numeric models with full scale tests. Based on the results further numeric studies will be carried out taking into account realistic load cases. Wind, snow and temperature loads are supposed to be considered, giving special attention to asymmetrical loads.

REFERENCES

[1] K. Berner, “Gekrümmte Sandwichpaneele”, *Stahlbau 79*, 2010; 5: 328-335.
[2] O. Jungbluth, “Weitgespannte Sandwichkuppel im Werkstoffverbundsystem Stahlfeinblech - Polyurethanschaum”, *IABSE congress report*: 1972, pages 501-510.
[3] A. Kurpelia, *Optimierung von Sandwichwandbauteilen mit PUR-Kern und Stahldeckschichten*, Technische Universität Darmstadt, Institute for Steel Structures and Materials Mechanics: 2013.
[4] J. Lange & K. Berner, “Sandwichelemente im Hochbau”, *Stahlbau Kalender 2010*, 2010: 643– 699.
[5] K. Stamm & H. Witte, *Sandwichkonstruktionen*, Springer-Verlag: 1974.

DOI: 10.5075/epfl-ICSS12-2018-143-145

A HYBRID CEMENTITIOUS BASED-G/CFRP SANDWICH PANEL: CONCEPT, DESIGN AND INITIAL OUTCOMES

José Sena-Cruz[1], Gonçalo Escusa[2], Diogo Figueira[3], Honeyeh Ramezansefat[4], Eduardo Pereira[5], Isabel Valente[6] and Joaquim Barros[7]
[1]ISISE, University of Minho, Portugal. jsena@civil.uminho.pt
[2] ISISE, University of Minho, Portugal. g.escusa@gmail.com
[3] ISISE, University of Minho, Portugal. diogo_silva@hotmail.com
[4] ISISE, University of Minho, Portugal. honeyrscivil@gmail.com
[5] ISISE, University of Minho, Portugal. eduardo.pereira@civil.uminho.pt
[6] ISISE, University of Minho, Portugal. isabelv@civil.uminho.pt
[7] ISISE, University of Minho, Portugal. barros@civil.uminho.pt

1. INTRODUCTION

Nowadays, the advantages of using fibre-reinforced polymers (FRP) in Civil Engineering structures are very well-known. In comparison to other materials, the FRPs show high strength-to-weight and stiffness-to-weight ratios, as well as high corrosion resistance [1]. Moreover, they can be easily moulded into complex shapes during the manufacturing process. Due to the slenderness of the cross section components and systems [2], and their significant initial cost [3], the FRPs are typically used along with other materials in composite structural elements. In the recent years, the FRPs have been increasingly used in composite sandwich panels designed for the building and housing industry [4]. However, in terms of flooring solutions, the sandwich panels still reveal some limitations for the most typical values of spans and loads in buildings [5].

In order to overcome the aforementioned drawbacks, the EasyFloor project was launched to develop enhanced composite sandwich panels for rehabilitation of floors in buildings. One of the important innovations included in the project relies on the use of both glass and carbon fibre roving (G/CFRP). This hybrid solution aims at improving significantly both the strength and stiffness. Furthermore, the top face of the panel is made of steel fibre reinforced self-compacting micro concrete (SFRSCMC), instead of the usual FRP compressive face, aiming to overcome face wrinkling issues. Additionally, this solution can provide higher ductility, fire endurance and impact resistance [6]. Furthermore, polycianurate (PIR) closed-cell foam is used as core material of the panel. Proper adhesion between G/CFRP and SFRSCMC is developed in order to obtain the full bending capacity of the composite solution. Finally, the FRP component is produced by pultrusion, taking all the advantages of this manufacturing process.

The final proposal for the hybrid sandwich panel was obtained through the use of genetic algorithms in the design, which consisted in optimizing the geometric and the mechanical properties of the panel, taking into account the following features: (i) structural and energy efficiency; (ii) durability, versatility of use, ease of handling, quick assembly and production; (iii) low maintenance needs and aesthetics.

The present work describes the design solution that resulted from the optimization procedure and subsequently presents initial experimental results regarding the mechanical characterization of the different materials, as well as the FRP/SFRSCMC interface. The experimental program comprised: (i) tensile and flexural tests on both the bottom and external ribs of the C/GFRP laminate skins; (ii) tensile, compressive and direct shear tests on both foam core materials (PIR); (iii) compressive and flexural tests on the SFRSCMC top face, and; (iv) pull-off tests for the characterization of the connection between the SFRSCMC and FRP using different types of adhesives.

2. CONCEPTION AND DESIGN

The design of the EasyFloor hybrid sandwich panels was addressed using Genetic Algorithms (GA). With this approach, a multi-objective function was defined with the target of minimizing (i) self-weight, (ii) total price and (iii) carbon-footprint of the solution. Taking into account the current needs in terms of rehabilitation market, a span of 5.0 m was considered for the panel, assuming simple supported conditions at the extremities. Values of 1.5 kN/m^2 and 2.0 kN/m^2 were used for other permanent and live loads, respectively. Additionally, due to technical limitations of the pultrusion equipment, a width of 500 mm was set. In order to create the random population and to continuously exclude the individuals outside the boundaries of the problem statement with GA, a set of boundary conditions (BC) were initially defined for avoiding "cripple" solutions. Some of the BC were set according to the requirements of the manufacturer (e.g. the width), while others were established to guarantee the fulfilment of the Structural Eurocodes 0 (EN 1990:2002) and 1 (EN 1991-1-1:2002) and the Italian recommendation CNR DT 205/2007 in terms of Ultimate Limit States (ULS) and Serviceability Limit States (SLS). Additionally, some building physics aspects were also considered, mainly thermal and acoustics. Further details about these aspects can be found in [7]. Moreover, a snap-fit type of connection between the panels was designed and studied by means of numerical and analytical models, where the structural behaviour of the

panels, force required for assembly, and load distribution among the floor's principal axes were taken into account in the joint's detailing and geometry [8].

Fig. 1 depicts the final solution for the hybrid sandwich panel with a total height of 140 mm, a width of 500 mm and a self-weight equal to 59.8 kg/m^2. The solution consisted on the following components: (i) a top face of SFRSCMC with a constant thickness of 20 mm in the middle of the cross-section and 36.5 mm at the extremities in order to improve the connection between the SFRSCMC and the remaining parts; (ii) face FRP sheets made of hybrid carbon fibre roving strands and glass fibre plies (G/CFRP) of 5 mm and 4 mm of thickness, for the case of bottom face and lateral ribs respectively; (iii) a foam core material made of polycianurate (PIR) closed-cell foam with a density of 40 kg/m^3; and, (iv) a GFRP skin between the PIR and the SFRSCMC with 3 mm of thickness, in order to prevent the damage of the PIR during the manufacturing production of the FRP component by pultrusion. In turn, the snap-fit joint (see Detail D1 and Detail D2 of Fig. 1) is 5 mm thick and has: (i) a latch 30 mm long, (ii) an overhang overlap of 1 mm, (iii) an overhang entrance angle of 4º, (iv) faces inclined at 2º and (v) a clearance of 0.25 mm.

Finally, the estimated thermal conductivity (U-value) for the hybrid sandwich panel is 0.19 W/m^2·K, which satisfies the legal requirements for thermal insulation in buildings for a heating flux below 0.30 W/m^2. Considering a room volume of 3.56×3.56×2.7 m^3, the estimated airborne and impact sound insulations are, respectively, 35.7 dB and 87.1 dB. These estimated values also fulfil 65% of Portuguese legal requirements, which are in agreement with the defined goals for the EasyFloor project.

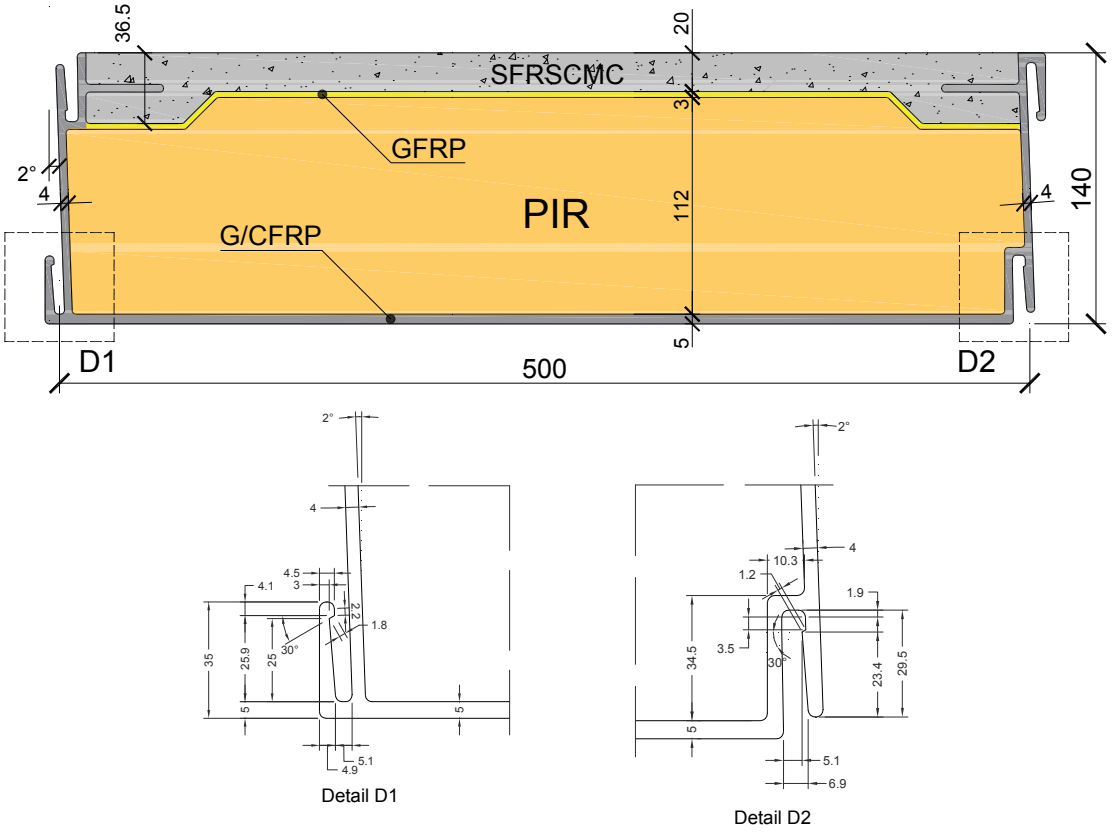

Fig. 1: Final geometry of the hybrid sandwich panel. Units in [mm].

3. MATERIAL CHARACTERIZATION TESTS

In the scope of the present paper the results of the material characterization carried out on the G/CFRP faces, foam and SFRSCMC are introduced, as well as the characterization of the interface between the GFRP skin and SFRSCMC face.

The direct tensile tests on the G/CFRP sheets comprised the longitudinal (0º), transverse (90º) and inclined (30º) directions, according to the ASTM standards D3039/D3039M-00. From the tests carried out, *E*-modulus of 50.2 GPa with a coefficient of variation (CoV) of 7.2%, of 13.9 GPa (6.5%) and of 8.87 GPa (11.8 %) were obtained for the specimens at, respectively, 0º, 30º and 90º directions, while the ultimate strength was, respectively, 545.0 MPa (8.2%), 115.8 MPa (3.6%) and 71.54 MPa (7.0%), with an ultimate strain of 0.982% (2.1%), 1.07% (8.2%) and 0.99% (12.4%), respectively.

Direct tensile, compressive and shear tests on PIR were executed according to the ASTM C297/C297M, C365/C365M and ASTM C273 standards, respectively. From these tests the following results were obtained: i) tension - *E*-modulus of 5.81 MPa (11.5%), ultimate strength of 0.22 MPa (10.7%), ultimate strain of 0.22 (2.9%); ii) compression - *E*-modulus of 4.79 MPa (10.0%), ultimate strength of 0.22 MPa (15.5%), ultimate strain of 0.054 (22.0%); iii) shear - *G*-modulus of 2.73 GPa (2.3%), ultimate strength of 0.19 MPa (6.5%), ultimate strain of 0.151 (13.0%).

The material characterization of the SFRSCMC was carried out at 7 and 28 days of age and comprised compression and flexural tests, according to the EN 12390-3:2001 and RILEM TC 162-TDF/2000, respectively. The rheological properties of the SFRSCMC were also assessed at fresh state. All the mixtures did not show any sign of segregation. From the compression tests at 28 days an *E*-modulus of 23.8 GPa (2.1%) and a compressive strength of 39.3 MPa (1.3%) were obtained. In terms of the flexural tensile properties, tested at 28 days, the following values were obtained: limit of proportionality of 4.16 MPa (5.2%); equivalent flexural strengths of $f_{eq,2}$=7.28 MPa (15.0%) and $f_{eq,3}$=6.69 MPa (15.4%); and, residual strengths of f_1=7.02 MPa (15.0%), f_2=7.47 MPa (13.7%), f_3=6.06 MPa (15.7%), and f_4=4.95 MPa (14.5%).

In general, all the results obtained for the material characterization of the G/CFRP sheets, PIR foam and SFRSCMC were in agreement with the required values at the design stage.

With the aim of studying the bond behaviour between the GFRP skin and SFRSCMC face, by using different surface treatments (without treatment, sandpaper with coarse aggregate size of 80 and 20) and adhesives (SikaTop® Armatec® 110 EpoCem, Sikadur® 32 EF, Mapei Eporip, Kerabuild® Eco Epoprimer) applied on the surface after the corresponding treatment and before casting the SFRSCMC, pull-off tests following the ASTM D 4541 standard were carried out. The best bond behaviour was observed in the series where the adhesives Sikadur® 32 EF and Mapei Eporip were used, independently of the roughness treatment applied. Moreover, in those series failure was cohesive and occurred always at the SFRSCMC substrate. This fact indicates that a complete composite action for the corresponding sandwich panel can be assumed in the design context.

4. CONCLUSIONS

The present work describes the design of a new hybrid sandwich panel for flooring applications in building industry. An hybrid sandwich panel was developed having a cross section of 500 mm of width and 140 mm height, with a span length of 5 m and a weight of 59.8 kg/m^2, able of supporting 1.5 kN/m^2 (other permanent loads) and 2.0 kN/m^2 (live loads) and fulfilling the design guidelines. The components of the hybrid sandwich panel, which resulted from the optimization procedure, are: (i) a top layer in SFRSCMC with 20 mm of thickness, (ii) bottom face and ribs on G/CFRP with thickness of 5 mm and 4 mm, respectively, (iii) PIR closed-cell foam as core, (iv) a GFRP skin between SFRSCMC and PIR, and (v) snap-fit connection between the panels.

An experimental program was carried out for material mechanical characterization. The results revealed that the required mechanical properties at the design stage were achieved by the adopted solutions. Finally, to improve the bond between the top face (SFRSCMC) and the core (PIR), adhesive Sikadur® 32 EF or Mapei Eporip should be used before casting the cementitious-based material.

ACKNOWLEDGMENTS

This work is part of the research project “EasyFloor – Development of composite sandwich panels for rehabilitation of floor buildings”, involving the company ALTO – Perfis Pultrudidos, Lda., CERis/Instituto Superior Técnico and ISISE/University of Minho, supported by FEDER funds through the Operational Program for Operational Program for Competitiveness and Internationalization (POCI) and the Portuguese National Innovation Agency (ANI) - project no. 3480 (POCI-01-0247-FEDER-003480). The authors would like to thanks the following companies for suppling the adhesives: KERAKOLL, MAPEI and SIKADUR.

REFERENCES

[1] S. Ahmed, K. Galal., “Effectiveness of FRP sandwich panels for blast resistance”, *Composite Structures*, 2017; 163: 454-464.
[2] B. D. Manshadi, et al., “Post-wrinkling behavior of webs in GFRP cell-core sandwich structures”, Composite Structures, 2016; 138: 276-284.
[3] J. R. Correia, F. A. Branco, J. Ferreira (2009). “GFRP-concrete hybrid cross-sections for floors of buildings”, Engineering Structures, 31, 1331-1343.
[4] S. Satasivam, Y. Bai, Y. Yang, L. Zhu, X. Zhao (2018). “Mechanical performance of two-way modular FRP sandwich slabs”, Composite Structures, 184, 904-916.
[5] H. Abdolpour, J. Garzón-Roca, G. Escusa, J. M. Sena-Cruz, J. A. O. Barros, I. B. Valente (2016). “Development of a composite prototype with GFRP profiles and sandwich panels used as a floor module of an emergency house”, Composite Structures, 153, 81-95.
[6] L. Zhang, Y. Bai, W. Chen, F. Ding, H. Fang (2017). “Thermal performance of modular GFRP multicellular structures assembled with fire resistant panels”, Composite Structures, 172, 22-33.
[7] G. Escusa, J. Sena-Cruz, F. Cruz, E. Pereira, I. Valente, J. Barros (2017). “The use of genetic algorithms for structural optimization of hybrid sandwich panels”. APFIS2017 – 6th Asia-Pacific Conference in FRP Structures, Singapore, 4 p.
[8] M. Proença, M. Garrido, J.R. Correia (2017) “Development of the panel-to-panel snap-fit joint” Project EasyFloor, Technical report no. CERIS DTC 11/2017.

DOI: 10.5075/epfl-ICSS12-2018-146-148

EXPERIMENTAL STUDY ON CRACKING BEHAVIOR OF GLASS-FRP REINFORCED PRECAST CONCRETE SANDWICH PANELS

Marcin M. Haffke[1]and Matthias Pahn[2]
[1] Technische Universitaet Kaiserslautern, Germany. marcin.haffke@bauing.uni-kl.de
[2] Technische Universitaet Kaiserslautern, Germany. matthias.pahn@bauing.uni-kl.de

1. INTRODUCTION

Precast concrete sandwich panels (PCSP) consist usually of two reinforced concrete wythes and a core layer composed of insulating material and mechanical connectors. The innovative solutions with integrated thermally insulating layer and non-metallic connectors can meet severe energy efficiency requirements and provide space for application of another high performance system. Application of glass fibre reinforced polymer (GFRP) rebars in concrete wythes of PCSP enables reduction of their thickness as a result of the reduced concrete cover of the rebars due to their excellent chemical properties and high durability. In this way, by application of GFRP materials as connectors and reinforcement of concrete wythes, thin and energy efficient sandwich panels can be constructed (see Fig.1). Such wall panels are competitive against known steel-reinforced panels, due to their high durability, good thermal properties and lower concrete consumption.

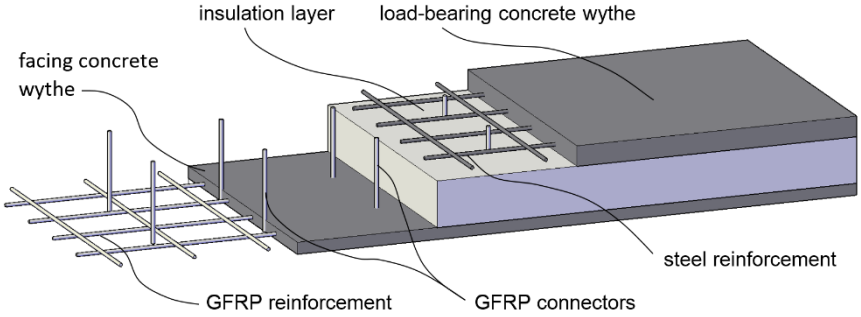

Fig. 1: Precast concrete sandwich panels (PCSP) with GFRP-reinforcement and connectors (specimens CS1 and CS2).

However, due to significantly different mechanical properties of GFRP from steel, their performance in thin concrete wythes needs to be investigated, so guidelines for optimal application can be developed. Furthermore it has been recognized that constructing panels with reduced thickness of wythes, contribution of the face wythe and the shear stiffness of insulation can provide significant reserves to the load-bearing capacity and overall flexural stiffness of the panel [1,2]. Use of GFRP reinforcement in prefabricated concrete panels allows to utilize their special properties. Due to the different bond characteristics and lower modulus of elasticity of GFRP bars the cracking behavior of GFRP reinforced structures remains one of the biggest limitation of its application. Since cracking of facing wythes of precast sandwich panels is of a great concern, investigation of the impact of the degree of composite action on the flexural cracking behavior of GFRP-reinforced panels is essential for an safe and economic design.

As it was reported in previous research [1,2] the contribution of the shear stiffness of insulation activated by bond to concrete can increase the overall flexural stiffness of panels even by 100% in the service load range in comparison to the panels with composite action provided only by connectors. However, since it is difficult to provide uniform quality of bond of insulation pressed into fresh concrete and insulation layer fails in shear cracking and subsequent debonding from concrete [3] the two crucial conditions were investigated. For specimen CS1 and CS3 good bond was provided by placing the EPS insulation plates in fresh concrete and compacting of the mixture. In case of specimen CS2 and CS4 PVC foil was placed during casting on both sides of the EPS insulation plates to prevent its bond to concrete. Created in this way two different conditions of actively shear-bearing and deactivated insulation influenced significantly cracks development in the facing wythes and overall flexural stiffness. The shear stiffness and composite action provided by GFRP connectors have constant values until their ultimate shear failure which occurs under much higher load than the shear failure of insulation and therefore constitute the majority of the panel's composite action after the shear failure of insulation. Although relatively a lot of research has been done on cracking behavior of GFRP-reinforced concrete members, the influence of the degree of composite action defined by the bond conditions of insulation to concrete on the cracking of facing wythe of sandwich panels has never been investigated.

2. EXPERIMENTAL INVESTIGATION

Aiming to investigate the cracks development and propagation a test series consisting of four test panels (width x length = 400 x 1700 mm) was conducted. Longitudinal reinforcement ratio of facing (bottom) wythe with reduced, efficient thickness of 40 mm (investigated in previous research [2]), was equal for each panel (ρ=0,031). The longitudinal

rebars where positioned with spacing 85 mm. In addition, transverse rebars where used, with spacing ~ 280 mm. Concrete cover of 10 mm was applied for longitudinal reinforcement in each specimen. In case of panels CS1 and CS2 facing wythes were reinforced with Schoeck Combar® GFRP rebars of nominal diameter 8 mm, while facing wythes of panels CS3 and CS4 were reinforced with conventional steel reinforcement of nominal diameter 8 mm. The load-bearing (top) wythe (70 mm thick in each specimen) were reinforced with conventional steel reinforcement of nominal diameter 8 mm. Connectors of diameter 12 mm (16 pcs per specimen, every 20 cm), with length equal to the thickness of the panel, were anchored by bond to the concrete along the length embedded in the concrete wythes (see Fig. 1). Tested mean cubic compressive strength of concrete used was 54,7 MPa, while maximum aggregate size was 8 mm, in order to ensure proper compaction of the mixture around the rebars. The middle-density (18 kg/m^3) expanded polystyrene (EPS) with thickness of 140 mm was used as a core material of the panels. The longitudinal E-modulus of the Schoeck Combar® rebars and connectors given by the manufacturer is equal to 60 GPa [4]. Their good bond characteristics are provided by grooves cut into the surface after curing. The steel-reinforced panels (CS3 and CS4) where tested as a reference in terms of stiffness as well as cracking and damage development. Simply supported panels with roller and pin, four point bending test configurations, were loaded in flexure, displacement controlled with servo hydraulic cylinders up to the ultimate failure of the concrete wythes. The extensive instrumentation, including measurement of the deflection along the panel (with linear variable displacement transducers), relative displacement of wythes and strains in reinforcement (strain gauges), were implemented. Load was applied in displacement controlled manner at the rate of 2 mm/min in order to investigate development of the crack pattern.

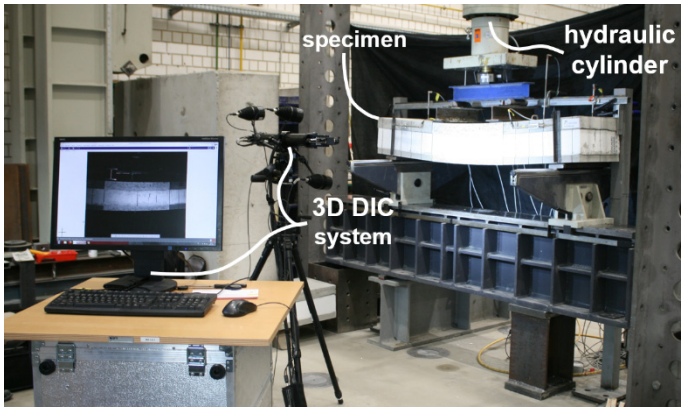

Fig. 2: Test set-up for measurement with Digital Image Correlation System.

The 3D Digital Image Correlation (DIC) technique was used for continuous measuring of crack widths of the facing wythe. The DIC system allows contactless determination of deformations and displacements of the surface of a specimen under loading. The system uses two high-resolution cameras and Aramis software [5]. The calculation of the surface deformation is based on comparison of two consecutive images taken at two different stages during the test. The captured field of the used 3D DIC system covered the middle area of the panel (see Fig. 3). The data were captured with two digital cameras acquiring frames at frequency of 0,5 Hz with a resolution of 2448 x 2050 pixels. The post-processing of images allowed the measurement of the 3D full field displacement on the front side of the facing wythe. For this purpose, that side of the specimen was painted white and randomly speckled with black acrylic paint.

3. RELATION OF CRACKING BEHAVIOUR OF FACING WYTHES AND DEGREE OF COMPOSITE ACTION

Conducted tests allowed continuous observation of crack pattern development of the thin GFRP-reinforced sandwich panels with comparison to the steel-reinforced reference specimens. It is important to mention that throughout the loading of the panels up to the ultimate failure, the cracks in facing wythes were growing slowly through these layers, never protruding the full depth of the wythes.

The analysis of crack development is done on a basis of mean crack width (MCW), calculated as a mean value of crack widths measured continuously during loading in the middle area of the panel between the loading points. Crack widths were calculated from the relative displacement of two points localized on both sides of the crack at the depth of the reinforcement axis. Figure 3 shows the fully developed crack pattern of the facing wythe (CS1) displayed as the strain map in the X direction and the middle area of the panel where the DIC technique was applied.

Since the degree of composite action is governed by the active shear contribution of the insulation to the flexural stiffness of sandwich panels, the quality of insulation to concrete bond is of a particular importance for cracking behavior. Figure 4(a) shows the difference in the flexural behavior of panels with actively contributing insulation - CS1, and reference panels with passive insulation - CS2.

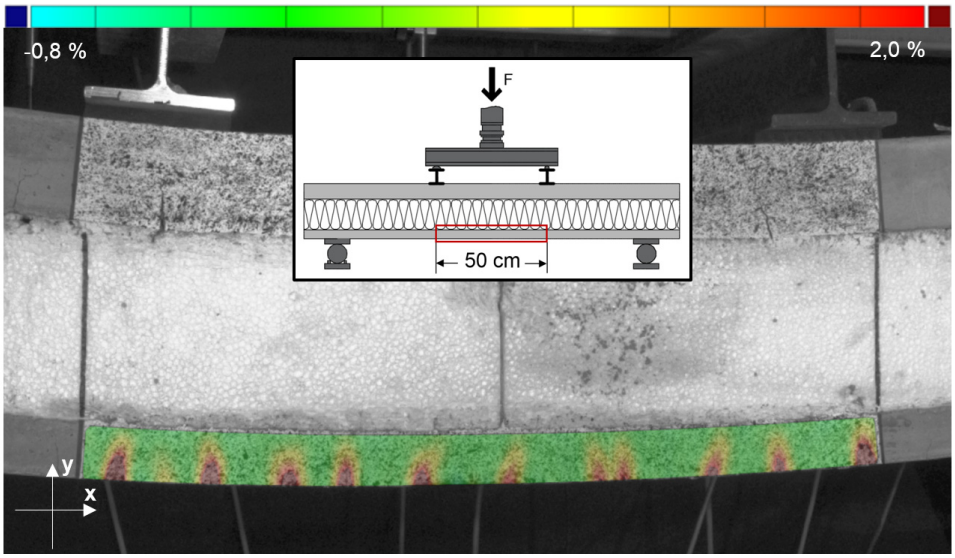

Fig. 3: Distribution of cracks in the facing wythe of CS1 specimen (stains in X-direction) under load of 46,6 kN and middle area.

The mean crack width measured with DIC system showed significantly different cracking behavior of GFRP and steel-reinforced facing wythes.

Although the cracking initiation starts at comparable load level for all specimens the MCW at the higher load is much larger for GFRP-reinforced specimens. The reducing influence of the active insulation on MCW can be observed as the shear cracking of insulation (for CS1 and CS3) results in its deactivation in terms of its contribution to the flexural stiffness and sudden increase of MCW and increase of its growing rate. This phenomenon is particularly clear for GFRP-reinforced panels, where MCW of the panel with active insulation (CS1) after shear failure and deactivation of insulation, exceeds the MCW of CS2 (see Fig. 4(b)). This indicates strong dependence of the crack width and crack pattern on the degree of the composite action. However in each test, the MCW was not exceeding 0,08 mm and maximum crack width 0,15 mm, values much below the recommended allowable crack widths in concrete structures reinforced with GFRP rebars. The presented test results confirm the positive impact of an actively shear-bearing insulation on the flexural stiffness as well as on the reduction of crack widths in sandwich panels.

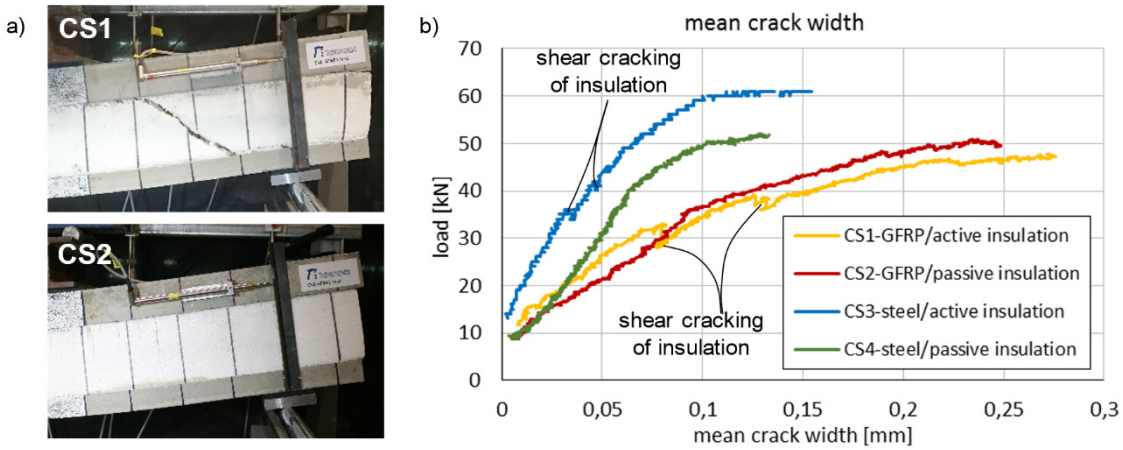

Fig. 4: Experimental mean crack width depending on the load.

REFERENCES

[1] Haffke, M.M.; Pahn, M.: "Flexural Behaviour of Thin GFRP-reinforced Concrete Slabs with Reduced Concrete Cover as a part of pre-cast Sandwich Panels", in: *Proceedings of the 8th Biennial Conference on Advanced Composites In Construction (ACIC-17)*, University of Sheffield, UK, 2017, pp. 267–272.

[2] Haffke, M. M.; Schmitt, A.; Pahn, M., "Experimental Investigation of Flexural Behaviour of Thin Sandwich Wall Panels Reinforced with GFRP Rebars" presented at the *8th International Conference on Fibre-Reinforced Polymer (FRP) Composites in Civil Engineering*, Hong Kong, China, 2016.

[3] Pahn, M., „Beitrag zur Ermittlung von Schnitt- und Verformungsgrößen bei mehrschichtigen Sandwichwandtafeln mit Verbindungsmitteln aus glasfaserverstärktem Kunststoff", Dissertation, Technische Universitaet Kaiserslautern, 2011.

[4] Schöck Combar®, Technical Information Schöck Combar® international. October 2016, Available: http://www.schoeck.de/.

[5] GOM GmbH: "Aramis v6.3" GOM optical measuring techniques, Braunschweig, Germany, 2015.

DOI: 10.5075/epfl-ICSS12-2018-149-151

EXPERIMENTAL INVESTIGATION ON THE BEHAVIOR OF FIBER REINFORCED LIGHTWEIGHT CONCRETE FILLED DOUBLE STEEL PLATE SHEAR WALL

Ghazaleh. Eslami[1] and Alireza Rahai[2]
[1] PhD candidate, Department of civil engineering, Amirkabir University of Technology, Iran. gh_eslami@aut.ac.ir
[2] Professor, Department of civil engineering, Amirkabir University of Technology, Iran. rahai@aut.ac.ir

1. INTRODUCTION

The behavior of tall buildings during earthquakes has been a significant concern in the recent decades. Different lateral load resisting systems can be used in steel structures, namely the braced frames, shear walls, and the moment resisting frames. In the past several years, Reinforced concrete (RC) shear walls have been used to resist earthquake loads. Later, steel plate shear walls were employed as a more economical system leading to the overall weight reduction of structure. Nowadays, concrete filled double-steel-plate (CFDSP) shear walls are introduced as a significantly efficient lateral load resisting system in which the steel faceplates delay the cracking of concrete panel while the concrete panel prevent the premature buckling of steel faceplates. Steel faceplates are connected to the concrete panel using shear connectors such as shear studs, bolts, and other profiles resulting in composite behavior. Zhang et al. [1] found that a 75 to 90% partial composite action can be expected if the stud spacing is designed to achieve target development lengths of three times the wall thickness or less. This would allow the steel faceplates to develop yielding before local buckling and will lead to wall's composite action. The plane composite truss model was investigated by Nie et al. [2] to evaluate the effective shear stiffness of the composite shear walls. Moreover, they observed that the failure mode will be flexural failure in walls with a shear span ratio of 2.0 and 1.5, whereas with a shear span ratio of 1.0, the failure mode will be a mixed failure of flexure and shear. To investigate the local buckling of steel plates in composite shear walls subjected to uniform axial compression, Qin et al. [3] proposed a methodology to predict the strength of steel plates considering restraint of both concrete and shear studs. Yang et al. [4] developed three-dimensional finite element (FE) models to simulate the behavior of double skin composite (DSC) panels subjected to compression, and found the FE results to be in good agreement with the observed buckling behavior during tests. The experimental and parametric studies conducted by Kurt et al. [5], investigating the effects of wall aspect ratio, reinforcement ratio, and wall thickness, showed that lateral load bearing capacity of steel-concrete composite (SC) wall piers with aspect ratios greater than or equal to 0.6 is governed by the flexural yielding of the steel faceplates in tension, and by local buckling of the steel faceplates and crushing of the concrete infill in compression. After all, the post cracking behavior of macro synthetic polypropylene fiber reinforced concrete was investigated by Amin et al. [6].

In this study, a fiber reinforced lightweight concrete filled double steel plate shear wall and -as a reference specimen- a plain concrete filled double steel plate shear wall were fabricated and tested under monotonic lateral loading. The effects of using fiber reinforced lightweight concrete on lateral load bearing capacity, stiffness, ductility, and failure characteristics of the composite shear walls were analyzed.

2. SPECIMEN DETAILS AND TEST SET-UP

The experimental program was developed at Amirkabir University of Technology, Tehran, Iran, with the purpose of studying the effects of adding "Fibercem P50" synthetic fiber to concrete mixture in concrete filled double-steel-plate (CFDSP) shear walls subjected to monotonic lateral load.

Experimental Specimens

In this study, monotonic tests were carried out on four 1:4 scaled elements. Two specimens were fiber reinforced lightweight concrete filled double-steel-plate shear walls and another two specimens were ordinary concrete filled double-steel-plate shear walls. The variables of the experimental program were related to the fiber contribution ratio while being designed using the guidelines provided by Astaneh Asl [7]. The efficient synthetic fiber contribution ratio was obtained from previous tests to be equal to 1 kg/m^3. The details of the two types of CFDSP are presented in Table 1.

Material Properties

To characterize the compressive strength and density of concrete, 6 concrete cube samples were made for either of synthetic fiber concrete or ordinary concrete. The sample test results with age of 28 days revealed the 25% compressive strength increase by adding synthetic fiber. The properties of synthetic fiber are presented in Table 2.

Test Setup

Four 1:4 scaled one-bay one-story specimens were fabricated and tested under monotonic lateral load. Designed walls were assumed as the first floor wall of a high rise building, so the specimens were designed as a cantilever wall fixed to a rigid column which was connected to the strong floor of the laboratory (Fig. 1). To eliminate the lateral load resistance contributed by the wall peripheral frame, beam-to-column joints were designed to be pin-jointed as shown in Fig. 1.

According to the AISC 341-10 [8], the stiffness of the boundary elements (IPE 14 and Box 12) shall be designed to allow the full yield zone to be developed across the diagonal area of the steel faceplates. Test specimens were rotated and the lateral loading was applied as a gravity point load at the top of the specimens by a servo controlled actuator. The rigid column was designed to have no lateral displacement during the test. All elements of the test setup (rigid column, connection to the rigid column), were analyzed and designed for the maximum probable moment value factored by 1.5.

Instrumentation

A load cell was mounted on the hydraulic actuator to monitor the lateral loads applied to the specimen. One linear variable differential transducer (LVDT) was used to measure the displacements along the lateral load. The location of LVDT is shown in Fig. 1. Several strain-gauges were used to measure the deformations of the steel plate and their locations are shown in Fig. 1.

Table 1: The experimental specimens details.

Model	Composite shear wall dimensions (mm^2)	Concrete panel thickness (mm)	Concrete cubic compressive strength (MPa)	Concrete density (kg/m^3)	Steel plates thickness (mm)	Steel yield strength (MPa)	Metal international code	Fiber contribution (kg/m^3)	Shear connector distance (mm)
CFDSP 1 CFDSP 2	750*750	50	27	1500	1.2	240	A36	0	150
CFDSP 3 CFDSP 4	750*750	50	35	1500	1.2	240	A36	1	150

Table 2: Synthetic fiber properties.

Length (mm)	Diameter (mm)	Tensile Strength (MPa)	Melting point (°C)	Modulus of elasticity (MPa)	Water absorption (%)	Compaction factor
50	0.07	600	230	3500	0.01-0.02	0.91

Fig. 1: Specimen configuration and test set-up.

3. RESULTS AND CONCLUSION

Results

The main objective of this research project was to investigate the effects of adding synthetic fiber to plain concrete in improvement of steel faceplate and concrete panel composite action and how the lateral load bearing capacity of CFDSP shear wall is affected by it. A comparison can be made regarding the strength of the specimens by analyzing the failure load and local buckling of steel faceplates (Figs. 2-3). Fig. 2 illustrates that increasing the concrete compressive strength has a positive effect on load-displacement response and failure load of the CFDSP walls. The first collapse mode of the CFDSP wall was cracking and spalling of the concrete panel, so by using fiber reinforced concrete, the cracking of the concrete panel happened with a delay indicated from the initial stiffness of load-displacement curves. Based on the results of strain gauges, both kinds of CFDSP shear walls had the same buckling mode, but the local buckling of steel faceplates was lagged by using fiber reinforced concrete with the same values of out of plane deformations. The CFDSP shear wall maintains its composite action with the delay in local buckling of steel faceplates due to the continuous presence of concrete panel out of plane support resulted from increase in lateral capacity of the concrete panel using fiber reinforced concrete. The more the CFDSP shear wall preserves its composite action, the higher the lateral load bearing capacity is.

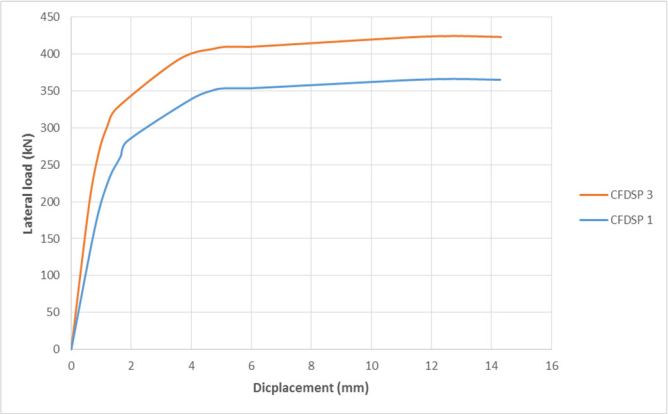

Fig. 2: Load-displacement curve of the two type specimens.

(a) (b)

Fig. 3: Buckling of the specimen after the test.

Conclusion

Composite shear walls consist of steel face plate and concrete panel that are connected in one or two sides of steel face plate. Compared to reinforced concrete shear walls, Composite shear walls of the same shear capacity, have smaller thickness and less weight. Moreover, in a composite shear wall, the concrete wall restrains the steel plate and prevents its before-yield premature buckling resulted by composite action between steel face plate and concrete panel [7]. The CFDSP shear wall was examined using various characteristics and subjected to various types of loading (axial, cyclic, impact, thermal, and combined) in some recent researches. In this research, monotonic lateral behavior of the CFDSP shear walls were investigated experimentally to study the effects of adding synthetic fiber to concrete mixture for better composite action. It was observed that:

1- Fiber reinforced concrete increase the initial stiffness of the CFDSP wall in lateral loading.

2- Utilizing fiber reinforced concrete delays the cracking and spalling of the concrete in panel. Therefore, the concrete panel continues the out of plane support of faceplates and the CFDSP shear wall maintains its composite action which leads to a 16% increase in lateral load bearing capacity.

3- Adding fiber in concrete mixture doesn't have any effects on failure mode or ultimate displacement of the wall while the local buckling of steel faceplates was lagged.

REFERENCES

[1] K. Zhang, A. H. Varma, S. R. Malushte, and S. Gallocher, "Effect of shear connectors on local buckling and composite action in steel concrete composite walls," *Nucl. Eng. Des.*, vol. 269, pp. 231–239, 2014.

[2] J. G. Nie, X. W. Ma, M. X. Tao, J. S. Fan, and F. M. Bu, "Effective stiffness of composite shear wall with double plates and filled concrete," *J. Constr. Steel Res.*, vol. 99, pp. 140–148, 2014.

[3] Y. Qin, G. P. Shu, S. G. Fan, J. Y. Lu, S. Cao, and J. H. Han, "Strength of double skin steel-concrete composite walls," *Int. J. Steel Struct.*, vol. 17, no. 2, pp. 535–541, 2017.

[4] Y. Yang, J. Liu, and J. Fan, "Buckling behavior of double-skin composite walls: An experimental and modeling study," *J. Constr. Steel Res.*, vol. 121, pp. 126–135, 2016.

[5] E. G. Kurt, A. H. Varma, P. Booth, and A. S. Whittaker, "In-Plane Behavior and Design of Rectangular SC Wall Piers without Boundary Elements," *J. Struct. Eng.*, vol. 142, no. 6, p. 4016026, 2016.

[6] A. Amin, S. J. Foster, R. I. Gilbert, and W. Kaufmann, "Material characterisation of macro synthetic fibre reinforced concrete," *Cem. Concr. Compos.*, vol. 84, pp. 124–133, 2017.

[7] A. Astaneh-asl, "Seismic Behavior and Design of Composite Steel Plate Shear Walls," 2002.

[8] American Institute of Steel Construction, "Seismic Provisions for Structural Steel Buildings," *Seism. Provisions Struct. Steel Build.*, no. 1, p. 402, 2010.

DOI: 10.5075/epfl-ICSS12-2018-152-154

CONTACT BEHAVIOR OF PREFABRICATED GFRP INFILL PANEL ON STEEL FRAME STRUCTURE

Jinsup Kim[1] and Minho Kwon[2]
[1]Dept. of Civil Engineering, ERI, Gyeongsang National University, South Korea. jinsup.kim@gnu.ac.kr
[2]Dept. of Civil Engineering, ERI, Gyeongsang National University, South Korea. kwonm@gnu.ac.kr

1. INTRODUCTION

Many researchers have developed seismic retrofitting technologies and performed research and development to improve the seismic performance of buildings. Some low- and mid-rise building frame structures have infill wall systems that are built and installed as partitions after the structural frame is completed, while other infill walls are constructed as part of the structural system. Seismic reinforcement technologies have been developed based on new reinforcement materials and methods. Practical applications of FRP composite materials have been attempted in the construction field recently. One of the challenges involved in creating new practical applications using FRP composite materials are still being addressed [1,2]. In this study, GFRP panels was developed to enhance the strength of the existing walls or to replace of the existing walls in the purpose of rapid construction and emergency repair. Compression behavior of glass-fiber reinforced polymer (GFRP) infill panels to enhance the strength of existing steel frame structure when they must be strengthened or reinforced was evaluated. Compression behavior data of GFRP infill panels is very useful to propose a design procedure applicable to the design of GFRP-composite panels. So, the compression behavior of GFRP infill panels on the steel-frame structures was evaluated experimentally. Compression behavior of GFRP infill panels was checked through the distribution of compression strain.

2. GFRP INFILL PANEL

The design goal for the GFRP infill panel was to increase the performance of steel frame structures under lateral loading. The panel is consisted of GFRP plates and stiffeners with an infill of Urethane foam. The cross-section of such a GFRP panel can be designed depending on the strengthening goals for the steel frame structure. The cross-sectional shape of the GFRP infill panel was considered as a box form, which it had advantages such as a symmetric cross-section, ease of increasing its moment of inertia and so on. The main loads for the design of cross-section were in-plane and buckling loads. The thickness is controlled by in-plane load, while the buckling load determines the moment of inertia, stiffener spacing and thickness. Fig. 1 shows the designed GFRP infill panels.

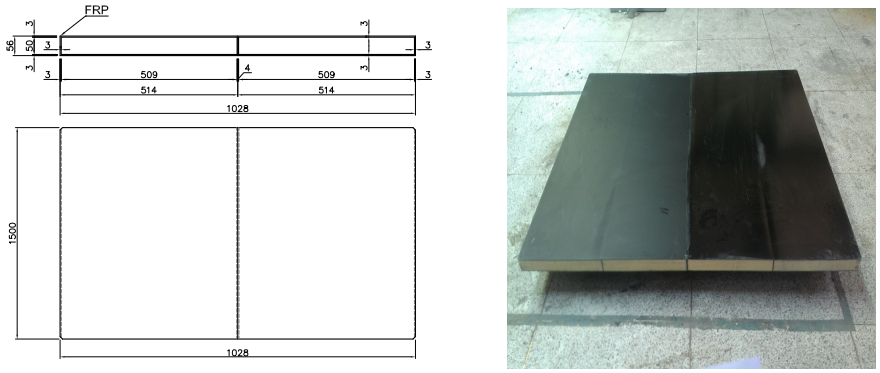

Fig. 1: Design of GFRP infill panel.

3. EXPERIMENTAL STUDY

Experimental instruments were set up to measure the performance of steel frame structure including linear variable differential transformers (LVDTs) and strain gauges. Fig. 2 presents the experimental test setup. Lateral loads were imposed on the top-loading block over the steel frame specimen using a 1,000-kN hydraulic actuator. The specimens and instruments were installed to a reaction wall and floor. The boundary conditions of the steel frame specimen were assumed to be hinges. Two LVDTs were placed on the upper and lower beams to measure lateral displacement, and inter-story drift and relative lateral displacement were calculated from the displacements measured at these two locations. The displacement load was applied through a loading arm over the specimen and was increased by 0.2 % of the drift ratio in each loading step. The steps were repeated twice for the accuracy. Through the experimental test, the compression strain distributions on GFRP infill panel were performed.

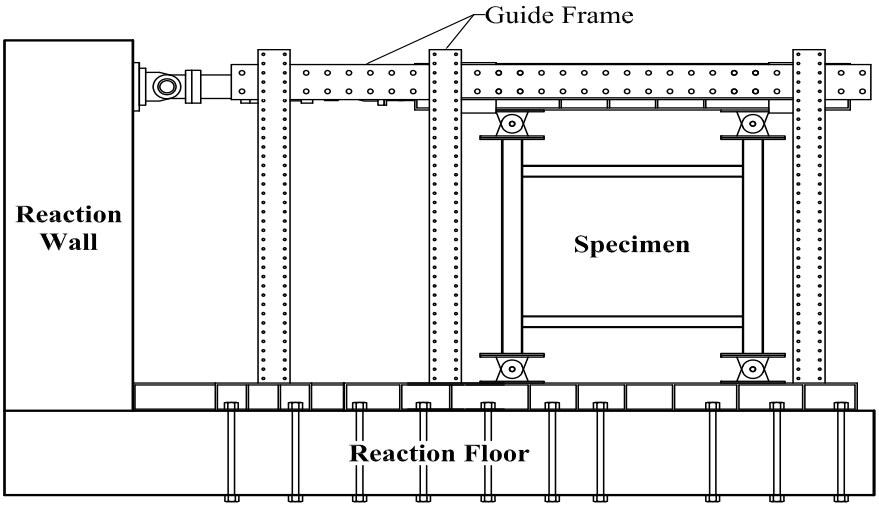

Fig. 2: Experiment test setup.

4. TEST RESULTS AND DISCUSSION

Deformed Shape

Fig. 3 shows the deformed shape of specimen (RSF2) under the final loading step. The top and bottom beam show flexural deformations. The deformation of the beam member was larger than that of the column member, and critical damage did not occur in the steel frame specimen. The RSF2 specimen was strengthened with the GFRP infill panels. Large plastic deformations were concentrated at both ends of the beam since the flexural and shear stress was much increased as the GFRP infill panel was resisted more force. The welded part of the beam section, located at the left bottom of the frame', was experienced the failure at the final loading step, and the failure of GFRP infill panel was located at the right corner.

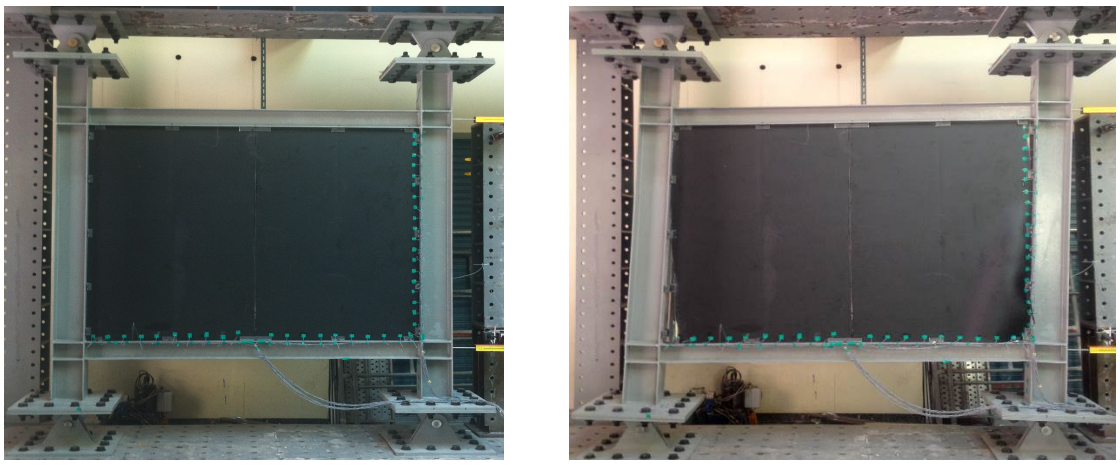

Fig. 3: Deformed shapes of specimen (RSF2).

Compression Strain of GFRP Infill Panel

Fig. 4 shows the compression strain of the GFRP infill panel at the peak of each load-step, by load direction. The compression strains at the corner of the GFRP infill panels were larger than the strains elsewhere. The compression strain distribution of GFRP infill panels reflected the diagonal compression behavior of the GFRP infill panels. Moreover, it is possible to determine indirectly the contact length between the GFRP infill panels and the steel frame, from the strain distribution of the GFRP infill panels. From the diagonal compression strain results, the effective width of the diagonal compressed struts in the GFRP infill panels was determined. In order to determine the effective width of the diagonal compressed struts, compression strain results that were greater than 0.002 were used. The effective contact-length ratio between the column and the GFRP infill panels was approximately 21.3%, and that between the beam and GFRP infill panels was approximately 2.5%. The steel-frame structures and GFRP infill panels were assumed to be in total contact in the design. However, they were not in perfect contact due to construction and manufacturing errors, and the boundary conditions of the GFRP infill panels also did not exactly match those specified in the design.

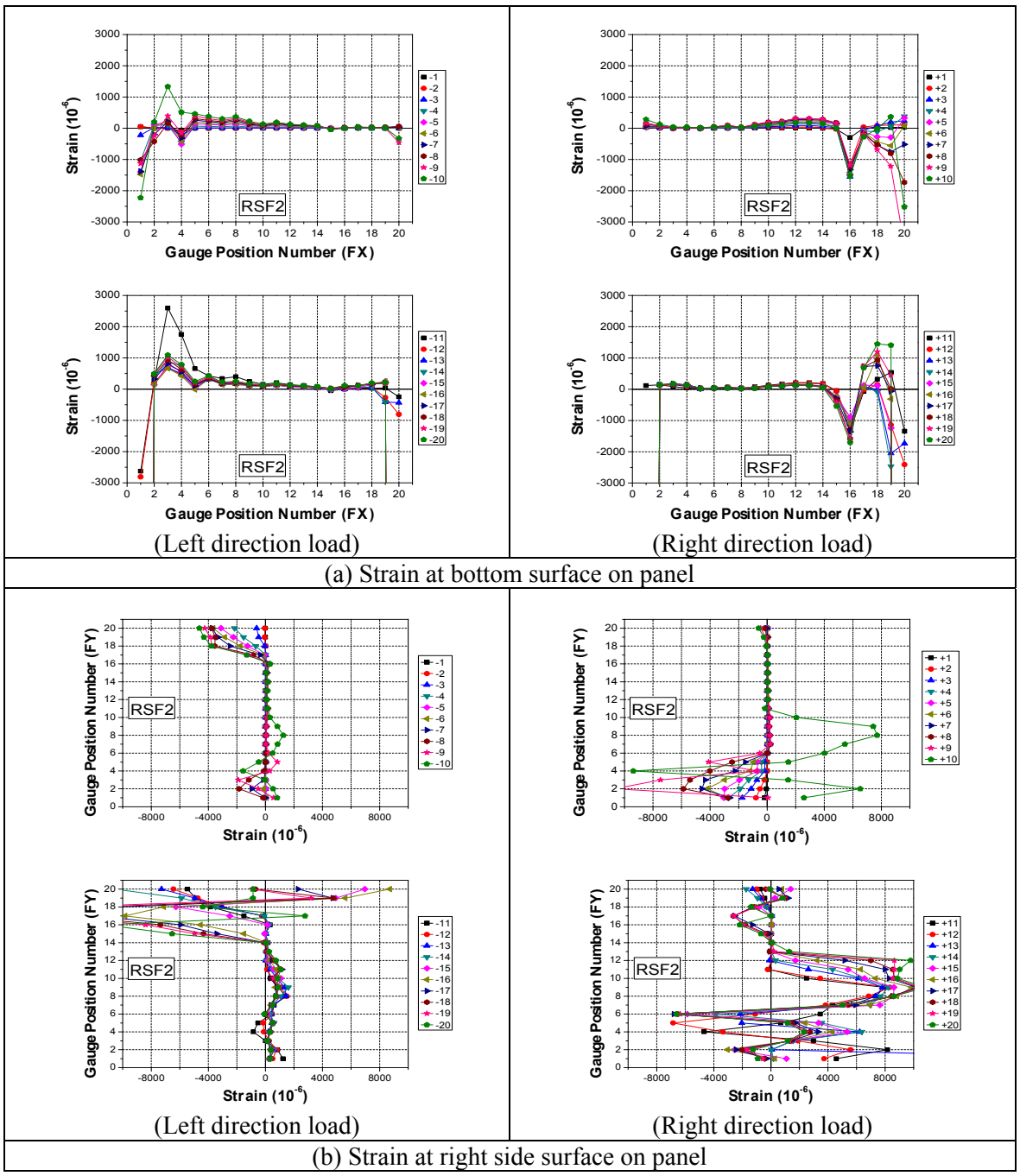

Fig. 4: Compression strains of GFRP infill panel.

5. CONCLUSIONS

In this study, the compression strain of GFRP infill panels was checked to determine the effective contact-length ratio between the GFRP infill panels and steel frame structure. Finally, it is possible to use to propose a design procedure for GFRP infill panels to apply in the construction field.

ACKNOWLEDGMENTS

This research was supported by a grant (18SCIP-B146946-01) from construction technology research program funded by Ministry of Land, Infrastructure and Transport of Korean Government.

REFERENCES

[1] Aref, A.J. and Jung, W.Y., "Advanced composite panels for response modification of existing structures", *J. Engineering Materials and Technology*, ASME, 2006, 128, 618-633.

[2] Kim, J.S., Kwon, M.H., Seo, H.S. and Jung, W.Y., "Performance evaluation of GIP wall systems for strengthening steel-frame structures." *Composite Structures*, 2015, 125, 228–238.

SESSION 7A: MANUFACTURING

DOI: 10.5075/epfl-ICSS12-2018-156-158

PROCESS EFFECTS ON THE PROPERTIES OF A SANDWICH PART MANUFACTURED BY PARTICLE FOAM INJECTION MOLDING

Kay A. Weidenmann[1,2], Hannah Kerrmann[2], Anja Dennard[2], Alexander Roch[2], Christoph Lohr[1] and Peter Elsner[1,2]
[1]Karlsruhe Institute of Technology, Institute for Applied Materials. Germany.
Kay.Weidenmann@kit.edu, Christoph.Lohr@kit.edu
[2]Fraunhofer Institute for Chemical Technology. Germany.
Hannah.Kerrmann@ict.fraunhofer.de, Anja.Dennard@ict.fraunhofer.de, Alexander.Roch@ict.fraunhofer.de,
Peter.Elsner@ict.fraunhofer.de

1. INTRODUCTION

Particle foams are shaped parts made from thermoplastic foam beads. Particle foams are characterized by very low densities in the range from 15 to 80 kg/m³ [1] as well as good dynamic properties, static shock resistance and an acoustic and heat-insulating effect [2,3]. With a tensile strength of up to 500 kPa, the tensile strength is far below that of solid plastics [4]. Basically the foaming of polyolefins (PP, PE) and polystyrene (PS) is based on the expansion process of foam particles. The foamed particles are further processed in a molding process. They are passed through with superheated steam and thus interact with each other resulting in a sintered particle foam part [5]. Injection molding is the preferred method for processing thermoplastics to molded parts. The injection molding process is characterized by a high degree of integratability of process sequence steps, whereby a wide variety of process combinations are possible. In this regard, particle foam composite injection molding (PVSG) was developed by Ruch Novaplast GmbH + Co. KG together with Arburg GmbH + Co KG and the Krallmann Group Kunststoffverarbeitung GmbH [6]. In this process, a substance-to-substance bond is formed between a particle foam inlay and a plastic component. For this purpose, the pre-foamed inlay is inserted into the injection molding machine. Due to the temperature of the melt, the surface of the particle foam is permanently bonded to the solid material during a subsequent injection molding step [7]. The combination of two plastic components with different properties creates a composite component that achieves high stiffness combined with low weight per unit volume [2].

In principle, the production of sandwich components using this process is also conceivable. However, some research questions have to be solved: The foam insert has to be fixed in the mold. The injection pressure used in injection molding must not cause the foam to collapse. The bond between the particle foam and the surface layers must be able to transfer loads under bending, for example. In this contribution, the process-impact on the properties of a particle foam injection molded sandwich part is investigated by means of mechanical tests.

2. EXPERIMENTAL

Manufacturing of Foam Inlays and Injection Molding of Sandwich Parts

The mold plates for the foam inserts were produced on an automatic molding machine from Erlenbach GmbH. The expanded polypropylene originated from the company JSP of the material types Arpro 1133 Dragonfruit and Arpro 5195, with bulk densities of 35 kg/m³ and 90 kg/m³. The slabs have a size of 500 × 500 × 50 mm³. After the plates were ejected from the molding machines, they were tempered at 80 °C for 4 hours. The slabs with a bulk density of 35 kg/m³ had a molded part density of 50 kg/m³. In the foam plates with a bulk density of 90 kg/m³, the mold was slightly overfilled during the filling process of the molded part, thus achieving a molding density of 100 kg/m³. The boards were then cut to the required insert size of 200×60×20 mm³ using a band saw.

In order to reduce the pressure in the cavity and hence preventing the foam from collapsing during injection molding, a groove with 2 mm in depth was subsequently inserted into the foam insert over the sprue width. With the help of this flow aid, the inlay of both high and low density was overflowed and the cavity was completely filled. The schematic geometry of the mold cavity including the gating is shown in Fig. 1. Polypropylene with an MFI 120 was chosen as the matrix material. Table 1 shows the respective process parameters for the different inlay foam densities.

Table 1: Process parameters for the particle foam injection molding.

Foam density	Mass temperature	Injection speed
50 kg/m³	180 °C and 200 °C	10 and 20 cm³/s
100 kg/m³	180 °C and 200 °C	10 and 30 cm³/s

The second stage of the injection speed corresponded to the maximum achievable speed, depending on foam density, without the insert being overmolded. For the foam density of 50 kg/m³ a speed of 20 cm³/s was chosen, for the foam density of 100 kg/m³ a speed of 30 cm³/s was chosen.

Mechanical and Microstructure Characterization

The samples were stored under standard climatic conditions for at least 48 hours prior to testing. In both cases the sample as a whole was tested. The sample dimensions are presented in Fig. 1.

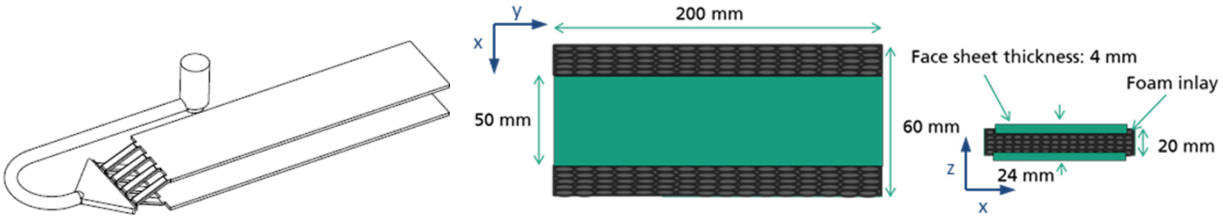

Fig. 1: Schematic drawing of the mold cavity (left), final specimen geometry (right).

The characterization of the interlaminar strength in the DCB test was carried out in the x-y-plane (c.f. Fig.1) of the sandwiches on the basis of ASTM D5528 which is a standardized testing procedure for composites. The load was applied in z direction. The procedure can also be used for sandwich structures [8] and was carried out on a universal testing machine with a constant crosshead velocity of 2 mm/min. The foam inserts were prepared prior to the injection molding process for the DCB test. At the end of the flow path, a 10 mm wide strip of polyimide adhesive tape covered the entire width of the inserts. Thus, it was ensured that a crack occurring during the test was introduced into the interface in a targeted manner. To clamp and test the specimen, two aluminum lids were glued on the PP surface using a two-component epoxy resin adhesive. The adhesive was cured according to the data sheet at 65 °C for 60 min.

Due to the specimen dimensions, three-point bending test could only be carried out in accordance with DIN EN ISO 178 at a constant test speed of 10 mm/min. The load was applied in z direction. The support diameters were 10 mm and the lower support distance 140 mm. The test was aborted when a failure of the surface layer or core occurred or when the travel of the testing machine had reached its maximum.

In order to analyze potential air inclusions in the samples, the distribution was investigated at a total of five points per sample. The sample was cut using a band saw. The surface layers of the samples were then sanded with 220 grit sandpaper and subsequently a 800 grit. The occurrence and the percentage volume distribution of the air inclusions were determined according to the line intersection method.

3. RESULTS

Mechanical Characterization

Due to the different sample height of the two foam densities and the associated change in the moment of inertia of the area the results of the 3-point bending test can only be compared qualitatively with each other. For each parameter combination, an example of a bending test specimen was selected that represents the average course of each parameter combination. Fig. 2 shows the bending curves of the two foam densities of 50 and 100 kg/m³.

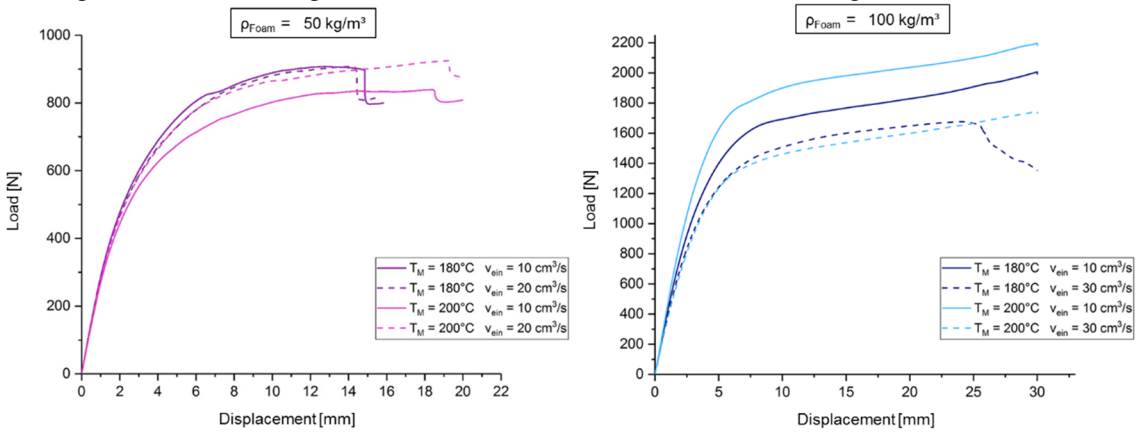

Fig. 2: Results from the 3-point bending tests for both foam inlay densities at different injection speeds (v_{ein}).

Comparing the curves of low density with each other, a similar curve can be observed for all of them. With a deflection of approx. 7 mm a short time force plateau is visible, followed by a further increase in force. All configurations suffer from surface layer failure. It should also be noted that the composites of low melt temperature (180 °C) have potentially a higher maximum force than those of the higher temperature. However, the tests with sandwiches manufactured at 200 °C reveal a higher deflection. Additionally, for the foam featuring the higher density, an impact of injection speed (v_{ein}) is visible.

The DCB test was used to investigate the interface between foam and injection molding material. Fig. 3 shows an example of the curves for the test results. In all samples, the crack has spread directly into the foam core after insertion of the defect. The force-displacement curves for the individual foam densities therefore characterize the strength of the particle foam. As a result, the interfacial strength is higher than that of the foam core.

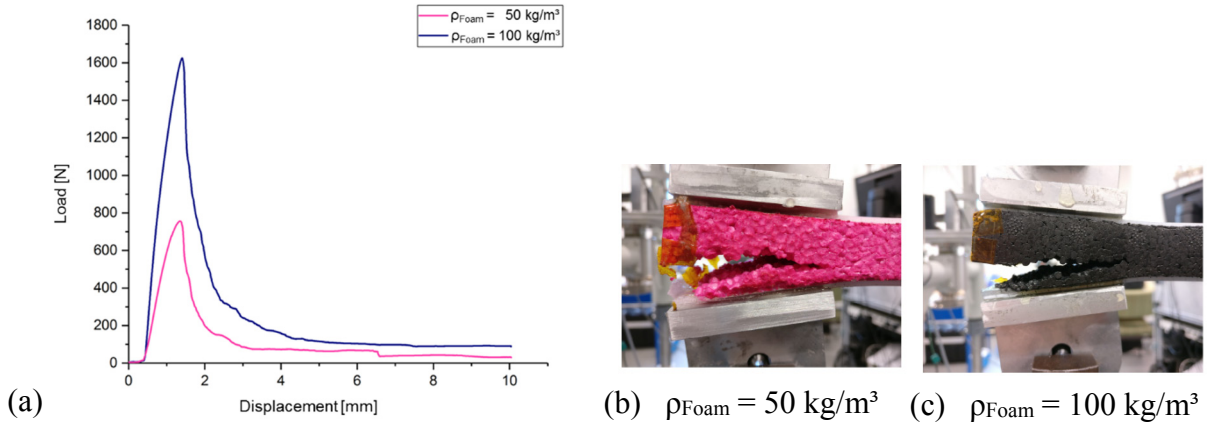

Fig. 3: Results from DCB tests (a) including the crack propagation observations (b,c).

Microstructure Characterization

Fig. 4 shows representative cross-sections for sandwiches with different foam densities at otherwise comparable process parameters. It can be seen that the low foam density results in a much higher share of air bubbles within the interlayer between foam inlay and face sheet. This suggests that, due to the higher compressibility of the foam, it is possible to increase the capacity of the foam to expand the escaping air from the molten particles. This allows the formation of larger air inclusions

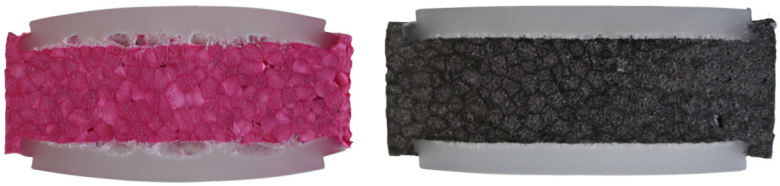

Fig. 4: Cross-sections (x-z-plane) for particle foamed injection molded sandwiches (T = 180 °C, v = 10 cm³/s) for the different inlay densities 50 kg/m³ (left) and 100 kg/m³ (right), dimensions c.f. Fig. 1.

4. SUMMARY

The production of a sandwich component by combining a particle foam as core material and an injection-molded top layer has shown to be feasible using a specially design injection molding tool. The bending properties of the particle foam can be significantly enhanced by the bonded compact surface layers. The connection between the foam insert and the top layer is not a weak point, but a low foam density leads to the formation of entrapped air bubbles at the interface between the inlay and top layer.

REFERENCES

[1] Neue Materialien Bayreuth GmbH: Partikelschaum-Verfahren. URL: http://www.nmbgmbh.de/verfahren/partikelschaumverfahren/.
[2] Arburg GmbH + Co. KG. *Partikelschaum-VerbundSpritzgießen: Leichtbau mit Funktionsintegration.* Arburg GmbH + Co. KG. URL: https://www.arburg.com/fileadmin/redaktion/sonstiges/arburg_pvsg_680864_de.pdf.
[3] E. Bürkle et.al., "Schäumen nach dem Spritzgießen". *Kunststoffe,* 2013; 2: 14-17
[4] A. Kauffmann et.al., "Particle Foams – Ways to Improve the Product Quality", *PPS21*: 2005
[5] A. Kauffmann, "Extruded particle foams – Material- and process investigations", *PPS23*: 2007
[6] I. Brexeler et.al. "Partikelschaum-Bauteil mit integrierter Befestigung und Verfahren zu seiner Herstellung", *Patent WO 2014/114449 A1*, 2014
[7] Th. Brinkmann. „Partikelschaum-Verbundspritzgießen - Ein neues Verfahren für den Leichtbau" URL: https://www.fachportal-produktentwicklung.de/de/sonstiges/aktuelles/nachricht/Partikelschaum-Verbundspritzgiessen-ein-neues-Verfahrenfuer-den-Leichtbau-224T/.
[8] ASTM International. "Standard Test Method for Mode I Interlaminar Fracture Toughness of Unidirectional Fiber-Reinforced Polymer Matrix Composites", 1, November 2013.

DOI: 10.5075/epfl-ICSS12-2018-159-160

PROCESS OPTIMIZATION FOR ULTRA-LIGHTWEIGHT POLYURETHANE/PET RESIN TRANSFER MOLDING (RTM) SANDWICH COMPONENTS

Gion A. Barandun[1], Lorenz Schüssler[1], Philipp Angst[2] and Hannes Eggenschwiler[2]
[1]HSR Hochschule für Technik Rapperswil, IWK Institut für Werkstofftechnik und Kunststoffverarbeitung, Oberseestrasse 10, CH-8640 Rapperswil, Switzerland. gionandrea.barandun@hsr.ch, lorenz.schuessler@hsr.ch
[2]Airex Speciality Foams, Industrie Nord 26, CH-5643 Sins, Switzerland. Philipp.Angst@3AComposites.com, Hannes.Eggenschwiler@3AComposites.com

1. INTRODUCTION

With their high stiffness-to-weight ratio, sandwich structures are ideal lightweight design components. Countless materials are available as core and face sheets – the appropriate combination for a given application might therefore be difficult. Material compatibility in terms of processing and application is however crucial for adequate properties. The combination of glass fiber reinforced polyurethane for the face sheets and low-density PET foams as core material are an ideal choice for structural components in all kind of transportation applications. An efficient processing route for the manufacture of such structures is the Resin Transfer Molding (RTM) process, where the dry preform, including face sheets and core, is placed in a cavity and resin is injected under pressure. Elevated temperature and pressure enable a fast curing, thus demolding of the finished part is possible within minutes. Within the EUREKA project PRISCA (Polyurethane Reaction Injection for Structural Composite Applications), materials and processes for the manufacture of PUR-RTM sandwich components have been established and characterized [1].

2. MATERIAL SELECTION

Glass fiber reinforcements are widely used in composite applications, either for monolithic structures or sandwich components. They combine excellent strength, good stiffness, low weight and relatively low material costs. For demanding structural application, the matrix system commonly used today is epoxy. Polyurethane is an interesting alternative to epoxy, as it offers similar mechanical properties but might come with additional advantages: a very broad bandwidth of tunable properties, better impact toughness and lower costs. For sandwich components, the processing is typically faster and the very low viscosity of polyurethane resin reduces the pressure required for the injection thus enables the use of very light foam cores.

In combination with a PET foam core, an ultra-lightweight, high performance yet very cost efficient sandwich is feasible. In fact, the combination of PET and PU enables new applications within the transport industry, where the price-performance ratio is crucial. PET foam cores are easy to thermoform (T=160°C) and do not show any spring back effects [2].

3. PROCESS DEVELOPMENT

Efficient production of sandwich parts may be done using different process routes:

- Hot pressing of dry preforms (thermoplastic face sheets)
- Wet press molding of dry preforms (thermoset resins)
- Resin injection of dry preforms (thermoset resins)

Within the context of this project, the latter method is used. Compared to the other processing routes, there are some advantages using the RTM process (Fig. 1):

- High performance parts are feasible (excellent impregnation and consolidation, high fiber volume content, low voids, excellent adhesion)
- Comparably low processing times thanks to fast resin injection (low viscosity) and fast curing (snap cure)
- Core limits prevent risk to equipment

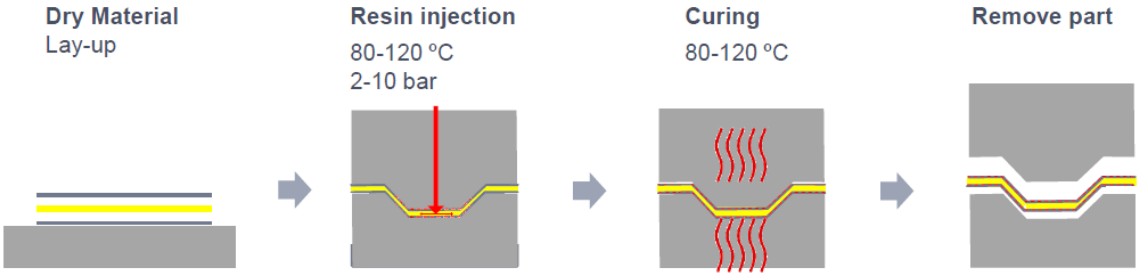

Fig. 1: RTM process to manufacture structural sandwich components [1].

However, the implementation of robust RTM processes is challenging, as effects such as fiber washing or race tracking might influence the fill pattern and turn a part unusable. The successful production of PUR-RTM sandwich components therefore depends on several process parameters. The objective is to manufacture (even larger) sandwich parts in the shortest possible time, without damaging the PET core due to the cavity pressure created by the resin injection. Thus, process parameters have to be adjusted in an appropriate range to enable such manufacturing cycles. This has been done by using a coupon tool to produce a sandwich specimen with dimensions 220 x 110 x 20mm (Fig. 2). By adapting resin system, core architecture and process parameters, an optimal combination for a robust production could eventually be identified.

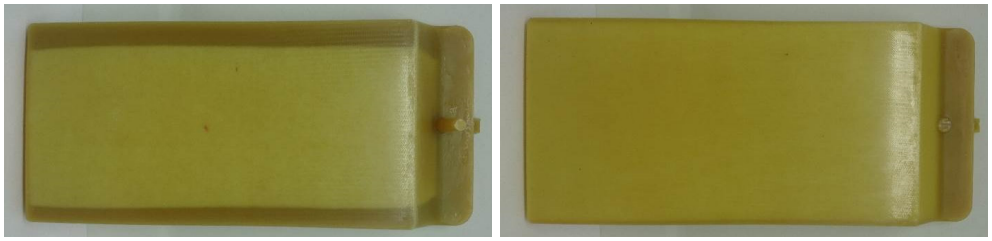

Fig. 2: Sandwich specimen (left: collapsed core; right: optimized processing).

In this context, based on a PET foam core and a low-viscosity PU resin system, the process parameters as illustrated in Table 1 have been optimized.

Table 1: process parameters for the manufacture of PET/PU sandwich structures.

Resin	Core	Fibers	Temperatures	Max. cavity pressure	Flow rate	Inj. time	Cycle time
Rühl Puropreg	AIREX TX.170	Glass fibers	Tool: 120°C Resin: 60°C	8bar	4g/s	20s	<5min

4. RESULTS

The main objective of this work was to develop appropriate processing technologies for the fast and robust manufacture of structural PUR-RTM sandwich parts. In terms of evaluation of the manufactured specimens, the flow front propagation inside the tool has been monitored using indicator marks, to be able to identify race tracking and potential dry spot formation. Fig. 3 shows a typical flow path, where it can clearly be seen that race tracking occurs along the vertical edges in direction of the pressure drop.

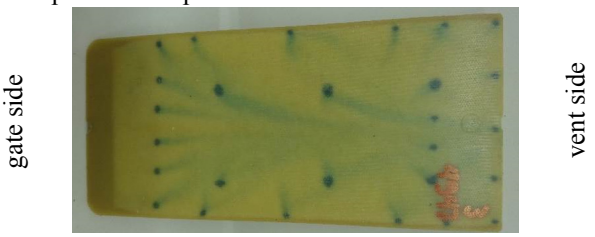

Fig. 3: Typical flow path marked by indicators with race tracking along the edges and back-flow towards the vent.

As with monolithic RTM parts, race tracking cannot be completely avoided and is a result of a gap between preform and mold. It is however possible to minimize the influence by adjusting process parameters (foam core cutting, processing temperatures, injection pressure) and thus obtain a reproducible part quality.

Further work will focus on the process optimization for curved sandwich components. As a robust and reproducible process has been reached on coupon-level, the next logical step is to transfer the technology to real-life geometries.

ACKNOWLEDGEMENTS

This work was granted under the EUREKA project 9183, BMWi in Germany (KF2198131EB4) and CTI in Switzerland (16956.1 PFIW-IW). The authors gratefully acknowledge the support by EUREKA, AIF/ZIM and CTI.

REFERENCES

[1] D. Hülsbusch et al., “PRISCA: Polyurethane as a matrix material for composite components”, FAPU EPJ, 2017, 38-40.
[2] P. Angst et al., “Weight-saving with Sandwich Design”, SKZ – Kunststofftrends im Automobilbau: 2017.

DOI: 10.5075/epfl-ICSS12-2018-161-163

THERMOPLASTIC SANDWICH STRUCTURES WITH BEAD FOAM CORE – NOVEL PROCESSING APPROACHES

Peter Schreier[1], Thomas Neumeyer[2], Johannes Knöchel[3], Mathias Mühlbacher[4] and Volker Altstädt[5,6]
[1] Neue Materialien Bayreuth GmbH, D-95448 Germany. Peter.Schreier@nmbgmbh.de
[2]Neue Materialien Bayreuth GmbH, D-95448 Germany. Thomas.Neumeyer@nmbgmbh.de
[3]Neue Materialien Bayreuth GmbH, D-95448 Germany. Johannes.Knöchel@nmbgmbh.de
[4]Neue Materialien Bayreuth GmbH, D-95448 Germany. Mathias.Mühlbacher@nmbgmbh.de
[5]Neue Materialien Bayreuth GmbH, D-95448 Germany. Volker.Altstaedt@nmbgmbh.de
[6]Department of Polymer Engineering, University of Bayreuth, D-95447 Germany. Altstaedt@uni-bayreuth.de

1. INTRODUCTION

Lightweight construction makes an important contribution to resource efficiency and furthermore allows improvement of functionality and reduction of costs regarding energy consumption as a result of reduced weight. The use of lightweight structures in aerospace sector is well known. The relevance of lightweight construction in further application fields like energy technology, construction and especially transportation has strongly increased in recent years. The light weight construction market in the transportation sector (in particular automobiles) will grow in the coming years to 2020 according to market forecasts at 140 billion euros [1]. Thermoplastic composite sandwich structures offer a great potential to meet the demands of lightweight structures as they provide low weight and high stiffness at the same time [2]. Using a thermoplastic foam core, particularly a bead foam core, offers further advantages like additional thermal insulation, elevated energy adsorption and thus improved crash behavior and enhanced recycling compatibility. Therefore, this approach will gain more significance in e-mobility [3]. Furthermore, the use of thermoplastic materials allows shorter cycle times in production compared to thermoset based systems as no curing step is needed. Another advantage is the integration of functional elements such as ribs or connecting elements by injection molding.

Nevertheless, there is a lack of established processes allowing the economic manufacturing of thermoplastic sandwich structures in high-volume production as necessary for automotive industry. Thus, this work deals with efficient and highly integrated processing solutions to meet the mentioned demands.

2. STATE OF THE ART

The sandwich concept can be expressed as increasing the bending stiffness of a panel without adding significant weight. By separating two stiff face sheets, the bending stiffness increases with rising distance between the sheets as a result of the increased moment of inertia about the beam centroid. To keep the face sheets separated usually core materials like honeycombs, polymer foams or balsa wood are used [4].

Polymer bead foams are lightweight materials consisting of fused microcellular beads. Their multiscale structure makes bead foams unique in terms of a free choice of shape combined with extreme low density down to 15 kg/m³. Further benefits of bead foams are good energy absorption properties, excellent impact resistance and their low thermal conductivity having values in the order of 0.03 W/m K. The processing of bead foam components is usually done by means of steam which enables the welding of the single beads. The best-known representatives are expandable polystyrene (EPS) and expanded polypropylene (EPP). Typical applications are insulation of buildings, packaging, load carriers and technical parts in automotive interior [5].

3. AIM OF STUDY

The main goal of the present study is the identification and establishing of economic processing technologies for large-scale production of thermoplastic sandwich structures with bead foam core.

4. PROCESSING APPROACHES

The manufacturing of thermoplastic sandwich structures with bead foam core can be realized by different processing routes. The conventional technique is compression molding of two thermoplastic face sheets (e.g. organo sheets, UD-tapes) and a thermoplastic foam core (e.g. semi-finished products). The joining by welding of the single components is initiated by preheating of the face sheets and if necessary of the core material too. By using compatible polymers there are no additional adhesive films necessary because a substance-to-substance bond with rather high strength can be achieved. In order to achieve a three-dimensional sandwich structure built up of two different face sheet geometries by the use of this technology, there are at least three different molds required (shown in Fig. 1). Furthermore, advanced handling and heating in both molds is necessary. Another disadvantage is given by the inhomogeneous compression of the foam core by different and complex shapes of the face sheets and resultant inhomogeneous properties.

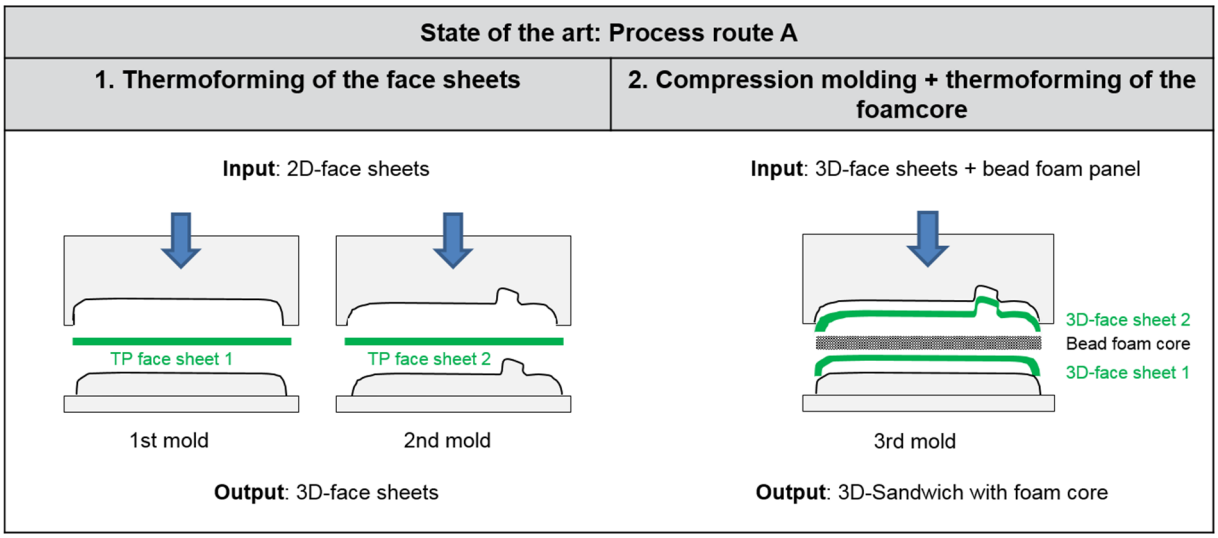

Fig. 1: Schematic sketch of conventional technology for manufacturing 3D-sandwich structures.

A second processing route for fabricating three-dimensional sandwich structures is given by using in-situ techniques which are more suitable for complex structures. For this purpose, 3D-face sheets are inserted and fixed in the mold and the foam core is fused directly by welding of foamed beads in-between the face sheets. By the use of bead foams like EPP, core densities between 20 kg/m³ and approx. 300 kg/m³ can be achieved. Bead foams allow for shaping very complex geometries and enable varying core thickness between 5 mm and several centimetres. Furthermore, theses closed-cell foams offer superior thermal insulation properties [3]. Besides the mentioned advantages of the in-situ bead foaming technology there are the same economical limits (primary the long cycle time) for high-volume production. Again, three different molds are necessary. The processing sequence is shown in Fig. 2.

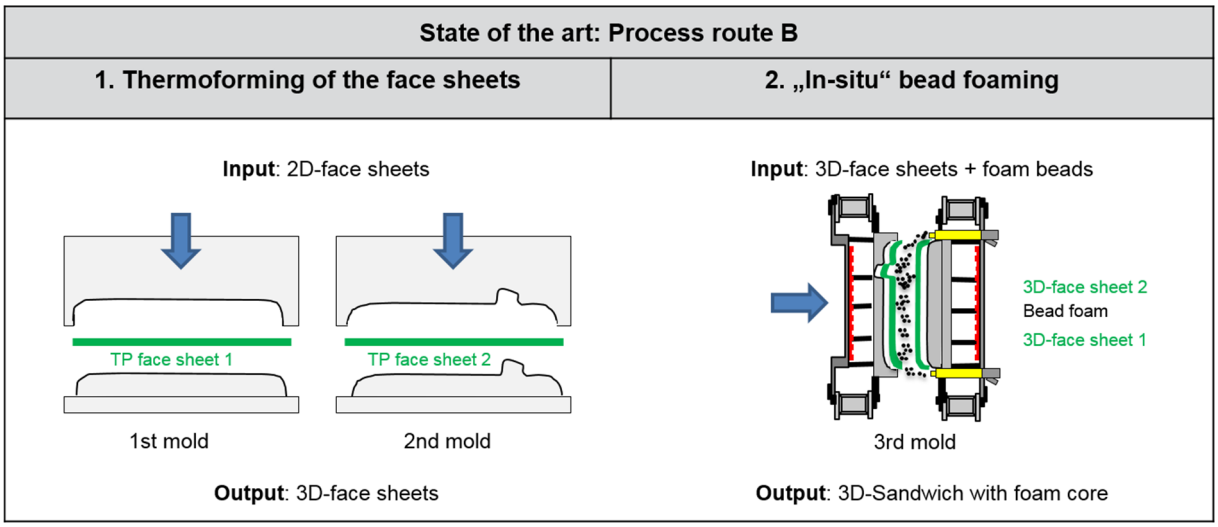

Fig. 2: Schematic sketch of in-situ bead foaming technology for manufacturing 3D-sandwich structures.

Following the specific requirements of high-volume production for automotive industry a more efficient process technology has been established that allows the production of 3D-sandwich components with additional functional integration realized by injection molding. At first the thermoplastic face sheets based on PP or PA6 are pre-heated by applying infrared radiation. By means of a suitable core dummy (made of steel) the two face sheets are thermoformed within one multi-stage mold and functional elements are attached via injection molding at the same time. Within few seconds the dummy is removed and the foam core (e.g. bead foam cores) is placed by a handling system between the functionalized face sheets. By closing the mold again the thermoforming of the core as well as the welding process of the face sheets and the core take place. If needed edge closures can be formend by subsequent injection molding within the same mold. The schematic sketch of this technique is shown in Fig. 3. With this innovative multi-stage process only one mold and one machine is necessary, and it is possible to produce components without any post-processing. The new intelligent process and tool design allows a high level of functional integration as well as short cycle times which leads to a suitable and economical process for large series production.

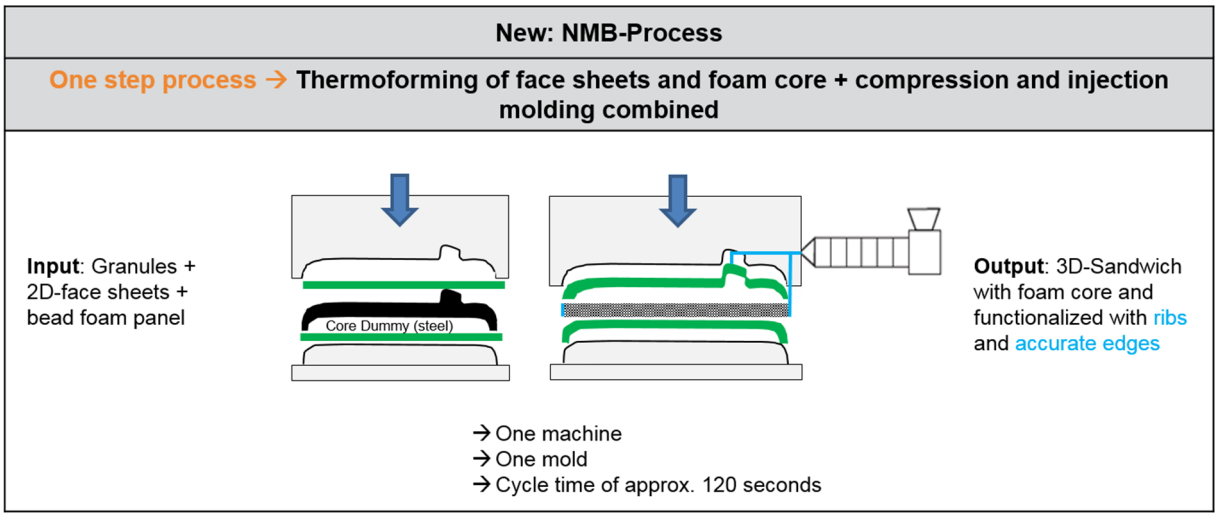

Fig. 3: Schematic sketch of the new NMB-processing technology for manufacturing functionalized 3D-sandwich structures within one mold.

In order to investigate the process capability of the new processing technology a demonstration part based on polypropylene with the dimension of approx. 350 x 450 mm was engineered and produced (Fig. 4).

Fig. 4: Demonstration part "Functionalized 3D-Sandwich with bead foam core" (CAD-view on the left and realized component on the right).

5. CONCLUSION AND OUTLOOK

The economic use of full thermoplastic sandwich structures in large-scale production like in automotive industry is only expedient if a high degree of functional integration and a short cycle times below 120 seconds can be realized. By means of the introduced NMB-processing technique a highly promising solution statement for an efficient manufacturing process for full thermoplastic sandwich structures is outlined. This innovative approach, especially with the use of bead foams as core material offers a great potential to meet the demands of prospective sustainable lightweight developments for the use in electromobility.

In order to reach an even higher degree of functional integration the combination of the shown process with the technique of additive manufacturing will be taken in account and investigated. The use of 3D printing processes enables the individualization of special functional variants (Fig. 4, right side - yellow screw boss) as well as design variants.

ACKNOWLEDGEMENTS

This work is largely performed in the framework of the project „MAI Sandwich - Entwicklung von thermoplastisch fügbaren Sandwichstrukturen unter Berücksichtigung eines sortenreinen und wiederverwertbaren Werkstoffeinsatzes", No. 03MAI32H, which is funded by the German Federal Ministry of Education and Research via the MAI Carbon Cluster as part of a program to support the joint industrial research and development. We thank all partners and all those who supported the present work.

REFERENCES

[1] A. Thielmann et al., *Leichtbau – Trends und Zukunftsmärkte*, Leichtbau BW GmbH: 2014, 6.
[2] J. Grünewald et al., "Manufacturing of thermoplastic composite sandwich structures", *Journal of Thermoplastic Composite Materials*, 2017; 30: 437-464.
[3] T. Neumeyer et al., "Thermoplastic sandwich structures – processing approaches towards automotive serial production", *ICCM-21*: 2017, 1.
[4] J. Knöchel et al., "Funktionsintegration in thermoplastische Sandwichstrukturen durch Spritzgießen", 8. Landshuter Leichtbau-Colloquium: 2017, 106-115.
[5] D. Raps et al., "Past and present developments in polymer bead foams and bead foaming technology", *Polymer*, 2015; 56: 5-19.

SESSION 7B: DESIGN

DOI: 10.5075/epfl-ICSS12-2018-165-167

STRUCTURAL DESIGN OPTIMISATION OF RECTANGULAR HONEYCOMB CORE SANDWICH PANELS UNDER OUT-OF-PLANE LOADING

Luis Santos[1], Alexander N. Nordas[2], Bassam A. Izzuddin[3] and Lorenzo Macorini[4]
Department of Civil and Environmental Engineering, Imperial College, London, SW7 2AZ, UK
[1]ls3715@ic.ac.uk, [2]an913@ic.ac.uk, [3]b.izzuddin@imperial.ac.uk, [4]l.macorini@imperial.ac.uk

1. INTRODUCTION

Sandwich systems are often used in applications where enhanced structural performance is required at minimal weight. Offshore deck systems stand to benefit from sandwich construction not only in relation to improved resistance to localised equipment loads and other distributed loads but also due to favourable manufacturing and assembly procedures.

Minimising weight, which is particularly important for offshore applications, requires a relatively accurate design method to be established, and to increase the applicability of sandwich panels, a design approach based on a practical methodology is required. Achieving a design methodology naturally evolves from an ability to assess candidate solutions, which requires an accurate and practical analysis method and a comprehensive understanding of all possible failure modes.

This paper proposes a methodology for optimising rectangular steel sandwich panels with a rectangular honeycomb core under combined uniformly distributed loads and patch loads. The analysis of sandwich panels is based on the first-order shear theory for isotropic sandwich plate bending [1] as well as the sandwich concept, where it is assumed that top and bottom plates resist bending moments and the core resists the shear forces. When compared to the more complex equations for orthotropic sandwich plate bending derived by Robinson [2], accurate results for panels with similar core shear stiffness in the x- and y-directions can be achieved. Moreover, isotropic sandwich plate bending equations allow for a relatively accurate optimisation sequence to run without recalculating the internal forces for every iterative step.

The internal forces obtained from the aforementioned analysis are used to generate the constraints of a structural optimisation problem to minimise weight, which is solved using the Method of Moving Asymptotes (MMA) [3]. These constraints are generated considering the various failure modes in the domain of the panel, including material yielding, plate buckling and deformation control.

The establishment of this methodology, based on trigonometric series for analysis and on a gradient-based method for optimisation, enables the optimal design of rectangular sandwich panels to be established, leading to the minimum weight panel that fulfils all the design constraints.

2. METHODOLOGY

Failure Modes

It is important to consider all possible failure modes to achieve a systematic performance assessment method at a local level. The critical failure modes considered for rectangular honeycomb core sandwich panels are face yielding, face intercellular buckling, core compressive yielding, core compressive buckling, core shear yielding, which includes punching shear, and core shear buckling. The deformation of the panel is also controlled.

Steel structures yield according to the von Mises yield criterion. According to the sandwich concept, the top and bottom plates are under a general stress state, while the plates of the core are under a pure shear stress state. In this study, the interaction of compression and shear stresses within the core is neglected.

For plate buckling failure modes, the critical buckling stress σ_{cr} can be generally expressed as:

$$\sigma_{cr} = k \cdot \frac{\pi^2 \cdot E}{12(1-v^2)} \cdot \left(\frac{t}{b}\right)^2 \tag{1}$$

where E is Young's modulus, set to 210 GPa, t is the plate thickness, v is the Poisson ratio, b is a dimension of the plate, and k is the buckling coefficient that is defined by the loading and support conditions along the plate boundaries.

Analysis

Consider a rectangular sandwich plate of sides a and b, simply supported on all edges. The deformed shape of a sandwich plate, which can be decomposed in partial deflections of bending $w_b(x,y)$ and shear $w_s(x,y)$ deformation [1], can be respectively computed by double trigonometric series according to:

$$w(x,y) = \sum_{m=1}^{\infty}\sum_{n=1}^{\infty} \frac{p_{mn} \cdot (1-v^2) \cdot sin\frac{m\pi x}{a} sin\frac{n\pi y}{b}}{D \cdot \pi^4 \cdot \left[\left(\frac{m}{a}\right)^2 + \left(\frac{n}{b}\right)^2\right]^2} + \sum_{m=1}^{\infty}\sum_{n=1}^{\infty} \frac{p_{mn} \cdot sin\frac{m\pi x}{a} sin\frac{n\pi y}{b}}{S \cdot \pi^2 \cdot \left[\left(\frac{m}{a}\right)^2 + \left(\frac{n}{b}\right)^2\right]} \tag{2}$$

where D is the sandwich plate flexural stiffness, S is the core shear stiffness, and p_{mn} are the coefficients of the double Fourier expansion that are respectively described for an uniformed distributed load (UDL) and a patch load (PL) according to:

$$p_{mn,UDL} = \frac{4p_0}{\pi^2 mn} \cdot [1 - \cos(m\pi)] \cdot [1 - \cos(n\pi)]; \quad p_{mn,PL} = \frac{16p_0}{\pi^2 mn} \sin\frac{m\pi\xi}{a} \sin\frac{n\pi\eta}{b} \sin\frac{m\pi u}{2a} \sin\frac{n\pi v}{2b} \tag{3}$$

where p_0 is the applied pressure, and ξ, η, u and v describe the location and size of the patch.
The internal forces in the domain of the panel can be easily derived from the deflected shape using similar double trigonometric series. Load combinations can be considered by superimposing the effects of each load, calculated separately, since the internal forces are assumed to be recovered accurately based on linear analysis.

From this analysis, the following quantities are computed: maximum equivalent von Mises bending moment, M_{vM}, for face yielding, obtained from the general planar von Mises stress combined with the sandwich effect; maximum bending moment in x- and y-directions at critical locations, M_x and M_y, for intercellular buckling; maximum shear forces in x- and y-directions, $V_{ed,x}$ and $V_{ed,y}$, for core shear yielding and buckling; maximum compressive stress, C_{ed}, for compressive yielding and buckling; the constants K_{bend} and K_{shear}, for serviceability, which are equal to $D{\cdot}w_{b,max}$ and $S{\cdot}w_{s,max}$, obtained from Eqs. 2 and 3.

Optimisation

At this stage, the MMA algorithm for optimisation can be established to minimize the weight function, given by:

$$W = 7850 \cdot \left[t_{f,top} + t_{f,bot} + h \cdot \left(\frac{t_{wx}}{l_x} + \frac{t_{wy}}{l_y} \right) \right] \tag{4}$$

where $t_{f,top}$, $t_{f,bot}$, h, t_{wx}, l_x, t_{wy} and l_y are the geometric variables that define the rectangular honeycomb core sandwich panel to be optimised, representing the thickness of the top and bottom plates, height of the panel and thicknesses and cell sizes in the x- and y-directions, respectively. The steel yield strength is represented by f_y, set to 235 MPa.
The problem constraints are generated from the aforementioned failure modes. Face yielding for the top plate is given by:

$$h \cdot t_{f,top} \cdot f_y \geq M_{vM} \tag{5}$$

Core shear buckling in the x-direction, for the case where h is greater than l_y, is given by:

$$\left(5.35 + 4 / \left(\frac{h}{l_y} \right)^2 \right) \cdot \frac{{t_{wx}}^3}{{l_y}^2} \geq V_{ed,x} \cdot \frac{12(1 - v^2)}{\pi^2 E} \tag{6}$$

Deflection control, assuming the maximum allowable displacement to be 1/360 of the smaller span, is given by:

$$E \cdot \frac{t_{f,top} \cdot t_{f,bot} \cdot h^2}{t_{f,top} + t_{f,bot}} / K_{bend} + G \cdot h \cdot \min\left(\frac{t_{wx}}{l_x}, \frac{t_{wy}}{l_y} \right) / K_{shear} \geq \frac{360}{min(a,b)} \tag{7}$$

Other constrains include face yielding of the bottom plate, face intercellular buckling, for which contribution of M_{xy} is neglected, core compressive yielding, core compressive buckling and core shear yielding.

3. RESULTS

A rectangular sandwich panel with an area of 5400×9000 mm^2 under a combination of distributed and patch loads is analysed and optimised using the proposed methodology. To improve the convergence of the method, the failure modes are rearranged to the following form:

$$\frac{A}{R} - SF \leq 0 \tag{8}$$

where, A stands for actions, R for resistance and SF for the target safety factor for the optimal panel. In this example, the target safety factors for all the failure models are kept as 1.0. A schematic view of the example is presented in Fig. 1(a), an illustrative example of a map of internal forces, obtained from the double Fourier series, is presented in Fig. 1(b) for the bending moment in the x-direction, and the detailed nonlinear FE model of the optimal panel is presented in Fig. 1(c), displaying the compressive stress maps in the x-direction.

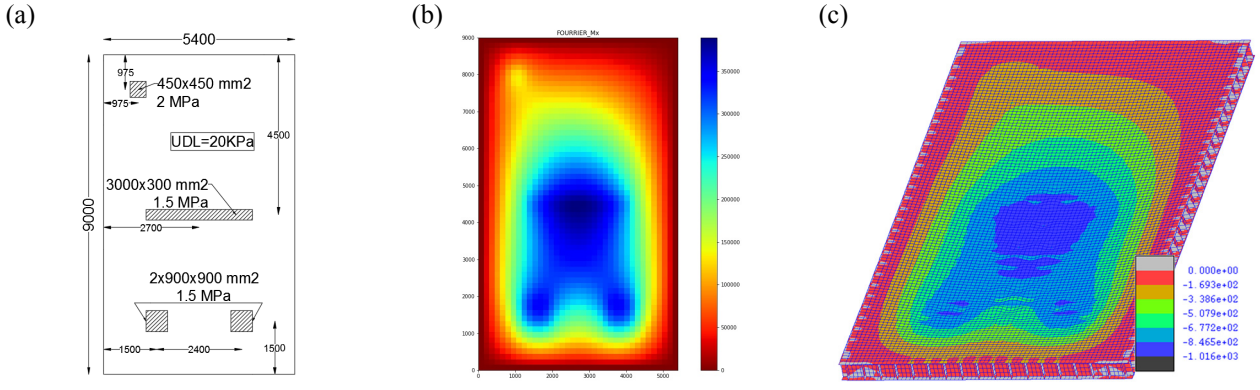

Fig. 1: (a) Description of load case (b) Example of stress map (c) Detailed FE Model.

Detailed nonlinear Finite Element models are developed in ADAPTIC [4] for verifying the results obtained from proposed approach. These models are built with 9-noded co-rotational shell elements [5] to discretise both the core and the facings while a triaxial elastoplastic material model is used for mild steel.

The main outcomes of the analysis are the maximum internal forces on the domain of the panel, which are presented in Table 1a and serve as input parameters for the optimisation sequence. The outcomes of the optimisation algorithm are the dimensions of the optimal panel and are presented in Table 1b, while the safety factors for the optimal panel are presented in Table 1c. It can be observed that several failure modes have a safety factor close to 1.0. The optimal panel is confirmed using exhaustive search in the vicinity of the solution.

Table 1: Presentation of results: (a) Material properties and internal forces (b) Optimal panel (c) Safety factors.

(a)

M_{vM} [N.mm/mm]	407000
M_x [N.mm/mm]	389000
M_y [N.mm/mm]	287000
$V_{ed,x}$ [N/mm]	467
$V_{ed,y}$ [N/mm]	452
C_{ed} [MPa]	2.02
K_{bend} [N.mm^2]	9.2e11
K_{shear} [N]	5.2e5

(b)

$t_{f,top}$ [mm]	6.17
$t_{f,bot}$ [mm]	4.97
h [mm]	348.1
t_{wx} [mm]	3.0
l_x [mm]	303.3
t_{wy} [mm]	2.97
l_y [mm]	303.3

(c)

Yielding Top	1.241
Yielding Bot	1.000
Shear yielding X	1.000
Shear yielding Y	1.022
Compressive yielding	2.289
Intercellular buckling	1.000
Shear buckling X	1.000
Shear buckling Y	1.000
Compressive buckling	1.621
Deformation control	1.000

The nonlinear response of the optimal panel (see Fig. 1(c)) is presented in Fig. 2.

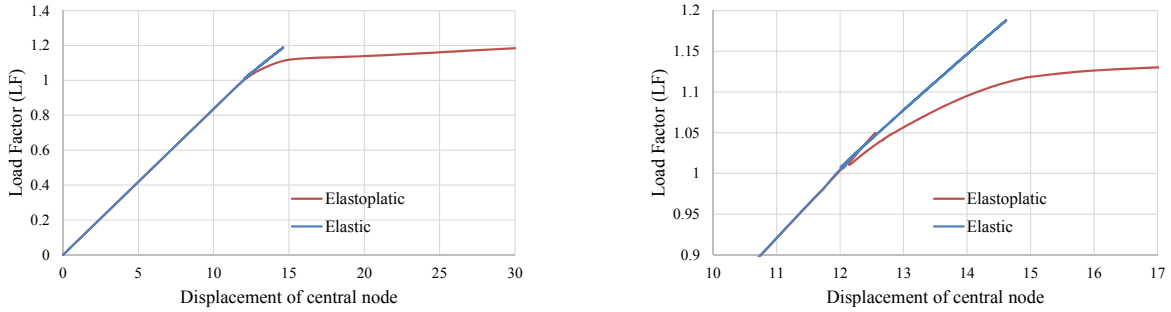

Fig. 2: Nonlinear response of the optimal panel.

From the deformed shape, it can be established that the critical failure mode is shear yielding and buckling on the core plates below the 900×900 mm^2 patch loads, at a load factor LF=1.01. The fact that this load factor is close to 1.0 indicates that the interaction between different failures modes is not significant. The results from an identical model with linear elastic material are shown so as to identify material yielding, which occurs at LF=1.02. At LF=1.0, the maximum displacement is 13.10 mm, complying with the serviceability limit of 15.0 mm (i.e. 5400mm/360). From the analysis of the post-failure response, the panel displays residual capacity to resist the applied loading.

4. CONCLUDING REMARKS

A methodology for design optimisation of rectangular honeycomb sandwich panels based on first-order shear theory for isotropic sandwich plate bending for structural analysis and the MMA algorithm for structural optimisation is proposed. Verification is undertaken against results of detailed nonlinear finite element analysis. The method is shown to provide relatively accurate results, rendering it useful for the development of an optimisation method for offshore deck systems composed of all-steel sandwich panels.

REFERENCES

[1] Zenkert D., "The Handbook of Sandwich Construction", EMAS Publishing, Worcestershire, 1997.
[2] Robinson J.R., "The Buckling and Bending of Orthotropic Sandwich Plates with all Edges Simply Supported", *Aero. Quart.,* Vol. 6, No 2, 1955, p 125-148.
[3] Svanberg K., "The Method of Moving Asymptotes – A new Method for Structural Optimisation", *International Journal for Numerical Methods in Engineering*, Vol. 24, 1987, p 359-373.
[4] Izzuddin, B.A., "Nonlinear Dynamic Analysis of Framed Structures", *PhD Thesis, Imperial College, University of London,* 1991.
[5] Izzuddin, B.A. and Liang, Y., "A Hierarchic Optimisation Approach towards Locking-free Shell Finite Elements", *Computers and Structures,* 2017, http://dx.doi.org/10.1016/j.compstruc.2017.08.010.

DOI: 10.5075/epfl-ICSS12-2018-168-170

IMPROVED FAILURE DESCRIPTION FOR AN ANALYTICAL DIMENSIONING APPROACH FOR INSERTS IN HONEYCOMB SANDWICH ELEMENTS

Johannes Wolff[1], Marco Brysch[2] and Prof. Dr. Ing. Christian Hühne[1]
[1]Institute of Composite Structures and Adaptive Systems, DLR, Braunschweig, Germany. Johannes.wolff@dlr.de
[2] Institute of Adaptronics and Function Integration, Technische Universität Braunschweig. Marco.Brysch@TU-Braunschweig.de

The major requirement for structures of aerospace and ground vehicles is a highly efficient lightweight design i. e. a high stiffness- and strength-to-mass ratio. Due to their outstanding specific bending and shear stiffness, sandwich elements composed of CFRP facings and aluminium honeycomb cores are frequently used as elements of e. g. satellite structures, race car monocoques or lightweight car bodies of passenger train concepts, Fig. 1. To fulfil assembly, maintenance, repair and recycling requirements, connections are often designed as removable, bolted connections. Sandwich core materials typically provide a low local compression resistance. Therefore, cylindrical supporting elements, so called "inserts", are commonly used to stabilize the core against the clamping force of the screw and to transfer loads into the structure, Fig. 2.

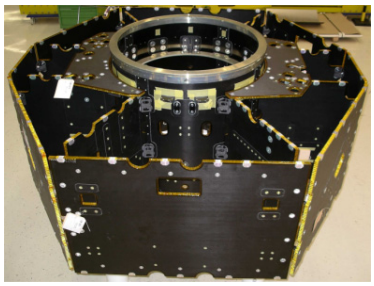

Fig 1: Sandwich structure of the Lisa Pathfinder satellite science module [1].

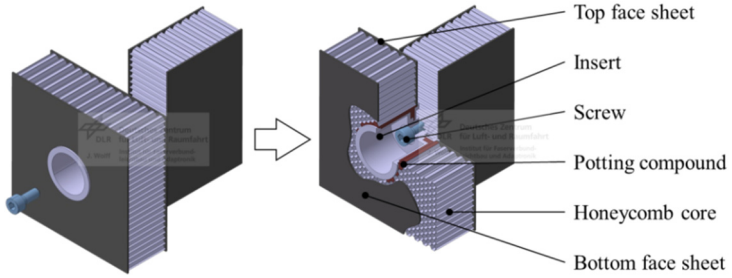

Fig. 2: Bolted t-connection between sandwich panels with a through-the-thickness insert element.

If huge numbers of such inserts are demanded (as e. g. communication satellites can contain insert with numbers up to 25.000, [2]) they can add a remarkable mass proportion to the overall weight of the structure. Since e. g. launching costs of space vehicles reach 10 - 50K$/kg [3–5], a mass minimization of the insert load introductions is worthwhile. In this regard, the objective of this work is to develop an analytical dimensioning method to minimize the diameter $d_i \rightarrow d_{i,min}$ of insert elements loaded with a force $F_{i,n}$, acting normal to the surface of the sandwich. Since through-the-thickness, core connected (resp. potted) inserts are recommended for structural applications, this type of insert is regarded exclusively herein by [6–8], Fig. 3.

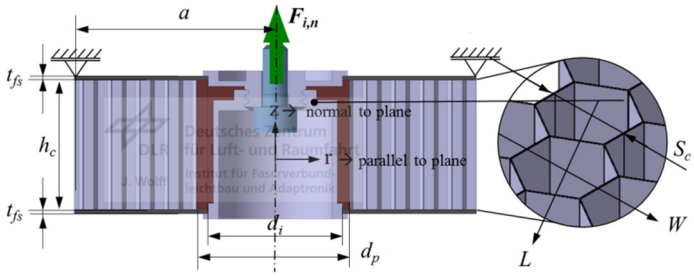

Fig. 3: Schematic insert load introduction with a core connected, two-piece, through-the-thickness insert element.

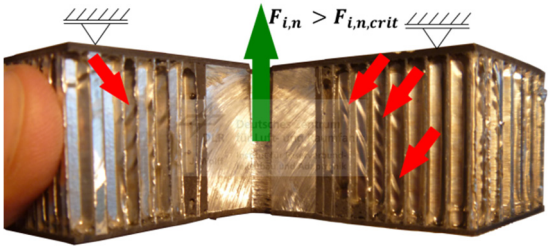

Fig. 4: Plastification of shear deformed cell walls adjacent to the insert (red arrows).

Primary structures of aerospace vehicles must stay undamaged (i. e. without permanent deformations causing a decrease in stability) after they have been exposed to their limit load, according e. g. to specification CS-25, [9]. Therefore, the failure strength ($F_{i,n,crit}$) of any insert load introduction must be superior to the acting force on the insert ($F_{i,ll}$) when the aerospace structure is exposed to its limit load. Therefore, the inserts failure strength, including a safety factor S_1 becomes $F_{i,n,crit} \geq F_{i,ll} \cdot S_1$. Summarizing recent literature, the preliminary damage of an insert load introduction exposed to $F_{i,n} > F_{i,n,crit}$ is a plastification of shear buckled honeycomb core cell walls around the insert, Fig. 4. Regarding ECSS [6] and Hertel [10], this plastification starts when the elastic shear strength of the core material ($\tau_{hc,crit}$), is reached. To avoid this irreversible decrease in stiffness of the insert load introduction, the highest shear stress in the core ($\tau_{c,max}$) may not exceed $\tau_{hc,crit}$. According to ECSS [6], the core shear stress ($\tau_c(r,z)$) increases with $1/r$ near to the insert, Fig. 5. Therefore, $\tau_{c,max}$ is located adjacent to the potting of the insert element, $\tau_{c,max} = \tau_c\left(r = d_p/2\right)$, Fig. 6. The minimal insert diameter is found when $\tau_{c,max}$ equals the shear strength of the core, $\tau_{c,max} = \tau_{hc,crit}$. The core shear stress $\tau_c(r,z)$ can also be described as the quotient of core shear force $Q_c(r)$ and related core shear area,

$\tau_c(r) = Q_c(r)/A_{c,\tau}(r)$, [6], Fig. 5. Under condition of $\tau_{c,max} = \tau_{hc,crit}$, the maximal core shear force becomes $Q_{c,max}(r = d_p/2) = Q_{c,ll}$. With $A_{c,\tau}(r) = \pi \cdot h_c \cdot d_p$, $\tau_{hc,crit}$ can be expressed as $\tau_{hc,crit} = Q_{c,ll}/\pi \cdot h_c \cdot d_p$.

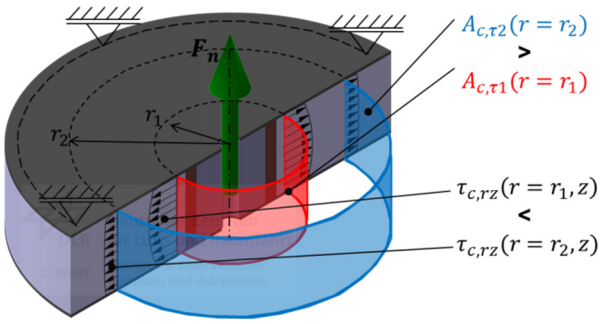

Fig. 5: Decreasing core shear area $A_{c,\tau}$ and increasing core shear stress towards the insert load introduction.

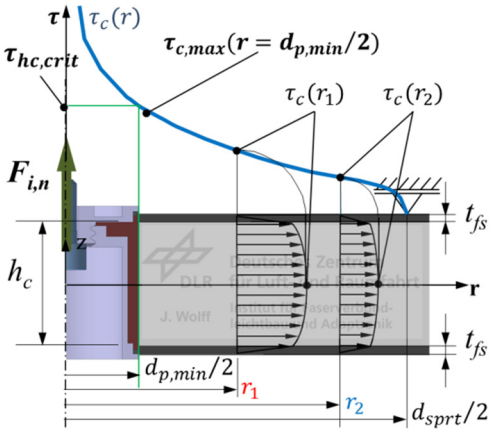

Fig. 6: Course of core shear stress around an insert load introduction.

For a preliminary, rough estimation, the maximal core shear force can be equated with the assumption of $Q_{,c,ll} \approx F_{i,o,crit}$, under condition that the sandwich element exhibits thin face sheets and/or a high core height, [6]. With this, an analytical relation between external normal force and insert diameter is found which can be used for a preliminary dimensioning of the insert diameter, Eq. 1.

$$d_{i,min} \approx d_{p,min} \approx \frac{F_{i,n,crit}}{\tau_{hc,crit} \cdot \pi \cdot h_c} \tag{1}$$

Hence, to gain more precise results, three additional factors have to be taken into consideration due to their influence on the minimal insert diameter, [10]. Firstly, there is the relation between the external force $F_{i,n}$ and the internal shear load $Q_c(r)$, secondly the relation of potting-to-insert diameter, $d_i = f(d_p)$ and thirdly the direction depending shear strength of common honeycomb materials, $\tau_{hc,crit,L} \neq \tau_{hc,crit,W}$, Fig. 3.

Regarding the relation of $F_{i,n}$ to $Q_{,c}(r)$, a significant mechanical characteristic of an insert-sandwich system, its statically over determination, has to be considered. It is characteristic for an overdetermined system that the internal loads are distributed to all elements of the system in certain proportions depending on the stiffness ratios between these elements. For this reason, in an insert-sandwich system with flexural rigid face sheets (configuration A, Fig. 7, left), the major proportion of the internal loads is transferred by the face sheets (Q_{fs}, M_{fs} ↑), while the load proportion in the core is significantly reduced (Q_c ↓). Compared to an insert-sandwich system with flexible face sheets (configuration A, Fig. 7, center), the critical shear strength is reached at a considerably smaller distance towards the center of the insert, $d_{p,min,B}/2 < d_{p,min,A}/2$, Fig 7, right.

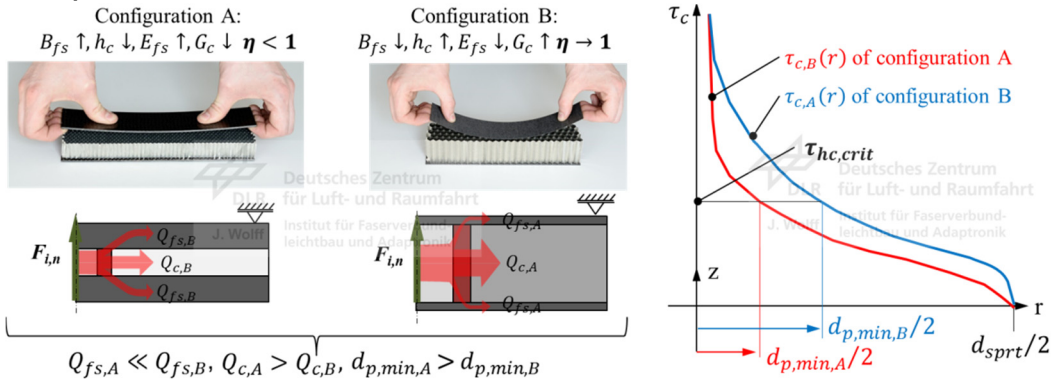

Fig. 7: Sandwich configuration B allows for a smaller insert diameter since the load proportion in the core is reduced.

Youngquist [11] introduced the core shear force reduction factor "k_3" in 1955 to consider the correct relation between $F_{i,n}$ and $Q_c(r = d_p/2)$ depending on the sandwich configuration, $Q_c = F_{i,n} \cdot k_3$ with $0 < k_3 \leq 1$. With k_3 is called η herein, Eq. 1 is extended to Eq. 2.

$$d_{i,min} \approx d_{p,min} = \frac{F_{i,n,crit} \cdot \eta}{\tau_{hc,crit} \cdot \pi \cdot h_c} \tag{2}$$

Due to the static over determination, the reduction factor η can only be determined with the help of either finite element models) or advanced mechanical-analytic models [7, 13, 15-17]. State-of-the-art mechanical-analytic approaches are basing on the higher order sandwich plate theory (HSAPT) due to its ability to solve statically indeterminate problems

by integrating additional, independent boundary conditions obtained from e. g. the principle of virtual work. Different HSAPT-models, allowing the calculation of η for different insert types, were provided by Ericksen [15], Thomsen [8] and Bozhevolnaya [18]. Although the Thomsen-model matches best with the specific insert type regarded herein, only the Ericksen- and Bozhevolnaya-models provide usable analytical solution formulations. Unfortunately, both models are only valid for through-the-thickness-inserts without a connection to the core in sandwich elements with only isotropic core materials. Yet Hertel, later cited by ECSS, recommends a modified version of the Ericksen-model usable also for inserts elements with a potted connection to the surrounding core in sandwich elements with honeycomb core material.

Concerning the relation of potting-to-insert diameter in honeycomb cores, it has to be recognized that the potting shape in a honeycomb core is not circular (Fig. 2) like in e. g. sandwich elements with foam core materials. Depending on the borehole center position, different cell numbers where cut and filled with potting afterwards. This results in a spectrum of possible irregular potting forms and quantities.

The irregular potting area can be "smeared" to a theoretically circular, "effective" potting diameter ($d_{p,eff}$), Eq. 3. Hertel [10] provided this analytical formulation, basing on a power function generated from test results. The factors a_1, a_2 and a_3 were derived by different authors independently [6, 10, 19].

$$\mathrm{d}_i = \frac{d_p}{a_1} - \frac{S_c}{a_1} + \frac{a_3}{a_1} \tag{3}$$

The typical manufacturing method of honeycomb materials causes different shear strength levels in the plane parallel directions of the honeycomb grid, $\tau_{hc,crit,L} > \tau_{hc,crit,W}$, Fig. 3. For this, Hertel [10] and Rodriguez [20] provide semi-analytical formulations to smooth the divergent shear strength values to an effective, average shear strength $\tau_{hc,crit,eff}$. Extending Eq. 2 with Eq. 3 and inserting $\tau_{hc,crit,eff}$ now allows the calculation of $d_{i,min}$ of core connected (potted) inserts in sandwich elements with honeycomb cores, Eq. 4.

$$\mathrm{d}_{i,min} = \frac{F_{i,n,crit} \cdot \eta}{a_{1,min} \cdot \tau_{hc,crit,eff3} \cdot \pi \cdot h_c} - \frac{a_{2,min}}{a_{1,min}} \cdot S_c + \frac{a_{3,min}}{a_{1,min}} \tag{4}$$

Yet, Wolff et al. [19] reveal that the results of Eq. 4 show high deviations from experimental results, caused by three reasons. Firstly, the applicability of the Hertel-modified version of the Ericksen-model onto core connected insert types, like it is claimed by Hertel and ECSS, is highly distrusted by the authors, since neither Hertel nor ECSS provide any explanations on their modifications. Secondly, the different approaches to smooth the anisotropic core shear strength of typical honeycomb materials by Hertel and Rodriguez deliver quite deviating results for $\tau_{hc,crit,eff}$. Thirdly, different references claim divergent characteristics of the experimental load-deflection curve to correspond to $F_{i,n,crit,exp}$. Consequently, inacceptable divergences result between the different definitions of $F_{i,n,crit,exp}$. At the ICSS 12, the third issue will be addressed: With the help of a test program, the damage process steps of insert-sandwich systems with core connected, through-the-thickness inserts in honeycomb sandwich elements with different configurations, are analyzed with the help of hysteresis load sequences and cutting samples. This will serve as a basis for a refined, distinct allocation of the critical load $F_{i,n,crit,exp}$ to a characteristic feature of the load-deflection curve. Furthermore, a comparison of experiments to results of an improved version of Eq. 4 will be carried out to show a potential improvement.

The work is financed by the German Aerospace Center within the core funded project Next Generation Train III.

REFERENCES

[1] ESA, „lisa pathfinder," Online, 27.06.2007. http://sci.esa.int/lisa-pathfinder/40832-science-module-structure.
[2] RUAG Schweiz AG, Automating inserts for sandwich panels, *Composites World Vol. 9*, RUAG Space, 2015, p. 12
[3] B. J. Kim et al., Characteristics of joining inserts for composite sandwich panels, *Composite Structures 86*, 2008, p. 55–60.
[4] B. J. Kim und D. G. Lee, Development of a satellite structure with the sandwich T-joint, *Composite Structures 92*, 2009.
[5] D. Brosius, Outer space: The "final frontier" is exciting again! *Composites World Vol. 9*, 2015, p. 6.
[6] ECSS, Space Engineering Insert Design Handbook, ECSS-E-HB-32-22A, *ESA-ESTEC*, 2011.
[7] O. T. Thomsen, Analysis of sandwich panels with through-the-thickness inserts using a HSAPT, *ESA*, 1994.
[8] O. T. Thomsen et al., Analysis and design of sandwich plates with inserts - a HSAPT approach, *Composites B 29B*, 1998.
[9] European Aviation Safety Agency, Certification Specifications for Large Aeroplanes CS-25, Amendment 21, 2007, p. 617.
[10] W. Hertel et al., Standardisation Programme on Design Analysis and Testing of Inserts, Final Report , *ESTEC*, 1981, p. 426.
[11] W. G. Youngquist et al., Stresses induced in a SW- Panel by Load applied at an Insert, *US Department of Agriculture*, 1955.
[12] P. Bunyawanichakul et al., Non-linear FEA of inserts in composite sandwich structures, *Composites B 39*, 2008.
[13] E. Bozhevolnaya et al., Local effects in the vicinity of inserts in sandwich panels, *Composite Structures 35*, 2004, p. 9.
[14] C. Burchardt, Fatigue of sandwich structures with inserts, *Composite Structures 40*, 1998, pp. 201 - 211.
[15] W. S. Ericksen, The bending of circular Sandwich Plate under normal Load, Report, *US Department of Agriculture*, 1953, p. 35.
[16] Y. Frostig et. al, High order theory for sandwich-beam behaviour with transversally flexible core, *J. of Eng. Mech. 118*, 1992.
[17] E. Bozhevolnaya et al., Local effects across core junctions in sandwich panels, *Composite Structures*, 2003, pp. 509-517.
[18] E. Bozhevolnaya et al., Local effects at core junctions of sandwich structures under different types of loads, *CS 73*, 2006.
[19] J. Wolff et al., Pilot study on an analytic sizing tool approach for insert load introductions in sw elements, *ECCM17*, 2016.
[20] J. D. D. Rodriguez Ramirez, Shear testing of honeycomb cores for inserts, *ICCS20*, 2017.

DOI: 10.5075/epfl-ICSS12-2018-171-173

CREEP RESISTANCE OF LOAD APPLICATION INSERTS FOR HYBRID THERMOPLASTIC SANDWICH STRUCTURES

Jörg Hohe[1] and Sascha Fliegener[2]
[1]Fraunhofer-Institut für Werkstoffmechanik IWM, joerg.hohe@iwm.fraunhofer.de
[2]Fraunhofer-Institut für Werkstoffmechanik IWM, sascha.fliegener@iwm.fraunhofer.de

1. INTRODUCTION

Structural sandwich panels are nowadays employed in a wide range of technological fields where extreme lightweight solutions are required. In addition to the classical fields of the aerospace industry or the wind energy sector, sandwich structures become increasingly popular in transport applications of both the rail and road sector (Kim et al. [1], Ning et al. [2]. In contrast to aerospace components or wind turbine blades with limited numbers of components to be manufactured, especially the automotive sector is characterized by industrial scale mass production with large numbers of components to be manufactured with an extreme demand for short cycle times. Furthermore, automotive applications usually involve a large number of fixtures for secondary parts, seats, safety belts, etc. For this purpose, polymeric composite and sandwich components consisting of thermoplastic base materials are promising candidates for future composite automotive designs. One of the major shortcomings of thermoplastic composites is the distinct tendency of thermoplastic polymers towards creep due to the limited crosslinking of their macromolecules. Due to local stress concentrations, creep deformation is an issue especially at loading spots. Aim of the present contribution is the design and evaluation of load application inserts for thermoplastic sandwich structures for an enhanced creep resistance.

2. DESIGN

Regarding general design options, a wide range survey has been provided in a previous contribution (Fliegener et al. [3]). In the multiple-step optimization procedure employed in this study, the design options “C” and “E” according to Fig. 1 had been identified as the most promising options under static loading conditions. In addition, option “A” has been considered further due to its more economic manufacturing properties. Fig. 1 shows the sketches of the initial design identified in a preliminary design study on the left hand side as well as the optimized versions on the right hand side.

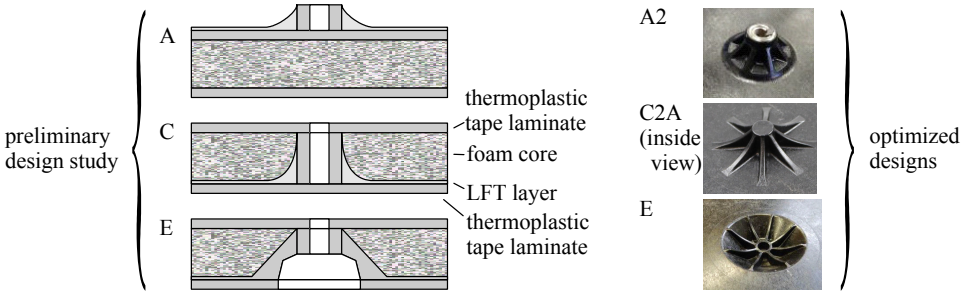

Fig. 1: Load application inserts considered in the present study.

In all three cases, the sandwich structures consist of laminated face sheets made from thermoplastic PA6 based tape with unidirectional carbon fiber reinforcement. The plies are arranged in a quasi-isotropic stacking sequence. The sandwich core consists of a polyurethane foam. For integration of the loading inserts (as well as for further functionalizations such as local stiffening ribs etc.), the face sheets were supplied with a thin layer of PA6-GF40 discontinuous long glass fiber reinforced thermoplastic (LFT), applied in a press molding process (Henning et al. [4]). By this means, a hybrid face sheet design consisting of plies with continuous fiber reinforcement (tape laminates) as well as plies with discontinuous fiber reinforcement (LFT) with integrated loading inserts are obtained.

3. MATERIAL MODEL

In a preliminary experimental investigation, the creep response of the individual tape plies as well as the LFT plies has been characterized. For this purpose, creep experiments under constant uniaxial loading conditions were performed, using standard plane ISO 3167 specimens. The creep load was applied at different load levels considering two different temperatures (23°C and 80°C). The overall creep time was 166.7 h (approximately one week). During the creep experiments, the axial strain in the gauge section of the specimens was recorded continuously using clip gauges. For the numerical simulation, an anisotropic creep model is defined. The model assumes linear elasticity in the fiber direction which is superimposed by an isotropic generalized 3-element Kelvin-Voigt approach representing the thermoplastic matrix response. The material model is implemented as a user-defined material model into the commercial finite element

program ABAQUS. For the LFT material ranges, a similar approach is used. The material parameters are determined by simulation of the creep experiments in conjunction with a reverse engineering approach. In Fig. 2, selected results are presented. In all cases, the experimental observation and the numerical prediction for the creep curves are found in a good agreement. Both, the spatial anisotropy of the material as well as the stress dependence of the creep curves are properly reproduced by the proposed material model. Full details on the model can be found in an oncoming contribution.

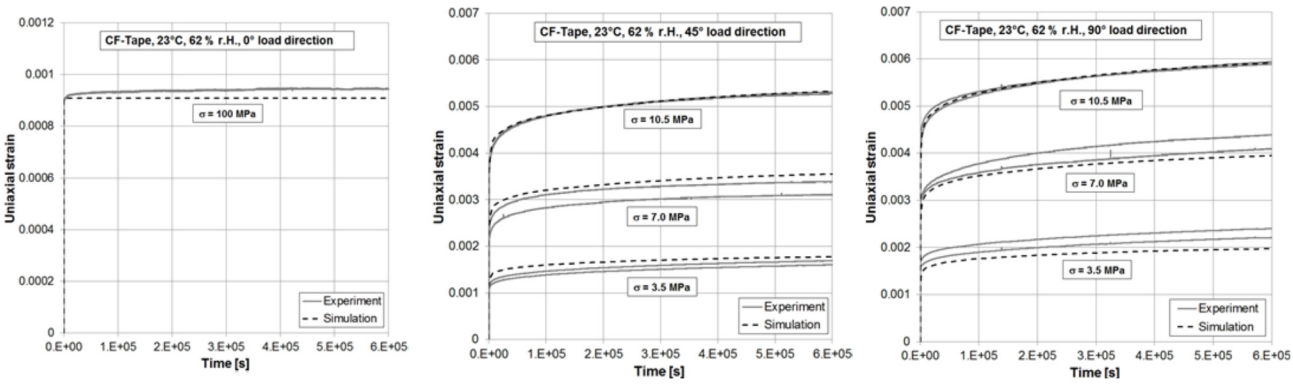

Fig. 2: Anisotropic creep material model.

4. FINITE ELEMENT PREDICTION

The material models defined and implemented in Sec. 3 are employed for a numerical simulation of the creep response of the loading inserts proposed in Fig. 1. For this purpose, circular three-dimensional finite element models with the respective loading insert located in the center according to Fig. 3 are employed. The finite element model is clamped around the external boundary and loaded by a constant force applied to the metal insert in the center. Using these models, the creep response for a creep time of approximately one week is computed.

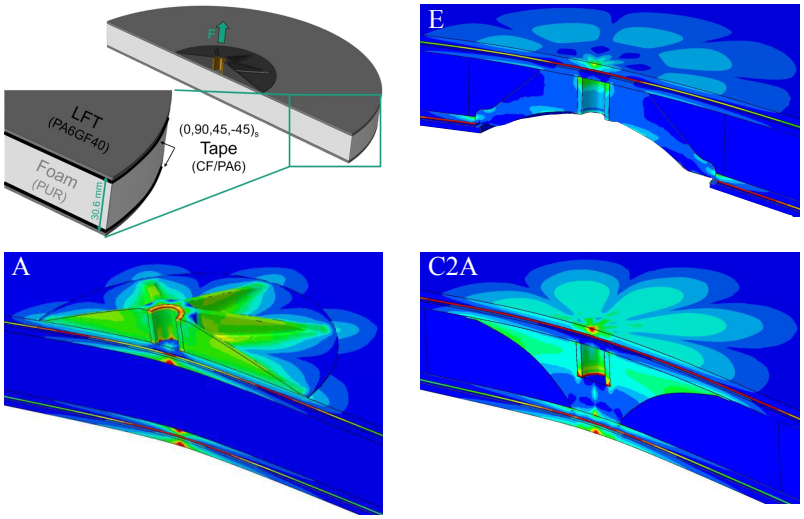

Fig. 3: Finite element model, schematic principle and details of loading inserts.

5. EXPERIMENTAL INVESTIGATION

In an experimental investigation, the three most promising design options have been examined experimentally. Using a fixture with a circular cutout, corresponding to the outer edge modelled in the finite element study, rectangular samples were loaded by a constant vertical force over a prescribed time. The samples for each design option were tested at three different load levels. Each of the three design options was tested at load levels of 2.5 kN and 5 kN applied over creep time intervals of 160 h and 80 h, respectively. In addition, a constant load close to the static strength was applied over an interval of 80 h. For options “A” and “C2A”, the corresponding load level was fixed at 6 kN whereas the statically much stronger design option E was loaded at 14 kN.

6. RESULTS

The numerical predictions for the creep curves are presented in Fig. 4 where the total displacement (i.e. elastic and creep displacement is plotted versus the loading time. As in the previous static investigations (Fliegener et al. [3]), design option “E” proves to be the design option with the highest stiffness and strength due to the contemporary distributed load transmission to both face sheets. Compared to the two other design options, option “E” also features the highest creep

resistance with the lowest creep deformation developing during the one week creep interval. Qualitatively similar results are obtained at 23°C and 80°C with higher creep rates and creep deformations developing at 80°C.

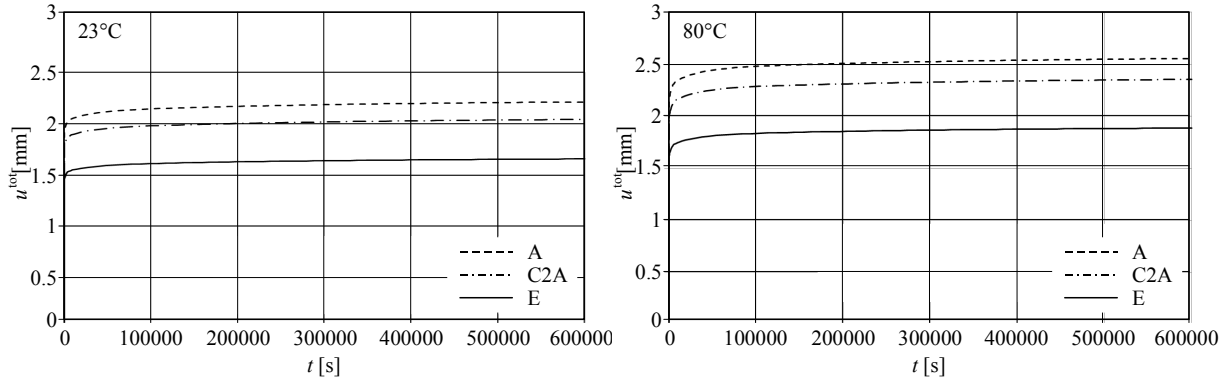

Fig. 4: Numerical prediction of the creep curves.

In Fig. 5, the creep curves for design options "C2A" and "E" at different applied load levels are presented in terms of the creep deformation (without initial elastic parts) plotted versus the creep time. Again, option "E" provides the highest creep resistance. The fact that at its highest load level of 14 kN, the specimen for design option "E" experienced larger amounts of creep deformation than option "C2A" derives from the higher applied load. The experimental findings are found in good agreement with the numerical predictions.

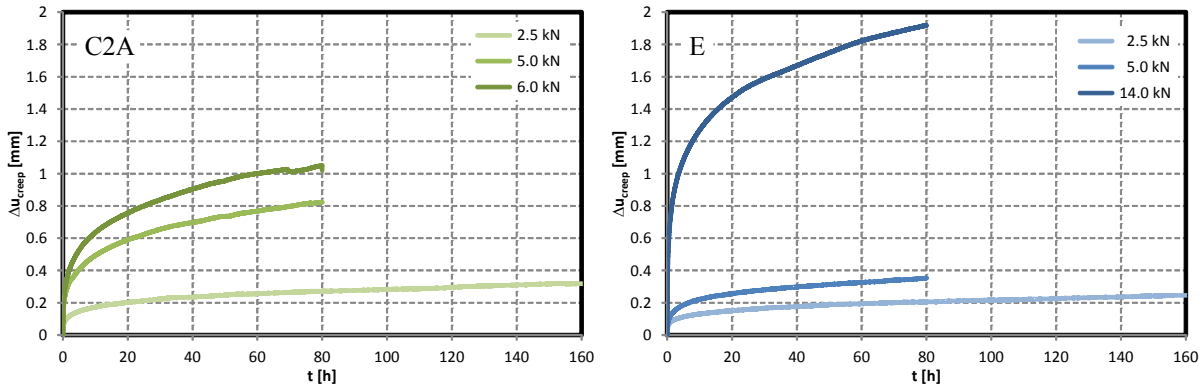

Fig. 5: Experimental results.

7. CONCLUSION

Different design options for loading inserts for thermoplastic sandwich structures have been examined with respect to their creep response, using a combined experimental and numerical approach. It is observed that substantial creep deformation might develop in the vicinity of the loading insert due to local stress concentrations. This creep deformation can be minimized by an appropriate design of the local geometry of the insert. Hence, in thermoplastic sandwich structures creep deformation forms an important design driver for such loading inserts.

ACKNOWLEDGEMENT

The present study has been financially supported by the German Federal Department of Education and Science (BMBF) under Grant No. 03X3041P. The financial support is gratefully acknowledged.

REFERENCES

[1] J.S. Kim. et al., "Numerical and experimental studies on the deformational behavior of a composite train carbody of the Korean tilting train", *Compos. Struct.*, 2007, 81, 168-175.

[2] H. Ning et al., "Thermoplastic sandwich structure design and manufacturing for the body panel of mass transit vehicle", *Compos. Struct.*, 2007, 80, 82–91.

[3] S. Fliegener et al., "Design and optimization of load application inserts for thermoplastic sandwich structures in automotive applications", *ICSS-11*, 2016.

[4] F. Henning, et al., "LFTs for automotive applications", *Reinf. Plastics*, 2005, 49, 24-33.

SESSION 8A: CORE MATERIALS

DOI: 10.5075/epfl-ICSS12-2018-175-177

DETERMINATION OF TRANSVERSE SHEAR MODULI OF COMPOSITE CORE MATERIALS THROUGH SANDWICH BEAM TESTS

Özgün Şener[1], Oğuzhan Dede[2], Oğuz Atalay[1], Mert Atasoy[3] and Altan Kayran[1]
[1] METU Center for Wind Energy, Ankara, Turkey. osener@metu.edu.tr, oguza@metu.edu.tr, akayran@metu.edu.tr
[2] Middle East Technical University, Ankara, Turkey. oguzhan.dede@metu.edu.tr
[3] ASELSAN Inc., Ankara, Turkey. matasoy@aselsan.com.tr

1. INTRODUCTION

The necessity for high performance and low weight structures have increased the demand for development of sandwich constructions. Nowadays, sandwich structures are predominantly used in various fields such as aerospace, automotive, satellite, and bridge construction. Due to the notable flexural stiffness to weight ratio, sandwich structures present lower lateral deformations, higher buckling loads, and greater natural frequencies compared to other structural configurations [1].

The interest in sandwich panels increased considerably in the 1960s. Allen published his book on sandwich structures that is considered as one of the milestones in the sandwich construction field [2]. Ha [3] reviewed finite element analysis methods for sandwich constructions. In the recent years, utilization of fiber reinforced composite materials as facing and/or core material is studied to take advantage of superior properties of composites. In 2000, Daniel and Abot [4] worked on the determination of flexural properties of composite sandwich constructions experimentally and compared the outcomes with the theoretical models. Moreover, the failure mechanisms of composite sandwich structures have been widely examined [5-7].

In this work, transverse shear moduli of composite core materials are determined through three-point bending tests of sandwich beams and compared with analytical and finite element solution. All-composite sandwich structures are produced by using carbon fiber reinforced plastics (*CFRP*) material. The CFRP core material has a nonconventional geometry and presents different shear properties depending on the core orientation with respect to the beam axis; therefore, the tests are carried out for different core material orientations. Results showed that outcomes of experimental, analytical, numerical solutions are comparable.

2. METHODOLOGY

Three-point bending tests are performed by following ASTM C393 [8] test standard for the sandwich structures that have 20 mm composite core with two different core orientations which are parallel and perpendicular to the beam axis, respectively. The experiments are validated with the theoretical solution and finite element analyses.

Analytical Method

Fig. 1 illustrates the geometry of a sandwich structure in a three-point bending test. A force with a magnitude P is introduced to the structure by the above circular cylindrical roller, and the beam deflects by u. In Fig.1, c and h denote the core thickness and total thickness of the sandwich, and the width of the beam is b. The support length is indicated with L, the overhang portion of both ends of the beam is H, and t_f represents the face thickness. The facesheet properties of the structure are determined by following several test procedures [9-10] and the details are not presented in this study. The relevant mechanical properties for facesheet material are modulus of elasticity and the axial strength and are denoted with E_f and σ_f, respectively. The pertinent properties for the core material are E_c, σ_c, and G_c, which are the Young's modulus, compressive strength, and transverse shear modulus of the core material, respectively.

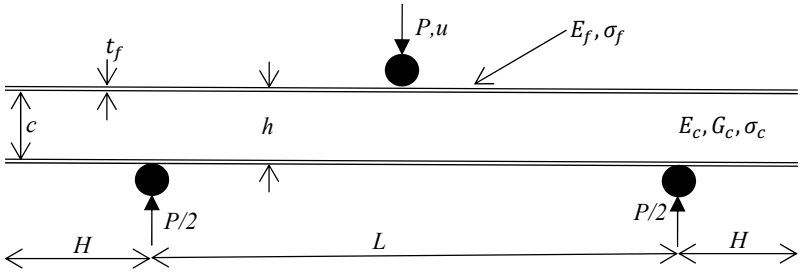

Fig. 1: Three-point bending test setup.

The flexural stiffness of the sandwich structure is determined by Eq. 1.

$$D = \frac{E_f b t_f^3}{6} + \frac{E_f b t_f d^2}{2} + \frac{E_c b c^3}{12} \tag{1}$$

In Eq. 1, the length d represents the distance between the centroids of facesheets and it is determined by Eq. 2.

$$d = \frac{h + c}{2} \tag{2}$$

Allen [4] formulized the transverse displacement due to the applied load P as in Eq. 3.

$$u = \frac{PL^3}{48D} + \frac{PL}{4A_{eq}G_c} \tag{3}$$

In Eq. 3, the term $A_{eq}G_c$ is described as the *shear rigidity* and A_{eq} is the equivalent cross-sectional area which can be determined by Eq. 4.

$$A_{eq} = bd^2/c \tag{4}$$

The axial stress applied on the mid-surface of the composite facesheet is determined by Eq. 5 [2]. In Eq. 5, θ symbolizes the angle that the upper facesheet makes with the horizontal at the support location as shown in Fig. 2.

$$\sigma_f = \frac{P}{bt_f(h+c)}\left(\frac{L}{2} + utan\theta\right) \tag{5}$$

Fig. 2: The angle at the support location.

A procedure has been followed to determine the transverse shear moduli of sandwich structures that have composite core materials placed parallel and perpendicular to beam axis, respectively [2]. In this methodology, the experiments should be conducted for at least two different span length: one span length selection must be short enough such that the displacement due to shear is dominant, and the other one should be sufficiently long such that the displacement is driven due to the bending. For this purpose, Eq. 3 brought into the form given by Eq. 6.

$$\frac{u}{PL^3} = \frac{1}{48D} + \frac{1}{4A_{eq}G_c}\left(\frac{1}{L^2}\right) = n_2 + m_2\left(\frac{1}{L^2}\right) \tag{6}$$

It is known that the compliance *C* can be determined as the inverse of the slope of load-displacement curve. Therefore, Eq. 6 can be written as in Eq. 7.

$$\frac{C}{L^3} = \frac{1}{48D} + \frac{1}{4A_{eq}G_c}\left(\frac{1}{L^2}\right) = n_2 + m_2\left(\frac{1}{L^2}\right) \tag{7}$$

In order to calculate transverse shear moduli of core materials, the slopes of load-displacement (*P*-*u*) curves are calculated for each support length configuration and the inverse of the slopes are stored as compliance values, *C*. Then, the plots of C/L^3 versus $1/L^2$ are drawn so as to obtain the slope of the curve, m_2. Transverse shear modulus (G_c) can then be calculated from Eq. 8.

$$m_2 = \frac{1}{4A_{eq}G_c} \tag{8}$$

Transverse shear moduli values are obtained by following the above-mentioned procedure through testing sandwich beams. With this method, realistic core shear moduli can be determined, as opposed to testing of pure core material since the effect adhesive used in the core-facesheet bonding is also reflected in the transverse shear modulus that is calculated. Transverse shear moduli calculated are then used to the draw load-displacement curves by employing analytical solution and finite element analyses for comparison purpose.

Experimental Setup

Three point bending tests are performed in METU Center for Wind Energy Composite Materials Laboratory with MTS 809 Axial/Torsional Tensile Testing system with special three-point bending fixture by utilizing ASTM C393 [8] test standard. The specimens have the dimensions of 380 mm in length, 50 mm in width, and 21.7 mm in thickness with a core thickness of 20 mm. The carbon composite core material has rather nonconventional geometry and its CAD drawing with primary axes and the actual photo are presented in Fig. 3. Additionally, the obtained experimental results are validated by measuring the displacement of the roller that introduces force via Digital Image Correlation (*DIC*) system so as to exclude the compliance of the actuator.

(a) ***(b)*** ***(c)***

Fig. 3: (a) CAD drawing and (b) actual photo of the core material and (c) three-point bending test setup including DIC system.

Finite Element Model

The model is created by using exactly the same dimensions and test configurations as the experimental setup in MSC.MARC. The finite element model is illustrated in Fig. 4. The FE model is created by assigning equivalent 3D orthotropic material properties to the solid elements which are used to model the core material in the sandwich beam. In the FE model, for the transverse shear moduli, experimentally determined values are used and the remaining elastic

constants are obtained through FE analysis of a representative volume of the core material. The upper and lower cylindrical rollers are represented by rigid elements and abbreviated as *SPC1* and *SPC2* in Fig. 4.

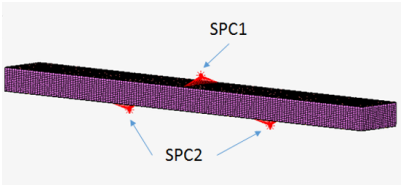

Fig. 4: 3D finite element model of the test configuration.

3. RESULTS AND CONCLUSION

The experiments are performed for three different span lengths and transverse shear moduli of sandwich test specimens are obtained as 99.7 MPa and 57.2 MPa for parallel (G_{13}) and perpendicular (G_{23}) core material orientations, respectively, from both actuator and DIC system. The obtained transverse shear moduli are used in both analytical and finite element models to generate and compare the load-displacement curves with the experimental data. Additionally, the experiments are also monitored with DIC system. Fig. 5 illustrates the load-displacement curves of sandwich structures with different support span lengths that have parallel and perpendicular core material orientation with respect to beam axis. Since the load-displacement curves obtained from the actuator and the DIC system coincide, the plots acquired from DIC system are omitted from Fig. 5 for the sake of clarity. The experimental, numerical, and analytical data produce one-to-one correspondence and validate the obtained transverse shear moduli values. For the 150 mm support span configuration, there is a curve shift which might have been occurred due to the slippage in the early phases of the experiment for the short span beams and this phenomenon is being investigated. For the three different support span lengths, slopes of the load displacement curves determined experimentally, analytically and through finite element analysis agree very well by the virtue of the accurate estimation of the transverse shear moduli through three point bending tests of the sandwich beam.

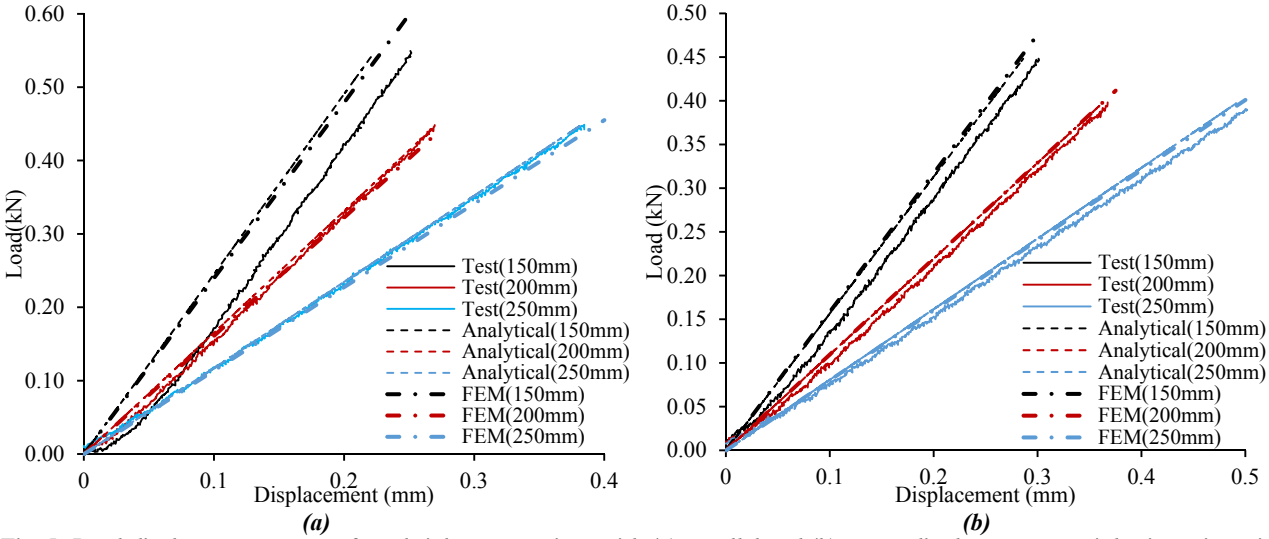

Fig. 5: Load-displacement curves of sandwich constructions with (a) parallel and (b) perpendicular core material orientation with different span lengths.

ACKNOWLEDGMENTS

This study is performed as a part of the project supported by The Scientific and Technological Research Council of Turkey (TUBITAK) TEYDEB.

REFERENCES

[1] J. R. Vinson, "Sandwich Structures," *Appl. Mech. Rev.*, vol. 54, no. 3, p. 201, 2001.
[2] H. G. Allen, *Analysis and Design of Structural Sandwich Panels*. Oxford: Pergamon Press, 1969.
[3] K. H. Ha, "Finite element analysis of sandwich plates: An overview," *Comput. Struct.*, vol. 37, no. 4, pp. 397–403, 1990.
[4] I. Daniel, "Fabrication, testing and analysis of composite sandwich beams," *Compos. Sci. Technol.*, vol. 60, no. 12–13, pp. 2455–2463, 2000.
[5] F. M. Shuaeib and P. D. Soden, "Indentation Failure of Composite Sandwich Beams," *Compos. Sci. Technol.*, vol. 57, no. 9–10, pp. 1249–1259, 1997.
[6] E. . Gdoutos, I. . Daniel, and K.-A. Wang, "Compression facing wrinkling of composite sandwich structures," *Mech. Mater.*, vol. 35, no. 3–6, pp. 511–522, 2003.
[7] I. M. Daniel, E. E. Gdoutos, K. –A. Wang, and J. L. Abot, "Failure Modes of Composite Sandwich Beams," *Int. J. Damage Mech.*, vol. 11, no. 4, pp. 309–334, 2002.
[8] ASTM Standard, "ASTM C393-06 Standard Test Method for Core Shear Properties of Sandwich Constructions by Beam Flexure," *ASTM Int.*, vol. i, no. C, pp. 1–7, 2010.
[9] ASTM International, "ASTM D3039 / D3039M-17, Standard Test Method for Tensile Properties of Polymer Matrix Composite Materials," *Stand. Test Method Tensile Prop. Polym. Matrix Compos. Mater.*, vol. 3, 2017.
[10] DIN EN 6031, "Determination of In-Plane Shear Properties (±45° Tensile Test)," Köln.

DOI: 10.5075/epfl-ICSS12-2018-178-180

ENERGY-ABSORBING HONEYCOMB STRUCTURES BASED ON CARBON FIBER REINFORCED PLASTICS

Alia R. Aziz[1], Shanmugam Kumar[1], Pradeep George[1] and Wesley James Cantwell[1]
[1]Khalifa University of Science and Technology (KUST),
127788 Abu Dhabi, United Arab Emirates.
alia.aziz@kustar.ac.ae, kshanmugam@masdar.ac.ae, pradeep.george@kustar.ac.ae and wesley.cantwell@kustar.ac.ae

1. ABSTRACT

As a result of their impressive mechanical properties and low density, sandwich structures are being widely used in a large range of engineering applications [1-3]. Recently, there has been a drive to develop new core designs that offer enhanced properties under extreme loading conditions. The present paper investigates the energy-absorbing properties and compression characteristics of a CFRP honeycomb core produced using vacuum assisted RTM. The lightweight cores were produced using a steel mold into which a series of hexagonal blocks were inserted. Initially, a unidirectional carbon fiber cloth was inserted into the gaps between the hexagonal blocks and the mold was wrapped in a vacuum bag and infused with a room-temperature curing epoxy resin. Following the twenty-four hour cure cycle, the steel blocks were removed from the mold to leave a repeating composite honeycomb structure. The compression and energy-absorbing properties of the cores were then determined through a series of quasi-static compression tests. Cores with their fibers oriented a several angles were also manufactured in order to understand the influence of stacking sequence on the compressive behavior.

2. EXPERIMENTAL

In this study, a CFRP honeycomb core is manufactured and tested. This type of structure has been selected since it offers the opportunity to combine the excellent energy-absorbing characteristics of composite materials with a continuous core architecture that is well-established in the design of energy-absorbing engineering components, namely a honeycomb structure.

The CFRP honeycomb cores study in this investigation were manufactured from a unidirectional (UD) carbon fiber cloth (Unitex UT-300/500) and a two-part epoxy resin (Prime^{TM} 20LV). The carbon fiber cloth has a thickness of 0.25 mm and an areal density of 290 g/m^2. The cores were produced using the mould shown in Fig. 1(a). Here, 27 mm high steel hexagons (face-to-face distance = 22 mm) were placed in slots that were machined into the base of the steel mould. Following this, 25 mm wide strips of carbon fibre cloth were positioned in the vertical gaps in the hexagonal structure. The mould was then placed on a large glass table and wrapped in a bagging film. A line injection was used to introduce the resin into the mould and a line vent was used to apply a vacuum. After infusion, the resin allowed to cure under 24 hours. The mould was removed from the bagging film, and the hexagonal blocks carefully pushed out to leave the uniform honeycomb structure shown in Fig. 1(b).

Honeycomb cores based on one, two, three and four fabric layers were manufactured in this investigation. Initially, UD cores where the fibres were arranged in the through-thickness 0^o direction were manufactured and tested. Using this technique allowed the fibre weight fraction, w_f, to be varied between approximately 0.15 and 0.51. Honeycomb cores were also produced with their central layers oriented at either +/-45^o or 90^o to give cores with stacking sequences of (0^o, +45^o, -45^o, 0^o) or (0^o, 90^o $_2$, 0^o).

The compression strength and energy-absorbing properties of the CFRP cores were characterized on a servohydraulic universal testing machine. Following testing, force and displacement data were used to determine the compression strength and specific energy absorption (SEA) properties of the composite cores.

3. RESULTS AND DISCUSSION

Following manufacture, a number of samples were scanned in an X-ray computed tomography machine to assess the quality of the manufactured parts and ass the level of voiding. These studies highlighted the uniformity of the cell wall thickness and the very low level of porosity (less than two percent).

Fig. 2 shows force-displacement plots following tests on samples based 1, 2 and 5 hexagons (cells). The weight fraction of fibers in all samples is 0.28. All curves exhibit similar characteristics, with the force increasing to a maximum value dependent on the number of cells in the specimen. The force decreases steadily before increasing as the samples begin to fully crush (i.e. densify) between the plattens. From the figure, it is clear that the densification threshold is similar in all three specimens.

Fig. 3 shows the variation of the compression strength as a function of fiber weight fraction in the core. The figure indicates that the strength of the core increases in a roughly linear manner with w_f. Indeed, the strength increases from approximately 18 MPa to 35 MPa as the fiber weight fraction passes from 0.14 to 0.4. Normalizing these values by the

density of the core gives for the specific compression strength that lie between 0.12 and 0.2 MPa.m^3/kg. Available data for the specific compression strengths of crosslinked PVC foams with densities of 200 and 250 kg/m^3 (i.e. comparable to those tested here) are similar, being approximately 0.025 MPa.m^3/kg. Similar data for an aluminum honeycomb with a density of approximately 190 kg/m^3 yields a specific compression strength of 0.097 MPa.m^3/kg. These comparisons highlight the impressive compression properties of the current carbon fiber/epoxy core materials.

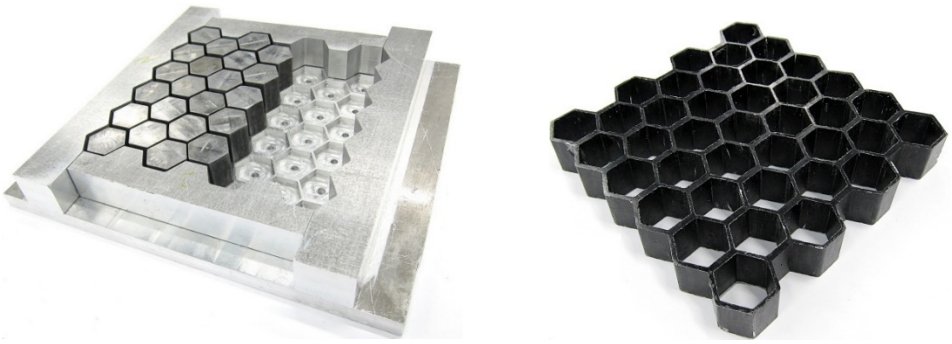

(a) *(b)*

Fig. 1: Photograph of the mould and a carbon fibre/epoxy honeycomb core.

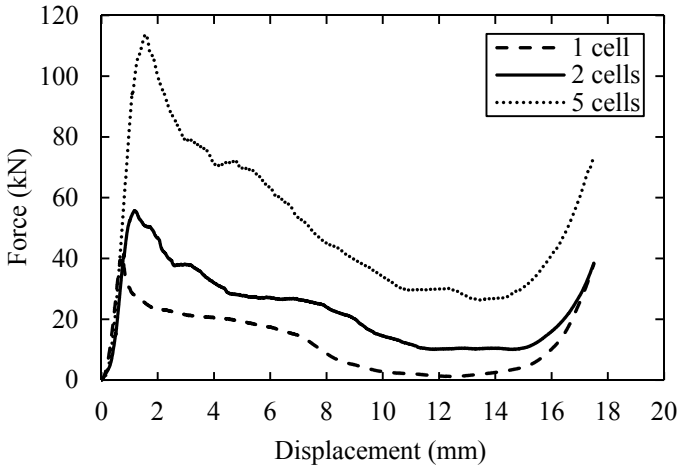

Fig. 2: Force-displacement traces following compression tests on samples containing one, two and five unit cells and a weight fraction of fibers = 0.28.

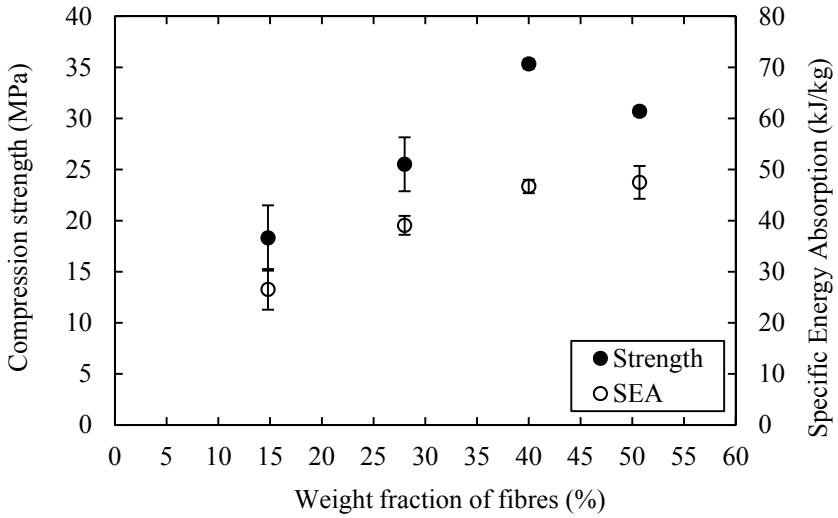

Fig. 3: The variation of compressive strength and specific energy absorption with weight fraction of fibers.

4. CONCLUSIONS

Carbon fiber reinforced epoxy composite honeycomb cores have been produced using a steel mold and the VARTM manufacturing technique. Compression tests on samples based on a unidirectional fiber arrangement have shown that the strength increased with increasing fiber content, reaching a maximum for a core based on $w_f = 0.4$. Further increases in the amount of fibers in the core resulted in a drop in strength, due to increased levels of porosity in the materials. The resulting values of specific compression strength surpassed those of aluminum honeycomb cores by a factor of approximately two. Similarly, the SEA of the composite honeycomb cores increased steadily to 46 kJ/kg, before remaining roughly constant at higher values of w_f.

A number of multidirectional cores based on (0^o,90^o,90^o,0^o) and (0^o,$+45^o$,-45^o,0^o) stacking configurations have also been manufactured and tested. Offsetting the fibers served to stabilize the force during the crushing process, although the measured values of SEA were lower than those recorded on the unidirectional samples. Finally, test data from impact tests on sandwich panels based on CFRP cores with CFRP skins will demonstrate the excellent impact resistance of these lightweight structures.

REFERENCES

[1] T. George, V. S. Deshpande, K. Sharp and H. N. G. Wadley, “Hybrid core carbon fiber composite sandwich panels: Fabrication and mechanical response”, *Composite Structures*, 2014,108: pp696–710.

[2] S. Kazemahvazi, D. Tanner and D. Zenkert, “Corrugated all-composite sandwich structures. Part 2: Failure mechanisms and experimental programme”, *Composites Science and Technology*, 2009,69: pp920–925.

[3] A. Stocchi, L. Colabella, A. Cisilino and V. Álvarez, “Manufacturing and testing of a sandwich panel honeycomb core reinforced with natural-fiber fabrics”, *Materials and Design*, 2014, 55: pp394–403.

DOI: 10.5075/epfl-ICSS12-2018-181-183

SHEAR NONLINEAR BEHAVIOR OF THE NOMEX HONEYCOMB CORE

Juan de Dios Rodríguez-Ramírez[1-a], Bruno Castanié[1-b] and Christophe Bouvet[1-c]
[1]Institut Clément Ader (ICA), Université de Toulouse, CNRS UMR 5312-INSA-ISAE-Mines Albi-UPS, Toulouse, France.
[a] jddrodri@insa-toulouse.fr
[a] castanie@insa-toulouse.fr
[c] christophe.bouvet@isae.fr

1. INTRODUCTION

Sandwich structures are widely used for many different applications since they offer exceptional benefits, providing a high bending stiffness with a very low weight. In aeronautics, sandwich panels are commonly made of Nomex honeycomb, and therefore this core has been studied for decades. Concerning the literature, most of the investigations on honeycomb cores are focused on to investigate the compression properties of the structure, for energy absorption applications or impacts on sandwich panels.

In the other hand, there are far fewer studies concerning the understanding of the shear nonlinear behavior of the honeycomb [1], this can be considered a major drawback, knowing that it's the core who absorbs most of the shear components when a bending force is applied.

To help fill this gap, this work focuses on to study the shear behavior of the honeycomb structure. Several experimental tests are conducted using different boundary conditions to observe the buckling of the cells. This helps to understand the causes of the phenomenological stages that appear when the honeycomb structure is submitted to shear loads.

Finally, a numerical approach is used to simulate the honeycomb response to be able to see on the interior cell walls and to better understand this phenomenon.

This work is a contribution to the understanding of the shear buckling of Nomex honeycomb cores.

2. EXPERIMENTAL STUDY

Testing with Double Lap Specimens

The first part of this research consisted into test 12 double lap specimens to determine the shear response of the honeycomb core; 6 specimens oriented in the W and other 6 oriented in the L direction. Of the 6 specimens, 3 were submitted to a continuum displacement, and the other 3 to an incremental cyclic displacement.

While the tests were performed a 3D-DIC was installed to be able to measure the buckling of the cells at the exterior surface of the honeycomb.

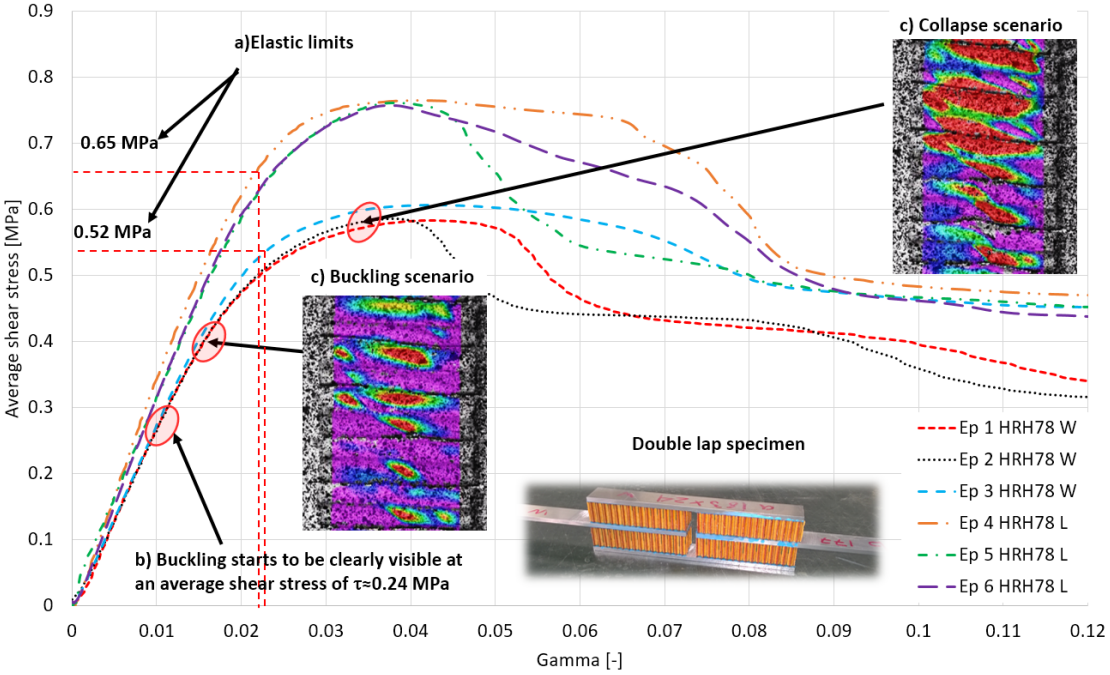

Fig. 1: Description of the shear behavior of the HRH-78 Nomex Honeycomb core (a) The elastic limits were detected trough an incremental cyclic testing, (b) The buckling of the cells is detected at a relatively low shear stress, (c) Buckling scenario of collapsing and non-collapsing cells.

The results shown that the buckling of the cells starts to be visible at relatively low shear stress considering that the shear strength was around 0.58 MPa. By looking the deepness of the buckles, it was observed that the cells buckled predominantly to the inside of the specimen.

Also, the incremental cyclic tests revealed that the honeycomb structure presented a nonlinear elastic behavior beyond the buckling point. Finally, it has been seen that the buckling scenario of the of the cells was very different at the bifurcation point and at the shear strength limit (0.58 MPa). To explain this behavior a hypothesis was made; this difference is attributed to two different phenomenological phenomena's, first the buckling and then the collapse of the cells. And so, an artificial neural network was ANN developed that was capable to detect the collapse of the alveolus based on the shape of the buckles.

Testing with Sandwich Beam Specimens with Lateral Stabilization

The second part consisted into tests other 6 specimens. This time, the specimens consisted on a sandwich beam that had potting at the borders and at the middle. This was made on propose to study how the lateral stabilization (provided by the potting) affected the behavior of the cells.

The sandwich beams were submitted to a classical 3 point bending test and the response of the specimens was compared to the double lap specimens.

It was detected that the initial behavior of both types of specimens was very similar as the shear modulus was the same. However, there were three principal differences; the linear behavior of the cells was extended, the shear strength was increased by approximately 16% and 35% for the W and L directions respectively, and the collapse of the cells was much more dramatic.

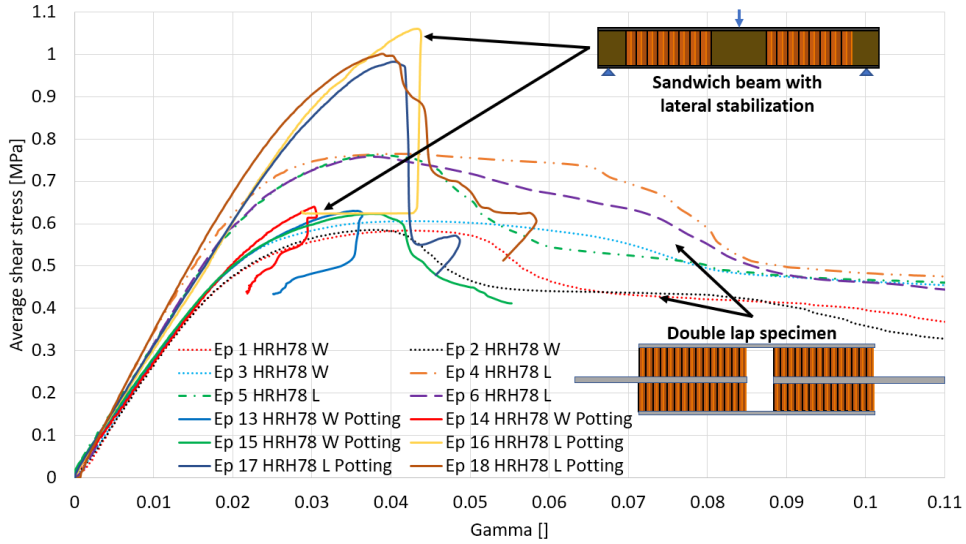

Fig. 2: Comparison of the shear behavior of the same honeycomb structure under two different boundary conditions; Double lap and sandwich bending with lateral stabilization.

The experimental study revealed important aspects of the shear behavior of the honeycomb structure; The shear behavior of the honeycomb structure is mainly a postbuckling behavior. The nonlinear response of the cells can be divided into two phenomenological stages, buckling and collapse. And finally, that the boundary conditions of the cells strongly modify the response of the honeycomb structure.

3. NUMERICAL STUDY

To complement this research, a numerical study was also performed by modeling the two types of test specimens that were used in the experimental part. This helps to see some aspects that were not very clear in the experimental part such as the buckling shape of the cells located at the interior of the core and to clarify the influence of the boundary conditions that modifies the nonlinear behavior of the cells.

The first part of this study was the modeling of the double lap test. The simulation revealed that the buckling shape of the cells of the exterior and interior part of the specimens were very different due to the lack of stabilization of the surrounding cells. Also, it was possible to find a relation between the shear stress and the rotation of the cell walls.

The second part was the modeling of the lateral stabilized honeycomb structure, where the buckling of the cells and the rotation of the cell walls was also obtained.

The comparison of both buckling shapes between the two types of specimens revealed that for the linear part the buckling is very similar but for the nonlinear behavior it's completely different, explaining the differences that were found on the experimental part.

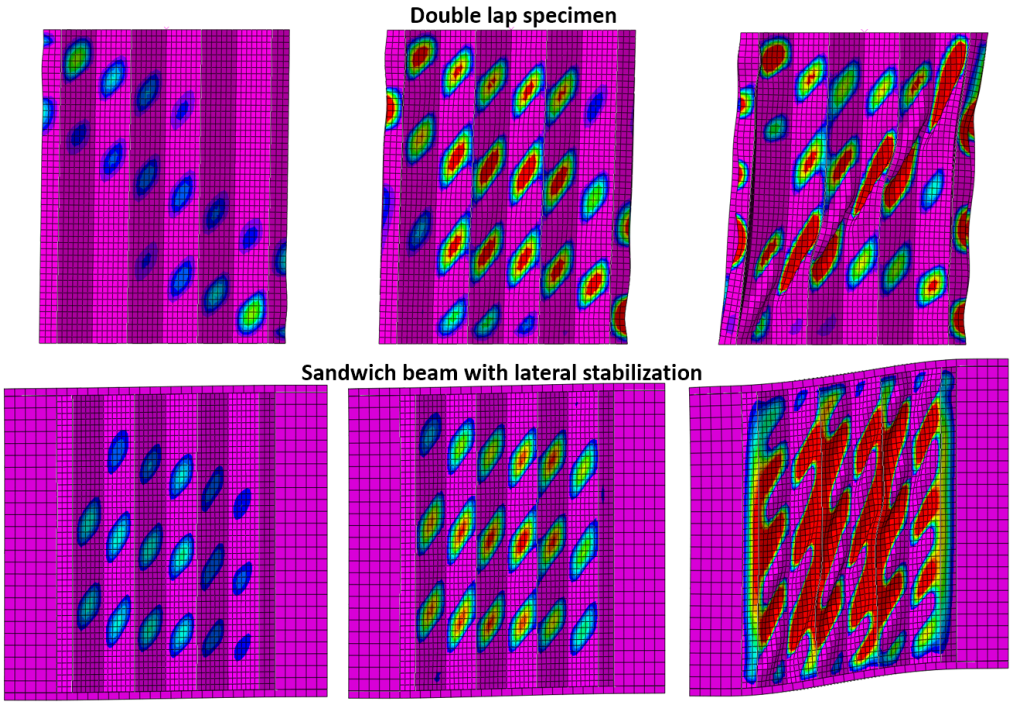

Fig. 3: Comparison of the buckling of the cells in the interior of the double lap specimen and the sandwich beam with lateral stabilization.

REFERENCES

[1] R. Seemann and D. Krause, "Numerical Modeling of Nomex Honeycomb Sandwich Cores at Meso-Scale Level," *Compos. Struct.*, 2016.

DOI: 10.5075/epfl-ICSS12-2018-184-186

IMPACT PERFORMANCE OF ENCAPSULATED SHEAR THICKENING FLUID INTEGRATED FOAM CORE SANDWICH COMPOSITES

Cigdem Caglayan[1,3*], Ipek Osken[2], Elif Ozden-Yenigun[2,3,4] and Hulya Cebeci[1,3**]
[1] Department of Aeronautical Engineering, Faculty of Aeronautics and Astronautics, Istanbul Technical University, Istanbul 34469, Turkey
[2] Department of Textile Engineering, Istanbul Technical University, Istanbul 34469, Turkey
[3] ITU Aerospace Research Center, Istanbul Technical University, Istanbul 34469, Turkey
[4] School of Design, Textiles, Royal College of Art, SW7 2EU, London, United Kingdom
* caglayanci@itu.edu.tr
** geyikh@itu.edu.tr

1. INTRODUCTION

Besides favorable properties of sandwich composites with high specific stiffness, good bending rigidity, thermal insulation, acoustic damping and ease of manufacturing, poor impact resistance is a major concern limiting their use in advanced technologies such as aerospace [1]. The impact loadings can be in a wide range from tool drops, runway debris to bird strikes and hailstorms implying the importance of crash absorbing property of these structures. These types of loadings can introduce damages on both face sheets and core materials which also can create debonding in between them. Using regular core materials such as honeycombs with lower surface area and poorer bonding to face sheet may decrease the properties of sandwich composites. Herein, a foam core material from polyurethane is used to provide an increased bonding within enhanced surface area between face sheet and core reducing debonding problems, and is a possible candidate having a closed cellular structure for impact resistivity. However, enhancing only the quality of bonding between face sheet and core is not enough since failure of sandwich composites initiates from its core under loading.

A local indentation or crack of foam core under impact load with a huge depth from collapsing vacancies between cells is not desired for the safety since crack initiation in core may grow and cause catastrophic failures during operation and its lifetime. Thus, latest researches have focused on a new approach based on rapid toughening and impact absorbing materials which are succeeded by embedding shear thickening fluids (STF) into composites [2, 3]. Particularly, STF impregnated Kevlar fabrics have been studied by many researchers for ballistic penetration performance [2, 4]. As stated, STF consist of nanoparticles in a carrier fluid forming a highly filled stabilized dispersion and nanoparticles stay in a randomly distributed position inside dispersion at rest and create clusters with an applied external stress increasing the viscosity substantially after a critical shear rate. In addition of their use in ballistic impact damper applications, STFs have also recently found a place to itself in porous structures as foams [3]. However, to the best of our knowledge, these studies are on the impact or dynamic compressive load damping performance of STF embedded open cell soft foams as a cushioning element for composite structures [3, 5].

In this work, rapid toughening effect of shear thickening fluids is used directly in closed cell rigid polyurethane (PU) foam cores to reduce the damage of sandwich composites under impact loads. Besides its expected benefits on impact performance of rigid foam core, embedding STF into foam also causes some problems as the difficulty of handling, integrating STF into structure and its stability during service life [6]. Thus, Zhang *et al.* studied the encapsulation of STF (e-STF) that is stiff enough to resist forces during synthesis process and behaves as a rubber like material under impact loads for an easy-to-apply impact resistant material [6]. This study aims to fulfill the need of literature studies on impact absorbing properties of sandwich composites by embedding STF microcapsules with a polyurethane compatible shell into closed cell rigid polyurethane foam core (e-STF/PU). Within this approach, by the encapsulation of STFs with polyurethane compatible shell, the impact resistivity of the sandwich composites will be studied.

2. EXPERIMENTAL

For shear thickening fluid, there are several studies explaining the STF structure as a concentrated colloidal suspension of silica particles and ethylene glycol [6, 9]. Thus, this study also repeated similar process to synthesize STF with a high weight fraction of silica particles in ethylene glycol. Materials for STF were commercially supplied from Sigma-Aldrich having a diameter of 12nm in the form of nano-powder and ethylene glycol. Silica particles are added to ethylene glycol gradually during mixing process by a mechanical stirrer at room temperatures. In order to have the most homogenous mixture, ultrasound sonication is also applied through the process when needed. Herein, two different weight fractions of silica particles are studied until now as 35% (STF-35) and 46% (STF-46). Further studies are going on to increase the silica loading capability inside ethylene glycol at least 50% by wt. Obtained STFs are tested by a rheometer of Anton Paar with 25mm parallel plate geometry at room temperatures performing a pre-shear loading first in order to eliminate bubbles and possible non-homogeneities. Shear thickening characteristic is clearly observed in Fig.1 for STF-46 while STF-35 does not show an obvious non-Newtonian behavior. This sharp increase in viscosity of STF-46, nearly threefold of initial

value, resulted from the agglomeration or disordering of silica particles inside carrier fluid as shown in Fig.2(b). Wherein for STF-35, loaded amount of silica particles was not enough to show thickening behavior due to lack of effective hydrodynamic forces between particles creating clusters.

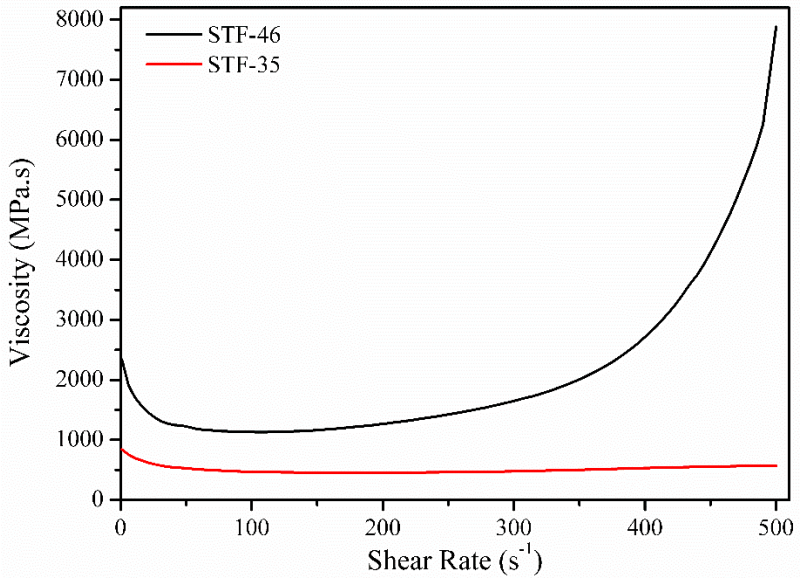

Fig. 1: The curves of viscosity vs shear strain rate for STF samples.

Following step of STF fabrication is identified as encapsulation where two major promising methods have been observed as solution polymerization and emulsion polymerization in literature. In a study, Chung *et.al.* synthesized microcapsules with a self-healing core by emulsion polymerization and successfully embedded into PU foam [7]. B.J.Blaiszik *et.al.* also studied polyureaformaldehyde (PUF) microcapsules prepared by in situ emulsion polymerization of urea and formaldehyde for shell and reactive solutions as self-healing materials for core [8]. Despite existing studies on microcapsules with self-healing material cores, there is still lack of studies on microcapsules containing shear thickening fluids, and particularly their integration into structure within existing processing techniques. Zhang *et.al.* successfully synthesized encapsulated STF to overcome the physical and chemical problems in handling of STF in polymers and found that e-STF does not lose its shear thickening effect to absorb impact energy [6]. In this study, both techniques stated above for microcapsule synthesis are performed since they both offer well-established capsules with liquid cores and a shell acting as a protective barrier from external environment. The optimized procedure and the best conditions are chosen to obtain the shear thickening fluid containing microcapsules embedded PU (e-STF/PU) cored sandwich composites. Morphology of the STF microcapsules are analyzed by scanning electron microscopy (SEM) and mechanical properties are examined.

Under impact, the protective shell of microcapsule behaves like a rubber like material and dampens the created impact energy. Silica particles increase the flow resistance and causes STF to behave like a solid after a critical shear rate. This behavior of STF in PU foam toughens the structure and eliminates the risk of a deep damage under impact in service preventing catastrophic failure of sandwich composite by modified foam.

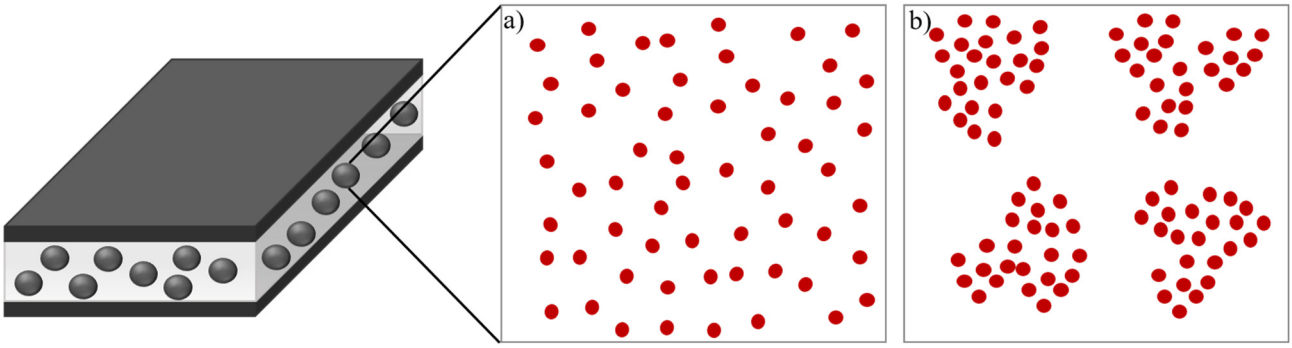

Fig. 2: Response of STF microcapsules after a critical stress (a) Particles at rest in STF, (b) Agglomerated particles under shear increasing the flow resistance, causing a shear-thickening behavior.

Prepared STF microcapsules are embedded in PU foam directly during foaming and STF microcapsules are mixed in polyol media by a mechanical stirrer at different stirring speeds. Then, remaining part of PU is added and mixed mechanically for foaming. STF microcapsules embedded rigid PU foams are placed in oven to perform polyurethane reaction. Two different core materials are used to fabricate sandwich composites as neat PU foam and e-STF/PU foam.

Foams are slimmed from top and bottom surfaces to get rid of non-homogeneities. Twill carbon fiber prepregs are used as face sheet for 4 plies each side. Sandwich composites are produced under pressure with a vacuum bag at 80°C for 4 h in oven for curing process of prepregs.

Response of e-STF/PU foams under quasi-static compression is studied according to ASTM C365-16 with 3 specimens for each case. Damage resistance properties of sandwich structures under impact are tested under impact to observe the rapid toughening effect of STF microcapsules in PU foam core.

3. CONCLUSION

Until now, microcapsules, shear thickening fluids and impact response of composites are studied by many researchers but none of these studies focused on integrating these three concepts to apply in sandwich composites. This study focuses on impact response of e-STF/PU cored sandwich in which impact load causes a huge increase in viscosity of STF, due to particle clusters after a critical shear rate, and toughens the polymer foam core. Fabricated STFs with a silica particle loading of 46% by wt. showed nearly threefold increase in viscosity and further studies are going on to achieve a better thickening mechanism by loading the carrier fluid with at least 50% by wt. fraction of particles. Stated mechanism is expected to prevent the catastrophic failure of sandwich structure by a modified core since damage starts from core first. Morphology and mechanical properties of e-STF/PU foam, neat PU foam and sandwich composites are studied through SEM, compression and impact tests.

REFERENCES

[1] M.V. Hosur et al., "Impact performance of nanophased foam core sandwich composites", *Materials Science and Engineering, A*, 2008; 498(1-2): p. 100-109.
[2] A. Srivastava et al., "Improving the impact resistance performance of Kevlar fabrics using silica based shear thickening fluid", *Materials Science and Engineering A*, 2011; 529: p. 224-229.
[3] M. Soutrenon et al., "Impact properties of shear thickening fluid impregnated foams", *Smart Materials and Structures*, 2014; 23(3): p. 035022.
[4] Young S. Lee et al., "The ballistic impact characteristics of Kevlar; woven fabrics impregnated with a colloidal shear thickening fluid", *Journal of Materials Science*, 2003; 38: p. 2825-2833.
[5] M. A. Dawson et al., "The dynamic compressive response of an open-cell foam impregnated with a non-newtonian fluid", *Journal of Applied Mechanics*, 2009; 76.
[6] Zhang, H. et al., "Encapsulation of shear thickening fluid as an easy-to-apply impact-resistant material", *Journal of Materials Chemistry A*, 2017; 5(43): p. 22472-22479.
[7] Chung, U.S. et al., "Polyurethane matrix incorporating PDMS-based self-healing microcapsules with enhanced mechanical and thermal stability", *Colloids and Surfaces A: Physicochemical and Engineering Aspects*, 2017; 518: p. 173-180.
[8] B.J. Blaiszik et al., "Microcapsules filled with reactive solutions for self-healing materials", *Polymer*, 2009; 50(4): p. 990-997.
[9] X.Z. Zhang et al., "The rheology of shear thickening fluid (STF) and the dynamic performance of an STF-filled damper", *Smart Materials and Structures*, 2008; 17(3): p. 035027.

SESSION 8B: DESIGN

DOI: 10.5075/epfl-ICSS12-2018-188-190

SHAPE OPTIMIZATION OF A SANDWICH PLATE WITH A NOVEL CORE DESIGN

Coskun Yalkilic, Fazil O. Sonmez, Fatih E. Oz and Nuri Ersoy
Department of Mechanical Engineering, Bogazici University, Email: sonmezfa@boun.edu.tr

1. INTRODUCTION

The objective of this study is to optimize the shape of a sandwich composite plate with a novel core design under three-point bending. The core has an egg-crate shape. The initially chosen geometric design is shown in Fig. 1. The material is epoxy reinforced with non-crimp E-glass fabric and the layup configuration is quasi isotropic for both the core and the face sheets.

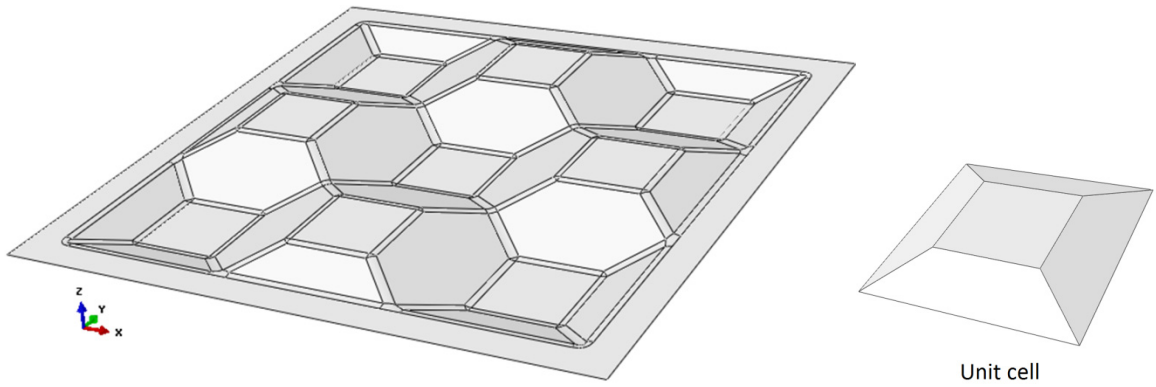

Fig. 1: The schematic representation of the initial core geometry and its unit cell [1].

2. TENSION TESTS

In the first stage of the study, the mechanical properties of the composite material are determined. A procedure is proposed to determine these properties using tension test and acoustic emission (AE) results for specimens with $[0/45/-45/90]_s$ and $[0/90]_{2s}$ layup sequences and a progressive failure model. Using this procedure, longitudinal and transverse tensile strengths, X_t and Y_t, shear strength, S, together with the stiffness properties can be obtained. Tension tests are conducted according to ASTM D3039 standard testing procedure. The strain of the specimen is measured by a video extensometer. Fig. 2 shows the peak frequency distribution as well as the energy levels of AE hits for a quasi-isotropic specimen, $[0/45/-45/90]_s$, together with the load-strain curve. Ply-failure load levels, which are indicated on the graph, are determined considering the changes in the load-displacement diagram as well as the AE signals. Fig. 3 shows a comparison between the experimental load-strain curves of cross-ply and quasi-isotropic tension test specimens and the curves predicted by the progressive model.

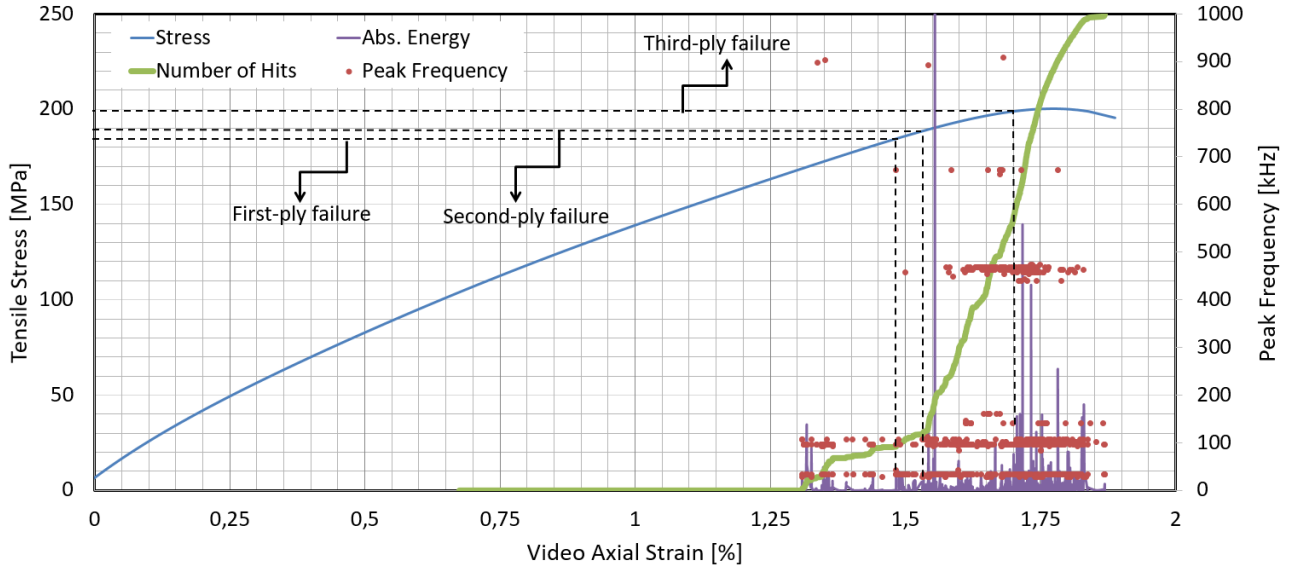

Fig. 2: The peak frequency distribution, the energy levels, and the cumulative counts of the AE hits and the stress vs. strain curve for quasi-isotropic tension test specimens with layup configuration $[0/45/-45/90]_s$.

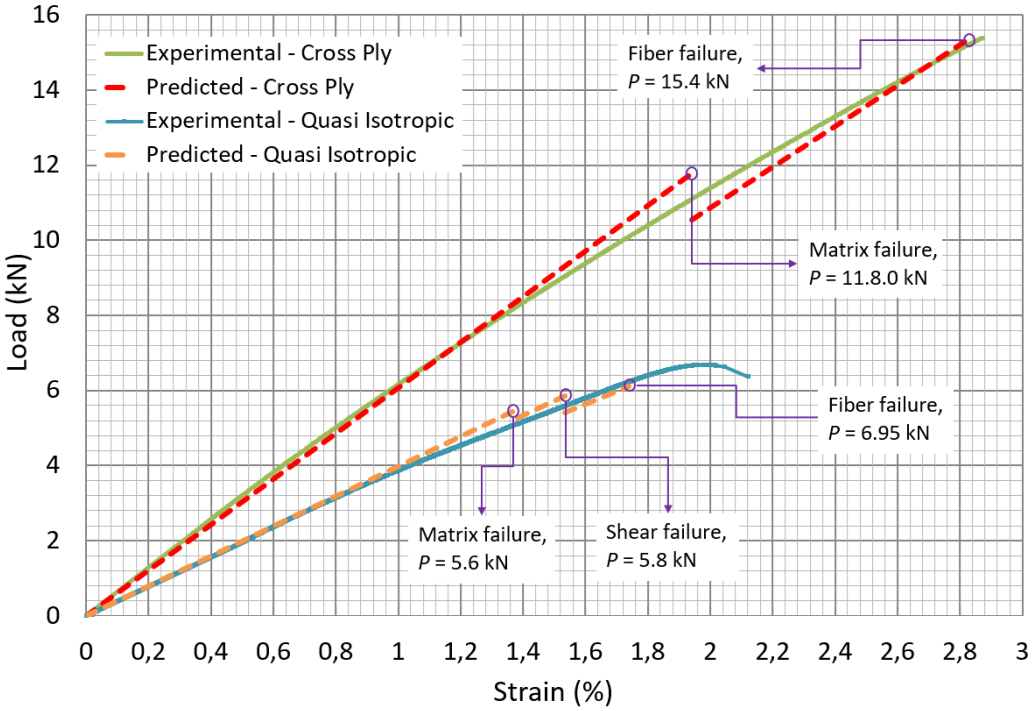

Fig. 3: Experimental load-strain curves of a tension test specimen with cross-ply, $[0/90]_{2s}$, and quasi-isotropic, $[0/45/-45/90]_s$, layup configurations and the curves predicted by the progressive damage model.

3. THREE-POINT BENDING OF SANDWICH SPECIMENS

In the second stage of the study, the failure behavior of the sandwich specimens is investigated via three-point bending tests. Acoustic emission (AE) monitoring is used to detect the progression of damage and identify the failure modes and failure load levels. A finite element model of the sandwich structure is also developed to predict the structural response and the failure behavior of the specimens under the loading conditions in the tests. A promising agreement between the results of the FE model and the experiments is observed. The force-deflection relation as well as the failure load level are accurately predicted.

4. DESIGN OPTIMIZATION

In the third stage of the study, the shape of the core is optimized using the experimentally validated FE model. Fig. 4 shows the geometry of a unit cell. There are basically three geometric parameters for the trapezoidal prism; the height of the prism, h, the angle between the base and side faces, θ, and the length of the top face, L_c, which is in contact with the face plates. The base length of the prism, L_b, is a dependent variable, which is a function of the other three independent parameters.

$$L_b = L_c + 2h/tan\theta \tag{1}$$

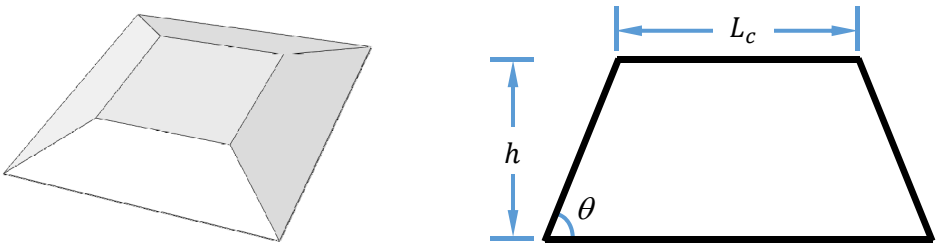

Fig. 4: The geometry of a unit cell.

Although fiber orientations are considered to be important design variables in composite optimization studies, for the structure considered in this study quasi isotropic layup configuration, $[(0/45/-45/90)_n]_s$, is considered to be preferable, because this structure is designed for applications in which high stiffness and high strength are desired in all directions. For this reason, only layer thickness or the number of plies in the layers, n, can be considered as design variable besides geometric parameters. The specimen tested previously is used as a benchmark in order to see the improvements in the performance of the optimized plate. For this reason, the thickness of the sandwich plate is taken to be constant and equal

to the thickness of the benchmark specimen. For comparison purposes, the layer thicknesses are also taken to be the same. Accordingly, two of the design variables, contact length, L_c, and the inclination angle, θ, are used as optimization variables.

Because the dimensions of the unit cells are changed during optimization, strength of the plate is normalized to compare different designs. Besides, it should also be normalized for the amount of composite material used as the following:

$$F_n = F_{all}\left(\frac{t_0}{t}\right)\left(\frac{L}{L_0}\right)^2\left(\frac{m_0}{m}\right) \tag{2}$$

where t_0, L_0, and m_0 are thickness of the core, length of the plate between the supports, and mass of the composite material for the reference configuration. t, L, and m are the respective parameters for the configurations generated during design optimization. F_{all} is the first-ply failure load level calculated for the generated configuration. F_n is the normalized value for the first-ply failure load. The thickness is taken as constant and the same as that of the initial geometry, which is 2.0 cm. Then, a parametric study is conducted to investigate the effects of the design parameters on the strength and the stiffness of the sandwich plate. After that, optimum values of the parameters are found using Nelder-Mead search algorithm. The objective function is chosen as the normalized failure load, F_n, given by Eq. 2. Table 1 presents optimum values of the design variables and the normalized failure load level and the respective values for the reference configuration shown in Fig. 1. As seen in the table, significant improvement is obtained in strength by optimization compared to the reference configuration.

Table 1: Comparison of the optimum configuration and the reference configuration.

	Angle, θ	Contact Length, L_c	Failure Load
Reference Design	21.8°	6.20	4.2 kN
Optimum design	47.7°	15 mm	9.7 kN

In order to manufacture and test the optimized core geometry, a mold is produced by 3D printing. The mold and the fiber forms on the mold are shown in Fig. 5. Soon experiments will be conducted on composite specimens with the optimum core shape and the strengths of the plates with the optimum core structure and the foam-core sandwich plates will be compared.

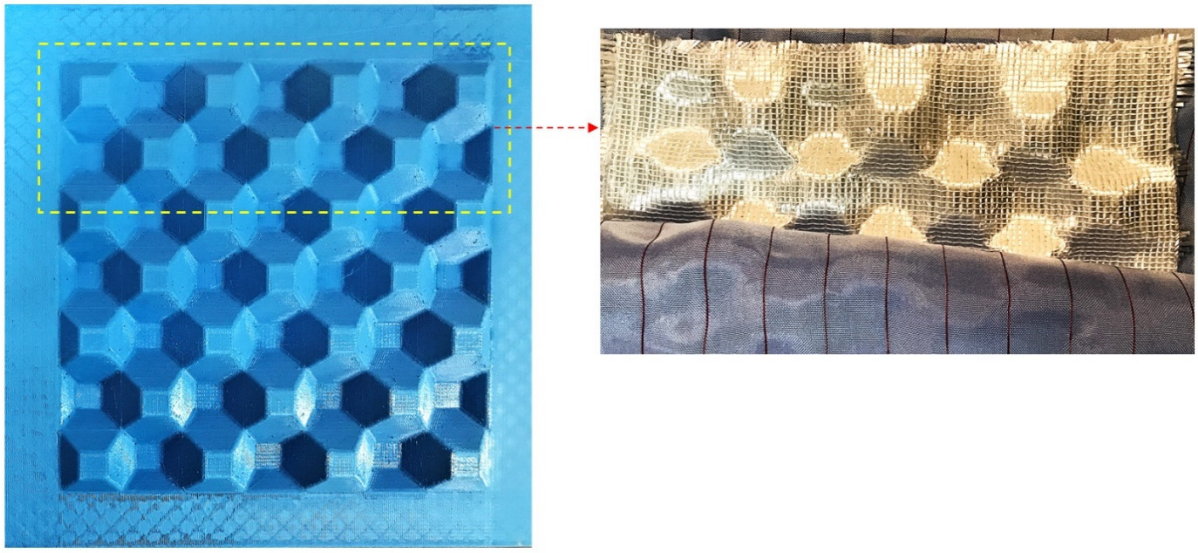

Fig. 5: 3D printed mold and the form of the fibers on it.

ACKNOWLEDGMENT

This paper is based on the study supported by Bogazici University Research Fund with grant number 11168-16A06P2.

REFERENCES

[1] A. Uzal, F.O. Sönmez, F.E. Oz, N. Ersoy, K. Cinar, "A composite sandwich plate with a novel core design," *Composite Structures*, 2018; 193: 198-211.

DOI: 10.5075/epfl-ICSS12-2018-191-193

STRUCTURAL DESIGN AND OPTIMIZATION OF FRP CURVED SANDWICH PANELS USED AS THE ENCLOSURE STRUCTURE OF A LARGE BRIDGE

Xinmiao Meng[1,2] and Peng Feng[3]
[1] Department of Civil Engineering, Beijing Forestry University, Beijing, China. mengxinmiao@bjfu.edu.cn
[2] Department of Civil Engineering, Tsinghua University, Beijing, China.
[3] Department of Civil Engineering, Tsinghua University, Beijing, China. fengpeng@tsinghua.edu.cn

1. INTRODUCTION

Non-linear architecture releases the imagination and creation of architects when designing the buildings and infrastructures [1]. However, when constructing the freeform appearance, the traditional construction techniques especially using concrete, face high construction cost and slow construction speed. FRP curved sandwich panels, composed of FRP (fibre-reinforced polymer) face sheets and PUR (Polyurethane) foam core, provide a better solution to the above issues. Such panels have the advantages of low density, high strength, convenient construction and excellent designability, and are suitable to construct non-linear architecture fast and economically. So it has been pioneered to build several non-linear architectures and infrastructure [2-3], such as the roof of the Yitzhak Rabin center in Israel [4], Novartis main gate building in Switzerland [5] and Wuhan factory gate building (China) [6].

This paper also presents a practical engineering application, a 9028.5 m^2 enclosure structure of a large bridge in Beijing, designed and manufactured with such panels [7]. The structural design and optimization process will be displayed here to give a reference to the similar projects.

2. PROJECT INFORMATION

The bridge with the 210-m length and five spans, located in Beijing, China, is composed of steel main structure and exterior enclosure structure. The appearance of the enclosure structure with 9028.5-m^2 area is highly non-linear, but impressive, as shown in Fig. 1. The main structure is made of steel arch and the enclosure structure is made of FRP curved sandwich panels with PUR foam core. To connect the enclosure structure and the steel arch, the steel brace system has to be designed. The enclosure structure is grouped into several parts according to each location, including bottom part, water platform and sidewalk parts as Fig. 2 shows. Each part is further divided into small components, from 3.5 m to 5.5 m, along the longitudinal direction. The total enclosure structure is divided into 968 panels. Each panel is unique and has to be designed individually. The main loads, includes 5.5-m water pressure at most, 2-kN/m^2 fundamental wind pressure, and 0.4-kN/m^2 fundamental snow pressure.

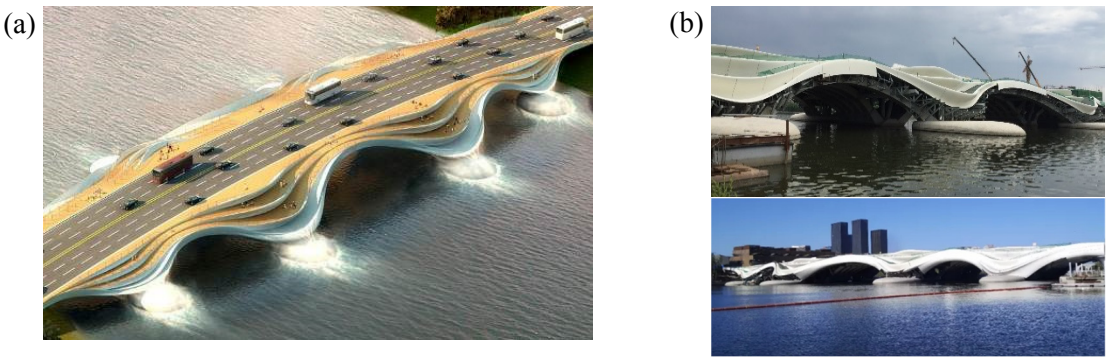

Fig. 1: Enclosure structure of FRP curved sandwich panels: (a) rendering; (b) partial installation.

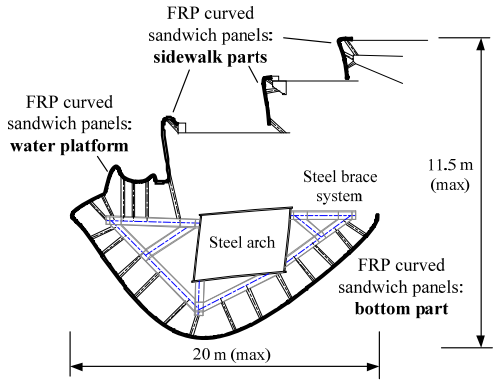

Fig. 2: The composition of the enclosure structure.

3. MATERIAL PROPERTIES

The FRP curved sandwich panel is composited of GFRP (glass fibre-reinforced polymer) laminate face sheets and PUR foam core. The GFRP laminate is designed as transverse isotropic and the PUR foam core is designed as isotropic. The material properties are listed in Table 1.

Table 1: Material properties of GFRP laminate and PUR foam core.

Materials	E_1 (GPa)	E_2 (GPa)	E_3 (GPa)	G_{12} (GPa)	G_{23} (GPa)	G_{13} (GPa)	ν_{12}	ν_{23}	ν_{13}
GFRP laminate	20	20	3.2	3	3	3	0.30	0.30	0.30
PUR foam core	$E=20\times10^{-3}$			$G=7.8\times10^{-3}$			$\nu=0.15$		

4. STRUCTURAL DESIGN

Design of sandwich panel

The sandwich panels have highly non-linear appearance, as shown in Fig. 3(a), making it impossible to design with theoretical method [8]. FEA (finite element analysis) provides an efficient approach to assist the structural design. In the enclosure system, most of the bottom part is submerged into the water when the water depth comes to 5.5 m. So it is chosen here to show the structural design process. The digital model of bottom part in Rhinoceros is saved as ACIS documents (.sat format). Shell 99 element is selected to simulate FRP curved sandwich panels in ANSYS, the shell is defined into three layers, including two layers of FRP face sheets and one layer of PUR foam core. The element size is about 0.4 m, and the total element number is 15903. Each panel is usually supported by 5 steel brace trusses through support joints. Adjacent panels are connected with assembly joints. The boundary conditions are defined by constraining the degrees of freedom at corresponding nodes. The water load is applied perpendicular to each element according to each location. The dead weight is also considered. The FEA is based on elastic analysis. The safety factor of strength is set as 3. The displacement of FEA results for bottom part is shown in Fig. 3(b). Based on the FEA results, the thicknesses of FRP face sheets and the foam core are adjusted to optimize the structural design. Final the thickness of FRP face sheets changes from 6 to 12 mm, the thickness of foam core changes from 40 to 100 mm according to the load conditions.

Fig. 3: FRP curved sandwich panels: (a) the groups and divisions; (b) the displacement of FEA results of bottom part.

Design of connection joints

The connection joints include support joints and assembly joints, as shown in Fig. 4(a). The support joints are embedded in the sandwich panels. To reduce the stress concentration, the support joint is designed as Fig. 4(b), in which the FRP ribs have the K-shape end. The assembly joint is designed to connect adjacent panels but let the water leak out at the same time. The load is transferred from the panels to the steel brace system through the support joints. The structural design is conducted with FEA in ANSYS. The safety factor of strength is set as 4. In the FEA, the FRP is simulated by solid 46, and the foam core is simulated by solid 45. The thickness and length of the components are optimized through analyzing the FEA results.

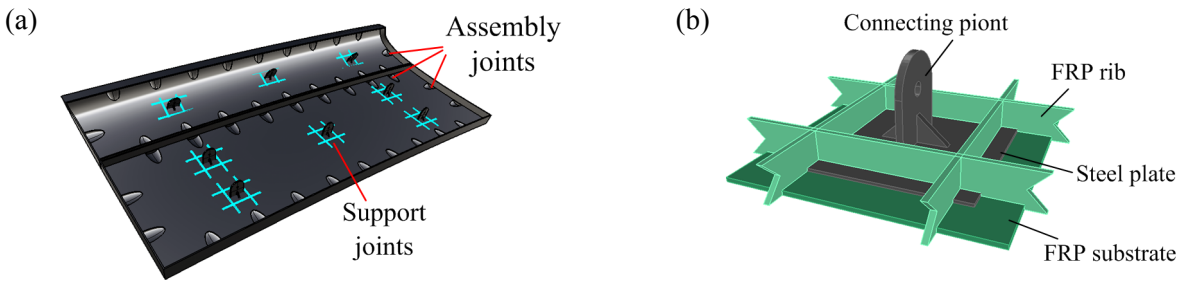

Fig. 4: Connection joints: (a) the sketch; (b) the details of support joints.

5. STRUCTURAL OPTIMIZATION AND MANUFACTURING

In this project, the 3D digital model built in Rhinoceros contains only the facade of the enclosure system, but not the thickness of the panel, which can be calculated and determined through FEA. Generally, the thickness of the panel is design to be uniform for a single panel in the current FEA process. However, the thickness can be further optimized to reduce the use of the materials as soon as possible. A parametric offset method is put forward here to realize the above objective. In this method, the offset is along the angular bisector direction, and the offset distance R is controlled with a function $f(j)$ as shown in Eq. 1, where the $f(j)$ is the function of the optimization variables defined in ANSYS.

$$R = f(j) + R_0 \tag{1}$$

The mismatch correction method is provided in the parametric offset process to ensure the finite element model built successfully for the facade with large curvature. The parametric offset and modeling process is shown in Fig.5. The nodes on the outer appearance were first chosen in Rhino and then were input into ANSYS. Then the nodes were offset one by one according to the distance function R. Finally, the finite element model was built up based on the solid model directly generated from the nodes as shown in Fig.5.

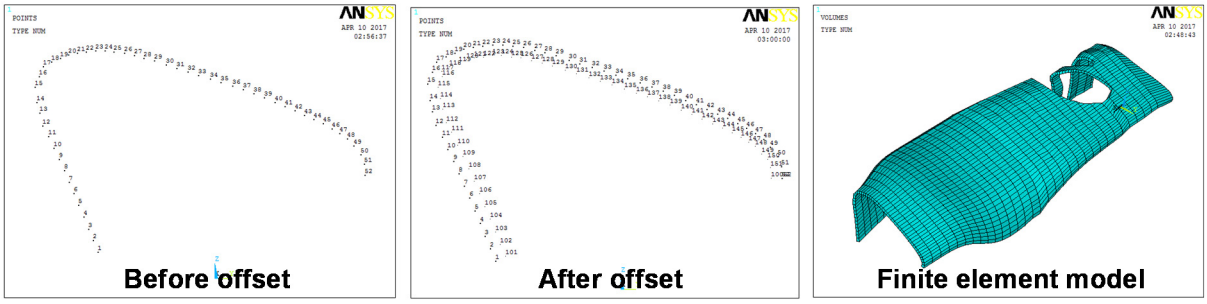

Fig. 5: Parametric offset and modeling using ANSYS.

The results of structural optimization are used to guide the manufacturing. To reduce the cost, two kinds of manufacturing processes are applied. For the overwater panels, the hand-lay-up technique is chosen because of the low level of loads. However, for the underwater panels, the VARTM (Vacuum Assisted Resin Transfer Molding) is chosen to provide high quality. In the process of hand-lay-up technique, the mold could be constructed with wood to further reduce the cost.

6. CONCLUSION

The following conclusions can be drawn from this study:

(1) The structural design and optimization are conducted through the design of FRP curved sandwich panels, connection joints.
(2) The FRP ribs and K-end are designed to reduce the stress concentration at the support joints.
(3) The variable thickness optimization for FRP curved sandwich panels is realized through parametric offset.

ACKNOWLEDGMENTS

The authors acknowledge funding supported by the Fundamental Research Funds for the Central Universities of China (No. BLX201706), and supported by the National Natural Science Foundation of China (No. 51278276 and No. 51522807).

REFERENCES

[1] N. Hu et al., “Structural art: Past, present and future”, *Eng. Struct.*, 2014;79:407-416.
[2] T. Keller, “FRP sandwich structures in bridge and building construction”, *CICE 2016*: 2016, 23-28.
[3] A. Manalo et al., “State-of-the-art review on FRP sandwich systems for lightweight civil infrastructure”, *J. Comps. Const.*, 2016;21:04016068.
[4] F.G. Roosenboom, “Building the future with FRP composites”. *Reinf. Plast.*, 2014;51:26-9.
[5] T. Keller et al., “Structural concept, design, and experimental verification of a glass fiber-reinforced polymer sandwich roof structure”, *J. Comps. Const.*, 2008;12:454-68.
[6] W. Xu, “Structural envelope”, *Archit. J.*, 2014:1-5.
[7] X. Meng et al., “The application to bridge enclosure structure of FRP curved sandwich panels with foam core”, *APFIS2017*: 2017,.
[8] Y. Frostig, “Bending of curved sandwich panels with a transversely flexible core-closed-form high-order theory”, *J. Sandw. Struct. Mater.*, 1999;1:4-41.

DOI: 10.5075/epfl-ICSS12-2018-194-197

ASSESSING THE IN-PLANE CORE SHEAR CONTRIBUTION OF COMPOSITE SANDWICH PLATES USING THE PICTURE FRAME TEST METHOD

Oludare E. Oluwabusi[1], Elias A. Toubia[2] and Susan Hill[3]
[1]Department of Mechanical and Aerospace Engineering, University of Dayton, USA. oluwabusio1@udayton.edu
[2]Department of Civil and Environmental Engineering and Engineering Mechanics, University of Dayton, USA. etoubia1@udayton.edu
[3]Structures and Materials Assessment, Research and Testing Lab, University of Dayton Research Institute, Dayton Ohio, USA. susan.hill@udri.udayton.edu

1. INTRODUCTION

Numerous structural members such as shear webs for wind turbine blades, shear walls, and plate girders etc. are mainly subjected to in-plane shear loading. Assessing the real contribution of the core to the in-plane shear capacity of the sandwich structure, can lead to a better realistic design and eventually to a reliable optimized structure. Few researchers have used experimental approach to study the in-plane shear behavior. [1] used biaxial method to evaluate two aluminum plate specimens, while [2] looked at in-plane shear tests of sandwich plates using two different experimental procedures. Recently, [3] investigated two different picture frame fixture configurations for in-plane shear strength of composites sandwich constructions. Shear frame test fixtures recently became adopted as a standard testing method in Europe and North America ([4] [5]). There exist a number of barriers to overcome before the wide adoptions of composite sandwich construction beyond the scope of research, particularly in civil infrastructure. Consequently, there are need for an established design methodology and data for composite-foam based materials for sandwich construction. Additionally, few of the available simplified design approaches need validations [6].

This paper discusses the in-plane shear characterization of shear load resistant structures. A systematic experimental approach coupled with both 2D and 3D digital image correlation (DIC) techniques were used to test and characterize 20 samples using the newly released ASTM picture frame test method. This research produced a new in-plane shear data along with a simplified analytical model that will assist designers and engineers to confidently size, design, and predict the in-plane shear capacity of sandwich structural members.

2. MATERIALS SELECTIONS AND MANUFACTURING

All composites sandwich plates and laminates tested in this experimental work were molded using E-glass double bias skin (E-BXM 1708 [±45/Mat]) and infused with Derakane 610C-200 vinyl ester resin. The Vacuum Assisted Resin Transfer Molding (VARTM) process was used to mold all samples. Experimental setup utilized the recently released ASTM D8067 standard test method (picture frame device) for in-plane shear properties of several sandwich panel configurations with varying core densities (C70.55, H80, and H100 foam core) and face-sheet layup (2 plies vs. 4 plies).

3. EXPERIMENTAL RESULTS

In this work, two predominant failure modes were identified for composite sandwich plates: global buckling (Fig. 1) and face sheet fracture. Core fracture was also observed in the plain H-series and C70.55 foam (Fig. 2). Global buckling was detected for the composite laminates only (Fig. 3).

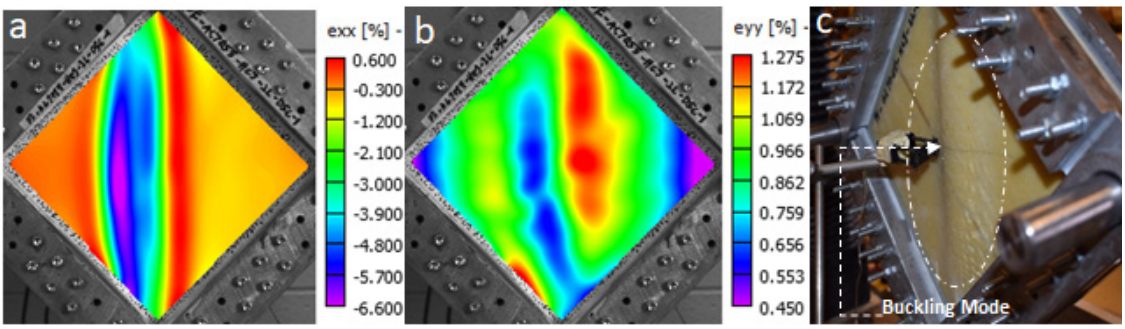

Fig. 1: Buckling mode of sandwich plate, Core: C70.55 with core joint, 12.7mm thick, Facings: [±45/mat]$_2$ (a) diagonal compression strain, (b) diagonal tension strain, (c) buckling mode.

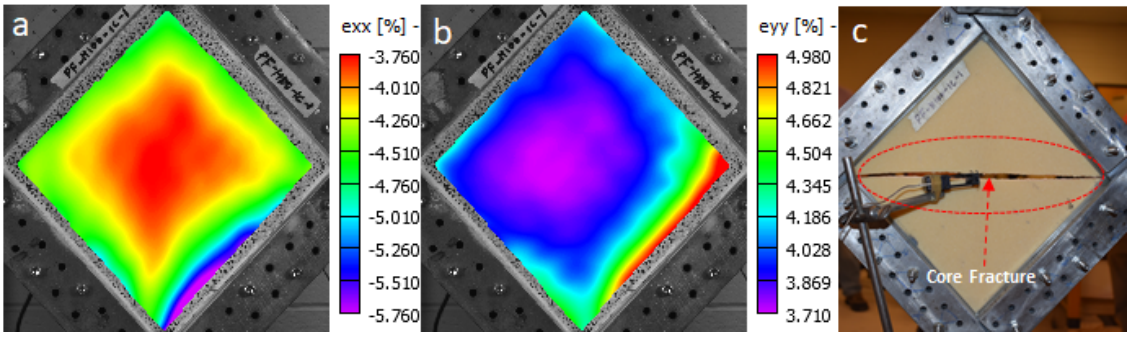

Fig. 2: Core fracture of foam panel, Core: H100, 25.4mm thick, (a) diagonal uniform compression strain, (b) diagonal uniform tension strain, (c) core fracture mode.

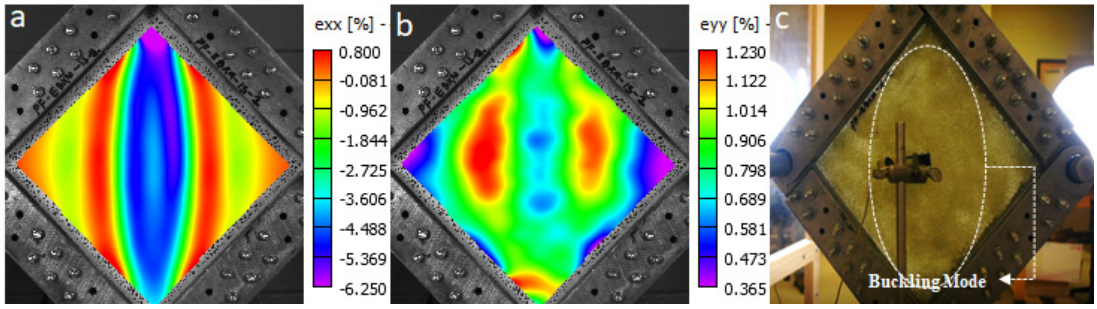

Fig. 3: Global buckling of 2 x EBXM ([±45/mat]$_2$) laminate (a) diagonal compression(DC) strain, (b) diagonal tension strain(DT), (c) buckling mode.

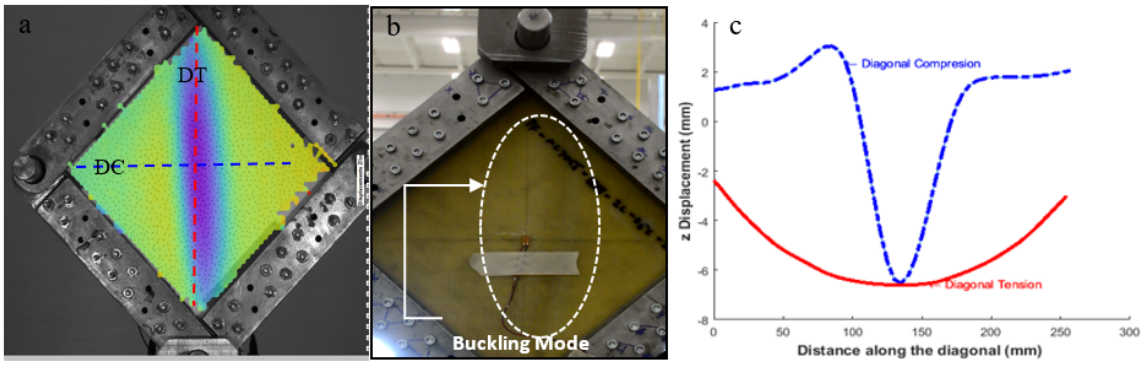

Fig. 4: (a) 3D DIC fringe pattern of buckling mode shape for C70.55 (12.7 mm thick core) and Facings: 2 x EBXM [±45/mat]$_2$, (b) onset buckling of the actual specimen, (c) Out-of-plane buckling mode shapes (z-direction) along the diagonals – one wavelength along the Tension vertical line, three wavelengths along the Compression horizontal line.
Note: DC (diagonal compression), DT (diagonal tension).

4. SIMPLIFIED MODEL

To obtain a realistic design, engineers need to assess the proportion of load carried by the core in the sandwich construction. The practical assumption that all of the in-plane applied load on sandwich construction is carried by the laminates is somewhat misleading. This section helps understand the influence of core to the mechanical performance of the panel.

A simplified predictive equation was developed to quantify the influence of core to the mechanical performance of the panel. This simplified analytical equation could be used to select, size, and predict the load capacity and failure mode of composite sandwich structures under in-plane shear loading. With this approach, the maximum failure load for each of the constituent components of sandwich can be predicted using the following Eq. 1.

$$P_s = P_c\left(1 + 2G_\phi\right) = P_f\left(2 + \frac{1}{G_\phi}\right) \quad (1)$$

Where $G_\phi = \frac{G_f t_f}{G_c t_c}$: Shear stiffness dimensionless parameter. G and t are shear modulus and thickness respectively.

P = Maximum load. The subscripts s, f, and c are sandwich, face skin and core respectively.

Using this Eq. 1, the effect of core shear modulus and thickness as well as the composites face-sheet shear modulus and thickness on in-plane sandwich performance is presented in Table 1 and Fig. 5. The dotted points represent the

experimental data where face-sheet fracture occurred at ultimate load. The sandwich specimen with the C 70.55 foam core (12.7 mm thick) samples (red cross-points) failed by buckling and then face-sheet fracture

Table 1. In-plane Shear Test Results and Failure modes (Foam and sandwich panels).

Plate Type	Foam Type	Thickness (mm)	No of plies	Max. Diagonal Compression Strain (%)	Max. Diagonal Tension Strain (%)	Max Load (kN)	Failure Mode
Foam	H100	12.7	Plain Foam	4.35%	4.37%	7	Core Fracture
		12.7		3.84%	3.51%	6	Core Fracture
		25.4		4.27%	4.02%	13	Core Fracture
		25.4		4.21%	4.05%	12	Core Fracture
	H80	12.7		3.82%	3.59%	7	Core Fracture
		25.4		4.19%	3.93%	10	Core Fracture
		25.4		3.60%	3.27%	10	Core Fracture
	C70.55	12.7		2.66%	3.16%	3.6	Core Fracture
		25.4		3.31%	3.63%	7.3	Core Fracture
		25.4		3.35%	3.55%	7.3	Core Fracture
Sandwich	H100	12.7	1 X EBXM	Not available		96	Face-sheet Fracture
		25.4	1 X EBXM	Not available		114	Face-sheet Fracture
		12.7	1 X EBXM	1.03%	1.15%	118	Face-sheet Fracture
		25.4	1 X EBXM	1.13%	1.31%	117	Face-sheet Fracture
		25.4	1 X EBXM	0.91%	1.03%	103	Face-sheet Fracture
	H80	25.4	2 X EBXM	0.86%	0.85%	168	Face-sheet Fracture
		25.4	2 X EBXM	0.87%	0.92%	184	Face-sheet Fracture
	C70.55	12.7	2 X EBXM	1.17%	0.95%	(152)	Global Buckling
		25.4	2 X EBXM	0.93%	0.92%	177	Face-sheet Fracture (Mixed Mode)
		25.4	2 X EBXM	0.86%	1.07%	183	Face-sheet Fracture

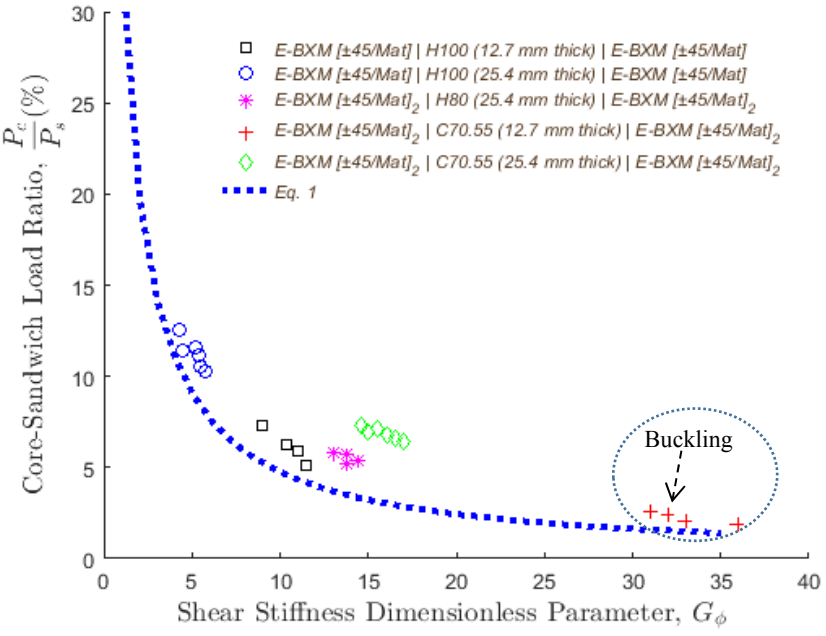

Fig. 5: Ratio of core load to sandwich load against shear dimensionless parameter.

5. CONCLUSION

This work reports a progressive systematic experimental approach for the in-plane shear contribution of sandwich core materials. A total number of 20 samples were tested using the picture frame device. Constituent materials, such as plain foam cores, laminates, and sandwich constructions featuring several foam core densities and face-sheets were tested using the in-plane picture frame. The major highlight from this experimental work is that that designers should not neglect the in-plane load carrying capacity of the core material. It was found that for stiff foam the load contribution of the core could be as high as 10 to 15 % of the total in-plane load. In addition, this test method is a reliable experimental tool to understand the true capacity of the core shear contribution to the overall structure. This test method is valid to detect the buckling load and could be extrapolated to predict the performance of large-scale non-load bearing shear walls for potential use in infrastructure applications.

REFERENCES

[1] H. G. Bush et al., "A biaxial method for inplane shear testing" NASA, 1978, pp 1-21
[2] M. Morgenthaler et al., "Dependence of inplane sandwich shear deformation on core material type and thickness", *ICSS:* 2005, pp 441-450
[3] F. Stoll et al., "In-plane shear characterization of sandwich laminates using a picture-frame test configuration", *ASC*: 2016, pp 1-14.
[4] DIN SPEC 4885, "Shear test method using a shear frame for the determination of the in-plane shear stress/shear strain response and shear modulus", *DIN:* 2014, pp 1-28
[5] ASTM D8067, "Standard Test Method for In-Plane Shear Properties of Sandwich Panels Using a Picture Frame Fixture", *ASTM:* 2017, pp 1-11
[6] A. Manalo et al., "State-of-the-Art Review on FRP Sandwich Systems for Lightweight Civil Infrastructure", *J. Comp Constr.*, 2017; 21: pp 1-16.

DOI: 10.5075/epfl-ICSS12-2018-198-200

MODELLING AND DESIGN OF COMPOSITE SANDWICH PANELS UNDER IN-PLANE COMPRESSION CRUSHING

Yuan Chen and Lin Ye*
Centre for Advanced Materials Technology (CAMT), School of Aerospace, Mechanical and Mechatronic Engineering, the University of Sydney, NSW 2006, Australia.
First author: augustu@163.com
*Corresponding author: lin.ye@sydney.edu.au (L. Ye).

1. INTRODUCTION

This study aims to simulate in-plane compressive crushing behaviour of a composite sandwich panel using the finite element analysis (FEA) and to maximise its in-plane crushing energy absorption by optimising some geometrical variables. The proposed model describes a number of damage mechanisms and deformation behaviours of the composite sandwich panel during in-plane compression. Subsequently, the FEA results are validated by experiments. Further, some geometrical variables of the composite sandwich panel are assessed for optimal design with the maximum in-plane crushing energy absorption.

2. EXPERIMENT

In the experiment, the face sheets were fabricated in a quasi-isotropic configuration with T300 carbon fibre plain woven fabric - epoxy prepreg (CF/EP), and the core material was honeycomb from Nomex series. A 1515-3 film adhesive was utilised to bond the face sheets and the core tightly. Finally, the manufactured panel was cut into specimens with a constant W = 60 mm, and an initial H =50 mm after set-up, as shown in Fig. 1. In addition, different bevel angles θ were introduced according to the design requirement, and chamfers were machined on the crushing edges for all specimens.

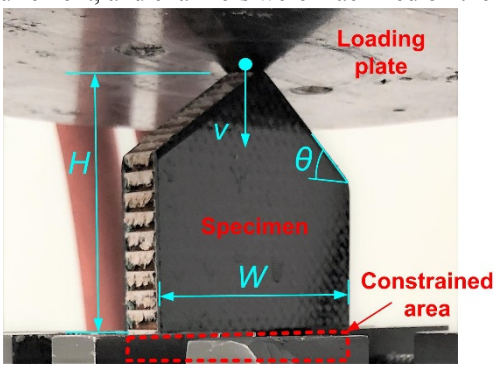

Fig. 1: Experimental set-up.

The quasi-static compression crushing tests were conducted on a MTS 810 material test system with a constant crushing rate of v=2 mm/min, as presented in Fig. 1. During compression, the load-displacement curve was recorded by a computer-instrumented data acquisition system, and the total absorbed energy (TAE) can be defined by integration of the load-displacement curve as

$$TAE = \int_0^S F(x)dx \tag{1}$$

where $F(x)$ is the crushing load as function of the displacement of x, S is the maximum crushing displacement. Additionally, the specific energy absorption (SEA) is defined by

$$SEA = \frac{TAE}{m} \tag{2}$$

where, m is the mass of crushed section.

3. FINITE ELEMENT ANALYSIS

The finite element analysis is integrated with a few mechanistic models that describe the damage and failure in the composite sandwich panels, including the continuum damage mechanics (CDM) model for the in-plane failure of composite face sheets, cohesive zone model (CZM) for interlaminar fracture in the composite face sheets and debonding between the face sheets and sandwich core, and elastic-plastic model for the sandwich core [1-4].

Continuum Damage Mechanics

CDM model expresses the damage defined by the degradation of the stiffness matrix of a composite with plain fabric of reinforcing fibres. The constitutive stress-strain relations are formulated as [1]:

$$\begin{Bmatrix}\sigma_{11}\\ \sigma_{22}\\ \sigma_{12}\end{Bmatrix}=\frac{1}{D}\begin{bmatrix}(1-d_1)E_1 & (1-d_1)(1-d_2)E_1v_{21} & 0\\ (1-d_1)(1-d_2)E_2v_{12} & (1-d_2)E_2 & 0\\ 0 & 0 & 2(1-d_{12})DG_{12}\end{bmatrix}\begin{Bmatrix}\varepsilon_{11}\\ \varepsilon_{22}\\ \varepsilon_{12}^{el}\end{Bmatrix} \quad (3)$$

In the equation, σ_{11}, σ_{22} and σ_{12} are the stresses, and ε_{11}, ε_{22} and ε_{12}^{el} are the elastic strains, respectively. D=1-(1-d_1)(1-d_2)$v_{12}v_{21}$, d_1 and d_2 are the damage variables in the two main fibre directions, d_{12} denotes the current shear damage state; E_1 and E_2 are Young's moduli in the two fibre directions, respectively, G_{12} is the in-plane shear modulus, and v_{12} and v_{21} are Poisson ratios. In this work, the damage variables were calculated based on the stress state in the fibre directions as

$$d_i = d_{i+}\frac{\langle\sigma_{ii}\rangle}{|\sigma_{ii}|}+d_{i-}\frac{\langle-\sigma_{ii}\rangle}{|\sigma_{ii}|},\ i=1,2 \quad (4)$$

where d_{i+}, d_{i-} and d_{12} are the damage variables that are assumed as a function of the corresponding effective stress. As for the initiation failure criteria, it is based on the ultimate strength. After the initiation failure criteria has been met, the damage evaluation will be implemented according to [4]. In the shear direction, plasticity is also considered using a classical plastic model [3].

Cohesive Zone Model

In terms of the interface damage and failure, a cohesive zone model (CZM) was utilised taking into account a damage initiation criterion and a damage evaluation law [3, 4].

Damage initiation criterion

$$\left\{\frac{\langle t_n\rangle}{t_n^0}\right\}^2+\left\{\frac{\langle t_s\rangle}{t_s^0}\right\}^2+\left\{\frac{\langle t_t\rangle}{t_t^0}\right\}^2=1 \quad (5)$$

Damage evaluation law

$$G_n^C+(G_s^C-G_n^C)\left\{\frac{G_S}{G_T}\right\}^{\eta}=G^C \quad (6)$$

where t_i (i=n, s, t) is the traction stress vector and t_i^0 (i=n, s, t) is the strength vector. G_S=G_s+G_t, G_T=G_n+G_S, G_i (i=n, s, t) is the total strain energy release rate; G^C is the corresponding fracture toughness. η is the cohesive property coefficient.

Elastic-plastic Model

With regards to the honeycomb core, there are also a number of studies that could be referred to establish the numerical model [5, 6]. The geometric parameters and modelling detail of aramid paper and phenolic resin were proposed and discussed in previous work [3].

4. DESIGN METHOD

After the analysis of the numerical and experimental results, important geometric factors (including the bevel angle θ and the height H) were selected as the variables for optimisation design. The mass and energy absorption were defined as the objectives. To acquire mathematic surrogate model for approximating the variables and objectives, an optimal surrogate modelling technique on the basis of a radius basis function (RBF) was utilised [7]. The form of the RBF to construct the approximation by $\tilde{f}(x)$ can be formulated as:

$$\tilde{f}(x)=\sum_{i=1}^{n}\lambda_i\phi(r_i) \quad (7)$$

where n is the number of the sampling points, $\phi(r_i)$ is the basis function, r_i is the Euclidean distance and λ_i is the coefficient. After the model has been built, non-dominated sorting genetic algorithm (NSGA-II) was carried out to solve such a multi-objective optimisation problem and acquire the optimal solutions. The specific design methods can be referred in [7].

5. RESULTS AND DISCUSSION

The numerical model was validated by experiments for specimens with different bevel angles, and the results for the specimens of 30° bevel and 50 mm height are shown in Fig. 2. It can be seen that the forces gradually climb to the peak ahead of a devastating drop, which indicates that there was sustained damage propagation when the composite panel failed progressively under in-plane crushing. Further, it implies that there must be an optimal bevel angle with a specific height that can perform optimally in mass reduction but enhanced energy-absorption.

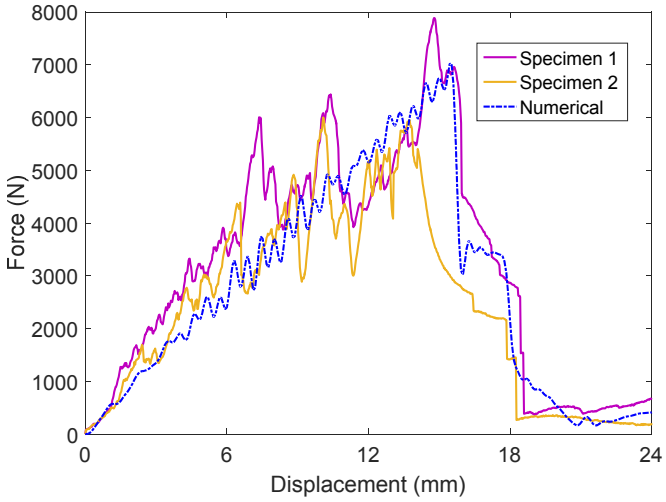

Fig. 2: Force-displacement plots of experimental and numerical results.

To acquire the optimal structural parameters, optimisation calculation was conducted as described before. Afterwards, with the aid of surrogate model, the optimal result was achieved, which was input into the numerical model for validation and analysis. It is found that the error of the objective responses between the surrogate model and numerical calculation were all below 10 %, indicating the effectiveness and reliability of the constructed model. To compare the performance of optimised result with other specimens within the design scope, the diagram of *SEA* versus crushed mass is depicted in Fig. 3. Clearly, the optimal composite sandwich panel, when the bevel angle is 36.5° and the height is 27 mm, can achieve the highest energy absorption by consuming comparatively less mass.

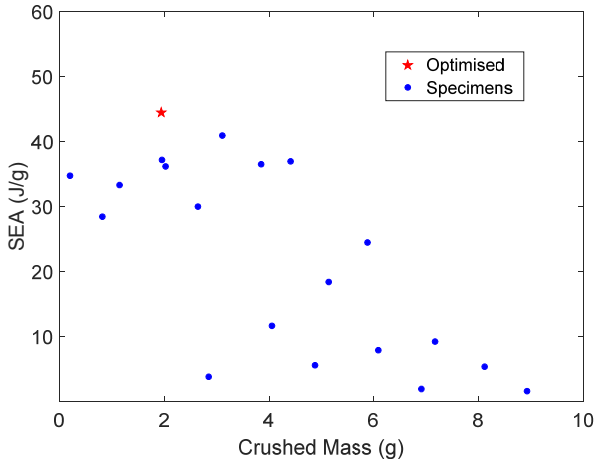

Fig. 3: SEA versus crushed mass of the optimised and other specimens.

REFERENCES

[1] A.F. Johnson, "Modelling fabric reinforced composites under impact loads", *Compos Part A Appl Sci Manuf*, 2001; 32: 1-2.
[2] I. Ivañez et al., "The oblique impact response of composite sandwich plates", *Compos Struct*, 2015; 133:1127-36.
[3] Y. Chen et al., "Low-velocity impact response of composite sandwich structures: Modelling and experiment", *Compos Struct*, 2017; 168: 322-34.
[4] V.S. Sokolinsky et al., "Numerical simulation of the crushing process of a corrugated composite plate", *Compos Part A Appl Sci Manuf*, 2011; 42: 1119-26.
[5] M. Giglio et al., "Investigations on sandwich core properties through an experimental-numerical approach", *Compos Part A Appl Sci Manuf*, 2012; 43:361-74.
[6] R. Seemann et al., "Numerical modeling of nomex honeycomb cores for detailed analysis of sandwich panel joints", *11th World Congress on Computational Mechanics (WCCM XI)*, 2014.
[7] Y. Chen et al., "Integrated design technique for materials and structures of vehicle body under crash safety consideration", *Struct Multidiscip Optim*, 2017; 56: 455-72.

SESSION 9A: FATIGUE / FRACTURE

DOI: 10.5075/epfl-ICSS12-2018-202-204

FATIGUE DAMAGE AND FAILURE ANALYSIS OF HONEYCOMB SANDWICH

Fahmi Alila[1], Pascal Casari[1] and François Bertrand[1]
[1]Université de Nantes, France.
Fahmi.alila@univ-nantes.fr
Pascal.Casari@univ-nantes.fr
Francois.bertrand@univ-nantes.fr

1. ABSTRACT

Fatigue behavior of sandwich structures with honeycomb core and GFRP skins is studied and failure mode is investigated through tomographic observations. The first S/N curves are presented. The second part discusses the failure modes observed during fatigue tests and responsible for stiffness decrease during fatigue tests.

2. INTRODUCTION

Fatigue of composite materials has been less studied during numerous years since these materials were known not to damage under cyclic loading (particularly entrenched reputation for materials-based carbon fiber in the world of aeronautics) [1–6]. Their use is being more and more important in many industries. However the increasingly occurrence of frequent and early failure in composite structure showed the necessity to design and study these structures also in fatigue. Thus the complex aspect of the fatigue phenomenon of composite materials and industrial interest have contributed to the further development of research on the subject over the past two decades [7–9]. In terms of complexity it can be cited for example failure modes and multi-axial stress state. The stress distribution in a composite material is often multi-axial even when subjected to a single load.

In aeronautics, the use of sandwich structures is being increased due to their weight-performance ratio. The challenge nowadays in aeronautics transport field is the reduction of energy consumption by reducing the weight of the airplane [10–12]. For equal reliability and durability and with significant weight savings compared to metal materials, new materials are trying to meet this challenge. Among these materials there may be mentioned the sandwich structures with foam or honeycomb core [13].

In this paper sandwich with GFRP faces and both L and W honeycomb orientations (Fig. 1) was studied in fatigue under 4 point bending test.

Fig. 1: Honeycomb panel sandwich and associate cells orientation.

The additional outcome of this study is the analysis of the cell orientation (L and W) effects on the fatigue life of the honeycomb structure and a tomography analysis of the honeycomb sandwich.

3. MATERIALS AND METHODS

The honeycomb sandwich beams are provided by the aircraft industry. Sandwich specimen dimensions are shown in Table 1.

Table 1: Sandwich specimen dimensions and boundary conditions.

L (length) (mm)	l (width)(mm)	h (mm)	b (mm)	tf (mm)	L2 (mm)	L1 (mm)
300	50	12.7	11.26	0.72	250	80

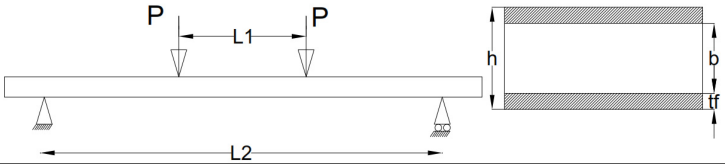

Fatigue tests were carried out through a developed four point bending testing fixture device that can test 3 specimens in the same time (Fig. 2).

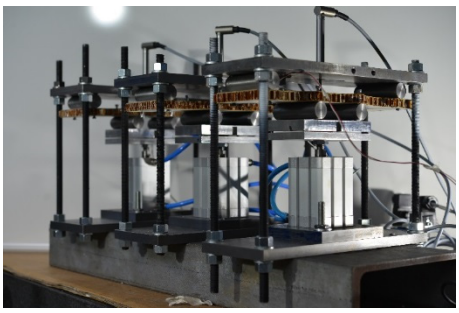

Fig. 2: Developed four-point test machine.

4. FATIGUE TEST RESULTS

Fatigue behavior of honeycomb sandwich structure is analysis based on S/N curves and fatigue damage modes. The fatigue tests were performed at conditioned temperature room made at 25°C. The test load frequency was f=2Hz and the load ratio was R=0.1. Fatigue lifetime of specimens is recognized by the number of cycles to ultimate failure. Moreover, the number of cycles from crack initiation to final fracture was in all cases short compared to fatigue life. While monitoring tests, degradation of stiffness was more affirmed due to the crack formation.

S/N curves illustrated in Fig. 3 show a qualitative comparison between the fatigue life-time of sandwich composites made of aramid fibers cores in L and W orientations cells. It appears that for honeycomb sandwich composites the lifetime of the L configuration is greater than in the W configuration at constant load level.

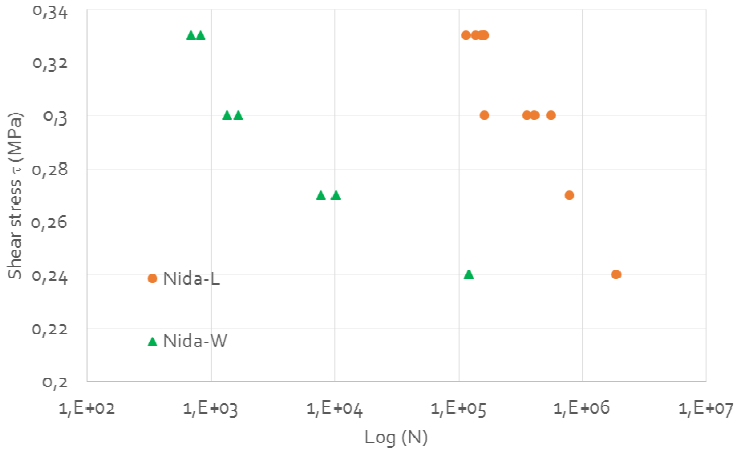

Fig. 3: S/N diagram of fatigue tests at f=2Hz.

During the fatigue test we followed the evolution of Force versus displacement in order to investigate the stiffness loss in the specimen. Different cycles were plotted in Fig. 4.

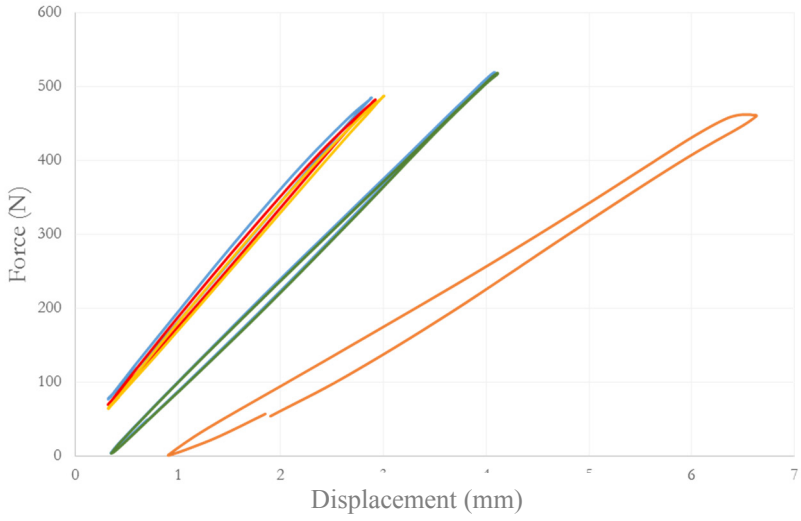

Fig. 4: Force versus displacement loops at different times during fatigue test of L type sandwich.

The loops or the hysteresis plotted in Fig. 4 demonstrate the stiffness loss of the sandwich structure during the fatigue tests. The hysteresis surface area is different from the first cycles to the last ones. This could help quantify the stiffness loss amount and also to predict the failure. The following discussions regarding the fatigue failure processes were only based on visual inspection of the damaged sections of the specimens. For our honeycomb sandwich specimens, both W and L configurations failed in shear with a crack propagation through the thickness of the core (Fig. 5) .The crack propagation in cells walls is always in the diagonal direction in the case of the L configuration and horizontal for the W one. In both cases, cracks or micro defects appear before any macro size crack is formed.

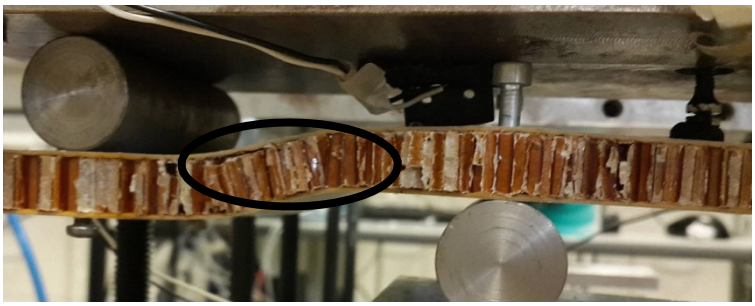

Fig. 5: Core shear failure in honeycomb sandwich at f=2Hz and 0.30 MPa.

Shear failure mode has been analysed with tomography images. 3D views are showing honeycomb cells before and after failure. One can notice cracks in the walls of the failed cell (Fig. 6).

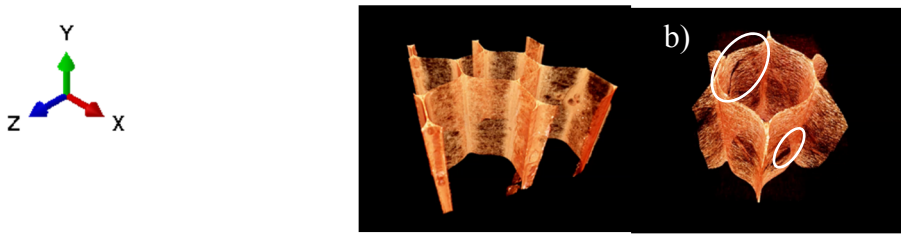

Fig. 6 : (a) 3D view of honeycomb cell before failure. (b) 3D view of honeycomb cell after failure.

5. CONCLUSION

In this paper, fatigue tests in four point bending were performed on two different honeycomb sandwich configurations. One in L cells orientation and the other in W cells orientation. The fatigue tests results were illustrated in standard S/N diagrams. It was concluded that the fatigue life time of L cells orientation is greater than W cells. Most of the specimens' failure mode was core shear failure based on cell walls cracking.

REFERENCES

[1] Jollivet T, Peyrac C, Lefebvre F. Damage of Composite Materials. Procedia Eng 2013;66:746–58. doi:10.1016/j.proeng.2013.12.128.
[2] Gibson LJ, Ashby MF. Cellular Solids: Structure and Properties. 2 edition. Cambridge University Press; 1999.
[3] Fatigue of Composite Materials: A Symposium Presented at December Committee Week, American Society for Testing and Materials, Bal Harbour, Fla., 3-4 Dec. 1973. ASTM International; 1975.
[4] An H, Chen S, Huang H. Optimal design of composite sandwich structures by considering multiple structure cases. Compos Struct 2016;152:676–86. doi:10.1016/j.compstruct.2016.05.066.
[5] Alila F, Fajoui J, Kchaou M, Casari P, Wali N, Gerard R. Mechanical characterization of sandwich composite structure using a new experimental approach. Adv Compos Lett 2016;25:117–20.
[6] Gerard R, Alila F, Fajoui J, Jacquemin F. Updated fatigue test methods for structural foams and sandwich beams. 5th High Perform Yacht Des Conf Auckl 2015.
[7] Allen HG. Analysis and Design of Structural Sandwich Panels. The Commonwealth and International Library: Structures and Solid Body Mechanics Division. Pergamon; 1969.
[8] Zenkert D. The handbook of sandwich construction. Engineering Materials Advisory Services Ltd; 1997.
[9] Dai J, Thomas Hahn H. Flexural behavior of sandwich beams fabricated by vacuum-assisted resin transfer molding. Compos Struct 2003;61:247–53. doi:10.1016/S0263-8223(03)00040-0.
[10] Carlsson LA, Kardomateas GA. First-Order Shear Analysis of Sandwich Beams. Struct. Fail. Mech. Sandw. Compos., Springer Netherlands; 2011, p. 85–101. doi:10.1007/978-1-4020-3225-7_4.
[11] Russo A, Zuccarello B. Experimental and numerical evaluation of the mechanical behaviour of GFRP sandwich panels. Compos Struct 2007;81:575–86. doi:10.1016/j.compstruct.2006.10.007.
[12] Sharma N, Gibson RF, Ayorinde EO. Fatigue of Foam and Honeycomb Core Composite Sandwich Structures: A Tutorial. J Sandw Struct Mater 2006;8:263–319. doi:10.1177/1099636206063337.
[13] Davies JM. Lightweight sandwich construction 2001:245.

DOI: 10.5075/epfl-ICSS12-2018-205-207

FATIGUE TESTING OF SANDWICH STRUCTURES USING THE SINGLE CANTILEVER BEAM TEST AT CONSTANT ENERGY RELEASE RATES

Marianne John[1], Ralf Schäuble[2] and Ralf Schlimper[3]
[1]Fraunhofer Institute for Microstructure of Materials and Systems IMWS, Germany, marianne.john@imws.fraunhofer.de
[2]Fraunhofer Institute for Microstructure of Materials and Systems IMWS, Germany, ralf.schaeuble@imws.fraunhofer.de
[3]Fraunhofer Institute for Microstructure of Materials and Systems IMWS, Germany, ralf.schlimper@imws.fraunhofer.de

1. INTRODUCTION

Cyclic Single Cantilever Beam (SCB) tests were used to characterize the fatigue behavior of interface fracture toughness of a foam core sandwich structure. First foam core sandwich structures were tested in SCB, where alternating loads were carried out. The cyclic alternating load tests were performed force-controlled with peak value control, resulting in a sinusoidal force curve and a nearly sinusoidal course of the path. Also classical fatigue tests are performed either under a constant force or constant displacement amplitude. Using this method of crack progress testing in the SCB test, the energy release rate (ERR) G increases significantly with increasing crack length until it exceeds the critical static value of the ERR and leads to unstable crack growth. In this way, only a few values within the area of stable crack growth can be determined. A better way to determine the crack growth under cyclic loads represents the Constant-G method. In this method, the crack tip is kept under almost constant stress. The necessary algorithms for this method were therefore developed. Afterwards it was implemented in the test control. Additional test specimens were tested and the method was validated on various sandwich specimens.

2. SINGLE CANTILEVER BEAM TEST

The concept of the Constant-G method is based on the experimental determination of the relationship between the compliance of the loaded sample and the crack length. The method allows calculating the ERR already during the current test from the force and displacement signals of the testing machine for each load cycle. By controlling the test force over the entire test duration, the ERR is kept constant during the crack growth (Fig. 1, left). Consequently, it is achieved that more values can be determined in the area of stable crack growth, so that a reliable determination of the fatigue crack growth by means of Paris [4] law is possible. In order to check the method, the actual crack length is recorded simultaneously on the basis of photographic documentation and then evaluated in a comparative manner .

Before the starting the test, a desired level of ERR can be set in the test software. For this, the critical ERR of the material must be known. If it is not known, preliminary tests must be carried out to determine critical ERR (G_{IC}). After each load cycle, the compliance is determined from the force and traverse path values of the testing machine. From the known relationship between compliance and crack length (see Fig.1 right), the present crack length in the sample can be calculated. Thus, it is again possible to calculate the ERR acting on the crack tip in this load cycle. In a further step, the test computer compares the calculated ERR with the default value. If both values match, a new load cycle is carried out with the same traverse path. If not, the minimum and maximum of the applied displacement must be adjusted. The basic procedure for the control is shown in Fig. 2. For two different sandwich materials (foam core and honeycomb core) the fitted equations of ERR depending on are shown.

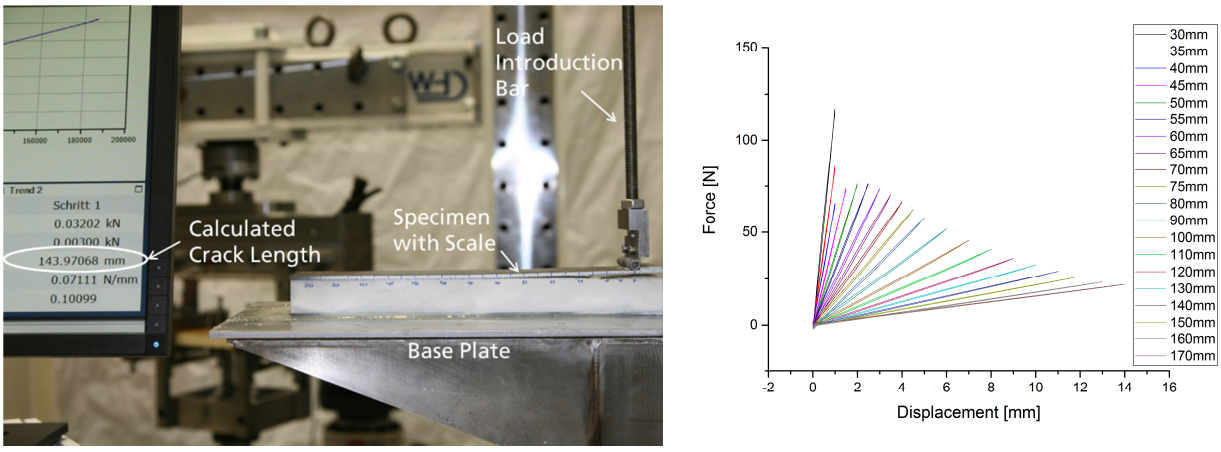

Fig. 1: Compliance of Foam Core (a) and Honeycomb Core Sandwich (b).

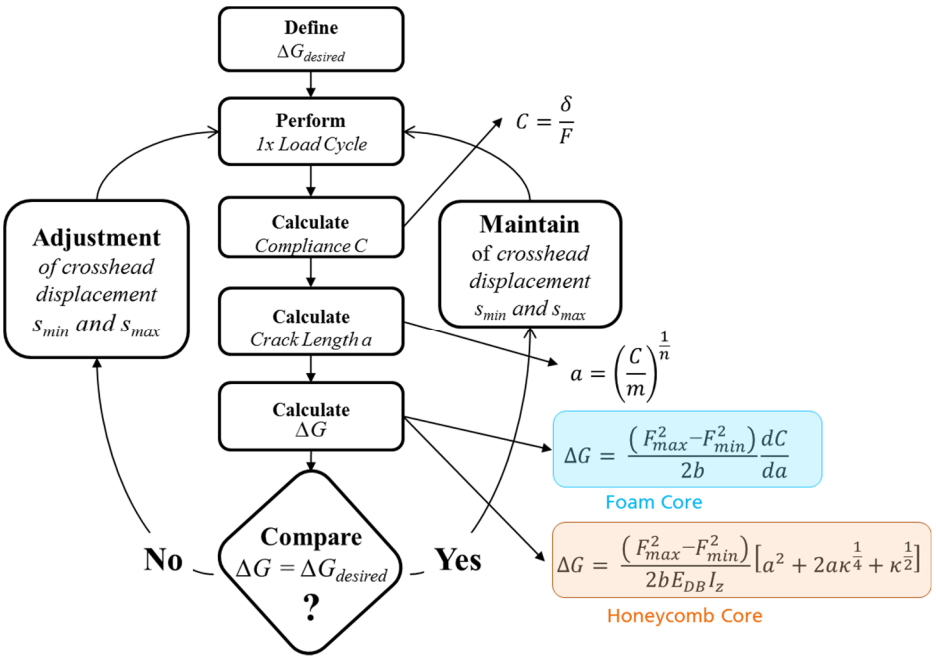

Fig. 2: Workflow of SCB-Test at constant Energy Release Rate.

In this study, all experiments were carried out path-controlled. A force-controlled procedure is also possible. In Fig.3, the control loop is illustrated by a block diagram. A setpoint of the ERR is given to the control software, which passes control signals to the test cylinder. The test cylinder extends and adjusts a traverse path, which sets a specific stress field at the crack tip. The random nature of the crack progression disturbs this stress field. This leads to a change in the actual ERR. The true ERR at the crack tip is determined indirectly via the measured force and displacement values of the testing machine. The calculated ERR is given back to the control software and compared with the setpoint to calculate the error. This closes the control loop and the control software calculates new control values for the test cylinder based on the deviation from the setpoint to actual value. The control software regulates the upper and lower limits of the traverse path _min and _max. For the upper limit, the control tries to reach _$G_{desired}$ and to select the lower limit at the same time, so that the desired force ratio R prevails. For the calculation of the ERR, three values are averaged to reduce measurement noise.

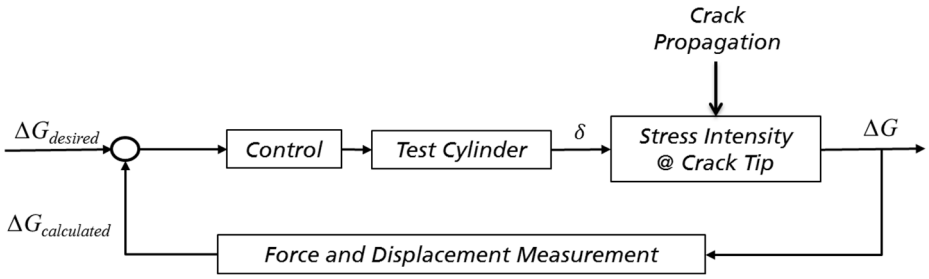

Fig. 3: Block diagram of the Constant-G method.

3. CRACK GROWTH RATE RESULTS

Analytic and experimental relationships between compliance and crack length can be used to determine the crack length. It has been shown that the calculation of the crack lengths, using the compliance of the cover layers, shows good agreement with the measured values. The ERR can be determined from these values. It is recalculated after each oscillation cycle. As a result of the experiment, the crack growth curves and the lifetime of the materials can be determined, see Fig. 4.

Overall, the Constant-G method can be seen as complementary to other fracture mechanics fatigue tests. It is particularly useful when the area of stable crack growth is very small and needs to be characterized with a high accuracy. Only a limited number of sample bodies were available for the experimental investigation. A larger sample size is recommended to optimize the method and to validate future experiments statistically.

For the exact determination of the prevailing ERR, it is important to be able to describe the correlation between compliance and crack length as precisely as possible. It turns out that this correlation differs from the calculated values, especially with large crack lengths. Dynamic measurement of the actual crack length during the SCB test would provide a more realistic view of the stress state of the crack tip. For this purpose, possible measuring methods were presented that

allow an automated determination of the crack length in sandwich materials. Time Domain Reflectometry, electrical resistance measurement, and acoustic emission measurement are promising [5,6]. The suitability and quality of these methods in relation to SCB experiments on sandwich samples should be investigated and quantified in further experiments. The range of constant crack growth that occurs for the tested material combinations within very narrow limits of ERR can be described by a higher number of measurements using the developed test method. It enables more reliable statements on crack progress behavior. This has contributed to a better understanding of the fatigue behavior of pre-damaged sandwich materials under global opening mode I loading. The applicability has been demonstrated for sandwich materials with PMI rigid foam.

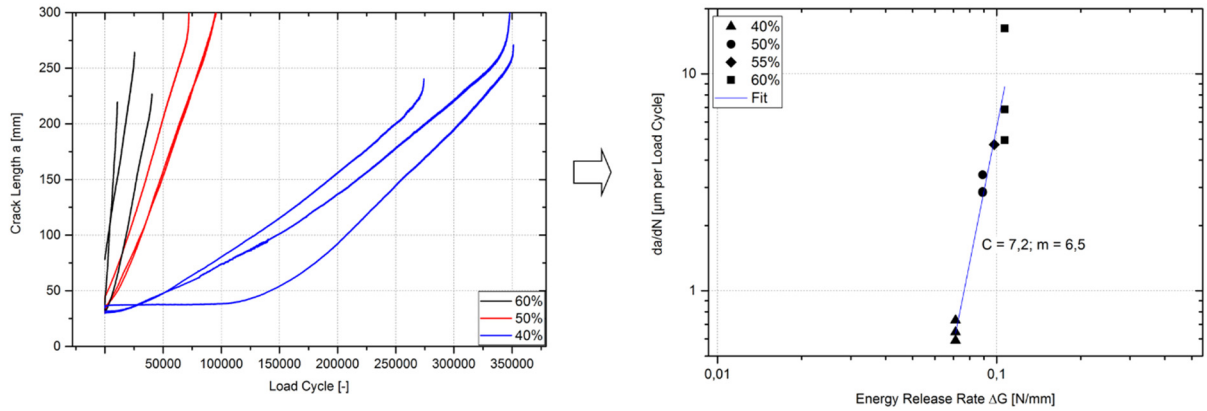

Fig. 4: Crack Length vs. Load Cycles (left), Crack Growth Diagram fitted by PARIS-law (right).

REFERENCES

[1] ASTM Draft SCB Standard, Interfacial Fracture Toughness of Peel Loaded Sandwich Constructions, Date of Revision: November 18, 2014.
[2] F. Avilés et al., Analysis Of The Sandwich DCB Specimen For Debond Characterization. Engineering Fracture Mechanics, 2008, Vol. 2, 153–168
[3] R. Krueger et al., Characterizing Facesheet/-Core Disbonding In Honeycomb Core Sandwich Structure - NASA/CR-2013-217959. 2013
[4] P. C. Paris et al., Service load fatigue damage - a historical perspective, International Journal of Fatigue, 1999, Vol.21, 35-46
[5] S. Yarlagadda et al.: An Automated Technique for Measuring Crack Propagation during Mode I DCB Testing. In: Conference: 2004 SEM X International Congress & Exposition on Experimental & Applied Mechanics Citeseer, 2004
[6] G. Deng et al.: Fatigue Crack Length Measurement Method With an Ion Sputtered Film. In: Proceedings of the 16th European Conference of Fracture, 2006, S. 1–8
[7] M. Manca et al., G-control fatigue testing for cyclic crack propagation in composite structures, Engineering Fracture Mechanics, Vol.149, p. 375-386.

DOI: 10.5075/epfl-ICSS12-2018-208-210

EXPLICIT SIMULATION OF CRACK GROWTH IN HONEYCOMB CORES OF SANDWICH STRUCTURES

Alexander Bugiel[1], Falk Hähnel[2] and Klaus Wolf[3]
Institute of Aerospace Engineering, Technische Universität Dresden, 01062 Dresden, Germany.
[1]Email: alexander.bugiel@tu-dresden.de, [2]Email: falk.haehnel@tu-dresden.de, [3]Email: klaus.wolf@tu-dresden.de

1. INTRODUCTION

High performance sandwich as used in aerospace structures typically consists of thin CFRP face sheets and Nomex honeycomb cores. Owing to the rather weak core material, this kind of structure is prone to a range of damages. While matrix cracks, fibre fracture and delamination occur in the face sheet, the cell walls of honeycomb cores are often wrinkled or crushed. Further loading of the damaged structure can initiate cracks in the core. During typical ground-air-ground cycles of airplanes, these cracks may grow further. In the worst case, this can lead finally to a complete failure of the sandwich component. Therefore, the fracture mechanical behaviour of honeycomb cores has to be considered in the damage tolerance and fatigue evaluation of aerospace sandwich structures. In this context, often the energy release rate is determined to assess the fracture behaviour of structures. This task is usually done utilizing experimental methods like the single or double cantilever beam (SCB or DCB) test [1, 2]. In order to reduce the experimental effort numerical methods are increasingly used to simulate the crack growth behaviour [3, 4]. Different fracture mechanics approaches such as the *Virtual Crack Extension* method (VCE), the *Virtual Crack Closure Technique* (VCCT) or the *Crack Surface Displacement* method (CSDE) can be applied in combination with finite element models to analyse the crack growth in honeycomb sandwich structures [4]. For the commonly used VCCT method, the structure is modelled by volumetric elements for both the core and the face sheets. Due to the large difference between the stiffness of the face sheets and the sandwich core, often large and unrealistic deformations are obtained with this approach [5]. Furthermore, previous works have shown that a homogenized model of the sandwich core cannot predict local failure behaviour correctly [6, 7].

In order to overcome these problems, this paper presents an improved approach, which is based on an explicit numerical method and a detailed sandwich core model to predict the crack growth in honeycomb sandwich structures. Layered shell elements are used to model the face sheets as well as the core cell walls. A test method has been developed and applied to characterise the crack growth of the basic core material. The investigations showed a non-negligible bridging effect of the material near the crack front. Based on this information, the material model describing the cell wall behaviour was enhanced. Finally, the structural behaviour of honeycomb sandwich specimens in SCB tests were numerically analysed.

2. MATERIAL CHARACTERIZATION

Cell Wall

The material data of the base core materials are required as input parameters for the simulation. Therefore, the mechanical material properties of the pure and the impregnated aramid paper were identified by various test methods. The in-plane tensile properties have been determined using the standardised tensile test for paper material according to DIN 1924-2. The material properties under compression and shear loading were obtained by the single curved compression test (SCCT) and the picture frame shear test [8, 9, 10].

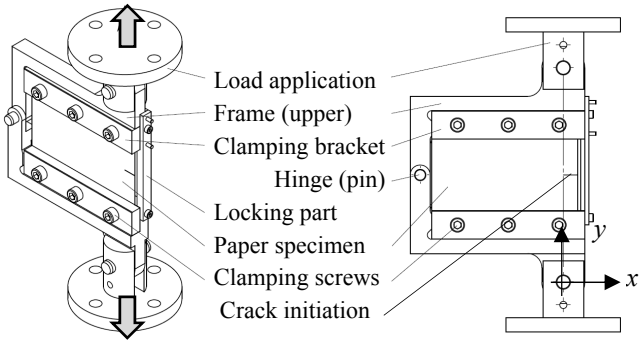

Fig. 1: Developed tear test device for paper and paper-like materials.

Investigations have shown that fibre bridging is important when failure mechanisms are considered (see Fig. 2(a)). The bridging occurs after a region reaches its maximum stress. Since the effective stiffness decreases and becomes negative, this behaviour cannot be observed using standard tensile tests. Hence, fracture toughness tests are necessary. Unfortunately, there are no suitable experimental methods for paper. Standards like the *Elmdorfer Tear* test according to ASTM D1424 and the *Brecht Imset* test according to DIN 53115 ensure only a mode III failure. Only the *Van den Akker*

tear test applies a mode I loading to paper [11]. However, due to the nature of this test the repeatability is low and the procedure is hard to simulate by finite element analysis. Therefore, a new tear test method has been developed (Fig. 1).

To ensure a pure in-plane loading, a planar test configuration has been chosen. The specimen is clamped on two frame members. An asymmetric hinge connects these parts and ensures that the clamped paper is loaded with a tensile stress distribution. Due to the hard clamping and the tensile stress distribution, it is not possible to measure the fracture toughness directly. However, the test setup can easily be simulated using finite element analysis, Fig. 2(b).

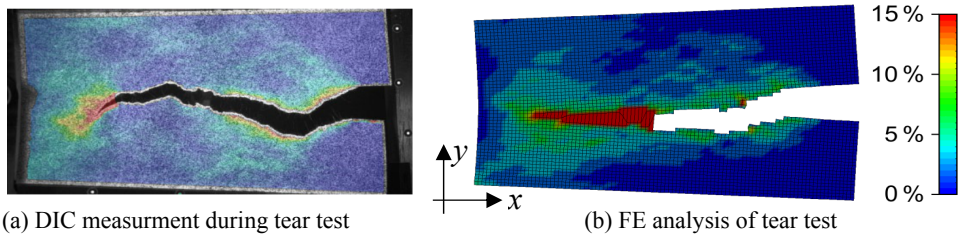

(a) DIC measurment during tear test (b) FE analysis of tear test

Fig. 2: y-strain distribution of test and simulation results for the developed tear test (y-strain).

Honeycomb Geometry

For the investigation a Nomex® honeycomb core Cormaster C1-4.8-32 provided by *Schütz GmbH* was used. The core has a cell size of 4.8 mm, a density of 32 kg/m³ and a height of 40 mm. To determine the geometrical parameters for the FE model, micro sections and pictures were made. As it turned out, the measured cross section geometry deviated considerably from an actual hexagon [6]. The investigated cores were slightly over-expanded and the single and double cell walls differed in length. In addition, local resin reservoirs existed in the transition zone from single to double walls.

CFRP Face Sheets Material

The face sheets consist of four layers of a CFRP fabric prepreg (Hexcel fabric 926 and epoxy resin 913) with an overall thickness of 1.4 mm. An AF163 adhesive film connects the face sheets with the core. The adhesive film forms a meniscus layer. Since the cracks normally grow in the honeycomb core, it can be assumed that the adhesive film does not influence the fracture mechanical behaviour.

The fabric composite material of the face sheets has been modelled using the LS-Dyna orthotropic material law for layered composites. The required mechanical properties were determined by standard test methods. Delamination interfaces between the layers were not considered, since no delamination has been observed in the experiments.

3. SCB TEST ON SANDWICH SPECIMENS

The *Fraunhofer Institute IMWS* (Halle) carried out the SCB tests [5]. The used test setup is shown in Fig. 3(a): the lower face sheet of the specimen is clamped onto a test fixture and a hinge is glued onto the upper face sheet. A rod and a loading cell connect the hinge with the upper part of a universal test machine. During the test a force F is applied to the hinge. At a critical load level, the crack starts to grow from the initiation point in positive W-direction. Once a crack length of 40 mm is reached, the upper frame part is moved back to its original position and the first loading cycle is completed. Subsequently, a second loading cycle starts until a total crack length of 80 mm. An example for the resulting force-displacement relationship is given in Fig. 3(b).

4. EXPLICIT SIMULATION

Material Model

A regressive failure model has been developed to enhance the applied user defined material model to describe the cell wall behaviour. The regressive failure process begins at the maximum stress, which is determined by a previously defined failure criterion (e.g. *Tsai-Wu* criterion). For this stress state the equivalent strain at failure $\hat{\varepsilon}_e$ is given by the effective strain

$$\varepsilon_e = \sqrt{\frac{2}{3}\varepsilon_{ij}\varepsilon_{ij}}\,. \tag{1}$$

The effective residual strain $d\varepsilon_e$ defines a region for which the material retains a residual stiffness throughout fibre bridging. In this region the stress state is attenuated. For this, a regressive attenuation factor is defined as follows:

$$f_R(\varepsilon_e) = \begin{cases} 1 & \varepsilon_e \le \hat{\varepsilon}_e \\ \left(1 - \left(\frac{\varepsilon_e - \hat{\varepsilon}_e}{d\varepsilon_e}\right)^{n_R}\right)^{1/n_R} & \hat{\varepsilon}_e \le \varepsilon_e \le \hat{\varepsilon}_e + d\varepsilon_e \\ 0 & \varepsilon_e \ge \hat{\varepsilon}_e + d\varepsilon_e \end{cases} \tag{2}$$

It becomes clear, that the regression exponent n_R defines the decreasing stress-strain behaviour for values greater than $\hat{\varepsilon}_e$ and smaller than $\hat{\varepsilon}_e + d\varepsilon_e$. Exponents greater than 1 lead to a progressive decay and values less than 1 to a digressive decay. By simulating the developed tear test, the parameters $d\varepsilon_e = 17{,}6\%$ and $n_R = 0{,}55$ could be determined, Fig. 2(b).

SCB Simulation

Simulations of the single cantilever beam test were conducted using the developed user-defined material model [8] in the explicit finite element tool LS-Dyna, see Fig. 3(c). The mesh was created with the help of the SandMesh 2.0 software which has been developed at the Institute of Aerospace Engineering of the TU Dresden. This tool allows to create finite element models including imperfections and irregularities, like those detected on the honeycomb specimens. The cell wall material has been modelled as a three-layer material with the stacking sequence phenolic resin / aramid paper / phenolic resin. Material parameters not determined in section 2 were taken from [7]. As shown in Fig. 3(b) the analysis results agree very well with the experimental data determined by *IMWS*.

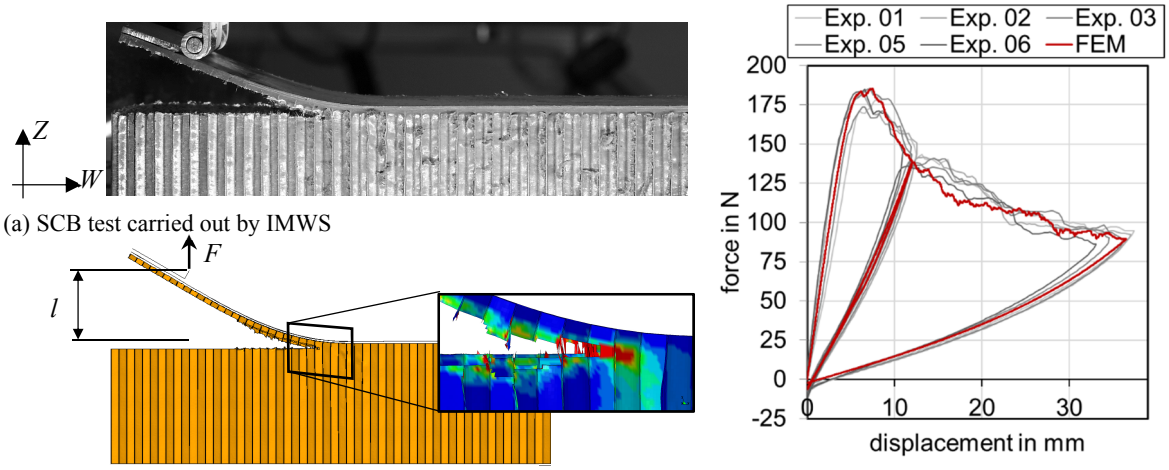

(a) SCB test carried out by IMWS

(c) FE simulation of the SCB test

(b) FEA (red) and test (grey) results

Fig. 3: Single-cantilever-beam (SCB) test, simulation and comparison of the results.

5. CONCLUSIONS

The numerical study performed in the presented research project provides an alternative to commonly used fracture mechanical analyses. The explicit simulation approach yields conclusive results and is in good agreement with experimental data. An advantage of the method is that no SCB testing is necessary to determine the energy release rate. In theory, it is possible to carry out such simulations based merely on the data of the constituent materials (i.e. aramid paper and phenolic resin) as well as on the core geometry. However, in practice it is necessary to calibrate the sandwich simulation by tensile or compressive tests of the sandwich core.

ACKNOWLEDGEMENTS

This research was performed within the project TFSanDis (03FS15017) funded by the German Federal Ministry for Economic Affairs and Energy. The simulations were performed on the Bull HPC-Cluster of the Center for Information Services and High Performance Computing (ZIH) of TU Dresden. Both the financial support and the computing capacity provided is gratefully acknowledged.

REFERENCES

[1] Martin Rinker, James G. Ratcliffe, Daniel O. Adams, R. Krueger: *Characterizing Facesheet/Core Disbonding in Honeycomb Core Sandwich Structure.* CR-2013-217959, NIA Report No. 2013-0115, Langley Research Center, Hampton, 2013.

[2] A.T. Nettles: *Measuring Core/Facesheet Bond Toughness in Honeycomb Sandwich Structures*, NASA Report, TP-2006-214713, Marshall Space Flight Center, Alabama, 2006.

[3] Z. M. Chen, R. Krueger, M. Rinker: *Facesheet/Core Disbond Growth in Honeycomb Sandwich Panels Subjected to Ground-Air-Ground Pressurization and In-Plane Loading*, ICSS-11, Florida Atlantic University, USA, 2016.

[4] C. Berggreen: *Damage Tolerance of Debonded Sandwich Structures*, PhD Thesis, Department of Mechanical Engineering, Technical University of Denmark, 2004

[5] R. Schäuble, M. Petersilge, R. Schlimper: *Single Cantilever Beam Test for Honeycomb Sandwich Materials with Very Thin Facesheets – Effects of Test Conditions and Material Properties*, ASTM Committee D30 Meeting, 2016, Williamsburg, Virginia

[6] C. Fischer et al., *Influence of Imperfections on the structural behaviour of honeycomb cores*, ECCM-17, 2016.

[7] F. Hähnel: *Ein Beitrag zur Simulation des Versagens von Honigwaben aus Meta-Aramid-Papier in schlagbelasteten Sandwichstrukturen*, PhD Thesis, TU Dresden, Shaker Verlag, 2016.

[8] A. Bugiel, F. Hähnel, K. Wolf, J. Strauß, T. Kuntzsch: *Enhanced test devices for the development of novel paper-like materials for sandwich-structures*, In: I'Anson, S. J.: Trans. XVIth Fundamental Research Symposium, Oxford, FRC, pp. 27 – 41, 2017

[9] A. Bugiel, P. Reichenbach, F. Hähnel, K. Wolf: *Prüfvorrichtung für Druckfestigkeit dünnwandiger Materialien*. Patent DE 102015100467 A1 pend., 2016.

[10] F. Hähnel, K. Wolf: *Vorrichtung für die mechanische Werkstoffprüfung zur Bestimmung der Schubkennwerte von Werkstoffen*. Patent DE 102010006163 A1, 2011.

[11] J. A.Van den Akker, W. A. Wink: *Tearing Strength of Paper. III. Tearing Resistance by the in-Plane Mode of Tear*. In: Tappi Journal 9 (1967), S. 466-470

SESSION 9B: DYNAMICS / THERMAL EFFECTS

DOI: 10.5075/epfl-ICSS12-2018-212-214

PEAK PROBABILITY FUNCTIONS FOR RANDOM DYNAMIC RESPONSE OF COMPOSITE PLATE WITH INITIAL GEOMETRIC IMPERFECTION RESTING ON ELASTIC FOUNDATIONS

Liu Liu[1] and Ming Jin[1]
[1]School of Aerospace Engineering, Beijing Institute of Technology, Beijing, PR China. liuliu@bit.edu.cn

1. INTRODUCTION

For high performance military aircrafts and future high-speed civil transport planes, certain structural skin components are subjected to very large acoustic loads under in thermal environments [1]. Some structural components are excited by the intense acoustic and thermal-mechanical loads (~1650 ºC temperature and ~180 dB Overall Sound Pressure Level, OASPL [2]). In order to protect substructure of hypersonic flight vehicle, a sandwich structure with two thin stiff and strong ceramic facesheets separated and a relatively thick, lightweight, and compliant aerogel thermal insulator has been developed as a thermal protection system (TPS). The facesheets and the relatively thick aerogel thermal insulator are bonded tightly. The current investigation focuses on the random dynamic response of the top facesheet for the TPS sandwich structure since the ceramic-based composite plate is structurally weak with low fatigue resistance and can fail easily. Thus the contribution of the relatively thick and compliant core and the bottom facesheet are treated as an equivalent elastic foundation, on which the top facesheet is resting on. Very few analyses and results have been reported regarding characterizations of strain process for thin plates subject to a combination of thermal and acoustic loadings. Peak probability function of strain process is related to acoustic fatigue life prediction [3-5]. Therefore it is of practical interest to understand in-plane strain process and peak probability function of thin top facesheet in the TPS sandwich structure under thermal and acoustic loadings. The influence of the thermal sealing material around the top facesheet in the thermal environments has been considered as the in-plane boundary constraints with the equivalent boundary compliance. Transverse initial geometric imperfection w^* in a stress-free state has been considered in the model to represent the imperfection due to plate manufacture [6].

2. THEORETICAL FORMULATION

Plate Model

The length, width and the thickness of the top facesheet plate are a, b and h, and the schematic model is shown in Fig. 1. A Cartesian coordinate $Oxyz$ is located in the middle surface of the rectangular plate with its origin at the left corner. Assume that (u, v, w) represent the displacements of an arbitrary point in the x, y and z directions, respectively. In-plane boundary constraint condition is specified only on the top facesheet of the TPS sandwich structure due to thermal sealing materials around it in thermal environments. The load-displacement relationship of the foundation is assumed to be $F = \bar{K}_1 w - \bar{K}_2 \nabla^2 w$, where F is the force per unit area, $\bar{K}_1$ is the Winkler foundation stiffness and $\bar{K}_2$ is the shearing layer stiffness, and ∇^2 is the Laplace operator in x and y.

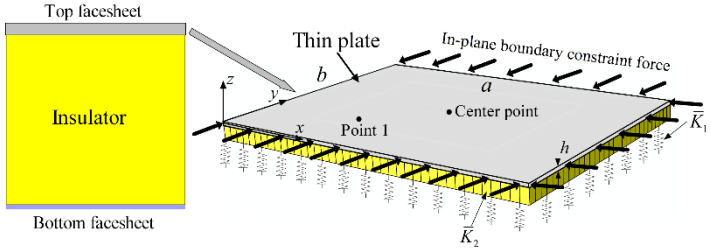

Fig. 1: The model configuration. The thin top facesheet of the sandwich TPS has been modeled as a thin plate resting on a two-parameter elastic foundation.

Modal Equations by Galerkin Procedure

The deflection function $w(x,y,t)$ is assumed to be:

$$w(x,y,t) = \sum_{i=1}\sum_{j=1} q_{ij}(t)\sin(i\pi\bar{x})\sin(i\pi\bar{y}) \tag{1}$$

where $\bar{x} = x/a$ and $\bar{y} = y/b$ and $i,j = 1,23...$are numbers of half waves in x and y directions, respectively. $q_{ij}(t)$ is the modal amplitude of the plate mode. For sake of simplicity, only sine type global type of imperfection is studied in the work. Thus,

$$w^*(x,y) = \eta\sin(\pi\bar{x})\sin(\pi\bar{y}) \tag{2}$$

The midplane nonuniform temperature field in the present work is assumed as a simplified illustration:

$$\bar{T}(x,y) = t_0 + t_0\delta\sin^2(\pi\bar{x})\sin^2(\pi\bar{y}) \tag{3}$$

Substituting Airy stress function $F(x, y, t)$ and the transverse deflection function into the governing equation, and a set of coupled nonlinear ordinary differential equations (ODEs) is developed utilizing Galerkin procedure under the classical theory of thin plates and the von Kármán type kinematic relation, and the reduced-order modal equation takes the form as following:

$$\ddot{\boldsymbol{q}} + \boldsymbol{C}\dot{\boldsymbol{q}} + (\boldsymbol{K} + \boldsymbol{G} + \boldsymbol{H} + \boldsymbol{\Theta})\boldsymbol{q} + \boldsymbol{f}(q_{ij}) = \boldsymbol{p} \tag{4}$$

Some noteworthy statements can be given from the explicit expression of the matrix term in the modal equation. For instance, $\boldsymbol{K}$ is the diagonal linear structural stiffness matrix. The diagonal linear stiffness matrix $\boldsymbol{H}$ is induced by the uniform temperature rising t_0. The symmetric and non-diagonal linear stiffness matrix $\boldsymbol{G}$ is introduced by the non-uniform temperature rising term $t_0\delta$. It is worth noting that the compliances $\boldsymbol{S}_x$ and $\boldsymbol{S}_y$ are only included in the linear stiffness matrices $\boldsymbol{H}$ and $\boldsymbol{G}$. The symmetric and non-diagonal linear stiffness matrix $\boldsymbol{\Theta}$ is induced by the geometric imperfection, and the terms are related to the imperfection η^2 size linearly. The column vector $\boldsymbol{f}(q_{ij})$ consists of the coupled nonlinear quadratic and cubic modal amplitude terms, which can be written as:

$$\boldsymbol{f}(q_{ij}) = \sum_i\sum_j\sum_k\sum_l R_{ijklrs} q_{ij} q_{kl} + \sum_i\sum_j\sum_k\sum_l\sum_m\sum_n S_{ijklmnrs} q_{ij} q_{kl} q_{mn}, i, j, k, l, m, n, r, s = 1, 2, 3... \tag{5}$$

R_{ijklrs} is the coefficient of the nonlinear quadratic modal amplitude term induced by the initial geometric imperfection, and it is linearly related to the geometric imperfection size η. $S_{ijklmnrs}$ is the coefficient of the nonlinear cubic modal amplitude term, which is induced by the coupling between in-plane stretching and transverse deflection. All nonlinear modal amplitude terms are independent with the equivalent elastic foundation stiffness and thermal effects.

In-Plane Strain Response

Total in-plane strain can be evaluated explicitly. As an illustration, the in-plane normal strain along x direction is shown as following:

$$\varepsilon_x = l_0 + \sum_i \sum_j \bar{l}_{ij} q_{ij} + \sum_i \sum_j \sum_k \sum_l \bar{\bar{l}}_{ijkl} q_{ij} q_{kl} \tag{6}$$

in which constant, linear and coupled quadratic modal amplitude terms are included. It is interesting to note that the uniform temperature rising t_0 can induce a constant in-plane strain due to the in-plane boundary constraints. The linear term is induced by the linear strain distribution due to Kirchhoff hypotheses. It includes two parts, the first part is linearly related to the out-of-plate coordinate z, and the second part is linearly related to the initial geometric imperfection size η. The foundation stiffness and the geometric imperfection effect are not included in the quadratic coefficients explicitly. It is worthy of noting that the thermal effects only contribute to the constant term l_0 and are not included in the linear and quadratic coefficients. Displacement and strain process can be given by solving the set of coupled nonlinear ODEs (Eq. 4). It is noteworthy that as the linear term $\bar{l}_{ij} q_{ij}$ dominates strain process, symmetric Gaussian displacement process results in Gaussian strain process. Thus spectral-based approaches such as Bendat's model and Dirlik narrow band model can be used to predict the sonic fatigue life. On the other hand, if strain process is governed by the quadratic term, Gaussian displacement process leads to non-Gaussian skewed strain process. Therefore the peak probability function of the strain process needs to be estimated for acoustic fatigue life prediction.

3. RESULTS

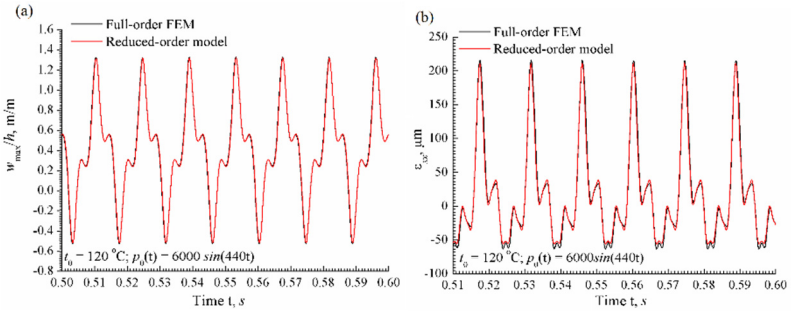

Fig.2: The displacement w_{max} and the associated in-plane strain process for the perfect plate without in-plane boundary constraints.

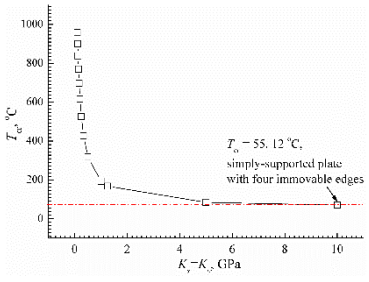

Fig.3: The critical buckling temperature variation with in-plane boundary stiffness.

The number of physical degrees-of-freedom for the structure has been reduced in the coupled modal equations using a series of basis functions to expand the deflection displacement field (Eq. 1). Thus the accuracy and efficiency of the present model depend on the number of series included in the displacement expansion function. Results showed the maximum normalized difference for the displacement is no more than 3% if four symmetric modes are included. In order to demonstrate the capability of the reduced four-mode model to yield accurate dynamic response, Fig. 2 shows the time history of the displacement w_{max} and the associated ε_x of the postbuckled plate at under the periodic excitation load. It is

noted that the displacement response as calculated by the four-degree reduced-order model is nearly identical to the solution of full-order FEA model, and only small difference can be noticed for the displacement and strain process.

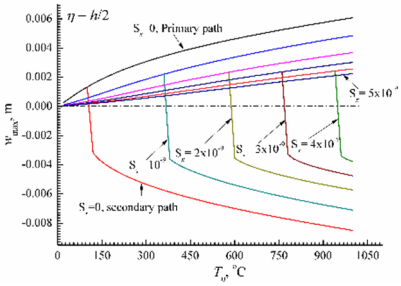

Fig.4: The displacement w_{max} and the associated in-plane strain.

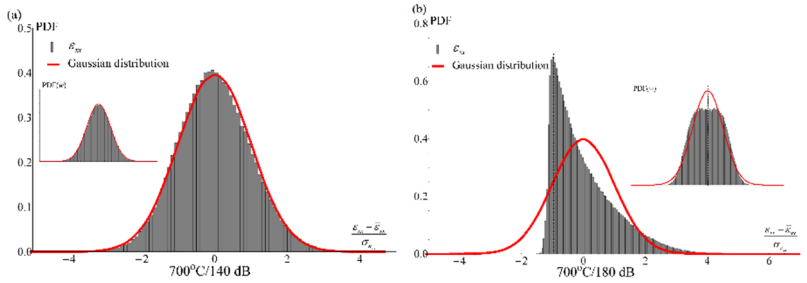

Fig.5: Histogram of in-plane strain process for the top facesheet with initial geometric imperfection and in-plane constraints. (a) 700°C/140dB; (b)700°C/180dB.

It is apparent that the thermal buckling of the perfect plate occurs when the resultant in-plane compressive force increases with an increasing of thermal effects. Both give rise to thermal expansion and induce a negative thermal stiffness under in-plane boundary constraints of the panel. The perfect plate remains flat as the applied temperature increases until it experiences a critical bifurcation (it buckles) at the critical point. Fig. 3 shows the critical buckling temperature T_{cr} variation with the equivalent in-plane boundary stiffness K_x with $S_x = 1/K_x$. It is clear that T_{cr} decreases with increasing K_x and it converges to the buckling temperature of simply supported plate with four immovable edges. The variation of the maximum deflection with the uniform temperature rising is provided for an imperfect plate in Fig. 4. Due to the effect of the initial geometric imperfection, the plate experiences a gradual deflection with t_0. Above a certain point, which is another critical state, a secondary stable equilibrium branch appears. The equilibria are unsymmetric and the occurrence of the imperfection actually postpones the onset of the critical state until a higher t_0. Fig. 5 demonstrates that due to dominant contribution of the quadratic modal amplitude terms in Eq. (5), the skewed non-Gaussian strain process can be observed for the top facesheet of a sandwich TPS structure subjected to a combination of thermal and acoustic loadings Therefore the peak probability function of the strain process is not Rayleigh distribution and a new peak probability function has to be determined.

4. CONCLUSIONS

This paper investigates the dynamic response of a thin facesheet of a TPS sandwich structure subjected to a combination of thermal and acoustic excitation. A simply-supported thin plate with initial geometric imperfection under in-plane boundary constraints resting on a two-parameter elastic foundation is proposed to characterize the behavior of the facesheet of the sandwich TPS for simplification. A theoretical reduced-order model is developed based on the thin-plate theory and the von Kármán-type relationship. Quadratic terms are included in the coupled modal equations due to initial geometric imperfection (initial curvature). It is clear that the critical buckling temperature decreases with increasing in-plane boundary stiffness. Due to the effect of the initial geometric imperfection, the plate experiences a gradual deflection with t_0. A secondary stable equilibrium branch appears above a certain point. The equilibria are unsymmetric and the occurrence of the imperfection actually postpones the onset of the critical state until a higher t_0. A skewed non-Gaussian strain process occurs due to the contribution of the quadratic term in the strain distribution. Thus the peak probability function of the steady-state strain process has to be estimated carefully with the extensive numerical analysis using the reduce-order model.

REFERENCES

[1] L. Liu, et al. "Thermal-Acoustic Fatigue of a Multilayer Thermal Protection System in Combined Extreme Environments", *Advances in Mechanical Engineering*, 2014; volume: 176891 page numbers 18.

[2] J. Lee, "Large amplitude plate vibration in an elevated thermal environment", *Applied Mechanics Reviews*, 1993;46(2): page 242-254.

[3] J-M M. Dhainaut, et al. "Nonlinear Response and Fatigue Life of Isotropic Panels Subjected to Nonwhite Noise", *Journal of Aircraft*, 43(4):975-979.

[4] A. Przekop, et al. "Nonlinear Response and Fatigue Life of Shallow Shells to Acoustic Excitation Using Finite Element", *44th AIAA/ASME/ASCE/AHS/ASC Structures, Structural Dynamics, and Materials Conferences.* 2003, 2003-1710.

[5] J. Locke, et al."Finite element large-deflection random response of thermally buckled beams", *AIAA Journal*, 28(12):2125-2131.

[6] M. Rafiee, et al. "Non-linear dynamic stability of piezoelectric functionally graded carbon nanotube-reinforced composite plates with initial geometric imperfection", *International Journal of Non-Linear Mechanics*, 2014; 59:37–51.

DOI: 10.5075/epfl-ICSS12-2018-215-217

THREE DIMENSIONAL TRANSIENT ANALYSIS OF FGM RECTANGULAR SANDWICH PLATE SUBJECTED TO THERMAL LOADING

Akbar Alibeigloo [1] and Ali Taheri Maslak[2]
[1] Department of Mechanical Engineering, Tarbiat Modares University, Tehran, Iran, abeigloo@modares.ac.ir
[2] Department of Mechanical Engineering, Tarbiat Modares University, Tehran, Iran, alith@modares.ac.ir

1. INTRODUCTION

In recent years with extensive progresses in science and technology, an extensive research has been conducted dealing with materials with novel structures. FGM materials are a new kind of composites that have been used extensively in aerospace, nuclear, biomechanics, electronic and etc. One of the main applications of FGM materials is in high temperature environments. So a major part of researches in literature have been focused on thermal stress analysis, thermal buckling, fracture mechanics and optimization, for instance Senthil and Batra [1] investigated transient thermal analysis of rectangular FGM plates using three dimensional elasticity theory, Zhong [2] analyzed the three dimensional behavior of FGM plates using state space equations. Tounsi et al.[3] Provided a static analysis of functionally graded sandwich plate using modified trigonometric shear deformation theory, Alibeigloo [4] carried out an time dependent analysis on sandwich plates based on Lord-Shulman formulation, using generalized coupled thermoelasticity. In the present study, a three-dimensional transient analysis of functionally graded rectangular sandwich plate under thermal load has been investigated. The functionally graded material is graded in thickness direction and follows exponential distribution. The plate with simply supported boundary conditions is under transient thermal load on the upper surface. The solution process is analytical and semi-analytical for simply supported boundary conditions.

2. PROBLEM DESCRIPTION

The geometry of the plate and the position of the coordinate system is shown in Fig. 1. The surface layers are made of metal and ceramics whereas the mid layer is of functionally graded material (FGM) with exponential function distribution. It is noted that the plate is under an uniform transient thermal load applied on the upper face of the sandwich plate.

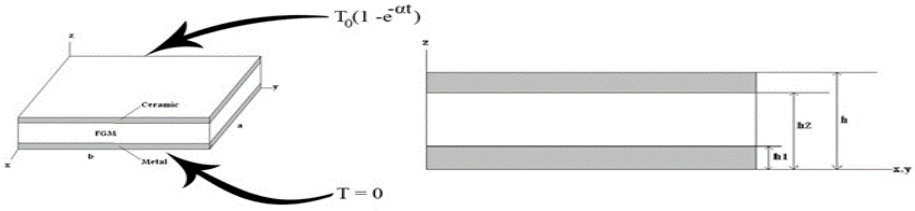

Fig. 1: Geometric diagram of sandwich plate.

Temperature Field

Heat distribution equation in the Cartesian coordinate system in General is:

$$k\frac{\partial^2 T}{\partial x^2}+k\frac{\partial^2 T}{\partial y^2}+\frac{\partial k}{\partial z}\frac{\partial T}{\partial z}+k\frac{\partial^2 T}{\partial z^2}=\rho c\frac{\partial T}{\partial t} \tag{1}$$

Properties of constituent material, Initial, and boundary conditions are:

$$b.c:\begin{cases} T=0 & t=0 \\ T=0 & z=0 \\ T=T_0(1-e^{-\alpha t}) & z=h \\ T=0 & x=o,a \\ T=0 & y=o,a \end{cases} \quad ,\{E,\rho,k,C\}=\left\{\hat{E},\hat{\rho},\hat{k},\hat{C}\right\}e^{\frac{p\times(z-h_1)}{h_f}} \tag{2}$$

And the ^ notation shows the properties of material and the P shows the index of material changes.

Now, with respect to the boundary conditions in x=0, a and y=0, b and consider the following Fourier expansion for temperature distribution and by applying Laplace transform and using Eq .2, the temperature for the FG layer and upper and lower layers of plate will be: (p2, p3, p4 shows the index of material changes.)

For FG layer:

$$T=\xi^{\frac{3-A}{2}}I(\frac{1}{2}\sqrt{1-2A+A^2+\frac{16w^2}{a^2}},\frac{2\xi}{a})\mathrm{C}_1+\xi^{\frac{3-A}{2}}K(\frac{1}{2}\sqrt{1-2A+A^2+\frac{16w^2}{a^2}},\frac{2\xi}{a})\mathrm{C}_2, A=3+\frac{2p_3}{p},$$

$$\mathrm{w}=\sqrt{{p_m}^2+{p_n}^2-a^2\left(\frac{1}{4}+\frac{p_3}{2p}\right)}, \xi=b.e^{\frac{a}{2}z}, b=\sqrt{\frac{\hat{c}\hat{\rho}s}{\hat{k}}e^{\frac{-ph_1}{h_f}}}, a=\frac{p}{h_f}, p=p_2+p_4-p_3 \tag{3}$$

For lower and upper layer respectively temperature is:

$$\begin{aligned} T_m &= C_3e^{\sqrt{K}z}+C_4e^{-\sqrt{K}z}, K=\mathrm{p}_m{}^2+{p_n}^2+\frac{C_m\rho_m s}{k_m}, p_m=\frac{m\pi}{a}, p_n=\frac{n\pi}{b} \\ T_c &= C_5e^{\sqrt{K'}z}+C_6e^{-\sqrt{K'}z}, K'=\mathrm{p}_m{}^2+{p_n}^2+\frac{C_c\rho_c s}{k_c} \end{aligned} \tag{4}$$

The parameters I and K are Bessel functions. Constants of (C1, C2, C3, C4, C5, and C6) are obtained from thermal boundary conditions.

State Space Equation Extraction

Using stress-displacement relations and governing equations of motion in the absence of body forces the state-space equations are obtained.

Analytical and Semi-Analytical Solution for a Simply Supported Plate

In the case of analytical solution, the Laplace transform is used for time, the Fourier series are used for the length and width of the plate and the state-space method is used in thickness direction. For the cases of semi-analytical solution, the differential quadrature method is used. In this case, by applying differential quadrature method in length and width directions, and by making use of state-space method in thickness direction, semi-analytical solution is presented. First, the matrix of the state space is calculated for each layer, then the boundary conditions between the layers and the continuity of the stress and displacement are applied and the general state space matrix is obtained. Finally, the equations are solved using the stress –displacement relations of the upper and lower surface of the plate. Assumed that the plate is under transient temperature on the upper surface. The boundary conditions at the upper and lower layers of the plate are:

$$\begin{aligned} &\sigma_z=0,\ \tau_{xz}=\tau_{yz}=0 \qquad z=0,\quad \sigma_x=0,\ V=W=0,\quad x=0,a \\ &\sigma_z=0,\ \tau_{xz}=\tau_{yz}=0 \qquad z=h,\quad \sigma_y=0,\ U=W=0,\quad y=0,b \end{aligned} \tag{5}$$

Vector δ and General solution of the state space equation for analytical and semi-analytical for point (i, j) respectively is

$$\frac{d\delta}{dz}=G\delta+KT,\ \delta=\left\{\bar{\sigma}_z \quad \bar{U} \quad \bar{V} \quad \bar{W} \quad \bar{\tau}_{xz} \quad \bar{\tau}_{yz}\right\}^T,\ \delta(z)=\frac{1}{\mu(z)}\left[\int_{z_0}^{z}\mu(z).k.\bar{\mathrm{T}}\mathrm{dz}+\delta(\mathrm{z}_0)\right],\ \mu(z)=e^{\int_{z_0}^{z}-Gdz} \tag{6a}$$

$$\frac{d\delta_{(i,j)}}{dz}=G_{(i,j)}\delta_{(i,j)}+kT,\ \delta_{(\mathrm{i,j})}=\left\{\sigma_{\mathrm{z_{(i,j)}}},\mathrm{U}_{(\mathrm{i,j})},\mathrm{V}_{(\mathrm{i,j})},\mathrm{W}_{(\mathrm{i,j})},\tau_{\mathrm{xz(i,j)}},\tau_{\mathrm{yz}_{(\mathrm{i,j})}}\right\}^{\mathrm{T}} \tag{6b}$$

Now consider the continuity of the boundary conditions between layers and then by applying the boundary conditions upper and lower layers of the plate transient bending of the plate will complete:

3. RESULTS AND DISCUSSION

In this section, the results obtained by solving the problem are discussed. Generally, validation and convergence are investigated. Material properties of sandwich plate of the lower surface (Aluminum) and upper surface (Silicon carbide) of the structure are listed in table 1.

Table 1: Material properties of sandwich plate.

Material	K[W/(mK)]	C[J/(KgK)]	E (GPa)	α(1/K)	ρ(kg/m^3)
SiC	65	670	427	4.3E-6	3100
AL	233	896	70	23.4E-6	2707

Besides, nondimensionalization of parameters is performed as follows:

$$t^*=\frac{t}{t_r},\mathrm{t_r}=1s,T^*=\frac{T}{T_i},U_{ij}{}^*=\frac{U_{ij}}{ph},\sigma_{ij}{}^*=\frac{\sigma_{ij}}{pk^*},\bar{\mathrm{z}}=z/\mathrm{h},\tau=\alpha t_r,a/b=1,a/h=10,T_0=200k$$

Where $p=\alpha_O\times T_0(\alpha_O=10^{-6}\frac{1}{k},k^*=1GPa)$ is valid for thermal load.

In the presented analysis, the number of terms in Fourier series is increased to converge the result of series to the final solution. In Figs .2(a) and 2(b), temperature convergence, Longitudinal displacement are illustrated respectively versus number of terms in Fourier series. In Figs. 3(a) and 3(b), the results of analytical solution and differential quadrature method for longitudinal displacement and transverse shear stress are illustrated. It can be observed that for longitudinal displacement and transverse shear stress for 9×9 and 11×11 nodes, the illustrated figures are so close which indicates acceptable convergence. By comparing the semi-analytical solution using differential quadrature method and the results obtained by analytical method, it can be inferred that the semi-analytical solution provides accurate results.

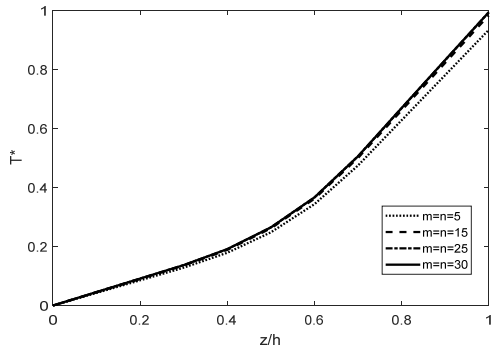

*(a) Temperature T**

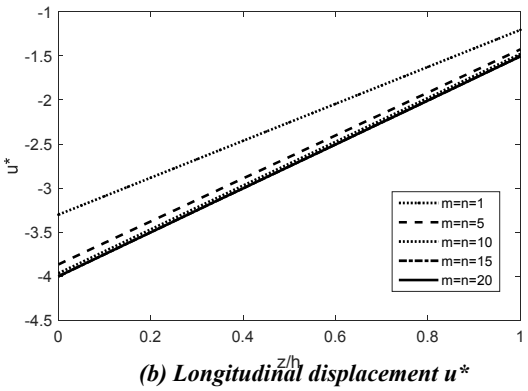

*(b) Longitudinal displacement u**

Fig. 2: Convergence of distribution, temperature, longitudinal displacement and shear stress in analytical solution.

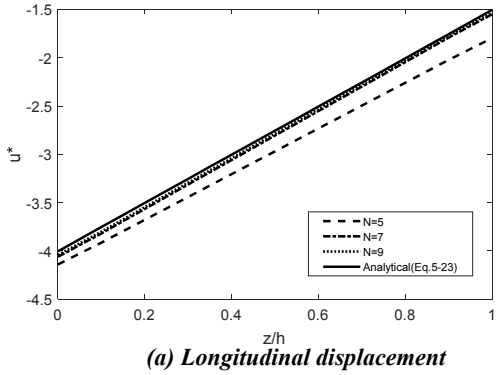

(a) Longitudinal displacement

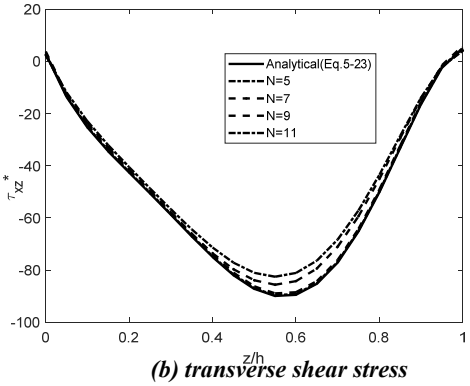

(b) transverse shear stress

Fig. 3: Convergence of distribution Longitudinal displacement and shear stress in semi-analytical solution and comparison with analytical solution at t=60s.

In order to provide validation, the results for scaled rectangular sandwich plate under thermal loading with simply supported are calculated and compared for a single layer plate according to the properties which are mentioned in reference [1]. As can be observed from Table. 2, the present results are in acceptable agreement with reference results. The differences between the values of displacement and shear stress are caused by adopting different methods for solving the problem

Table 2: Comparison of result transverse displacement obtained from analytical solution with the reference [1].

Time	0	0.25	0.5	0.75	1	1.25	1.5
Present	0	0.311	0.322	0.324	0.323	0.322	0.321
Ref [1]	0	0.318	0.32	0.32	0.32	0.32	0.32

CONCLUSIONS

The obtained results indicate that Rapid convergence is achieved in differential quadrature method, and the obtained results are in acceptable agreement with the results of analytical method.

REFERENCES

[1] Vel, S.S., Batra, R, "Three-dimensional analysis of transient thermal stresses in functionally graded plates", Int J Solids Struct, 2003; 40:7181-7196.

[2] Liu, W., Zhong, Z., "Three-dimensional analysis of simply supported functionally graded plate with arbitrary distributed elastic modulus", Tsinghua Sci Technol, 2009; 14:58-63 .

[3] Tounsi, A., Houari, M.S.A., Benyoucef, S, "A refined trigonometric shear deformation theory for thermoelastic bending of functionally graded sandwich plates", Aerosp Sci Technol, 2013; 24: 209-220.

[4] Alibeigloo, A., "Three dimensional coupled thermoelasticity solution of sandwich plate with FGM core under thermal shock", Compos Struct, 2017; 177:96-103.

DOI: 10.5075/epfl-ICSS12-2018-218-219

THERMAL NON-LINEAR RESPONSE OF SANDWICH PANELS WITH TEMPERATURE DEPENDENT PROPERTIES – AN EXTENDED HIGH-ORDER APPROACH

Yeoshua Frostig[1] and George A. Kardomateas[2]
[1]Technion-Israel Institute of Technology, Israel, cvrfros@technion.ac.il
[2]Georgia Institute of Technology, USA, george.kardomateas@aerospace.gatech.edu

The non-linear geometrical response of a sandwich panel when subjected to thermal induced deformations field with and without external loads within the framework of high-order theories such as the High-Order Sandwich Panel Theory (HSAPT) and the extended high-order theory (EHSAPT). The proposed analysis takes into account the differences in the coefficients of the thermal expansion of the face sheets and the core and considers the effects of the properties degradation with rising temperatures on the response. The mathematical formulation is based on the EHSAPT model. It includes the thermal field effects through the kinematic relations on one hand and the degradations of the properties of the core through the definition of the stress resultant – displacements relations, see similar formulation in Frostig and Thomsen [1-2]. Please notice that the constitutive relations within the core consist of moduli of elasticity and shear that are coordinate dependent. A numerical study on a specific sandwich panel is conducted and its results consist of displacements, interfacial stress and stress resultants along the panel and through its depth. A comparison with other theories such as Classical, First-Order Shear Deformation Theory (FOSDT), Ordinary Sandwich Panel Theory (OSPT) and the High-Order Sandwich Panel Theory (HSAPT). In addition, equilibria curves of temperature or load versus extreme quantities of these structural quantities along the panel are presented. The thermo-mechanical response is demonstrated for a combination of specific defined external and rising temperatures with and without degrading mechanical properties. In general, this kind of combination cause an early failure due to loss of stability.

Two cases of load transfer are investigated. In the first one the compressive in-plane load is transferred through the core only, yielding a non-uniform in-plane displacement of the entire section of the panel at its edges, and in the second case the in-plane loads are applied at the face sheets and the core simultaneous leading to a uniform end-shortening.

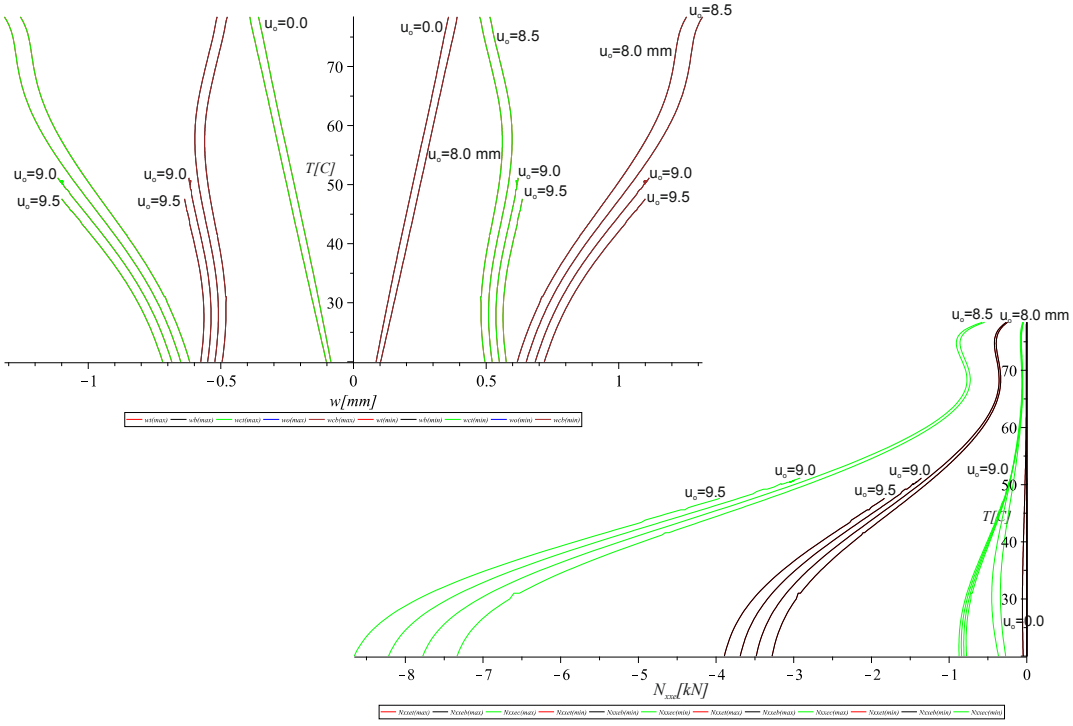

Fig. 1: Temperature versus extreme displacements for various in-plane load levels for load applied at core only, (uo=0 – temp. loading only, uo=9.5mm - 65% of failure load).

In both cases, an early failure occurs, prior to the collapse of the panel, due to temperature rise only, see Figs. 1 and 2.

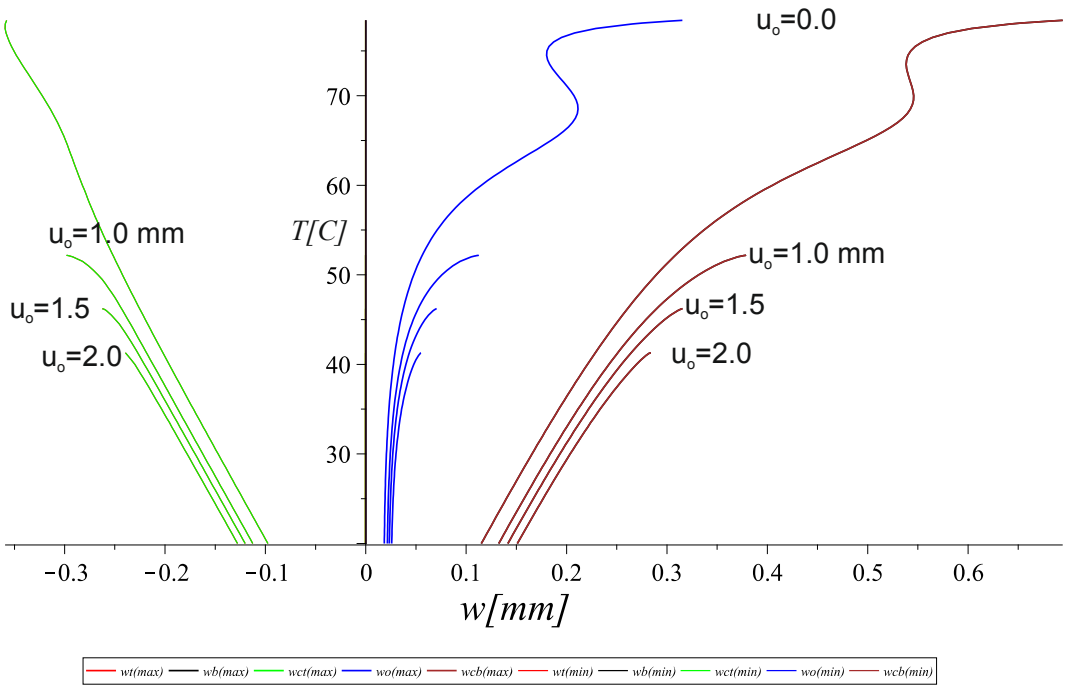

Fig. 2: Temperature versus extreme displacements for various in-plane load levels, end shortening load transfer, (uo=0 – temp. loading only, uo=2.0mm - 50% of failure load).

Please notice that the initial loss of stability (wrinkling), in both cases, occurs at temperature between 40-50ºC when external loads are applied simultaneous. Hence, the combination of load-temperature and degrading mechanical properties due to temperature must be considered simultaneously and not separately.

REFERENCES

[1] Frostig, Y. and Thomsen, O.T (2008a), "Non-linear Thermal Response of Sandwich Panels with a Flexible Core and Temperature Dependent Mechanical Properties", *Composites Part B: Engineering* (Special Issue, Ed. Y.D.S. Rajapakse, ONR), 39(1**),** 2008, pp. 165-184.

[2] Frostig Y. and Thomsen O.T (2008b) "Thermal Buckling and Post-Buckling of Sandwich Panels with A Transversely Flexible Core", *AIAA Journal*, 46 (8), Aug 2008, pp. 1976-1989

SESSION 10A: DELAMINATION / DISBOND

DOI: 10.5075/epfl-ICSS12-2018-221-222

MIXED-MODE FRACTURE CHARACTERIZATION OF HONEYCOMB CORED SANDWICH COMPOSITES USING THE DCB-UBM TEST METHOD

Christian Berggreen[1] and Vishnu Saseendran[2]
[1]Department of Mechanical Engineering, Technical University of Denmark, Denmark. cbe@mek.dtu.dk
[2] Department of Mechanical Engineering, Technical University of Denmark, Denmark. vsas@mek.dtu.dk

1. INTRODUCTION

The face/core disbond or debond problem in honeycomb core sandwich composites employed in the aerospace industry has been studied widely in recent years [1, 2]. The interface fracture toughness in a sandwich must be characterized over a wide range of mode mixities. The Double Cantilever Beam loaded with Uneven or Unequal Bending Moments (DCB-UBM) specimen, which was first introduced by Sørensen et al. [3] for monolithic laminate composite specimens and later extended for sandwich composites by Lundsgaard-Larsen et al. [4] (see Fig.1), has been proven to be robust for mixed mode fracture characterization of a typical face/core interface [5, 6]. In this work, interface fracture characterization of honeycomb cored sandwich composites is studied using the DCB-UBM test method in a recently presented novel test rig. The obtained fracture toughness values will aid in creation of reliable damage assessment models for sandwich structures in aircrafts.

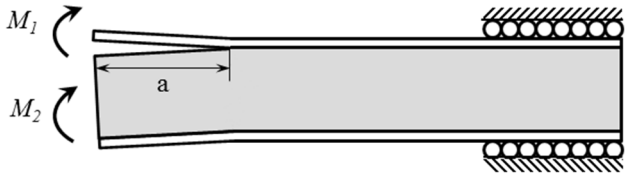

Fig. 1: Schematic illustration of DCB-UBM sandwich specimen.

The original design of the DCB-UBM test rig consisted of long wires and rollers, which made it difficult to achieve a wide range of mode-mixities. A modified novel test rig capable of applying moments to the specimen was developed and utilized for fracture characterization in this study [7]. The proposed rig consisted of two independent torsional actuators supported on rails. The actuators are able to slide independently upon crack propagation (see Fig.2). Hence, the new rig is stand-alone, compact and is able to apply high magnitudes of moment values. In addition, the current rig is able to operate in fatigue loading. It should be noted that in any DCB-UBM test rig, the mode-mixity (often expressed in terms of a phase angle, ψ) can be altered by changing the ratio of moments between the two arms, $MR = M_1/M_2$.

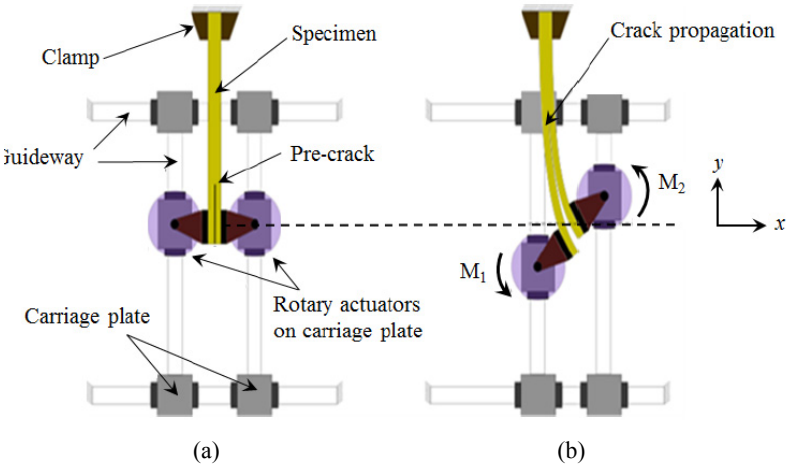

Fig. 2: Principle of the modified DCB-UBM test rig with torsional actuators mounted on rails (a) prior to start of test with a pre-crack and, (b) application of moments M_1 and M_2 causing crack propagation and crack flank displacements.

2. SPECIMEN PREPERATION AND FRACTURE CHARACTERIZATION

The sandwich specimens studied in this paper consisted of aerospace grade honeycomb cores manufactured by Schütz GmbH. Cormaster C1 type core material comprising of Nomex® T412 paper was employed with three different density classes (32, 64 and 96 kg/m^3). The cell size of all chosen cores grades was 4.8 mm. The face sheets comprised of plain weave CFRP prepreg. The DCB-UBM specimens were cut from sandwich panels which were manufactured using a one shot curing process in an autoclave. The specimens comprised of a constant core thickness (h_c = 40 mm), and two face sheet thicknesses (h_f = 0.35 and 1.4 mm) were also chosen.

In order to perform fracture testing at a constant mode-mixity phase angle, the moment ratio (MR) across the two arms must remain constant throughout the test. A dedicated controller operating based on CASCADE control was utilized which ensured that the moment ratio, MR, remained constant. When rotation is applied to Arm 1 (corresponding to M1), the CASCADE algorithm ensures that a moment M_2 is applied such that the MR is held constant. The MR value was provided as input prior to start of each test, and testing was carried out in angle control mode at a fixed rate of 10 °/min. The selection of MR corresponding to a particular mode-mixity phase angle (ψ) is based on the numerical mode-mixity method, the Crack Surface Displacement Extrapolation (CSDE) [8] method. A map of MR vs. ψ for the range of tested sandwich systems was generated using the CSDE method (see example in Fig.3(a)). The energy release rate, G, was calculated from the applied moments using the *J*-integral expressions for a DCB-UBM sandwich specimen [4]. A phenomenological expression provided by Hutchinson and Suo [9] was used to fit the experimental data (by eye).

$$\Gamma(\psi) = G_{1c}\left(1+\tan^2\left[(1-\Lambda)\psi\right]\right) \tag{1}$$

where G_{1c} is the mode I fracture toughness and Λ is dimensionless parameter.

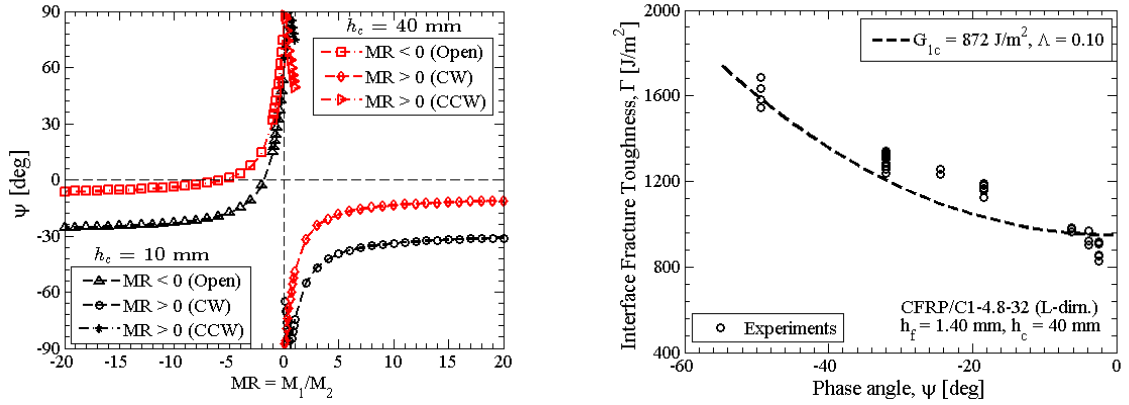

Fig. 3: (a) Moment ratio (MR), vs. phase angle (ψ) map, for a 32 kg/m^3 honeycomb core specimen (h_f = 1.40 mm), (b) interface fracture toughness (Γ) vs. phase angle (ψ) for a CFRP/C1-4.8-32 honeycomb core sandwich specimen with h_f = 1.40 mm and h_c = 40 mm, for crack propagation in the L- direction.

Interface crack propagation was observed for most of the tested specimen configurations. The variation of G vs. ψ for a CFRP/C1-4.8-32 sandwich case is provided in Fig.3(b). In order to understand the influence of core density, cell size and core paper properties on the fracture toughness, results will be provided for various classes of sandwich systems.

REFERENCES

[1] E. H. Glaessgen et al., "Debonding Failure of Sandwich-Composite Cryogenic Fuel Tank with Internal Core Pressure," J. Spacecraft and Rockets, 2005, vol. 42, no. 4, pp. 613-627.

[2] M. Rinker et al., "Characterizing Facesheet/Core Disbonding in Honeycomb Core Sandwich Structure": NASA/CR-2013-217959 NIA Rep. No. 2013-0115, 2013.

[3] B. F. Sørensen et al., "DCB-specimen loaded with uneven bending moments." International Journal of Fracture, 2006, vol. 141, no .1, pp. 163-176.

[4] C. Lundsgaard-Larsen et al.,"A modified DCB sandwich specimen for measuring mixed-mode cohesive laws". Engineering Fracture Mechanics, 2008, vol. 75, no. 8, pp. 2514-2530.

[5] V. Saseendran et al. "Fracture Characterization of PVC Foam Core Sandwich Specimen Using the DCB-UBM Test Method.", 21st International Conference on Composite Materials (ICCM-21). 2015.

[6] V. Saseendran et al. "Honeycomb Sandwich Face/Core Fracture Toughness Measurements using the DCB-UBM Test Method – DoSS Project", 2017, Technical Report, Dept. of Mechanical Engineering, Technical University of Denmark.

[7] C. Berggreen et al. "A Modified DCB-UBM Test Method for Interfacial Fracture Toughness Characterization of Sandwich Composites", 2017(manuscript under review)

[8] C. Berggreen et al. "Experimental and Numerical Study of Interface Crack Propagation in Foam-cored Sandwich Beams". Journal Composite Materials, 2007, vol. 41, no. 4, pp. 493–520.

[9] Z. Suo et al. "Mixed Mode Cracking in Layered Materials", Advances in Applied Mechanics, 1991, vol 29, pp: 63-191.

DOI: 10.5075/epfl-ICSS12-2018-223-225

ANALYSIS OF THE SCB TEST PROCEDURE APPLIED TO HONEYCOMB SANDWICH WITH THIN FACE SHEETS UNDER REPRESENTATIVE TEST CONDITIONS

Ralf Schäuble[1] and Matthias Petersilge[2]
[1]Fraunhofer Institute for Microstructure of Materials and Systems IMWS, Halle, Germany, ralf.schaeuble@imws.fraunhofer.de
[2]Fraunhofer Institute for Microstructure of Materials and Systems IMWS, Halle, Germany, matthias.petersilge@imws.fraunhofer.de

1. INTRODUCTION

Sandwich structure comprising of low density honeycomb core and thin CFRP face sheets can offer superior mechanical performance and excellent stiffness-to-weight ratio. Therefore, high performance honeycomb core sandwich construction is widely used in aerospace applications. However, this type of structure can exhibit severe damage and failure modes. One of the primary failure mechanisms of a sandwich component is face sheet/core disbonding. The face sheet can locally separate from the core structure, for example, as a result of a critical impact load. If not detected or prevented by design features, the disbond can extent to a critical size which poses a threat to the integrity of the entire structure. In recent years, numerous efforts were made to develop reliable methods to assess the damage tolerance of sandwich structures with disbond.

The disbond, or plane interface crack, respectively, can be appropriately described by means of fracture mechanics. Crack propagation is predicted if the load at the crack tip exceeds the corresponding fracture toughness of the material. The resistance of the material against crack propagation along the weakest path not only depends on the absolute load but also on the mode mixity along the crack front. The crack opening fracture mode (mode I) is assumed to be the most critical one, as known from many other composite materials. The fracture toughness of the specific sandwich material regarding a disbond damage must be determined experimentally. The Single Cantilever Beam Test (SCB), Fig. 1, is seen to be the most simple and robust test method available to determine the critical energy-release rate G_{IC} under peel load. Motivated by the high relevance of damage tolerance analysis of complex shaped and loaded lightweight sandwich structures, e.g. for aerospace application, the SCB test has been widely investigated over the last years and guidelines are available to properly apply the SCB test to various kinds of sandwich materials. Standardization of the test method is currently being prepared [1].

Nevertheless, particularly in the case of lightweight honeycomb sandwich materials with very thin face sheets, various effects are observed, which are not yet entirely understood. The proposed test conditions are still under discussion [2]. The present study was initiated not only to define optimal test condition for this specific sandwich class but mainly to understand the effect of inadequate test conditions which, for some cases, cannot be avoided. For example, if the test rig must be installed within a climate chamber, the recommended minimal length of the loading rod often cannot be realized due to limited space. Furthermore, the shape of the load/displacement response of the specimen diverges from an assumed, nominal shape, e.g. see Fig. 2, where the data reduction is based on. The reason for the deviating behavior can be the material characteristics itself, but also induced by handling errors or barely detectable, minor malfunctions of the test assembly while testing in ambitious environment, e.g. at sub-zero temperature.

In this study, typical real conditions and inadequacies were identified from a large number of SCB tests performed on honeycomb sandwich as well as examined by means of detailed Finite Element Analysis. Furthermore, proposals for suitable solutions were derived.

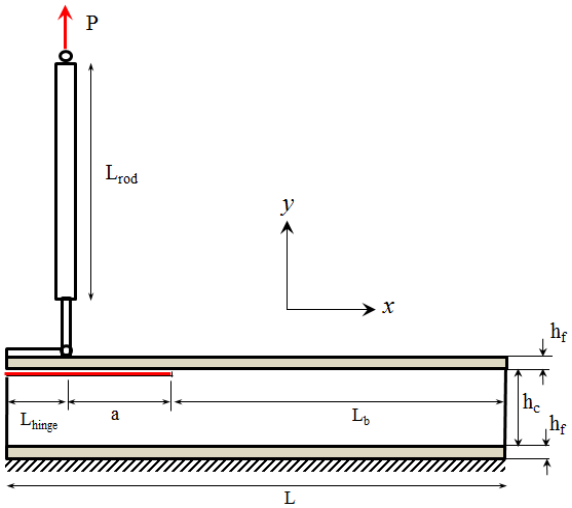

Fig. 1: Schematic illustration of the SCB test assembly.

2. SCB TEST PROCEDURE

The upper face sheet of the sandwich specimen was connected to a movable loading rod of variable length using a piano hinge. Alternatively, to avoid undesired face sheet bending near the piano hinge caused by out-of-plane torque in case of thin and flexible face sheets, a clamping device was designed to position the pivot axis in line with the neutral fiber of the cantilever beam. The lower face of the specimen is fixed to the base plate of the test rig. The specimen is loaded via the loading gear in displacement control until the crack propagates by Δa, followed by unloading the face sheet to the origin at zero displacement. The procedure is repeated several times for subsequent load cycles. Both load and displacement are recorded for each cycle, and the critical energy-release rate or fracture toughness, respectively, is obtained using the area method (AM) [1]. Images from both the left and right specimen side are recorded by two single lens reflex cameras to keep track of the crack propagation and to determine the crack length exactly after test termination. Within the first cycle, crack growth is initiated starting from a manufactured pre-crack and is converted to a natural crack in terms of shape and location. The propagation length Δa of the second and subsequent cycles are varied in order to study the influence of various test parameters. The width of the specimen is 50 mm, following the recommendations in [1], and the length is chosen to be at least 300 mm to avoid undesired shear deformation of the specimen. Fig. 3 shows a snapshot of the loaded specimen, depicting sub-interface crack propagation. The test temperature is 80°C. The sandwich is made of 32 kg/m^3 density core Cormaster C1 from Schütz GmbH and 4-layer CFRP fabric face sheet (h_f = 1.4 mm). In Fig. 2 the resulting load/displacement curve is presented.

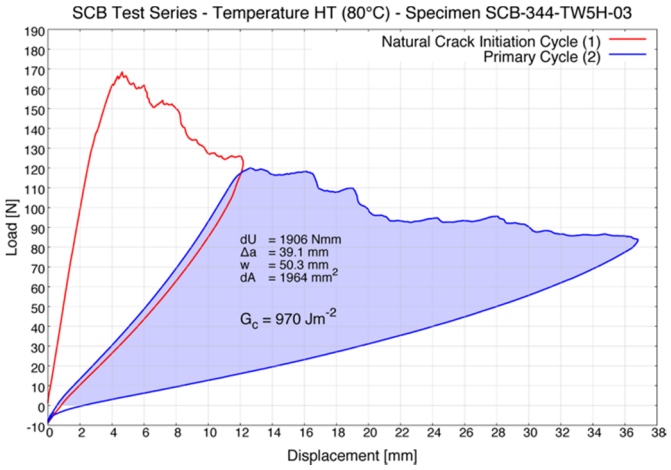

Fig. 2: Load vs. displacement curve of a 1.4 mm thick face sheet sandwich specimen from SCB test at elevated temperature.

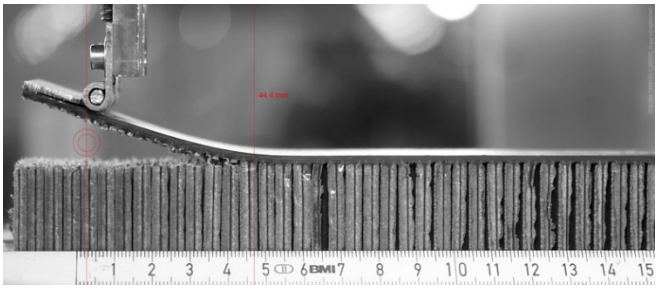

Fig. 3: Face sheet deflection at maximum stroke in load cycle 1 (1.4 mm face sheet sandwich specimen according to Fig. 2).

3. NUMERICAL MODEL OF THE SCB SPECIMEN

The SCB specimen is modelled by means of 3-dimensional solid elements for the core as well as for the face sheets using *Abaqus/Standard FEA* code. The honeycomb structure of the core is represented by a homogenized 3-d continuum. A separate study has been conducted to determine the complete set of orthotropic elastic constants as exact as possible for the honeycomb core types under consideration [3]. In particular, the in-plane Poisson's ratio of a homogenized honeycomb structure actually is close to one, $\nu_{xy} \cong 1.0$ [4], which also prevents extensive element distortion at the crack tip in case of numerical modeling. Otherwise, the Virtual Crack Closure Technique (VCCT), used to calculate the mode related parts G_I, G_{II}, and G_{III} of the total energy-release rate G, can be corrupted. Fig. 4 provides a representation of the FE model as well as detail view on element deformation at the crack tip at an intermediate load level. The graph shows simulated load/displacement curves (black) at certain crack lengths as well as corresponding energy-release rate levels. The blue graph was obtained from an experiment for comparison.

The model was designed to simulate disbond propagation both exactly at the face sheet/core interface as well as in the core underneath the adhesion layer. Various load introduction scenarios, like a piano hinge connection as well as a loading

block, can be simulated to study typical experimental assemblies. Furthermore, slip-out of the specimen from the base plate clamping jaws can be studied.

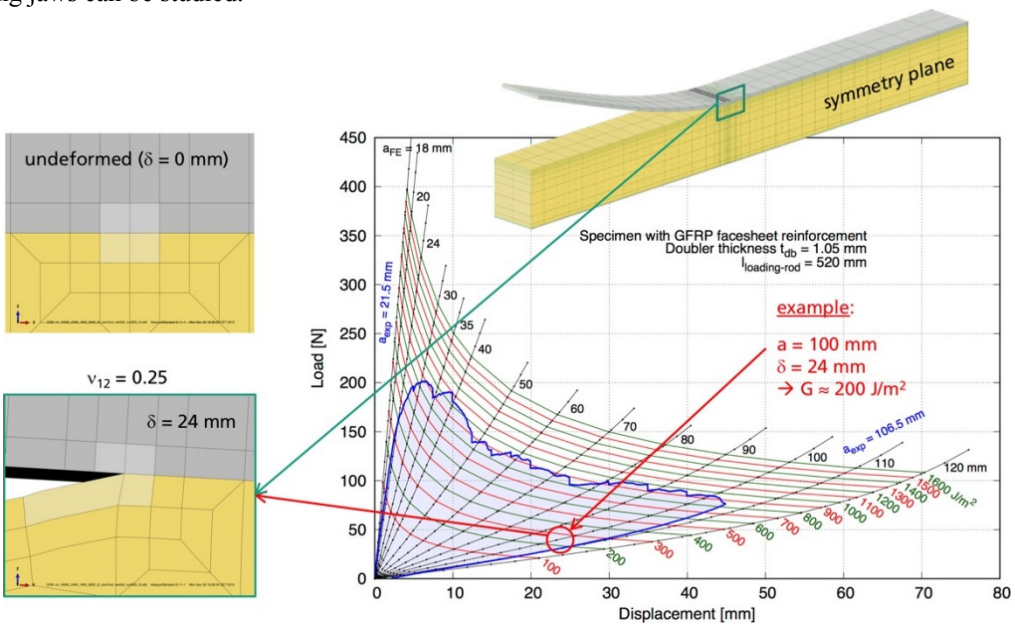

Fig. 4: 3-d FE solid model of a SCB specimen and numerically simulated behavior, compared to experiment (blue curve).

4. CONCLUSIONS

In this study, the performance of the SCB test was examined in detail by means of experimental and numerical methods to understand influencing boundary conditions and to identify the limits of applicability for low density honeycomb sandwich with very thin face sheets. The first part of the investigations was focused on certain adjustable test parameters, e.g. the loading rod length, and its effect on mode mixity for various material combinations. In the second part, typical measuring and handling errors that can occur while testing were identified and examined from a large amount of SCB tests conducted at Fraunhofer IMWS as well as based on an international round robin [5]. Examples include (a) misalignment of the piano hinge; (b) partially insufficient clamping of the specimen to the base plate; (c) bending of the face sheet at the load introduction point; and, (d) play or friction in the bearings (e.g. at sub-zero or elevated temperatures within a climatic chamber). Some of these faults are barely detectable during a running test, but can be identified from the load/displacement plot afterwards and corrected before applying the data reduction procedure. Furthermore, based on the comparison of numerous experimental and numerical results, influencing parameters of a laboratory specific test assembly on the recorded load/displacement curve - and finally on the fracture toughness - could be clearly separated from the mechanical response caused by the sandwich material. As a result, for example, an experimental procedure can be proposed to determine the proportion of energy typically dissipated during unloading, due to a mismatch of the adjacent crack surfaces, but is not related to the disbond process. This proportion then can be excluded from the data reduction, otherwise the fracture toughness will be overestimated by a certain amount. It can be shown that, for aramid honeycomb core, the fracture toughness typically is overestimated by approximately 3 up to 10 per cent when using the standard AM data reduction method without correction.

ACKNOWLEDGEMENT

This study was conducted under the ambit of *Thin Face Sheet Sandwich Disbond (TFSanDis)* project, supported with funds from the Federal Ministry for Economics and Energy, Germany.

REFERENCES

[1] D. Adams et al., “Standard Test Method for Interfacial Fracture Toughness of Peel Loaded Sandwich Constructions”, ASTM Draft Standard, 2017
[2] R. Schäuble et al., “Single Cantilever Beam Test for Honeycomb Sandwich Materials with Very Thin Facesheets – Effects of Test Conditions and Material Properties”, Proc. of the ASC: 31st Technical Conference, Williamsburg, Virginia, 2016, Paper 3208.
[3] F. Hähnel et al., “Determination of macroscopic properties of different aramid paper based honeycomb cores”, Technische Universität Dresden, Chair of Aircraft Engineering, Internal report ILR/LFT-IR17-19, Dresden, 2017
[4] L. J. Gibson et al., “Cellular Solids: Structure and Properties”, Cambridge University Press, 1999.
[5] Krueger et al., “Characterizing Face Sheet/Core Disbonding Using the Single Cantilever Beam Test: Results from an International Round Robin”, NASA Report, to be published.

DOI: 10.5075/epfl-ICSS12-2018-226-228

FRACTURE TOUGHNESS TESTING OF FOAM AND HONEYCOMB CORE SANDWICH USING THE SINGLE CANTILEVER BEAM (SCB) TEST

Mohammad Tauhiduzzaman[1], Seyed Morteza Sabet[2] and Leif A. Carlsson[3]
[1]Florida Atlantic University, FL, USA. mtauhiduzzam2016@fau.edu
[2]Florida Atlantic University, FL, USA. ssabet@fau.edu
[3]Florida Atlantic University, FL, USA. carlsson@fau.edu

1. INTRODUCTION

Sandwich structures are widely used as weight-efficient structural components, offering high stiffness-to-weight ratio. In recent years, sandwich structures are found in aerospace vehicles, aircrafts and naval structures. The applications will dictate selection of core and face sheets materials. Typical core materials are foam, honeycomb and balsa wood. Foams are open or closed cell structures depending on the processing conditions. Most applications use closed-cell foams. Honeycomb cores consist of thin walled hexagonal cells that provide sandwich panels with a very high stiffness-to-weight ratio. The performance of sandwich structures depends strongly on the bond between the face and core (F/C), and the performance may be severely reduced by propagation of a F/C debond [1]. Hence, it is important to be able to determine the debonding resistance of sandwich structures. Measurement of the static debond fracture for sandwich composites has been approached by several test methods. The SCB tests, shown in Fig. 1, is considered for ASTM standardization [2]. The SCB test consists of a sandwich specimen with a partially debonded upper face sheet. The lower face sheet is attached to the base of the test machine. A concentrated load is applied to the edge of the debonded upper face sheet and increased until the debond propagates. The test allows determination of the face/core debond toughness, expressed as the critical energy release rate, G_C .

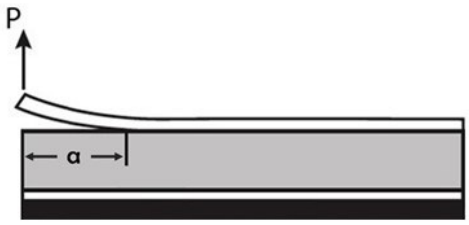

Fig. 1: Schematic of SCB test.

The aim of the present study is to investigate the face/core debonding fracture toughness of foam and honeycomb core sandwich specimens using the SCB test. Various combination of aluminum face sheets, core materials and two types of adhesives will be examined.

2. EXPERIMENTAL

PVC H100 foam core panels of 25.4 *mm* thickness were provided by DIAB. HC core panels of the type ECA- HC $3/16^{"}$ with 12.7 *mm* thickness was provided by Eurocomposites. Top face sheets made from 6061-T6 aluminum alloy of 4.76 and 6.35 *mm* thickness were used. The bottom face was also made from aluminum, same for all specimens, 3.20 *mm* thick. Some properties of face and core materials are presented in Table 1.

Table 1: Material properties of sandwich elements.

Materials	Mechanical Properties	Density (kg/m^3)
Facesheets (6061-T6 Aluminum)	$E = 68.9GPa$ $\sigma_y = 240MPa$	2700
PVC-H100 Core	$E_c = 130MPa$	100
ECA- HC $3/16^{"}$ Core (Cell Size = 4.8 *mm*)	$E_c = 140MPa$ (out of plane)	48

Sandwich SCB specimens were prepared. All HC core specimens were prepared with the L direction of the core along the specimen. The 5.1 *cm* width of the SCB specimen includes about 10 cells across the width (cell size is 4.8 *mm*). Foam and honeycomb cores were cut from large panels using a band saw. Face sheets were abraded with 120 grit

sandpaper and rinsed with acetone. The face and core materials were joined with two types of adhesives, viz. Araldite 2015, a ductile epoxy adhesive and Hysol LOCTITE EA 9309.3NA, a structural paste epoxy adhesive. The length of all SCB specimens prepared by Araldite was $305\ mm$. The SCB specimen assembled with Hysol adhesive was $203\ mm$ in length. An artificial precrack was defined by placing a ($250\ \mu m$) Teflon film of $3.18\ cm$ length between the core and upper face sheet at the edge of the specimen. To accommodate load application, a hinge was mechanically attached to the top face sheet at the precracked end of the specimen.

A WTF SCB test fixture was mounted to the base of a Tinis-Olsen test frame of $133\ kN$ load capacity. A $30\ cm$ long loading rod pinned at both ends attached to the moving crosshead of the test machine and the loading tab at the edge of the face sheet. Displacement was measured by a linear voltage differential transducer (LVDT). Load was recorded by a $13.3\ kN$ load cell mounted on the moving crosshead. The test matrix is presented in Table 2.

Table 2: Test program of sandwich specimens.

Sandwich Specimen	# Replicate Specimens	Core Thickness (mm)	Specimen Designation	Adhesive	Top Face Thickness (mm)	Length (mm)
PVC H100 Foam Core	3	25.4	PVC 1	Araldite	6.35	305
			PVC 2			
			PVC 3			
	2	25.4	PVC 4	Hysol	4.76	203
HC Core $3/16"$	2	12.7	HC 1	Araldite	6.35	305
			HC 2			305
	2	12.7	HC 3	Hysol	4.76	203

Testing was conducted at a crosshead speed of $2.5\ mm$/min. Load-displacement data was recorded throughout the test using a LabVIEW data acquisition system. Crack growth was monitored by visual observation of the crack tip region on both sides of the specimen. The location of the crack front was marked by pencil after each cycle to allow subsequent determination of the crack length. Although the first load-unloading cycles tented to be unstable, subsequent cycles were more stable, and the crack was allowed to grow in increment of about $1-2\ cm$. Crack length was measured on both sides of the SCB specimens. For each cycle, the difference in crack lengths on both sides of the specimen should be less than $10\ mm$.

SCB testing on sandwich specimen produces a number of loading-unloading cycles. The load-displacement curves were evaluated in terms of compliance and critical load. Fracture toughness is here expressed as the critical value of the energy release rate, G_C. Modified beam theory (MBT) and area methods [2-4] were used to determine G_C. The MBT toughness value, G_C, is referred to as initiation toughness. The area method provides a direct measure of G_C from the energy dissipation required to achieve a disbonded area increment ΔA. The fracture toughness G_C represents an average value including both initiation and propagation of the crack.

3. FRACTURE TOUGHNESS RESULTS

The fracture toughness was evaluated for all SCB specimens tested to date. Table 3 summarizes the fracture toughness results for the six tested SCB specimens and mode of crack propagation. MBT fracture toughness values are less than those reduced using the area method. Part of the reason for the low G_C values is the definition of P_C (onset of nonlinear response). The nonlinear response of the HC core specimens, also contributed to uncertainly in the compliance determination.

The crack propagation behavior in the PVC1 and PVC2 specimens reveal substantial extent of interfacial debonding followed by kinking of the crack into the core. The interface propagation corresponds to very low G_C values. In the PVC3 specimen, crack propagation occurred inside the core resulting in high G_C values. Similarly, for the PVC4 specimen, the crack propagated inside the core which provides very high G_C values. For the HC1 and HC2 specimens, the crack front consistently traveled through the face/core interface. Crack propagation at the face/core interface and the low G_C values indicate that the adhesive bonding is weak.

Table 3: Summary of face/core fracture toughness.

SCB Specimens	MBT G_C (kJ/m^2)	Area G_C (kJ/m^2)	Mode of Crack Propagation
PVC 1	0.351	0.606	Interfacial + Kinking
PVC 2	0.179	0.364	Interfacial + Kinking
PVC 3	0.734	0.956	Kinking
PVC 4	~	(2.68)*	Growth into Core
HC 1	0.133	0.346	Interfacial
HC 2	0.116	0.291	Interfacial

*) questionable due to nonlinear response.

Fracture toughness results (Table 3) may be compared with previously published fracture toughness data for similar sandwich specimens. Li and Carlsson [5] conducted TSD tests on PVC H100 foam core sandwich specimens. Compliance calibration method was utilized to determine G_C values that raged from $180-415$ J/m^2, in reasonable agreement with our results. Ratcliffe and Reeder [6] tested SCB specimens with carbon and glass fiber face sheets and Nomex honeycomb cores. The G_C values obtained from MBT method ranged between $960-1420$ J/m^2, much higher than our results, which points to inadequate adhesive bonding in our HC core specimens. This was also evidenced by lack of propagation inside the HC core specimens. Rinker et al. [1] conducted SCB tests on Nomex HC core specimens with 3.2, 4.8, 6.4 and 9.5 mm cell size. The crack propagation in the specimens with 3.2 and 4.8 mm cell size occurred near the face/core interface within the core. The fracture toughness was in the range from 700-800 J/m^2. Hence, these results seem to further support weak bonding in our HC core specimens.

ACKNOWLEDGEMENT

Support from NIA/FAA and ONR is gratefully appreciated. The NIA program manager, Dr. Ronald Krueger, and FAA program manager Dr. Zhi-Ming Chen provided also useful technical support. This research is partly managed by Dr. Yapa Rajapakse from ONR. We also wish to thank DIAB (James Jones) and Euro-Composites (Barry Millward) for donation of core materials.

REFERENCES

[1] M. Rinker et al., "Characterizing Facesheet/Core Disbonding in Honeycomb Core Sandwich Structure", *NASA Technical Publication* TP-2013-21 2013.

[2] ASTM Standard XXXXX-XX, Draft Standard "Interfacial Fracture Toughness of Peel Loaded Sandwich Constructions," American Society for Testing and Materials, March 9, 2017.

[3] ASTM Standard D5528- 01, "Mode I Interlaminar Fracture Toughness of Unidirectional Fiber-Reinforced Polymer Matrix Composites," *American Society for Testing and Materials*, 2007; ASTM Annual Book of Standards, Vol. 15.03.

[4] K. Shivakumar et al., "In situ fracture toughness testing of core materials in sandwich panels", *Journal of Composite Materials*, 2004; 38(8):655-668.

[5] X. Li et al., "The tilted sandwich debond (TSD) specimen for face/core interface fracture characterization", *Journal of Sandwich Structures and Materials*, 1999; 1(1):60-75.

[6] J. Ratcliffe et al., "Sizing a single cantilever beam specimen for characterizing facesheet–core debonding in sandwich structure", *Journal of Composite Materials*, 2011; 45(25):2669-2684.

DOI: 10.5075/epfl-ICSS12-2018-229-231

FRACTURE CHARACTERIZATION OF AEROSPACE GRADE HONEYCOMB CORE SANDWICH USING SCB AND DCB-UBM TEST METHODS – A COMPARISON

Ralf Schäuble[1], Yannick Albertone[2], Vishnu Saseendran[3], Christian Berggreen[4] and Ralf Hilgers[5]
[1]Fraunhofer Institute for Microstructure of Materials and Systems IMWS, Halle, Germany. ralf.schaeuble@imws.fraunhofer.de
[2]DuPont International Operations, Geneva, Switzerland. yannick.albertone@dupont.com
[3]Department of Mechanical Engineering, Technical University of Denmark, Denmark. vsas@mek.dtu.dk
[4]Department of Mechanical Engineering, Technical University of Denmark, Denmark. cbe@mek.dtu.dk
[5]Airbus Operations GmbH, Hamburg, Germany. ralf.hilgers@airbus.com

1. INTRODUCTION

Honeycomb core sandwich composites are attractive for aerospace applications due to its high specific bending stiffness. The sandwich technology has been widely utilized in flight control surfaces and interior of the aircraft, which have accumulated significant amount of flight hours. In addition, a considerable proportion of the modern day commercial aviation fleet comprises of sandwich constructions, employed both in primary as well as secondary aircraft structures. One of the primary failure mechanisms of a sandwich component is face sheet/core debonding, which can pose a risk to compromise of the integrity of the entire structure. In recent years, several structural failures have been caused due to debonding [1]. The disbond growth is influenced primarily by face sheet and core material characteristics, interface properties, face sheet and core thicknesses, geometric dimensions as well as the operating conditions.

The operating loading conditions determine the inclination of the crack to propagate along the interface or to kink into the core. Therefore, the interface fracture toughness must be ascertained accurately to be used in the development of reliable sandwich damage assessment tools. Due to the inherent elastic mismatch across the sandwich face sheet/core interface, the crack propagation will be invariably under mixed mode conditions [3]. Hence, the fracture toughness must be mapped for a range of mode mixity conditions, spanning from pure mode I to mode II. As with laminates, a peel load scenario corresponding to a mode I dominant loading is the most critical failure mode in sandwich composites. The Single Cantilever Beam (SCB) sandwich specimen [4] applied to sandwich composites has been found as the most suitable test method to obtain peel dominant interface fracture toughness. In addition, the Double Cantilever Beam loaded with Uneven or unequal Bending Moments (DCB-UBM) specimen, which was first introduced by Sorensen et al. [5] for laminate composites and later extended to sandwich composites by Lundsgaard-Larsen et al. [6] have been proven to be effective for mixed mode fracture characterization. Fig. 1 provides a schematic illustration of both SCB and DCB-UBM sandwich specimens.

In this study, interface fracture toughness of aerospace grade honeycomb core specimens is investigated for a variety of material combinations and environmental conditions using SCB sandwich specimens. DCB-UBM tests were carried out on a subset of specimens and adjusted to constant mode I loading for the purpose of validation. The study aims to understand the influence of honeycomb core density, crack propagation direction, face sheet thickness and honeycomb core material on the interface fracture toughness. Moreover, mode I fracture toughness is also compared against room, sub-zero and elevated temperatures. The investigated sandwich specimens comprised of Cormaster C1 and CN1 type cores from Schütz. The face sheets were made from CFRP prepreg (Hexcel fabric with HexPly®913 epoxy resin).

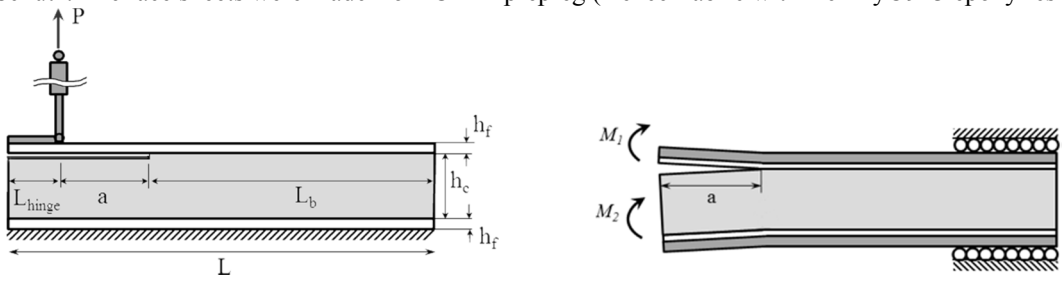

Fig. 1: Schematic illustration of (a) SCB sandwich specimen, (b) DCB-UBM specimen reinforced with doubler layers.

2. SCB TEST PROCEDURE

The SCB test involves loading the upper face sheet in displacement control until the crack propagates by certain Δa, followed by unloading the face sheet to a zero displacement level. Both, load and displacement, are recorded for each cycle, and the critical energy-release rate or fracture toughness is obtained using the area method (AM) [7]. An image recording device is used to ascertain the crack location. A two-cycle loading/unloading approach is adopted. The first cycle with Δa = 20 mm is made such that the manufactured pre-crack is converted to a natural crack front. The second cycle consists of Δa = 40 mm, which is used to deduce the fracture toughness. Fracture testing of SCB specimen was

conducted by loading the face sheet at a constant rate of 5 mm/min. Fig. 2 (a) shows interface crack propagation in a Cormaster C1 core specimen with a 4-layer CFRP fabric face sheet (h_f = 1.4 mm).

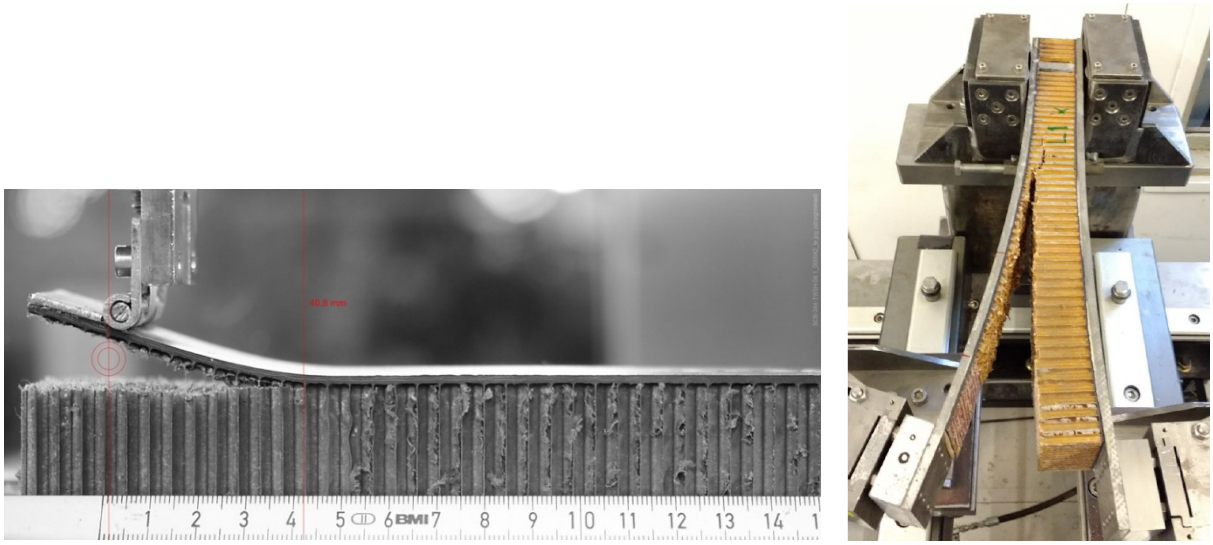

(a) *(b)*

Fig. 2: Interface crack propagation in Cormaster C1 honeycomb core, (a) SCB, (b) DCB-UBM sandwich specimen.

3. DCB-UBM TEST PROCEDURE

In the DCB-UBM test procedure, pure moments are applied on the crack flanks, see Fig. 1 (b). The mode-mixity, expressed using phase angle (ψ) is held constant by keeping the ratio of moments between the two arms constant. A numerical mode-mixity method, Crack Surface Displacement Extrapolation Method (CSDE) [8] is used to select the moment ratio (MR) corresponding to a mode-mixity phase angle (ψ). A unique test rig capable of applying edge moments based on independent torsional actuators is employed. The MR value obtained for each sandwich configuration is provided as input prior to each test. The test rig is programmed such that the ratio of moments is held constant throughout the crack propagation. For the DCB-UBM sandwich specimen, a dedicated crack monitoring device is not necessary as the energy-release rate in a moment loaded specimen is independent of crack length. Steel doubler layers were attached to both sides of the specimen, which reduced the excessive rotation of the specimen. The specimen is loaded at a constant rate of 10 deg/min and unloaded manually when the crack propagates approximately 10 mm. Interface crack propagation in a Cormaster C1 core DCB-UBM specimen is shown in Fig. 2 (b).

4. CONCLUSIONS

The mode I fracture toughness data can be seen to be consistent at room, sub-zero and elevated temperatures. It was found that production process can influence the performance of sandwich structures along with the operating environment. The investigation carried out signifies the impact of environmental factors, such as humidity and temperature, have on the interface fracture toughness. The crack path was observed to shift slightly depending on the test temperature. At room temperature, the crack was found to advance just beneath the meniscus layer (face sheet/core transition region). Fig. 3 presents a summary of the impact of temperature on fracture toughness G_{IC} for different sandwich materials in the range of -55°C to 135°C. The SCB test results were validated exemplarily at room temperature for the Cormaster C1 and CN1 4.8 mm cell width core types by using the DCB-UBM test method, adjusted to mode I condition. Fig. 4 summarizes the effects of the core density and core orientation at room temperature for sandwich specimen comprising a 4-layer CFRP face sheet and Cormaster C1 cores with densities of 32 kg/m^3, 64 kg/m^3 and 96 kg/m^3. The study was carried out throughout three different labs (marked with colors green, black and red in Fig. 4). The majority of specimen was tested without preconditioning using SCB and DCB-UBM procedures. Furthermore, a number of SCB specimen was preconditioned at 60% relative humidity before testing. It can be seen that, for all considered core densities, disbond propagation in L (ribbon) direction yields lower fracture toughnesses than in W (expansion) direction. Increased humidity can reduce the fracture toughness, albeit the effect evidently seems to depend on the specific cell wall material. Moreover, for higher density core the measured fracture toughness became more sensitive to the test method. In general, due to the use of stiff steel doublers in DCB-UBM test the face sheet bending deformation in the immediate vicinity of the crack tip is significantly lower than in the case of SCB specimen, which obviously can affect the fracture process. Moreover, from the comparative study it can be remarked that the interface fracture toughness is a material property.

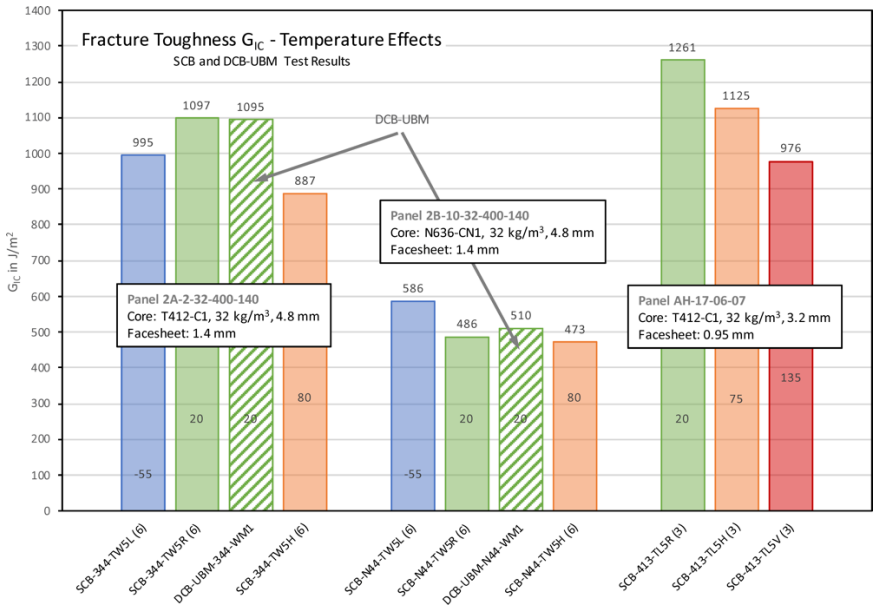

Fig. 3: Summary of temperature impact on fracture toughness G_{IC} for different core types with same density.

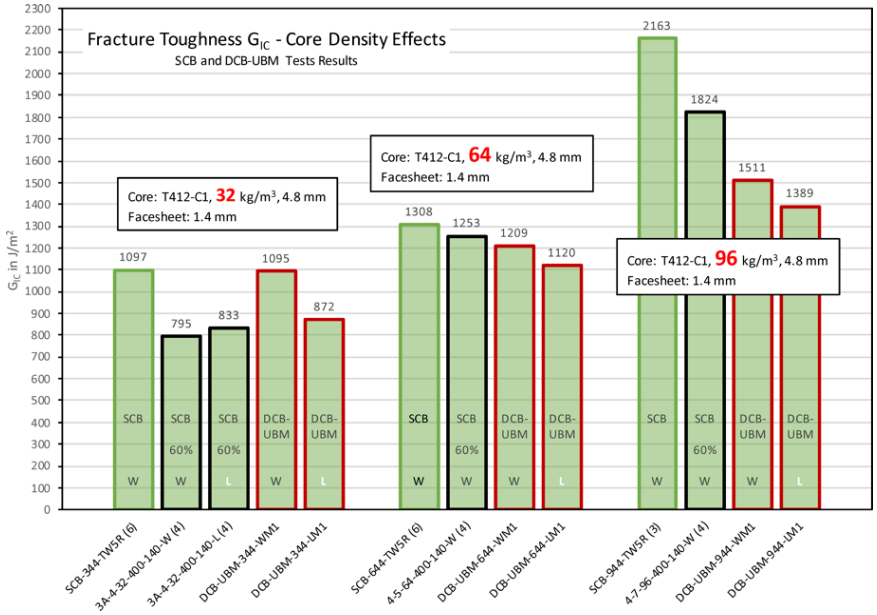

Fig. 4: Summary of core density, core orientation and humidity impact on fracture toughness G_{IC}.

ACKNOWLEDGEMENT

This study was conducted under the ambit of *Disbond of Sandwich Structures* (DoSS) project, funded by the European Aviation Safety Agency (EASA), as well as in collaboration with the *Thin Face Sheet Sandwich Disbond* (TFSanDis) project, supported with funds from the Federal Ministry for Economics and Energy, Germany.

REFERENCES

[1] Transportation Safety Board of Canada, "Loss of Rudder in Flight", Aviation Investigation Report A05F0047: Minister of Public Works and Government Services, Canada, 2007.
[2] E. H. Glaessgen et al., "Debonding Failure of Sandwich-Composite Cryogenic Fuel Tank with Internal Core Pressure", JSR, 2005, vol. 42, no. 4, pp. 613-627.
[3] J. W. Hutchinson et al., "Mixed mode cracking in layered materials", Adv. Appl. Mech., 1991, vol. 29, pp. 63-191.
[4] W. J. Cantwell et al., "A test technique for assessing core-skin adhesion in composite sandwich structures", J. Mater. Sci. Let., 1994, vol. 13, no. 3, pp. 203-205.
[5] B. F. Sørensen et al., "DCB-specimen loaded with uneven bending moments", Int. J. Fract., 2006, vol. 141, no .1, pp. 163-176.
[6] C. Lundsgaard-Larsen et al., "A modified DCB sandwich specimen for measuring mixed-mode cohesive laws", Eng. Fract. Mech., 2008, vol. 75, no. 8, pp. 2514-2530.
[7] "Preliminary Round Robin SCB Test Procedure - ASTM Preliminary Standard", 2015.
[8] C. Berggreen et al., "Experimental and numerical study of interface crack propagation in foam-cored sandwich beams", J. Compos. Mater., 2007, vol. 41, no.4, pp 493-520.

DOI: 10.5075/epfl-ICSS12-2018-232-234

MIXED-MODE QUASI-STATIC FRACTURE BEHAVIOR OF GFRP/BALSA SANDWICHES

Moslem Shahverdi[1,2,3,*], Anastasios P. Vassilopoulos[1] and Thomas Keller[1]
[1]Composite Construction Laboratory CCLab, EPFL, Station 16, CH-1015 Lausanne, Switzerland
[2]Empa, Swiss Federal Laboratories for Materials Science and Technology, Switzerland
[3]School of Civil Engineering, University of Tehran, Iran
E-mails: moslem.shahverdi@empa.ch; anastasios.vasilopoulos@epfl.ch; thomas.keller@epfl.ch

1. INTRODUCTION

Fiber-reinforced polymer (FRP) decks are resistant to corrosion, while being lightweight and allow the rapid installation of new, and widening or upgrading of existing bridges by replacing heavy concrete decks [1]. FRP decks include two main categories: pultruded decks and sandwich decks. Sandwich decks frequently exhibit significant technical advantages over pultruded decks, such as greater geometrical flexibility. Sandwich decks consist of two face sheets and either honeycomb or foam cores reinforced with internal FRP webs for shear resistance. Compared to the honeycomb structure and sandwich structures with foam core, an alternative material that has high shear capacity and can provide uniform support to the face sheets in composite sandwich bridge decks is balsa wood. This material has been used for the construction of the Avançon Bridge deck, installed in Bex, Switzerland, 2012 [2].

Although this material configuration (FRP/Balsa) is widely used in several applications, numerous questions regarding its fracture behavior still need to be addressed. Understanding and modeling of the fracture behavior of these systems is necessary for the efficient design of engineering structures. Mixed-Mode fracture is observed in actual loading conditions, of sandwich structural components. The most commonly used specimen for the characterization of the mixed-Mode I/II fracture behavior of composite sandwiches is the mixed-Mode bending (MMB) specimen. The MMB specimen proposed by Reeder and Crews [3] is a combination of the double cantilever beam (DCB) and the end notched flexure (ENF) specimen, both standardized specimens for measuring pure Mode I and Mode II interlaminar fracture of unidirectional laminates respectively. A wide range of Mode I and Mode II loading combinations can be experimentally investigated by the MMB configuration. The partitioning of the experimentally obtained total strain energy release rate, G_{tot}, into the G_I and G_{II} when mixed-Mode conditions exist is challenging [4-5], especially in asymmetric specimens.

In the current study, quasi-static mixed-Mode fracture experiments have been performed in order to study the behavior of bridge deck sandwich panels composed of GFRP skins and balsa wood core. In the current study, the components of strain energy release rate were calculated using the extended global method that was developed for the asymmetrical mixed-Mode specimens in [4].

2. EXPERIMENTS

The specimens were designed based on a sandwich bridge deck installed in the area of Bex, Canton of Vaud, Switzerland in 2012. The specimens were produced by infusion technique at the facilities of 3A Composites. All experiments were performed at the Composite Construction Laboratory (CCLab) at the Ecole Polytechnique Fédérale de Lausanne (EPFL), Switzerland. The specimens had a total length of 600 mm, from which 68 mm was occupied by a pre-crack between the upper skin and the balsa core created by the positioning of a Teflon layer during fabrication.

A mixed-Mode bending experimental device (see Fig. 1), developed at CCLab, was used to apply different controlled mode-mixity ratios with either Mode I or Mode II dominant fracture components. Nine specimens were investigated with half span lengths, L, between 170 and 200 mm in order to study the fracture behavior at different mode-mixity ratios.

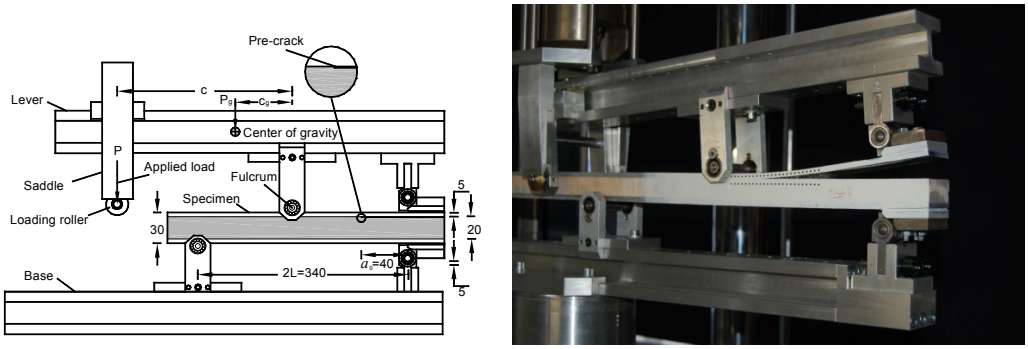

Fig. 1: Photo and schematic of the MMB fixture used.

The MMB experiments were performed under displacement control at a constant rate of 1 mm/min using a 25 kN MTS machine, calibrated to 20% of its capacity. The load was applied at the lever, via in-house developed piano hinges, at a distance c from the fulcrum, see Fig. 1. The position of the loading lever determines the mode-mixity for the experiment [6]. The lever, with a bending stiffness significantly higher than that of the MMB specimen, was assumed to be rigid. The applied load, the mid-span load, and the left support reaction are applied via bearing-mounted rollers to reduce frictional force. The applied loads and displacements were continuously recorded. The MMB experiments were performed with three different lever lengths, c=227, 197, and 80 mm, achieving mode mixities (G_I/G_{II}) between 0.13 and 6.47. The crack length was measured by means of a video extensometer. All experiments were performed at ambient environmental conditions. Representative, experimental results are presented in Fig. 2 for specimens with mode-mixity of G_I/G_{II}=6.47.

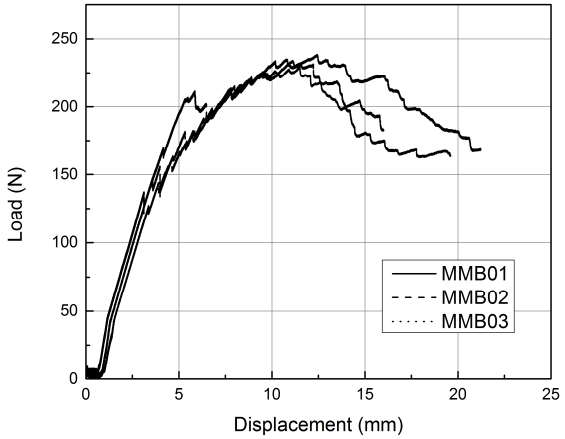

Fig. 2: Load-displacement diagram for c=227mm and L=170mm, specimens MMB01-MMB03.

The total strain energy release rate can be calculated by the experimental compliance method, ECM, based on experimentally derived values of loads, displacements, and crack lengths, as follows:

$$G = \frac{P^2}{2B}\frac{\mathrm{d}C}{\mathrm{d}a} \tag{1}$$

where P is the applied load, C is the compliance of the specimen, a is the crack length and B is the specimen width. The MMB specimen compliance is defined as:

$$C = \frac{\delta_P}{P} \tag{2}$$

where δ_p is the load-point displacement. From among different models for fitting compliance-crack length curves, Eq. (3) was selected because it better fits the experimental results:

$$C = C_0 + ma^3 \tag{3}$$

The "extended global method" [4], has been used for the mode partitioning of the examined specimens. Typical results for two different mode-mixities of 6.47 and 3.92 in the form of the G-α (or R-curves) are presented in Figs. 3 and 4. A mixed-Mode failure criterion can therefore be derived by plotting the results from all experiments as shown in Fig. 5. Appropriate interpolation between known values of mode-mixity allows the estimation of other combinations between G_I and G_{II}, see [5] for details.

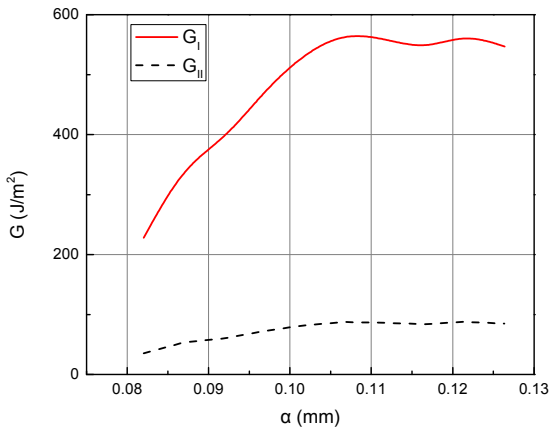

Fig. 3: R-curves of a MMB specimen with mode-mixity, G_I/G_{II}=6.47.

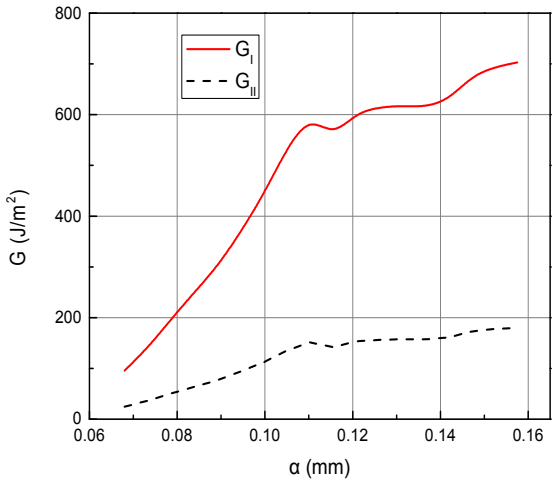

Fig. 4: R-curves of a MMB specimen with mode-mixity of G_I/G_{II}=3.92.

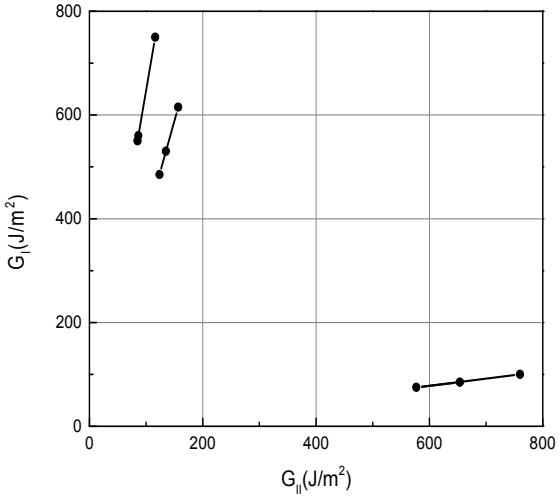

Fig. 5: Mixed mode failure criterion.

3. CONCLUSIONS

The fracture behavior of sandwich beams composed of GFRP skins and balsa wood core has been investigated. The quasi-static mixed-mode behavior has been characterized by experiments using the mixed-mode bending (MMB) fixture of CCLab. In total nine specimens at three different mode-mixities have been acquired. By implementation of the derived quasi-static data, a mixed-Mode failure criterion can be established. Such failure criterion can be used for the estimation of other mode-mixities by interpolation between known values. By the same experimental setup, fatigue crack growth curves can also be derived, and used for the definition of the fatigue threshold, the value of strain energy release rate (corresponding to a value of applied load) below which no crack propagation is expected to happen.

ACKNOWLEDGEMENTS

The material for the study has been provided, and all specimens were manufactured by 3A Composites. All experiments were performed at the Composite Construction Laboratory, CCLab, at the Ecole Polytechnique Fédérale de Lausanne (EPFL), Switzerland.

REFERENCES

[1] T. Keller, J. Rothe, J. De Castro and M. Osei-Antwi. “GFRP-Balsa Sandwich Bridge Deck: Concept, Design, and Experimental Validation” J Compos Construct, 2014;18(2):04013043

[2] M. Osei-Antw, Structural performance of complex core systems for FRP balsa composite sandwich bridge decks” Thesis No 6192, 2014, EPFL, Switzerland.

[3] Reeder JR, Crews JR. “Mixed-mode bending method for delamination testing” AIAA J 1990;28(7):1270–6.

[4] M Shahverdi, A. P. Vassilopoulos, T. Keller. “Mixed-Mode I/II fracture behavior of asymmetric adhesively-bonded pultruded composite joints” Eng Fract Mech, 2014;115:43-59.

[5] M Shahverdi, A. P. Vassilopoulos, T. Keller. “Mixed‐mode quasi‐static failure criteria for adhesively‐bonded pultruded GFRP joints” Compos Part A-Appl S, 2014;59:45-66.

[6] M. Shahverdi, Mixed-Mode Static and Fatigue Failure Criteria for Adhesively-Bonded FRP Joints” Thesis No 5728, 2013, EPFL, Switzerland.

SESSION 10B: IMPACT

DOI: 10.5075/epfl-ICSS12-2018-236-238

QUANTIFICATION OF CORE CRUSH CHARACTERISTICS IN AIRCRAFT HONEYCOMB SANDWICH PANELS SUBJECT TO LOW-VELOCITY IMPACT

Diane Wowk[1], Tyler Reyno[2] and Catharine Marsden[3]
[1,2]Department of Mechanical and Aerospace Engineering, The Royal Military College of Canada, Canada.
[1]diane.wowk@rmc.ca, [2]tylerreyno@gmail.com
[3]Faculty of Engineering and Computer Science, Concordia University, Canada. c.marsden@concordia.ca

1. INTRODUCTION

Honeycomb sandwich structures are widely used for aircraft panels in such locations as the floors, exterior body and the wings due to their high stiffness to weight ratios. One drawback of these panels is that they are susceptible to damage from low-velocity impact events such as tool drops, runway debris or hail in the form of surface dents and plastic deformation in the core. The damage to the core is of particular interest because it is more difficult to detect and monitor than surface damage and it has been shown that core damage is a major contributor to the loss of residual strength of the panel [1]. Numerical simulations can be used to predict the reduction in residual strength, but only if the damage to the core is known. There is therefore a need to be able to anticipate the damage to the core based on the visible surface damage and panel configuration (skin thickness and core density). Finite element simulations performed by our research group indicated that for a given panel configuration, the depth of the core damage underneath dents of various sizes is constant and independent of the dent depth [2], but these predictions had not been validated experimentally. McQuigg *et al.* [1] also observed constant core damage depth in their experimental test results but the actual depth was not measured. In the study presented here, a retired aircraft sandwich panel with a dented aluminum face-sheet and an aluminum honeycomb core was sectioned to expose the core damage resulting from low-velocity impacts. The depth of the damage to the core was measured and it was confirmed that for the 20 dents in this particular panel it was constant and independent of the dent depth. Additional characteristics of the damaged core were also examined such as the number of lobes that developed in the cell walls and the interaction between the cell walls and the adhesive in order to better understand the relationship between the surface damage and the depth of core damage.

2. METHODOLOGY

The sandwich panel considered in this study was a 12.7mm (0.5”) thick, flat honeycomb aircraft panel as shown in Fig. 1(a). The panel had been dented during service and was retired when the allowable damage limits specified in the standard repair manual (SRM) were exceeded. A retired panel was used as opposed to experimental coupons so that a range of damage states resulting from natural variations of in-service impact events (oblique impact, impactors with different shapes, masses, and velocities) could be examined. The Al 7075-T6 top face sheet was 0.51mm (0.02”) thick and the Al 5052 core had a cell size of 3.2mm across the flats with a wall thickness of 0.025mm. The panel was sectioned across the largest diameter of 20 dents using a diamond blade saw at a cut rate of 1mm/s and a blade speed of 200rpm. Only dents with cutting planes that did not interfere with another dent were chosen. The dent depths ranged from 0.12 to 0.69mm with widths between 2.8 and 36mm measured using previously developed 3D laser scanning techniques [3]. The sectioned panel pieces were examined via optical microscope with 6.3-40 times zoom capability and photographed via a detachable digital camera for image processing in the open source software ImageJ. A 0.5 mm resolution ruler was aligned to the panel sections within the images to set the pixel/mm scale. The damaged cross section of the panel was identified by three regions as shown in Fig. 1(b); the surface damage region that includes the dent, the undeformed adhesive fillet region and the core crush region.

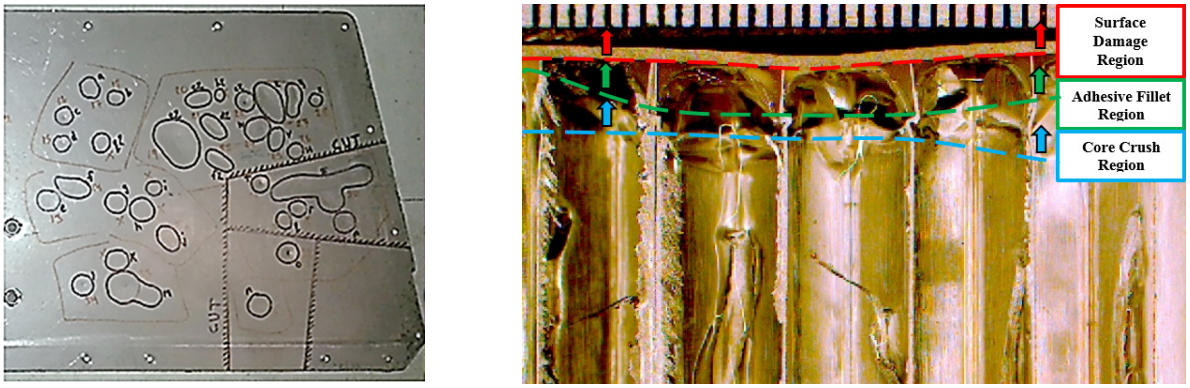

Fig. 1: (a) Retired aircraft panel with dented top face sheet. (b) Three distinct regions of the damaged panel.

3. RESULTS

Core Damage Depth

All of the damage to the core was concentrated within a region directly underneath the adhesive fillet as shown in Fig. 2(a). The concept of damage depth is introduced to describe the distance measured between the top of the undamaged face sheet and the maximum depth of the visibility identifiable core crush as illustrated in Fig. 2(a). For all 20 dents, the damage depth was observed to be constant and independent of the dent depth as shown in Fig. 2(b), with an average depth of 2.66 ± 0.85 mm (95%). The vertical axis in Fig. 2(b) is scaled to the thickness of the panel. This shows that for the 20 dents considered in this panel, different shapes or sizes of impact objects at different velocities or impact angles always produced the same damage depth.

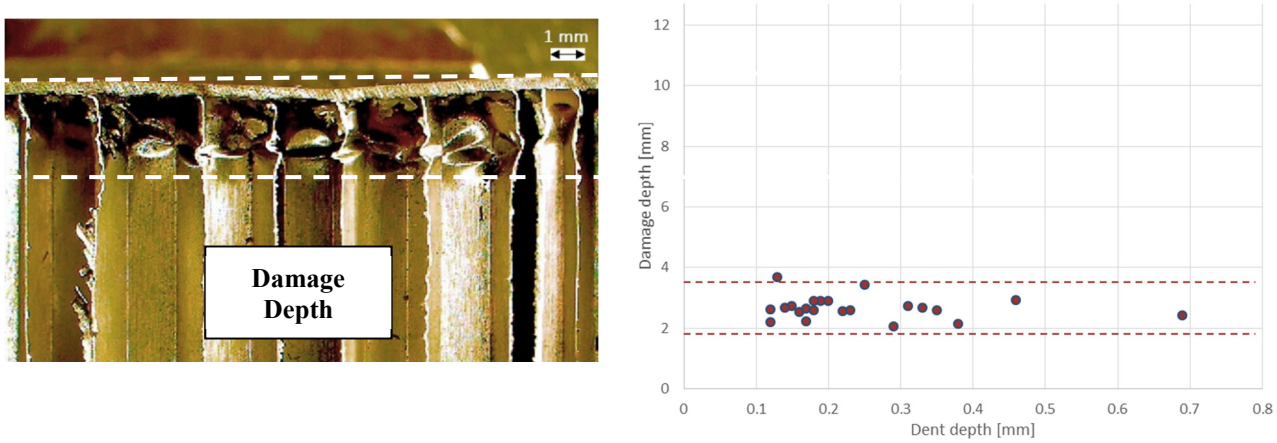

Fig. 2: (a) Damage depth dimension for damaged honeycomb sandwich panel with surface denting and core crushing. (b) Core damage depth plotted against dent depth; dashed lines represent a 95% confidence band.

Number of Lobes

Aminanda *et al.* [4] described the crushing process as the propagation of alternating cell wall folding from one side to the other, referred to as multi-lobe folding with the term "lobe" referring to the fold corner or plastic hinge of a buckled cell wall as shown in Figs. 3(a) and (b). Only 1-, 2- and 3-lobe folding was observed within the core of the panel. The number of lobes had no relation to the dent depth, and 1, 2 or 3 lobes could occur within the same dent. It was noted however, that 3-lobe folding typically occurred in cells with a smaller fillet radius and that 1-lobe folding occurred in cells with a larger fillet radius as shown by the graph in Fig 3(c).

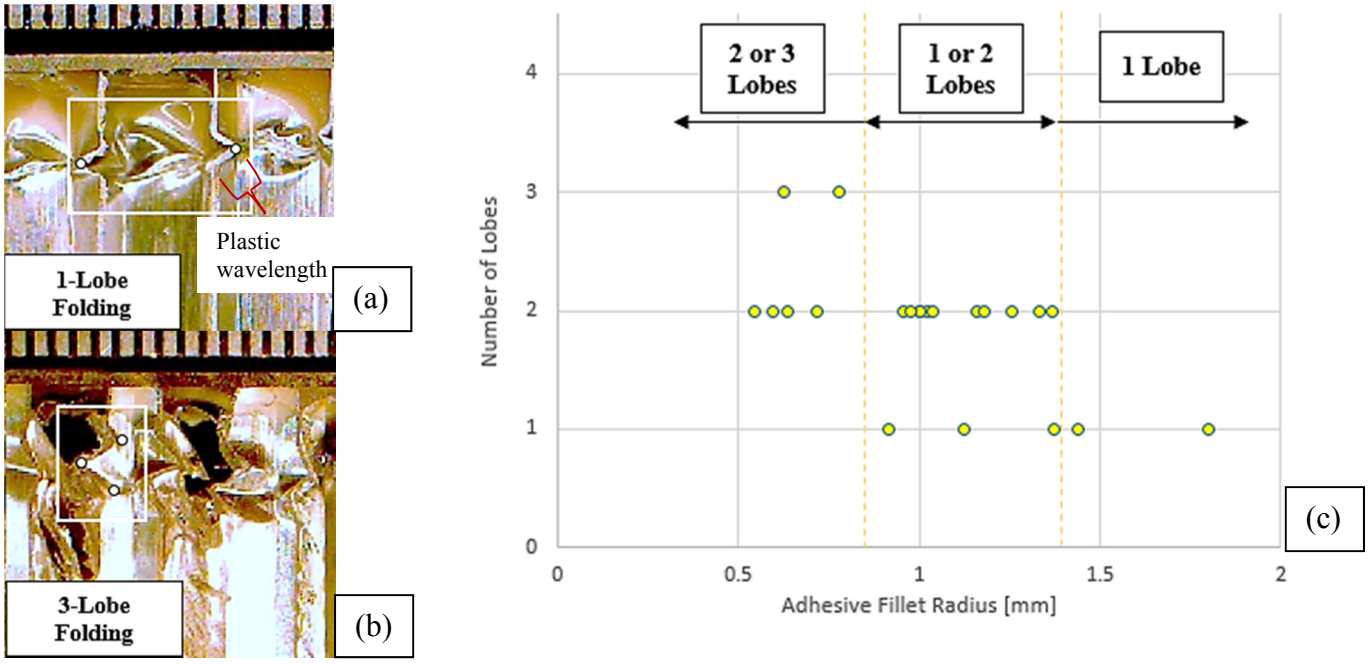

Fig. 3: (a) 1-lobe folding. (b) 3-lobe folding. (c) The number of lobes seen in a cell wall in relation to the fillet radius of the same cell.

4. DISCUSSION

Since the adhesive joining the facesheet to the core does not deform and the depth of the core damage is constant, each cell wall is only able to buckle or fold over the distance between the bottom of the adhesive fillet and the bottom of the damage depth. This means that the mechanisms of cell wall deformation must be able to accommodate the different lengths over which the cells have to deform, referred to here as the *effective length* and illustrated in Fig. 4(a). With the fillet radius being 1.07 ± 0.51 mm and the damage depth being 2.66 ± 0.85 mm, the effective length could theoretically vary between 0.23 and 2.95mm leading to many different modes of cell wall deformation. When a larger adhesive fillet radius is present, the effective length is smaller which resulted in cell walls with fewer folds as shown in Fig. 3(a). On the contrary, in Fig. 3(b), a smaller adhesive fillet radius resulted in a larger effective length and produced 3-lobe folding. Fig. 4(b) shows another deformation mode where the cell wall folded in a manner where the portion of the cell wall encased in the adhesive was not aligned with the undeformed cell wall below the damage region. The two lobes were positioned beside each other and exhibited a shear type of folding. Wu et al. [5] quantified core crushing based on the length of the folds in the cell walls, referred to as the plastic wavelength and labelled in Fig. 3(a). For the 96 folds present within the 20 dents, the average plastic wavelength was determined to be 0.56 ± 0.55 mm, but no clear trends could be identified with respect to the relationship with effective length. The angle of the folds was also measured, but again no trends could be identified.

While the core damage depth was consistent between dents and within dents, the number of lobes and the plastic wavelength revealed a high level of variability even within a single cell. Variability can be attributed to factors such differences in the adhesive fillet radius and the geometric irregularities observed within the honeycomb core. The adhesive fillet radius could be different on each side of a single cell wall, affecting the way the cell wall buckles. The cells in the honeycomb core were not perfectly hexagonal, and in some cases they appeared to be more of a diamond shape. In addition, the ribbon direction of the core has cell walls that are twice the thickness of those in the perpendicular direction leading to non-uniform buckling for the walls within a cell. The location of the cutting plane also added to the variation in the plastic wavelength and the fold angles as the cuts were not all positioned along the same cell orientation. It is important to keep in mind that in a numerical analysis the core is typically represented by an ideal geometry which buckles in a predictable and uniform manner, but physical aircraft panels show a high degree of variability in the deformation of the individual cell walls.

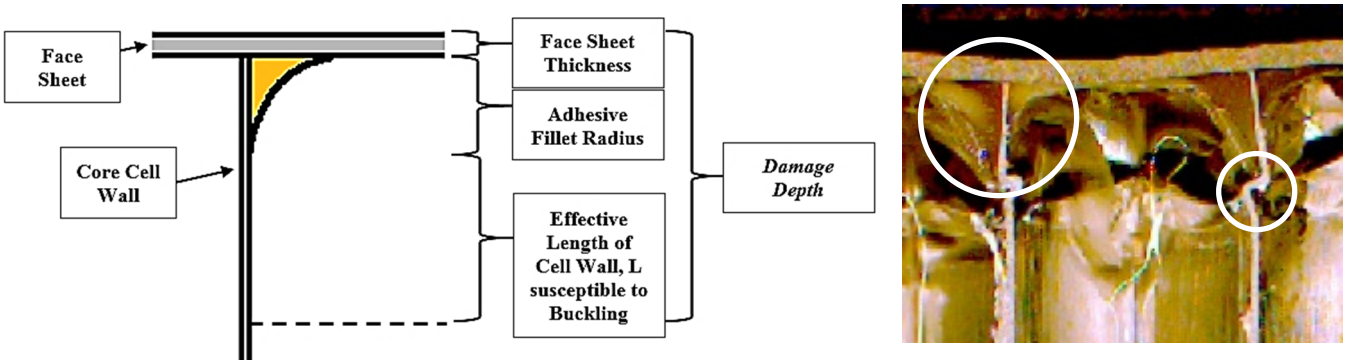

Fig. 4: (a) Definition of the effective length. (b) Cell walls deforming with a shear type of folding; uneven adhesive fillet radii on either side of a single cell wall.

5. CONCLUSION

Confirmation that the damage depth is constant for all dents within a panel is a key finding with regards to using numerical analysis to evaluate the effects of low-velocity impact damage on the residual strength of a honeycomb panel. It is expected that the size and shape of the damage to the core could be determined solely based on the core configuration and the thickness of the face sheet, facilitating the representation of core damage in a numerical model.

REFERENCES

[1] T. D. McQuigg, R. K. Kapania, S. J. Scotti and S. P. Walker "Compression After Impact Experiments on Thin Face Sheet Honeycomb Core Sandwich Panels", *J. Spacecr Rockets*, 2014; 51: 253-266.

[2] G. C. Clarke, "Characterization of Low Velocity Impact Damage in Metallic Honeycomb Sandwich Aircraft Panels Using Finite Element Analysis", Masters Thesis, The Royal Military College of Canada, 2017.

[3] T. Reyno, "Methods for Characterizing Surface and Core Damage in Aluminum Honeycomb Sandwich Aircraft Panels", Masters Thesis, The Royal Military College of Canada, 2017.

[4] Y. Aminanda, B. Castanie, J. Barrau, P. Thevenet "Experimental Analysis and Modeling of the Crushing of Honeycomb Cores", *Appl. Compos. Mater.*, 2005; 12: 213-227.

[5] E. Wu, W. Jiang, "Axial crush of metallic honeycombs". *Int J Impact Eng,* 1997, 19, 439-456.

DOI: 10.5075/epfl-ICSS12-2018-239-241

INTERACTION MECHANISM OF HONEYCOMB SANDWICH PANELS UNDER IMPACT LOADING

Fatemeh Hassanpour Roudbeneh[1], Gholamhossein Liaghat[2], Hadi Sabouri[3], Homayoun Hadavinia[4] and Ali Liaghat[5]
[1] Department of Mechanical Engineering, Tarbiat Modares University, Tehran, Iran. fatemehhassanpour05@gmail.com
[2] Department of Mechanical Engineering, Tarbiat Modares University, Tehran, Iran. & Kingston University, London, UK. ghlia530@modares.ac.ir, g.liaghat@kingston.ac.uk
[3] Department of Mechanical Engineering, Kharazmi University, Tehran, Iran. h_sabouri@khu.ac.ir
[4] Department of Aerospace and Aircraft Engineering, Kingston University, London, UK. h.hadavinia@kingston.ac.uk
[5] Department of Civil Engineering, Sharif University of Technology, Tehran, Iran. alilia95@gmail.com

1. INTRODUCTION

Owing to the increasing development in automotive, transportation and aeronautics engineering, analyzing the energy absorption capacity in structures has become an important field of research [1]. Sandwich panels are one of the most important types of energy absorbers which can be defined as constructions which have light and complex structure with two limited plates on both sides and a light thick core made of different materials as well as several shapes in the middle of structure [2]. They are high-strength and low-weight structures with a wide variety due to the geometrical shape and material type of their core. Despite the remarkable lightness of them, these panels have great resistance against all types of pressure and impact loading [3].

In this paper, numerical studies of impact loading on the sandwich panels with the foam filled honeycomb core and unfilled honeycomb core have been conducted. The structural elements used in this research were aluminum plate, aluminum 5052 honeycomb structure, and polyurethane foam which honeycomb cores were filled with this foam. Numerical modelling and analysis of high velocity penetration process was carried out by a nonlinear explicit finite element code, LS-DYNA. The impact loading was simulated and analyzed on unfilled and foam filled sandwich panels by flat ended projectile. In addition, the destruction mechanisms and damage modes, the ballistic limit velocities and the energy absorption were studied. Also, the effect of foam filling on impact loading response of the honeycomb sandwich panels was discussed. The results of numerical simulation are compared with impact loading experiments.

2. MATERIALS

Aluminum Plate

The aluminum plate used in this project was 1200 Arak with 0.5 mm thickness. This aluminum plate was subjected to tensile measurement according to the ASTM E8M-04. The test results are, E=76 GPa, σ_y=131.33 MPa, σ_u=133 MPa, ϵ_u=0.08 and ρ=2637 kg/m^3.

Honeycomb Structure

The honeycomb structure was constructed by 5052-H38 aluminum with corrugated process. The properties of 5052-H38 aluminum are, E=70 GPa, σ_y=255 MPa, σ_u=290 MPa, τ_u=165 MPa, ν=0.3 and ρ=2680 kg/m^3.

Polyurethane Foam

Commercially available closed-cell polyurethane foam (SKC501) was utilized in the current study. The apparent density of polyurethane foam which is selected for filling of honeycomb panel is 137.13 kg/m^3. Density of foam is determined based on ASTM D1622 standard.

3. NUMERICAL ANALYSIS

In this study, the numerical analysis was carried out by a nonlinear explicit finite element code, LS-DYNA. Also, the geometric modeling consists of two parts; first the projectile, second the target and its components. The modelled projectile was rigid and flat-ended cylinder with 15 mm length and 10 mm diameter. The projectile was modeled with 8 node solid elements. The modelled aluminum skins were 75×75 mm^2 with 0.5 mm thickness. The aluminum skins were modeled with 4 node shell elements. The modelled honeycomb structure was 75×75×19.15 mm^3 and the geometry of a cell is demonstrated Fig. 1. The honeycomb structure was modeled with 4 node shell elements. The polyurethane foam was modeled with 8 node solid elements. Material model 20 (*MAT_RIGID) was chosen for projectile. Aluminum skins, aluminum honeycomb structure and polyurethane foam were modeled with material model 3 (*MAT_PLASTIC_KINEMATIC), material model 3 (*MAT_PLASTIC_KINEMATIC) and Material model 63 (*MAT_CRUSHABLE_FOAM) respectively.

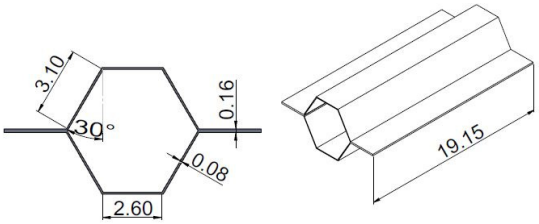

Fig. 1: The geometry and dimension of a honeycomb cell (all dimensions are in mm) [4].

4. RESULTS AND DISCUSSION

Process of Destruction

According to Fig. 2(a), the numerical analysis of perforation in the honeycomb structure was similar to that observed in experimental tests. The projectile, after colliding with upper of the honeycomb structure, created a stress wave and began to damage the structure. Because of the lattice structure and the adhesive bonding between the walls of each cell, the entire structure was resilient; this condition was completely visible in the numerical analysis at lower velocities than the ballistic limit velocity. At higher velocities than the ballistic limit velocity, the projectile passed through the target, compressed the honeycomb core and finally caused to cut and crumple the projectile surrounding cells.

In the numerical analyses of the unfilled honeycomb sandwich panel, at first step, the projectile perforated aluminum skin and formed a plug on it. Then, a local debonding happened between aluminum skin and core due to the projectile high velocity. Subsequently, the projectile along with the plug and the damaged parts of core exited from the rear aluminum skin and formed petals. Fig. 2(b) shows that the asymmetric petal shape of unfilled sandwich panel in both experimental and numerical analyses were similar to each other.

Fig. 2(c) shows the cut out view of the sandwich panel filled with foam. The destruction steps of the foam filled sandwich structure resembled unfilled ones with the difference that the foam was increased the strength of core. The destruction of the core led to a large local debonding between the core and the rear skin, which was completely visible in both experimental and numerical modes.

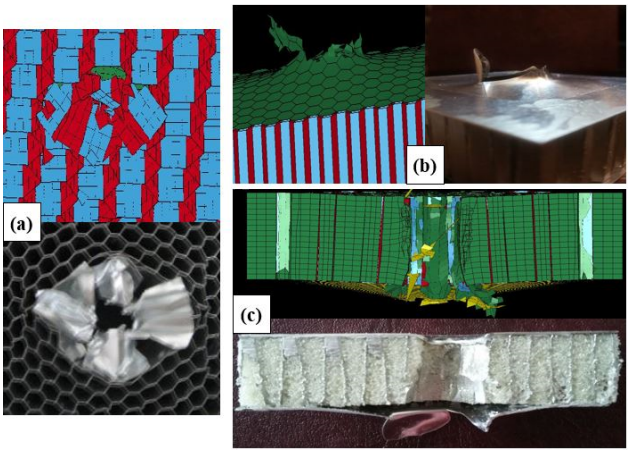

Fig. 2: The specimens (a) Honeycomb structure, (b) Unfilled honeycomb sandwich panel (c) Foam filled honeycomb sandwich panel.

Ballistic Limit Velocity

According to Table 1, the ballistic limit velocities of the numerical findings were in good agreement with experimental data. Obviously, the ballistic limit velocities of foam filled sandwich panel is more than unfilled ones. This is due to the interaction effect among the aluminum skins, the honeycomb core and the polyurethane foam.

The Absorbed Energy Corresponding to the Ballistic Limit

Using the ballistic limit velocity and the projectile mass, the ballistic energy is calculated from the kinetic energy of projectile ($E = mv^2 / 2$).

The numerical and experimental absorbed energy of each structure is given in Fig. 3. The interaction between foam and honeycomb structure as well as the interaction between foam and face sheets caused the significant increase in energy absorption and strength of the sandwich panel. Accordingly, foam filled sandwich structure as one of the suitable energy-absorbing structures could be proposed in various industries.

Table 1: Results of ballistic limit velocity of the specimens.

Specimens	Numerical Ballistic limit velocity (m/s)	percentage change with respect to honeycomb structure (numerically)	experimental Ballistic limit velocity (m/s)	percentage change with respect to honeycomb structure (experimentally)
Honeycomb structure	45.38	-	50.50	-
Sandwich panel with unfilled honeycomb core	63.11	39	72.75	44
Sandwich panel filled with foam	82.00	82	98.25	95

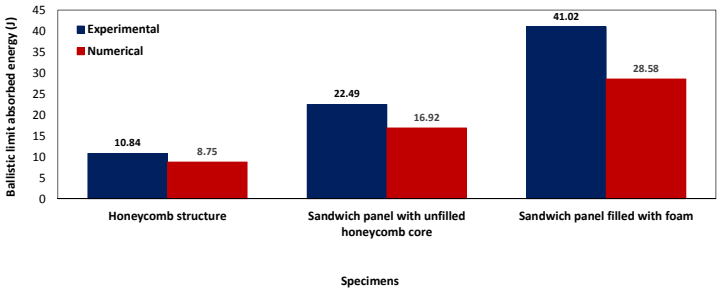

Fig. 3: Comparison of the energy absorption for each specimen.

5. CONCLUSIONS

In this study, the effect of polyurethane foam as filler material in the honeycomb structure used in the sandwich panel was investigated numerically. The results of numerical simulation are compared with impact loading experiments. This research is about the ballistic limit conditions under impact loading. Ballistic limit velocity, destruction shape and ballistic limit energy absorption in sandwich structures with unfilled and foam filled honeycomb core were obtained. The results of this research are as follows:

The dynamic strength of sandwich structure was increased using the polyurethane foam. The absorbed energy of foam filled sandwich panels would be enhanced by increasing the foam density. Indeed, the interaction effect between foam and honeycomb core, as well as the interaction between aluminum skins and foam, enhanced the energy absorption considerably.

Comparison of the unfilled and foam filled sandwich panels with honeycomb structure indicates that the numerical ballistic limit velocity of unfilled and foam filled sandwich panels are 39% and 82% more than honeycomb structure, respectively.

Comparison of the unfilled and foam filled sandwich panels with honeycomb structure indicates that the experimental ballistic limit velocity of unfilled and foam filled sandwich panels are 44% and 95% more than honeycomb structure, respectively.

The difference between the amount of experimental and numerical energy absorption related to honeycomb structure, unfilled and foam filled sandwich panels are 19%, 25%, and 30%, respectively.

Using foams and honeycomb structures each alone causes some limitations that make their using scope less than when they are utilized together. In this study, it was found that combining these two materials together results in produce of structures with superior properties and resistance.

REFERENCES

[1] A. Niknejad et al., "Experimental study of Poly-orthan foam filler on hexagonal honeycomb structure behavior under axial load with constant rate", *10th Iran Aerospace Conference, AERO2011, Tarbiat Modares University*: 2011.
[2] A. Petras, "Design of sandwich structures. Diss. University of Cambridge", 1999.
[3] YS. Tian et al., "Optimal design of compression corrugated panels", *Thin-walled structures*, 2005; 43: pp. 477-498.
[4] F. Hassanpour Roudbeneh et al., "Experimental investigation of impact loading on honeycomb sandwich panels filled with foam", *International Journal of Crashworthiness*, 2018; ISSN: 1358-8265: pp. 1-12.

DOI: 10.5075/epfl-ICSS12-2018-242-244

EFFECT OF CORE ORIENTATION ON LOW VELOCITY IMPACT RESPONSE OF HONEYCOMB SANDWICH BEAMS

Kemal Arslan[1*] and Recep Gunes[2]
[1]Graduate School of Natural and Applied Sciences, Erciyes University, Turkey. karslan@erciyes.edu.tr
[2]Department of Mechanical Engineering, Erciyes University, Turkey. recepg@erciyes.edu.tr

1. INTRODUCTION

Sandwich structures are playing an important role in many engineering fields because of their excellent high flexural stiffness to weight ratio compared to conventional monocoque structures. Accordingly, sandwich constructions exhibit a better mechanical performance than other constructions [1]. Another characteristic feature of sandwich structures is high energy absorption capability that is extremely important for impact applications. Sandwich structures can be exposed to a wide range of impact loads, and it is quite necessary to determine their impact characteristics. For this purpose, different studies are performed on the impact response of sandwich structures designed by various face sheets and core materials using analytical, numerical, and experimental techniques [2-7].

Honeycomb is one of the most popular core material in engineering applications where especially high energy absorption and high mechanical strength are needed. In this study, the effect of core orientation on the low velocity bending impact response of honeycomb sandwich beams is investigated using finite element modeling, and the results are evaluated in terms of contact force, total absorbed energy, and permanent central deflection.

2. STATEMENT OF THE PROBLEM

The structural behavior of sandwich structures depends on the geometrical parameters as well as material properties of the face sheets and core material [8,9]. Accordingly, the main goal of this study is to investigate the effect of core orientation on the low velocity bending impact response of honeycomb sandwich beams. A honeycomb core has two main directions in plane, length in the ribbon direction (L) and width in the direction of expansion (W) (Fig. 1). Therefore, two types of sandwich beam are constructed depending on these directions. The types of sandwich beam are based on L and W directions of the honeycomb core aligned with the length of the sandwich beam, named L-type and W-type beams, respectively (Fig. 2).

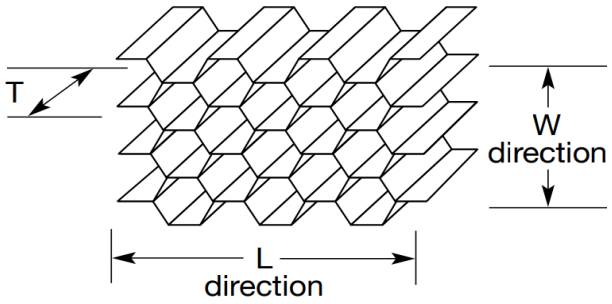

Fig. 1: The description of the in-plane directions of a honeycomb core [10].

To investigate the effect of core orientation, a sandwich beam consisting of two identical aluminum alloy face sheets and an aluminum alloy honeycomb core is considered. The sandwich beam is exposed to low velocity bending impact load by a semi-cylindrical rigid impactor that can properly create the bending deformation.

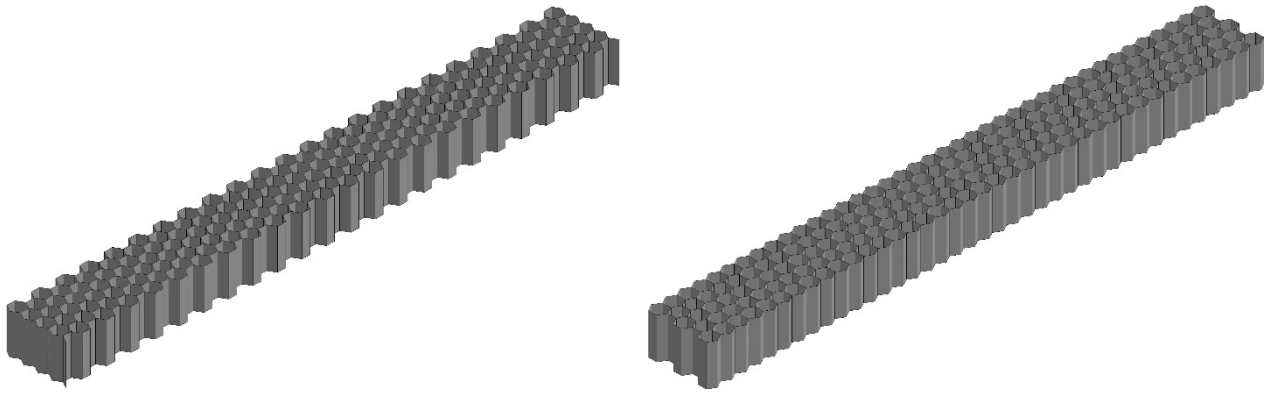

(a) L-type (b) W-type

Fig. 2: The types of sandwich beam.

3. FINITE ELEMENT MODELING

Modeling of the problem is performed using the nonlinear explicit finite element code, LS-DYNA®. The sandwich beam is considered in dimensions of 30x250 mm and consists of Al2024-T3 face sheets with a thickness of 1 mm and Al3003-H19 honeycomb core with a height of 18 mm. The geometry of this problem is the beam form of the sandwich panel that is investigated in our previous study [11]. In our previous study, the finite element model is verified in good agreement with the experimental tests. Accordingly, the same procedure is utilized in this study, and additionally, a similar concept is used in terms of boundary conditions (clamping supports).

Low velocity bending impact is modeled considering the actual geometry of the honeycomb sandwich beam (Fig. 3). The double wall thickness of the honeycomb cells is also considered in the finite element model. The elastoplastic material behavior of the face sheets and core material is represented with the piecewise-linear-plasticity material model. The behavior of the impactor and clamping supports is assumed to be rigid. The face sheets and honeycomb core are modeled with four-node shell elements, and the impactor and clamping supports are modeled with eight-node solid elements. An automatic-surface-to-surface contact algorithm is defined between the impactor and top face sheet, and an automatic-single-surface contact algorithm is defined for self-contacting surfaces. The contacts between core and face sheets are assumed to be perfectly bonded and defined by tied-nodes-to-surface contact algorithm. The boundary conditions are provided with a clamping force by the top supports according to our previous study [11]. The sandwich beam is subjected to a central bending impact by the semi-cylindrical rigid impactor having a diameter of 10 mm, and the analyses are performed for the impact energies of 2.64, 10.58, 23.80 J.

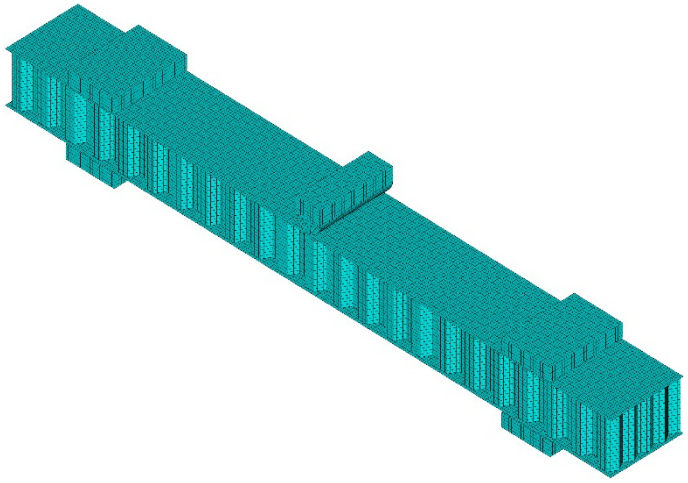

Fig. 3: The finite element model of the sandwich beam, impactor, and clamping supports.

4. RESULTS

The results are examined in terms of contact force, total absorbed energy, and permanent central deflection. The contact force and kinetic energy histories are shown in Fig. 4. L-type beam exhibits higher peak contact force values than W-type beam in analogy to a static four-point bending test of a honeycomb sandwich beam [12]. The difference between the peak contact forces of L-type and W-type beams are about 8.1%, 8.9, and 8.8% for increasing impact energy. The peak contact force is not strongly influenced by the impact energy. However, some fluctuations are observed in the contact force history by increasing the impact energy depending on the plastic deformation occurred in the honeycomb cells. The core orientation has almost no influence on the energy absorption capacity of the sandwich beam. Namely, the differences between the total absorbed energy are below 2% for all impact energies.

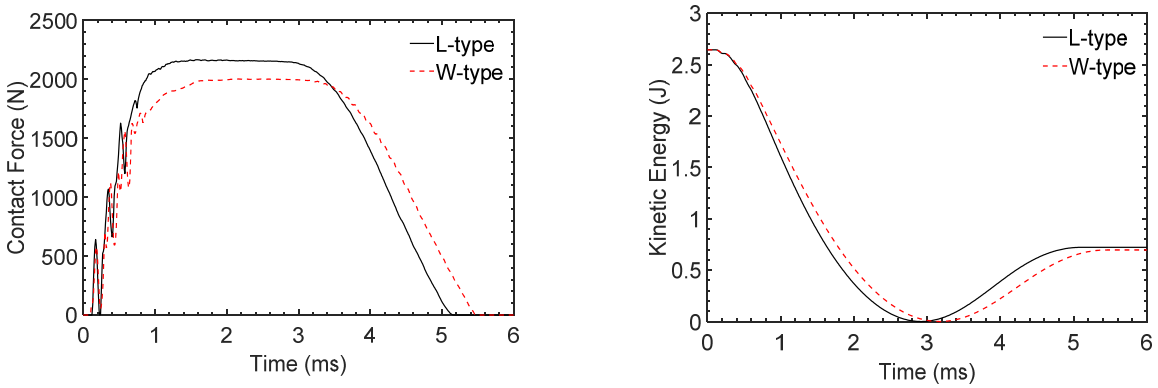

(a) 2.64 J

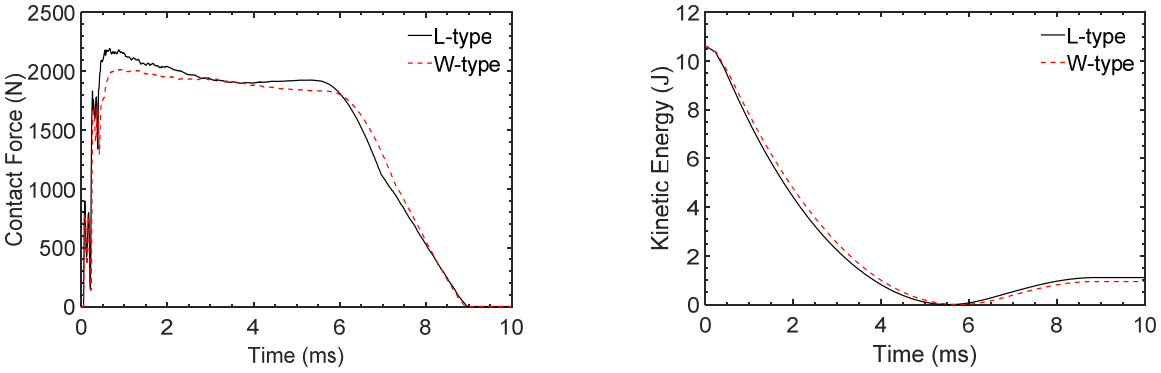

(b) 10.58 J

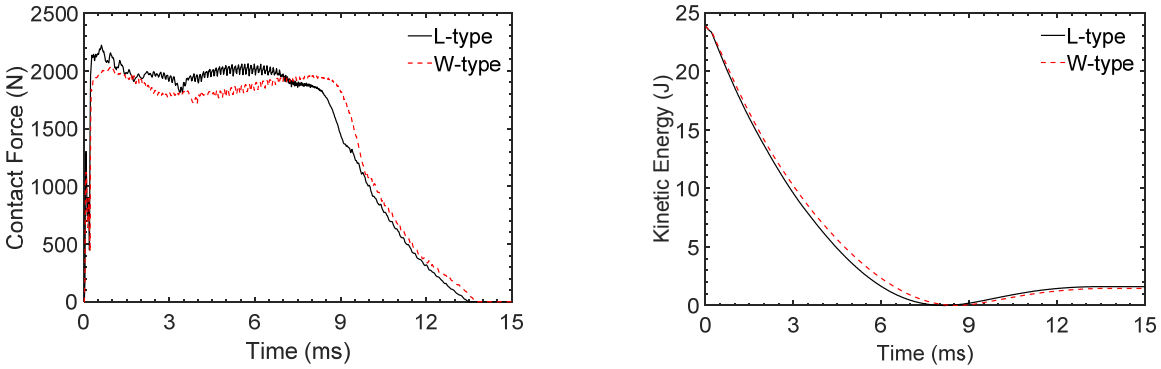

(c) 23.80 J

Fig. 4: The contact force and kinetic energy histories of the sandwich beams for different impact energy levels.

The permanent deformation views of the sandwich beams are given in Fig. 5 for 23.80 J impact energy. W-type beam shows about 11.8% more permanent central deflection and more plastic buckling deformation than L-type beam.

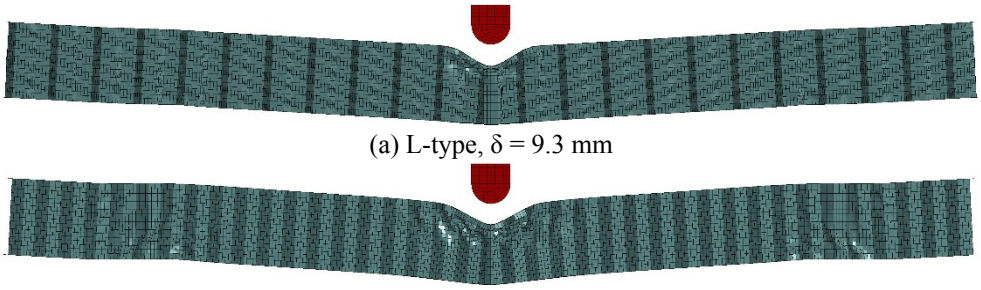

(a) L-type, δ = 9.3 mm

(b) W-type, δ = 10.4 mm

Fig. 5: The permanent deformation views of the sandwich beams.

REFERENCES

[1] J.R. Vinson, *The behavior of sandwich structures of isotropic and composite materials*, CRC Press: 1999.
[2] L. Jing et al., "The dynamic response of sandwich beams with open-cell metal foam cores", *Compos. Part B*, 2011; 42: 1-10.
[3] I. Ivañez et al., "Numerical modelling of the low-velocity impact response of composite sandwich beams with honeycomb core", *Compos. Struct.*, 2013; 106: 716-723.
[4] L. St-Pierre et al., "The low velocity impact response of sandwich beams with a corrugated core or a Y-frame core", *Int. J. Mech. Sci.*, 2015; 91: 71-80.
[5] J. Zhang et al., "A theoretical study of low-velocity impact of geometrically asymmetric sandwich beams", *Int. J. Impact Eng.*, 2016; 96: 35-49.
[6] J. Zhang et al., "Dynamic response of slender multilayer sandwich beams with metal foam cores subjected to low-velocity impact", *Compos. Struct.*, 2016; 153: 614-623.
[7] S.H.A Sabah et al., "Comparative low-velocity impact behavior of bio-inspired and conventional sandwich composite beams", *Compos. Sci. Technol.*, 1996; 49: 155–99.
[8] H.G. Allen, *Analysis and design of structural sandwich panels*, Pergamon Press: 1969.
[9] S. Abrate, *Impact on composite structures*, Cambridge University Press: 1998.
[10] HexWeb® Honeycomb Attributes and Properties, 2016.
[11] R. Gunes et al., "Development of numerical realistic model for predicting low-velocity impact response of aluminium honeycomb sandwich structures", *J. Sandwich Struct. Mater.*, 2016; 18: 95-112.
[12] S. Belouettar et al., "Experimental investigation of static and fatigue behaviour of composites honeycomb materials using four point bending tests", *Compos. Struct.*, 2009; 87: 265-273.

10.5075/epfl-ICSS12-2018-245-246

SOFT IMPACT OF LAMINATED GLASS USED FOR AIRCRAFT WINDSHIELDS

Iman Mohaghegian[1], Yi Wang[1], Jie Zhou[1], Long Yu[1], Xintao Guo[2], Yue Yan[2], Maria Charalambides[1] and John P. Dear[1]
[1]Department of Mechanical Engineering, Imperial College London, London, SW7 2AZ, United Kingdom, j.dear@imperial.ac.uk
[2]Beijing Institute of Aeronautical Materials, Beijing, 100095, China

1. INTRODUCTION

Front facing components of aircraft such as windshields, nose cones, wings and engine blades are always in danger of bird strike during flight time. This risk is increased at time of landing [1]. Engine ingestion is recognized as the major threat to transport jets, however for smaller aircraft, bird strike against the windshield is the main safety concern. This type of strike accounts for 52% of all fatal accidents [1]. Similar figures have been reported elsewhere in literature. Reference [2] details that amongst the 51 fatal accidents identified as being caused by bird strike between 1962 and 2009, 27 strikes were against the windshield. The majority of these fatal windshield strikes occurred on smaller aircraft. The focus of this paper is to study the impact damage of windshields caused by bird strike.

2. EXPERIMENTAL METHODS

To investigate the performance of laminated glass plates under soft projectile impact, laboratory scale impact experiments were performed using a gas gun apparatus. Projectile velocities between 100 and 180 ms^{-1} were adopted. Silicon rubber and gelatin cylindrical projectiles with flat and hemi-spherical noses were used to generate hydrodynamic loading. This is a similar type of loading to the load a windshield experiences under bird strike. A variety of laminated glass constructions, using different types of glass and polymer interlayer, were used to investigate the effects of various design parameters. The plates consist of two layers of glass and one layer of polymer which were laminated using an autoclave at Beijing Institute of Aeronautical Materials (BIAM). Two types of the strengthened alumina silicate glass were used for lamination: thermally and chemically strengthened. All tests were performed such that the target was oriented normal to the gas gun barrel. High speed 3D digital image correlation has effectively been employed to extract the full-field deformation and strain on the back surface of the specimens during impact. Finite element analysis was used to simulate the mechanical response of the laminated glass windows under impact loading. Due to symmetry, only one quarter of the target was modelled. Smoother Particle Hydrodynamic (SPH) was used for modelling the soft impact.

3. RESULTS AND CONCLUSIONS

Different phases of deformation were identified for the deformation of the laminated glass window under high velocity soft impact. Phase 1 where both displacement and strain are increasing, Phase 2 where the displacement continues to increase but the strain does not change much, Phase 3 where the displacement still continues to increase whilst strain is decreasing and Phase 4 where both displacement and strain are decreasing. The maximum strain in the center of the rear glass layer occurs early in the impact due to highly localized deformation, unlike the central out-of-plane displacement. This can be seen in the data captured by the high speed cameras shown in Fig. 1. This figure shows the results for a laminated glass sample, with a thermally strengthened front face, as often employed in the aircraft industry. Fig. 1(a) shows the deformation of the projectile. The contact duration is short and the projectile flows radially as expected. At this velocity only the front layer breaks and the rear layer remains intact. Fig. 1(b) displays out-of-plane displacement of the target calculated using DIC. Fig. 5(c) shows the major principal strain calculated by DIC.

For the laminated glass structures investigated, the damage inflicted is strongly sensitive to the nose shape of the projectile. A flat-fronted projectile causes the most damage. In addition, two threshold velocities have been identified for impact damage associated with the front-facing layer and secondly the rear glass layer breaking. The front glass layer was found to act as a sacrificial layer and protects the rest of the structure from premature failure. Additionally, the thickness of the glass layers affects the impact performance. When a thicker glass layer is placed in the front, both glass layers break. At the same impact speed, however, when a thinner glass layer is facing the projectile, only the front layer fractures and no damage appears in the thick rear glass layer. It can be concluded that the laminated glass window performs better if a thinner front layer is implemented.

Good agreement between the experimental and numerical results were observed. An example of a soft impact simulation for a rubber projectile with a hemi-spherical nose, impacting at a velocity of 158 ms^{-1} is shown in Fig. (2).

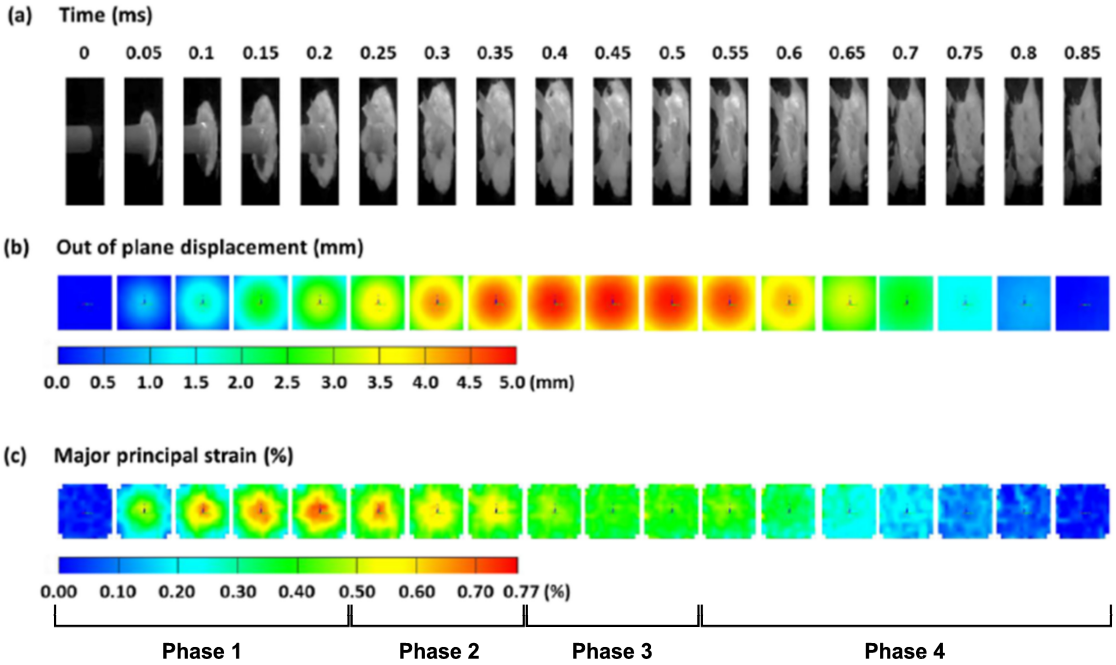

Fig. 1: Soft impact results of a laminated glass window at the velocity of 170 ms^{-1}: (a) shows the projectile deformation; (b) and (c) display the out-of-plane displacement and major principal strain contours over the observation area, calculated using DIC.

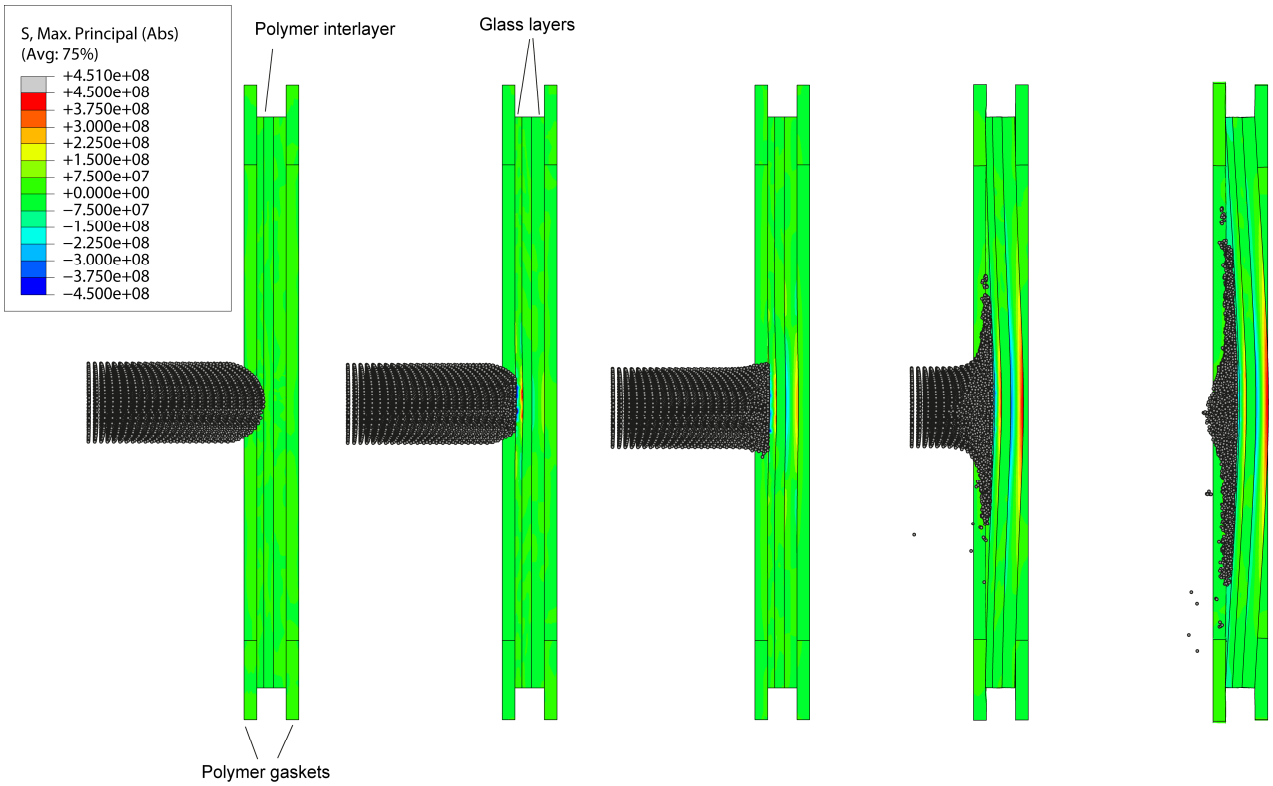

Fig. 2: Soft impact simulation on a laminated glass window impacted by a hemi-spherical projectile at a velocity of 158 ms^{-1}.

ACKNOWLEDGEMENTS

Much appreciated is the strong support received from AVIC Beijing Institute of Aeronautical Materials (BIAM). The research was performed at the AVIC Centre for Materials Characterisation, Processing and Modelling in the Department of Mechanical Engineering at Imperial College London.

REFERENCES

[1] J. Thorpe, "Fatalities and destroyed civil aircraft due to bird strikes, 1912-2002", *Int. Bird Strike Committee,* 2003, 26th Meet: p. 1-28.

[2] N. Dennis et al., "Bird strike damage & windshield bird strike final report", 2008.

SESSION 11A: THERMAL AND ENVIRONMENTAL EFFECTS / ONR

DOI: 10.5075/epfl-ICSS12-2018-248-250

EFFECT OF THERMAL CYCLING ON COMPOSITE HONEYCOMB SANDWICH STRUCTURES

Sandesh Rathnavarma Hegde and Mehdi Hojjati
Concordia Centre for Composites, Department of Mechanical and Industrial Engineering, Concordia University, Montreal, Quebec, Canada, H3G 1M8
* Corresponding author (sandeshrhegde@gmail.com)

1. INTRODUCTION

Composites sandwich structures offer features like higher bending stiffness, light weight, superior dimensional stability, low thermal conductivity and acoustic insulation, which makes them an attractive option for aerospace applications. There is a significant demand in spacecraft industry to reduce structural weight, thus choosing materials with higher strength-to-weight ratios which also satisfy other operational requirements such as the ability to withstand extreme temperature in space, is of primary importance. During a spacecraft's operation, it can experience temperature variations as high as ± 185 °C. Therefore, materials used in its structure such as solid laminates and sandwich structures with honeycomb core are likely to experience major problems, notably microcracking in resin [1], and delamination at the interfaces due to the freeze-thaw mechanism [2] which could result in premature failure.

This paper is focused on studying the effect of thermal cycling on composite honeycomb sandwich structures. Samples were subjected to a space-like thermal cycling, and crack formation and growth were monitored and quantified after repeated thermal cycles.

2. MATERIAL AND TEST PLAN

The sandwich panel was made of 6.4 mm (0.25inch) thick phenolic resin coated Kevlar honeycomb core with 0.25 mm thick facesheets made of 5HS carbon fiber fabric with cyanate ester resin. The facesheets were cured at the laminate level and are then bonded to the core using a structural film adhesive (FM300). The cure cycle was 90 minutes at 120 °C under autoclave pressure of 1.5 atm. There were no voids present in the facesheet when the sample cross-sections were observed under the optical microscope.

Test Plan

Four sandwich samples were cut into 25.4 mm by 25.4 mm pieces and then subjected to thermal cycling. To achieve cold case condition temperature, liquid nitrogen was used. The test samples were placed in a convection oven to achieve hot case condition. Two test setups were developed for the cold case. The first setup involves direct dipping of samples in LN2 (Liquid Nitrogen, for higher rate of cooling), which is comparable to the condition experienced by sandwich materials used in cryogenic fuel tank [3], where the cryogenic fuel is in direct contact with the material. The second setup involves non-contact cooling, where samples are subjected to cryogenic temperature environment, without direct contact with LN2. This condition simulates the thermal environment (lower rate of cooling) experienced by the materials used in spacecraft primary structures and support brackets in eclipse region of the orbit. A thermocouple was installed inside the core of a spare sample to monitor the change in temperature.

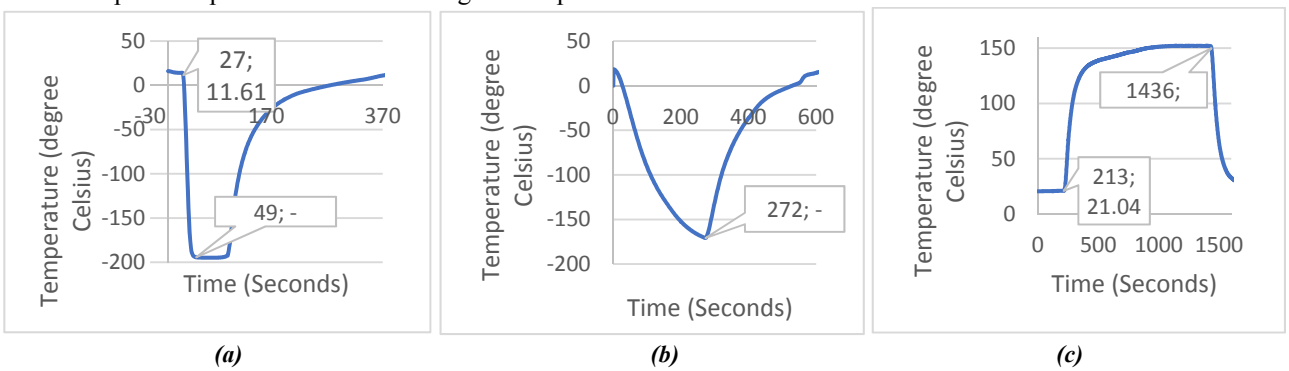

Fig. 1: Time vs temperature profiles of sample for direct dipping in LN2 (a), non-contact cooling (b) and hot cycle (c).

The change in temperature with respect to time for the thermal conditioning is shown in Fig. 1. It can be noted from Fig. 1 (a), that it takes 20 seconds for the samples to reach -194 °C when directly dipped in LN2, and approximately 5 minutes to reach -170 °C for samples subjected to non-contact cooling. For the hot case condition, it takes approximately 15 minutes to reach +150 °C, however the cycle time was extended to 20 minutes, which serves as buffer. One complete cycle consists of one cold and one hot cycle. Out of four, two samples were subjected to direct dipping in LN2 followed by hot cycle. The second set of two samples were subjected to non-contact cooling followed by hot cycle. This was done to simulate the condition as described in the test plan.

3. MICROSCOPIC INSPECTION

The samples were observed under the microscope after every half cycle, to investigate the part of the cycle (hot or cold) that contributes more towards the formation and propagation of microcracks. As the honeycomb sandwich material consists of both geometric and material anisotropy, the microscopic inspection was done on two cross-sectional sides perpendicular to each other, one on ribbon direction side (the side where the cut was made along the ribbon), and the other on transverse ribbon direction side of the core. The results after subsequent cycles are as shown below.

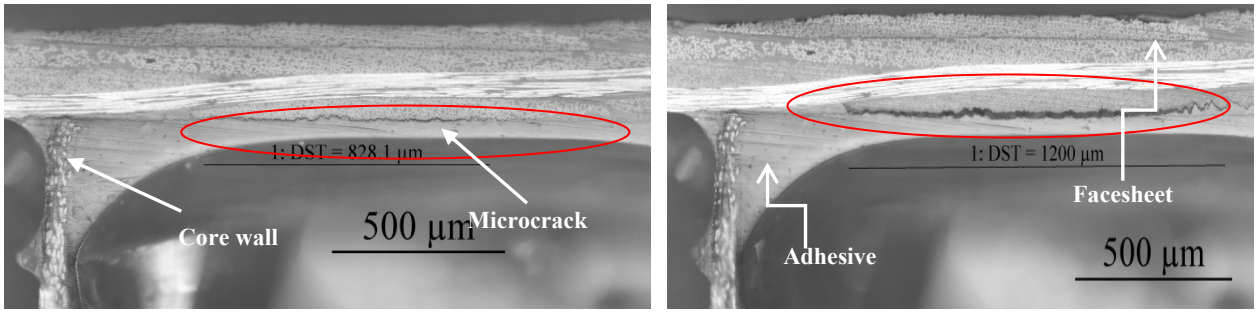

Fig. 2: Microscopic images of sandwich cross section taken after 2nd cycle (left) and 10th cycle (right).

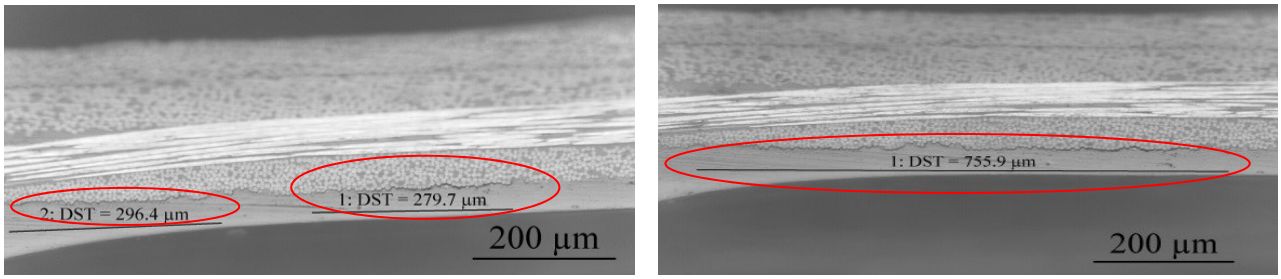

Fig. 3: Magnified microscopic images of sandwich cross section taken after 1st cycle-hot cycle (left) and 1.5 cycle- cold cycle (right).

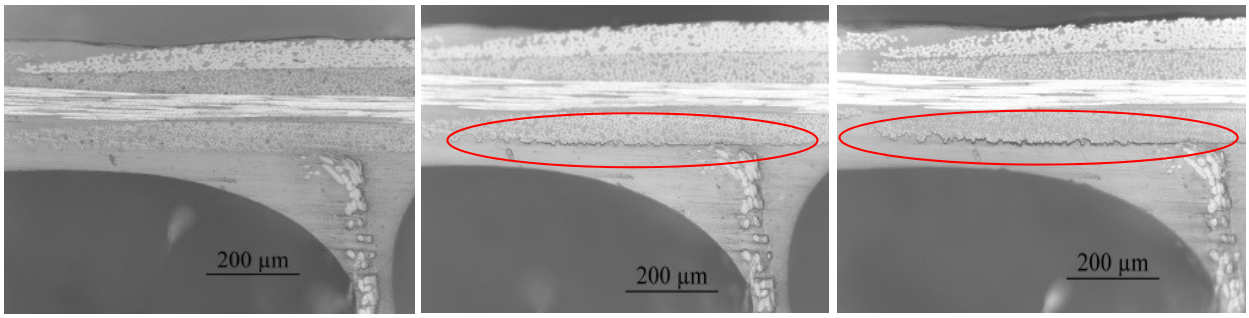

Fig. 4: Images taken after 0.5 cycle-cold cycle (left), 5th cycle (middle) and 10th cycle (right).

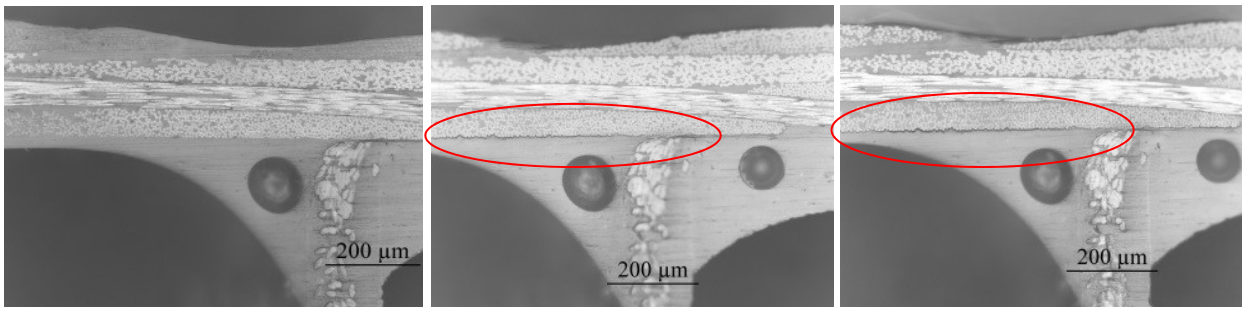

Fig. 5: Images taken after 0.5 cycle-cold cycle (left), 5th cycle (middle) and 10th cycle (right).

Microcrack Formation and Propagation

Fig. 2 clearly shows various aspects of honeycomb sandwich composite such as core wall, facesheet, adhesive fillet area and an example of a microcrack. Fig. 3 shows examples of magnified images of crack progression. The microscopic image as shown in Fig. 4 (left) was captured after cold cycle (0.5 cycle), the same position was again observed under microscope after subsequent cycles. A facing delamination crack was found at the interface between the adhesive layer and facesheet. Most cracks appeared after hot cycle which indicates that the influence of hot cycle is more severe for crack formation, in the first two thermal cycles. It is also interesting to note that crack formation in cold cycle is lower,

however thicker cracks grows in length (propagates) as shown in Fig. 3 (right, after cold cycle). Multiple cracks were observed at different part of sample with similar patterns as shown in Figs. 4 and 5, most cracks form between 90 degree tow and adhesive layer.

4. QUANTIFICATION OF CRACKS

Cracks were quantified using parameters such as crack density [1] and crack length, the former corresponds to number of cracks per unit area (cracks/mm^2) per sample and the later corresponds to summation of length of all the cracks observed per sample. The plot of change in crack density with respect to number of cycle is shown in the image below. Crack density was higher on ribbon direction side compared to transverse ribbon direction side as indicated by the plots in Fig. 6. This is mainly due to the anisotropic behavior of the sandwich core. The core's ribbon direction coefficient of thermal expansion is higher compared to the transverse ribbon direction CTE [5].

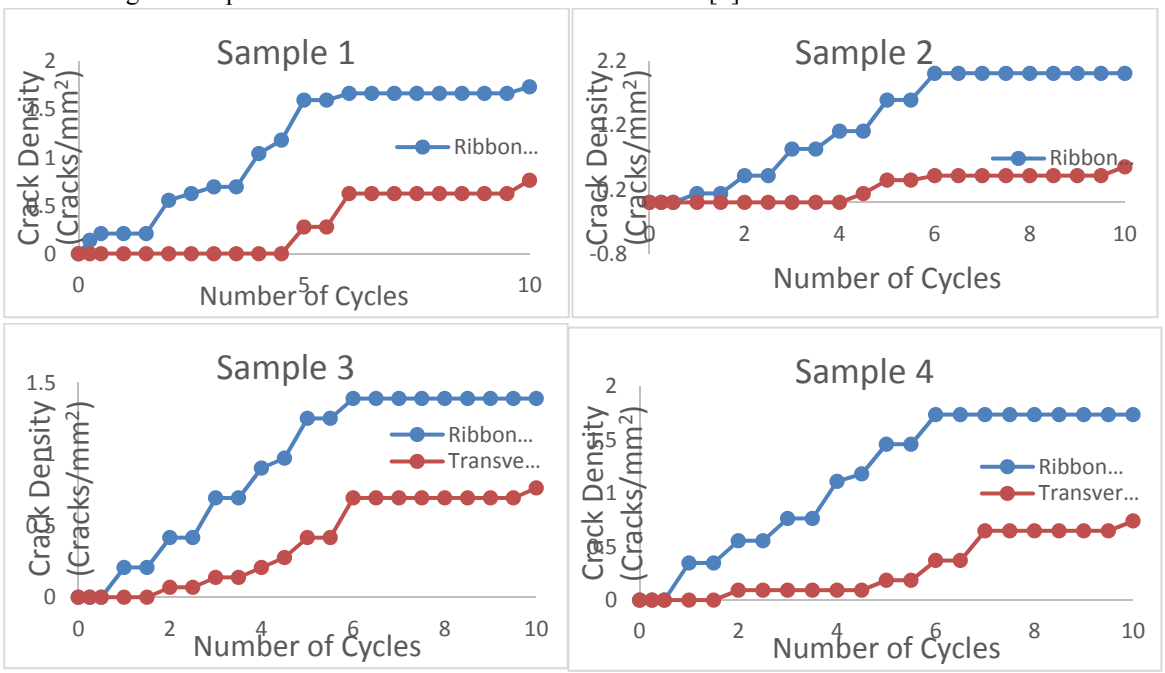

Fig. 6: Variation in crack density with respect to number of cycles of the four samples.

5. CONCLUSION

A methodology of quantifying microcracks on sandwich composite material subjected to thermal cycling is developed. For statistical significant data, four samples were observed after hot and cold cycles, with two samples each for different rate of cooling. Longitudinal microcracks were observed at the region between facesheet and core, indicating that the adhesive layer is the weak link. The variation in crack density with cycles is almost constant for all samples, with slight variance owing to the minor difference in local geometry of observation. A model is being developed to correlate the crack density vs number of thermal cycle.

ACKNOWLEDGMENT

The authors would like to acknowledge the financial support from the Natural Sciences and Engineering Research Council of Canada (NSERC), Consortium de Recherche et D'innovation en Aérospatiale au Québec (CRIAQ), MDA Corporation and Stelia North America.

REFERENCES

[1] John F. Temmerman et al., "Matrix and fiber influences on the cryogenic microcracking of carbon fiber/epoxy composites", *Elsevier Science Ltd.*, 2002; Composites Part A: 323-329.

[2] J.E. Shefizadeh et al., "Evaluation of the In-Service Performance Behaviour of Honeycomb Composite Sandwich Structures", *Journal of Materials Engineering and Performance.*, 1999; Volume 8(6): 661-668.

[3] Brian W. Grimsley et al., "Hybrid Composites for LH2 Fluid Tank Structure", NASA Technical Report Server https://ntrs.nasa.gov/search.jsp?R=20040086019.

[4] Thomas S. Gates et al., "Facesheet delamination of composite sandwich materials at cryogenic temperature", Elsevier Ltd, *Composites Science and Technology,* 2006; 66: 2423-2435.

[5] H. Chen et al., "Thermal Expansion of Honeycomb Sandwich Panels", Reprinted from Thermal Conductivity 25- Thermal Expansion 13-June 13-16,1999.

DOI: 10.5075/epfl-ICSS12-2018-251-253

EFFECT OF LOCALIZED FIRE DAMAGE ON FAILURE MODE SHIFTS IN SANDWICH STRUCTURES

Abraham Elmushyakhi[1], Elias A. Toubia [2] and Alexander B. Morgan[3]
[1]Northern Border University, Mechanical Engineering, KSA. Abraham.Elmushyakhi@nbu.edu.sa
[2]University of Dayton, Civil Engineering and Engineering Mechanics, USA. etoubia1@udayton.edu
[3]University of Dayton Research Institute, Energy Technology and Materials Division, USA. alexander.morgan@udri.udayton.edu

1. INTRODUCTION

Common damage encountered during the service life of the structure spans from a simple tool drop to localized fire damage. Assessing the damage and understanding their effects on structural performance is crucial to design a safe and durable composite structure. Composite sandwich structures with closed-cell foam cores are commonly used in marine and civil engineering structures. When such panels are subjected to localized heat damage due to low-intensity fire or excessive heat, several failure modes could be encountered. Depending on the induced heat flux and damage propagated into the face-sheet or core, the sandwich compression strut could potentially fail by face sheet instability at the location of the damage, or by core shear instability (shear crimping). This shift in failure modes of sandwich structures is directly related to the amount heat transferred into the core, and consequently, decomposing and charring the sandwich structure. This experimental work presents the post-fire failure mechanisms and residual properties of sandwich structures when subjected to axial loads. Using the cone calorimeter test apparatus, coupled with thermocouples on both sides (top and bottom) of the samples , measured temperature profiles are presented for the PVC foam cores (H80 and H200) and sandwich structures for the induced 10 and 30 kW/m^2 heat fluxes.

2. BACKGROUND AND EXPERIMENTAL TESTING

For an undamaged sample, the axial load resisted by the structure results in equal axial deformations of the facings and core, thus facesheet fracture and even global or local instability occur under “controlled axial displacements”. Several researchers already investigated these failure modes. However, in a post-fire scenario, the axial load will be redistributed to the stiffer part of the structure (undamaged facing/core), leading to local 3D-dimensional effects near the heat-damaged zone. This “controlled force loading” phenomenon leads to loss of strength prior to elastic stability failure. Several researchers investigated the post-fire mechanical properties of sandwich structures [1] and wrinkling at high temperature [2]. Specifically, Birman et al. [2] developed a theory where a desirable variation of the stiffness can be achieved by varying the mass density through the thickness of the core. Their specific application targeted wrinkling in a functionally graded core. This work investigates the failure modes related to low-to-medium localized fire exposure, and use the Digital Image Correlation (DIC) technique to measure the strain field and displacement prior to failure. The materials selected to manufacture the composite panels are shown in Table 1. The water jet technique was used to cut the panels into the desired dimensions (Fig. 1). For the tensile test samples, the two end sections were tabbed with G10 Epoxy on each side of the specimens using urethane adhesive (Lord adhesive 7150A/B H, LORD corporation) and then prepared according to testing protocol proposed by Toubia et al.[3]. Fig. 1 shows the dimensions and geometry of the test samples.

Table 1: Materials selection and sandwich construction.

Facesheet Construction/Areal Weight	Core	Resin	Catalyst	Fabric Architecture	Molding Process
4 Plies E-BXM-1708 E-Glass, 883 gr/m^2 total. [+45°(304 gr/m^2), -45°(304 gr/m^2), Chopped Mat (275 gr/m^2)] (Vectorply Corporation®)	H80 and H200 PVC foam (Divinycell® Inc.)	DERAKANE 610 C-200 Epoxy Vinyl Ester Resin (Ashland Inc.)	1.25% Organic Peroxide, Cadox®	Double bias, ±45° [+45/-45/Mat]	VARTM Infusion with 28 Hg Vacuum Pressure

To control the region of thermal decomposition at the center of the samples, the specified specimens for tensile and edgewise compression tests were wrapped in Aluminum foil on all sides except for the top middle section (Fig. 1) facing the heater. The ignition spark was exactly centered over the unwrapped area and the shutters were left open until either the sample ignited or maximum time of 7 minutes if the sample did not ignite. Following exposure, the samples were cooled to room temperature under an exhaust hood and were covered with a stainless steel snuffer. Char thickness through the samples was then measured before performing post-fire mechanical testing. Fig. 1 below shows couple of

representative samples using thermocouples to measure through-the-thickness temperature. Localized damaged was induced using the cone calorimeter heater. It is worth mentioning that at 10 kW/m^2 flux, a discoloration of the facesheet followed by facesheet-core interface debond occurred, while at a flux of 30 kW/m^2, partial damage/char of the core was noticeable.

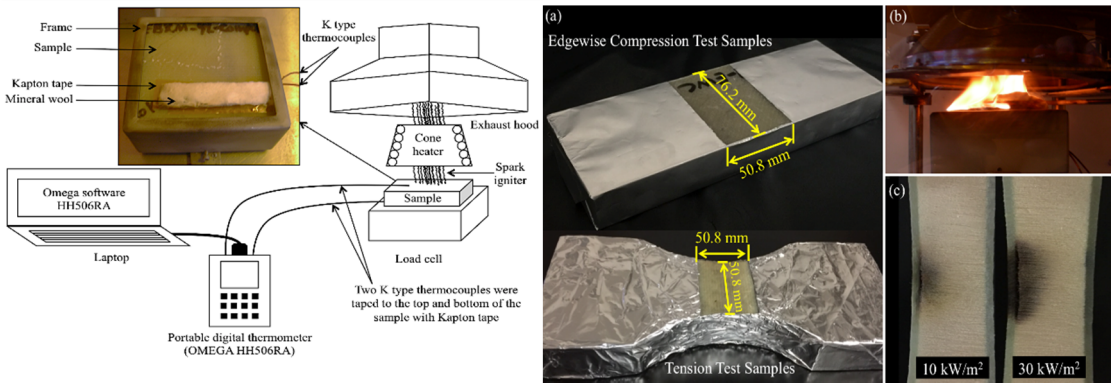

Fig.1: Left: Cone Calorimeter experimental procedure, Right: (a) Samples partially covered with aluminum foil except for a 25 cm^2 on top exposed area, (b) tested sample was placed 25 mm under the cone heater on an Aluminum foil wrapped ceramic brick, (c) samples clearly ignited and burned through-the-thickness.

Fig.below shows some representative experimental data on the compression behavior of several heat treated samples. The baseline sample experienced global buckling, whereas samples exposed to one sided heat exposure exhibited skin wrinkling and core shear instability (10 kW/m^2 and 30 kW/m^2, respectively). This shift in failure modes in the presence of damage must be taken into account to assess the service life of the structure, or even if a repair or replacement is attempted.

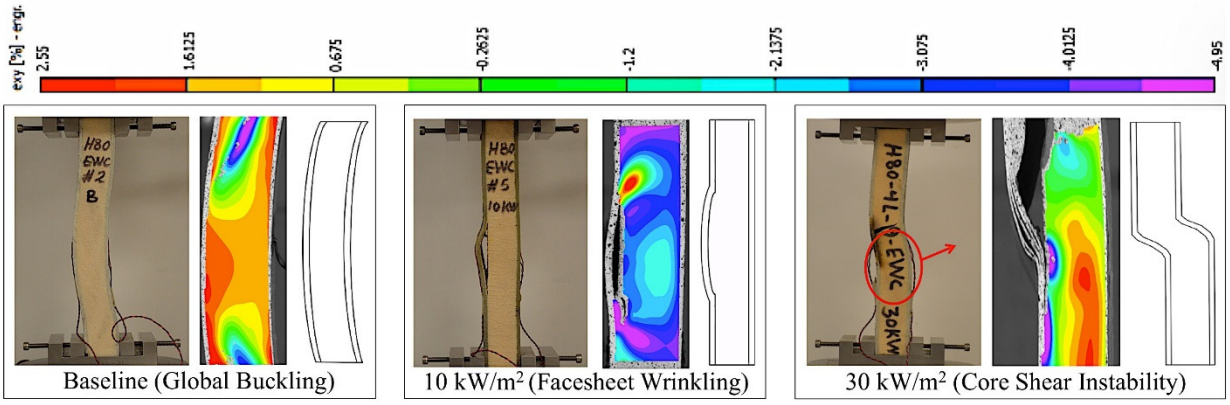

Fig.2: Edgewise compression and DIC images showing side view and shear strain distributions at incipient compression failure.

3. RESULTS AND CONCLUSIONS

The performed experimental tests demonstrated that the post-fire behavior of sandwich construction is governed by dependent sets and variables: the density of foam, the thermal conductivity and diffusivity of the foam core, and the amount of damage penetrating the core (char depth). The presented results revealed that depending on the heat damage propagating into the sandwich panel, a switch in failure modes will occur from global to local buckling modes. The foams significantly affected the measured temperatures, as well as the char depths. The H200 foam is a denser foam and therefore conducts heat better than the H80 foam (which is a better insulator), and this explains the results presented in Fig. 3. In addition, the sandwich panels with H200 foam core experienced less reduction in axial tensile modulus and strength than the sandwich samples with H80 foam core (Fig. 4).

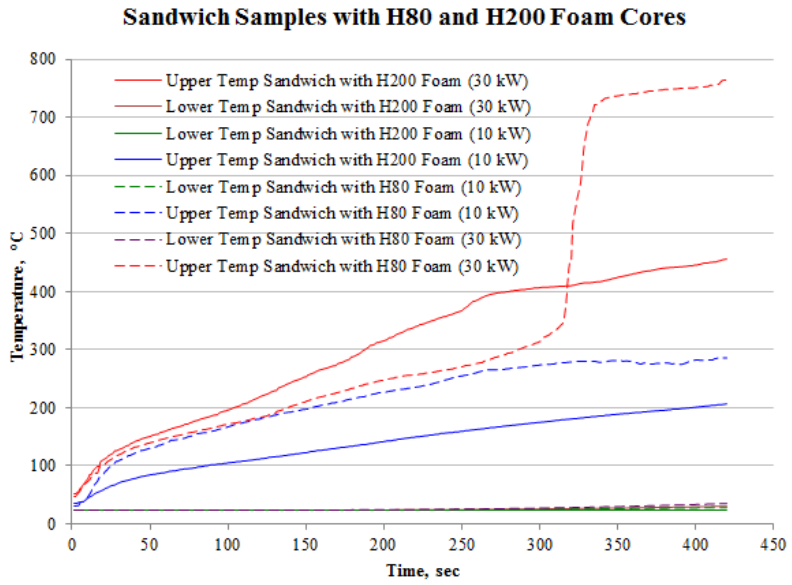

Fig.3: Upper (top facesheet) and lower (bottom facesheet) temperature profiles for sandwich samples with H80 and H200 foam cores.

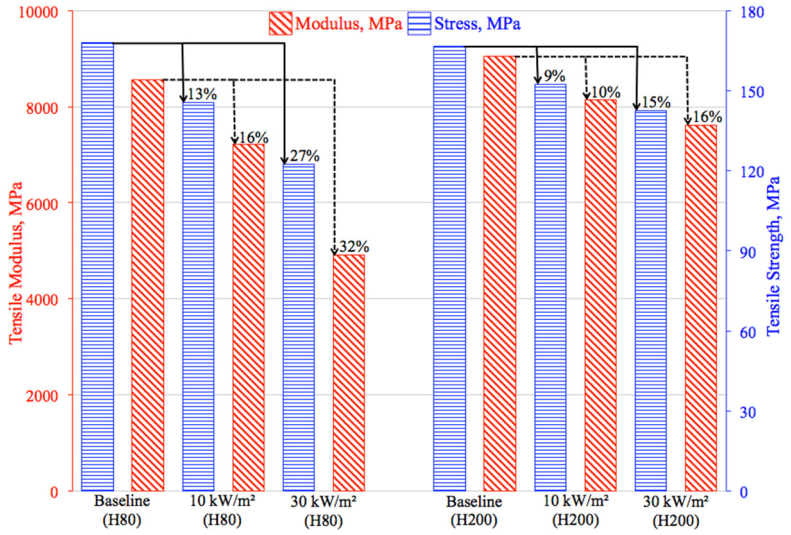

Fig.4: Tensile strength and modulus for sandwich samples with H80 and H200 foam cores (percentage reduction shown with respect to the undamaged baseline samples)

REFERENCES

[1] A. Anjang, et al., "Post-fire mechanical properties of sandwich composite structures." Composite Structures, 2015;132: 1019-1028.

[2] V. Birman, et al. "Wrinkling in Sandwich Structures With a Functionally Graded Core." Journal of Applied Mechanics,2017; 84(2): 021002

[3] E. Toubia, et al. “Influence of core joints in sandwich composites under in-plane static and fatigue loads”. Materials & Design. 2017;131:102-11.

DOI: 10.5075/epfl-ICSS12-2018-254-256

MECHANICAL PROPERTIES OF A BALSA WOOD VENEER CORE MATERIAL AT ELEVATED TEMPERATURES

Chao Wu[1,a], Niloufar Vahedi[2,b], Anastasios P. Vassilopoulos[2,c] and Thomas Keller[2,d]
[1] School of Transportation Science and Engineering, Beihang University, China
[2] Composite Construction Laboratory (CCLab), École Polytechnique Fédérale de Lausanne (EPFL), Switzerland
[a] wuchao@buaa.edu.cn
[b] niloufar.vahedi@epfl.ch
[c] anastasios.vasilopoulos@epfl.ch
[d] Corresponding author E-mail: thomas.keller@epfl.ch

1. INTRODUCTION

High strength-to-weight and stiffness-to-weight ratios make Balsa wood a preferred material for cores of sandwich structures [1, 2]. The major disadvantage of this system is the heat damage and softening that occurs in the event of fire. The stiffness and strength properties of the Balsa core and laminate skins are reduced by thermal softening, heat damage and decomposition [3]. Goodrich et al. [2] performed an experimental study on mechanical properties, physical degradation, and decomposition of Balsa wood at high temperatures. It was found that the compression strength of Balsa decreased at a quasilinear rate with increasing temperature up to 250°C. The reduction was attributed to the softening of the hemicellulose and lignin above 120°C. The authors also claimed that the loss in strength up to the point of decomposition was reversible for short-term fire exposure and the strength could fully recover when samples cooled back to room temperature. Since the mechanical properties of Balsa wood vary considerably, new configurations composed of veneer layers of different fiber orientations, which are adhesively-bonded together, were developed. The behavior of such materials at elevated temperature has not yet been investigated.

2. EXPERIMENTAL INVESTIGATION

Materials

The Balsa wood used in the current study was BALTEK® VBC provided by 3A Composites Core Materials at Sins, Switzerland. This product consists of Balsa veneer layers, which were produced through a rotary peeling process of Balsa trunks using a roller pressing bar. Each veneer layer had a nominal thickness of 6 mm. They were alternatingly stacked in 0°/90° grain orientations and bonded together with a one component cold curing and foaming Polyurethane (PU) adhesive, Jowapur 687.22. The veneer layers were compressed and cured at room temperature for at least twenty four hours.

Tensile, Compression and Shear experiments under Elevated Temperature

Considering all possible load directions which could be developed in the core of the sandwich panel, three tensile configurations (Fig. 1 (a)), three compressive configurations (Fig. 1(b)) and four shear configurations (Fig. 1(c)) were selected. The dimensions were determined according to ASTM D3500-14 [4], ISO 22390:2010 [5], ASTM D3501-05 [6] and ASTM D5379-12 [7]. The selected temperatures were ambient/laboratory temperature (27~31°C), 100°C, 150°C, 200°C and 250°C. For each temperature, at least 5 specimens were examined. Before the mechanical experiments, all specimens were stored in a condition room with a constant temperature of 20°C and a relative humidity of 65%. The temperature in the chamber was first increased to the target temperature. The specimen was then installed and left under the constant target temperature for 20 mins to ensure that the temperature of the specimen is uniform and equal to the target temperature. The load was then applied at a rate of 2 mm/min until failure of specimen.

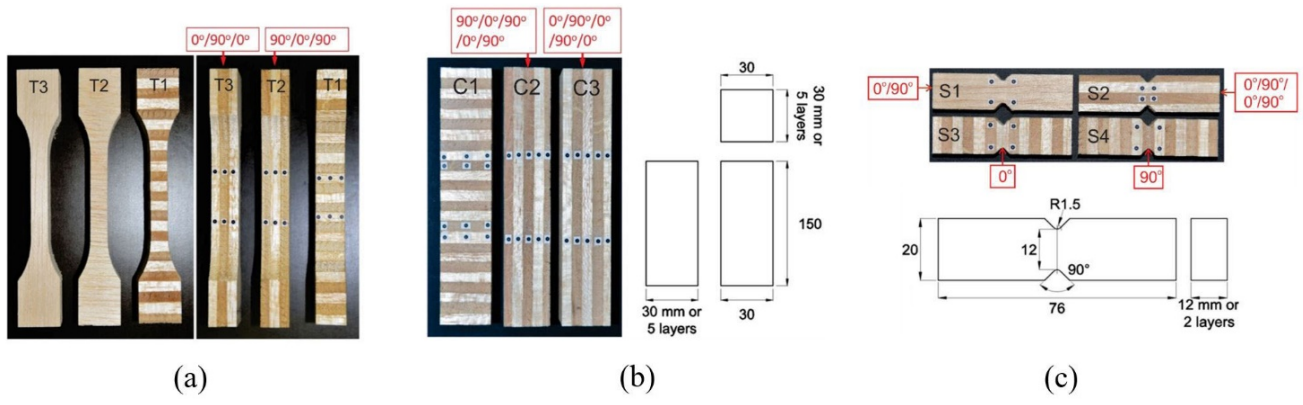

Fig. 1: (a) Tensile specimens, (b) Compressive specimens, (c) Shear specimens.

3. EXPERIMENTAL RESULTS AND DISCUSSION

Tensile Properties under Elevated Temperatures

The temperature-dependent modulus and strength responses of the three tensile configurations are shown in Fig. 2. All properties basically decreased with increasing temperature; at 250°C modulus and strength approached zero. The decreases were not linear however: in T1 specimens even an increase occurred up to 100°C; in T2 specimens, after a first decrease, an increase between 100 and 150°C was exhibited too; while the T3 specimens showed a reduced slope of decrease between 150 and 200°C. This partially recovery or deceleration of decrease could be attributed to moisture evaporation [8], which occurred differently, depending on the specimen configuration. The rate of evaporation depended on the area of surfaces cut perpendicular to the fiber direction. Evaporation along the fibers was faster than perpendicular to the latter. T1 specimens exhibited, proportionally, the highest amount of areas perpendicular to the fibers, followed by T2 and T3. Accordingly, the associated recovery was seen already at the beginning in T1 and prevailed the degradation due to temperature. In T2, evaporation was delayed and recovery occurred later, while evaporation in T3 was slowest, resulting only in the change of slope. Depending on the amount of fibers in the loading direction, the properties of T3 were higher than those of T2; T1 exhibited the lowest values.

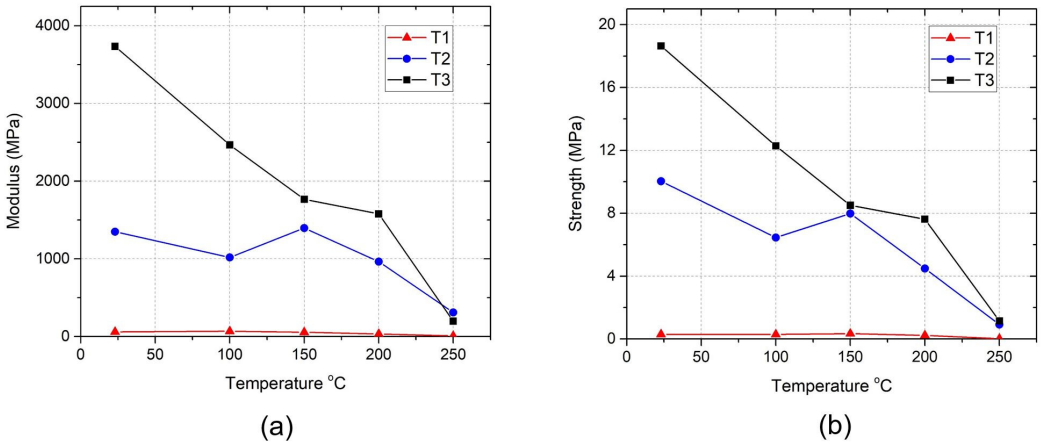

Fig. 2: Degradation of (a) modulus and (b) strength of T1, T2 and T3 configuration against elevated temperatures.

Compressive Properties under Elevated Temperatures

Fig. 3 shows the reduction in mechanical properties of the C1, C2 and C3 configurations with increasing temperature. It is obvious that samples lost most of their strength and modulus at 250°C. Configuration C3 exhibited higher strength and modulus than the other configurations at each temperature. The reason was again related to the orientation of fibers. C3 had three layers loaded in the strong direction, whereas C2 had only two layers. C1 was loaded in the weakest direction (transverse direction), therefore, it exhibited noticeably lower strength and modulus compared to C2 and C3. The effect of moisture was not as pronounced as in the tensile configurations since the specimens were more compact.

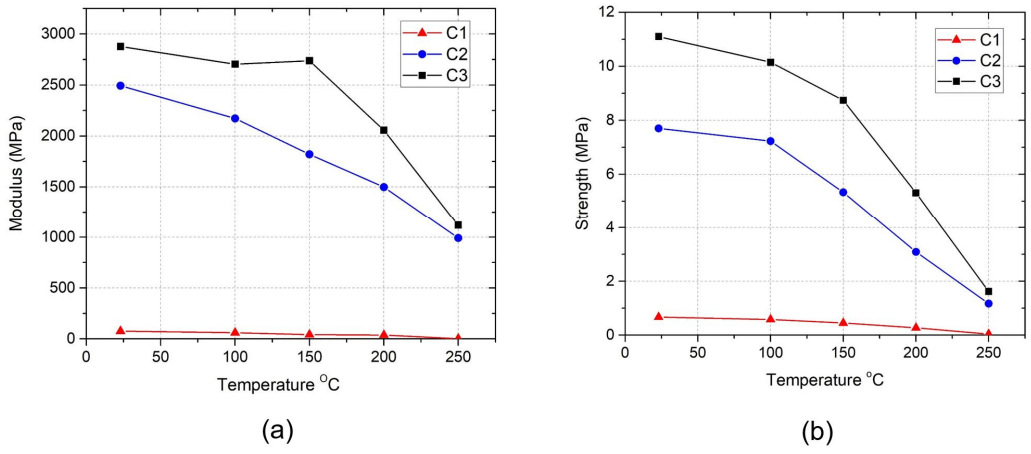

Fig. 3: Degradation of (a) modulus and (b) strength of C1, C2 and C3 configuration against elevated temperatures.

Shear Properties under Elevated Temperatures

Fig. 4 compares the degradation of modulus and strength of shear samples against elevated temperatures. A similar continuous degradation of the properties was exhibited as in tension and compression. Again moisture effects occurred with associated phases of recovery, depending on the specimen configuration. Therefore, the experiments at 100°C were repeated using dried specimens. The specimens were left in an oven at 105°C for 48 hours before the experiments. By drying specimens, modulus and strength increased approximately 11% and 25%, respectively (not shown in Fig. 4).

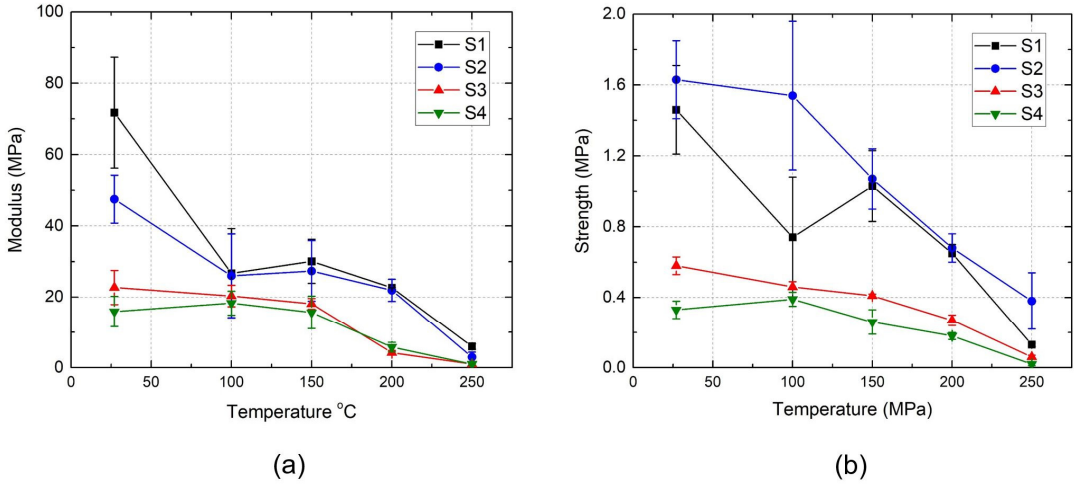

Fig. 4: Degradation of (a) modulus and (b) strength against elevated temperature of shear specimens.

4. CONCLUSIONS

This paper presents a comprehensive experimental study to characterize the tensile, compressive and shear properties of a veneered Balsa wood product, BALTEK® VBC, under elevated temperature. The following conclusions were drawn:

1. For tensile, compressive and shear specimens, the properties (modulus and strength) significantly decreased due to the effect of temperature. At 250°C, the material almost lost the load carrying capacity. Some specimens even started burning.
2. The effect of moisture content on the thermomechanical behavior was particularly noticed in the tension and shear experiments and was largely dependent on the specimen configuration, i.e. the portion of areas with cut fibers.
3. The results demonstrated that failure modes, stress-strain behaviors, modulus and strength values varied significantly and were closely associated with the fiber and loading directions.

REFERENCES

[1] Osei-Antwi M, De Castro J, Vassilopoulos AP, Keller T. Shear mechanical characterization of Balsa wood as core material of composite sandwich panels. Construction and Building Materials. 2013 Apr 1; 41: 231-8.

[2] Goodrich T, Nawaz N, Feih S, Lattimer BY, Mouritz AP. High-temperature mechanical properties and thermal recovery of Balsa wood. Journal of wood science. 2010 Dec 1; 56(6):437-43.

[3] Giancaspro J, Balaguru PN, Lyon RE. Use of inorganic polymer to improve the fire response of Balsa sandwich structures. Journal of materials in civil engineering. 2006 Jun;18 (3):390-7.

[4] ASTM D3500-14, Standard Test Methods for Structural Panels in Tension, ASTM International, West Conshohocken, PA, 2014, www.astm.org.

[5] ISO 22390:2010, Timber structures - Laminated veneer lumber-Structural properties, ISO/TC 165 Timber structures, ASTM International, West Conshohocken, PA, 2014, www.astm.org.

[6] ASTM D3501-05a(2011), Standard Test Methods for Wood-Based Structural Panels in Compression, ASTM International, West Conshohocken, PA, 2011, www.astm.org.

[7] ASTM D5379 / D5379M-12, Standard Test Method for Shear Properties of Composite Materials by the V-Notched Beam Method, ASTM International, West Conshohocken, PA, 2012, www.astm.org.

[8] Gerhards CC. Effect of moisture content and temperature on the mechanical properties of wood: an analysis of immediate effects. Wood and Fiber Science. 2007 Jun 27; 14(1):4-36.

DOI: 10.5075/epfl-ICSS12-2018-257-259

SEAWATER EFFECTS ON THE COMPRESSION BEHAVIOR OF CARBON FIBER VINYLESTER BASED NAVAL COMPOSITES AND MULTISCALE MECHANICS

Dayakar Penumadu[1] and Vivek Chawla[2]
[1]Fred N. Peebles Professor and Joint Institute for Advanced Materials Chair of Excellence, [2]Graduate Student, University of Tennessee, Knoxville, Tennessee, USA, dpenumad@utk.edu

1. INTRODUCTION

The effect of sea water on the compression behavior of Vacuum Assisted Resin Transfer Molding (VARTM) based Carbon Fiber Vinyl Ester (CFVE) composites of relevance to US Navy has not been studied in the past and the most important aspect that has been neglected in the past is the role of microstructure on compressive loading. Evaluation of compression response for fiber reinforced composites has led to lot of scatter in the reported measurements and often assumed be partially coming from loading fixture misalignment and/or test procedures, without much consideration to local microstructure effects largely due to an inability to noninvasively probe the related multi-scale features governing the deformation mechanics. Degradation from exposure to harsh marine environment (seawater effects and temperature) observed for this CFVE material system under tension during the recent studies sponsored by US Office of Naval Research is proving to be further exacerbated in compression. This study provides the compression response of laminate facings that correspond to sandwich structures with PVC foam core and seawater effects.

2. MATERIALS, SPECIMEN PREPARATION, AND TESTING SETUP

The composite laminates were reinforced with carbon stitch bonded fabric (LT650-C10-R2VE from Devold AMT AS, Sweden), an equi-biaxial fabric produced using Toray's T700 12 K carbon fiber tow with a vinyl ester compatible sizing. The resin matrix used is Dow Chemical's DERAKANE 520A-40, a brominated vinyl ester formulated for the vacuum assisted resin transfer molding process and included post-curing after infusion. The VARTM process, offers a cost-effective way of manufacturing large and complex parts with appreciable consistency as per the US Navy experiences to date. Stitching has been shown to improve the inter-laminar fracture toughness in mode I and mode II and impact damage tolerance with minimal effects on the in-plane properties. The fiber tows were stitched with 14 g/m^2 polyester knitting as shown in the photographs of this biaxial fabric in Figs. 1(a) and 1(b).

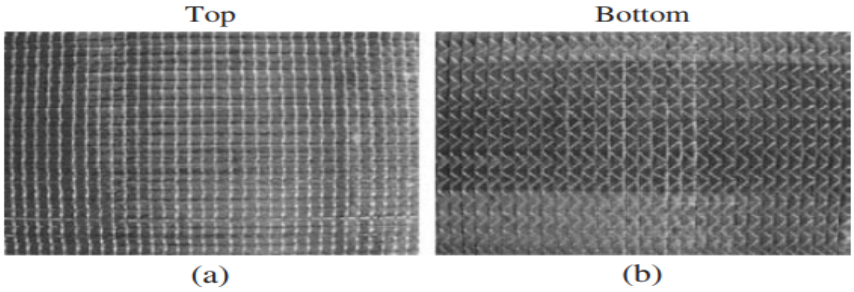

Fig. 1: T700 carbon fiber based equi-biaxial fabric: (a) fill (horizontal); (b) warp (vertical).

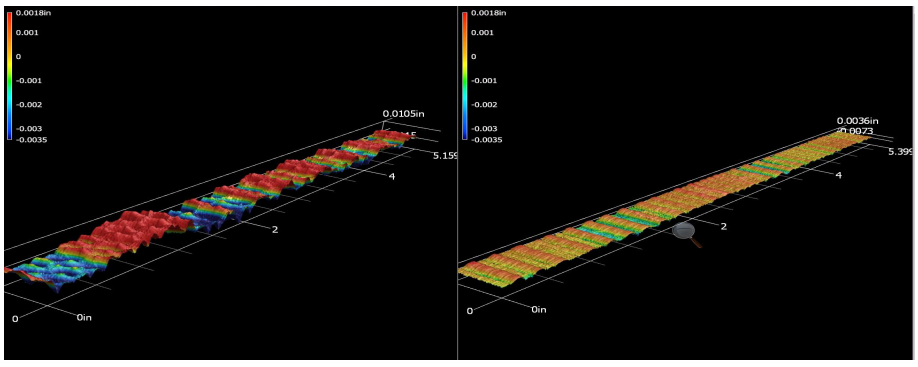

Fig. 2: Laser scan profiles of vacuum bag side versus mold side of the laminate showing substantially different microscale surface features on the top (B-side) and bottom (A-side) surfaces with impact on compression response.

VARTM process was used to fabricate composite panels by combining individual layers of the biaxial fabric using symmetrical lay-up. The total thickness of the panels obtained varied by 5% with an average thickness value of 2.7mm. Fig. 2 shows the difference of the surface roughness across the two faces (vacuum bag side and mold side) of the carbon fiber vinyl ester composite, measured using a Keyence 3D laser scanning instrument with violet laser for exceptional

precision. The top face (towards vacuum bag) shows significantly more roughness compared to the bottom face (mold plate side). This difference in roughness can be primarily attributed to the infusion where the facing in contact with the mold is smoother because of the resin settling down due to gravity before curing and the top face is rougher with interface to the vacuum bag during the infusion process. Tensile testing of Carbon Fiber Vinyl Ester composite was done as per ASTM D3039 with an extensional displacement rate of 2mm/min. Rectangular coupons of 200 x 25.4 x 2.7 mm are cut from the panels and tabbed at the ends as per the standard. Fig. 3(a) shows an example of a tabbed tensile specimen with dimensions. Compressive properties of carbon fiber vinyl ester composite (CF/VE) facings consisting of fiber dominated samples of $[0/90]_{2s}$ and matrix dominated samples of $[\pm45]_{2S}$ orientation are evaluated using ASTM D6641. Fig. 3(b) shows the compressive specimen dimensions, used without tabs as per the standard procedures. A gauge length of 12.7mm (0.5") was used to eliminate the size effects and to ensure that the failure does not happen because of the stress concentration at the ends of the gauge length. To determine the effects of fill, warp and shear, the laminates are cut along fill, warp and off-axis at 45^0 to give a laminate layup of $[0/90]_{2s}$, $[90/0]_{2s}$ and $[\pm45]_{2S}$ respectively.

Fig. 3: (a) Specimen dimensions in tension; (b) specimen dimensions in compression.

3. EFFECT OF SEAWATER AND COMPRESSION BEHAVIOR

Compression behavior of fiber reinforced composites has proven to be a very important but poorly understood aspect fiber reinforced composites and over the years there has been a considerable lack of understanding on best ways to measure it experimentally. This led to the development of Combined Load Compression (CLC) approach as the test fixture is easier to use, repeatable to manufacture, and less massive than the Illinois Institute of Technology Research Institute (IITRI) developed compression fixture. Standards exist for both approaches (ASTM D 6641 and D 3410). CLC test fixture is more recently widely adopted by the composites industry as the fixture is small, relatively easy to fabricate, and the combined use of end loading and shear loading in the grip region leads to more uniform state of compressive stress in the gage section, thus was used for this initial phase of this research. Specimens from two different panels were evaluated as shown in Table 1. Part of the specimens were time aged (dry) while other specimens from a given panel and location and orientation were soaked in sea water at 40^0C for several weeks (wet) till the moisture uptake reached saturation equilibrium monitored by periodic weight gain data.

Table 1: Summary results of compression behavior and sea water effects.

Panel	Environment	Specimen Orientation	Compression Modulus (GPa)	Compression Strength (MPa)	Compression Strength Reduction due to Sea Water Exposure (%)
Panel 1	Dry	0	49.35	399	
Panel 2	Dry	0	49	461	
Panel 1	Wet	0	43.75	269	32
Panel 2	Wet	0	57.4	349	24.3
Panel 1	Dry	45	11.6	127	
Panel 2	Dry	45	14.96	124	
Panel 1	Wet	45	11.55	118.5	7
Panel 2	Wet	45	14.55	118.1	4.7
Panel 1	Dry	90	46.96	422	
Panel 2	Dry	90	55.5	489	
Panel 1	Wet	90	47.35	415	1.6
Panel 2	Wet	90	56.1	444	9.2

In the absence of global buckling, polymer laminates in which most fibers are aligned with the external load, fail in compression by one of the three mechanisms: delamination, kink band formation or fiber collapse. Stitching causes significant distortion of both in-plane fibers and fibers within the stitches [1]. Due to the presence of localized defects and mis-orientations, fiber collapse is rarely the controlling failure mode for stitched laminates. The buckling stress can be estimated accounting for shear deformation and compliance of end condition [2].

The failure mechanism in tension is governed by the cluster of fiber breaks. The initial loading causes localized damage or local fiber breakage which is further arrested by the adjacent fibers. Since the ratio of the length of an individual fiber to its critical length, typically an aspect ratio of 100 is sufficient to fully mobilize interfacial shear stress for this particular sizing for the T700 carbon fiber with considered sizing, the tensile stress transfer is optimal leading to multiple locations of fiber breaks, leading to a coalescence of tow breaks and eventual failure. This failure mechanism in tension suggest less dependence upon the microstructural defects in the composite such as resin pockets and fiber misorientation. The tensile strength will certainly be affected by the misalignment of fibers due to stitching, but for fill and warp directions, the local misorientation due to stitching is much more critical for compression strength as can be seen from Fig. 4 which shows a decrease in fiber dominated directions along fill and warp of 60% when compared to tensile strength. Noticeable knock down was also observed for the modulus values. The matrix dominated laminate orientation is much less prone for reduction in compression response compared to tensile behavior.

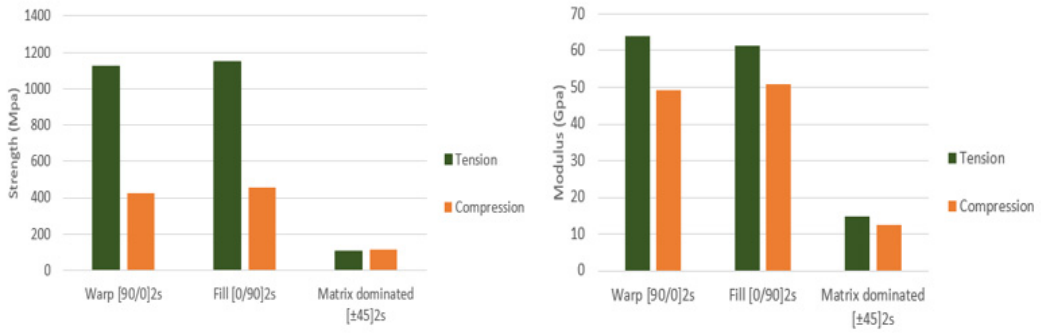

Fig. 4: Mechanical properties in tension and compression.

High resolution X-ray computed tomography show the importance of local microstructure on the observed differences in the compression response for warp and fill directions (Fig. 5).

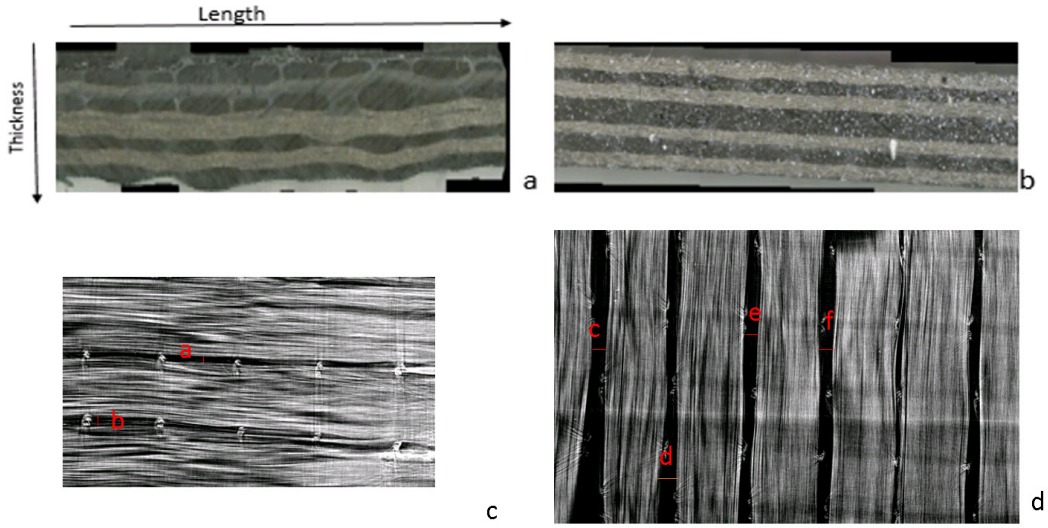

Fig. 5: Fiber waviness comparison: (a) Laminate cut parallel to warp; (b) laminate cut paralle to fill (X-ray CT Results); (c) front view of fabric showing straight stitched pattern; (d) back view of fabric showing zig-zag stitched pattern.

4. CONCLUSIONS

Compression behavior of carbon fiber based vinyl ester composites is largely dependent on the local fiber mis-orientations which were found to be significantly different along warp and weft directions for stitched fabric infused laminates. Largest degradation in the mechanical properties is observed along fiber direction with reductions as high as 32% due to long-term sea water exposure corresponding to post-'Fickian' moisture saturation state.

REFERENCES

[1] Reeder J. R. (1995) Stitching vs. a toughened matrix: compression strength effects. Journal of Composite Materials, 29(18), pp. 2464–2487.

[2] Mouritz A. P, Cox B. N. (2000) Mechanistic approach to the properties of stitched laminates. Composites part A: Applied Science and Manufacturing, 31(1), pp. 1–27.

SESSION 11B: IMPACT

DOI: 10.5075/epfl-ICSS12-2018-261-263

IMPACT RESISTANCE AND DAMAGE TOLERANCE ASSESSMENT OF COMPOSITE SANDWICH MATERIALS FOR AIRCRAFT

Moeen S. Rajput, Magnus Burman and Stefan Hallström
Department of Aeronautical and Vehicle Engineering, Division of Lightweight Structures,
KTH Royal Institute of Technology, SE 100 44, Stockholm, Sweden
mudsra@kth.se, mburman@kth.se, stefanha@kth.se

1. INTRODUCTION

Composite materials constitute a prime prospect to reduce the weight of aero engines and are now considered for several parts in modern turbofan engines. Polymer matrix composites are primarily used for components in the engines' cold section. KTH and GKN Aerospace perform research to develop technology for structural engine sandwich components. Being part of the load carrying structure in the aircraft engine, these components have to be designed for damage tolerance. With respect to the classic definition of sandwich structures the face-sheets (in the present study) cannot be considered as thin in relation to the foam core. An extensive experimental investigation on the damage tolerance of sandwich composite panels has been performed and an overview is presented in this work. Flat composite sandwich panels are subjected to low velocity impact at several energy levels in order to establish barely visible impact damage (BVID) and visible impact damage (VID) levels. According to aircraft airworthiness requirement, a component having either a BVID or VID impact damage should still be damage tolerant and airworthy to fly without jeopardizing the functionality of the aircraft [1,2]. The damage from impact in terms of dent depth, peak contact force, peak displacement and absorbed energy is measured.

2. MATERIAL SYSTEM

The face-sheets are quasi-isotropic carbon fiber, Tenax HTS45, NCF composites and three different thicknesses – 1.6, 2.4 and 3.1 mm – are investigated. The foam core is Rohacell 200Hero and a core thickness of 9 mm is used consistently for all configurations. All the test panels are manufactured using vacuum infusion with an epoxy (Araldite LY556) resin.

3. IMPACT TESTING

In order to perform the impact testing a state of the art, vibration-free, instrumented drop weight impact rig (DWR) was designed and built [3,4]. The working principle of the DWR is to separate the crosshead from the impactor assembly once the impactor tip comes in contact with the specimen. By doing so, dynamic oscillations from the drop rig are prevented to disturb the load cell attached to the impactor assembly during impact, meaning that the true impact response can be recorded relatively unaffected by noise.

The drop weight rig test setup is shown in Fig.1 (left) together with the force vs. time impact response (right) for different impact energies. The impact response is virtually free from adulteration from external vibrations and it is thereby possible to distinguish details related to different damage mechanisms from the force-time response.

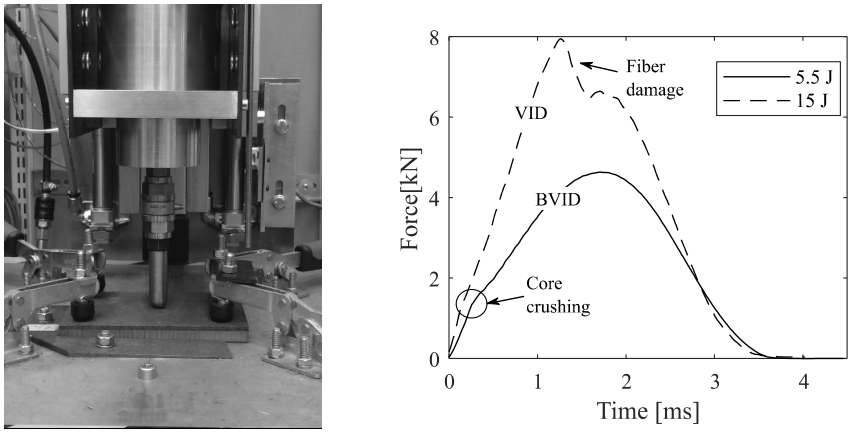

Fig. 1: Drop weight rig test setup (left) and force-time impact response for two different impact energies (right).

As seen in the graph in Fig.1 (right) the response is elastic for low energy impact (5.5 J) and does not show any significant load variation other than a hump near the start of a loading curve. This hump corresponds to the ultimate strength of the core material and is caused by core crushing [5,6]. In cases of higher impact energy (15 J in Fig. 1), a significant load drop is observed near the maximum contact force, which can be attributed to significant face-sheet damage in the specimen.

In order to understand the damage mechanism for both BVID and VID impact damage, a destructive inspection technique is used where by the impacted samples are sectioned in various directions with respect to the face-sheet ply orientations. The cut samples are polished and then inspected under a microscope. Fig. 2 shows examples of microscopy images from cut samples, where half of the impact area, around the point of impact, is shown for both BVID and VID damage samples.

For the BVID damage the main failure mode is delamination with multiple transverse shear cracks. Some core crushing and face-core de-bonding can also be noticed.

In case of a VID damage, several types of damage are observed. In addition to delamination and transverse shear cracks, significant fiber breakage and core crushing is visible. The magnitude of delamination also increases through the thickness. The delaminations predominantly grow along plies with radial fiber orientation with respect to the impact site. This significant damage in VID is also observed in the load-time response (Fig.1).

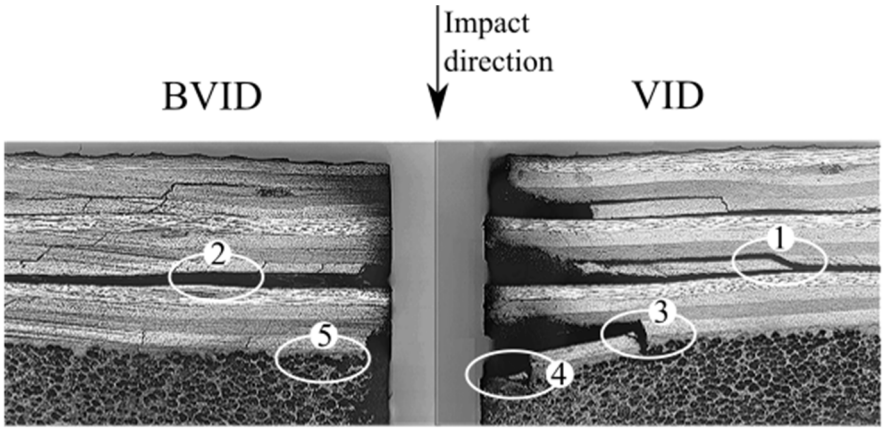

Fig. 2: Microscopy images of BVID and VID impact damages
1: Transverse shear crack, 2: delamination, 3: fiber breakage, 4: core damage, 5: Face-core de-bonding.

4. COMPRESSION AFTER IMPACT TESTING

A damage tolerance assessment of the impacted specimens is performed by subjecting the panels to in-plane compression. Instead of compressing the whole sandwich cross-section, only the impacted face-sheet cross-section is compressed in-plane. This is done to avoid the compressive by-pass load through the non-impacted side of the face-sheet and thus to prevent possible over-estimation of the residual compressive strength. Fig. 3 shows both the classical sandwich specimen compression and also compression after impact (CAI) in a single skin test case. CAI single skin specimens are manufactured by cutting the edge of the core material and the non-impacted face-sheet. The remaining core then provides sufficient lateral support to prevent global buckling without significantly affecting the load-bearing capacity. The loaded ends of the impacted face-sheet are tabbed in order to prevent local crushing and the compressive load is applied by gripping the tabbed ends.

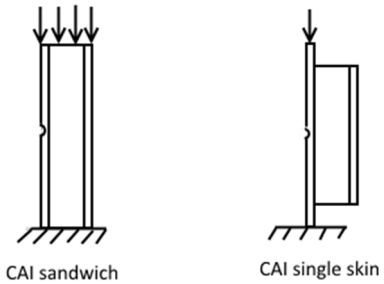

Fig. 3: Type of test configuration for compression after impact test.

Fig. 4 (left) shows the normalized residual strength vs. impact energy for all three specimen configurations. For each face-sheet configuration three impact damage levels are shown, i.e. LLD, BVID and VID, whereas their residual strengths are normalized with the strength of their non-impacted specimens, i.e. the ultimate load of the respective reference configuration. The residual strength decreases with increased impact energy. For BVID damage the knock down strength for the three face-sheet thicknesses, 1.6, 2.4 and 3.1 mm, came out as 14%, 20% and 25%, respectively, and for VID impact damage the measured loss of residual strength was 28%, 25% and 30%, respectively.

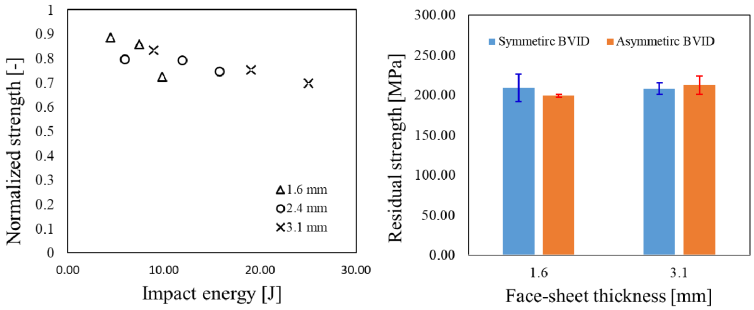

Fig. 4: Normalized residual strength vs impact energy for different face-sheet thicknesses (left), and effect of symmetry on the residual strength of the impacted specimens (right).

In addition to the symmetric sandwich specimens, asymmetric specimens were also manufactured and tested both under low velocity impact and damage tolerance testing. Asymmetric specimens are manufactured with varying face-sheet thicknesses, i.e. one face-sheet side with a thickness of 1.6 mm and the other with a thickness of 3.1 mm. Impact testing is performed on each side of the face-sheet separately and left the other side un-impacted. Damage tolerance testing is performed on the impacted samples by compressing the impacted side alone. The effect of symmetry on the residual strength was studied and the results are shown in Fig. 4 (right) where the residual strength of two different face-sheet configurations are plotted. There is no significant difference in residual strength for asymmetric sandwich specimens compared to the symmetric ones.

5. NUMERICAL STUDY

A finite element model was developed in Abaqus Explicit and the low velocity impact event was simulated for the different face-sheet configurations. The face-sheets were modeled with continuum shell elements whereas the core was modeled with 3D solid elements. For intra-laminar failure, the Hashin damage initiation criterion was used, whereas inter-laminar failure was modeled by inserting cohesive surface elements between each ply in the face-sheet laminates. In Fig. 5 the numerical impact force-time response from FE model is compared with the experimental results. The FE model predicts the peak load with good accuracy and the model is also able to capture the sudden drop in load for the VID impact damage.

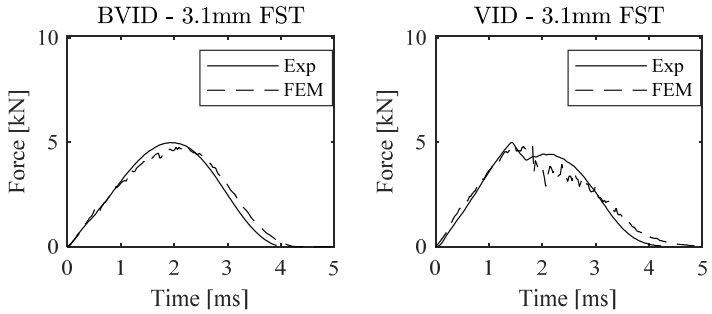

Fig. 5: Force-time impact response, comparison of results from FE simulations and experiments.

6. CONCLUSION

Impact and damage tolerance assessment of sandwich components with relatively thick face-sheets was performed. A vibration free drop weight impact testing rig successfully captured the true impact response. Impact testing is performed to identify the impact energies causing BVID and VID damage. Fractography inspection shows different types of damage in VID specimen whereas delamination is prominent for the BVID case. Thorough testing of compression after impact shows how the residual strength decreases with increasing impact energy and the developed FE models predict the impact response with good accuracy.

REFERENCES

[1] AC 25.571-1D - Damage Tolerance and Fatigue Evaluation of Structure. (https://www.faa.gov/regulations_policies/)
[2] X. Jian, L. Yao, Study on Airworthiness Requirements of Composite Aircraft Structure for Transport Category Aircraft in FAA, Procedia Eng. 17 (2011) 270–278. doi:10.1016/j.proeng.2011.10.028.
[3] M.S. Rajput, Design and evaluation of a novel instrumented drop-weight impact test rig, (n.d.).
[4] M.S. Rajput, S. Hallstrom, M. Burman, Impact testing apparatus, n.d.
[5] M.S. Rajput, M. Burman, J. Köll, S. Hallström, Compression of structural foam materials – Experimental and numerical assessment of test procedure and specimen size effects, J. Sandw. Struct. Mater. (2017) 1–29. doi:10.1177/1099636217690500.
[6] M.S. Rajput, M. Burman, S. Hallström, Distinguishing between strain measurement procedures during compressive testing of foam materials, 20th Int. Conf. Compos. Mater. Cph. (2015).

DOI: 10.5075/epfl-ICSS12-2018-264-266

LOW-VELOCITY IMPACT RESPONSES AND CAI PROPERTIES OF SYNTACTIC FOAM SANDWICH COMPOSITES

Jun Wang[1], Hota GangaRao[2], Ruifeng Liang[3] and Weiqing Liu[4]
[1]College of Civil Engineering, Nanjing Tech University, Nanjing, People's Republic of China, wangjun3312@njtech.edu.cn
[2]Department of Civil and Environmental Engineering, West Virginia University, Morgantown, WV, USA, Hota.Gangarao@mail.wvu.edu
[3]Department of Civil and Environmental Engineering, West Virginia University, Morgantown, WV, USA, Ruifeng.Liang@mail.wvu.edu
[4]College of Civil Engineering, Nanjing Tech University, Nanjing, People's Republic of China, wqliu@njtech.edu.cn

1. INTRODUCTION

Sandwich composites usually serve the dual function of carrying loads and absorbing energy, due to their prominent advantages of light weight, high flexural and transverse shear stiffness, and environmental resistance [1-3]. However, they are susceptible to low-velocity impacts because the internal damages induced by impacts often result in a sudden destruction of the structures [4]. Syntactic foam consisted of hollow particle fillers in polymer matrix is one of promising core materials for sandwiches, in which the syntactic foam provides superior compressive strength, high damage tolerance and energy absorption ability [5]. The increasing applications of syntactic foam sandwich composites in marine structures, transportations and civil infrastructures require full understanding of the mechanism of impact responses and reliable assessment of damage tolerance.

The use of a syntactic foam as sandwich core can increase the stiffness and strength of sandwiches significantly without a large weight increase [6-8]. However, there is little work concerned on the evaluation of damage and residual strength of syntactic foam sandwich composites after impact. Therefore, the present study focuses on characterizing the impact damage and CAI strength of sandwich panels with GFRP facesheets and syntactic foam core. Influences of the number of GFRP skin layers, syntactic foam density and the existing of lattice webs, as well as the applied impact energy were discussed.

2. EXPERIMENTAL PROGRAM

Materials and Specimens

E-glass bidirectional woven fabrics with fiber orientation angle 0/90° and vinyl ester resin were used in facesheets and lattice webs. The macrosphere syntactic foams, supplied by Engineered Syntactic Systems, USA, with density of 450 kg/m3 and 480 kg/m3 were used in this study. Vacuum assisted resin infusion process was used to manufacture GFRP-syntactic foam sandwich panels. Total 40 specimens were prepared including 8 bare syntactic foam panels, 16 GFRP-syntactic foam sandwich panels without webs, and 16 GFRP- syntactic foam sandwich panels with lattice webs. The distance between the webs is 50 mm. All the test specimens are of the same width of 100 mm, length of 150 mm and core height of 50 mm.

Impact Testing

DTM1203 drop-weight impact testing machine was used to impact the specimens at room temperature. The maximum drop height is 2 m. The steel impactor has a semicircular nose with a diameter of 16 mm and weight of 5.5 kg. During testing, the impactor is raised automatically by an automatic control system. Three different drop heights were used (0, 0.8 m, 1.2 m and 2 m), in which the applied energy can be varied from 0 J to 108 J. Each specimen was impacted only once. Four corners of the test specimens were clamped to avoid slippage and rotation. Fig. 1(a) shows the test set up of low-velocity impact.

The time histories of impact load were captured with a piezoelectric sensor mounted onto the drop hammer. The maximum penetration depth (MPD) was measured by a micrometer gauge with a resolution of 0.01 mm just after impact.

CAI Testing

A universal testing machine with 600 kN capacity was used for testing edgewise compressive strength of damaged and undamaged specimens. The test was conducted in strain control with a loading rate of 1.25 mm/min. During testing, the compressive load was applied through a very stiff steel top panel, and was collected via a load cell mounted directly above the top panel. The displacement of crosshead was recorded by the actuator automatically. Steel fixture systems were applied to both ends of the sandwich columns to minimize the stress concentrations of the facesheets at the contact with loading panels and to ensure uniform load transfer. In accordance with ASTM D7137/7127M-12 [26], all the specimens were loaded until the maximum load was reached and load had dropped off about 30% from the maximum. The test set-up of edgewise compression was shown in Fig.1 (b).

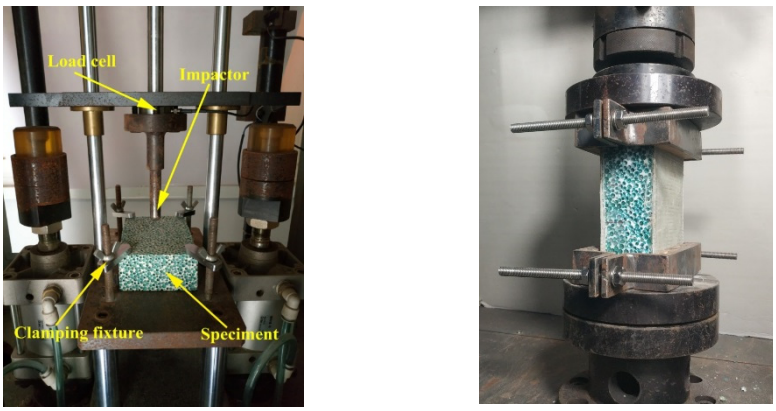

(a) Low-velocity impact (b) Edgewise compression

Fig.1: Test set-up.

3. RESULTS AND DISCUSSION

Impact Responses

The bare syntactic foam panels exhibited a circular dent on the impact face. The increase in applied impact energy from 41 J to 108 J leads to 33% increments in the peak load of impact and 61% ~ 76% increments in the MPD for bare syntactic foam panels, respectively. Under the same applied impact energy, the MPD of syntactic foam panels with foam density of 450 kg/m^3 was 20%~40% higher than the panels with foam density of 480 kg/m^3.

For GFRP- syntactic foam sandwich panels without webs under the applied impact energy 41 J, the damage is concentrated in the facesheets and has a diamond shape due to the breakage of fibers in the longitudinal and transversal directions. The deformation of the core in the impact zone was insignificant. However, with the increase in applied impact energy, the shape of damage turned to be a circle due to the crushing of resin and delamination between FRP layers, and the facesheets in the loading location was penetrated resulting in a deeper MPD in the foam core. The MPD of sandwich panels was much smaller than that of bare syntactic foam panels.

The damage mode of GFRP- syntactic foam sandwich panels with webs was similar with those sandwiches without webs. However, the sandwich panels with webs have smaller damage width and penetration depth than the counterparts without webs.

Given the same thickness of core and skins, the peak load of impact of GFRP-syntactic foam sandwiches was about two times that of GFRP- polymethacrylimide (PMI) foam sandwiches under 40 J in Ref [9], and the corresponding MPD of GFRP-syntactic foam sandwiches was much smaller than that of GFRP- PMI foam sandwiches.

Damaged Sandwich Panel Compression

Fig.2 shows the condition of damaged specimens after edgewise compression. The cracks of damaged syntactic foam columns were initiated from the impact dent due to the stress concentration in this region, and then propagated in transversal and vertical directions. For damaged sandwich columns without webs, widespread debonding between the facesheets and core occurred on both sides accompanied by vertical crack propagation in the foam core. The sandwich columns without webs were failed due to the facesheets being buckled into a half-wave and shear buckling of the foam core. The failure mode of damaged sandwich columns with webs is comprised by the debonding of facesheets, core being crushed between two webs, as well as delamination in GFRP layers, especially in the facesheets contained impact damage. The debonding area of panels with webs was much smaller than that of panels without webs because the debonding between the facesheets and the foam was controlled by the webs. Meanwhile, wrinkling occurred at the intersection of facesheets and webs. The indention of the facesheets under edgewise compression propagated from the top surface of facesheets to the intersection of facesheets and the top web until this intersection reached to the critical location, resulting in local buckling at the top intersection. Then the indention continued to propagate to the intersection of facesheets and the bottom web and caused local buckling at this intersection. This wrinkling process not only causes the delamination of facesheets, but also results in shear buckling of the foam core between two webs.

The ultimate load of damaged bare syntactic foam panels after 108 J was only reduced less than 8% in comparison with the undamaged panels. Although the damage depth of sandwich panels was much lower than that of bare syntactic foam panels, the ultimate load of damaged sandwich panels with and without webs after 108 J was reduced by about 8%~14% in comparison with the undamaged panels. This is attributed to the fact that the impact dent aggravates the debonding of facesheets and core and delamination of GFRP layers.

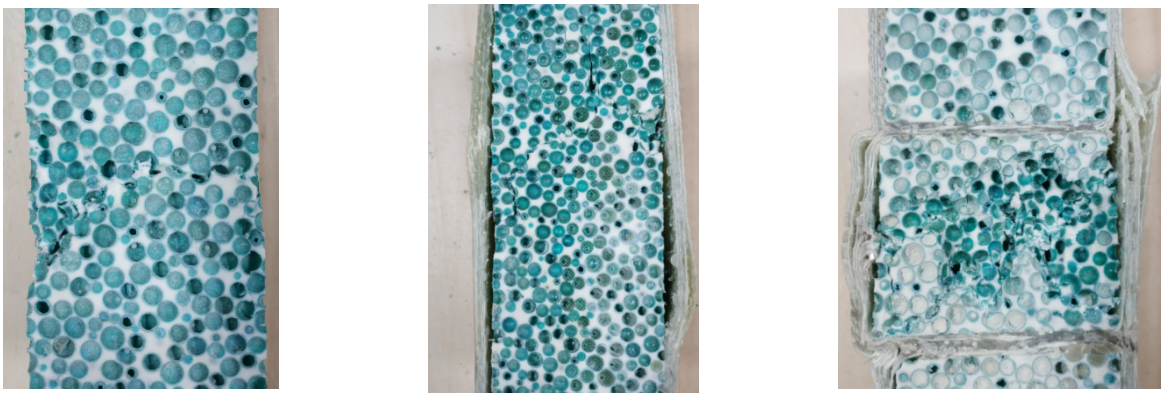

(a) Bare foam panels (b) Sandwich panels (c) Sandwich panels with webs

Fig.2: Edgewise compressive failure mode of damaged specimens.

4. CONCLUSIONS

The impact and post impact behavior of GFRP- syntactic foam sandwich panels were investigated. The results obtained from this study are summarized as follows:

(1) The damage shape of sandwich panels under impact is relative to the applied impact energy and layers of GFRP facesheets. The GFRP- syntactic foam sandwich panels have a diamond damage shape for specimens with 2 or 4 layers of facesheets after 41 J due to the fracture of fibers in orthogonal directions. Further increasing the number of GFRP layers or impact energy resulted in resin crushing and debonding of the facesheets and foam core, thus causing a circular damage on the impacted facesheets. The MPD of sandwich panels is much smaller than that of bare syntactic foam panels. Moreover, the existing of lattice webs contributes to decrease the MPD of sandwich panels. This is because the core in the central of the panel is confined by GFRP, resulting in the increase in the strength and stiffness of the core.

(2) The cracks of damaged syntactic foam panels under edgewise compression were initiated from the impact dent due to stress concentration, and then propagated in transversal and vertical directions. The damaged sandwich panels without webs failed predominantly by debonding between facesheets and core, the buckling of facesheets and the shear buckling of the foam. The existing of lattice webs contributes to prevent the debonding of the facesheets from the foam core, and delamination and local buckling of facesheets prevailed in sandwich panels with webs.

(3) All the sandwich panels, with and without webs, exhibited a four-phase displacement: linear-elastic phase, plastic phase, foam compaction phase and facesheets buckling phase. However, the sandwich panels with webs exhibited much larger plastic deformation than the sandwich panels without webs. After 108 J, the ultimate load of damaged bare syntactic foam panels was only reduced less than 8% in comparison with the undamaged panels, while the ultimate load of damaged sandwich panels with and without webs after 108 J was reduced by about 8%~14%. This is attributed to the fact that the impact dent aggravates the debonding of facesheets and core and delamination of GFRP layers.

REFERENCES

[1] Walsh J. et al., "Low velocity impact resistance and energy absorption of environmentally friendly expanded cork core-carbon fiber sandwich composites", *Compos. Part A-Appl. S.*, 2017; 101:290-296.

[2] Liu C. et al., "Tensile properties and failure mechanism of 3D woven hollow integrated sandwich composites", *Appl. Compos. Mater.*, 2017; 24: 1151-1163.

[3] Satasivam S.et al., "Mechanical performance of bolted modular GFRP composite sandwich structures using standard and blind bolts", *Compos. Struct.*, 2014; 117: 59-70.

[4] Ude A.U. et al., "Impact damage characteristics in reinforced woven natural silk/epoxy composite face-sheet and sandwich foam, coremat and honeycomb materials", *Int. J. Impact. Eng.*, 2013; 58:31-38.

[5] Gupta N. et al., "Compression properties of syntactic foams: effect of cenosphere radius ratio and specimen aspect ratio", *Compos. Part A-Appl. S.*, 2004; 35: 103-111.

[6] Kumar S.J.A. et al., "Compression behavior and energy absorption capacity of stiffened syntactic foam core sandwich composites", *J. Reinf. Plast. Comp.*, 2013; 32: 1370-1379.

[7] Omar M.Y. et al., "Syntactic foam core metal matrix sandwich composite: compressive properties and strain rate effects", *Mat. Sci. Eng. A*., 2015; 643: 156-168.

[8] Corigliano A. et al., "Experimental characterization and numerical simulations of a syntactic-foam/glass-fibre composite sandwich", *Compos. Sci. Technol.*, 2000; 60: 2169-2180.

[9] Shipsha A. et al., "Compression-after-impact strength of sandwich of sandwich panels with core crushing damage", *Appl. Compos. Mater.*, 2005; 12: 149-164.

DOI: 10.5075/epfl-ICSS12-2018-267-269

DESIGNING AND BUILDING FOR IMPACT: QUANTITATIVE DYNAMIC SHEAR STRENGTH OF SANDWICH CORE MATERIAL

Mark Battley[1], Thomas Basset[2], Tom Allen[1], John Weber[1] and Raphael Gerard[2]
[1]University of Auckland, New Zealand. m.battley@auckland.ac.nz, tom.allen@auckland.ac.nz, jweb106@aucklanduni.ac.nz
[2] Gurit Composite Engineering, New Zealand. thomas.basset@gurit.com, raphael.gerard@gurit.com

1. INTRODUCTION

When considering structural failure during an impact, the energy that can be absorbed by the material can be more important than its ultimate static strength. Often the dynamic energy absorption is assumed to be approximated by the strain energy accumulated during a quasi-static test before failure, which depends as much on the elongation at break as on the maximum load sustained. As a result, for core materials, the shear elongation at break has thus become considered to be as important a property as ultimate shear strength [1].

Nonetheless, it has also been found that the transient nature of impact loads can cause stress and strain rates that are high enough to affect the behaviour of the core material, including the resulting strength, particularly for polymeric foams [2]. As a result, the static energy absorption is still a qualitative indication of the likely dynamic behaviour of a core material, but cannot be taken as a quantitative measure of the dynamic property by itself. The aim of this paper is to undertake characterisation of the dynamic shear strength of cores at various loading rates, in order to build a quantitative database of material performance

2. EXPERIMENTAL METHODOLOGY

Summary

A drop weight dynamic 4pt bending test was used to characterise core materials across a range of chemistry, densities, and strain rates. The different chemistries included in this study are cross-linked polyvinyl chloride (PVC, 80, 100 and 130 kg/m^3), polyethylene terephthalate (PET, 90, 110 and 135 kg/m^3) and styrene acrylonitrile foams (SAN, 80, 100 and 130 kg/m^3), representing a range of different levels of ductility and maximum elongation. Quasi-static 4pt bending was also undertaken of the same specimen types to provide benchmark static data.

Specimens

The nominal specimen geometry was 60 x 500 x 33mm (W x L x T). The upper fiberglass beam skins were thicker in the regions where the loading bars contact the specimen to prevent minimise the likelihood of localized skin failure. Specimens were manufactured by Gurit with 12 specimens provided for each core material and density.

Dynamic Beam Testing System

The high-rate beam testing was undertaken in an IMATEK IM10 Drop Weight Impact Testing system as shown in Fig. 1. Four point load and support spans of 133 and 330mm respectively were used to test the specimens. Impacts of the SAN and PVC cored beams were performed at 3.5 m/s with an impacting mass of 34.7 kg. Impacts of the PET cored beams were performed at 2.0 m/s with an impacting mass of 14.7 kg due to the low failure energy of the PET. Rubber and steel pads were placed on top of the fiberglass pads to reduce dynamic signal noise during the impact event. A high speed camera was used to record the failure process and assist in identifying and comparing failure modes.

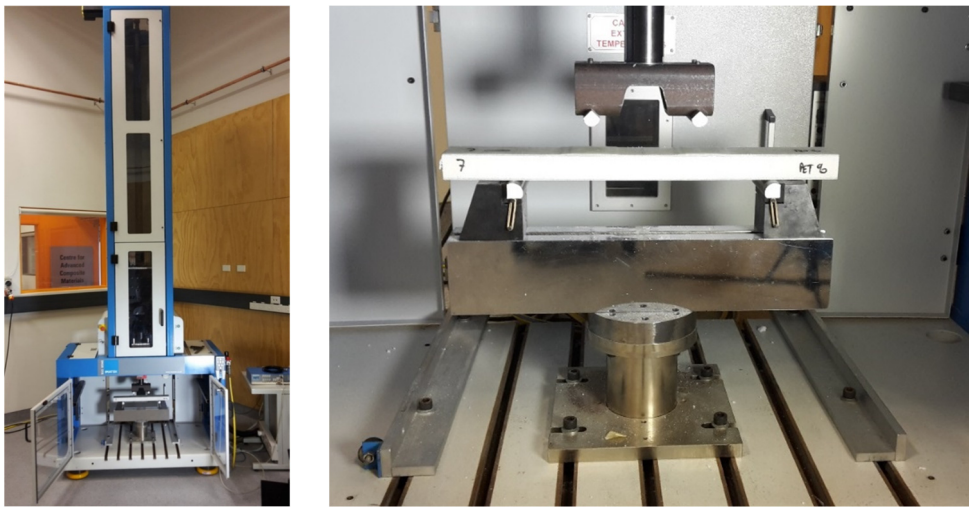

Fig. 1: Drop weight impact testing system.

3. RESULTS

Failure Modes

Under dynamic loading all of the core types failed by transverse shear as expected, however the shear failure differed between materials. The SAN foam was the most ductile, undergoing significant plastic deformation before failing in transverse shear fracture. The PVC core had some plastic deformation before also failing in transverse shear fracture. The PET cores failed as brittle transverse shear fractures. Fig. 2 compares failure modes for 100J impacts, with only plastic deformation for the SAN 100 core (top), a single crack transverse shear fracture for PVC 100 (middle) and complex multiple shear fractures for the PET (bottom).

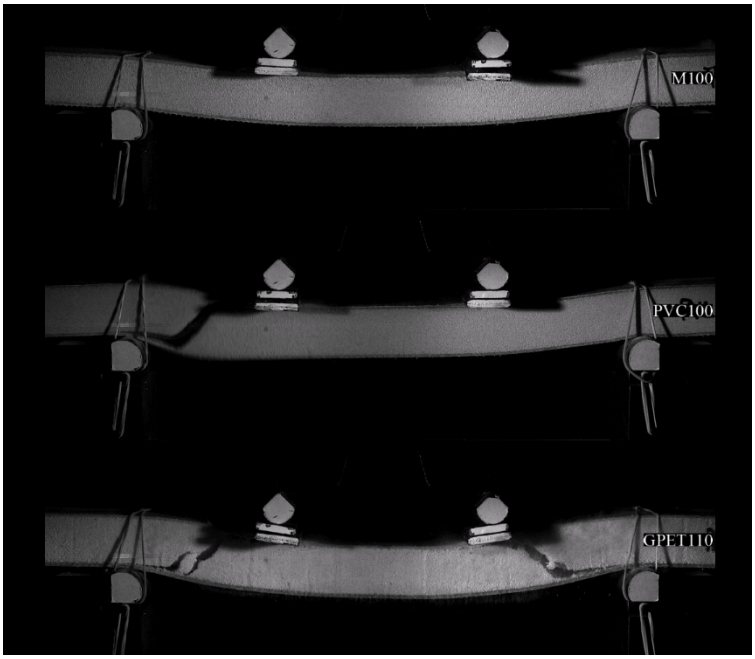

Fig. 2: Failure modes for 100J impacts.

Shear Strength and Energy to Failure

Fig. 3 presents typical load displacement curves for static and dynamic tests, taking as an example the 100 J impacts shown above for the SAN and PET samples. The high-speed camera images were used to identify the time at which fracture occurred for the energy calculations.

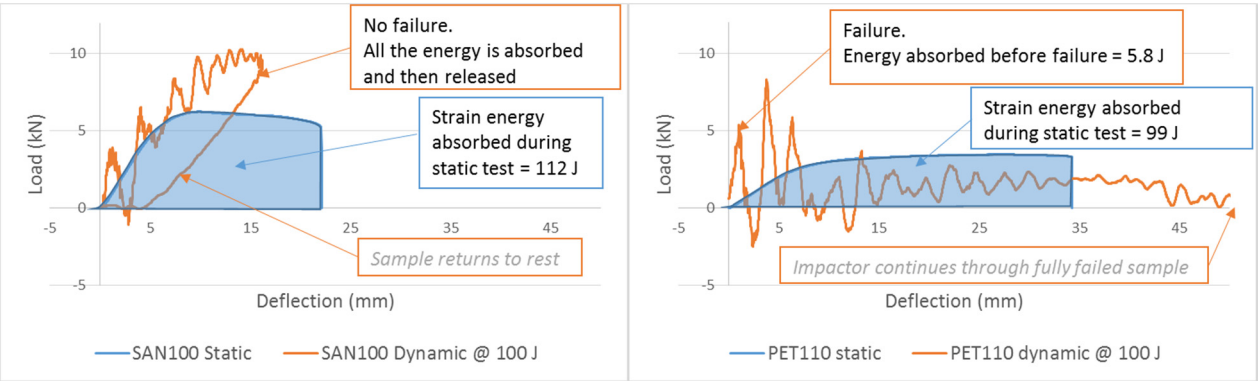

Fig. 3: Load Displacement curves for 100J impacts.

Fig. 4 compares the static and dynamic transverse shear strength and energy to failure for each of the materials. While the failure load (apparent shear strength) is higher dynamically than statically for almost all materials, the true ability of the material to sustain these loads in an impact scenario (energy absorption) varies greatly across the three material types. The SAN foam is able to absorb more energy in a dynamic impact than in a quasi-static test, whereas the PVC cannot sustain the same energy as statically, and the PET suffers a large reduction in its ability to absorb energy in a dynamic loading scenario.

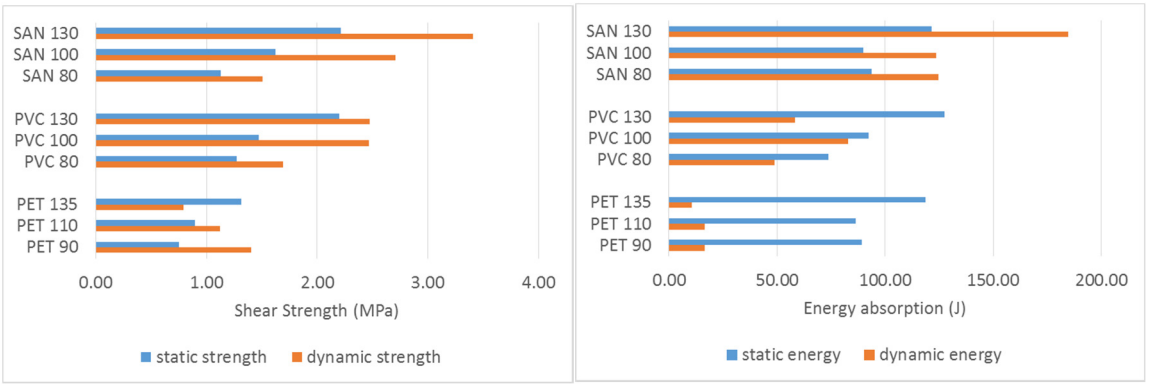

Fig. 4: Static and dynamic transverse shear strength (left) and failure energy (right).

The static shear strength increases with density for all materials, but the dynamic shear strength increases with density only for the SAN material. It plateaus at 100 kg/m3 for the PVC material, and decreases for PET, which results in PET 135 having a lower dynamic shear strength than static, actually only marginally higher than the static shear strength of PET 90.

Across material types, the static energy absorption is of a similar order of magnitude, and only follows a definite trend as a function of density for the PVC material, where it increases with increasing density. For SAN and PET the 130 (rep. 135) density is better than the 80 and 100 (respectively 90 and 110), which are close together. Overall the SAN 130, PVC 130 and PET 135 form a group of high static energy absorption materials at around 120J, SAN 100, SAN 80, PVC 100, PET 110 and PET 90 have a medium level of static energy absorption at around 90J, while PVC 80 is the material able to absorb the least energy in a static test, at 74J. The range of static energy absorption is thus 1.7 (PVC 80 at 74 J to PVC 130 at 127 J)

The dynamic energy absorption varies greatly across material types, increasing from PET to PVC to SAN, with a ratio of 17 between the material able to absorb the least energy, PET 135 at 11J, and the material able to absorb the most, SAN 130 at 185J. Within a material type, there is also no clear trend relating dynamic energy absorption ability to density: For PET, the dynamic energy absorption ability for the 135 density is lower than for the 90 and 110 densities, which have similar dynamic energy absorption ability. For PVC, 100 is higher than 130, itself higher than 80. For SAN, the dynamic energy absorption ability for the 130 density is higher than for the 80 and 100 densities, which have similar dynamic energy absorption ability.

4. CONCLUSIONS

There are significant differences in the dynamic transverse shear strength and failure energy of cores depending on the type of material. Very ductile cores such as SAN have significantly higher strengths and failure energies dynamically than statically and the dynamic strength increases with density. For moderately ductile materials such as PVC the relative dynamic strength depends on the particular density, with higher density cores not necessarily resulting in greater strengths, and the energy absorption is lower dynamic than statically. More brittle cores such as PET can have lower strengths dynamically than statically, particularly at higher densities, and can have very low energy to failure during impact loading.

The results also demonstrate that the static shear strength and strain energies to failure are not good indicators of the core material's performance during impact loading, and highlight the need to better understand the behavior of polymeric core materials during dynamic loading. Consideration also needs to be given to how best to incorporate this behaviour into material selection and design processes.

REFERENCES

[1] M. Burman et al., "Characterisation of ductile core materials", *J. Sandwich Structures and Materials*, 2010; 12-2: 237-252
[2] M. Battley, et al., "Shear Strength of Sandwich Core Materials Subjected to Loading Rates Relevant to Water Slamming", *J. Reinforced Plastic and Composites*, 2014 33-6: 506-513

DOI: 10.5075/epfl-ICSS12-2018-270-272

IMPROVEMENT OF THE IMPACT BEHAVIOUR OF FOAM CORE SANDWICH THROUGH THE USE OF A CORK LAYER AS IMPACT SHIELD

M. Adli Dimassi[1], Tim Dunker[2], Christian Brauner[3] and Sawsane Nakouzi[4]
[1]Faserinstitut Bremen e.V., Germany. dimassi@faserinstitut.de
[2]University of Bremen, Germany. tdunker@gmx.de
[3] University of Applied Sciences Northwestern Switzerland, Switzerland. christian.brauner@fhnw.ch
[4] University of Applied Sciences Northwestern Switzerland, Switzerland. sawsane.nakouzi@fhnw.ch

1. INTRODUCTION

Foam core sandwich structure made of two stiff and strong face sheets and separated, by a low-density closed cell foam core, exhibit higher specific stiffness and strength compared to monolithic composites [1]. Since standard sandwich structures with honeycomb or foam core are susceptible to low-velocity impact and foreign object damage (FOD), its use in aerospace is limited to non-carrying structures like the elevator and the high lift devices [2].

Impacts on foam core sandwich may create invisible damages consisting of skin delaminations, face sheet debonding, core crushing and core shear cracks. Most critical are shear cracks, as they degrade the residual compressive strength of an impact-damaged composite structure and could lead to the loss of the structure integrity [3].

Substituting traditional foam materials with a cork core has a high potential to be used in FOD endangered sections of an aircraft. Cork core sandwich structures show better impact damage tolerance, remarkable natural damping behaviour and higher energy absorption compared to Polymethacrylimid (PMI) foams [4]. Thanks to the cellular structure and the viscoelastic properties of the cork, cork core materials show superiority when used as thermal/sound insulating panels or for vibration damping purposes [5]. Moreover, due to its high temperature withstanding property the use of cork agglomerates is very well established in rocket boosters and re-entry space vehicles [6]. Nevertheless, because of lower specific properties of cork composite compared to foam core sandwich with PMI foams (for instance Rohacell®) the use of cork in aircraft structures is very limited.

In order to make benefits of the impact damage resistance of the cork and to fulfil the stiffness requirements of an aerospace structure, a new hybrid sandwich layout is proposed. In this work, sandwich specimens made up of two CFRP-facings and a core composed of foam material and a cork layer on the impact loaded side of the test specimens have been manufactured, the impact behaviour was investigated and compared to a reference sandwich configuration without cork layer.

2. EXPERIMENTAL TESTS AND MATERIALS

Materials and Manufacturing

The vacuum assisted resin infusion (VARI) process was used for the manufacturing of the sandwich specimens. The face skins consist of two layers Toho Tenax HTS40 carbon fibre Non-Crimp Fabrics (NCF) impregnated by EPICOTE™ RESIN MGS™ RIMR035c. All the tested specimens have a face sheet thickness of about 0.75 mm. The PET100 3D|Core™ foam core with integrated honeycomb structure was chosen as reference core. The Amorim CoreCork NL 20 with a thickness of 3 mm and a density of 200 kg/m³ was used to manufacture the hybrid sandwich. The cork layer was perforated at predefined intervals to ensure the bonding of the cork to the foam core during the resin infusion. Moreover, the honeycomb perforation of the 3D|Core™ enables a better bonding of the cork layer compared to standard foam core.

Fig. 1 shows the VARI-setup to manufacture the hybrid sandwich panel. Two resin inlets were used to ensure the impregnation of the face sheets and the bonding of the cork layer. For the manufacturing of the reference panels without cork layer, only one resin inlet on the top face of the sandwich panel was used as the honeycomb-like perforation in the 3D|Core™ enables the resin to flow from the top face to the bottom face of the sandwich.

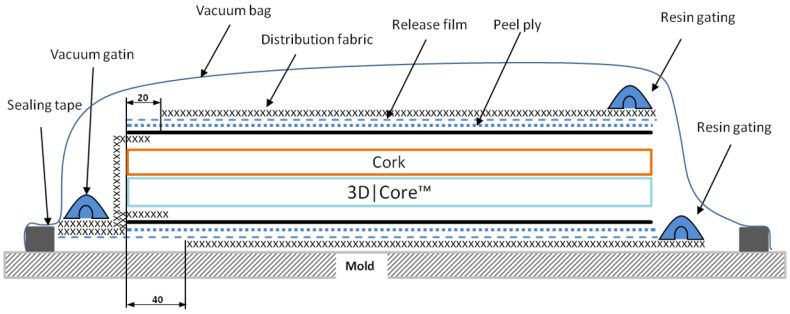

Fig. 1: Vacuum infusion set-up of the hybrid sandwich panel.

Test Setup and Specimen

Impact testing was performed using a stationary drop-impact testing machine custom-built at the Faserinstitut Bremen. The flat sandwich panels of size 330x220 mm were clamped at two edges with steel bars and impacted in the centre using a hemispherical impactor of diameter 25.4 mm. Three different configurations were investigated: "3D_7" with a 7 mm 3D|Core^{TM} core, "3D_10" with a 10mm 3D|Core^{TM} core and "cork" with a core consisting of 7 mm 3D|Core^{TM} and 3mm cork layer. Every test configuration was tested at 39 J and 53 J impact energies. After the impact, the damage was assessed using water coupled C-scan.

3. EXPERIMENTAL RESULTS

The aim of the impact tests is to investigate the effect of the cork layer on the impact behaviour of the foam core sandwich. The damage was inspected visually and using water coupled C-scan for the specimens with invisible core cracks. The detected damages are summarised in table 1. At 39 J-impact energy all the tested specimens have only local damages (small dent or/and face sheet rupture). The performed C-scans (Fig. 2) shows large damage areas in the foam core sandwich panels, which is typically a sign of shear cracks in the core, while the cork panel has no detectable damage. Moreover, a large rebound of the impactor was observed after the impact of the cork-panel.

Table 1: Summary of the detected impact damages.

Configuration	39 J-impact	53 J-impact
3D_7	Small dent; C-scan: core shear cracks	Small dent, visible core shear cracks
3D_10	Face sheet rupture; C-scan: core shear cracks	Small dent, visible core shear cracks
Cork	Small dent; C-scan: no core cracks	Face sheet rupture, C-scan: no core cracks

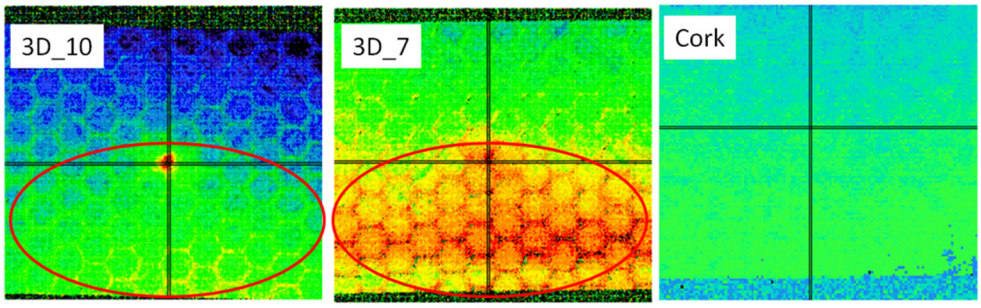

Fig. 2: Impact damages at 39J-impact.

At 53 J-impact visible shear cracks were detected in the panels 3D_7 and 3D_10 (Fig. 3) and a permanent global deformation could be observed. The impact energy was mainly dissipated by occurrence of damage mechanisms in the skins and the foam core. Considering the panel with the cork layer, only a small dent with minor face sheet damage could be observed and a rebound of the impactor took place. The C-scan in Fig. 3 shows a small damage surface in the centre of the panel and no sign of core cracks. The addition of the cork layer to the foam core led to the conversion of the impact energy mainly into elastic and rebound energy, which reduces the probability of catastrophic structure damages.

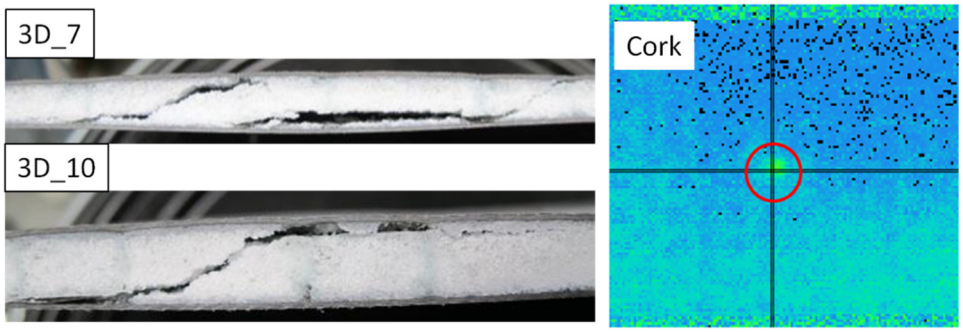

Fig. 3: Impact damages at 53J-impact.

These results shows that adding a cork layer to the foam core on the impact loaded side of the sandwich structure leads to a remarkable improvement of the impact behaviour. The core cracks were completely suppressed in the specimens with cork layer and only small dents with light face sheet damages were detected. While the impact energy is mainly dissipated through conversion in core cracks and face sheet damage for the foam core specimens, the hybrid specimens with cork

layer dissipate the impact energy by impactor rebound, oscillation damping and elastic deformation, which reduce the amount of energy that has to be absorbed by the structure during the impact.

4. CONCLUSIONS

The aim of this work was to explore the feasibility of improving the impact behaviour of foam core sandwich by using a hybrid foam cork core layout. This design enables to benefit from the good energy absorption properties of the natural cork without significant increase of the structure weight or stiffness degradation compared to a sandwich with cork core. The performed impact tests showed that only a thin cork layer is sufficient to suppress the core cracks and to improve the impact resistance of the structure. The rebound effect during the impact and the high-energy absorption of the cork layer lead to significant energy dissipation, which reduces the amount of energy absorbed by the rest of the structure.

New impact tests with honeycomb cork core are necessary to verify whether the cork layer leads to the same effects observed with the foam material. Moreover, static tests are planned to investigate the effect of the cork layer on the sandwich stiffness.

The proposed design of the sandwich structure could be an efficient solution for aircraft structures susceptible to foreign object damage like the landing gear doors or the radome. However, further investigations are required regarding the manufacturing process and other mechanical properties of the sandwich structure like structure stiffness and debonding of the cork layer.

ACKNOWLEDGMENTS

The authors would like to thank the companies 3D|Core GmbH & Co. KG for delivering the 3D|Core foam panels and Amorim Cork Composites for delivering the cork material.

REFERENCES

[1] D. Zenkert, *The Handbook of Sandwich Constructions*, EMAS Publishing, 1997.
[2] A.S. Herrmann et al., “Sandwich structures technology in commercial aviation”, *7th International Conference on Sandwich Structures*: 2005, 13-26.
[3] M.A. Dimassi et al., “Experimental study of the mechanical behaviour of pin-reinforced foam core sandwich materials under shear load”, *18th Chemnitz seminar on materials engineering*: 2016, 268-275.
[4] J.M. Silva et al., “Cork: Is it a good material for aerospace structures?”, *52nd* AIAA/ASME/ASCE/AHS/ASC Structures, Structural Dynamics and Materials Conference: 2011.
[5] L. Gill, “Cork Composite: a Review”, *Materials,* 2009; 2:776-789.
[6] J.M. Bouilly et al., “Ablative thermal protection systems for entry in Mars atmosphere. A presentation of materials solutions and testing capabilities”, *4th International Planetary Probe Workshop*: 2006.

LIST OF AUTHORS